# Behaviour of extended shear tab connections under combined axial and shear forces

By

Mohammad Motallebi Nasrabadi



Department of Civil Engineering and Applied Mechanics

McGill University

Montreal, Quebec, Canada

August 2018

A thesis submitted to McGill University in partial fulfillment of the requirements of the degree of Doctor of Philosophy

# **Dedication**

To my family for their unconditional love and support.

## **Abstract**

The configuration of a shear tab connection depends greatly on the location and geometry of the supported and supporting structural members. In comparison to the short (conventional) shear tab, the long (extended) shear tab is considered as a more economical solution to join a simply supported beam to the web of a supporting girder or column. Despite a long history of use of the extended shear tab in the USA and Canada, both the American and Canadian steel design codes provide no design recommendation for extended shear tabs under combined axial and shear forces. The Steel Construction Manual of the American Institute of Steel Construction (AISC) provides a procedure for the design of extended shear tabs under gravity induced shear force, while the Handbook of Steel Construction of the Canadian Institute of Steel Construction (CISC) is silent.

To address this shortcoming, a series of full-scale tests was performed in the Jamieson Structures Laboratory at the McGill University. The tested specimens consisted of two stiffened and four unstiffened extended shear tabs. These specimens varied in the number of vertical bolt lines and bolt rows, the bolt size, the depth and thickness of the shear plate, the offset of the bolt group from the face of the support, and the applied axial force. The test results shaped a baseline for validation of the finite element models and a subsequent parametric study. In addition to the various geometric parameters of the shear tab, the impact of the axial force with varied magnitude and direction was investigated for both unstiffened and stiffened configurations of the extended shear tab connection. Based on the experimental-numerical results, modifications to the current AISC procedure for the design of the extended shear tabs are introduced, and applied in the case of coupled axial and shear demands.

## Résumé

La configuration d'une connexion de plaque de cisaillement dépend grandement de l'emplacement et de la géométrie des éléments de structure supportés et de supports. Comparée à la plaque de cisaillement courte (conventionnelle), la plaque de cisaillement longue (étendue) est considérée comme une solution plus économique pour joindre une poutre simplement supportée à l'âme d'une poutre ou d'une colonne de support. Malgré une longue histoire d'utilisation de la plaque de cisaillement étendue aux États-Unis et au Canada, les guides de conception en acier américains et canadiens n'offrent aucune recommandation de la conception pour les plaques de cisaillement étendues sous des forces axiales et de cisaillement combinées. Le manuel de la construction en acier par l'American Institute of Steel Construction (AISC) fournit une procédure pour la conception de plaques de cisaillement étendues sous les charges de cisaillement induites par la gravité, tandis que le manuel de la construction en acier par l'Institut canadien de la construction en acier (ICCA) reste silencieux.

Pour combler cette lacune, une série de tests à grande échelle a été effectuée au laboratoire de structures Jamieson à l'Université McGill. Les spécimens testés constituaient de deux plaques de cisaillement étendues raidies et de quatre non-raidies. Ces spécimens variaient en nombre de lignes de boulons verticaux et de rangées de boulons, la taille des boulons, la profondeur et l'épaisseur de la plaque de cisaillement, le décalage du groupe de boulons de la face du support et la force axiale appliquée. Les résultats des tests ont servi à la validation de base des modèles d'éléments finis et à une étude paramétrique ultérieure. En plus des divers paramètres géométriques de la plaque de cisaillement, l'impact de la force axiale avec une amplitude et une direction variées a été étudié pour les configurations non-raidies et raidies de la connexion de plaque de cisaillement étendue. Fondé sur les résultats expérimentaux et numériques, des modifications de la procédure actuelle

de l'AISC pour la conception des plaques de cisaillement étendues sont introduites, et appliquées dans le cas de demandes axiales et de cisaillement couplées.

# Acknowledgements

First, I would like to express my deepest gratitude to my supervisors, Professor Colin Rogers and Professor Dimitrios Lignos, for providing me the opportunity to work on this research project under their supervision. Their patience, guidance and feedback along every stage of this research program were invaluable.

I would like to thank the Natural Sciences and Engineering Research Council of Canada (NSERC) as well as ADF Group Inc. and DPHV Structural Consultants for their financial and technical support, which made this research possible. The finite element computations were conducted using the Guillimin and Graham supercomputers. I would also like to acknowledge Calcul Québec and Compute Canada for providing access to these clusters.

I would like to convey my appreciation for the day-to-day assistance of Andrea Iachetta, Keith Lee, Estella Miao and David Pizzuto, who made the laboratory testing possible. I would also like to thank Dr. William Cook and John Bartczak, the coordinator and staff of the Jamieson Structures Laboratory, for all the support in the laboratory as well as their innovative solutions to the problems faced during the laboratory testing.

Special thanks to Jorge Sayat, the network technician of the Civil Engineering Department, for his support during software and hardware issues. I am also thankful to all fellow graduate students in our research group, especially Dr. Alireza Mirzaei for his mentorship and friendship.

Last but not the least; I would like to express my great appreciation to my family for their continuous love and support throughout my studies. Without their sacrifice and advice, I could not achieve anything.

## **Preface**

## **Contribution of Authors**

This thesis is presented in a manuscript-based format in accordance with the requirement of McGill University. It contains five journal papers in addition to the three chapters of introduction, literature review, and conclusion. The contribution of the authors of these five paper is as follows:

## • Chapter3:

Mohammad Motallebi <sup>a</sup>, Dimitrios G. Lignos <sup>b</sup>, Colin A. Rogers <sup>b</sup>, "Behaviour of stiffened extended shear tab connections under gravity induced shear force", Journal of Constructional Steel Research, 148 (2018) 336-350, https://doi.org/10.1016/j.jcsr.2018.06.011

## • Chapter 4:

Mohammad Motallebi <sup>a</sup>, Dimitrios G. Lignos <sup>b</sup>, Colin A. Rogers <sup>b</sup>, "Design considerations - stability of stiffened extended shear tab connections", Journal of Construction Steel Research (2018), Under Review (Submission No: JCSR\_2018\_58)

#### • Chapter 5:

Mohammad Motallebi <sup>a</sup>, Dimitrios G. Lignos <sup>b</sup>, Colin A. Rogers <sup>c</sup>, "Full-scale testing of stiffened extended shear tab connections under combined axial and shear forces", Engineering Structures (2018), Under Review (Submission No.: ENGSTRUCT\_2018\_528)

<sup>&</sup>lt;sup>a</sup> conducting the numerical studies as well as writing the manuscript

<sup>&</sup>lt;sup>b</sup> supervising the research and editing the manuscript

<sup>&</sup>lt;sup>a</sup> conducting the numerical studies as well as writing the manuscript

<sup>&</sup>lt;sup>b</sup> supervising the research and editing the manuscript

<sup>&</sup>lt;sup>a</sup> conducting the laboratory tests as well as writing the manuscript

<sup>&</sup>lt;sup>b</sup> supervising the research and editing the manuscript

<sup>c</sup> supervising the laboratory tests and the research as well as editing the manuscript

## • Chapter 6:

Mohammad Motallebi <sup>a</sup>, Dimitrios G. Lignos <sup>b</sup>, Colin A. Rogers <sup>b</sup>, "Parametric study of stiffened extended shear tab connections under combined axial and shear forces", Intended to be submitted to Engineering Structures

<sup>a</sup> conducting the numerical studies as well as writing the manuscript

<sup>b</sup> supervising the research and editing the manuscript

## • Chapter 7:

Mohammad Motallebi <sup>a</sup>, Dimitrios G. Lignos <sup>b</sup>, Colin A. Rogers <sup>c</sup>, "Unstiffened Extended Shear Tabs under Combined Axial and Shear Forces", Intended to be submitted to the Journal of Construction Steel Research

<sup>a</sup> conducting the laboratory tests and the numerical studies as well as writing the manuscript

<sup>b</sup> supervising the research and editing the manuscript

<sup>c</sup> supervising the laboratory tests and the research as well as editing the manuscript

## Contribution to original knowledge

The original contribution of this research can be described as follows:

- The current AISC method for the design of extended shear tabs was evaluated comprehensively
  and modifications were introduced to make its predictions more accurate in the case of the
  unstiffened and full-depth stiffened configurations of extended shear tabs under gravity shear
  demand.
- Required modifications to the current AISC design method were introduced in order to implement this method for design of the unstiffened and full-depth stiffened extended shear tabs under combined axial and shear forces.

# **Table of Contents**

A	bstr	ract	i
R	lésun	mé	ii
A	ckno	owledgements	iv
P	refac	nce	v
T	able	e of Contents	vii
L	ist of	of Figures	XV
L	ist of	of Tables	xxi
1	C	Chapter 1: Introduction	1
	1.1	Overview	1
	1.2	Objectives and research methodology	5
	1.3	Outline	7
	1.4	References	9
2	C	Chapter 2: Literature Review	12
	2.1	Introduction	12
	2.2	Previous research	12
	2.	2.2.1 Extended shear tabs under gravity induced shear force	12
		2.2.1.1 Moore and Owens-1992	12
		2.2.1.2 Sherman and Ghorbanpoor-2002	14
		2.2.1.3 Goodrich-2005	16
		2.2.1.4 Metzger-2006	16

2.2.1.5 Muir and Hewitt-2009	18
2.2.1.6 Thornton and Fortney-2011	19
2.2.1.7 Dowswell and Whyte-2014	19
2.2.1.8 D'Aronco-2013	23
2.2.1.9 Hertz-2014	24
2.2.1.10 Goldstein Apt 2015	26
2.2.1.11 Abou-zidan and Liu-2015	27
2.2.1.12 Fortney and Thornton-2016	28
2.2.1.13 Suleiman et al2017	30
2.2.2 Extended shear tabs under Combined Axial and Shear Forces	31
2.2.2.1 Thomas-2014	31
2.2.2.2 Johnston-2015	34
2.2.2.3 Salem-2016	36
2.3 Current design procedures	37
2.3.1 CISC Handbook of Steel Construction	37
2.3.2 AISC Steel Construction Manual-2017	39
2.3.2.1 Conventional configuration	39
2.3.2.2 Extended Configuration	40
2.3.3 Eurocode	42
2.4 Summary	43

	2.5	References	45
3	Cha	apter 3: Behaviour of Stiffened Extended Shear Tab Connections under Gra	vity
In	duced	Shear Force	49
	3.1	Introduction	51
	3.2	Brief description of full-scale laboratory testing at McGill University	56
	3.3	Finite element simulation of extended beam-to-girder shear tab connections	61
	3.3.	1 Comparison of numerical and experimental results	63
	3.4	Observed failure modes of extended beam-to-girder shear tab connections	65
	3.4.	1 Single-sided shear tabs	66
	3.4.	2 Double-sided shear tabs	69
	3.5	Discussion	71
	3.5.	1 Load transfer mechanism	72
	3.5.	2 Effective eccentricity	76
	3.6	Conclusions	80
	3.7	Acknowledgments	82
	3.8	References	82
Li	ink bet	tween Chapter 3 and Chapter 4	87
4	Cha	apter 4: Design Considerations - Stability of Stiffened Extended Shear	Tab
C	onnect	ions	88
	4.1	Introduction	90
	4.2	Brief description of full-scale laboratory tests	92

	Fin	ite element simulation	94
4.3	.1	Comparison of numerical and experimental results	94
4.3	5.2	Finite element model simulation results	96
4.4	Par	ametric study	99
4.4	.1	Load transfer mechanism	102
4.4	.2	Observed failure modes	106
4.4	.3	Bolt group shear capacity	112
4.5	Coı	nclusions	116
4.6	Acl	knowledgments	117
4.7	Ref	Perences	117
Link be	etwee	n Chapter 4 and Chapter 5	122
5 Ch	napte	r 5: Full-scale Testing of Stiffened Extended Shear Tab Connections u	nder
	_	r 5: Full-scale Testing of Stiffened Extended Shear Tab Connections units and Shear Forces	
	ned A		123
Combii	ned A	axial and Shear Forces	<b>123</b> 125
Combin 5.1	ned A Intr	oduction	123 125 128
5.1 5.2	Intr	oductionl-scale laboratory testing	123 125 128
5.1 5.2 5.2	Intr Ful	description of test specimens	<b>123</b> 125 128 129 134
5.1 5.2 5.2 5.2	Intr Ful 2.1 2.2	Description of test specimens  Test setup	123 125 128 129 134
5.1 5.2 5.2 5.2 5.2	Intr Ful 2.1 2.2 2.3	Description of test specimens  Test setup  Instrumentation	123 125 128 129 134 135

5.3.1	Model validation	144
5.3.2	Simulation results	146
5.4 D	iscussion	150
5.4.1	Shear plate yielding	150
5.4.2	Shear plate internal forces along the interior bolt line	152
5.4.3	Effect of axial force	155
5.4.4	Evaluation of the current design procedure	156
5.5 Co	onclusions	158
5.6 A	cknowledgments	159
5.7 Re	eferences	160
Link betwe	en Chapter 5 and Chapter 6	165
6 Chapt	er 6: Parametric Study of Stiffened Extended Shear Tab Connect	
_	er 6: Parametric Study of Stiffened Extended Shear Tab Connect	ions under
Combined		ions under 166
Combined 6.1 In	Axial and Shear Forces	ions under 166
Combined 6.1 In	Axial and Shear Forcestroduction	ions under
Combined 6.1 In 6.2 Fi	Axial and Shear Forces	ions under
6.1 In 6.2 Fi 6.1.1 6.1.2	Axial and Shear Forces	ions under
6.1 In 6.2 Fi 6.1.1 6.1.2	Axial and Shear Forces	ions under
6.1 In 6.2 Fi 6.1.1 6.1.2 6.3 Di	Axial and Shear Forces  troduction  nite element simulations  Numerical parametric study.  Simulation results	ions under

6.3.4	Shear plate resistance under tension	191
6.3.5	Shear plate resistance under compression	191
6.3.6	Effects of ht/hw ratio	192
6.3.7	Effect of the gap between beam and girder	193
6.3.8	Effect of axial force	193
6.3.9	Shear plate internal forces along the bolt line	199
6.3.10	The net section fracture	206
6.3.11	Design procedure	208
6.4 Con	nclusions	214
6.5 Acl	knowledgments	217
6.6 Ref	ferences	217
Link betwee	en Chapter 6 and Chapter 7	221
7 Chapte	r 7: Unstiffened Extended Shear Tabs under Combined Axia	al and Shear
Forces		222
7.1 Inti	oduction	224
7.2 Ful	l-scale laboratory testing	229
7.2.1	Description of test specimens	229
7.2.2	Test Setup	233
7.2.3	Loading Protocol	234
7.2.4	Instrumentation	234
7.2.5	Experimental Results	235

	7.3	Finite element simulation	244
	7.3.1	1 Description of FE models	245
	7.3.2	2 Model Validation	247
	7.3.3	3 FE Parametric study	249
	7.3.4	4 Simulation Results	252
	7.4	Discussion	258
	7.4.1	1 Ultimate resistance under gravity induced shear force	258
	7.4.2	2 Shear capacity of the bolt group	260
	7.4.3	3 Yielding of the shear plate under shear force	261
	7.4.4	4 Shear plate buckling	265
	7.4.5	5 Gross section rupture	267
	7.4.6	6 Net section rupture	268
	7.4.7	7 Connection resistance under axial force	269
	7.4.8	8 Effect of axial force	270
	7.5	Conclusions	278
	7.6	Acknowledgments	281
	7.7	References	281
8	Cha	apter 8: Summary and conclusions	289
	8.1	Summary	289
	8.2	Conclusions	290

8.3	Original contribution	294
8.4	Recommendations for future research	295
Append	lix A: Design Calculations	297
Append	lix B: Fabrication Drawings	340
Append	lix C: Instrumentation	356

# **List of Figures**

Fig. 1-1 Various configurations of the shear tab connection:	3
Fig. 2-1. Test setup for shear tab tests [1]	3
Fig. 2-2. Typical test setup for beam-to-girder shear tabs [2]	5
Fig. 2-3- Schematic of test setup [5]	7
Fig. 2-4. Different types of the stabilizer plates: a) Type I, b) Type II, c) Type III [21] 2	9
Fig. 2-5 Setup for shear tab testing at the University of Alberta [24]	1
Fig. 2-6. Failure modes of unstiffened shear tabs: (a) weld tearing, (b) bolt fracture [23] 3	3
Fig. 2-7. Failure modes of stabilized shear tabs: (a) out-of-plane deformation of shear plate	Э,
(b) tearing at tensile re-entrant corner of shear plate [23]	4
Fig. 3-1.Extended beam-to-girder shear tab connections	1
Fig. 3-2. Full-depth stiffened extended beam-to-girder shear tab	4
Fig. 3-3. Full-depth stiffened extended beam-to-column shear tab	4
Fig. 3-4. Laboratory tests of beam-to-girder shear tabs	7
Fig. 3-5. Laboratory tests of beam-to-girder shear tabs	8
Fig. 3-6. Laboratory test of beam-to-girder shear tab specimen BG3-2-13-F 5	9
Fig. 3-7. Test results6	1
Fig. 3-8 Finite element model specifics	2

Fig. 3-9. Numerical model verification
Fig. 3-10. Predictions of numerical models for shear tab connection BG3-2-10-F
Fig. 3-11. Predictions of numerical models for shear tab connection BG3-2-13-F
Fig. 3-12. Prediction of model FE-E-SH of BG3-2-10-F
Fig. 3-13. FE models for double-sided shear tabs
Fig. 3-14. Prediction of model FE-Pl-Imp of BG3-2-10-F
Fig. 3-15. Free body cuts from FE models
Fig. 3-16. Predictions of the developed axial force at the stiffener
Fig. 3-17. Prediction of elastic FE models of BG3-2-10-F for vertical force
Fig. 3-18. Predictions of numerical models for shear force
Fig. 4-1. Extended beam-to-girder shear tab connections
Fig. 4-2. Test specimens: (a) BG3-2-10-F, (b) BG3-2-13-F, (c) BG6-2-10-F
Fig. 4-3. Finite element model predictions: (a and b) specimen BG3-2-10-F, (c and d)
specimen BG3-2-13-F, (e and f) specimen BG6-2-10-F
Fig. 4-4. Finite element model predictions
Fig. 4-5. Finite element model predictions of specimen BG6-2-10-F
Fig. 4-6. Finite element predictions using models with elastic material properties99
Fig. 4-7. Response of elastic FE models
Fig. 4-8. Finite element model predictions for bolt group eccentricity
Fig. 4-9. Predictions of FE models for α ratio

Fig. 4-10. Response of FE models	107
Fig. 4-11. Response of FE models of: BG3-2-10-F configuration with varied: (a) $h_t/h_w$ ra	atic
(Group 2), (b) $h_w/t_w$ ratio (Group 3), (c and d) Gap distance (Group 4)	108
Fig. 4-12. Bending moment equilibrium at top portion of the shear plate	109
Fig. 4-13. Response of <i>E-Bo</i> FE models	113
Fig. 4-14. Bolt group eccentricity of E-Bo models	114
Fig. 5-1.Single-sided extended shear tab configurations	126
Fig. 5-2. Double-sided configuration of test specimens: (a) BG3-2-13-F-200C, (b) BG6-2-	19.
F-500C	129
Fig. 5-3. Details of test specimens: (a) BG3-2-13-F-200C, (b) BG6-2-19-F-500C	130
Fig. 5-4. Specimens: (a & b) BG3-2-13-F-200C, (c&d) BG6-2-19-F-500C	131
Fig. 5-5. Laboratory tests: (a) test setup, (b) axial load application system	135
Fig. 5-6. Instrumentation of Specimen BG3-2-13-F-200C: (a) targets of optical CMM systems of the control of the	em
(b) LVDTs, (c) strain gauges	136
Fig. 5-7. Measured response vs. connection rotation: (a) connection shear force, (b) shear pl	late
out-of-plane deformation	138
Fig. 5-8. Specimen BG3-2-13-F-200C	138
Fig. 5-9. Specimen BG3-2-13-F-200: (a) binding between beam and shear plate, (b	)-d]
deformed shape at end of test	139

Fig. 5-10. Bearing deformation and fracture along the interior bolt line of specimen BG3-2-
13-F-200C at
Fig. 5-11. Specimen BG6-2-19-F-500C: (a) bolt bearing at plate top half, (b) bolt bearing at
plate bottom half, (c) diagonal crack at bottom re-entrant corner
Fig. 5-12. Finite element model specifics
Fig. 5-13. FE model verification
Fig. 5-14. Simulated response of Specimen BG3-2-13-F
Fig. 5-15. Simulated response of Specimen BG6-2-19-F
Fig. 5-16. Neal's Interaction equation (Eq. (5-3))
Fig. 5-17. Shear plate equivalent plastic strain (PEEQ) corresponding to the net section
fracture at: (a) BG3-2-1-13-F-200C, (b) BG6-2-1-9-F-500C
Fig. 5-18. FE model predictions
Fig. 5-19. Bolt group under an eccentric shear force
Fig. 5-20. Bolt under: (a) shear force, (b) shear and tension, (c) shear and compression 154
Fig. 6-1. Configuration of single-sided extended shear tab connections
Fig. 6-2. Specimen BG3-2-13-F-200: (a) FE model verification, (b) deformed shaped at end
of analysis, (c) deformed shape at end of test
Fig. 6-3. FE model predictions for: shear force of configurations (a) BG3-2-10-F and (b) BG3-
2-13-F, bending moment of configurations (c) BG3-2-10-F and (d) BG3-2-13-F

Fig. 6-4. Deformed shape of shear tab at end of analysis for models: (a) BG3-2-10-F, (b) BG3
2-13-F
Fig. 6-5. FE model predictions for: (a) connection shear force, (b) shear plate out-of-plane
deformation
Fig. 6-6. Plastic strain propagation corresponding to capping strength
Fig. 6-7 P <sub>n</sub> /P under combined axial and shear forces
Fig. 6-8. Interior vertical bolt line under: (a) concentric shear force, (b) tension and concentric
shear, (c) compression and concentric shear
Fig. 6-9. Interaction equation at the plate net section for FE models BG3-2-10-F 203
Fig. 7-1. Different configurations for unstiffened extended shear tabs
Fig. 7-2. As built dimensions of the specimens: (a) BC3-2-10, (b) BC3-2-10-200C, (c) BC6
2-16, (d) BC6-2-16-500C
Fig. 7-3. Specimens: (a) BC3-2-10, (b) BC3-2-10-200C, (c) BC6-2-16, (d) BC6-2-16-500
Fig. 7-4. Specimen BC6-2-1-6-500C: (a) test setup, (b) axial load application system 233
Fig. 7-5. Instrumentation of Specimen BC6-2-16-500C: (a) strain gauges, (b) targets of optical
CMM system, (c) LVDTs
Fig. 7-6. Damage propagation of Specimen
Fig. 7-7. Deformed shape of Specimens: (a-c) BC3-2-10, (d-f) BC3-2-10-200C
Fig. 7-8. Deformed shape of Specimens: (a-c) BC6-2-16, (d-f) BC6-2-16-500C

Fig. 7-9. The interior vertical bolt line of Specimen BC6-2-16	240
Fig. 7-10. The interior vertical bolt line of Specimen BC6-2-16-500C	240
Fig. 7-11. Details of FE model	246
Fig. 7-12. Finite element model predictions of connection shear force vs. connection	n rotation
and shear plate vertical deformation	248
Fig. 7-13. Deformed shape of FE model: (a) BC3-2-10, (b) BC3-2-10-200C, (c) BC6-	-2-16, (d)
BC6-2-16-500C	249

# **List of Tables**

Table 3-1 AISC predicted strength of shear tab test specimens	59
Table 3-2-Features and targeted behavioural aspects of FE models	65
Table 3-3-Bolt shear strength based on predictions of the model FE-E-Bo	79
Table 4-1. Stiffened and extended shear tab connection configurations for parametric FE stu	ıdy
	01
Table 4-2. Elastic buckling strength based on predictions of the FE models E	.05
Table 4-3. Shear strength based on predictions of the FE models	.11
Table 4-4. Bolt shear strength based on predictions of the FE models E-Bo	15
Table 5-1. Material properties of connection components	31
Table 5-2. AISC predicted strength of shear tab test specimens	34
Table 5-3. Calculated plastic capacities of shear tab test specimens	46
Table 5-4. FE model predictions for connection resistance	.55
Table 5-5. Connection resistance to different failure modes	.57
Table 6-1. Connection configurations for parametric FE study	.73
Table 6-2. Material properties of connection components	75
Table 6-3. Predicted plastic capacities of shear tab connection specimens	.77
Table 6-4. Connection response under gravity induced shear force	.78
Table 6-5.bolt shear strength based on FE-E-Bo models	81

Table 6-6. FE models predictions for connection axial capacities	182
Table 6-7. FE models predictions for connection capacities under combined axia	l and shear
forces	183
Table 6-8. Gross section yielding strength	187
Table 6-9. Connection capacities under combined axial and shear forces	197
Table 6-10. Net section yielding strength of connection under gravity shear	202
Table 6-11. Net section yielding strength of the connections under combined axia	ıl and shear
force	205
Table 6-12. Shear strength corresponding to net section fracture	207
Table 6-13. Ultimate capacity of the connections under gravity shear force	211
Table 6-14. Ultimate capacity of the connections under combined axial and shear	forces . 212
Table 7-1. Material properties of connection components	231
Table 7-2. AISC predicted shear strength of shear tab test specimens	232
Table 7-3 Specimen measured response	241
Table 7-4. Weld line resistance under an eccentric shear force	243
Table 7-5 Observed and predicted failure modes and corresponding resistances	244
<b>Table 7-6.</b> Unstiffened shear tab connection configurations for parametric FE students.	ły 250
Table 7-7. Connection response under gravity induced shear force based on FE an	alyses . 254
Table 7-8. FE models predictions for connection axial capacities	256
Table 7-9. Connection response under gravity induced shear force based on FE an	alysis 257

Table 7-10. Ultimate strength of the connection with A325 bolts under gravity shear demand
Table 7-11. Ultimate strength of the connection with A490 bolts under gravity shear demand
Table 7-12. Yielding of the plate's critical gross section
Table 7-13 Yielding of the plate's critical net section
Table 7-14 Plate buckling strength
Table 7-15. Connection resistance corresponding to gross section rupture
Table 7-16. Connection resistance corresponding to net section rupture
Table 7-17. Ultimate capacity of shear tabs under combined axial and shear force 273
Table 7-18 buckling strength under combined axial and shear forces
Table 7-19 Rupture strength of the critical gross section under combined axial and shear
demands
Table 7-20. Rupture strength of the critical net section under combined axial and shear forces

# 1 Chapter 1: Introduction

## 1.1 Overview

Structural steel connections are classified, based on their stiffness, into three main categories; the simple shear connection, the partially restrained (PR) moment connection, and the fully restrained (FR) moment connection. Shear connections have low stiffness and allow relative rotation between the connected members without developing significant bending moment. In contrast, fully restrained moment connections transmit significant bending moment under small relative rotation due to their large stiffness. Partially restrained connections transfer significant bending moment while experiencing large relative rotation. The Commentary on the AISC 360 Specification [1] considers  $K_s = 2EI/L$  as the maximum allowable stiffness of a shear connection at the service load level, whereas 20EI/L is considered as the minimum K<sub>s</sub> value for a fully restrained moment connection. In addition to the connection stiffness, the AISC 360 Specification allows designers to expand the definition of shear connections to those that transfer less than 20% of the plastic moment resistance of the supported beam. The Canadian steel design standard (CSA-S16) [2] implements similar terms for connection classification; simple, semi-rigid, and rigid connections. However, it provides no quantitative procedure to aid in this classification. In addition to the AISC procedure, researchers such as Bjorhovde [3] have proposed alternative schemes for connection classification. In the analysis of the structure, the shear and fully restrained moment connections are replaced respectively by the idealized pin and fixed connections; whereas, the real moment vs. rotation behaviour of the partially restrained connection would have to be included in the analysis.

Although the shear connections are permitted to deform (rotate), they are also required to have enough shear strength to resist the end reactions of the supported beam. Furthermore, they should have enough ductility to endure the rotational demand of the supported beam end. Among the various possible configurations for shear connections, the shear tab is widely used in steel construction in the USA and Canada due to its simplicity in terms of fabrication and erection. This connection consists of a steel plate, which is shop-welded to the supporting girder or column, and then bolted to the supported beam in the field. The shear tab can be used to connect a beam into the flange of a supporting column (Fig. 1-1a). Further, the shear tab can be used to connect a beam to the web of a supporting girder (Fig. 1-1b). Although the short shear tab can be implemented easily for beam-to-column flange connections, coping of the beam's flange(s) is necessary if the plate is joined to the web of the supporting member. In comparison to the short (conventional) shear tab, the long (extended) shear tab is considered as a more economical solution to join a simply supported beam to the web of a supporting girder or column (Fig. 1-1c and 1-1d, respectively). The long plate moves the bolts clear of the support; as such, there is access to install the bolts, and also, no need for coping of the beam's flange(s). In addition to the unstiffened extended configuration, a stiffened extended shear tab may be used to address the need to stabilize the beam or the shear plate itself (Fig. 1-1e and 1-1f).

The supporting member can be classified based on the rotational stiffness that it provides to the shear plate, i.e. rigid or flexible. The column flange support scenario (Fig. 1-1a) and the double-sided connection configurations (Figs. 1-1g & 1-1h) are typically assumed to provide a rigid support for the shear plate. The single-sided configuration of the beam-to-supporting web connections (girder and column) is typically classified as a flexible support.

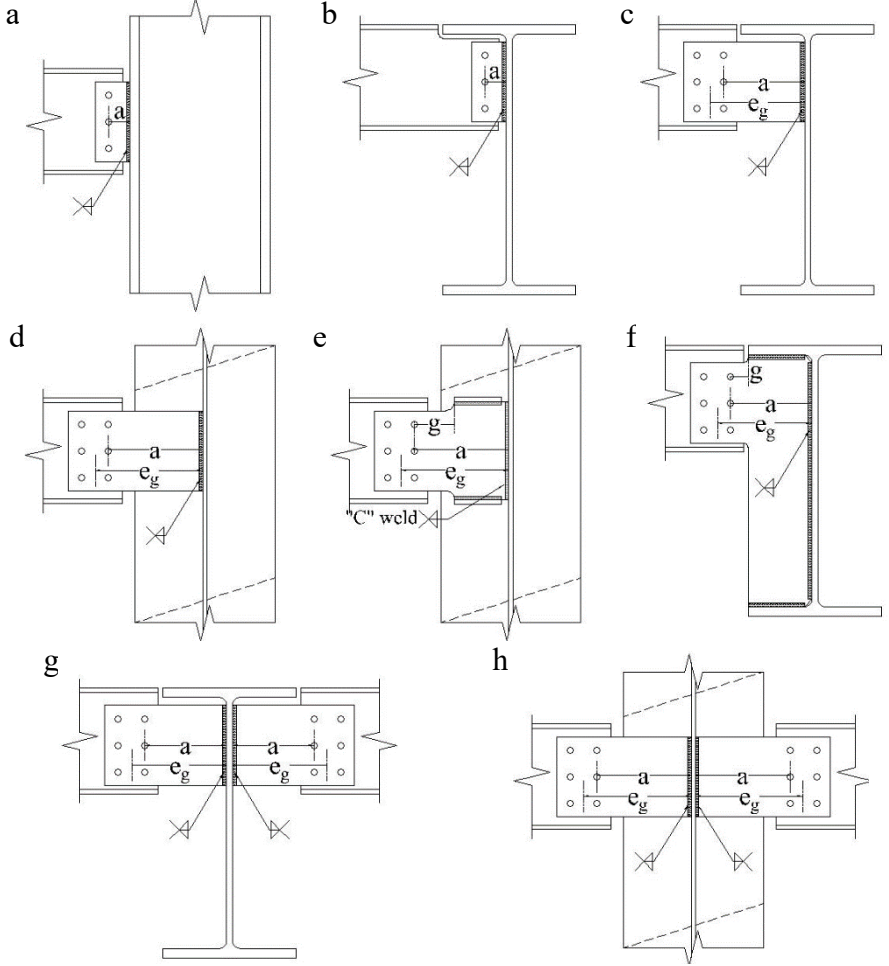


Fig. 1-1 Various configurations of the shear tab connection: (a) conventional beam-to-column flange, (b) beam-to-girder web with coped beam, (c) unstiffened extended beam-to-girder, (d) unstiffened extended beam-to-column, (e) stiffened extended beam-to-girder, (g) double-sided beam-to-girder, (h) double-sided beam-to-column

The current AISC Steel construction Manual [4] classifies the shear tab connection into two main categories: conventional and extended. The distance between the weld line and the single vertical bolt line (a distance in Fig. 1-1-a) is limited to 89 mm (3.5 in.). Furthermore, the number of bolts should be between 2 and 12. The extended shear tab can have multiple vertical bolt lines, while there is no limitation for the number of bolt rows or the a distance. The current CISC Handbook of Steel Construction [5] provides a design table for limited configurations of shear tabs; i.e. shear tabs with a single vertical line of two to seven bolts and a 75mm distance between the weld and bolt lines. This design table, developed based on a design procedure of conventional

shear tab connections dating back to the experimental study of Astaneh et al. in 1989 [6], does not represent the current state of practice for steel construction in which more complex shear tab connections with multiple vertical bolt lines are common.

Although the AISC Steel Construction Manual has illustrated the use of the extended plate configuration since 1992 [7], the AISC introduced a design procedure for the extended shear tab connection for the first time in 2005 [8, 9]. Although the AISC method was developed for design of unstiffened extended shear tabs under gravity induced shear force, practicing structural engineers use this method for design of stiffened extended shear tabs owing to the lack of a validated comprehensive design procedure. Of note, this design procedure is applicable only to connections that are subjected to gravity induced shear force. Contrary to the traditional perspective on these shear connections, it may be necessary to design them under combined axial and shear (gravity) forces. Large axial force may develop in a shear connection when the supported beam performs as the lateral brace of the supporting column, or is a component in the lateral force resisting load path. The gravity load may also cause an axial force in the shear connection of supported inclined beams in a stair frame, rafter or a gable-framed building, for example. Further, a simple shear connection may be subjected to an axial force due to wind and/or earthquake loads, while it continues to resist gravity-induced shear force. Furthermore, extreme loading scenarios, such as the removal of a column, lead to the development of significant axial tension in these connections.

Of note, codes and standards used in the design of steel structures [1, 10-13] specify tie force requirements as the minimum tensile forces for tightening of structural elements together to take necessary precautions for reducing the progressive collapse possibilities following a column loss. However, there is a great discrepancy regarding the tie force value and its application. Despite the

need, there is little guidance in the literature for the design of shear connections under combined axial and shear forces [14, 15]. Although the AISC Steel Construction Manual [4] addresses the shear tab connection only under gravity shear demand, the Steel Connection Handbook (Section 2.5.3) [14] and AISC Design Examples (Example IIA-19B) [15] make a few minor adjustments to the AISC design method in order to implement it for design of extended shear tabs under combined axial and shear forces. To take into account the impact of the axial force on the connection behaviour, this adjusted design method [14, 15] combines the existing equation for the interaction of bending and shear in shear tabs with the design requirement of Section H1.1 of the AISC 360 Specification [1] for doubly symmetric members subjected to flexure and axial force. This recommendation is based on engineering judgment and needs to be verified by laboratory tests and additional finite element analyses.

Despite a long history of use, limited research has been conducted on extended shear tab connections. Most past studies focused mainly on the behaviour of the unstiffened extended shear tab under gravity induced shear force [16-19]. Regarding the extended shear tabs under combined axial and shear forces, a few researchers have studied the behaviour of relatively long shear tabs in the presence of small axial force [20-22]. Further research is needed to determine the impact of large axial force on the behaviour of extended shear tab connections.

## 1.2 Objectives and research methodology

The aim of this research is to develop design recommendations for extended shear tab connections subjected to combined axial and shear forces. These extended shear tabs can be classified into two main categories: 1) full-depth stiffened beam-to-girder shear tab connections, and 2) unstiffened extended beam-to-column shear tab connections. This main objective is divided into four sub-objectives as follows:

#### Full-depth stiffened extended beam-to-girder shear tab connections

- Objective 1: Characterize the behaviour of the full-depth stiffened extended beam-to-girder shear tab under gravity induced shear force, evaluate the response to loading with respect to the current AISC design method and propose modifications to this design method if warranted.
- Objective 2: Study the impact of axial force on the behaviour of the full-depth stiffened extended beam-to-girder shear tab and propose required design recommendations for this configuration and loading scenario.

#### Unstiffened extended beam-to-column shear tab connections

- Objective 3: Evaluate the influence of various parameters on the behaviour of the unstiffened extended beam-to-column shear tab, subjected to gravity induced shear force.
- Objective 4: Investigate the behaviour of the unstiffened extended shear tabs under combined axial and shear forces to recommend requirements for their design.

## **Research Methodology**

The listed sub objectives were attained following the methodology described below:

- Objective 1: This objective was achieved through parametric finite element (FE) simulations. First, the FE models were developed in the commercial software ABAQUS-6.11-3 [23] based on full-scale stiffened extended shear tabs, previously tested under gravity shear demand in the Jamieson Structures Laboratory at McGill University [24, 25]. The validated FE models then were implemented in a parametric study that incorporated the number of vertical bolt lines and bolt rows, the thickness of the shear plate, the depth of shear plate and supporting girder, the slenderness of the girder web, and the offset of the bolt group from the girder web.
- Objective 2: To achieve this objective, laboratory tests were conducted in addition to parametric FE simulations. First, the author tested two full-scale specimens of the full-depth

stiffened extended shear tab connection under combined shear and axial compression. The test specimens were chosen to represent the double-sided configuration due to its ability to provide a load path for pass-through forces, allowing the connection to experience a wide range of axial and shear forces. Considering the symmetry of a double-sided shear tab along the girder axis, the laboratory specimens consisted of only half of the connection, i.e. a single beam connected to a simulated girder. The test results shaped a baseline for validation of the FE models and a subsequent parametric study. In addition to the various geometric parameters of the shear tab, the impact of the axial force with varied magnitude and direction was investigated.

- Objective 3: This objective was achieved through an experimental-numerical study. Two full-scale unstiffened extended beam-to-column shear tabs were tested under gravity induced shear force. Based on the measured response, a FE model was calibrated and a parametric FE study was carried out to determine the dependence of the connection's response to gravity shear demand on a number of shear tab parameters; i.e. the number of vertical bolt lines and bolt rows, the bolt size and bolt grade, the depth and thickness of the shear plate, and the offset of the bolt group from the column face.
- Objective 4: As a first step to achieve this objective, the author tested two specimens under combined shear and axial compression. These two specimens were identical to those tested under gravity shear demand, in order to determine the impact of the axial force on the connection behaviour. Further, the validate FE models of the tested specimens were used to conduct a parametric study and determine the dependence of the connection response on the magnitude and direction of the axial load as well as the offset of the bolt group from the column face.

### 1.3 Outline

This manuscript-based thesis consists of eight chapters, including the Introduction (Chapter 1). Chapter 2 gives a brief background on the extended shear tab connections. In addition to describing the current AISC and CISC design procedures for extended shear tab connections, the existing related literature is summarized.

Chapter 3 focuses on the load transfer mechanism of single- and double-sided configurations of the full-depth stiffened extended beam-to-girder shear tab connection. This chapter is based on the results of FE simulations, validated based on the results of the laboratory tests which were previously conducted at McGill University.

Chapter 4 contains a presentation of the results of a parametric FE study, conducted on the single-sided configuration of the full-depth stiffened extended beam-to-girder shear tab connection. The influence of a number of parameters on the connection behaviour is evaluated; among them, the number of the vertical bolt lines and bolt rows, the thickness of the shear plate, the offset of the bolt group from the girder face, the depth of shear plate and girder web, and the slenderness of the girder web. Further, recommendations are presented for design of this configuration of extended shear tab connections. Objective 1 of this research was achieved through Chapters 3 and 4.

Chapter 5 reports on the results of two full-scale laboratory tests of the double-sided configuration of the full-depth stiffened extended beam-to-girder shear tab connection. The test specimens were subjected to combined gravity shear and axial compression. In addition to the experimental results, results of complementary FE simulations are presented.

Chapter 6 provides the results of a parametric FE study on the double-sided configuration of the full-depth stiffened extended beam-to-girder shear tab connection. This chapter first presents the influence of various parameters on the connection behaviour under gravity induced shear force.

Then, the FE models are subjected to coupled shear and axial forces to determine the impact of the magnitude and direction of the axial force on the connection response. Objective 2 of this research was achieved through Chapters 5 and 6.

Chapter 7 presents the results of full-scale laboratory tests and parametric FE simulations, conducted on the unstiffened extended beam-to-column shear tab connection. In addition to the gravity induced shear force, the connection behaviour is studied under combined axial and shear force. Based on the experimental-numerical results, modifications to the current AISC procedure for the design of the extended shear tabs are introduced, and applied in the case of coupled axial and shear demands. Objectives 3 and 4 of this research were achieved through Chapter 7.

Chapter 8 provides a summary of the research and a listing of the main findings. In addition, recommendations are presented for future research on extended shear tab connections.

## 1.4 References

- [1] AISC 360-16, Specification for structural steel buildings, American Institute of steel Construction, Chicago, IL, 2016.
- [2] CSA-S16-14, Design of steel structures, Canadian Standards Association, Mississauga, ON., 2014.
- [3] R. Bjorhovde, A. Colson, J. Brozzetti, Classification system for beam-to-column connections, J. Struct. Eng. ASCE, 116(11) (1990) 3059-3076.
- [4] Steel construction manual, 15<sup>th</sup> edition, American Institute of steel Construction, Chicago, IL, 2017.
- [5] CISC, Handbook of steel construction, Canadian Institute of Steel Construction, Markham, ON., 2016.

- [6] A. Astaneh, S.M. Call, K.M. McMullin, Design of single plate shear connections, Eng. J. AISC, 26(1) (1989) 21-32.
- [7] Manual of steel construction, volume ii connection, 9th asd edition/1st lrfd edition, American Institute of steel Construction, Chicago, IL, 1992.
- [8] Steel construction manual, 13<sup>th</sup> edition, American Institute of steel Construction, Chicago, IL, 2005.
- [9] L.S. Muir, C.M. Hewitt, Design of unstiffened extended single-plate shear connections, Eng. J. AISC, 46(2) (2009) 67-80.
- [10] UFC 4-023-03, Unified facilities criteria, design of buildings to resist progressive collapse, U.S. Department of Defence, Washington, DC., 2013.
- [11] IBC-2015, International building code,, International Code Council, Falls Church, VA., 2015.
- [12] BS EN 1991-1-7: 2006, Eurocode 1: Actions on structures, part7: General actions-accidental actions, British Standards Institution, London, England, 2010.
- [13] ASCE 7-16, Minimum design loads for buildings and other structures, American Society of Civil Engineers, Reston, VA, 2016.
- [14] A.R. Tamboli, Handbook of structural steel connection design and details, Third edition, McGraw-Hill, New York, NY., 2016.
- [15] Design examples companion to the aisc steel construction manual, version 15.0, American Institute of steel Construction, Chicago, IL, 2017.
- [16] D.B. Moore, G.W. Owens, Verification of design methods for finplate connections, The Struct. Eng., 70(3) (1992).
- [17] D.R. Sherman, A. Ghorbanpoor, Design of extended shear tabs, University of Wisconsin-Milwaukee, Milwaukee, WI, 2002.

- [18] W. Goodrich, Behavior of extended shear tabs in stiffened beam-to-column web connections, Master's Thesis, Vanderbilt University, Nashville, TN, 2005.
- [19] K.A. Baldwin Metzger, Experimental verification of a new single plate shear connection design model, Master's Thesis, Virginia Polytechnic Institute and State University, Blacksburg, VA, 2006.
- [20] K. Thomas, Design and behaviour of extended shear tabs under combined loads, Master's Thesis, University of Alberta, Edmonton, AB, 2014.
- [21] K. Thomas, R.G. Driver, S.A. Oosterhof, L. Callele, Full-scale tests of stabilized and unstabilized extended single-plate connections, Structures, 10 (2017) 49-58.
- [22] P. Salem, Unified design criteria for steel cantilever plate connection elements, PhD Thesis, University of Alberta, Edmonton, AB, 2016.
- [23] ABAQUS 6.11-3, [Computer software], Dassault Systemes Simulia Corp., Providence, RI.
- [24] J. Hertz, Testing of extended shear tab connections subjected to shear, Master's Thesis, McGill University, Montreal, QC, 2014.
- [25] N. Goldstein Apt, Testing of extended shear tab and coped beam-to-girder connections subject to shear loading, Master's Thesis, McGill University, Montreal, QC, 2015.

# 2 Chapter 2: Literature Review

# 2.1 Introduction

A brief presentation of the existing knowledge of extended shear tab connections has been provided in this chapter. A review of the findings from previous research studies on shear tab connections is first included. The focus is primarily on recent research studies of extended shear tab connections. In the second part, the current design procedures of shear tab connections used in Canada and the United States are presented.

## 2.2 Previous research

## 2.2.1 Extended shear tabs under gravity induced shear force

## 2.2.1.1 Moore and Owens-1992

To investigate the behaviour of shear tab connections, 11 full-scale specimens were tested by Moore and Owens [1]. These tests consisted of six extended configurations, while the remaining five specimens represented the conventional configuration. Among these six specimens of extended shear tabs, the beam was framed into the column web in three tests. There was a single vertical bolt line, while the number of horizontal bolt lines varied. Hereafter, only the experimental results of extended shear tabs will be discussed. Referring to Fig. 2-1, both ends of the test beam were connected to the supporting columns using a shear tab connection. The span-to-depth ratio of the test beam was equal to 20 for all specimens. The test beams, laterally supported at regular intervals along their entire length, were subjected to two concentrated forces. The location of these concentrated forces was determined based on elastic analysis to resemble the rotational demand at the ends of a simply supported beam under a uniformly distributed load. Of note, this was a critical

step to insure that the shear tab was subjected to a real world load scenario, i.e. a coupled rotation, bending moment and shear force.

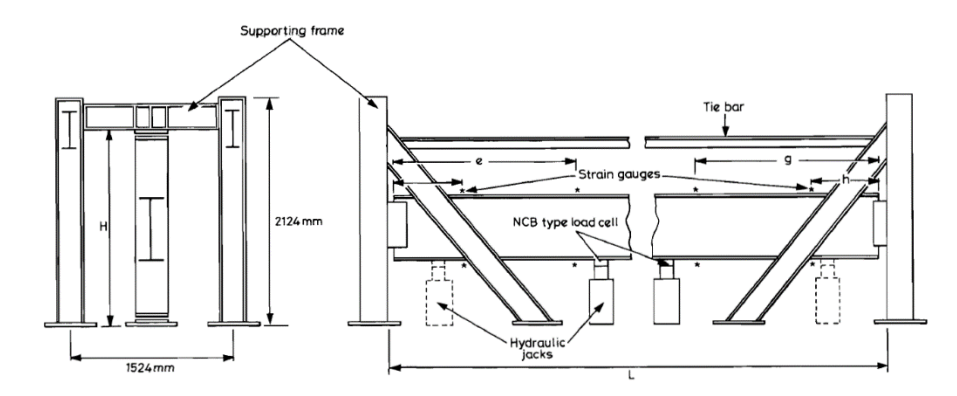


Fig. 2-1. Test setup for shear tab tests [1]

The specimens were loaded in two phases. In the first phase, the elastic characteristics of the specimens were determined by loading them up to the anticipated unfactored dead and live load. The load was removed as the test beam showed signs of yielding due to the bending. In the second phase of loading, the concentrated forces were moved closer to the connections to guarantee that failure would occur at the connection instead of the test beam. The specimens then were loaded up to failure of the connection. However, it should be noted that this action was not a conservative move because the connection was subjected to a smaller bending moment and rotation in comparison to a real world loading protocol. The first phase demonstrated that the mid-span deflection of the test beams was much larger than the analytical estimate and the beam serviceability limits (L/360). This observation was attributed to the large rotation and vertical deformation of the shear plate, e.g. the shear tabs, which framed into the column web, experienced 0.12 rad rotation.

Based on the results of the second phase, the bolt and weld lines were identified as the critical points along the shear plate. The shear plate failed at either of these points due to the interaction of shear and bending moment. Short shear tabs had a tendency to fail at the bolt line while long

shear tabs would fail at the weld line. Twisting of the plate was also determined as a failure mode of extended shear tabs. The authors suggested that the serviceability of the supported beam should be considered as a failure mode in design and detail of the extended shear tabs.

#### 2.2.1.2 Sherman and Ghorbanpoor-2002

The main goal of this research was to establish a design procedure for the extended shear tab connection. To this end, Sherman & Ghorbanpoor [2] tested 31 full-scale extended shear tabs under gravity induced shear force. In these tests, the shear tab was framed into the web of its supporting member (either column or girder). These tests included 14 stiffened beam-to-column shear tabs, nine stiffened beam-to-girder shear tabs, two unstiffened beam-to-girder shear tabs, and five unstiffened beam-to-column shear tabs. Of note, the shear tab was extended to the bottom flange of the girder in only two stiffened beam-to-girder shear tabs. Although only a single vertical bolt line was used in these specimens, the remaining parameters were varied; i.e. the shear plate depth, the web slenderness of the of the supporting member, the span-to-depth ratio of the supported beam, the number of the horizontal bolt lines, the type of the bolt holes, the weld configuration, and the size of the stiffeners. To load these specimens, a concentrated force was applied to the test beam (Fig. 2-2). The location of the concentrated load was determined through elastic analysis to replicated the expected bending and rotation at the ends of a uniformly loaded simply supported beam.

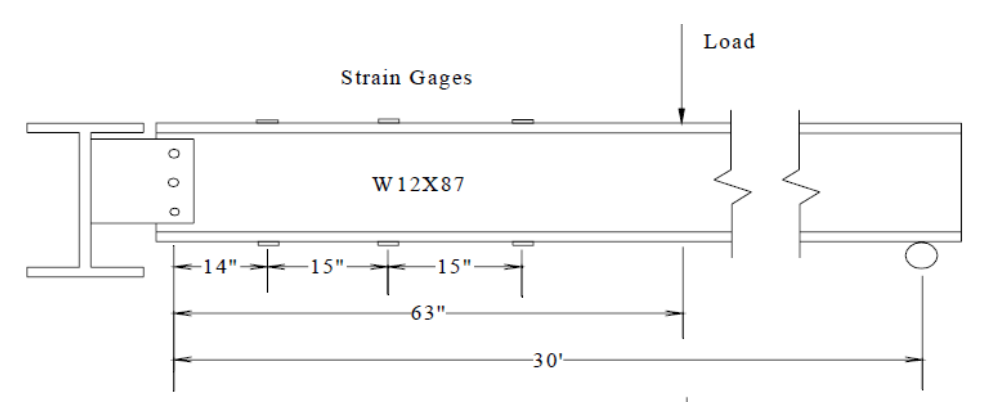


Fig. 2-2. Typical test setup for beam-to-girder shear tabs [2]

The experiments highlighted a number of important aspects. In particular, the stiffened extended shear tab had much larger shear capacity than the similar unstiffened shear tab. The stiffened extended beam-to-girder shear tabs with full depth of the stiffener failed due to the buckling of the stiffened portion of the shear plate. The primary failure mode of unstiffened extended shear tabs connected to supporting members with high web slenderness was web yielding. Shear Plate twisting was observed as either a primary or secondary failure mode in unstiffened extended shear tab. Restriction of the lateral deformation of the beam flanges in the vicinity of the connection decreased the plate twist. Although the weld between the stiffeners and the column flanges was necessary, there was no need to weld stiffeners to the column web. Providing the lateral bracing near the applied concentrated load did not affect the connection capacity. The bolt tightening did not affect the connection's ultimate capacity. The type of the bolt hole had negligible effect on the ultimate capacity of the extended shear tabs for the snug tightened bolts in standard or short slotted holes. The connection shear resistance drove no benefit from implementation of stiffeners, thicker than the shear plate, increase of the stiffener thickness beyond the thickness of the shear plate.

Regarding the design method, the authors considered a serviceability limit for the vertical deformation of unstiffened extended shear tabs (6mm (1/4 in.)). Furthermore, they recommended that plate twisting and web yielding of the supporting member should be considered in design of

the unstiffened extended shear tabs. For the stiffened extended shear tabs, the authors suggested to design the bolt group based on the distance between the inflection point and the centre of the bolt group, determined through a regression equation. However, it should be noted that this method was only applicable to stiffened extended shear tab with a single vertical line of two to ten bolts.

#### 2.2.1.3 Goodrich-2005

To investigate the behaviour of stiffened extended shear tabs, Goodrich conducted an experimental-numerical study [3]. In this study, three configurations of stiffened extended beam-to-column shear tabs were tested. Each configuration was tested two times. All specimens had a single vertical bolt line, while the number of horizontal bolt lines varied. All specimens failed due to the buckling of the stiffened portion of the shear plate, and the buckling capacity was more than twice the design (factored) strength. The design strength was calculated based on the assumption that the extended portion of the shear plate could be designed as a conventional shear tab.

#### 2.2.1.4 Metzger-2006

The main goal of this research was to examine the AISC design procedure [4] for shear tab connections. Metzger [5] tested eight full-scale beam-to-column flange shear tabs including four conventional and four extended configurations. The results from the extended shear tabs are only discussed hereafter. The tested specimens varied in the number of horizontal and vertical bolt lines, the a distance (distance between weld line and bolt line), and the weld size. Referring to Fig. 2-3, one end of the test beam was connected to the column by a shear plate while the other end was supported by a simple roller system on a load cell. The test beam was loaded by applying two concentrated loads at nominal third points of the beam length. The tested beam was laterally supported at both the top and bottom flanges. For two tests with 76 mm (3 in.)< a, additional lateral braces were installed on the beam near the connection.

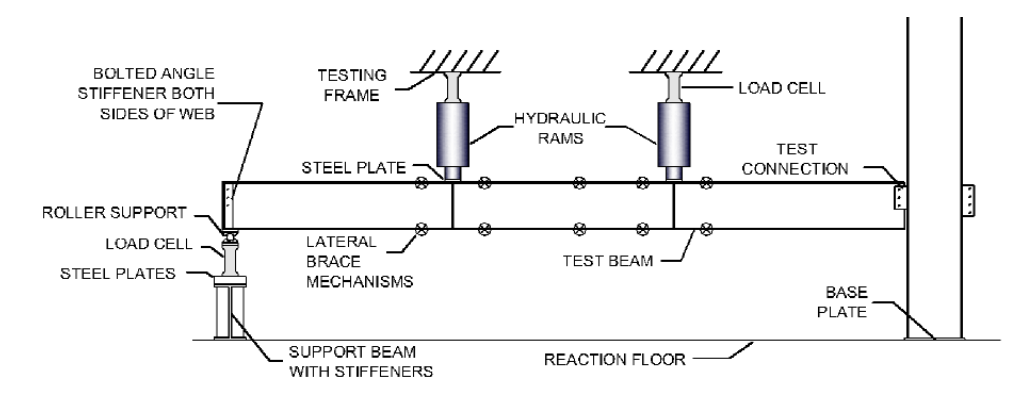


Fig. 2-3- Schematic of test setup [5]

Although the AISC method predicted the bolt shear strength as the governing failure, these specimens failed due to either weld tearing or beam lateral-torsional buckling. However, the AISC design procedure predicted conservatively the connection capacity in all configurations. Two specimens with  $a_w = t_p/2$  failed due to the weld tearing, while the shear plate was still elastic. The observed weld rupture capacity was lower than the concentric shear capacity of the weld line. The average test-to-predicted ratio would increase to 1.10 if the geometric eccentricity (e distance: the distance between weld line and centre of the bolt group) was taken into account in the calculation of the weld line shear capacity. It should be noted that these calculations were conducted based on the nominal rupture strength of E70 electrodes (483 Mpa (70 ksi)). The other two specimens whose weld size satisfied the AISC requirement for the minimum weld size ( $5t_p/8 \le a_w$ ) [4] failed due to the beam lateral buckling, while minor plate yielding was observed. As the beam buckling preceded the weld tearing, the validity of the AISC requirement for the minimum weld size ( $5t_p/8 \le a_w$ ) [4] could not be evaluated.

Regarding the design procedure, the author found the AISC design method as a conservative procedure. Furthermore, the capacity of the weld line should be calculated by considering the eccentricity of shear force, the distance between the weld line and centre of the bolt group. To validate the minimum weld size, further test were needed.

## 2.2.1.5 Muir and Hewitt-2009

Muir and Hewitt [6] outlined the background and development procedure of the AISC design method [4] for extended shear tab connections. The authors considered the main uncertainty in the design of shear tab connections to be the bending moment that develops in the connections. Given this, a simple beam supported by shear tab connections can be imagined as an indeterminate system. The bending moment at each end of the beam depends greatly on the relative stiffness of the beam, the connections, and the supporting members. The stiffness of the shear tab connection itself is a function of the plate dimensions, bolt configuration, and bolt slippage. Furthermore, the connection stiffness as well as the moment distribution may change due to yielding of the plate and bolts. Due to the abovementioned issues, a lower bound theorem was implemented to create a safe and simple design method for shear tab connections. The AISC design method assumes a pinned-end beam model for the behaviour of shear tabs in which the shear tab transfers only shear force to the support. By satisfying all probable failure modes, the connection would have enough ductility for the force redistribution, a requirement for the lower bound theorem.

Based on the assumed model, the inflection point was assumed to occur at the support face, and the distance between the weld line and the bolt group center was used to design the bolt group. To provide the required ductility, the weld line and bolt group were designed to fail only after full yield of the shear plate had taken place. The minimum required plate thickness was determined based on the flexural and shear limit states corresponding to the rupture of the plate's net section, as well as yield of the gross section of the plate. Furthermore, the interaction of the shear force and bending moment was considered as a failure mode for the gross section of the shear plate. In addition to the block shear rupture of the plate, plate buckling was also controlled. The design

method was evaluated to physical testing available in the literature [2, 5]. The test-to-unfactored strength ratio varied between 1.0 and 2.16.

## 2.2.1.6 Thornton and Fortney-2011

Thornton and Fortney [7] aimed to provide a procedure to evaluate the need for stiffening of extended shear tabs. To this end, two cases were studied: lateral-torsional buckling of the plate and twisting of the plate due to the lap eccentricity (the offset between the beam and shear plate longitudinal axes). To develop an equation for the lateral-torsional capacity of extended shear tabs, the genuine similarity between the extended shear tabs and double-coped beams was implemented. Previous research [8] showed that the lateral-torsional buckling of double-coped beams primarily occurred at the coped section; whereas, the uncoped section of the beam behaved like a rigid body. Furthermore, it was assumed that the beam was laterally supported along its entire length. In the proposed method, two equations were introduced for the shear plate resistance corresponding to the plate's clastic lateral-torsional buckling and twisting due to the lap eccentricity. The author suggested to implement horizontal stabilizer plates in the case where the applied shear force was larger than the connection strength, calculated based on these two equations [7]. Of note, the proposed method was based on principles of structural mechanics and was not evaluated through either FE simulations or laboratory tests.

## **2.2.1.7 Dowswell and Whyte-2014**

This paper's objective was to expand the applicability limits of the existing AISC's design procedure for double-coped beams in which the high shear and bending stresses at the cope face caused local buckling and limited the beam capacity. For many years, the AISC Steel Construction Manual [9] used Eqs. 2-1, 2-2, and 2-3, developed by Cheng et al. [8], to determined the local buckling stress at the coped region of double-coped beams. In Eq. 2-2, the theoretical solution for

lateral-torsional buckling of a rectangular section was adjusted by the  $f_d$  factor to account for the shape of the bending moment diagram along the coped region. The adjustment factor (Eq. 2-3) was developed based on the results of 14 elastic FE analyses. This equation was only applicable for configurations placed in the range of these analyses; double coped beam with the same top and bottom copes in which the cope length was not greater than two times the beam depth ( $c \le 2d_b$ ) and the cope depth was less than 0.2 of the beam depth ( $d_c \le 0.2d_b$ ). However, it is common to have a different cope depth at the top and bottom flanges of a double-coped beam. Furthermore, unequal cope length is also required in some connections.

$$M_n = F_{cr} S_{net} \tag{2-1}$$

$$F_{cr} = 0.62\pi E f_d \frac{t_w^2}{ch_0} \le F_y$$
 (2-2)

$$f_d = 3.5 - 7.5(\frac{d_{ct}}{d_b}) \tag{2-3}$$

in which  $M_n$  is the nominal bending capacity of the coped region,  $F_{cr}$  is the buckling stress at the cope face, c is the cope length,  $d_{ct}$  is the cope length, and  $d_b$  is the beam depth.

In cases that  $d_{ct} > 0.20$ , the coped capacity could be determined based on inelastic plate-type buckling [10]. In this method, the critical buckling stress was determined as a fraction of the plate yield stress (Eq. 2-4). The Q reduction factor was determined based on the cope slenderness,  $\lambda$  as suggested by Eq. 2-8. If  $\lambda \le 0.70$ , the coped section may experience yielding (Eq. 2-5). Inelastic buckling would occur in the plate if  $0.70 < \lambda \le 1.41$ . In this case, the Q reduction factor could be determined based on Eq. 2-6 If  $1.41 < \lambda$ , elastic buckling governs the behaviour, and the reduction factor can be calculated based on Eq. 2-7.

$$F_{cr} = F_{y}Q \tag{2-4}$$

$$Q = 1 \tag{2-5}$$

$$Q = 1.34 - 0.486\lambda \tag{2-6}$$

$$Q = \frac{1.30}{\lambda^2} \tag{2-7}$$

$$\lambda = \frac{h_0}{10t_w} \sqrt{\frac{F_y}{475 + 280(\frac{h_0}{c})^2}}$$
 (Imperial unit) (2-8)

In addition to the above mentioned equations, Section F11 of the AISC 360 Specification [11] comprises a comprehensive method to determine the flexural capacity of rectangular beams in their strong axis. Based on this method, a rectangular beam could reach its plastic bending moment (Eq. 2-9) if  $L_b d_{pl}/t_{pl}^2 \leq 0.08 E/F_y$ . In the case of  $0.08 E/F_y < L_b d_{pl}/t_{pl}^2 \leq 1.9 E/F_y$ , inelastic lateral-torsional buckling would govern the beam's bending capacity (Eq. 2-10). The beam's flexural capacity would be governed by elastic lateral-torsional buckling (Eqs. 2-11 and 2-12) if  $1.9 E/F_y < L_b d_{pl}/t_{pl}^2$ . The  $C_b$  factor was determined based on Eq. 2-13. It should be note that Eq. 2-12 was identical to Eq. 2-2 by substituting  $t_{pl}$ = $t_w$ ,  $d_{pl}$ = $t_0$ ,  $L_b$ = $t_0$ ,  $t_0$ = $t_0$ .

$$M_n = M_p = F_y z \le 1.6 M_y \tag{2-9}$$

$$M_n = C_b [1.52 - 0.274 \frac{L_b d_{pl}}{t_{pl}^2} \frac{F_y}{E}] M_y \le M_p$$
 (2-10)

$$M_n = F_{cr} S_x \le M_p \tag{2-11}$$

$$F_{cr} = \frac{1.9EC_b}{\frac{L_b d_{pl}}{t_{rl}^2}}$$
 (2-12)

$$C_b = \frac{12.5M_{\text{max}}}{2.5M_{\text{max}} + 3M_A + 4M_B + 3M_C}$$
 (2-13)

in which  $M_{max}$  is the absolute value of the maximum moment in the unbraced length,  $M_A$  is the absolute value of the bending moment at the quarter point of the unbraced length ( $L_b/4$ ),  $M_B$  is the absolute value at the mid-length of the unbraced length ( $L_b/2$ ), and  $M_C$  is the bending moment at three-quarter point ( $3L_b/4$ ). Equation 2-13 resulted in value of 1.67 for the case of a double-coped beam as it was assumed that the inflection point formed at the support face.

Dowswell & Whyte [12] conducted a parametric FE study to develop a new procedure to predict the local capacity of double-coped beams. They conducted elastic analyses (54 configurations) and gathered the simulation results in three main groups: 30 configurations with equal length at both compressive and tensile copes, 12 configurations in which the compressive cope was longer than the tensile one, and 12 configuration with longer tensile copes. Each group contained configurations with varied equal or unequal depth of copes. The compressive flange (top flange) was laterally braced at the face of the cope section in all analyses.

The cope region showed a similar deformed shape in all analyses: in addition to the torsion of the coped region, the compressive edge (top edge) of the coped region showed much larger lateral deformation as compared with the cope's tensile edge (bottom edge). This observation was consistent with previous analyses conducted by Cheng et al [8]. This deformed shape resembled several independent buckling modes including lateral-torsional buckling, shear buckling, and local buckling. Although shear buckling was the governing failure mode in the short copes, the long copes were affected greatly by lateral-torsional buckling. They developed a new expression [12] to calculate the lateral-torsional buckling modification factor C<sub>b</sub> based on regression analysis to the FE results. In addition to these equations, they proposed simplified equations to predict C<sub>b</sub>.

Based on the assumption that the inflection point formed at the support face, the required moment at the face of the cope was calculated as  $M_r = V_r e_{\min}$ ; in which  $V_r$  is the reaction shear force at the beam's end and  $e_{\min}$  is the minimum of the  $e_t$  and  $e_b$ , which are the distances from the support face to the face of the top and bottom copes, respectively. The interaction of the bending moment and the shear force at the cope face would not allow a double-coped beam to reach its plastic bending strength  $(M_p)$ . Neal's equation [13], (Eq. 2-14), was implemented to take into account the interaction.

$$\frac{M_r}{M_p} + (\frac{P_r}{P_y})^2 + \frac{(V_r/V_y)^4}{1 - (P_r/P_y)^2} \le 1.0$$
(2-14)

The proposed design procedure could accurately predict the buckling capacity of the FE analyses; a mean of 1.02 for the observed-to-predicted ratio with a standard deviation of 0.0665 were reported. Although the accuracy of the design procedure decreased when the simplified equations were implemented, it was still more accurate than the design procedure recommended by Cheng et al.

#### 2.2.1.8 D'Aronco-2013

D'Aronco [14] conducted ten full-scale tests of shear tabs with multiple vertical bolt lines. The specimens consisted of four beam-to-column flange shear tabs and six stiffened extended beam-to-column shear tabs. The number of vertical and horizontal bolt lines was varied, as were the plate thickness, and the distance between the weld line and bolt line (the *a* distance). Although the beam-to-column flange connections had a short *a* distance (51mm (2 in.)), they could not be designed based on AISC's method for conventional shear tabs due to the multiple vertical lines of bolts. These four beam-to-column flange specimens consisted of two bolted and two welded configurations. Each of the welded specimens was identical to one of the bolted specimens, except that a partial C-shaped weld was used to connect it to the beam web. The partial C-shape weld is a possible retrofit method when a shear tab cannot bolted to the beam web due to misalignment of the bolt holes. The retrofitted weld group was detailed in the way that its factored resistance was equal to the factored capacity of the corresponding bolted connection. The top flange of the test beam was laterally supported along its entire length.

All specimens were designed based on AISC's design method for extended shear tabs [9]. It should be noted that the inflection point was assumed to form at the toe of the stiffener (column

flange), and the extended potion of the shear plate was design based on g eccentricity, the distance between the stiffener's toe and the interior bolt line (51 mm (2 in.)). Either net section shear fracture or the yield of the shear plate due to the interaction of shear force and bending moment was predicted as the governing failure mode. All specimens were able to reach their target rotation except a stiffened extended shear connection in which the column experienced significant yielding due to minor axis bending. Significant rotation was observed in the columns supporting the stiffened extended shear tabs due to the bending moment applied to each column through the stiffened extended shear tab. The observed bending moment was slightly lower than that calculated from the product of the shear force and the half width of the column flange.

The AISC design method resulted in reasonably conservative predictions for the capacity of connections. The mean test-to-predicted value was 1.15 with a 7.7% standard deviation. All bolted shear tabs failed due to shear rupture of the plate along the interior bolt line; no damage was observed in their bolts. The welded shear tabs failed due to shear yielding and excessive shear deformation. The partial C-shaped weld imposed larger rotational restrained on the shear plate. Implementation of the *g* distance (the distance between the toe of the stiffener and the interior bolt line) in the design of the extended portion of the stiffened extended shear tabs led to reasonably conservative estimate of the connection ultimate strength.

#### 2.2.1.9 Hertz-2014

In order to investigate the behaviour of extended shear tabs, Hertz et al. [15, 16] tested twelve extended shear tab specimens including. four extended beam-to-column flange shear tabs and eight beam-to-girder configurations. The beam-to-girder specimens included three stiffened shear tabs with a full-depth stiffener, four stiffened shear tabs with a partial-depth stiffener, and one connection with two side plates which were bolted through a single vertical bolt line in both the

beam web and a full-height stiffener within the supporting girder. Two of specimens with the partial-depth extended shear tab were further reinforced by partial-depth stiffeners at the backside of the girder. None of the beam-to-girder specimens satisfied the CSA-S16 compactness requirement [17] for plate girder stiffeners ( $200/\sqrt{F_y}=10.7$ ).

All configurations had two vertical bolt lines and a 10 mm (3/8 in.) shear plate, while there various numbers of horizontal bolt lines, and different *a* distances. All configurations were designed based on the AISC design procedure for extended shear tabs [9]. The same setup and loading procedure with the one used in D'Aronco (2013) was utilized. The top flange of the test beam was supported laterally along its length while the bottom flange was laterally brace at the location of the tip actuator, far from the connection. Based on the AISC design method for extended shear tabs, bolt shear fracture was predicted as the governing failure mode of all specimens, other than three configurations with deep shear tab. In these three specimens, ASTM F3125 Grade A325 bolts [18] with size of 22 mm (7/8 in.) were implemented while 19 mm (3/4 in.) bolts were used in all others.

Although the weld size satisfied the requirements of the AISC for minimum weld size  $(5t_p/8 \le a_w)$  [9], weld tearing was observed in all beam-to-column shear tabs. As the weld strength was lower than the concentric shear capacity of the weld line, the eccentricity of shear force should be taken into account in the calculation of the weld line capacity. Furthermore, the AISC requirement for the minimum weld size  $(5t_p/8 \le a_w)$  [9] should be increased in order to take into account the probable yield stress  $R_y F_y$  of the shear plate. For ASTM A572 Gr 50 plates with  $R_y=1.1$  and E70 electrodes, the minimum weld size should be increased to  $11t_p/16$ .

All three extended beam-to-girder shear tabs failed due to the buckling of the stiffened portion of the shear plate along the lower re-entrant corner of the plate's extended part. The inflection

point formed away from the girder web. The author suggested the stiffened portion of the shear plate should be control for biaxial buckling. For the four extended shear tabs with a partial-depth stiffener, the damage and deformation mainly focused at the web and flange of the girder in the vicinity of the shear plate. Implementation of the partial-depth back stiffener significantly delayed the girder web yielding in the girder with thin web ( $t_w$ =11.9 mm) while it was not effective in the girder with thicker web ( $t_w$ =16.6 mm). The author concluded that the girder web mechanism should be considered as a failure mode for the partial depth extended beam-to-girder shear tabs.

#### 2.2.1.10 Goldstein Apt 2015

Goldstein Apt [19] conducted 13 full-scale beam-to-girder connections. The tested specimens included nine connections with coped beams and four stiffened extended shear tabs. The extended shear tabs were divided into two main categories: two specimens with full-depth stiffeners and two specimens with partial-depth stiffeners. The same loading protocol and lateral bracing system used in prior testing programs at McGill was employed. [15]. A pseudo-concrete slab was installed to restrict the in-plane rotation and out-of-plane deformation of the girder top flange. Both full-depth specimens were identical to Specimen 5 of Hertz testing program [15], except the thickness of the shear plate was increased to the meet CSA-S16 requirement for compactness of the plate girder stiffener,  $200/\sqrt{F_y}$ =10.7 [17].

Although implementation of the pseudo-concrete slab decreased the girder rotation, it could not prevent the girder web deformation. Extended shear tabs with full-depth compact stiffener showed a very ductile behaviour. Although yielding and out-of-plane deformation of the stiffener and the girder web were observed, these configurations reached a shear force much larger than the expected value as determined using the AISC design method [9]. Yielding concentrated at the girder web in the partial-depth shear tab (Specimen 6J), even in the presence of the pseudo-

concrete slab. The horizontal reinforcement is likely to decrease the out-of-plane deformation of the shear tab. However, girder web yielding is still likely to occur. The test results showed that reinforced partial-depth shear tab could reach a greater shear force than the predicted value. Regarding the design procedure, the author suggested that the shear plate should satisfy the compactness requirement of the plate girder stiffeners. In this case, the AISC design method predicted the connection strength conservatively. This recommendation should be evaluate for double-sided configuration of the extended beam-to-girder shear plate.

#### 2.2.1.11 Abou-zidan and Liu-2015

A numerical study including 20 FE analyses was conducted to investigate the behaviour of unstiffened extended shear tabs under gravity induced shear force [20]. Several parameters of beam-to-column web connections were studied including the thickness of the shear plate, the number of horizontal and vertical bolt lines, the distance between centre of the interior bolt line and the weld line (*a* distance), the beam lateral restraint, and the web slenderness of the supporting column. Other than two models, the studied models did not satisfy the AISC requirement for the maximum thickness of the plate [9]; they were detailed to failed in bolt shear in advance of the plate yield. The reference model was subjected to a concentrated force while the far end of the beam was restrained against transversal displacements; the weld lines were not included in the FE simulations. The top flange of the beam was laterally braced along the beam length.

In order to determine the bolt shear fracture, the shear stress along the bolt centerline was monitored during the analyses. An irreversible decrease in this monitored shear stress was considered as the fracture criterion for the bolts. Of note, this failure criterion is not necessarily an ideal indicator of bolt fracture, because other failure modes resulting in a decrease in applied load could also result in an irreversible decrease of the bolt shear stress.

FE analyses showed that an increase in the slenderness of the column web resulted in a decrease of the connection capacity due to the larger bolt group eccentricity (e<sub>b</sub>: the distance between the inflection point and the centre of the bolt group). It was observed that the increase of the *a* distance (the distance between the weld line and the interior bolt line) led to a decrease of the connection capacity. Change of the plate thickness had no significant effect on the e<sub>b</sub> value. However, it should be noted that the mentioned bolt group capacity corresponding to the bolt shear fracture, occurred in advance of the full yield of the shear plate. In the absence of the beam lateral bracing, the unstiffened extended shear tab failed soon after the yielding due to twisting of the shear plate. In order to prevent the twist of the shear plate, restraining the beam's out-of-plane deformation at the connection's locations was as effective as providing the lateral brace all over the beam length. The authors found the AISC design method over conservative for connections with either three or four bolt rows. They also recommended that the bolt group should be designed for a shorter eccentricity.

## 2.2.1.12 Fortney and Thornton-2016

Fortney and Thornton [21] aimed to establish a design procedure for the stabilizer plates of stiffened extended shear tabs. They introduced design and detailing recommendations for three different types of stabilizer plates (stiffeners). Further, recommendations were introduced in order to take into account the effects of the stabilizer plates on the design of the shear plate and the supporting column. The authors classified the stabilizer plates based on their implementation as well as their role in transferring the connection shear force. Referring to Fig. 2-4, Types I and II can be used in beam-to-column connection, when there is no need for the continuity plates due to the moment connection in the column strong axis. Otherwise, Type III shall be used. The behaviour of shear plate in the Type III connection is quite similar to the stiffened beam-to-girder shear tabs.

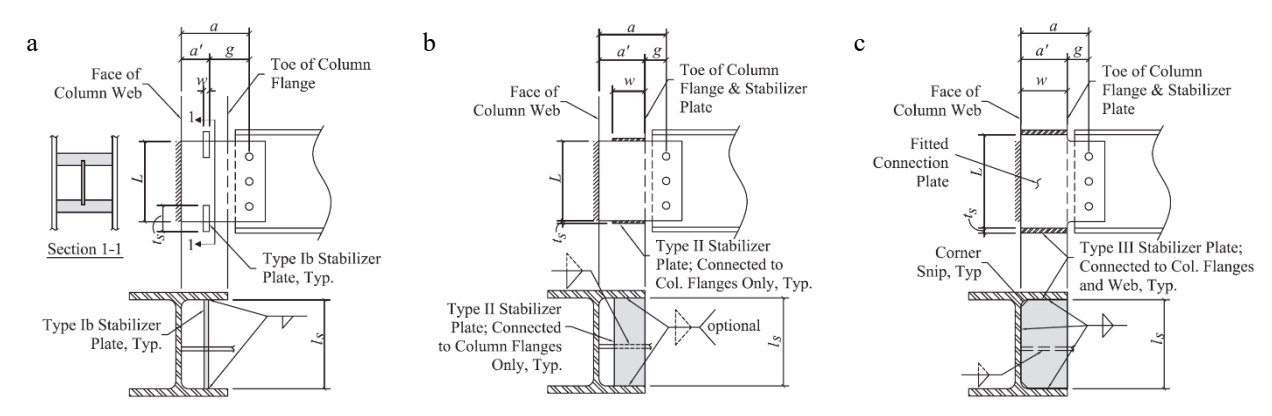


Fig. 2-4. Different types of the stabilizer plates: a) Type I, b) Type II, c) Type III [21]

The presence of the stabilizer plates increases the rotational stiffness of the connection, which is undesirable in simple shear connections as it may lead to the development of larger bending moment at the support, which has not been considered in design of the support. To eliminate this concern, the authors suggested not to attach the stabilizer plate to the column flange. This method could be used in Type I and II stabilizer plates. In this case, the length of the stiffener was equal to the clear span between the column flanges. It was connected only to the shear plate and could move (float) relative to the column flange. The axial force of the stiffener (P<sub>s</sub>), required to provide lateral support to the shear plate, would transfer to the column flange through bearing and its buckling should be taken into account. If the weld was used to connect the stiffener to the column flange, the axial force would be transferred through both ends of the stiffeners and buckling would not occur. The required axial strength of the stabilizer plate was determined based on AISC-360 Specifications [11] requirements for nodal bracing.

Type I stiffener was notched around the shear plate and the required axial force would be transferred through bearing of the shear plate and the notch portion of the stabilizer plate. This configuration did not introduce extra torsional restraint on the shear plate and consequently did not contributed in transferring the shear force. The shear plate would be design based on the AISC design procedure for extended shear tabs [9]. As both ends of the stabilizer plates are welded to

the column flange, buckling of the stiffener is not a concern. The authors of the paper provided recommendations for detailing of the stiffeners [21], and the thickness of the stabilizer plated was determined based on the interaction of the axial and bending moment at the net section, as well as the bearing at the notch.

Type II stabilizer plates would contribute in transfer of the shear force if they were welded to the column flange. In this case, the authors assumed that the inflection point formed at the toe of the stabilizer plate. The extended portion of the shear plate should be designed based on the AISC design method for the extended shear tab [9], but the *g* distance (distance between the interior bolt line and the toe of the stiffeners) should be used instead of *a* in all equations. Furthermore, there was no need to satisfy the AISC requirement for minimum weld size and maximum plate thickness [9]. Type III stabilizer plate could be designed based on the design procedure of the Type II stiffener, except that there is no need to control the bending of the stabilizer plate.

## 2.2.1.13 Suleiman et al.-2017

In order to determine the need for stiffeners in laterally braced unstiffened extended shear tabs, a parametric FE study was carried out including 17 beam-to-column flange shear tabs [22]. Furthermore, they evaluated the accuracy of AISC equation [9] to determine a need for stiffeners, which was proposed by Thornton and Fortney [7] based on the structural mechanics. Regarding the FE models, all configurations were design based on AISC requirements for extended shear tabs [9]; with the neutral axis of the beam and shear plate at the same height. The FE simulation procedure was verified by comparison with the results of two tests of extended shear tabs [2, 5]. In order to detect the bolt shear fracture, distribution and magnitude of the shear stress along the bolt centerline was monitored during the analysis.

The authors concluded that there was no need for stiffeners in connections that satisfied all other AISC requirements for extended shear tabs if the beam was laterally supported. Although large lateral displacement was observed at ultimate load, the lateral displacement remained small under service load. The torsional rotation of the shear plate increased as the shear force got closer to the predicted value of the AISC equation. However, this equation failed to determine if the plate twisting was the ultimate failure mode.

#### 2.2.2 Extended shear tabs under Combined Axial and Shear Forces

#### 2.2.2.1 Thomas-2014

In order to study the behaviour of extended shear tab connections under combined axial and shear forces, 23 full-scale specimens were tested at the University of Alberta [23, 24]. All tested specimens had two vertical bolt lines, which were used to connect the web of the supported beam to the web of the supporting column. Among them, 13 specimens represented unstiffened extended shear tab connections while the remaining 10 specimens were extended shear tab connections with stabilizer plates. The specimens varied in the thickness of the shear plate, and the number of horizontal bolt rows, while the *a* distance was kept constant. Three actuators (Fig. 2-5) were incorporated in the setup to apply the connection rotation, shear and axial forces simultaneously.

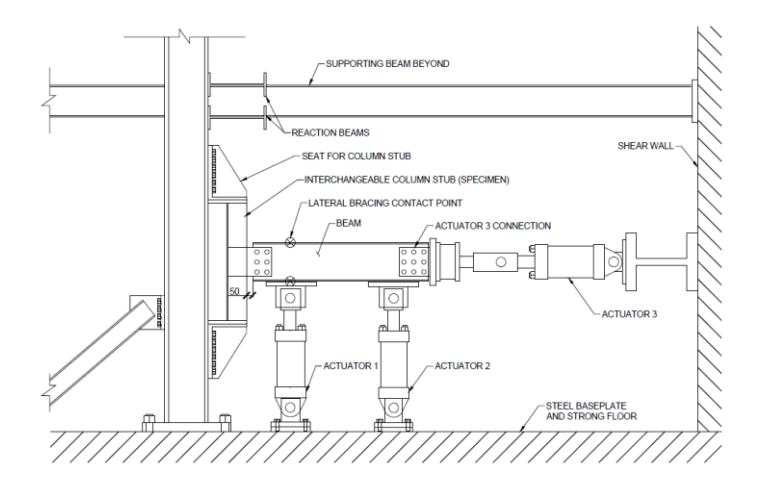


Fig. 2-5 Setup for shear tab testing at the University of Alberta [24]

The loading protocol consisted of three steps: applying rotation, horizontal force application, and applying vertical force. In the first step, the beam was subjected to 0.03 rad rotation, while the connection horizontal and vertical forces were kept near zero. During the second step, the horizontal force was applied to the connection, while the vertical force was held near zero and the beam rotation was kept constant (0.03 rad). In last step, the connection horizontal force, as well as the beam rotation, were kept constant while the connection vertical force was increased up to the failure of the connection.

Regarding the unstiffened extended shear tabs, the plate yielded while the vertical force in the connection increased up to its peak value, at which time the primary failure mode (CFM: Critical Failure Mode) occurred. In eight specimens, yielding was observed along the vertical bolt line, the closest to the weld line. Either weld tearing (Fig. 2-6a) or bolt fracture (Fig. 2-6b) was observed as the critical failure mode. As the primary failure modes, bolt fracture resulted in a more sudden drop of the connection vertical force as compared to the weld tearing. In four cases the weld tearing propagated significantly, and as such was classified as the critical failure mode, even though the weld size satisfied the AISC requirement [9] for minimum weld size  $(5/8t_p \le a_w)$ . In other cases, weld tearing became stable and was limited to a short distance. In most cases, the column web yielded due to out-of-plane bending. As the beams were braced adjacent to the connection, plate twisting did not occur. In general, applying a horizontal load (either tension or compression) resulted in a decrease in the ability of the connection to resist vertical force.



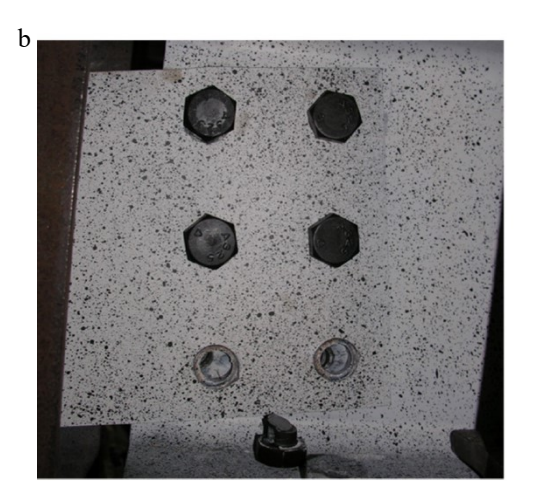


Fig. 2-6. Failure modes of unstiffened shear tabs: (a) weld tearing, (b) bolt fracture [23]

For the stiffened extended shear tabs, the yielding was first observed at the compression reentrant corner of the shear plate. The out-of-plane deformation of the plate began as yielding
propagated in the shear plate. In some specimens, the shear plate yielded over its full depth in
advance of the plate's out-of-plane deformation. The critical failure mode was out-of-plane
deformation in all tests (Fig. 2-7a). The interior bolts at this location were subjected to high prying
force in addition to the in-plane forces; consequently, bolt shear failure was observed in six
specimens. For two specimens without compression force, the tensile re-entrant corner of the shear
plate tore after the connection experienced its peak vertical load and large out-of-plane
deformation (Fig. 2-7b). This re-entrant corner resembles the re-entrant corner of coped beam
where high stress concentration exists due to cross-section discontinuity.

In comparison to the unstiffened extended shear tabs, the connections with stabilizer plates reached a higher vertical force especially in the absence of compressive horizontal force. In the presence of a large compression force, the shear capacity of the stabilized shear tab was close to the capacity of the representative unstiffened shear tab. This observation can be attributed to the horizontal compression force, which accelerated the critical failure mode and out-of-plane deformation, and decreased the connection shear capacity.



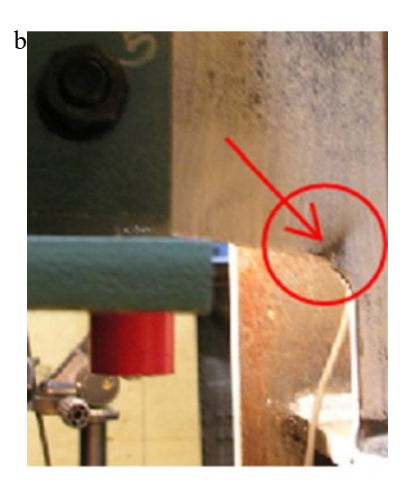


Fig. 2-7. Failure modes of stabilized shear tabs: (a) out-of-plane deformation of shear plate, (b) tearing at tensile re-entrant corner of shear plate [23]

Regarding the design method, the author found the current AISC design method for extended shear tabs overly conservative. The connection eccentricity was much shorter than the value assumed in design. Based on the experimental results, Thomas proposed refinement [24] to the current AISC design method to take into account the effect of the axial force. Furthermore, the minimum plate thickness was introduce to prevent shear plate buckling.

#### 2.2.2.2 Johnston-2015

This research study [25] aimed to characterize the the behaviour and local strength of double-coped beams under combined axial and shear forces through 29 full-scale laboratory tests. All tested beams had a relatively thin web to assure that the local instability occurred in advance of the full yield of the coped section. The length and depth of the coped section, rotational stiffness of the supporting girder (i.e. flexible or rigid support), end rotation of the coped beam, and the axial force's magnitude and direction were other parameters that were examined as part of the testing program. The coped beams were connected to the supporting girder using two methods; a welded end-plate, and a direct weld of the beam to the girder. Both top and bottom flanges of the beam were laterally supported in the vicinity of the connection.

The inelastic behaviour was observed in all specimens, even though these specimens were detailed to assure local instability prior to the full yield of the coped section. In the 18 specimens, failure occurred when yielding propagated into the coped section and its out-of-plane deformation gradually increased. These results demonstrated that most of the stability issues could be eliminated if the double-coped beam was detailed with the minimum size of the cope (depth and length). Bending moment developed at the support even in the connections with flexible supports. Therefore, the assumption that the inflection point forms at the face of the support was untrue. In comparison to the connections with flexible support, the double-coped beam resisted higher shear force when it was connected to a rigid support with higher rotational constraint. Applying axial tension increased the connection capacity as it stabilized the coped region while axial compression decreased the connection capacity due to its destabilizing effect. Of note, the observed behaviour was limited to the axial force smaller than 32% of axial yield strength ( $P_y=F_yA_g$ ).

The test results were compared with their predicted unfactored shear capacities, calculated based on four different design procedures; 14<sup>th</sup> version of AISC steel manual [9], Section F11 of AISC 360 Specification [11], Dowswell's and Whyte's method [12], and the design procedures used by the fabricator of the specimens (Waiward Steel Fabricators Ltd., Edmonton, Alberta). The comparison demonstrated that all methods were conservative in predicting the capacity of the coped section. Among these design methods, the AISC 360 Specification method [11] to determine the flexural capacity of a rectangular section was the most accurate, with mean value of 1.28 for the test-to-predicted strength ratio and a coefficient of variation (C.O.V) of 27%. In order to increase the accuracy of the design methods, the geometric eccentricity was replaced by the effective eccentricity, measured during the test. In this case, Dowswell's & Whyte's design method resulted in the best predictions with a mean test-to-predicted of 1.10 and C.O.V of 25%. The

requirements of AISC 360 Specification over-estimated the connection capacity; the mean value for the test-to-predicted strength ratio was 0.92 while the coefficient of variation was 29%.

#### 2.2.2.3 Salem-2016

In order to determine the behaviour of steel cantilever plate connections (i.e. a shear plate with two unrestrained horizontal edge or connections with double-coped beams), an experimental and numerical research study was conducted by Salem [26] at the University of Alberta. During the laboratory phase of this research, 17 full-scale specimens were tested. Other than the rotational stiffness of the supports, the connection configurations were identical to Thomas' tests of unstabilized shear tabs [23]. To resemble rigid support condition, two different configurations were implemented: a) welding the shear tab to the column flange, and b) connecting the shear tab to the column web while the stabilizer plates were welded to the backside of the column. The results of these tests and test data from Thomas' research [23] were used to validate FE models of the extended shear tab. Furthermore, FE models of connections with double-coped beams were validated by comparison with Johnston's test data [25]. Then the validated FE models were used to do a parametric study and address the influences of other design parameters on the behaviour of cantilever plate connections.

The experimental and numerical results demonstrated that the connection's shear capacity depends greatly on the rotational stiffness of the supporting element. In the connections with a flexible support, the inflection point formed close to the support face because of the support's low rotational stiffness. Therefore, the net section (cope face in the case of a doubly coped beam) was subjected to a shear force with a large eccentricity. In connections with a rigid support, firstly the inflection point formed away from the support. Therefor, the gross section of the shear plate near the support face was subjected to a larger eccentricity as compared with the net section. As the

shear force increased, the gross section yielded gradually under interaction of the bending moment and shear force. Due to yielding of the shear plate's gross section, the inflection point moved toward the support face, which was followed by yielding of net section under the interaction of shear force and enhanced bending moment. A sharp degradation of the connection stiffness followed the yielding of the shear plate's net section.

The author suggested to consider yielding of the net section as the design limit state of the shear plate, when supported by either a rigid or flexible support. Furthermore, Neal's equation (Eq. 2-14) [13] was used to take into account the shear-bending-axial force interaction for the yield of both the gross and net sections of the shear plate. In addition, different values were proposed as the connection effective eccentricity to calculate bending demand corresponding to the failure modes. In addition to the failure mode, these values depend on the connection configuration as well as the failure mode. The finding of this research should be evaluated for a wider range of connection configurations including medium-length extended shear tabs. Further, the impact of the axial force on the connection response should be evaluated for larger axial forces. The design recommendation should be evaluated for the loading protocol, better representative of a real world scenario.

# 2.3 Current design procedures

The section outlines the current design procedures of shear tab connections in the USA and Canada.

## 2.3.1 CISC Handbook of Steel Construction

The CISC Handbook of Steel Construction [27] provided a design table (Table 3-41) instead of a detailed design procedure. This table was developed based on the findings from an

experimental study conducted by Astaneh et al. [28]. The implemented design methodology consisted of following steps:

- Calculation of the bolt group eccentricity based on empirical values reported by Astaneh et al.
   [28].
- 2. estimation of the bolt group capacity based on the calculated eccentricity
- 3. prediction of the plate thickness to ensure adequate shear resistance including shear yielding, shear fracture, bolt bearing, block shear rupture
- In order to provide ductility, the maximum thickness of the shear plate is limited to d<sub>b</sub>+2mm.
   Further, the shear plate should be at least 6mm.
- 5. The weld size should be enough to allow the shear plate to yield in order to satisfy the required ductility. Astaneh et al. [28] concluded that the weld line with size of 3/4t<sub>p</sub> was adequate for this purpose.

It should be noted that reported design strength values in Table 3-41 were calculated based on the following assumptions and limitations:

- 1. Single vertical line of two to seven bolts
- 2. Shear plate of G40.21 300W steel
- 3. A325 bolts of size 19mm (3/4 in.) or 22 mm (7/8 in.) (shear plane intercepted the threads)
- 4. E49 electrodes
- 5. 75 mm distance between the bolt line and the support
- 6. 80 mm as the bolt distance
- 7. 35mm as the horizontal and vertical edge distances

As a summary, this design table, developed based on a design procedure of conventional shear tab connections dating back to the experimental study of Astaneh et al. in 1989 [28], does not represent

the current state of practice for steel construction in which more complex shear tab connections with multiple vertical bolt lines are common.

### 2.3.2 AISC Steel Construction Manual-2017

The 15<sup>th</sup> edition of the AISC Steel Construction Manual [29] contains two methods for the design of shear tab connections: a simplified procedure for conventional shear tabs and a comprehensive procedure for extended shear tabs. The AISC manual classifies shear tab connections into these two categories (conventional and extended shear tabs) based on their geometries.

## 2.3.2.1 Conventional configuration

The AISC manual considers a shear tab connection as being conventional if it satisfies the following limitations, upon which the simplified method was developed:

- 1. The weld between the shear plate and the supporting element should be sized as 5/8t<sub>p</sub>.
- 2. The connection has only a single vertical line of two to twelve bolts.
- 3. The a distance is equal to or lower than 89 mm (3.5 in.).
- 4. In addition to standard holes (STD), short-slotted holes (SSLT) are permitted if slots are perpendicular to the direction of the resultant reaction force of the supported beam.
- 5. The vertical edge distance should satisfy the requirements of AISC 360 Specification (Table J3.4) [30] while the horizontal edge distance is not smaller than two times the bolt diameter (2d<sub>b</sub>)
- 6. Either the beam web or the shear plate satisfies the maximum thickness requirement outlined in the AISC Manual.

The following design checks should be made for conventional shear tabs:

- 1. Calculation of the bolt shear capacity based on the reaction force (R) and the corresponding bending moment (Re).
- 2. Control of the plate bearing and tearout resistance based on the concentric reaction force (R)
- 3. No need for control of the plate buckling

## 2.3.2.2 Extended Configuration

This method could be used for connections that do not meet the limitations of the conventional configuration. In addition to the extended configuration shear tabs, this method could be used to design connections with multiple vertical bolt lines. The extended shear tab should satisfy the following limitations:

- 1. The weld between the shear plate and the supporting element should be sized as 5/8t<sub>p</sub>.
- 2. The bolt holes satisfy requirements of AISC 360 Specification (Section J3.2) [30]. Of note, the use of short-slotted holes is allowed in extended shear tabs even when the bolts are designed to transfer the shear force by bearing.
- 3. The vertical and horizontal edge distances satisfy the requirements of AISC 360 Specification (Table J3.4) [30].
- 4. There is no limitation on the number of bolts or the *a* distance.

The extended shear tab is designed based on following design checks:

- 1. Calculation of the connection capacity for bolt shear fracture, plate bearing and plate tearout based on the reaction force (R) and the corresponding bending moment (Re). The *e* value is the distance between the weld line and the centre of the bolt group.
- 2. The shear plate should not be thicker than the maximum allowable value. This value is determined such that the flexural strength of the shear plate does not surpass the moment capacity of the bolt group.

- 3. The plate should be checked for shear yielding, flexural yielding, shear rupture, flexural rupture, and block shear rupture.
- 4. The shear plate should be checked for shear buckling and yielding due to the interaction of shear and bending by using elliptical yield criterion.
- 5. The buckling of the shear plate was controlled based on the existing procedure for double-coped beams ( $\phi M_n$ = 0.90  $M_n$ ). In this procedure, it is assumed that the beam is laterally braced near the connection. Of note, the method to control buckling of the double-coped beam was changed in the 15<sup>th</sup> version of the AISC steel manual. In this method the buckling strength was determined in accordance with requirements of AISC 360 Specification (Section F11) [30] for the flexural strength of a rectangular beam.
- 6. It was necessary to provide lateral support for the beam near the connection. If it was not supported, the method proposed by Thornton and Fortney [7] should be implemented to check the need for horizontal stiffeners.
- 7. If the shear tabs were designed based on the AISC procedure [29] for extended shear tabs, i.e. design based on the geometric eccentricity (e<sub>g</sub>), the column would be designed for axial force without eccentricity. However, this eccentricity could be decreased by an assumption that a bending moment equal to 5% of the column weak-axis flexural strength (M<sub>py</sub>) was transferred to the column through the extended shear tabs. This assumption allows for a decrease in the eccentricity for design of the bolt group, but this assumes that the bending moment should be considered in the design of the column.
- 8. Although the AISC Steel Construction Manual [29] addresses the shear tab connection only under gravity shear demand, the Steel Connection Handbook (Section 2.5.3) [31] and AISC Design Examples (Example IIA-19B) [32] make a few minor adjustments to the AISC design

method in order to implement it for design of extended shear tabs under combined axial and shear forces. In this adjusted method, the capacity of bolt group and weld lines is controlled for the resultant force of axial and shear demands. The interaction of axial and shear forces is taken into account for control of the block shear rupture. The main adjustment is introduction of an equation to consider the axial-shear-bending interaction to control the gross section yield and the net section rupture of the shear plate. This equation was based on elliptical yield criterion and design requirement of Section H1.1 of the AISC 360 Specification [30] for doubly symmetric members subjected to flexure and axial force. Neither published laboratory tests nor finite element analyses have been provided to validate these adjustments.

## 2.3.3 Eurocode

Eurocode 3 part 1-8 [35] uses component method to provide detailed recommendations for design of fully and partially restrained moment connections. In this analytical method, the joint is considered as a set of individual basic components. First, the active components of the connection are determined under the applied loading. The stiffness and strength of each component is then evaluated. The stiffness and strength of the connection is estimated through the assembly of the response of active components. However, this standard does not provide practical guidelines for design of simple shear connections. To fill this gap, the European Convention for Constructional Steelwork (ECSS) published a practical guideline [36] for design of simple shear connections such as shear tab connections, called as fin plate connections in Europe.

The shear tab is designed based on following design checks:

1. The shear plate should satisfy the geometric requirements, developed to assure sufficient rotational capacity of the connection.

- 2. The weld size should be detailed to prevent premature weld rupture
- 3. The bolt group capacity should be designed for an eccentric shear force. The geometric eccentricity, the distance between support face and the centre of the bolt group, was assumed as the bolt group eccentricity.
- 4. Bolt bearing in the shear plate should be controlled.
- 5. Shear plate should be controlled for shear yielding, flexural yielding, net section rupture, and block shear rupture.
- 6. Buckling of the shear plate should be controlled.
- 7. Bolt bearing in the beam web should be assessed.
- 8. Beam web should be controlled for shear yielding, net section rupture, and block shear rupture.
- 9. To ensure required ductility for stress redistribution, the guild line [36] required that the governing failure mode should occur in advance of bolt shear fracture or plate buckling. Furthermore, the bearing resistance of the shear plate or the beam web should be smaller than the shear resistance corresponding to the bolt shear fracture.

# 2.4 Summary

Several research programs were conducted to study the behaviour of extended shear tab connections under gravity induced shear force. They demonstrated the effect of the supporting member's flexibility on the response of the connections. In unstiffened configurations with rigid supports, higher demands were applied to the weld line, while the bolt group was subjected to higher demand if the unstiffened configuration was connected to a flexible support. Furthermore, it was observed that stiffening significantly changed the behaviour of extended shear tabs and made the buckling of the stiffened portion of the shear tab as the governing failure mode. However,

these observations should be evaluated for a wider range of connection configurations, commonly used in steel construction. To develop a design procedure for full-depth stiffened extended shear tabs, there is still a need for a comprehensive study on beam-to-girder shear tabs under gravity shear demand.

Research on extended shear tab connections under combined axial and shear forces was limited to research studies conducted by Thomas [23] and Salem [26]. Further, Johnston's experimental observations of double-coped beams under combined axial and shear forces could be extrapolated to the extended shear tabs. Bolt shear fracture and weld tearing were observed as the ultimate failure mode for unstiffened extended shear tabs with flexible supports while stiffened extended shear tabs failed due to the large out-of-plane deformation. For connections with rigid support, bolt shear fracture observed after large yielding and out-of-plane deformation of the shear plate. However, these findings should be evaluated for a wider range of connection configurations, e.g. the shear tab connections in which the stiffened portion should be extended to the continuity plate along the bottom flange of the orthogonal beam. Furthermore, the abovementioned studies all called for further research under higher axial force as they studied the connection behaviour under a relatively low axial force. As a conclusion, experimental and numerical studies are still needed to expand our knowledge of the behaviour of extended shear tabs.

The current CISC design table for shear tab connections [27] is limited to only a few conventional configurations. Its design recommendations do not represent the current state of practice for steel construction in which more complex shear tab connections with multiple vertical bolt lines are common. In contrast to the CISC Handbook of Steel Construction [27], the AISC Steel Construction Manual [29] provides a design method for extended shear tab connections. Although the AISC method was developed for design of unstiffened extended shear tabs under

gravity induced shear force, practicing structural engineers use this method for design of stiffened extended shear tabs owing to the lack of a validated comprehensive design procedure. For instance, Fortney's and Thornton's design recommendations [21] for stiffened extended shear tabs are not validated through either experimental or numerical study. Furthermore, the design recommendations for extended shear tabs under combined axial and shear forces, implemented in Steel Connection Handbook [31] and AISC Design Examples [32], are not validated as well. To address these shortcomings, further experimental and numerical study should be carried out.

## 2.5 References

- [1] D.B. Moore, G.W. Owens, Verification of design methods for finplate connections, The Struct. Eng., 70(3) (1992).
- [2] D.R. Sherman, A. Ghorbanpoor, Design of extended shear tabs, University of Wisconsin-Milwaukee, Milwaukee, WI, 2002.
- [3] W. Goodrich, Behavior of extended shear tabs in stiffened beam-to-column web connections, Master's Thesis, Vanderbilt University, Nashville, TN, 2005.
- [4] Steel construction manual, 13<sup>th</sup> edition, American Institute of steel Construction, Chicago, IL, 2005.
- [5] K.A. Baldwin Metzger, Experimental verification of a new single plate shear connection design model, Master's Thesis, Virginia Polytechnic Institute and State University, Blacksburg, VA, 2006.
- [6] L.S. Muir, C.M. Hewitt, Design of unstiffened extended single-plate shear connections, Eng. J. AISC, 46(2) (2009) 67-80.

- [7] W.A. Thornton, P.J. Fortney, On the need for stiffeners for and the effect of lap eccentricity on extended single-plate connections, Eng. J. AISC, 48(2) (2011) 117-125.
- [8] J.-J. Cheng, J. Yura, C. Johnson, Design and behavior of coped beams, University of Texas at Austin, Austin, TX, 1984.
- [9] Steel construction manual, 14<sup>th</sup> edition, American Institute of steel Construction, Chicago, IL, 2011.
- [10] L. Muir, W. Thornton, A direct method for obtaining the plate buckling coefficient for double-coped beams, Eng. J. AISC, 41 (2004) 133-134.
- [11] AISC 360-10, Specification for structural steel buildings, American Institute of steel Construction, Chicago, IL, 2010.
- [12] B. Dowswell, R. Whyte, Local stability of double-coped beams, Eng. J. AISC, 51(1) (2014) 43-52.
- [13] B.G. Neal, The effect of shear and normal forces on the fully plastic moment of a beam of rectangular cross section, Journal of Applied Mechanics, 28(2) (1961) 269-274.
- [14] M. D'Aronco, Behaviour of double and triple vertical rows of bolts shear tab connections and weld retrofits, Master's Thesis, École Polytechnique de Montréal, Montreal, QC, 2013.
- [15] J. Hertz, Testing of extended shear tab connections subjected to shear, Master's Thesis, McGill University, Montreal, QC, 2014.
- [16] J. Hertz, D.G. Lignos, C.A. Rogers, Full scale testing of extended beam-to-column and beam to-girder shear tab connections subjected to shear, 8th International Conference on Behavior of Steel Structures in Seismic Areas, Shanghai, China, 2015.

- [17] CSA-S16-14, Design of steel structures, Canadian Standards Association, Mississauga, ON., 2014.
- [18] ASTM F3125 / F3125M-15a, Standard specification for high strength structural bolts, steel and alloy steel, heat treated, 120 ksi (830 mpa) and 150 ksi (1040 mpa) minimum tensile strength, inch and metric dimensions, ASTM International, West Conshohocken, PA, 2015.
- [19] N. Goldstein Apt, Testing of extended shear tab and coped beam-to-girder connections subject to shear loading, Master's Thesis, McGill University, Montreal, QC, 2015.
- [20] A. Abou-zidan, Y. Liu, Numerical study of unstiffened extended shear tab connections, J. Constr. Steel Res., 107 (2015) 70-80.
- [21] P.J. Fortney, W.A. Thornton, Analysis and design of stabilizer plates in single-plate shear connections, Eng. J. AISC, 53(1) (2016) 1-28.
- [22] M.F. Suleiman, B.M. Shahrooz, H.L. Bill, P.J. Fortney, W.A. Thornton, 3-d finite element modeling of extended single plate shear connections: Predicting the mode of failure, International Journal of Steel Structures, 17(2) (2017) 525-534.
- [23] K. Thomas, Design and behaviour of extended shear tabs under combined loads, Master's Thesis, University of Alberta, Edmonton, AB, 2014.
- [24] K. Thomas, R.G. Driver, S.A. Oosterhof, L. Callele, Full-scale tests of stabilized and unstabilized extended single-plate connections, Structures, 10 (2017) 49-58.
- [25] G. Johnston, Strength and behaviour of double-coped steel beams under combined loads, Master's Thesis, University of Alberta, Edmonton, AB, 2015.
- [26] P. Salem, Unified design criteria for steel cantilever plate connection elements, PhD Thesis, University of Alberta, Edmonton, AB, 2016.

- [27] CISC, Handbook of steel construction, Canadian Institute of Steel Construction, Markham, ON., 2016.
- [28] A. Astaneh, S.M. Call, K.M. McMullin, Design of single plate shear connections, Eng. J. AISC, 26(1) (1989) 21-32.
- [29] Steel construction manual, 15<sup>th</sup> edition, American Institute of steel Construction, Chicago, IL, 2017.
- [30] AISC 360-16, Specification for structural steel buildings, American Institute of steel Construction, Chicago, IL, 2016.
- [31] A.R. Tamboli, Handbook of structural steel connection design and details, Third edition, McGraw-Hill, New York, NY., 2016.
- [32] Design examples companion to the aisc steel construction manual, version 15.0, American Institute of steel Construction, Chicago, IL, 2017.

# 3 Chapter 3: Behaviour of Stiffened Extended Shear Tab Connections under Gravity Induced Shear Force

Published in Journal of Constructional Steel Research, Volume 148, September 2018, Pages

336–350, https://doi.org/10.1016/j.jcsr.2018.06.011

Mohammad Motallebi<sup>1</sup>, Dimitrios G. Lignos<sup>2</sup>, Colin A. Rogers<sup>3</sup>

<sup>&</sup>lt;sup>1</sup> Graduate Research Assistant, Department of Civil Engineering and Applied Mechanics, McGill University, Montreal, QC. Email: mohammad.motallebinasrabadi@mail.mcgill.ca

<sup>&</sup>lt;sup>2</sup> Dimitrios G. Lignos, Associate Professor, School of Architecture, Civil and Environmental Engineering, Swiss Federal Institute of Technology, Lausanne (EPFL), Switzerland, Email: dimitrios.lignos@epfl.ch

<sup>&</sup>lt;sup>3</sup> Corresponding author
Colin A. Rogers, Associate Professor, Department of Civil Engineering and Applied Mechanics, McGill University,
Montreal, QC. Email: colin.rogers@mcgill.ca
817 Sherbrooke Street West
Montreal QC, Canada, H3A 0C3
Tel. 514 398-6449
Fax. 514 398-7361

# **Abstract**

Stiffened extended shear tab connections (either in full-depth or partial-depth configurations) are widely used to connect simply supported beams to the web of supporting girders or columns. Full-scale laboratory tests of stiffened extended shear tab connections underscored the differences between their observed and expected design strength calculated according to current design specifications. In particular, the design procedure of such connections neglects the influence of the out-of-plane deformation of the supporting girder web on yielding and inelastic buckling of the shear plate. These are the main governing failure modes for the full-depth configurations of stiffened extended shear tabs, when placed on one side of a supporting girder or column. The research described in this paper aims to develop a better understanding of the load transfer mechanism and failure modes of extended beam-to-girder shear tab connections. The findings are based on finite element (FE) simulations validated with full-scale experiments on beam-to-girder shear tab connections. The influence of girder web flexibility on the behaviour of single-and double-sided shear tabs is assessed. The stiffened portion of the full-depth extended shear tabs yielded due to the interaction of horizontal shear and vertical axial force. Due to the flexibility of the girder web of the single-sided shear tab, its stiffened portion experienced much larger vertical axial force in comparison to that of the double-sided configuration.

**Keywords**: extended shear tab, connection, plate buckling, design, effective eccentricity, finite element simulation

# 3.1 Introduction

Extended shear tab connections are widely used in steel construction practice due to their ease of fabrication and erection. They consist of a steel plate, which is shop-welded to the supporting girder or column and then bolted to the supported beam in the field. The increased shear tab length allows the beam to be connected to the girder web without coping the beam's flanges (Fig. 3-1). The shear plate may be welded to the girder web alone, i.e. unstiffened configuration (Fig. 3-1a), or may be connected either to the top flange, i.e. partial-depth stiffened configuration (Fig. 3-1b) or to both the top and bottom flanges, i.e. full-depth stiffened configuration (Fig. 3-1c). Similarly, connection to the minor axis of a W-shape column can benefit from the use of an extended shear tab.

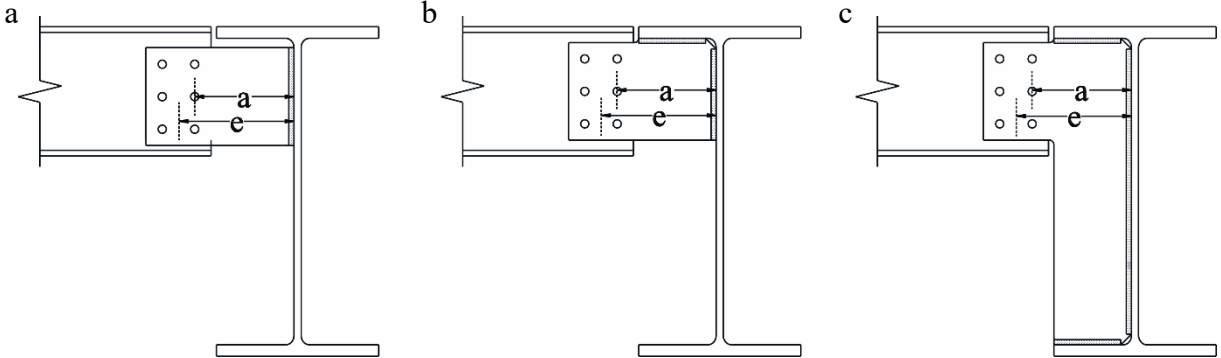


Fig. 3-1.Extended beam-to-girder shear tab connections: (a) partial-depth unstiffened, (b) partial-depth stiffened

The potential failure modes of unstiffened extended shear tab connections are summarized in the 15<sup>h</sup> Edition of the AISC Steel Construction Manual [1]. The plate thickness and the weld throat are proportioned to develop plate yielding prior to bolt shear and weld tearing such that a stable behaviour can be achieved for the imposed loading. The 15<sup>th</sup> Edition of the AISC Steel Construction Manual [1] uses the rectangular plate buckling model [2,3] to account for flexural buckling of the shear plate, while the 14<sup>th</sup> Edition of the AISC Steel Construction Manual [4]

implements equations corresponding to the flexural buckling resistance of a doubly coped beam [5-6].

The AISC design method [1] was originally developed for unstiffened extended shear tabs connected to rigid supports. The same method was further applied to unstiffened extended shear tabs connected to flexible supports by considering the out-of-plane deformation of the supporting element's web (either girder or column) as a serviceability issue for the supported beam [7]. The AISC design method was not originally developed for use with the partial-depth or full-depth stiffened extended shear tab. The shear tab in this case, may impose higher rotational demands to the supporting member (girder or column), which are typically not considered in frame analysis. This raises concern about the desirability of using stiffened extended shear tabs [8]. Nonetheless, practicing structural engineers do use stiffened extended shear tabs, typically, when an increase in the thickness of the shear plate is not a reasonable option to address the need to stabilize either the beam or the shear plate itself. The stiffened detail may be chosen because an upper limit is placed on the thickness of the shear plate to ensure its yielding prior to shear fracture of the bolts. Hence, an increase in thickness of the shear plate to improve its stability may not be permitted.

Further, specific to a beam-to-column connection, the column may also need continuity plates if there exists a fully restrained beam-to-column moment connection in the perpendicular direction. This allows for the possibility of attaching the extended shear tab to these plates as a lateral stability bracing. As well, even when continuity plates are not required, horizontal stabilizer plates may be added to laterally support the extended shear tab attached in the minor direction of a W-shape column. Moreover, if the supporting members are part of the primary lateral load-resisting system, their behaviour under gravity and lateral loads may be adversely affected by a potential out-of-plane deformation of the respective columns and/or girders. This may be particularly concerning

when deep members are utilized in the lateral load resisting system [9]. Stiffened shear tab connections may also be chosen for this reason. Given these situations, in which extended shear tabs are stiffened, there exists the need to better understand their behaviour under load, and ultimately to ascertain whether existing design methods are appropriate. As a first step, the design method found in the AISC Manual [1] can be utilized to identify the potential failure modes of these shear tab connections.

In the design of extended shear tabs the current AISC Manual [1] suggests the inflection point to be located at the face of the supporting member, i.e. the girder web in this case (Fig. 3-2a). The design shear force and flexural moment for the bolt group (Figs. 3-2b and 3-3a) are the shear force at the beam end (R) and the resultant eccentric moment (M=R × e), respectively. Furthermore, the vertical weld line, which connects the shear plate to the girder web (or the column web as shown in Fig. 3-3a), is designed to resist the shear force (R) alone. The horizontal weld lines, that connect the shear plate to the girder flanges (the stabilizer plates in Fig. 3-3a), are not considered as load carrying welds; as such, they are detailed having a minimum size. Of note, Figs. 3-2b and 3-3a show the symmetric configuration where the centreline of the supported beams is located midway between the girder flanges (the two stabilizer plates in Fig 3-3a). This configuration may not be applicable if a supported beam is connected to a deeper supporting girder (Fig. 3-2c). Further, the symmetric configuration may not be applicable in the presence of continuity plates of a fully restrained moment connection joining a deeper beam to the column in the orthogonal direction (Fig. 3-3b).

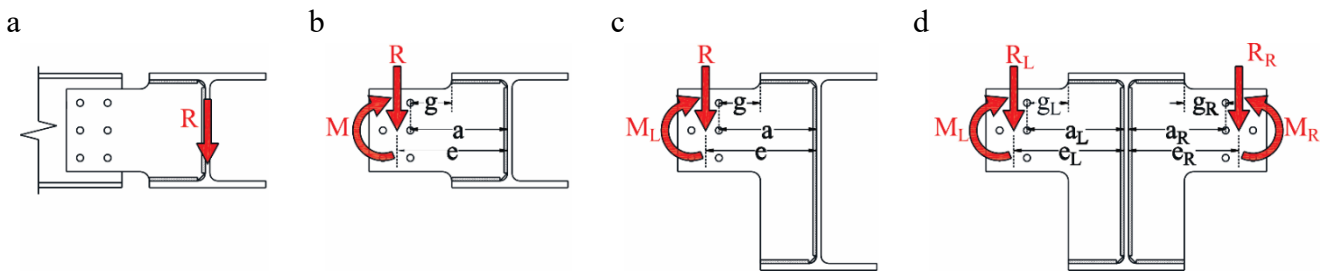


Fig. 3-2. Full-depth stiffened extended beam-to-girder shear tab: (a) location of inflection point, (b) single-sided (the beam and girder have the same depth), (c) single-sided, (d) double-sided

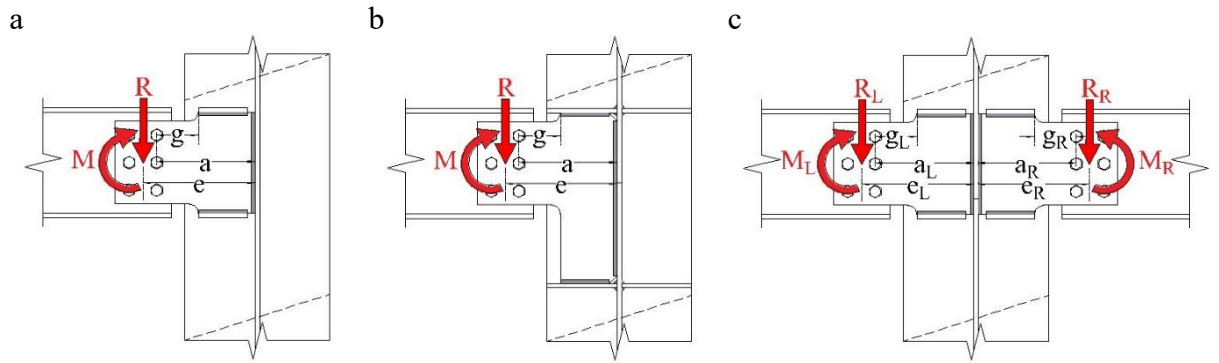


Fig. 3-3. Full-depth stiffened extended beam-to-column shear tab: (a) single-sided, (b) single-sided with continuity plates, (c) double-sided

For a girder or column, which supports a beam on both sides (Figs. 3-2d and 3-3c), each connection is designed for its corresponding shear force ( $R_R$  and  $R_L$ ) and a portion of the net flexural moment ( $M_R$ - $M_L$ = $R_R$ × $e_R$  -  $R_L$ × $e_L$ ) determined based on the engineer's judgement [1]. For the design of other connection elements, i.e. the shear plate and stabilizer plates, the current AISC Manual gives no explicit recommendations.

It is often the case that the design procedure of stiffened beam-to-girder shear tabs follows that of the unstiffened ones; the bolt group and the gross section of the plate are designed for the connection shear force (R) and the resultant eccentric bending moment (R  $\times$  e and R  $\times$  a, respectively). This leads to either bolt shear fracture or yielding of the extended portion of the shear plate as the governing failure mode of the stiffened shear tab connection if the current AISC design approach [1] is followed. However, this is not consistent with the observed behaviour of such connections from laboratory tests [10-12].

Findings from past experimental and finite element studies [10-13] reveal that bolt shear fracture is not deemed to be critical in the context of the connection configurations that were evaluated. Plate buckling is the governing failure mode for stiffened full-depth configurations of either beam-to-girder [10] or beam-to-column shear tab connections [11, 12]. Notably, in stiffened extended beam-to-girder shear tabs with a partial-depth shear plate, shear plate yielding and twisting were the governing failure modes [10, 13]. Although the girder web mechanism was evident, it was a secondary failure mode that mostly occurred in deep connections, i.e. shear tab connections with a single vertical line of six or more bolts [10,13].

In order to improve the current design provisions for full-depth stiffened extended shear tabs, Fortney and Thornton [14] recommended that the distance between the bolt line and the toe of a stabilizer plate should be used as the bolt group eccentricity for the design of extended shear tabs with stabilizer plates. Neither published laboratory tests nor finite element analyses were provided to fully explain this recommendation. Although the design calculations based on the aforementioned eccentricity result in a higher prediction for the bolt shear strength, they still overestimate the shear plate buckling strength, which is the governing failure mode observed in laboratory tests [10-12].

The test results of extended beam-to-girder shear tabs are limited to a few configurations with a single vertical row of bolts, although shear tabs with multiple bolt lines are common in current steel construction practice. Multiple bolt lines may decrease the shear plate buckling strength because the shear plate is loaded farther from its support, the weld line. Furthermore, most of the experimental studies on stiffened beam-to-column shear tabs [12] were limited to the configuration similar to that shown in Fig. 3-3a. Nevertheless, this configuration would need to be modified if continuity plates were incorporated into a fully restrained beam-to-column connection (Fig. 3-3b),

resulting in a full-depth stiffened shear tab connection. As such, conflicting opinions exist regarding the design of stiffened extended shear tabs, and the definition of the eccentric loading.

To further our understanding on how unstiffened and stiffened extended shear tab connections behave under gravity-induced shear forces, a research program was carried out at McGill University. Full-scale laboratory tests of extended and various other shear tabs were first conducted [15-22]. These test results allow for a better comprehension of the nonlinear behaviour of shear tab connections under monotonic loading. The testing program was complemented with detailed finite element (FE) simulations. Several parameters were interrogated to further our understanding of the behaviour of extended shear tab beam-to-girder connections. This paper presents the findings from the corroborating finite element analysis of the research program for two specific beam-to-girder extended stiffened shear tab connections. The main objective was to gain insight into the differences in load transfer mechanism of single- and double-sided stiffened full-depth extended shear tabs.

# 3.2 Brief description of full-scale laboratory testing at McGill University

Fifty-five full-scale laboratory tests were conducted at McGill University [15-22] to characterize and further understand the behaviour of shear tab connections, including both standard and extended configurations, beam-to-column and beam-to-girder arrangements, as well as bolted and welded details. The connection configurations reflect the current practice in North America. Among these tests, two specimens of stiffened full-depth extended beam-to-girder shear tabs with two vertical rows of three bolts (Figs. 3-4a and 3-4b) were selected to develop finite element models to further our understanding regarding their behaviour under gravity-induced shear forces; BG3-2-10-F [19] and BG3-2-13-F [20]. These specimens were nominally identical except for the

thickness of the respective shear plate; the shear plate was 10 mm thick for Specimen BG3-2-10-F, and 13 mm for BG3-2-13-F. In particular, the thickness of the shear plate of Specimen BG3-2-13-F was increased to satisfy the current compactness criteria for the stiffener of a plate girder as per CSA S16 [23]  $(200/\sqrt{F_y})$ . This corresponds to the AISC 360 [2] width-to-thickness ratio for unstiffened elements subjected to axial compression (Table B4.1a,  $0.45\sqrt{E/F_y}$ ). Of note, the shear plate compactness is not part of the AISC shear tab design method [1]; this method addresses unstiffened shear tab connections where plate local buckling is not a concern.

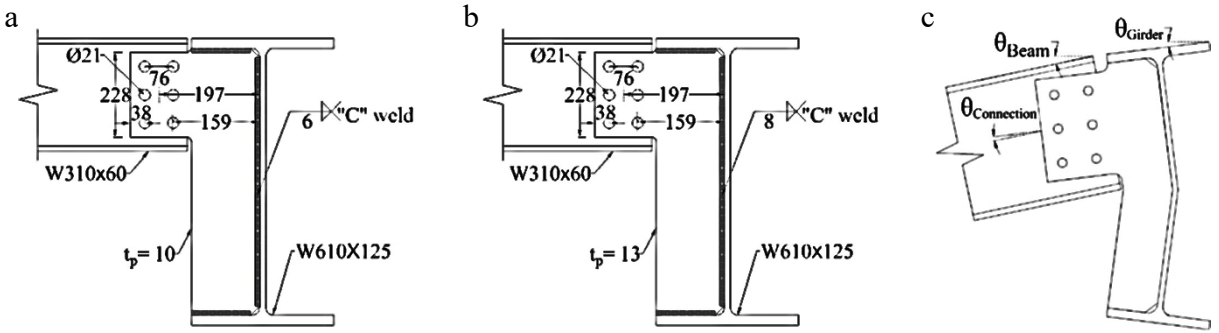


Fig. 3-4. Laboratory tests of beam-to-girder shear tabs: (a) details of Specimen BG3-2-10-F, (b) details of Specimen BG3-2-13-F, (c) measured rotations of specimens (dimensions in mm)

The beam and girder were fabricated from ASTM A992 Grade 50 steel [24], while the shear plates were made of ASTM A572 Grade 50 steel [25]; for both grades the nominal F<sub>y</sub>=345 MPa and F<sub>u</sub>=448 MPa. To attach the shear tab to the supporting girder, an E71T (nominal F<sub>u</sub>=490 MPa) electrode was used in a flux-cored arc welding process with additional shielding gas (CO<sub>2</sub>) to provide a fillet weld on both sides of the plate. Each beam was snug tightened to the shear tab using 19 mm (3/4 in.) ASTM F3125 Grade A325 bolts [26] in standard size holes (20.6 mm (13/16 in.)). The test setup (Fig. 3-5) consisted of a 12 MN and a 445 kN hydraulic actuator, a lateral bracing system for the steel beam, and supporting elements for the girder. The 12 MN actuator, located near the shear tab connection, developed the main shear force in the connection. The 445 kN actuator, placed at the far end of the beam, facilitated the vertical displacement control of the

beam tip, as well as the connection rotation. The relative rotation between the beam and the girder was defined as the connection rotation (Fig. 3-4c). The lateral bracing system was installed to restrict the lateral displacement of the beam, without affecting its vertical displacement. This test setup, to apply simultaneous shear force and rotation to the connection, is based on that used in prior research of shear tab connections [27].

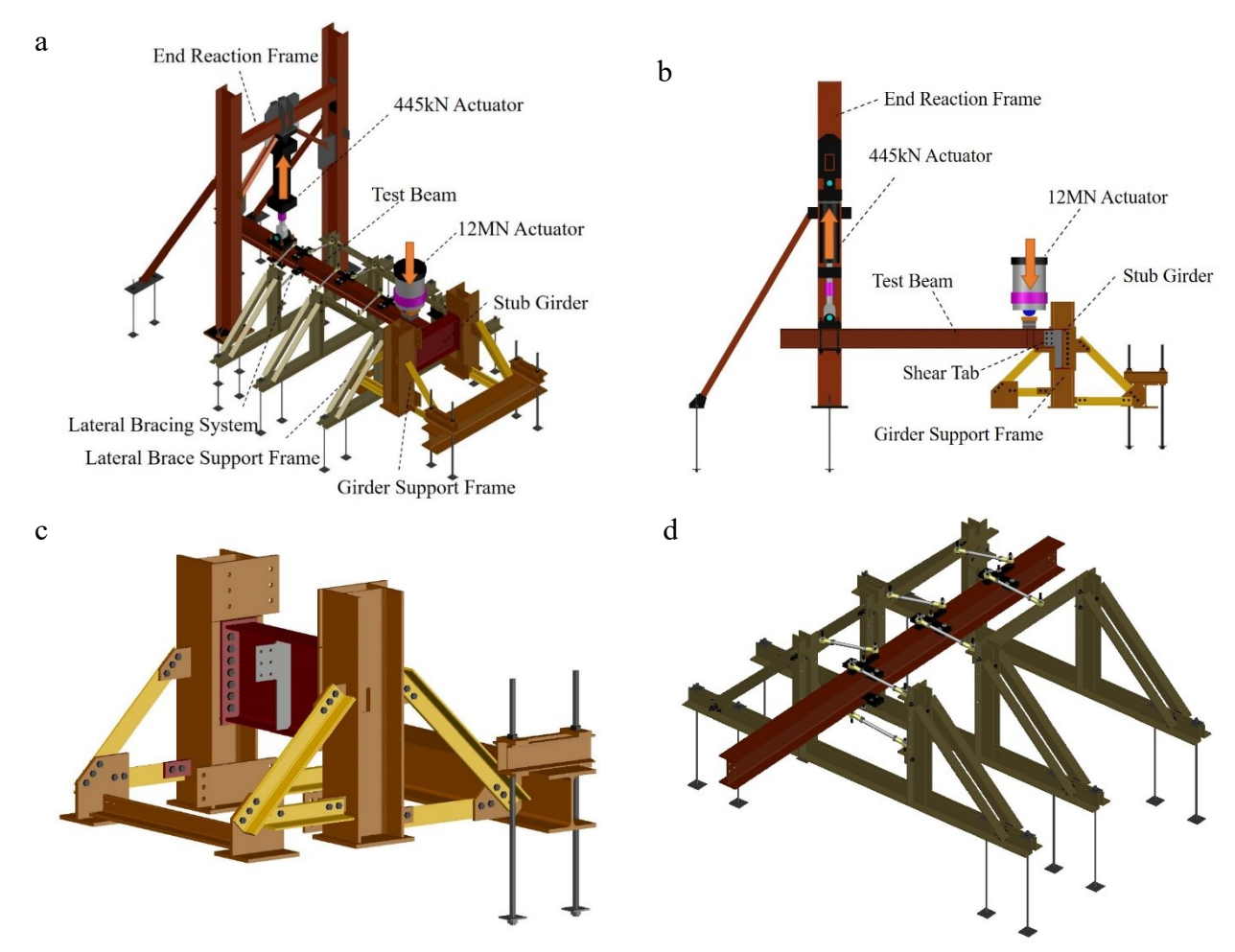


Fig. 3-5. Laboratory tests of beam-to-girder shear tabs: (a) overall test setup, (b) elevation view (lateral bracing system was not shown for clarity), (c) close-up view of the shear tab connection, girder, and its supporting frame, (d) view of the test beam and its lateral bracing system

Linear Variable Differential Transformers (LVDTs) were installed to measure the out-of-plane deformation of the beam, as well as that of the shear plate and of the girder web (Fig. 3-6). Inplane rotation of the beam and girder were measured using inclinometers (Fig. 3-6). A complete description of the test programs can be found in [19, 20].

On the basis of the current AISC design procedure [1], Table 3-1 contains a summary of the calculated connection strengths corresponding to the probable failure modes. The contact between the shear plate and girder flanges was ignored; the shear plate was designed as would be done for an unstiffened shear tab. Hence, the distance between the girder web and the interior bolt line (the *a* distance) was conservatively considered to be the unbraced length of the shear plate. Of note, this method resulted in a more conservative prediction for the shear plate buckling as compared to Fortney and Thornton's recommendation [14] for the connection eccentricity.

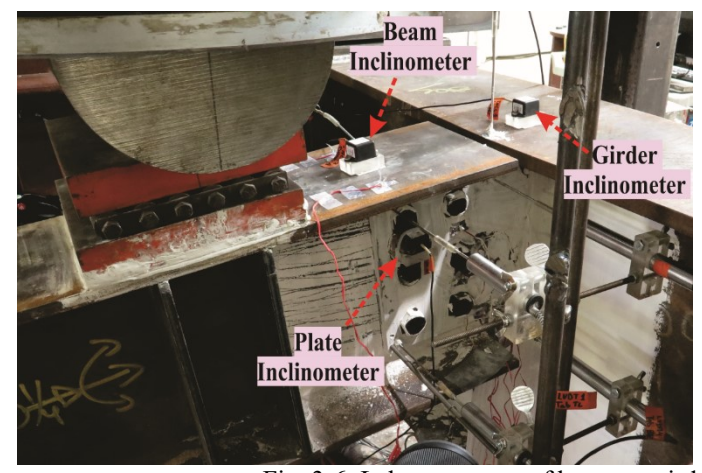




Fig. 3-6. Laboratory test of beam-to-girder shear tab specimen BG3-2-13-F

Table 3-1 AISC predicted strength of shear tab test specimens

		BG3-2-10-1	F	BG3-2-13-F			
Failure mode	Design strength (kN)	Expected strength <sup>1</sup> (kN)	Expected strength <sup>2</sup> (kN)	Design strength (kN)	Expected strength <sup>1</sup> (kN)	Expected strength <sup>3</sup> (kN)	
Flexural and shear yielding of shear plate	214	255	307	281	334	390	
Shear yielding of shear plate	450	495	596	591	650	758	
Bolt bearing	191	280	305	191	280	290	
Buckling of shear plate	243	297	357	319	390	455	
Rupture at net section of shear plate	318	509	496	417	667	654	
Bolt shear	182	270	270	182	270	270	
Weld tearing	1035	1380	1380	1294	1725	1725	

<sup>&</sup>lt;sup>1</sup>Expected strength based on probable material properties i.e.R<sub>y</sub>F<sub>y</sub> (1.1 F<sub>y</sub>) and R<sub>T</sub>F<sub>u</sub> (1.2 F<sub>u</sub>) for steel plates [27]

buckling [1] and buckling of the double coped beam [4]. Both methods predicted that buckling

<sup>&</sup>lt;sup>2</sup>Expected strength based on measured material properties i.e F<sub>y</sub>=456MPa and F<sub>y</sub>=525MPa for 10mm plate

<sup>&</sup>lt;sup>3</sup>Expected strength based on measured material properties i.e F<sub>v</sub>=442MPa and F<sub>v</sub>=527MPa for 13mm plate

The buckling strength of the shear plate was calculated using two methods: rectangular plate

would not prevent the shear plate from reaching its nominal plastic flexural capacity ( $M_p=F_yZ_p$ ). In addition to the nominal and expected material properties, the measured properties (coupon tests [19, 20]) of the steel beam, girder and plate were used to conduct these AISC-based calculations, whereas the nominal properties of the bolts and welds were relied on in this process.

Regarding the shear plate-to-girder weld, its size meets the AISC minimum requirement ( $a_w \ge 5/8t_p$ ), and the reported weld tearing strength is the concentric shear capacity of the vertical weld line. To ensure yielding of the shear plate in advance of bolt shear fracture, the AISC requirement for maximum shear plate thickness was controlled using the nominal yield stress of the shear plate, as well as its expected and measured material properties. Although both configurations meet this requirement, the bolt shear fracture was predicted as the governing failure mode in all cases, other than for calculations based on the expected material properties of Specimen BG3-2-10-F.

Referring to Fig. 3-7a, both specimens showed very ductile response; these tests were terminated due to binding between the beam's bottom flange and the shear plate. The binding took place at 271 kN (0.073 rad) and 520 kN (0.129 rad) for Specimens BG3-2-10-F and BG3-2-13-F, respectively. However, it should be noted that it would be imprudent to rely on these ultimate shear resistances in the design of extended shear tabs because the large rotation, needed to develop this shear force, would be detrimental to the serviceability of the supported beam.

The yielding and out-of-plane deformation of the girder web and the stiffened section of the shear tab (Figs. 3-7b and 3-7c), which was confined between the girder web and flanges, were observed as failure modes. The stiffness of specimen BG3-2-10-F degraded significantly at 221 kN shear force (82% of the connection expected strength, i.e., 270 kN), while the stiffness of specimen BG3-2-13-F decreased at 390kN shear force (144% of the connection expected strength, i.e., 270 kN). Contrary to the design predictions, bolt shear failure did not occur in any of the full-

scale tests, nor did the bolts exhibit damage. It was observed that the inflection point formed away from the girder web and close to the centre of the bolt group. As such, the bolt group eccentricity was much smaller than the AISC assumption, the distance between the weld line and the centre of the bolt group (the geometric eccentricity). Further discussion of this aspect is provided in Section 3.5.2.

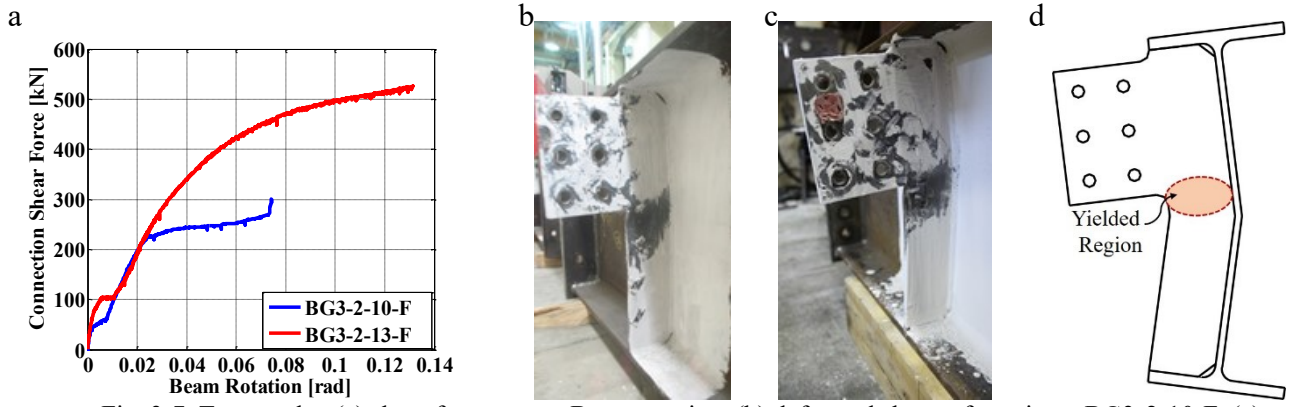


Fig. 3-7. Test results: (a) shear force versus Beam rotation, (b) deformed shape of specimen BG3-2-10-F, (c) deformed shape of specimen BG3-2-13-F, (d) girder web mechanism

# 3.3 Finite element simulation of extended beam-to-girder shear tab connections

The finite element (FE) models were developed in the commercial software ABAQUS-6.11-3 [29] to obtain a better understanding of the behaviour of extended beam-to-girder shear tab connections with full-depth stiffeners under gravity-induced shear forces. The main features of the FE models (Fig. 3-8) were chosen to be representative of those seen in the laboratory experiments; including geometry, boundary conditions, material properties, element size and element type, contacts and interactions, and the imposed loading protocol. The employed material properties were defined based on the engineering stress-strain curves obtained from tensile coupon tests, directly extracted from the various components of the tested subassemblies. These were then converted to true stress-strain curves. The material properties for the bolt and welds were defined based on typical stress-strain curves, obtained from Kulak et al. [30] and Gomez et al. [31],

respectively, which were scaled to meet the minimum specified values. Of note, all constitutive material models were defined up to the ultimate strain.

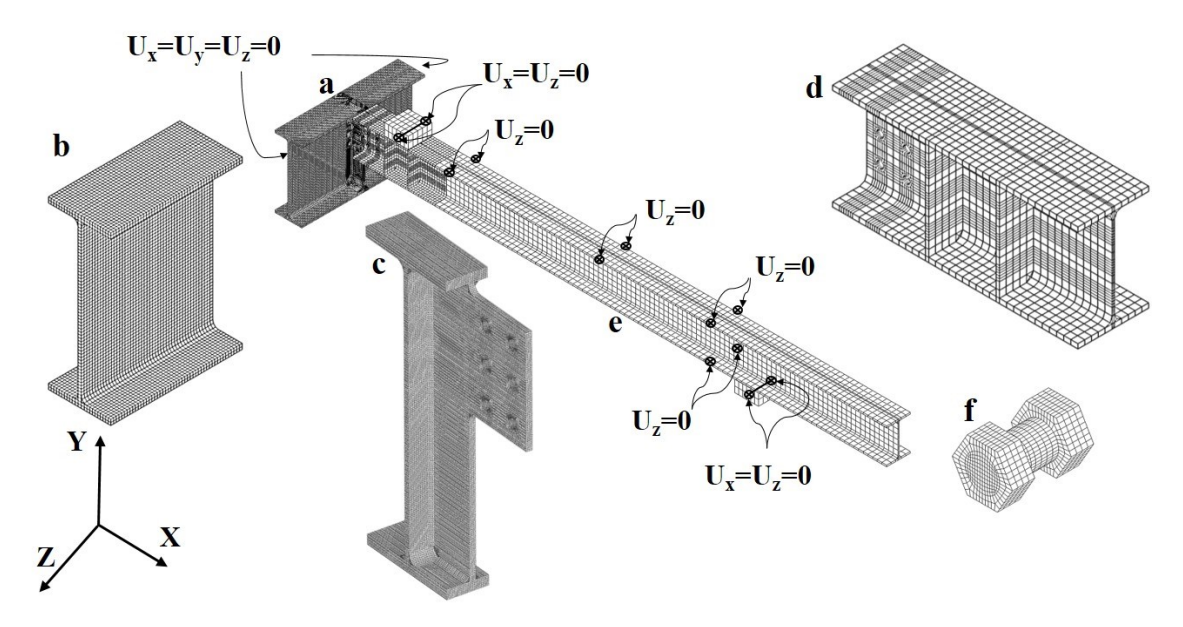


Fig. 3-8. Finite element model specifics: (a) overall model, (b) girder mesh (typical element size of 10 mm), (c) shear plate mesh (typical element size of 3 mm), (d) mesh of the beam in the vicinity of connection (typical element size of 20 mm), (e) beam mesh (typical element size of 40 mm), (f) bolt mesh (Typical element size of 1.5 mm)

First-order fully-integrated 3D solid elements were utilized to mesh the FE models of the shear tabs (Fig. 3-8). The element size was determined based on a mesh sensitivity analysis. The stub columns (Fig. 3-5c) were replaced by idealized fixed boundary conditions to create a computationally efficient FE model. To simulate the lateral braces (Fig. 3-5d) of the beams, the lateral displacement of the beam flanges at the locations of the braces was restricted. The loading protocol was simulated by applying the displacements of the two actuators, recorded during the tests, to the centerline of the load cubes, while the horizontal (U<sub>x</sub>) and out-of-plane deformation (U<sub>z</sub>) of the load cubes' centerline were prevented. To allow transmission of tangential force between the components in contact, a friction coefficient of 0.3 was used for all surface-to-surface contact pairs, except those between the load cubes and the flanges of the beam where frictionless interaction was defined. The normal behaviour of contacts, allowing separation after closure, was defined

using a hard contact formulation with a penalty constraint enforcement method. Furthermore, to trigger possible local instabilities of the shear tab connection, local imperfections were introduced into the shear plate and girder. In order to define the local imperfections, the nodal coordinates of the shear plate and girder were modified by scaling appropriate buckling mode shapes, obtained from eigenvalue buckling analysis. These local imperfections were proportioned to the limits of manufacturing tolerances for the web of W-sections (d/150) [32-34]. This approach was found to be satisfactory in prior FE studies by Elkady and Lignos [35] to simulate the onset of local and/or member geometric instabilities.

## 3.3.1 Comparison of numerical and experimental results

In order to evaluate the accuracy of the numerical models, their predictions were compared to test results. Among others, the developed shear force of the connection and the girder web out-of-plane deformation were chosen as the primary model verification criteria as shown in Fig. 3-9.

Referring to Figs. 3-9a to 3-9d, the predicted shear force response deviated from the test measurements only in the initial increments of the applied loading. This discrepancy is due to uncertainties related to the contact between the bolt shanks and the bolt holes for each specimen due to fabrication tolerances and installation of the respective test specimens. The shear tab connections were snug-tightened, hence, bearing between the bolt shanks and bolt holes transferred the shear force between the beam and the shear plate. Further, the initial position of each bolt in its hole was not controlled during testing, leading to an unknown slip before contact bearing. In the FE model, the bolts were consistently placed at the bolt hole centre, resulting in an initial 0.8 mm (1/32 in.) gap around the entire perimeter of the bolt shanks, which matches the fabrication tolerance of standard 21 mm (13/16 in.) holes. To prevent rigid body motion of the

beam, and consequently to overcome issues with numerical convergence of the FE model, a small amount of bolt pretension, i.e. 50 MPa, was applied as suggested in prior related studies [36].

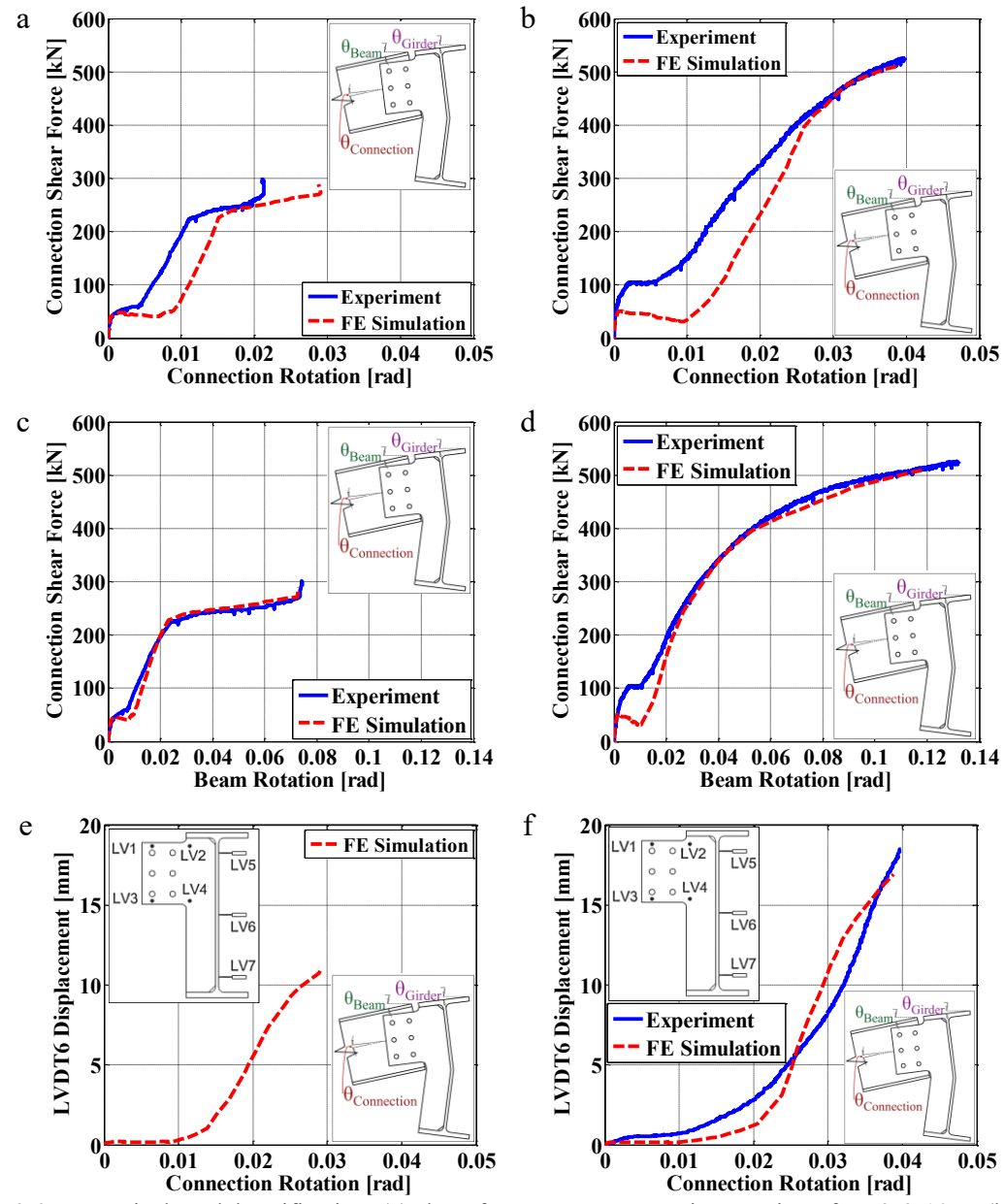


Fig. 3-9. Numerical model verification: (a) shear force versus connection rotation of BG3-2-10-F, (b) shear force versus connection rotation of BG3-2-13-F, (c) shear force versus beam rotation of BG3-2-10-F, (d) shear force versus beam rotation of BG3-2-13-F, (e) girder web out-of-plane deformation versus connection rotation of BG3-2-13-F (f) girder web out-of-plane deformation versus connection rotation of BG3-2-13-F

Figure 3-9f suggests that the FE models predict reasonably well the out-of-plane deformations of the girder web of connection BG3-2-13-F. For shear tab connection BG3-2-10-F (Fig. 3-9e),

the girder web out-of-plane deformation was not accurately measured due to the malfunction of one of the LVDTs (LVDT6).

# 3.4 Observed failure modes of extended beam-to-girder shear tab connections

It is rather challenging to observe the individual failure modes of shear tab connections addressed in the AISC Steel Construction Manual [1] by solely conducting physical experiments. This is due to the failure mode coupling after the connection exhibits inelastic behaviour. As such, a numerical study was conducted in which the strength of the connection components (beam, shear plate, bolts, and girder) were determined. The calibrated FE models for shear tab configurations BG3-2-10-F and BG3-2-13-F served as baseline models.

The features and the targeted behavioural aspects associated with each individual FE model are presented in Table 3-2, and are further discussed in Sections 3.4.1 and 3.4.2.

Table 3-2-Features and targeted behavioural aspects of FE models

Table 3-2-1 catures and targeted behavioural aspects of PL models						
Model Notation	Features	Behavioural Aspect				
FE-E	All components elastic	Elastic stiffness and elastic buckling				
	7 m components clastic	strength				
FE-E-G	All components elastic except girder	Out-of-plane bending capacity of girder				
	All components clastic except girder	web				
FE-E-Be	All components elastic except beam	Effect of beam yielding on response of				
	An components clastic except beam	connection				
FE-E-Bo	All components elastic except bolts	Shear capacity of bolt group				
FE-E-SH	All components elastic except shear plate	Strength of shear plate				
FE-Pl	Yieldable material properties assigned to	Strength of connection and interactions				
	all components	between failure modes				
FE-Pl-Imp	Yieldable material properties assigned to	Effect of initial imperfection on behaviour of shear tab				
	all components. Initial imperfections					
	assigned to trigger buckling of shear tab					

In the FE-E model, all the material properties were assumed to be elastic such that the elastic stiffness of the shear tab connection could be computed. The FE models with damageable components advanced our understanding in the load redistribution due to material nonlinearity

and/or geometric instabilities occurring within a connection. Both single- and double-sided shear tabs were investigated.

### 3.4.1 Single-sided shear tabs

The results of the numerical FE study for shear tab connections BG3-2-10-F and BG3-2-13-F are illustrated in Figs. 3-10 and 3-11, respectively. The shear force of BG3-2-10-F is presented versus the connection rotation and the beam rotation in Figs. 3-10a and 3-10b, respectively. Displacements of LVDT 4 and LVDT 6 (Figs. 3-9e and 3-9f) are presented versus the connection rotation in Figs. 3-10c and 3-10d, respectively.

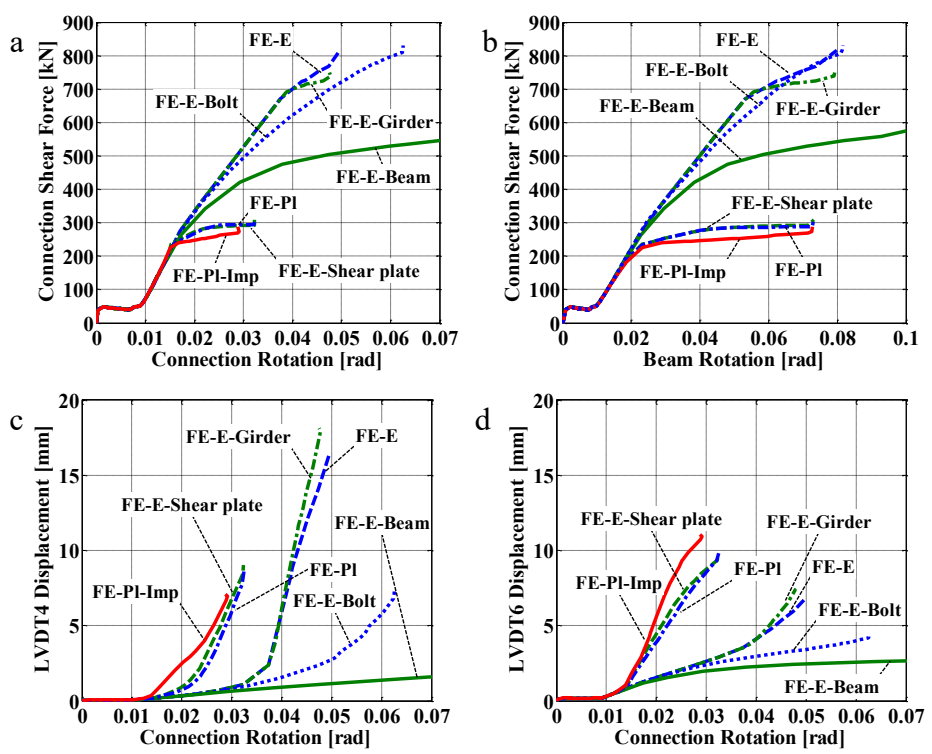


Fig. 3-10. Predictions of numerical models for shear tab connection BG3-2-10-F

Referring to Figs. 3-10 and 3-11, the FE-E model suggests a near bilinear response. In general, a significant loss in stiffness is identified when the slope of the curve representing the out-of-plane deformation of the shear plate (LVDT4) versus connection rotation (Fig. 3-10c) exhibits a sudden increase. This stiffness change is associated with the bifurcation point due to elastic buckling.

Figures 3-10d and 3-11d show a substantial increase in the girder web out-of-plane deformation slope (LVDT6) following elastic buckling of the shear plate. A comparison between the FE-E model and the model with a yieldable girder (FE-E-G), demonstrated that their response was approximately identical prior to the onset of girder web yielding. For the slender shear tab (BG3-2-10-F), Fig. 3-10a shows that the connection with a yieldable girder lost its stiffness and reached its capping strength soon after the shear plate buckled. The strength plateau of the FE-E-G model was attributed to yielding of a large part of the girder web, due to the out-of-plane bending, and formation of a mechanism in the girder web (Fig. 3-7d).

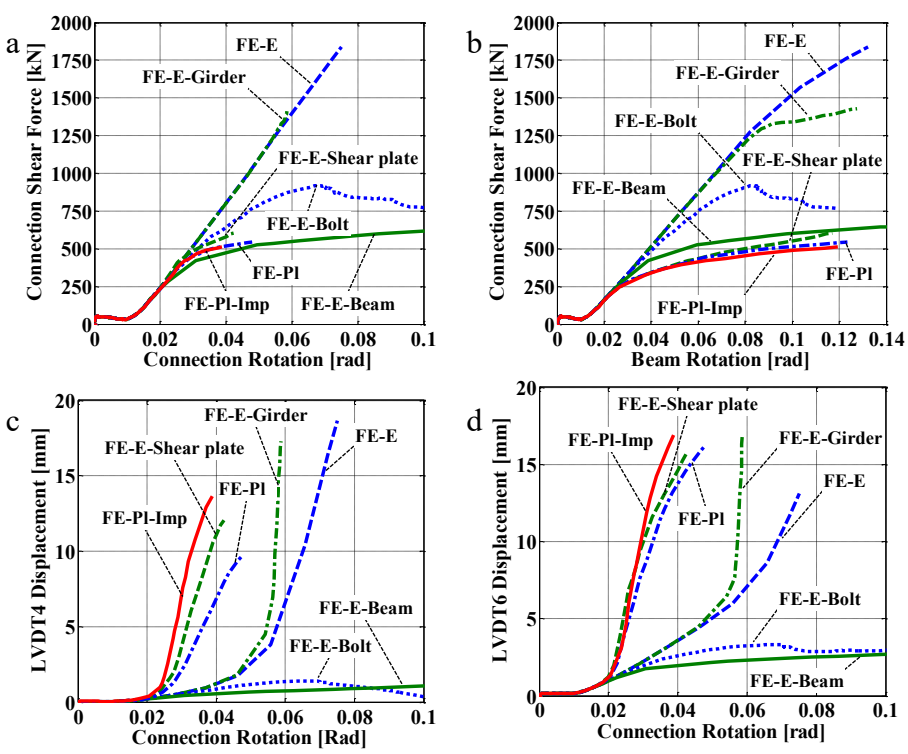


Fig. 3-11. Predictions of numerical models for shear tab connection BG3-2-13-F

In contrast, Fig. 3-11a shows that the FE-E-G model of the compact shear tab (BG3-2-13-F) lost its stiffness prior to the shear plate elastic buckling due to the shear yielding of the bottom part of the girder web.

Figures 3-10 and 3-11 demonstrate the great dependency of the connection response on the yielding of the shear plate. The yieldable shear plate, i.e. shear plate of models FE-E-SH, FE-Pl, and FE-Pl-Imp, began to yield at the lower re-entrant corner (Figs. 3-12a and 3-12b), while its out-of-plane deformation was negligible. As the shear force increased, the yielding propagated to the stiffened part of the shear plate, while the out-of-plane deformation of the plate increased. Referring to Fig. 3-10a, the slender shear plate (BG3-2-10-F) lost its stiffness when yielding propagated through the full width of its stiffened portion (Figs. 3-12c and 3-12d). In contrast, Fig. 3-11a shows that the compact shear tab (BG3-2-13-F) was able to continue resisting shear after yielding of the stiffener, although its stiffness slightly decreased at this point.

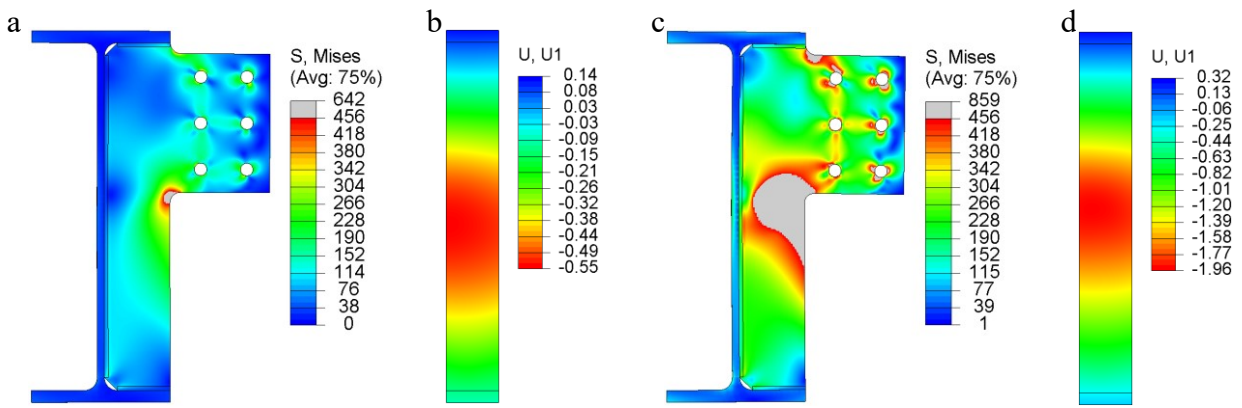


Fig. 3-12. Prediction of model FE-E-SH of BG3-2-10-F for: (a) stress of shear plate at  $\theta$ =0.0115 rad, (b) out-of-plane deformation of girder web at  $\theta$ = 0.0115 rad, (c) stress of shear plate at  $\theta$ = 0.0155 rad, (d) out-of-plane deformation of girder web at  $\theta$ = 0.0155 rad (The grey colour represents yielded regions)

In comparison to the FE-E-SH model, the girder web of the FE-Pl model began to yield soon after yielding of the stiffener, which resulted in a slightly lower shear force at the end of the analysis. Referring to Figs. 3-10 and 3-11, the shear plate and the girder web of the model incorporating imperfections experienced a larger out-of-plane deformation at the same level of shear force as compared with model FE-Pl. In comparison to model FE-Pl, this imperfection resulted in a slight decrease in the capping strength (9% and 5% for BG3-2-10-F and BG3-2-13-F, respectively) of the model FE-Pl-Imp.

#### 3.4.2 Double-sided shear tabs

As presented in the Section 3.4.1, the girder web out-of-plane deformation influenced the failure mode of single-sided shear tabs. However, the contribution of this failure mode may be insignificant for double-sided shear tab connections, where two beams, one framed to each side of the girder, counterbalance the moments of each other. To investigate the behaviour of double-sided shear tabs, a series of FE analyses, as described in Table 3-2, was conducted for shear tab connections BG3-2-10-F and BG3-2-13-F. To decrease computational costs, symmetric boundary conditions were implemented along the girder axis; a beam and half of a girder section were included in these FE models. The FE results for connections BG3-2-10-F and BG3-2-13-F are presented in Fig. 3-13.

Referring to Figs. 3-13a and 3-13b, the bifurcation point due to elastic buckling of the shear plate was observed in the slender shear tab (BG3-2-10-F), while the stiffness of the connection with a compact shear plate (BG3-2-13-F) remained constant, even though its shear plate experienced large out-of-plane deformations. The response of the FE model with a yieldable girder was identical to the elastic model up to the yielding of the girder web. The out-of-plane deformation of the girder web was restrained, which led to yielding of the girder web due to the applied shear force. This girder web yielding mechanism is distinct from the yielding mechanism of the single-sided configuration, in which the yielding of the girder's web began mainly due to its out-of-plane bending. For the numerical model containing a yieldable shear plate, the onset of yielding occurred at the re-entrant corner of the shear plate when its out-of-plane deformation was negligible. Unlike the single-sided connections, the yielding propagated along the bolt line instead of through the stiffened part of the shear plate. The total height of the shear plate along the bolt line, closest to the girder, yielded and the connection stiffness decreased significantly at this point.

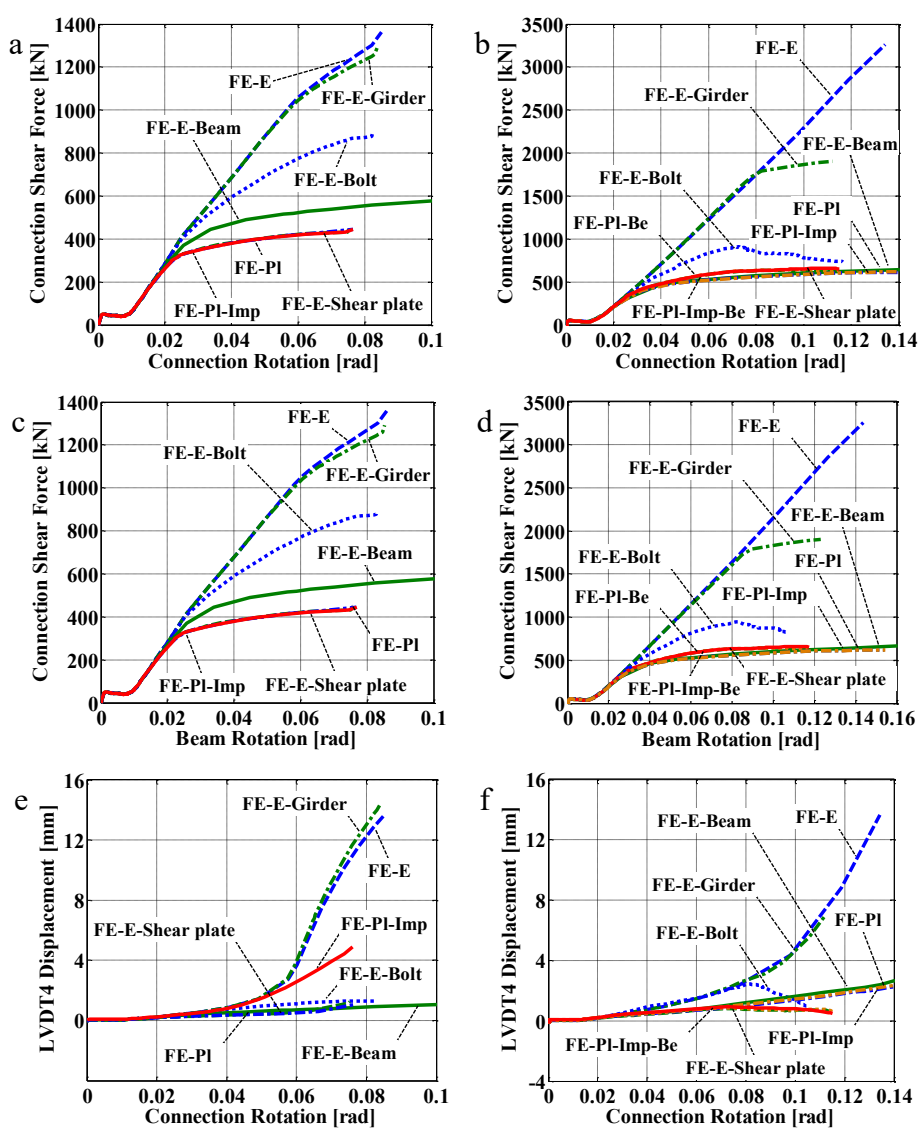


Fig. 3-13. FE models for double-sided shear tabs: (a) prediction for shear force versus connection rotation of BG3-2-10-F, (b) prediction for shear force versus connection rotation of BG3-2-13-F, (c) prediction for shear force versus beam rotation of BG3-2-13-F, (e) prediction for out-of -plane deformation of shear plate versus connection rotation of BG3-2-10-F, (f) prediction for out-of -plane deformation of shear plate versus connection rotation of BG3-2-13-F

Figure 3-13 shows that the predictions of the FE-Pl and FE-Pl-Imp models of BG3-2-10-F were close to those of the model with a yieldable shear plate. This occurred because the corresponding shear force demand was not sufficient to develop yielding in the girder web, as shown in Fig. 3-14. However, after yielding of the full depth of the shear plate along the interior bolt line of model FE-Pl-Imp (Fig. 3-14a), yielding propagated from the stiffened portion of the

shear plate (Fig. 3-14c), and the out-of-plane deformation of the plate increased. Referring to Fig. 3-13b, the results of models FE-Pl and FE-Pl-Imp of BG3-2-13-F deviated from the results of the model FE-E-SH due to the yielding of the beam's web along the net section of the vertical row of bolts, farthest from the girder. As the main purpose of this study was to investigate the behaviour of the shear tab connection, the effect of beam yielding was prevented from dominating the results of the numerical model FE-Pl-Be by assigning elastic material properties to the beam, while the other components were defined to experience yielding. Figure 3-13b shows that the results of this model and model FE-Pl-Imp-Be, were identical to the model with a yieldable shear tab because the level of shear force was not sufficient to initiate yielding of the girder web.

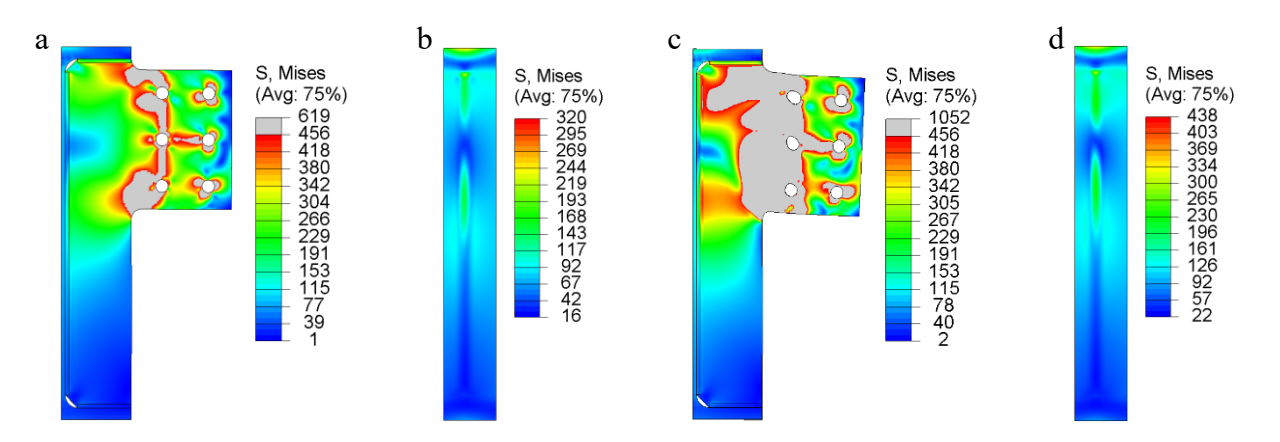


Fig. 3-14. Prediction of model FE-Pl-Imp of BG3-2-10-F for stress of: (a) shear plate at  $\theta$ =0.0223 rad, (b) girder web at  $\theta$ =0.0223 rad, (c) shear plate at  $\theta$ =0.0603 rad, (d) girder web at  $\theta$ =0.0603 rad (The grey colour represents yielded regions)

## 3.5 Discussion

A comparison of the measured and FE simulated results for the single-sided shear tabs and the double-sided shear tabs demonstrated that the expected failure mode is different for the two configurations. Figure 3-15a shows a free body cut for selected sections of the shear plate. This method of evaluation was employed to examine the different load transfer mechanisms in single and double-sided shear tabs. Using these free body cuts, the location of the inflection point was determined (Fig. 3-15b) and its distance to the centreline of the girder web, i.e. the effective

eccentricity ( $e_{eff}$ ), and the centroid of the bolt group, i.e. the bolt group eccentricity ( $e_b$ ), were calculated. The results of the free body cuts are presented and discussed in Sections 3.5.1 and 3.5.2.

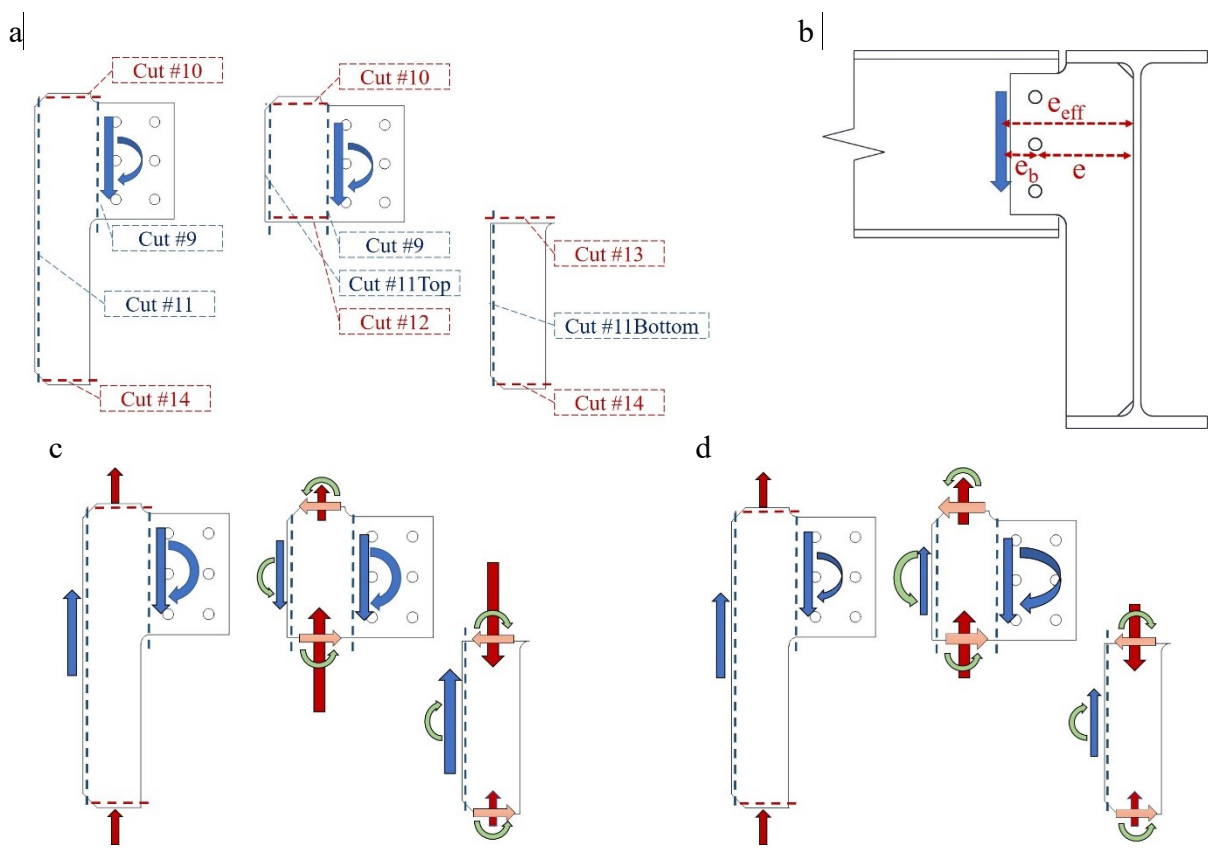


Fig. 3-15. Free body cuts from FE models (a) defined sections for Free body cuts, (b) connection eccentricity, (c) freebody diagram of single-sided shear tab, (d) freebody diagram of double-sided shear tab

#### 3.5.1 Load transfer mechanism

Figures 3-16a and 3-16c show that the compressive axial force, which developed in the stiffened portion of the shear tab (Cut #12), was larger than the connection shear force of the single-sided shear tabs. In contrast, this compressive axial force was smaller than the connection shear force in the double-sided shear tabs (Figs. 3-16b and 3-16d). For the FE-E models of shear tab connections BG3-2-10-F and BG3-2-13-F, the ratio between the stiffener axial force and the connection shear force was 1.67 and 0.48 for single-sided and double-sided shear tabs, respectively. As these ratios remained constant for both the slender and compact shear tabs, it can

be concluded that they result from the different loading transfer mechanisms for single and doublesided shear tabs.

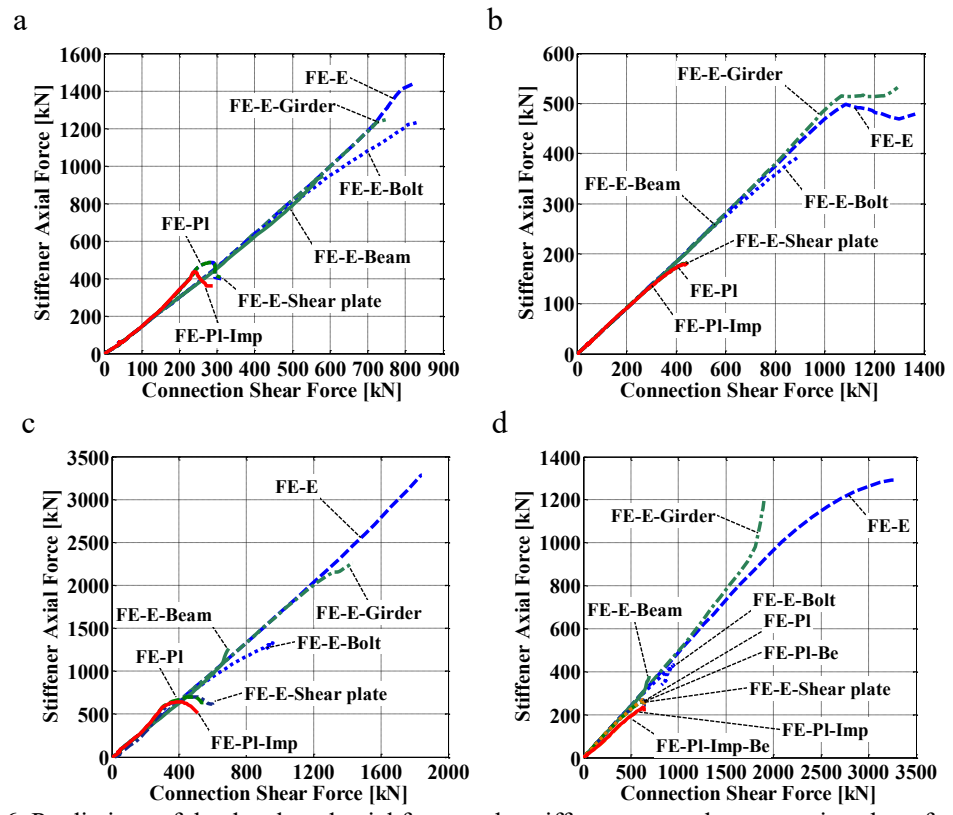


Fig. 3-16. Predictions of the developed axial force at the stiffener versus the connection shear force for: (a) single-sided configuration of BG3-2-10-F, (b) double-sided configuration of BG3-2-10-F, (c) single-sided configuration of BG3-2-13-F, (d) double-sided configuration of BG3-2-13-F

In order to determine the load transfer mechanism, the forces, developed through different portions of the shear plate, were also studied. Regarding the elastic models of BG3-2-10-F (including single-sided and double-sided), the vertical forces at the shear plate are presented versus the beam rotation in Fig. 3-17. A large component of the connection shear force of single-sided shear tabs (i.e. Cut #9) was transferred to the girder web (i.e. Cut #11) as a shear force, while the girder flanges (Cut #10 and Cut #14) carried 20% of the connection shear.

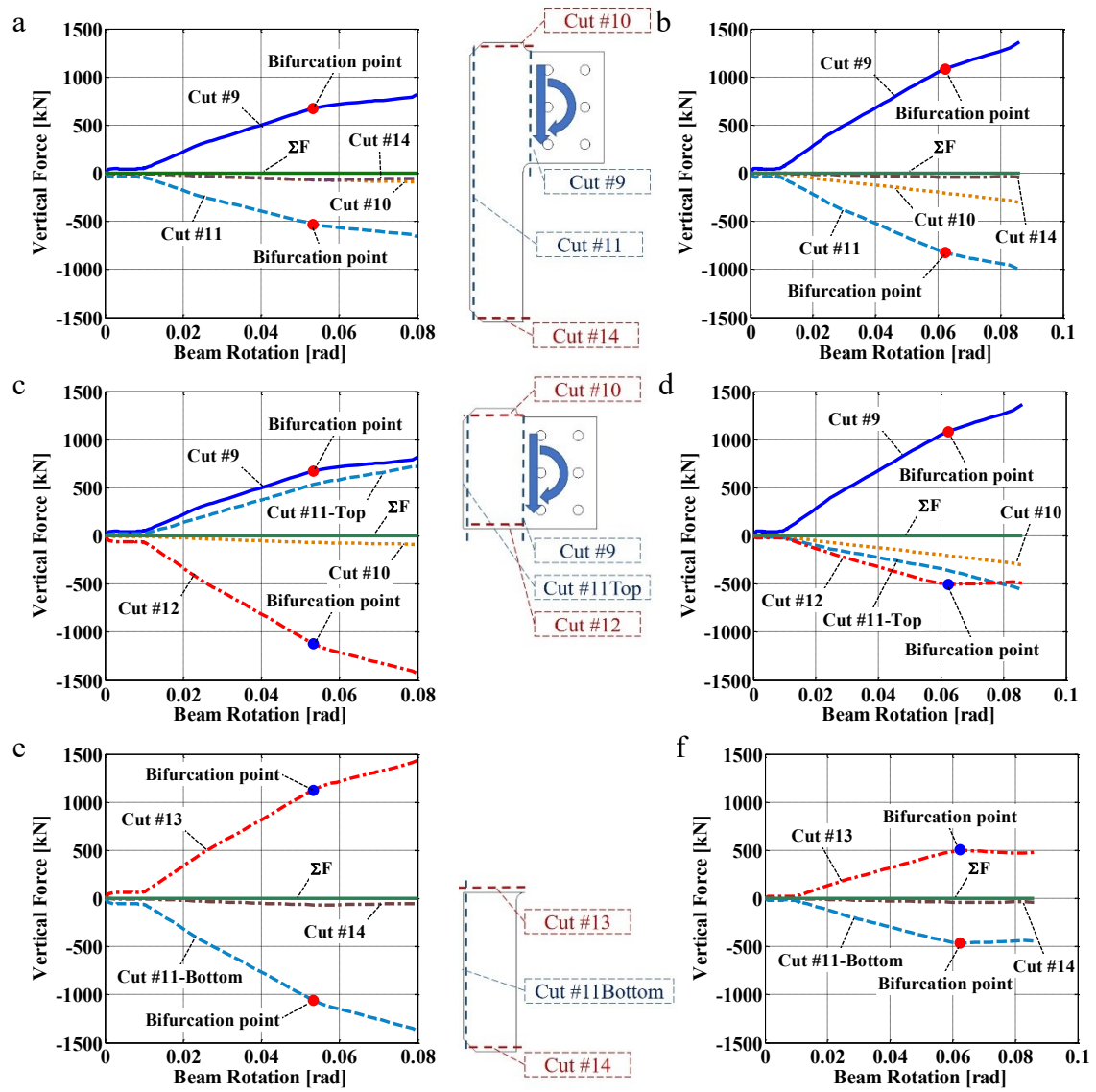


Fig. 3-17. Prediction of elastic FE models of BG3-2-10-F for vertical force at: (a) stiffener of single-sided connection, (b) stiffener of double-sided connection, (c) top part of the stiffener of single-sided connection, (d) top part of the stiffener of double-sided connection, (e) bottom portion of the stiffener of single-sided connection, (f) bottom portion of the stiffener of double-sided connection

Notably, the shear force was not distributed uniformly over the girder web depth, which contradicts the assumptions made in the design procedure of the shear tab connection. Referring to Figs. 3-15c and 3-17c, the shear force at the top part of the stiffener (Cut #11Top) developed in the downward direction to counterbalance the moment, mobilized due to the existing eccentricity of the external shear force. Further, horizontal forces developed at the stiffener, along the edges of the extended portion of the shear plate, to counterbalance the bending moment applied to the shear plate

at Cut #9 (Fig. 3-15c). Referring to Fig. 3-17c, the slope of the curve representing the axial force of the stiffener decreased significantly at 1129 kN compression, which corresponds to a connection shear force equal to 672 kN (0.0375 rad).

Referring to Figs. 3-15d and 3-17d, unlike the single-sided shear tabs, the shear force that was developed at the top portion of the stiffener (Cut #11Top) of the double-sided shear tabs was an upwards force that counterbalanced a significant portion of the connection shear force; therefore, the stiffener was subjected to a lower compression force although the double-sided connection was subjected to a higher level of applied shear force in comparison to the single-sided shear tab. The shear tab buckled at 508 kN compression force, which is half the buckling force observed in the single-sided shear tab. This is due to the larger horizontal shear stress along the bottom re-entrant corner of the connection. The horizontal shear stress was mobilized in the stiffener because of the bending moment that developed in the shear tab connection. Due to the higher stiffness of the doublesided shear tab, its inflection point formed farther from the girder as compared to the single-sided shear tab. The upward shear force along Cut #11-Top and the applied shear force along the Cut#9 formed a shear force couple, which caused an extra moment on the stiffener that was counterbalanced by the horizontal force developed in the stiffener. Therefore, the stiffener of the double-sided shear tab was subjected to a much higher horizontal shear stress as compared to the single-sided shear tab. The top flange of the girder resisted 20% of the connection shear force, while the bottom flange negligibly contributed to transfer the connection shear force.

Note that the yielding of the shear plate affected the load transfer mechanism. In single-sided shear tabs, the stiffened portion of the shear plate yielded locally in advance of its elastic buckling. This local yielding resulted in the application of a transverse force to the girder web, which was resisted by out-of-plane bending. Yielding occurred due to the limited out-of-plane bending

capacity of the girder web, which resulted in the formation of the girder web mechanism. Comparisons between the results of the single-sided connections illustrated the shear plate's susceptibility to inelastic buckling when the compactness limit for stiffeners was not met. The slender stiffener (BG3-2-10-F) became unstable and reached its strength plateau as soon as it yielded locally, while the compact stiffener (BG3-2-13-F) reached a higher shear force after the local yielding of the shear plate, which is a stable failure mechanism.

The yielding of the shear plate along the net section of the vertical row of bolts, closest to the girder, was observed as the governing failure mode for double-sided shear tabs. The observed strength of double-sided shear tabs for configurations BG3-2-10-F and BG3-2-13-F (430 kN and 630 kN, respectively) was close to the predictions for the rupture of their shear plate at the net section (496 kN and 654 kN for BG3-2-10-F and BG3-2-13-F, respectively). Notably, after yielding along the bolt line, yielding propagated to the stiffener of BG3-2-10-F, and its out-of-plane deformation started to increase. This observation demonstrates that inelastic buckling of the stiffener may also occur in double-sided configurations; which prevents the connection from reaching the shear force corresponding to rupture along the net section.

# 3.5.2 Effective eccentricity

Based on the shear force and bending moment developed in the shear plate and the bolt group, the location of the inflection point was determined. To calculate the connection eccentricity ( $e_{eff}$ = M/V), the bending moment and shear force at the outer ends of the re-entrant corners of the shear plate were determined directly using the Free body option available in Abaqus. Figure 3-18 illustrates the distance between the inflection point and the centroid of the girder web, i.e. the effective eccentricity ( $e_{eff}$  in Fig. 3-15b), for the various connection configurations. In contrast to the current design assumption, the inflection point forms away from the girder web, beyond the

centre of the bolt group (Fig. 3-18); which means  $e \le e_{eff}$ . As shown, the shear plate buckling, yielding of the shear plate, yielding of bolts, and the girder web yielding decreased the connection's stiffness and pushed the inflection point toward the girder. The only exception to this observed trend is the FE-E-G model of the double-sided configuration of BG3-2-13-F, for which the shear force reached the girder's shear yielding capacity.

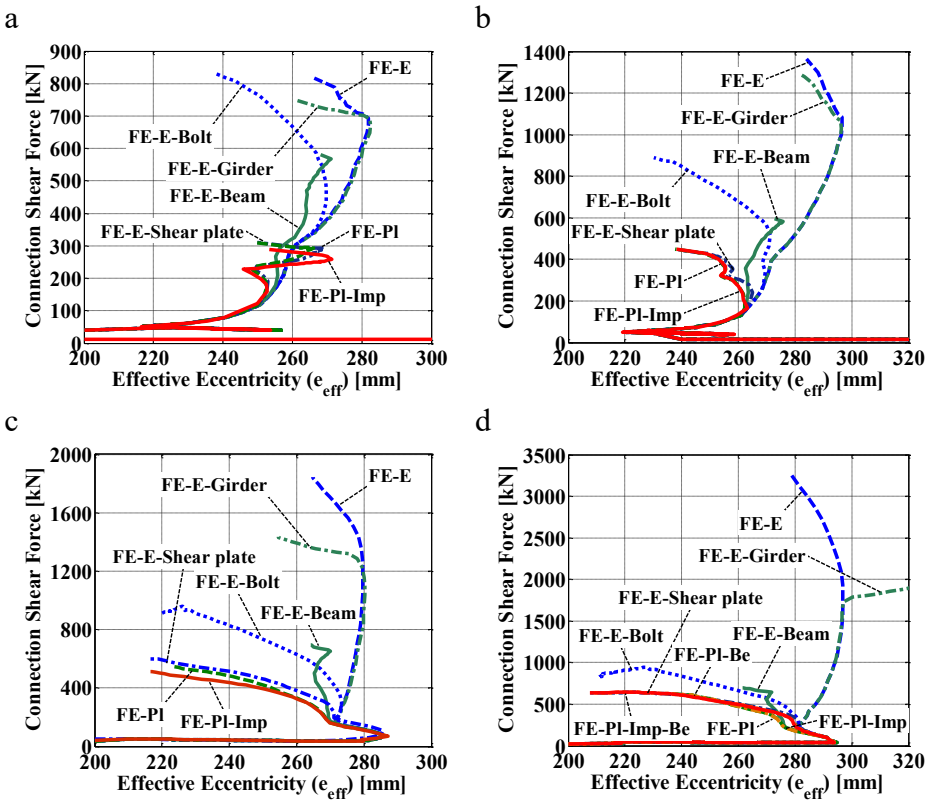


Fig. 3-18. Predictions of numerical models for shear force versus effective eccentricity at: (a) single-sided configuration of BG3-2-10-F, (b) double-sided configuration of BG3-2-10-F, (c) single-sided configuration of BG3-2-13-F, (d) Double-sided configuration of BG3-2-13-F

Comparisons between the single and double-sided configurations of BG3-2-10-F (Figs. 3-18a and 3-18b) and BG3-2-13-F (Figs. 3-18c and 18d) demonstrated the larger eccentricity of the double-sided configuration at the same level of shear force. This observation can be attributed to the higher stiffness of the double-sided configuration in comparison with the single-sided one. Moreover, the implementation of a thicker shear tab plate for BG3-2-13-F resulted in a higher stiffness and a larger eccentricity under the same level of shear force.

The comparison between predictions of the model with a yieldable bolt group (FE-E-Bo) and the model with the yieldable components (FE-Pl) demonstrated that the shear strength of the bolt group was much higher than the shear capacity of the connection. The FE model prediction was compared with available bolt shear experiments [37, 38] in order to ensure the capability of the FE model to detect accurately the bolt shear strength. Although the FE model accurately captured the bolt's strength plateau (continuous increase of the bolt deformation while the bolt force remained constant) in the shear test, it was not possible to capture the bolt's post ultimate (softening) response. This may result in concern regarding the capability of the FE model to capture the shear capacity of the bolt group under an eccentric shear force, in which the bolts would experience shear fracture progressively. To address this issue, the force-deformation response of each individual bolt was monitored during the analysis; the minimum level of the connection shear force corresponding to the time when the first bolt reached its strength plateau was considered as the shear capacity of the bolt group.

Furthermore, as shown in Table 3-3, the observed bolt shear strength of models FE-E-Bo was much higher than the AISC predictions based on the instantaneous centre of rotation (ICR) method. This over-strength can be attributed to the eccentricity of the bolt group ( $e_b$  distance in Fig. 3-15b) being much smaller than the AISC recommendation for eccentricity (e distance in Fig 3-15b). This observation mirrored the nature of the AISC method as it relies on the lower bound theorem [7] to provide a conservative, straight forward, and simple to use method for the design of extended shear tabs. However, the AISC Design Manual allows for an alternative bolt group eccentricity consideration if justified by rational analysis [1]. Based on these observations, the bolt shear strength of the connection could be determined based on the bolt group eccentricity ( $e_b$ ) that is equal to the distance between the location of the inflection point and the centre of the bolt group.

Notably, the observed bolt group eccentricity should not be extended to a configuration with a different bolt pattern; previous research [27] has demonstrated that the connection eccentricity is a function of the bolt pattern depth. Further studies are needed to propose an equation for the bolt group eccentricity.

Table 3-3-Bolt shear strength based on predictions of the model FE-E-Bo

	FE Model		Current design eccentricity			Revised eccentricity <sup>a</sup>		
Specimen	Inflection point b (mm)	V <sub>u</sub> Shear Strength (kN)	Eccentricity (mm)	V <sub>SH</sub> Shear Strength (kN)	$\frac{V_{_{u}}}{V_{_{SH}}}$	Bolt Group Eccentricity (mm)	V <sub>SH</sub> Shear Strength (kN)	$\frac{V_u}{V_{SH}}$
BG3-2-10-F-S.S °	252	709	197	270	2.63	49	667	1.06
BG3-2-10-F-D.S <sup>d</sup>	251	718	197	270	2.66	48	672	1.07
BG3-2-13-F–S.S <sup>c</sup>	258	674	197	270	2.50	55	641	1.05
BG3-2-13-F-D.S <sup>d</sup>	259	670	197	270	2.48	56	637	1.05

<sup>&</sup>lt;sup>a</sup> Based on the observed eccentricity in the model FE-E-Bo

As shown in Table 3-3, this revised definition of the bolt group eccentricity resulted in a reasonably conservative prediction of the bolt shear strength of the connection (the ratio between FE result and prediction based on the revised eccentricity was between 1.05 and 1.07). The smaller ratio between the FE and the analytical predictions for BG3-2-13-F was attributed to the fact that the thicker shear plate provided higher rotational stiffness and the inflection point formed farther from the bolt group centre in comparison to the specimen with the more slender shear tab (BG3-210-F).

Furthermore, the experimentally measured strength of the single-sided BG3-2-13-F (520 kN) was much larger than the design strength, which was based on the shear failure of the bolt group calculated using the instantaneous centre of rotation analysis method with the eccentricity equal to the distance between the centre of the bolt group and the weld line (270 kN), i.e. as per the current

<sup>&</sup>lt;sup>b</sup> Distance between the location of inflection point and the centre of girder web

<sup>&</sup>lt;sup>c</sup> Suffix S.S refers to single-sided configuration

<sup>&</sup>lt;sup>d</sup> Suffix D.S refers to double-sided configuration

practicing design method. This observation further validated the prediction of the FE models with respect to the formation of the inflection point along the exterior bolt line.

## 3.6 Conclusions

Owing to the lack of a comprehensive published procedure for the design of stiffened extended shear tab connections, practicing engineers often use the current AISC design procedure, even though it was originally developed for unstiffened extended shear tabs. This method assumes that the inflection point forms at the face of the supporting girder or column and that the weld attachment between the shear plate and the girder flanges (i.e., stabilizer plates) is ignored. Experiments on stiffened extended shear tabs have demonstrated that these weld attachments influence the load transfer mechanism within the connection. Therefore, there is concern with respect to the validity of the aforementioned design assumptions.

To better understand the behaviour of stiffened extended shear tabs (full-depth stiffeners), full-scale laboratory tests and complementary finite element simulations were conducted. This paper contains a summary of the finite element studies of two beam-to-girder shear tab configurations. The numerical models were validated with previously conducted full-scale experiments on representative connections. The main findings of the corroborating FE study are summarized as follows:

• The inflection point of extended beam-to-girder shear tabs with full depth shear plates is away from the girder centreline (i.e. beyond the centre of the bolt group) in both the single- and double-sided configurations. Hence, the current practice for design of these connections may not be always conservative as it underestimates the force demands on the stiffened portion of the shear tab as well as the bending demands on the supporting element.

- The stiffened portion of extended beam-to-girder shear tabs with full-depth shear plates (including single-sided and double-sided configurations) is subjected to vertical axial and horizontal shear forces simultaneously. This is not considered in the current design procedure. The axial and shear force demands are strongly dependent on the out-of-plane stiffness of the girder web and the connection eccentricity.
- Single-sided extended beam-to-girder shear tabs with full-depth shear plate experience yielding in their stiffened portion along the bottom re-entrant corner. Out-of-plane deformations tend to increase in such case.
- Single-sided extended beam-to-girder shear tabs with full-depth shear plates experience shear forces much higher than those anticipated based on design values representative of shear failure of the bolt group. This is an indication that the bolt group eccentricity may be significantly smaller than the assumed value, i.e. the distance between the weld line and the centre of the bolt group.
- The ultimate shear capacity of the bolt group can be determined by calculation on the basis of the bolt group eccentricity, the distance between the inflection point and the centre of the bolt group. For the studied bolt pattern (i.e., two vertical lines of three bolts), the inflection point formed beyond the vertical bolt line, farthest from the girder. Of note, this location is not representative of connections with different bolt pattern because the location of the inflection points is a function of the bolt pattern depth. Additional studies are necessary to develop an empirical equation for the bolt group eccentricity.
- In the absence of a robust method to predict the buckling strength of the stiffened portion of the shear plate, the local buckling failure mode of the shear plate should be considered. The use of shear plates that satisfy the CSA S16 compactness ratio for stiffeners  $(200/\sqrt{F_y})$  results in a stable shear tab connection behaviour.
- The behaviour of double-sided extended beam-to-girder shear tabs with full-depth shear plates differs
  from that of single-sided connections. In comparison to the single-sided connections, a much lower
  compressive force develops in the stiffener of a double-sided connection while the connection is

subjected to a higher shear force. In advance of yielding of the stiffened portion of the shear plate, these connections experience shear plate yielding at the net section of the vertical row of bolts, closest to the girder.

To extend this research to the point where recommendations for design can be made a numerical parametric study is needed to validate the observations described herein for a greater range of stiffened extended shear tab connections. This work is ongoing.

# 3.7 Acknowledgments

The authors would like to thank the ADF Group Inc. and DPHV Structural Consultants for their generous technical and financial support, as well as the Natural Sciences and Engineering Research Council of Canada. The authors also thank Jacob Hertz and Nathan Goldstein Apt for sharing their experimental results for extended shear tabs. The finite element computations were conducted on the McGill University supercomputer Guillimin, which is managed by Calcul Québec and Compute Canada. The supercomputer operation is funded by the Canada Foundation for Innovation (CFI), NanoQuébec, RMGA and the Fonds de recherche du Québec - Nature et technologies (FRQ-NT).

# 3.8 References

- [1] Steel Construction Manual, 15<sup>th</sup> edition, American Institute of steel Construction, Chicago, IL, 2017. (Chapter 7: pp.6-8, Chapter 9: pp.6-10, Chapter 10: pp.87-91 & 127-132)
- [2] AISC 360-16, Specification for Structural Steel Buildings, American Institute of Steel Construction, Chicago, IL, 2016.
- [3] B. Dowswell, R. Whyte, Local stability of double-coped beams, Eng. J. AISC, 51(1) (2014), pp. 43–51.
- [4] Steel Construction Manual, 14<sup>th</sup> edition, American Institute of steel Construction, Chicago, IL, 2011. (Chapter 9: pp.6-10)

- [5] J.J. Cheng, J.A. Yura, C.F. Johnson, Design and behavior of coped beams, University of Texas at Austin, Austin, TX, 1984.
- [6] L.S. Muir, W.A. Thornton, Direct method for obtaining plate buckling coefficient for double coped beams, Eng. J. AISC, 41 (3) (2004), pp. 133–134.
- [7] L.S. Muir, C.M. Hewitt, Design of unstiffened extended single-plate shear connections, Eng. J. AISC, 46 (2) (2009), pp. 67-79.
- [8].W.A. Thornton, P.J. Fortney, On the need for stiffeners for and the effect of lap eccentricity on extended single-plate connections, Eng. J. AISC, 48(2) (2011),pp. 117-125.
- [9] A. Elkady, D.G. Lignos, Full-scale testing of deep wide-flange steel columns under multiaxis cyclic loading: loading sequence, boundary effects, and lateral stability bracing force demands, J. Struct. Eng. ASCE, 144 (2) (2018), 04017189.
- [10] D.R. Sherman, A. Ghorbanpoor, Design of extended shear tabs, University of Wisconsin-Milwaukee, Milwaukee, WI, 2002.
- [11] W. Goodrich, Behavior of extended shear tabs in stiffened beam-to-column web connections," M.Sc. Thesis, Vanderbilt University, Nashville, TN, 2005.
- [12] K. Thomas, R.G. Driver, S.A. Oosterhof,, L. Callele, Full-scale tests of stabilized and unstabilized extended single-plate connections, Structures, 10 (2017), pp.49-58.
- [13] M. Mahamid, A. Rahman, A. Ghorbanpoor, The analyses of extended shear tab steel connections part II: stiffened connections, Eng. J. AISC, 44 (2) (2007), pp. 133-146.
- [14] P.J. Fortney, W.A. Thornton, Analysis and design of stabilizer plates in single-plate shear connections, Eng. J. AISC, 53 (1) (2016), pp. 1-28.
- [15] M. Marosi, Behaviour of single and double row bolted shear tab connections and weld retrofits," Master's Thesis, McGill University, Montreal, QC, 2011.

- [16] M. Marosi, M. D'Aronco, R. Tremblay, C.A. Rogers, Multi-row bolted beam-to-column shear tab connections, 6th European Conference on Steel and Composite Structures, Budapest (2011).
- [17] M. D'Aronco, Behaviour of double and triple vertical rows of bolts shear tab connections and weld retrofits," Master's Thesis, École Polytechnique de Montréal, Montreal, QC, 2013.
- [18] A. Mirzaei, Steel shear tab connections subjected to combined shear and axial forces, PhD Thesis, McGill University, Montreal, QC, 2014.
- [19] J. Hertz, Testing of extended shear tab connections subjected to shear, Master's Thesis, McGill University, Montreal, QC, 2014.
- [20] N. Goldstein Apt, Testing of extended shear tab and coped beam-to-girder connections subject to shear loading, Master's Thesis, McGill University, Montreal, QC, 2015.
- [21] J. Hertz, D.G. Lignos, C.A. Rogers, Full scale testing of extended beam-to-column and Beam-to-girder shear tab connections subjected to shear, 8th International Conference on Behavior of Steel Structures in Seismic Areas, Shanghai (2015).
- [22] C.A. Rogers, Marosi M., Hertz J., Lignos D., Tremblay R., D'Aronco M., Performance of weld-retrofit beam-to-column shear tab connections, Connections VIII, 8<sup>th</sup> International Workshop on Connections in Steel Structures, Boston, MA (2016).
- [23] CSA-S16-14, Limit States Design of Steel Structures, Canadian Standards Association, Toronto, ON, 2014.
- [24] ASTM A992 / A992M-11(2015), Standard Specification for Structural Steel Shapes, ASTM International, West Conshohocken, PA, 2015.
- [25] ASTM A572 / A572M-15, Standard Specification for High-Strength Low-Alloy Columbium-Vanadium Structural Steel, ASTM International, West Conshohocken, PA, 2015.

- [26] ASTM F3125 / F3125M-15a, Standard Specification for High Strength Structural Bolts, Steel and Alloy Steel, Heat Treated, 120 ksi (830 MPa) and 150 ksi (1040 MPa) Minimum Tensile Strength, Inch and Metric Dimensions, ASTM International, West Conshohocken, PA, 2015.
- [27] A. Astaneh-Asl, K.M. McMullin, S.M. Call, Behavior and design of steel single plate shear connections, J. Struct. Eng. ASCE, 119 (8) (1993), pp. 2421-2440.
- [28] AISC 341-16, Seismic Provisions for Structural Steel Buildings, American Institute of Steel Construction, Chicago, IL, 2016.
- [29] ABAQUS 6.11-3, [Computer software], Dassault Systemes Simulia Corp., Providence, RI.
- [30] G.L. Kulak, J.W. Fisher, H.A. Struik, Guide to design criteria for bolted and riveted joints, 2<sup>nd</sup> Edition. American Institute of Steel Construction, Chicago, IL, 2001.
- [31] I.R. Gomez, A.M. Kanvinde, Y.K. Kwan, G.Y. Grondin, Strength and ductility of fillet welds subjected to out of plane bending, American Institute of Steel Construction, Chicago, IL, 2008.
- [32] ASTM A6/A6M-04b, Standard specification for general requirements for rolled structural steel bars, plates, shapes, and sheet piling, American Society for Testing and Materials, West Conshohocken, PA, 2004.
- [33] CSA-G40.20-13/G40.21-13, General requirements for rolled or welded structural quality steel/structural quality steel, Canadian Standards Association, Toronto, ON, 2013.
- [34] CISC, Handbook of steel construction, 11<sup>th</sup> edition, Canadian Institute of Steel Construction, Markham, ON, 2016.
- [35] A. Elkady, D.G. Lignos, Analytical investigation of the cyclic behavior and plastic hinge formation in deep wide-flange steel beam-columns, Bull. Earthq. Eng., 13 (4) (2015), pp. 1097-1118. [36] H. Daneshvar, One-sided steel shear connections in column removal scenario," PhD. Thesis, University of Alberta, Edmonton, AL, 2013.

[37] J.J Wallaert, J.W. Fisher, The shear strength of high-strength bolts, Lehigh University, Bethlehem, PA,1964.

[38] J.J Wallaert, J.W. Fisher. Shear strength of high-strength bolts, J. Struct. Div. ASCE, 91 (3) (1965), pp. 99-126.

## Link between Chapter 3 and Chapter 4

The focus of Chapter 3 was to determine the impact of the girder web flexibility on the load transfer mechanism of the full-depth stiffened extended beam-to-girder shear tabs. As its findings were limited to only two connections, a parametric study was needed to validate the findings of Chapter 3 for a wider range of configurations for the single-sided full-depth extended beam-to-girder shear tabs. The studied connections varied in the number of the vertical bolt lines and bolt rows, the depth of the shear tab and girder web, and the offset of the bolt group from the girder web, and the slenderness of the shear plate. Chapter 4 contains a presentation of the results of this parametric study and includes recommendations for design of the single-sided configuration of the full-depth extended beam-to-girder shear tabs.

# 4 Chapter 4: Design Considerations - Stability of Stiffened Extended Shear Tab Connections

Journal of Construction Steel Research (2018), Under Review, (Submission No: JCSR 2018 58)

Mohammad Motallebi<sup>1</sup>, Dimitrios G. Lignos<sup>2</sup>, Colin A. Rogers<sup>3</sup>

<sup>&</sup>lt;sup>1</sup> Graduate Research Assistant, Department of Civil Engineering and Applied Mechanics, McGill University, Montreal, QC. Email: mohammad.motallebinasrabadi@mail.mcgill.ca

<sup>&</sup>lt;sup>2</sup> Dimitrios G. Lignos, Associate Professor, School of Architecture, Civil and Environmental Engineering, Swiss Federal Institute of Technology, Lausanne (EPFL), Lausanne, Switzerland, Email: dimitrios.lignos@epfl.ch

<sup>&</sup>lt;sup>3</sup> Corresponding author
Colin A. Rogers, Associate Professor, Department of Civil Engineering and Applied Mechanics, McGill University,
Montreal, QC. Email: colin.rogers@mcgill.ca
817 Sherbrooke Street West
Montreal QC, Canada, H3A 0C3
Tel. 514 398-6449
Fax. 514 398-7361

## **Abstract**

An investigation of the behaviour and stability requirements of full-depth extended shear tab connections, carried out by means of a parametric finite element (FE) study, is presented in this paper. In such connections, the inelastic buckling of the shear plate is a concern. The FE modeling procedure was validated with available full-scale experiments of such connections. Using the FE simulations, the load transfer mechanism and the buckling resistance of the stiffened portion of the full-depth shear tab were determined. Furthermore, the potential for shear fracture of the bolt group was assessed. The parametric study suggests that the buckling of the stiffener is strongly influenced by the shear plate depth and thickness, the girder web depth and thickness, as well as the connection eccentricity. This is dependent on the distance between the centroid of the bolt group and the girder web, as well as the number of horizontal and vertical bolt lines. A set of equations for predicting the shear strength corresponding to inelastic buckling of the shear plate and bolt fracture is proposed.

**Keywords**: extended shear tab, stability, stiffened shear tab connections, plate buckling, effective eccentricity

## 4.1 Introduction

Extended shear tab connections are widely used in beam-to-girder connections due to their ease of fabrication and erection. The shear plate can be solely welded to the girder web in unstiffened configurations of partial-depth shear tabs (Fig. 4-1a), or to the top flange of the girder (Fig. 4-1b) in stiffened configurations. In the full-depth configuration (Fig. 4-1c), the shear plate is typically fillet-welded to the web, as well as to the top and bottom flanges of the girder.

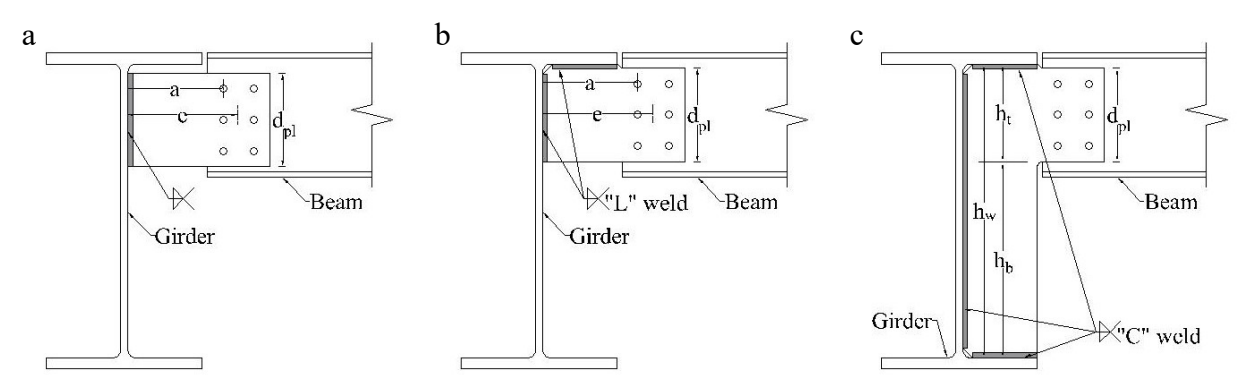


Fig. 4-1. Extended beam-to-girder shear tab connections: (a) partial-depth unstiffened, (b) partial-depth stiffened, (c) full-depth stiffened (h<sub>w</sub> definitions based on CSA-S16 [1])

Design engineers prefer the unstiffened configuration to the stiffened extended shear tab because the low rotational stiffness of the unstiffened connection properly satisfies the assumption made for frame analysis; a shear connection can be considered as a flexural hinge. However, the stiffened configuration may be the only available solution for the instability of the beam and shear plate where the stability issues require a thick shear plate, surpassing the upper limit that is placed on the thickness of the shear plate to ensure its yielding prior to shear fracture of the bolts. Further, in full-depth shear tabs the out-of-plane bending demands on the girder web are typically reduced compared to those in partial depth shear tabs [2, 3]. However, when a beam is placed only on one side of a supporting girder [4] the girder web flexibility influences the load transfer mechanism and the failure modes of full-depth shear tabs. In the case of double-sided shear tabs, where a girder

supports a beam on each side, the shear tab behaviour is largely independent from the girder web flexibility [4].

Although the stiffened extended shear tab has been used in steel construction, no comprehensive procedure exists for its design. In response to this shortcoming, the design engineer may make a conservative assumption and design the stiffened extended shear tab based on the design procedure of the unstiffened extended shear tab, such as the AISC design procedure [5]. Therefore, design engineers conservatively ignore the effect of the weld attachment between the shear plate and girder flanges. As such, the inflection point is assumed to be at the girder web, and the bolt group is designed for the shear force at the beam end (R) and its eccentric moment  $(R \times R)$ e). According to the above mentioned design practice, the predicted failure mode for stiffened extended shear tabs is typically bolt shear fracture or flexural-shear yield of the shear plate. Previous laboratory tests [6-8] demonstrated that the above mentioned assumption resulted in underestimated predictions for the ultimated resistance of stiffened extended shear tabs, always failed due to the shear plate buckling. The 14<sup>th</sup> edition of the AISC Steel Construction Manual [9] considers the doubly coped beam design equations [10, 11] to determine the flexural buckling strength of the shear plate. In the 15th edition of the AISC Steel Construction Manual [5], these equations were replaced with those corresponding to the lateral torsional buckling of a rectangular section [12]. The buckling modification factor in this case,  $C_b$  should be calculated according to Dowswell and Whyte [13]. Although recent full-scale experimental [2,3] and numerical [4] studies suggest that the influence of the flexibility of the girder web on the load transfer mechanism and associated failure modes of full-depth extended shear tabs should be accounted for in the design process, this is currently not done in practice. Therefore, the design approach for extended shear tabs should be refined to better predict the strength and failure mode of such connections.

However, the findings of the recent studies [2-4] was limited to a few connections and should be evaluated for a wider range of the configurations to be adequate for design recommendations. The authors of this paper tried to answer this need through parametric finite element simulations.

This paper presents the results of comprehensive parametric finite element (FE) simulations from 28 configurations of full-depth extended beam-to-girder shear tab connections. In these analyses, emphasis was placed on the single-sided configuration where the shear tab was placed on one side of the girder web. Their load transfer mechanism was determined in addition to their elastic and inelastic buckling strength, as well as their bolt shear strength. Several parameters and failure modes were investigated, including the depth and thickness of the shear plate, the depth and thickness of the girder web, and the number of horizontal and vertical rows of bolts. Equations for predicting the shear strength corresponding to inelastic buckling of the shear plate and bolt fracture are proposed to refine the existing design procedure for stiffened extended shear tab connections.

## 4.2 Brief description of full-scale laboratory tests

To comprehend the behaviour of shear tab connections, 55 full-scale experiments have been conducted to date at McGill University [2, 3, 14-19]. These tests included both standard and extended configurations, beam-to-column and beam-to-girder arrangements, as well as bolted and welded details. The connection configurations reflect the current design practice in the USA and Canada. Two actuators were implemented to apply simultaneous shear and rotation to the shear tab based on the shear connection's loading protocol, proposed by Astaneh [20]. During the laboratory tests, the rates of the two actuators were adjusted in an attempt to have the connection reach its expected shear capacity at target rotation, usually 0.02 rad of the relative rotation between the beam end and the supporting member (connection rotation). The actuator rates were kept

constant after this point to observe the inelastic behaviour of the shear tabs. Results from three extended beam-to-girder bolted shear tab connections (Fig. 4-2) were selected to validate a FE model. These specimens varied with respect to the shear plate dimensions, i.e. length, depth, and thickness, the girder web depth and thickness, as well as the number of bolt rows. To summarize the specimen geometry, an alphanumerical ID was implemented. For instance, in Specimen BG3-2-10-F: BG stands for beam-to-girder configuration, 3 represents the number of bolt rows, 2 shows the number of vertical bolt lines, 10 demonstrates the shear plate thickness (mm), and F indicates a full-depth shear plate.

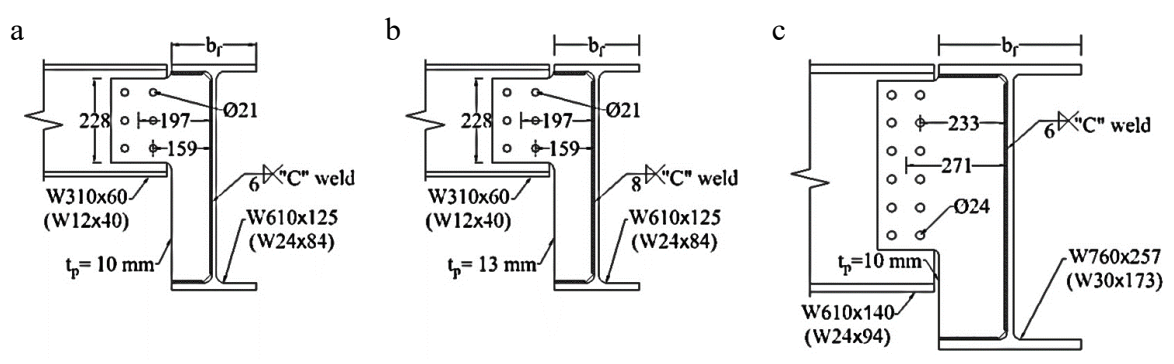


Fig. 4-2. Test specimens: (a) BG3-2-10-F, (b) BG3-2-13-F, (c) BG6-2-10-F (dimensions are in mm)

A comparison between specimens BG3-2-10-F and BG3-2-13-F illustrated the effect of stiffener compactness on the beam-to-girder connection stability. The slenderness ratio of the shear plate of specimens BG3-2-10-F and BG6-2-10-F (i.e.  $b_p/2t_{pl}$ =11.5 and 19.1, respectively) did not satisfy the CSA-S16 [1] compactness requirement for plate girder stiffeners (200/ $\sqrt{F_y}$  = 10.7), while the stiffener of specimen BG3-2-13-F ( $b_p/2t_p$ =8.8) did. Notably, the shear plate compactness is not addressed in the AISC's requirements for extended shear tab connections because local buckling is not a concern for an unstiffened extended shear tab. A comparison between specimens BG3-2-10-F and BG6-2-10-F allowed for the demonstration of the dependency of their behaviour on geometric parameters including the number of bolt rows, the depth of the shear plate and the girder web height.

The girder and beam were made of ASTM A992 Grade 50 steel [21], while the shear plates were fabricated from ASTM A572 Grade 50 steel [22]; for both grades the nominal  $F_y$ =345 MPa and  $F_u$ =448MPa. The shear plates were snug-tightened to the beam using ASTM F3125 Grade A325 bolts [23]. To weld the shear tab to the supporting girder, an E71T ( $F_u$ =490 MPa) electrode was used through the flux-cored arc welding process with additional shielding gas (CO<sub>2</sub>). Details of the test setup can be found in [2-4, 14].

### 4.3 Finite element simulation

Finite element simulation was adopted to obtain a deeper understanding of the behaviour of extended beam-to-girder shear tab connections under gravity-induced force. Through the FE simulations, the main parameters that influence the load transfer mechanism of the connection were identified. The FE models were developed in the commercial program ABAQUS-6.11-3 [24]. The features of the model, including the geometry, boundary conditions, material properties, element size and type, contacts and interactions, and the loading protocol, were chosen to be representative of the laboratory tests. A detailed description of the FE models can be found in [4, 25]; it is not presented herein due to space limitations.

## 4.3.1 Comparison of numerical and experimental results

The FE model predictions were compared with the laboratory test measurement in Fig. 4-3. The simulated connection shear force deviated from the test measurements in the initial increments of loading.

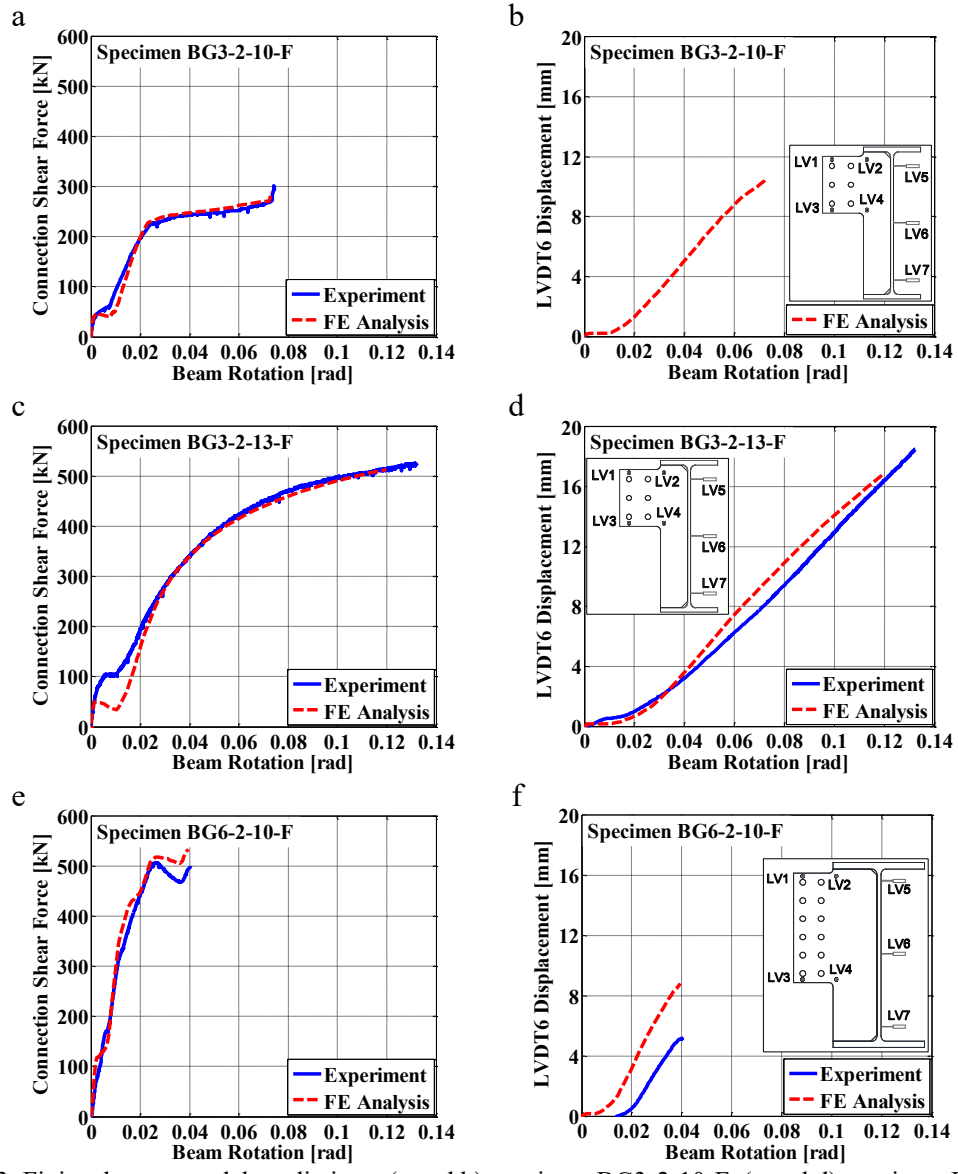


Fig. 4-3. Finite element model predictions: (a and b) specimen BG3-2-10-F, (c and d) specimen BG3-2-13-F, (e and f) specimen BG6-2-10-F

This discrepancy arose from the different contact conditions between the bolt shanks and the bolt holes assumed in the FE model and those present in the laboratory. The bolts in the shear tab connections were snug-tightened. Bearing between the bolt shanks and bolt holes transferred the shear force between the beam and the shear plate. Therefore, the initial response of a snug-tightened connection depended greatly on the contact between the bolt shanks and bolt holes. The contact conditions observed in the tests were not measured *a priori* due to the complexity of such

measurements. In the FE model, the bolts were placed at the centre of the bolt hole, resulting in a 1 mm (1/32 in.) gap around the entire bolt hole perimeter, which was consistent with the respective fabrication tolerance.

Referring to Fig. 4-3e, the FE model representing the BG6-2-10-F specimen slightly overestimated the shear force corresponding to the point of stiffness reduction. This discrepancy can be attributed to the specimen's sensitivity to the local imperfections of the shear plate due to its high slenderness ratio ( $b_f/2t_{pl}$ ). Such imperfections were not measured for the shear plate and the girder web or the girder flanges. However, it was rational to assume that they were proportioned to the limits of manufacturing tolerances for the web and flange of wide flange sections [26-28], respectively. This is consistent with prior FE studies [29].

Referring to Figs. 4-3d and 4-3f, the FE models predicted reasonably well the out-of-plane deformation of the girder web for specimens BG3-2-13-F and BG6-2-10-F, respectively. The out-of-plane deformation of the girder web for specimen BG3-2-10-F (Fig. 4-3b) was not accurately measured due to a malfunction of LVDT6.

#### 4.3.2 Finite element model simulation results

The FE results for the connection eccentricity and the out-of-plane deformation of the shear plate (LVDT4 in Fig. 4-3) are shown in Fig. 4-4. It should be noted that the effective eccentricity ( $e_{eff}$ ) of the connection was the distance between the inflection point and the girder web.

The FE models indicated that the shear plate yielding propagated similarly in these connections. Yielding initiated at the lower re-entrant corner of the shear plate under a small shear force. As the shear force increased, yielding continued through the stiffened section of the shear plate, which was confined between the girder web and flanges. In tandem, the out-of-plane deformation of the shear plate increased. For connections with slender shear plates (i.e. BG3-2-10-F and BG6-2-16-F), the

connection stiffness decreased as the full width of the stiffener yielded along the bottom re-entrant corner; further, the slope of the curve representing the shear plate's out-of-plane deformation showed a large increase. The connection with a compact shear plate (BG3-2-13-F) experienced only a slight decrease of the connection stiffness as the full width of the stiffener yielded.

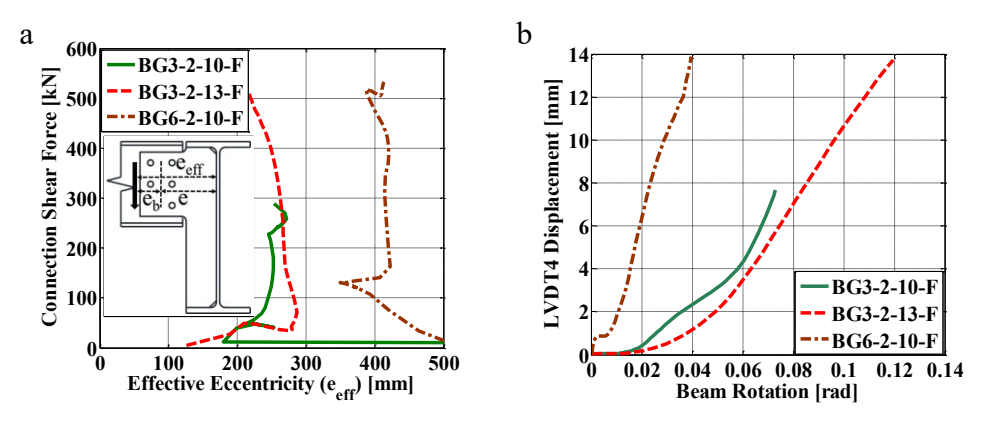


Fig. 4-4. Finite element model predictions: (a) shear force versus connection eccentricity, (b) out-of-plane deformation of shear plate versus beam rotation.

The stiffener's post yielding behaviour depended on its slenderness. The connection with a compact shear plate could resist a much larger shear force after the stiffener yielding; in comparison, the slender shear plates reached their strength plateau shortly after the stiffener yielding. Of note, the girder web yielding followed the stiffener yielding in all FE models. As an illustration of this behaviour, the initiation and progression of yielding for specimen BG6-2-10-F is shown in Fig. 4-5.

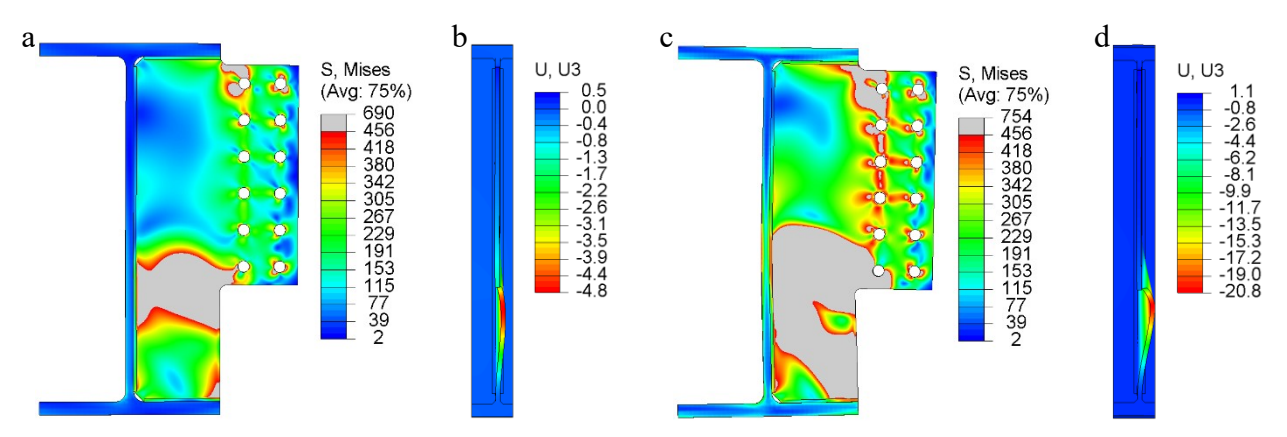


Fig. 4-5. Finite element model predictions of specimen BG6-2-10-F: (a) stress at  $\theta$ =0.0124 rad, (b) out-of-plane deformation at  $\theta$ =0.0124 rad, (c) stress at  $\theta$ =0.0274 rad, (d) out-of-plane deformation at  $\theta$ =0.0274 rad, (The grey colour represents yielded regions; displacement and stress values are in mm and MPa, respectively).

The load transfer mechanism of the connection was determined based on the internal force of the stiffener, obtained by using the free body cut option of the Abaqus software. A detailed description of the load transfer mechanism can be found in [4,25] and is not presented herein for purposes of brevity. As illustrated in Fig. 4-5a, the full width of the stiffener yielded because of the interaction of axial and shear forces along the bottom re-entrant corner of the shear plate. This compressive axial force was developed in the stiffener with a greater magnitude, as compared to the applied shear force. This was due to a non-uniform distribution of the shear force over the depth of the girder web, which is not consistent with the assumptions of the original design procedure for extended beam-to-girder shear tab connections [5]. This non-uniform distribution greatly depended on the geometry of the shear plate; this relationship was determined by conducting additional elastic FE simulations of the three connection configurations. Figure 4-6 shows the response of these elastic models.

As shown in Fig. 4-6, the stiffened portion of the shear plate buckled due to the interaction of axial and shear forces along the bottom re-entrant corner of the shear plate. Notably, the ratio between the stiffener's axial force and the connection's shear force,  $\alpha$  ratio, remained constant up to the bifurcation point. The comparison between the response of specimens BG3-2-13-F and BG3-2-10-F demonstrated that the  $\alpha$  ratio was independent from the thickness of the shear plate. Their  $\alpha$  ratio was almost equal, although the shear plate of Specimen BG3-2-13-F was 30% thicker than that of Specimen BG3-2-10-F. However, the  $\alpha$  ratio decreased significantly from 1.65 to 1.05 due to the different geometry of the shear plate in Specimens BG3-2-10-F and BG6-2-10-F, respectively.

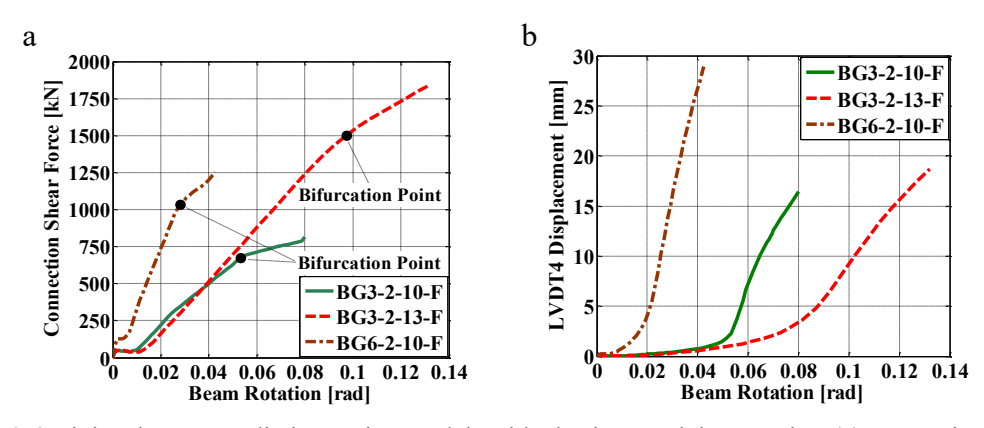


Fig. 4-6. Finite element predictions using models with elastic material properties: (a) connection shear force versus beam rotation, (b) out-of-plane deformation of shear plate versus beam rotation

## 4.4 Parametric study

The FE simulations demonstrated the influential parameters of the load transfer mechanism and its representative  $\alpha$  value, which was defined as the ratio between the stiffener's axial force and the connection's shear force,  $F_{\alpha}/V$ . Although the shear plate height and length significantly influenced the  $\alpha$  ratio, the shear plate thickness did not. These observations were further explored through a FE parametric analysis, which was limited in scope to the load transfer mechanism and the connection capacity of the single-sided configuration, i.e. a girder supporting a beam on one side. The FE simulation matrix included 25 different configurations, each represented by three model classes. The first class included elastic FE models (noted as E models). This was done to further understand the load transfer mechanism. The second class (noted as E-Bo models) was employed to determine the shear capacity of the bolt group. In this model class, only the bolts could experience yielding. In the third class of models (noted as PL models), all connection components could exhibit inelastic behaviour. These models were employed to determine the connection capacity, as well as the interactions between different failure modes.

The 25 configurations were divided into four groups to facilitate the interpretation of the FE simulations (Table 4-1). The first group contained configurations with different numbers of vertical and bolt rows, while all other aspects were identical to specimen BG3-2-10-F. The main

goal of this group was to determine the effect of the number of bolt lines on the connection eccentricity and the shear capacity of the bolt group. The second group included connections with different girder web depth and thickness, while other parameters, including the  $h_w/t_w$  ratio were set to be the same as those of specimen BG3-2-10-F. The aim of studying this group was to investigate the dependency of the load transfer mechanism on the ratio between the height of the top part of the stiffener and the height of the girder web  $(h_t/h_w)$ , as shown in Fig. 4-1. This ratio represented the relative distance between the bottom edge of the extended portion of the shear plate and the bottom flange of the girder. As this ratio approached unity, the bottom edge of the extended portion of the shear plate became closer to the bottom flange of the girder. The shallowest member corresponded to the depth of the shear plate (having two vertical lines of three bolts, 229 mm (9 in.) while the deepest member was 203 mm (8 in.) deeper than the deepest available AISC section (W1100×499). Of note, the girder of the second group connections did not represent the available AISC sections. They were identical to W610×125 section other then the height and thickness of the web, changed to study the effect of the  $h_t/h_w$  ratio on the connection behaviour. The thickness of the girder web was kept constant to keep their  $h_w/t_w$  ratio equal to W610×125. The members of the third group were identical to specimen BG3-2-10-F, except for the thickness of the girder web. The purpose of this group was to determine the effect of the girder web thickness on the load transfer mechanism and the connection capacity. The girder web was varied to meet the slenderness range for available AISC W610 sections. The fourth group included connections with a different gap between the beam and girder flanges, while other features were identical to specimen BG3-2-10-F. This group was included to investigate the impact of the gap distance on the shear plate stability, given that a large gap might result in buckling of the extended portion of the shear plate in advance of the stiffener. The gap distance ranged between 13 mm (specimen

BG3-2-10-F) and 50 mm, i.e. the worst-case scenario when a large gap was required due to fireproofing between the beam and girder [8].

Table 4-1. Stiffened and extended shear tab connection configurations for parametric FE study

			extended shear t	Giro		l es		Centroid			
	ID.	Beam Section	Section	h <sub>w</sub> (mm)	t <sub>w</sub> (mm)	$\frac{h_{t}}{h_{w}}$	$\frac{\mathrm{h_{_{\mathrm{w}}}}}{\mathrm{t_{_{\mathrm{w}}}}}$	Vertical Bolt Lines	Bolt Rows	of Bolt Group <sup>a</sup> (mm)	d <sub>pl</sub> <sup>b</sup> (mm)
	BG2-1-10-F	W250×49	W610×125	573	11.9	0.30	48.1	1	2	165	152
	BG3-1-10-F	W310×60	W610×125	573	11.9	0.43	48.1	1	3	165	229
	BG4-1-10-F	W410×74	W610×125	573	11.9	0.56	48.1	1	4	165	305
	BG5-1-10-F	W460×82	W610×125	573	11.9	0.70	48.1	1	5	165	381
ıp 1	BG6-1-10-F	W530×82	W610×125	573	11.9	0.83	48.1	1	6	165	457
Group 1	BG2-2-10-F	W250×49	W610×125	573	11.9	0.30	48.1	2	2	203	152
	BG3-2-10-F <sup>d</sup>	W310×60	W610×125	573	11.9	0.43	48.1	2	3	203	229
	BG4-2-10-F	W410×74	W610×125	573	11.9	0.56	48.1	2	4	203	305
	BG5-2-10-F	W460×82	W610×125	573	11.9	0.70	48.1	2	5	203	381
	BG6-2-10-F	W530×82	W610×125	573	11.9	0.83	48.1	2	6	203	457
	BG3-2-10-F-GD0.93	W310×60	W610×125bc	264	5.5	0.93	48.1	2	3	203	229
	BG3-2-10-F-GD0.80	W310×60	W610×125bc	308	6.4	0.80	48.1	2	3	203	229
2	BG3-2-10-F-GD0.60	W310×60	W610×125bc	410	8.5	0.60	48.1	2	3	203	229
Group	BG3-2-10-F-GD0.30	W310×60	W610×125bc	821	17.1	0.30	48.1	2	3	203	229
5	BG3-2-10-F-GD0.27	W310×60	W610×125bc	900	18.7	0.27	48.1	2	3	203	229
	BG3-2-10-F-GD0.24	W310×60	W610×125bc	1027	21.3	0.24	48.1	2	3	203	229
	BG3-2-10-F-GD0.20	W310×60	W610×125bc	1232	25.6	0.20	48.1	2	3	203	229
	BG3-2-10-F-GW57.3	W310×60	W610×125bc	573	10.0	0.43	57.3	2	3	203	229
$\omega$	BG3-2-10-F-GW40.0	W310×60	W610×125bc	573	14.3	0.43	40.0	2	3	203	229
Group.	BG3-2-10-F-GW30.0	W310×60	W610×125bc	573	19.1	0.43	30.0	2	3	203	229
5	BG3-2-10-F-GW20.0	W310×60	W610×125bc	573	28.6	0.43	20.0	2	3	203	229
	BG3-2-10-F-GW14.8	W310×60	W610×125bc	573	38.6	0.43	14.8	2	3	203	229
4	BG3-2-10-F-G25	W310×60	W610×125	573	11.9	0.43	48.1	2	3	216	229
Group 4	BG3-2-10-F-G38	W310×60	W610×125	573	11.9	0.43	48.1	2	3	229	229
Ğ	BG3-2-10-F-G50	W310×60	W610×125	573	11.9	0.43	48.1	2	3	241	229

<sup>&</sup>lt;sup>a</sup> Distance between centroid of bolt group and the centre of girder web

The second and third group were denoted by adding suffixes "-GD( $h_t/h_w$  ratio)" and "-GW( $h_w/t_w$  ratio)" to the regular alphanumerical label of the specimens. The fourth group was

<sup>&</sup>lt;sup>b</sup> Depth of the extended portion of the shear plate

<sup>&</sup>lt;sup>c</sup> The girder section is created based on W610×125. Although girder web is different, width and thickness of the girder flange is same as W610×125 section ( $b_f$ =229mm,  $t_f$ =19.6mm).

<sup>&</sup>lt;sup>d</sup> Tested specimen

labeled by adding the suffix "G(Gap distance)" to the label of specimen BG3-2-10-F. It should be noted that the thickness of shear plate was kept constant 10 mm (3/8 in.) in all configurations.

#### 4.4.1 Load transfer mechanism

Figure 4-7 shows the response of the configurations with a single line and two vertical lines of bolts based on the *E* models.

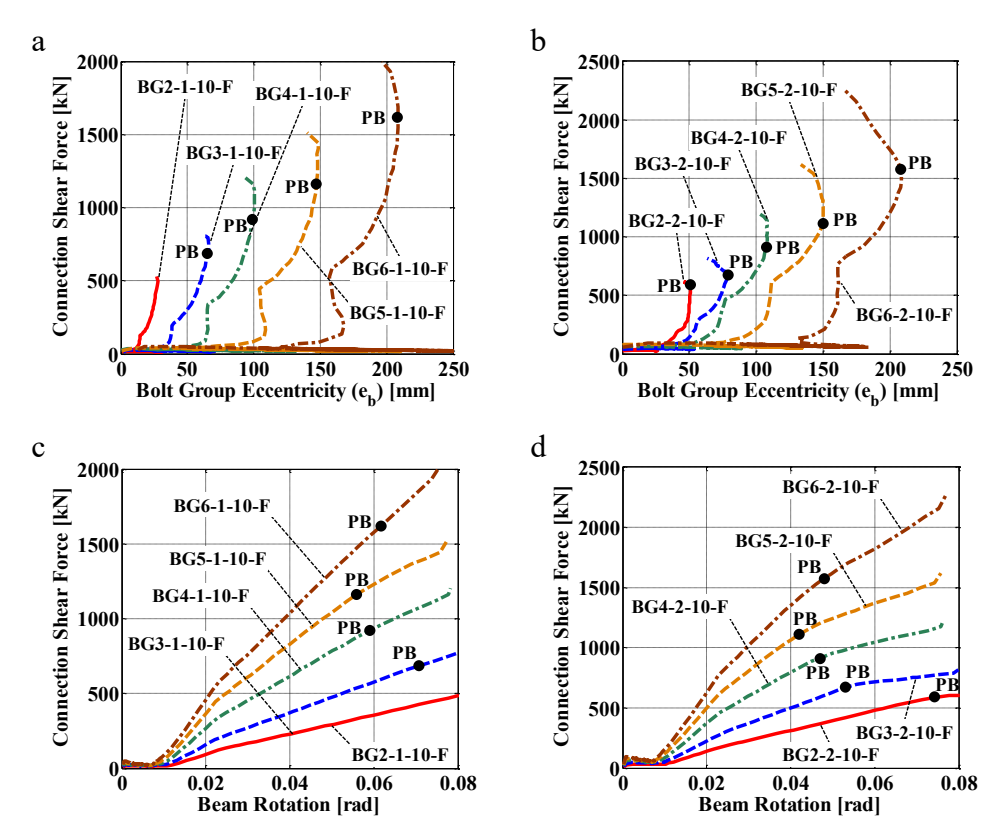


Fig. 4-7. Response of elastic FE models for: (a and c) specimens with a single vertical line of bolts, (b and d) specimens with two vertical lines of bolts (PB represents buckling of shear plate)

Referring to Figs. 4-7a and 4-7b, the distance between the inflection point and the bolt group centre (bolt group eccentricity,  $e_b$ ) increased with the number of horizontal lines of bolts. Although adding a second vertical bolt line increased  $e_b$  for connections with either two or three horizontal bolts lines, this was not the case for connections with more than three bolt rows. For connections with a single vertical line of four bolts or more, the distance between the inflection point and the

centre of the bolt group was almost equal to  $e_b$  of the connections with two vertical lines of bolts. However, in comparison to connections with a single vertical line of bolts, the centre of the configuration with two vertical lines of bolts is placed farther from the girder. This resulted in a larger bending moment demand to the shear plate; hence, plate buckling (Figs. 4-7c and 4-7d) occurred at a lower shear strength as compared to the corresponding connections with a single vertical line of bolts. Referring to Figs. 4-7a and 4-7b, the inflection point moved toward the girder soon after elastic buckling of the shear plate (PB points). Referring to Fig. 4-8, an empirical equation is proposed for predicting the bolt group eccentricity corresponding to the elastic buckling of the shear plate as a function of the number of horizontal lines of bolts, n, found to be the statistically significant variable at the 95% level based on standard t-tests and t-test. The coefficient of determination, t-2=0.947. The range of applicability of Eq. (4-1) is t-2 t-2 t-2 t-3.

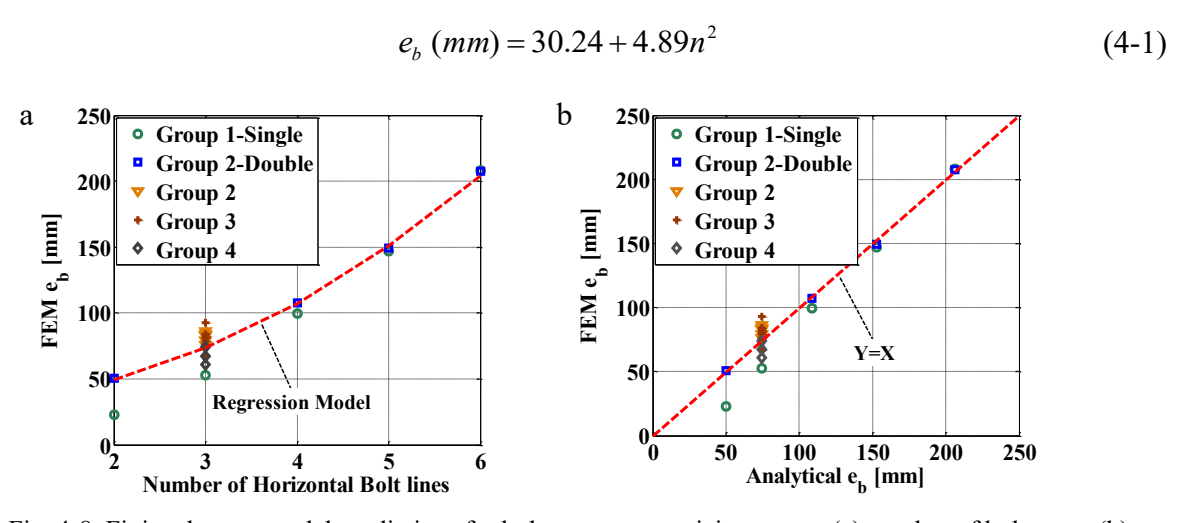


Fig. 4-8. Finite element model predictions for bolt group eccentricity versus: (a) number of bolt rows, (b) predicted eccentricity based on Eq. (4-1)

The results of the parametric study were consistent with the experimental observations (Section 4.2), as well as those from supplemental FE analyses (Section 4.3.2) regarding the load transfer mechanism. Referring to Fig. 4-9a, the connection with two vertical bolt lines had a larger  $\alpha$  ratio as compared to the corresponding connections with a single vertical bolt line. Although the two

connections were similar, the one with two vertical bolt lines exhibited a larger effective eccentricity. The out-of-plane stiffness of the girder web is influenced by the  $h_U/h_W$  and  $h_W/t_W$  ratios. The first parameter represented the location of a lower horizontal force along the girder depth. Similar to a beam subjected to a point load, the out-of-plane stiffness of the girder web increased as the position of this force became closer to the girder flanges. Referring to Fig. 4-9b, the maximum  $\alpha$  ratio was observed at  $h_U/h_W = 0.30$ ; this ratio decreased as  $h_W/t_W$  approached either zero or one. Furthermore, connections with more bolt rows had a larger  $h_U/h_W$  ratio, and consequently a lower  $\alpha$  ratio, as shown in Fig. 4-9a. The out-of-plane stiffness of the girder web decreased while the  $h_W/t_W$  ratio increased. This lead to an increase of the axial force ( $\alpha$  ratio) at the stiffener (Fig. 4-9c).

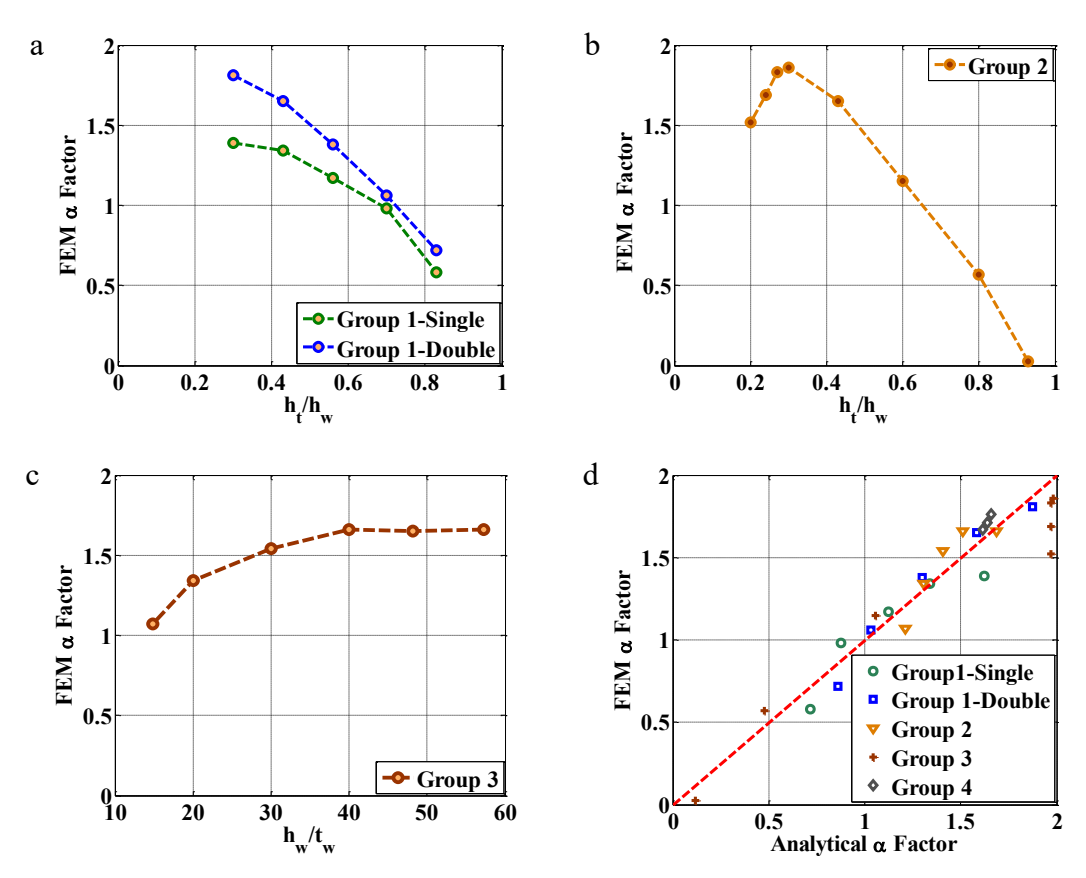


Fig. 4-9. Predictions of FE models for α ratio versus: (a) h<sub>t</sub>/h<sub>w</sub> of first group of configurations, (b) h<sub>t</sub>/h<sub>w</sub> of second group of configurations, (c) h<sub>w</sub>/t<sub>w</sub> of third group of configurations, (d) prediction of regression model (Eq. (4-2))

The results obtained from analyzing the Elastic FE models are summarized in Table 4-2. Notably, the stiffened portion of the shear plate buckled in Group 4 (i.e., larger gap between the beam and girder flanges). In comparison to specimen BG3-2-10-F with a 13mm gap distance, a larger gap resulted in a larger  $\alpha$  ratio due to increasing the a distance, as well as the larger bending moment.

Table 4-2. Elastic buckling strength based on predictions of the FE models E

	1 4010	∠ <del>T</del> -2, L1	astic ouc	Kling strength b	asca on pred	ictions of	the L L	ioucis i		ew
						FE mod	els		Recomn	nendatio
	ID									n
	ID.	h <sub>t</sub> /h <sub>w</sub>	$h_{\mathrm{w}}/t_{\mathrm{w}}$	Centroid of Bolt Group <sup>a</sup> (mm)	Inflection point b (mm)	e <sub>b</sub> (mm)	V <sub>FE</sub> c (kN)	α	e <sub>b</sub> (mm)	α
	BG2-1-10-F	0.30	48.1	165	188	28		1.39	51	1.73
	BG3-1-10-F	0.43	48.1	165	218	65	685	1.34	75	1.43
	BG4-1-10-F	0.56	48.1	165	264	99	921	1.17	109	1.17
_	BG5-1-10-F	0.70	48.1	165	312	147	1161	0.98	153	0.91
Group 1	BG6-1-10-F	0.83	48.1	165	373	208	1619	0.58	206	0.72
Ťo	BG2-2-10-F	0.30	48.1	203	254	51	589	1.81	51	1.88
0	BG3-2-10-F d	0.43	48.1	203	282	79	672	1.65	75	1.57
	BG4-2-10-F	0.56	48.1	203	311	108	912	1.38	109	1.31
	BG5-2-10-F	0.70	48.1	203	353	150	1112	1.06	153	1.05
	BG6-2-10-F	0.83	48.1	203	411	208	1575	0.72	206	0.86
	BG3-2-10-F-GD0.93	0.93	48.1	203	296	93		0.02	75	0.06
	BG3-2-10-F-GD0.80	0.80	48.1	203	287	84	1150	0.57	75	0.45
Group 2	BG3-2-10-F-GD0.60	0.60	48.1	203	279	76	808	1.15	75	1.06
lno	BG3-2-10-F-GD0.30	0.30	48.1	203	282	79	689	1.86	75	1.97
Ġ	BG3-2-10-F-GD0.27	0.27	48.1	203	284	81	699	1.83	75	1.97
	BG3-2-10-F-GD0.24	0.24	48.1	203	270	63	838	1.69	75	1.97
	BG3-2-10-F-GD0.20	0.20	48.1	203	285	82	841	1.52	75	1.97
	BG3-2-10-F-GW57.3	0.43	57.3	203	283	80	614	1.66	75	1.67
Group 3	BG3-2-10-F-GW40.0	0.43	40.0	203	286	83	808	1.66	75	1.48
lno	BG3-2-10-F-GW30.0	0.43	30.0	203	287	84	871	1.54	75	1.37
Ġ	BG3-2-10-F-GW20.0	0.43	20.0	203	290	87	1019	1.34	75	1.26
	BG3-2-10-F-GW14.8	0.43	14.8	203	279	76	1051	1.07	75	1.21
4	BG3-2-10-F-G25	0.43	48.1	216	290	74	668	1.67	75	1.62
Group 4	BG3-2-10-F-G38	0.43	48.1	226	296	67	663	1.71	75	1.67
Ğ	BG3-2-10-F-G50	0.43	48.1	241	302	61	641	1.76	75	1.72

<sup>&</sup>lt;sup>a</sup> Distance between the centre of bolt group and the centre of girder web

In order to predict the  $\alpha$  value, Eq. (4-2) is proposed based on the statistically significant variables defined by a standard t- and F-test. The coefficient of determination is  $R^2$ =0.947,

<sup>&</sup>lt;sup>b</sup> Distance between the inflection point and the centre of girder web

<sup>&</sup>lt;sup>c</sup> Prediction for resistance corresponding to the shear plate buckling

<sup>&</sup>lt;sup>d</sup> Tested specimen

$$\alpha = 1.293 + 0.875(e_{eff}/b_f) - 3.043(h_t/h_w) + 0.011(h_w/t_w)$$
 (4-2)

in which,  $e_{\it eff} = e + e_b$  is the distance between the inflection point and the centre of the girder web while e is the distance between the bolt group centre and the girder web (Fig. 4-1). The range of applicability of Eq. (4-2) is  $0.82 \le e_{\it eff} / b_f \le 1.80 \, , 0.30 \le h_t / h_w \le 0.93 \, , \ 14.84 \le h_w / t_w \le 57.28 \, .$  Referring to Table 4-2, if  $h_t/h_w = 0.30$  then Eq. (4-2) would conservatively overestimate the  $\alpha$  value for connections with  $h_t/h_w \le 0.30$ .

#### 4.4.2 Observed failure modes

The inelastic (PL) models demonstrated that shear plate inelastic buckling was the critical failure mode in most configurations. Referring to Figs. 4-10a and 4-10b, prior to yielding and buckling of the stiffened portion of the shear plate, shear plate yielding along the interior bolt line resulted in a significant decrease of the stiffness in five configurations summarized in Table 4-3. For all other configurations, yielding of the full width of the stiffened portion of the shear plate (PY points in Fig. 4-10) resulted in a marked decrease of the connection stiffness. Because of their slenderness, these shear tabs buckled (PB points in Fig. 4-10) shortly after they had yielded.

Referring to Figs. 4-10c and 4-10d, after inelastic buckling of the shear plate had occurred, the connection eccentricity increased due to force redistributions occurring within the connection, while the shear force remained constant or decreased slightly. However, the comparison between the elastic (E) and the inelastic models (PL), Fig. 4-7 and Fig. 4-10, respectively, demonstrated that  $e_b$  of the PL models was smaller than the E models due to yielding of connection components, among them the shear plate. In comparison to the connection with two vertical bolt lines, the corresponding connection with a single vertical bolt line had smaller eccentricity, and consequently buckled under larger shear force (Figs. 4-10a and 4-10b).

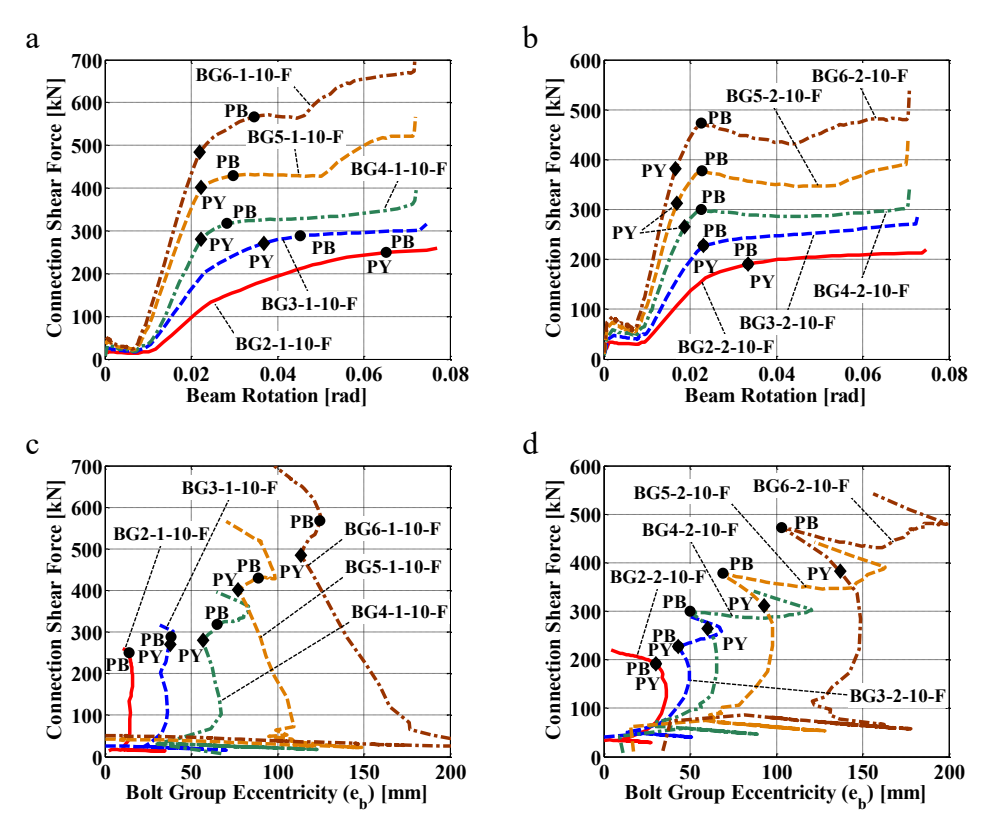


Fig. 4-10. Response of FE models for: (a and c) specimens with single vertical line of bolts, (b and d) specimens with double vertical lines of bolts (PY represents yielding along full width of the stiffener while PB represents buckling of shear plate)

Referring to Figs. 4-11a and 4-11b, the buckling shear force decreased with respect to the  $\alpha$  ratio and increased with respect to the  $h_w/t_w$  ratio, respectively. Referring to Figs. 4-11c and 4-11d, larger gaps decreased the buckling strength slightly due to the increase in the effective eccentricity.

As illustrated in Fig. 4-12, the stiffener yielded along the lower edge of the extended portion of the shear plate due to the interaction of the shear and axial forces. The stiffener axial force,  $F_a$ , was determined based on the  $\alpha$  value (Eq. (4-3)), while the horizontal shear force,  $F_v$ , was calculated based on the connection bending moment (Eq. (4-4)).

$$F_a = \alpha V \tag{4-3}$$

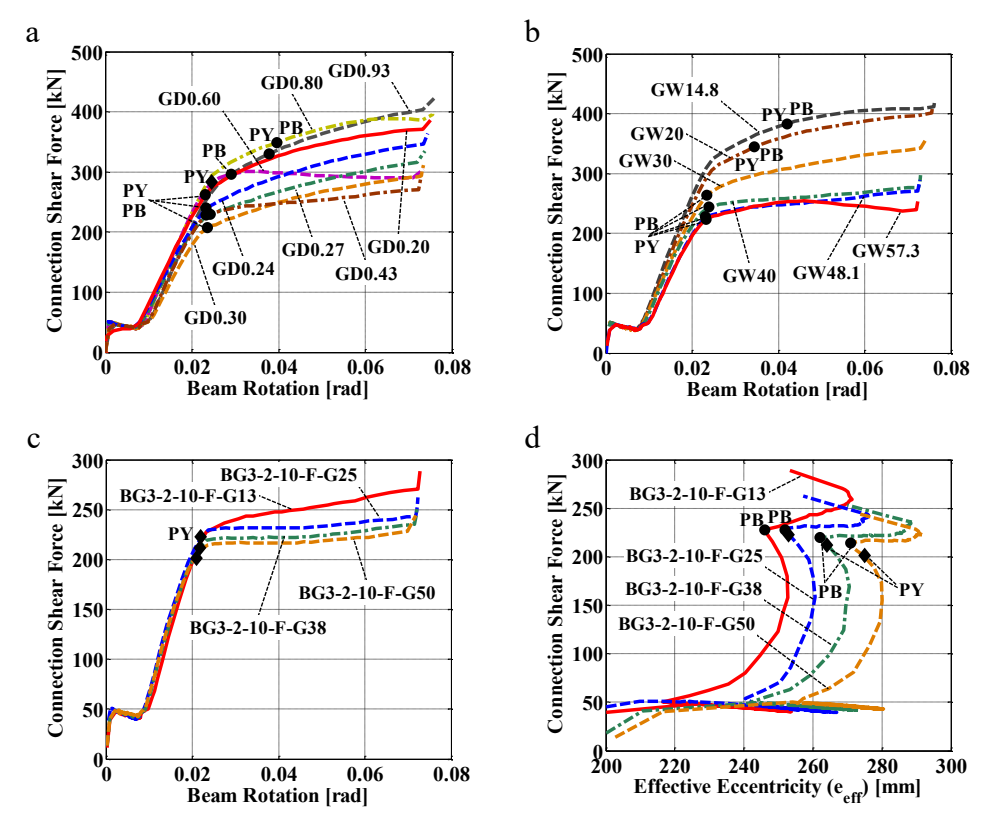


Fig. 4-11. Response of FE models of: BG3-2-10-F configuration with varied: (a) h<sub>t</sub>/h<sub>w</sub> ratio (Group 2), (b) h<sub>w</sub>/t<sub>w</sub> ratio (Group 3), (c and d) Gap distance (Group 4)

The horizontal shear force can be calculated based on equilibrium of the bending moment at the top portion of the stiffener with respect to the intersection point of the girder web and the midepth of the upper portion of the shear plate. It should be noted that Eq. (4-4) conservatively overestimated the horizontal shear force  $(F_{\nu})$  due to its dependence on the connection eccentricity, which corresponds to the elastic buckling of the shear plate (Eq. (4-1)). Furthermore, the contribution of the vertical force of the top flange, as well as the bending moments of all components were ignored conservatively in Eq. (4-4).

$$F_{v} = \left(\frac{e_{eff} - \alpha b_{f} / 4}{d_{pl}}\right) V = \beta V \tag{4-4}$$

in which,  $F_v$  is the shear force at the critical section of the stiffener; V is the connection shear force;  $e_{eff} = e + e_b$  is the distance between the inflection point and the centre of the girder web;  $b_f$  is the

width of the girder flange;  $d_{pl}$  is the depth of the extended portion of the shear plate;  $\alpha$  is the ratio between axial force of the stiffener and the connection shear force (Eq. (4-2));  $\beta$  is the ratio between the shear force of the stiffener and the connection shear force (Eq. (4-4)).

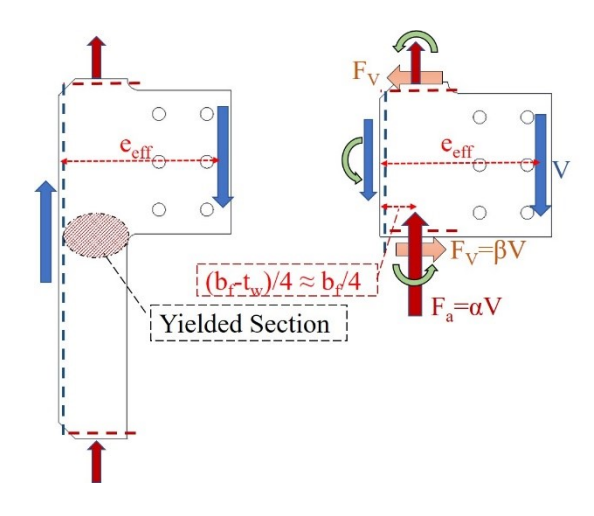


Fig. 4-12. Bending moment equilibrium at top portion of the shear plate

To control the shear and axial force interaction, the Von Mises yield criterion was implemented,

$$\left(\frac{f_a}{F_y}\right)^2 + \left(\frac{f_v}{F_y/\sqrt{3}}\right)^2 = 1 \tag{4-5}$$

This equation can be rewritten based on the connection shear force as follows,

$$\left[ \frac{F_a}{(t_{pl}b_f/2)} \right]^2 + \left[ \frac{F_v}{(t_{pl}b_f/2)} \right]^2 = 1$$
(4-6)

Finally, the connection shear force corresponding to yielding of the stiffened portion of the shear tab can be determined based on Eq. (4-7),

$$V = \frac{F_{y}t_{pl}b_{f}}{2}(\frac{1}{\sqrt{\alpha^{2} + 3\beta^{2}}})$$
(4-7)

In the absence of an equation to predict accurately the inelastic buckling strength of the shear plate, the shear force corresponding to the yielding of the stiffened portion of the shear plate can be used as a conservative prediction for inelastic buckling of the shear plate.

Referring to Table 4-3, Eq. (4-7) conservatively predicted the buckling shear force in all cases. However, this equation significantly underestimated the buckling shear force in configurations for which shear plate yielding along the interior bolt line occurred prior to the stiffener yielding. In these cases, shear plate yielding resulted in the movement of the inflection point toward the girder; hence, the effective eccentricity was much smaller than that of the corresponding elastic model, which was used to predict the  $\alpha$  value. Furthermore, the effect of the shear force eccentricity should be considered in design of the supporting girder, if the connection was designed based on Eq. (4-7).

The FE shear strength prediction for yielding ( $V_{FE}^{NY}$ ) was much smaller than the shear yielding predictions along the interior bolt line ( $F_yA_{net}$ ); for instance, the PL model of BG3-1-10-F yielded under 302 kN shear force, 30% lower than the expected value for shear yielding along the net section, 431 kN. This is due to the interaction of bending moment and shear force along the net section of the shear plate, which is not considered in the current AISC design approach. This aspect is outside the scope of the present study, which is concerned with the stability of stiffened beamto-girder connections subjected to gravity loading.

In contrast to Eq. (4-7), the current AISC design approach significantly overestimated the buckling strength of the shear tab connection. Notably, these predictions were the minimum values of the three buckling models: lateral-torsional buckling of a doubly coped beam, plate type buckling of a doubly coped beam [9], and lateral-torsional buckling of a rectangular section [5, 12]. To use these equations, the distance between the weld and bolt lines, *a* distance, conservatively

were considered as the unbraced length of the shear tab. However, the connections were subjected to relatively large bending moment in comparison to the shear connections in previous test [6-8].

Table 4-3. Shear strength based on predictions of the FE models

-		Table		strength b	aseu on		Design				
			FE mo			Met	hod	New Recommendations			
	ID.	$V_{\text{FE}}^{PY}{}_{a}$	$V_{\text{FE}}^{\text{PB}_{\text{b}}}$	$V_{\text{FE}}^{ ext{NY}\ c}$	$\frac{V_{FE}^{PB}}{V_{FE}}$	V <sub>A</sub> <sup>PB</sup> <sub>b</sub>	$\frac{V_{\text{FE}}^{\text{PB}}}{V_{\text{BB}}}$	β	$V_{\scriptscriptstyle A}^{\scriptscriptstyle PY a}$	$\frac{V_{FE}^{PY}}{V_{FE}}$	$\frac{V_{\text{FE}}^{\text{PB}}}{V^{\text{PY}}}$
		(kN)	(kN)	(kN)	$\frac{V_{\mathrm{FE}}^{\mathrm{FE}}}{V_{\mathrm{FE}}^{\mathrm{PY}}}$	(kN)	$\overline{V_{\scriptscriptstyle A}^{\scriptscriptstyle PB}}$	,	(kN)	$\overline{V_{A}^{PY}}$	V <sub>A</sub>
	BG2-1-10-F	250	250	253	1.00	158	1.58	0.76	227	1.10	1.04
	BG3-1-10-F	271	288	302	1.06	357	0.81	0.69	265	1.02	1.06
	BG4-1-10-F	280	318	d	1.14	400	0.79	0.68	298	0.94	1.09
_	BG5-1-10-F	401	429	d	1.07	579	0.74	0.70	326	1.23	1.36
dn	BG6-1-10-F	484	567	d	1.17	777	0.73	0.72	342	1.42	1.76
Group 1	BG2-2-10-F	191	191	178	1.00	158	1.20	0.96	197	0.97	1.02
$\cup$	BG3-2-10-F <sup>e</sup>	228	228	269	1.00	357	0.64	0.82	232	0.98	1.05
	BG4-2-10-F	265	300	d	1.13	400	0.75	0.78	263	1.01	1.20
	BG5-2-10-F	312	378	d	1.21	579	0.65	0.78	289	1.08	1.37
	BG6-2-10-F	382	473	d	1.24	777	0.61	0.79	305	1.25	1.64
	BG3-2-10-F-GD0.93	330	330	296	1.00	357	0.92	1.20	237	1.39	1.39
	BG3-2-10-F-GD0.80	349	349	298	1.00	357	0.98	1.10	252	1.39	1.39
Group 2	BG3-2-10-F-GD0.60	283	296	270	1.05	357	0.83	0.95	252	1.12	1.17
lno	BG3-2-10-F-GD0.30	207	207	279	1.00	357	0.58	0.72	212	0.98	0.98
Ġ	BG3-2-10-F-GD0.27	230	230	282	1.00	357	0.64	0.72	212	1.08	1.08
	BG3-2-10-F-GD0.24	240	240	299	1.00	357	0.67	0.72	212	1.13	1.13
	BG3-2-10-F-GD0.20	262	262	299	1.00	357	0.73	0.72	212	1.11	1.11
	BG3-2-10-F-GW57.3	224	224	d	1.00	357	0.63	0.79	228	0.98	0.98
Group 3	BG3-2-10-F-GW40.0	244	244	263	1.00	357	0.68	0.84	237	1.03	1.03
lno	BG3-2-10-F-GW30.0	264	264	290	1.00	357	0.74	0.87	242	1.09	1.09
Ġ	BG3-2-10-F-GW20.0	345	345	306	1.00	357	0.97	0.90	246	1.40	1.40
	BG3-2-10-F-GW14.8	383	383	309	1.00	357	1.07	0.91	248	1.54	1.54
4	BG3-2-10-F-G25	223	228	243	1.03	332	0.69	0.86	225	0.99	1.01
Group 4	BG3-2-10-F-G38	212	220	233	1.04	308	0.71	0.91	217	0.98	1.01
<u> </u>	BG3-2-10-F-G50	201	214	d	1.07	288	0.75	0.95	210	0.96	1.03
					Mini		0.58			0.94	0.98
					Me		0.80			1.13	1.20
					Maxi		1.58			1.54	1.76
		Standard deviation			0.22			0.17	0.22		
				COV			0.27			0.15	0.18

<sup>&</sup>lt;sup>a</sup> Prediction for shear resistance corresponding to yielding of the stiffened portion of the shear plate

The imposed bending moment was due to the implemented loading protocol in which 0.02 rad relative rotation between the beam and girder was set as the target rotation. In contrast, the end rotation of the supported beam would be accommodated through rotation of the girder in single-

<sup>&</sup>lt;sup>b</sup> Prediction for shear resistance corresponding to buckling of the stiffened portion of the shear plate

<sup>&</sup>lt;sup>c</sup> Prediction for shear resistance corresponding to yielding of the interior net section of the shear plate

<sup>&</sup>lt;sup>d</sup> Yielding was not observed along the interior net section of the shear plate

<sup>&</sup>lt;sup>e</sup> Tested specimen

sided beam-to-girder shear tab connections due to low torsional stiffness of the girder. Therefore, to achieve the target rotation, large bending moment was applied to the connection. The comparison between the results of previous experiment on extended shear tabs [6-8] with those implemented in this study [2, 3] demonstrated that the implemented loading protocol was conservative.

## 4.4.3 Bolt group shear capacity

The bolt shear fracture was observed in none of the studied connections, whereas the inelastic deformation was mostly concentrated in the shear plate. This observation was consistent with conclusions from previous research on full-depth stiffened extended shear tabs [2, 3, 8]; the buckling of the shear plate was determined as the governing failure mode. In the case of full-depth stiffened extended shear tabs, implementation of the current AISC design method resulted in an underestimation of the bolt group capacity. For instance, Specimen BG3-2-13-F experienced nearly double the shear force as predicted by the AISC bolt shear strength (520 kN shear force versus 270 kN), while no noticeable bolt deformation was observed. This was due to the AISC design method considering the bolt group eccentricity to be the distance between the weld line and centre of the bolt group, i.e. e distance in Fig. 4-1. This assumption would be overly conservative for full-depth stiffened shear tabs; in contrast, it was reasonably conservative for unstiffened shear tab connections, for which the design method was developed. To determine the bolt shear capacity of the stiffened shear tabs, the E-Bo FE models were utilized. Notably, the FE modeling procedure was implemented to simulate available bolt shear experiments [30, 31]. Although the FE model accurately captured the bolt's strength plateau (continuous increase of the bolt deformation while the bolt force remained constant) in the shear test, it was not possible to capture the bolt's post ultimate (softening) response. This may result in concern regarding the capability of the FE model to capture the shear capacity of the bolt group under an

eccentric shear force, in which the bolts would experience shear fracture progressively. To address this issue, the force-deformation response of each individual bolt was monitored during the analysis; the minimum level of the connection shear force corresponding to the time when the first bolt reached its strength plateau was considered as the shear capacity of the bolt group. Figure 4-13 shows the response of configurations with a single bolt line and two vertical bolt lines.

Referring to Figs. 4-13a and 4-13b, the shear capacity of a connection with a single vertical line of bolts was slightly more than half the shear capacity of a connection containing two vertical lines of bolts (same number of bolts per line). Referring to Figs. 4-13c and 4-13d, adding to the number of rows of bolts increased the bolt group eccentricity. The comparison between the eccentricity of the *E*-and the *E-Bo* models demonstrated that yielding of the bolts resulted in a decrease of the bolt group eccentricity.

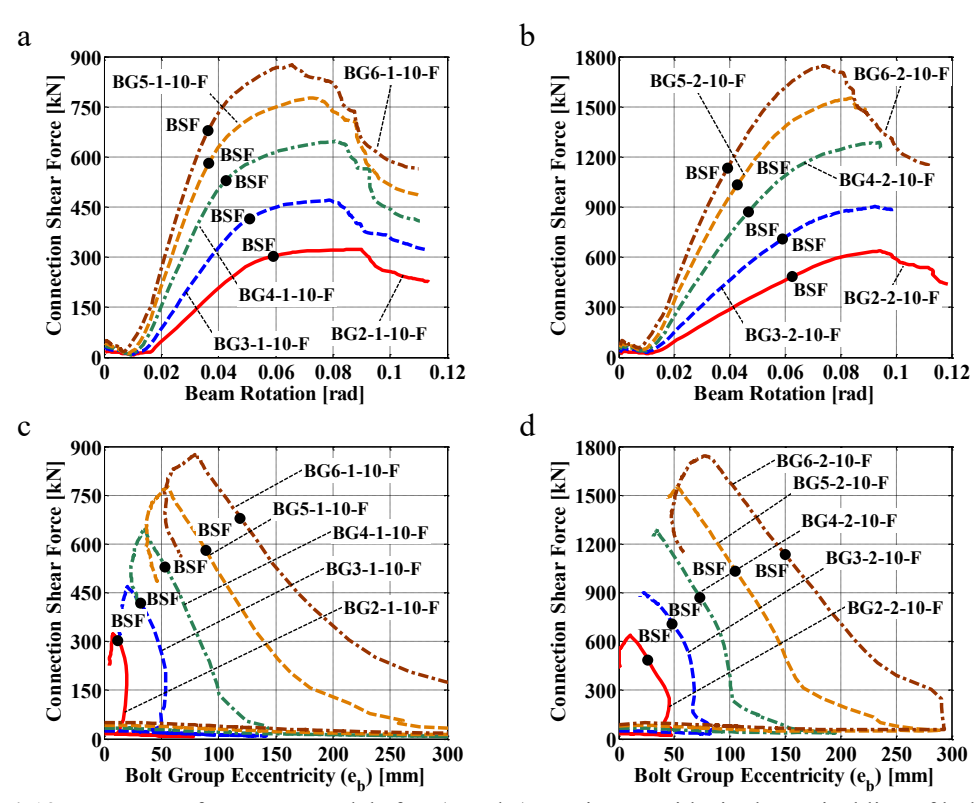
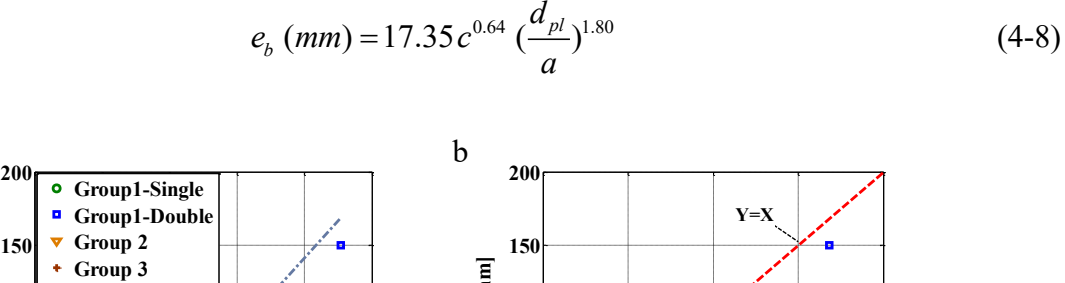
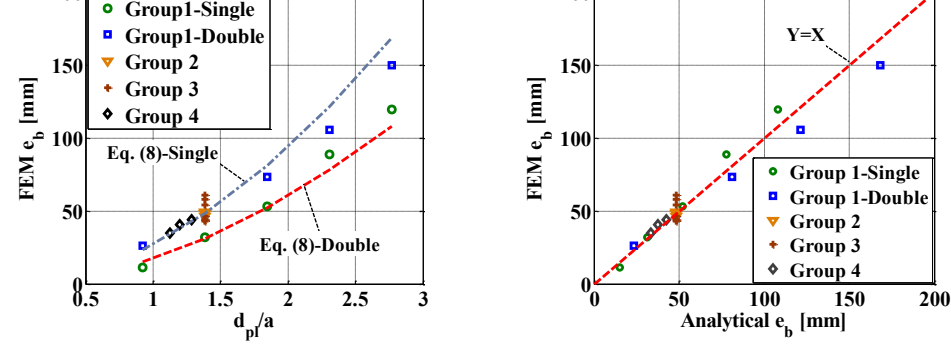


Fig. 4-13. Response of *E-Bo* FE models for: (a and c) specimens with single vertical line of bolts, (b and d) specimens with double vertical lines of bolts (BSF represents bolt shear fracture failure mode).

Figure 4-14a shows the FE model predictions for the eccentricity of a bolt group versus the  $d_{pl}/a$  ratio of the plate when bolt shear fracture was observed. It was concluded that the eccentricity of the bolt group was strongly influenced by the  $d_{pl}/a$  ratio of the shear plate. Of note,  $d_{pl}$  is the depth of the extended portion of the shear plate, while a is the distance between the girder web and the interior bolt line (Fig. 4-1). To estimate the distance between the inflection point and the bolt group centre, Eq. (4-8) is proposed. Referring to Fig. 4-14b, the proposed equation predicted the bolt group eccentricity with a  $R^2$ =0.945 and a range of applicability of  $0.92 \le d_{pl}/a \le 2.77$  and c=1 & 2.





a

Fig. 4-14. Bolt group eccentricity of E-Bo models: (a) versus the number of horizontal lines of bolts, (b) predicted eccentricity based on Eq. (4-8).

The shear capacity of the bolt group was calculated in accordance with the Instantaneous Centre of Rotation (ICR) method while the predicted  $e_b$  was used as the eccentricity of the shear force. Referring to Table 4-4, the proposed eccentricity resulted in a reasonably conservative prediction of the bolt shear strength, compared to the current design recommendations. Referring to Table 4-4, in the current AISC design recommendations it is assumed that the bolt group eccentricity is given by the distance between the bolt group centre and the girder web; which when

used for the strength calculation of the test specimens resulted in a substantial underestimation of the bolt group capacity. This issue is more evident in bolt groups with a single vertical line of bolts.

Table 4-4. Bolt shear strength based on predictions of the FE models E-Bo

			FE 1	models	Currer	Current Design Method			New Recommendations		
	ID.	Inflection point a (mm)	e <sub>b</sub> (mm)	V <sub>FE</sub> b (kN)	e <sub>b</sub> (mm)	V <sub>A</sub> BSH (kN)	$\frac{V_{FE}^{BSH}}{V_{A}^{BSH}}$	e <sub>b</sub> (mm)	V <sub>A</sub> BSH (kN)	$\frac{V_{\text{FE}}^{\text{BSH}}}{V_{\text{A}}^{\text{BSH}}}$	
	BG2-1-10-F	177	12	303	159	68	4.45	15	262	1.15	
	BG3-1-10-F	197	32	417	159	138	3.02	31	383	1.09	
	BG4-1-10-F	219	53	530	159	246	2.16	52	485	1.09	
	BG5-1-10-F	254	89	581	159	370	1.57	78	569	1.02	
tp 1	BG6-1-10-F	285	119	679	159	508	1.34	109	640	1.06	
Group 1	BG2-2-10-F	229	26	485	197	146	3.32	23	491	0.99	
_	BG3-2-10-F <sup>c</sup>	252	48	709	197	270	2.63	49	671	1.06	
	BG4-2-10-F	276	73	872	197	445	1.96	82	816	1.07	
	BG5-2-10-F	309	105	1034	197	647	1.60	122	909	1.14	
	BG6-2-10-F	353	150	1134	197	885	1.28	169	987	1.15	
	BG3-2-10-F-GD0.93	250	47	714	197	270	2.65	49	671	1.07	
	BG3-2-10-F-GD0.80	249	46	729	197	270	2.70	49	671	1.09	
7	BG3-2-10-F-GD0.60	252	49	708	197	270	2.62	49	671	1.06	
Group	BG3-2-10-F-GD0.30	253	49	702	197	270	2.60	49	671	1.05	
Ġ	BG3-2-10-F-GD0.27	252	48	715	197	270	2.65	49	671	1.07	
	BG3-2-10-F-GD0.24	264	61	634	197	270	2.35	49	671	0.95	
	BG3-2-10-F-GD0.20	261	58	643	197	270	2.38	49	671	0.96	
	BG3-2-10-F-GW57.3	257	54	666	197	270	2.47	49	671	0.99	
$\alpha$	BG3-2-10-F-GW40.0	249	46	711	197	270	2.63	49	671	1.06	
Group 3	BG3-2-10-F-GW30.0	247	44	732	197	270	2.71	49	671	1.09	
Ġ	BG3-2-10-F-GW20.0	246	43	745	197	270	2.76	49	671	1.11	
	BG3-2-10-F-GW14.8	247	44	738	197	270	2.73	49	671	1.10	
4	BG3-2-10-F-G25	260	44	731	210	255	2.87	42	697	1.05	
Group 4	BG3-2-10-F-G38	269	41	747	223	242	3.09	38	719	1.04	
Ġ	BG3-2-10-F-G50	276	35	766	235	231	3.32	33	737	1.04	
					Minimum		1.28			0.95	
						Mean	2.55			1.06	
					Ma	ıximum	4.45			1.15	
				St	andard de		0.68			0.05	
						COV	0.27			0.05	

<sup>&</sup>lt;sup>a</sup> Distance between the inflection point and the centre of girder web
<sup>b</sup> Prediction for shear resistance corresponding to the shear fracture of the bolt group

<sup>&</sup>lt;sup>c</sup> Tested specimen

To calculate the shear capacity of the bolt group, the authors suggest implementing the ICR method with the bolt group eccentricity as obtained with the *E-Bo* models (Eq. (4-8)), which accounts for bolt yielding. This recommendation is conservative because the FE models with yieldable components have smaller bolt group eccentricity than the *E-Bo* models at the same level of shear force.

## 4.5 Conclusions

This paper presents the results of a parametric finite element study on the single-sided configuration of extended beam-to-girder shear tab connections with full depth shear plates. The intent is to further understand the shear load transfer mechanism and to propose improved design procedures. The FE models were validated with prior full-scale experiments of such connections. The main findings are summarized as follows:

- The critical section of the stiffened portion of the shear plate (section along the bottom edge of the extended part of the shear plate) is subjected to high axial and shear force resulting in local yielding of the shear plate and connection stiffness reduction.
- The force demands developed at the shear plate's critical section are strongly influenced by the girder web flexibility and the relative distance between the girder bottom flange and the bottom edge of the extended part of the shear plate. Eqs. (4-1) to (4-4) were developed to determine these forces prior to yielding of the critical section.
- To determine the connection shear force corresponding to yielding of the critical section, the Von Mises yield criterion was used to detect the force interaction developed at this section (Eq. (4-7)).

- The critical section of the stiffened portion of the shear plate experiences inelastic buckling shortly after its local yielding, if the shear plate does not satisfy the CSA S16 compactness ratio for bearing stiffeners ( $200/\sqrt{F_y}$ ).
- The shear resistance corresponding to yielding of the stiffened portion of the shear plate (Eq. (4-7)) can be used as a conservative prediction for the inelastic buckling strength of the slender shear tab.
- It is recommended that the ICR method be implemented to calculate the shear capacity of the bolt group with the bolt group eccentricity as obtained from Eq. (4-8).
- In the case of the single-sided configuration of the full-depth stiffened extended shear tab connection, the effect of the eccentricity of the shear force should be taken into account in the design of the supporting girder.

## 4.6 Acknowledgments

The authors would like to thank the ADF Group Inc. and DPHV Structural Consultants for their generous technical and financial support, as well as the Natural Sciences and Engineering Research Council of Canada. The authors also thank Jacob Hertz and Nathan Goldstein Apt for sharing their experimental results for extended shear tabs. The finite element computations were conducted at the McGill University's supercomputer Guillimin, which is managed by Calcul Québec and Compute Canada. The supercomputer operation is funded by the Canada Foundation for Innovation (CFI), NanoQuébec, RMGA and the Fonds de recherche du Québec - Nature et technologies (FRQ-NT).

### 4.7 References

- [1] CSA-S16-14, Design of steel structures, Canadian Standards Association, Mississauga, ON., 2014.
- [2] J. Hertz, Testing of extended shear tab connections subjected to shear, Master's Thesis, McGill University, Montreal, QC, 2014.
- [3] N. Goldstein Apt, Testing of extended shear tab and coped beam-to-girder connections subject to shear loading, Master's Thesis, McGill University, Montreal, QC, 2015.
- [4] M. Motallebi, D.G. Lignos, C.A. Rogers, Behaviour of stiffened extended shear tab connections under gravity induced shear force., J. Constr. Steel Res., 148 (2018) 336-350.
- [5] AISC Steel construction manual, 15<sup>th</sup> edition, American Institute of steel Construction, Chicago, IL, 2017.
- [6] D.R. Sherman, A. Ghorbanpoor, Design of extended shear tabs, University of Wisconsin-Milwaukee, Milwaukee, WI, 2002.
- [7] W. Goodrich, Behavior of extended shear tabs in stiffened beam-to-column web connections, Thesis, Vanderbilt University, Nashville, TN, 2005.
- [8] K. Thomas, R.G. Driver, S.A. Oosterhof, L. Callele, Full-scale tests of stabilized and unstabilized extended single-plate connections, Structures, 10 (2017) 49-58.
- [9] AISC Steel construction manual, 14<sup>th</sup> edition, American Institute of steel Construction, Chicago, IL, 2011.
- [10] J.-J. Cheng, J. Yura, C. Johnson, Design and behavior of coped beams, University of Texas at Austin, Austin, TX, 1984.

- [11] L. Muir, W. Thornton, A direct method for obtaining the plate buckling coefficient for double-coped beams, Eng. J. AISC, 41 (2004) 133-134.
- [12] AISC 360-16, Specification for structural steel buildings, American Institute of steel Construction, Chicago, IL, 2016.
- [13] B. Dowswell, R. Whyte, Local stability of double-coped beams, Eng. J. AISC, 51(1) (2014) 43-52.
- [14] J. Hertz, D.G. Lignos, C.A. Rogers, Full scale testing of extended beam-to-column and beam to-girder shear tab connections subjected to shear, 8th International Conference on Behaviour of Steel Structures in Seismic Areas, Shanghai, China, 2015.
- [15] M. Marosi, M. D'Aronco, R. Tremblay, C.A. Rogers, Multi-row bolted beam to column shear tab connections, 6th European Conference on Steel and Composite Structures, Budapest, Hungary, 2011.
- [16] M. Marosi, Behaviour of single and double row bolted shear tab connections and weld retrofits, Master's Thesis, McGill University, Montreal, QC, 2011.
- [17] M. D'Aronco, Behaviour of double and triple vertical rows of bolts shear tab connections and weld retrofits, Master's Thesis, École Polytechnique de Montréal, Montreal, QC, 2013.
- [18] A. Mirzaei, Steel shear tab connections subjected to combined shear and axial forces, PhD Thesis, McGill University, Montreal, QC, 2014.
- [19] C.A. Rogers, M. Marosi, J. Hertz, D.G. Lignos, R. Tremblay, M. D'Aronco, Performance of weld-retrofit beam-to-column shear tab connections, 8th Int. Workshop on Connections in Steel Structures, Boston, MA., 2016.

- [20] A. Astaneh, Demand and supply of ductility in steel shear connections, J. Constr. Steel Res., 14(1) (1989) 1-19.
- [21] ASTM A992 / A992M-11(2015), Standard specification for structural steel shapes, ASTM International, West Conshohocken, PA, 2015.
- [22] ASTM A572 / A572M-15, Standard specification for high-strength low-alloy columbium-vanadium structural steel, ASTM International, West Conshohocken, PA, 2015.
- [23] ASTM F3125 / F3125M-15a, Standard specification for high strength structural bolts, steel and alloy steel, heat treated, 120 ksi (830 MPa) and 150 ksi (1040 MPa) minimum tensile strength, inch and metric dimensions, ASTM International, West Conshohocken, PA, 2015.
- [24] ABAQUS 6.11-3, [Computer software], Dassault Systemes Simulia Corp., Providence, RI.
- [25] M. Motallebi, D.G. Lignos, C.A. Rogers, Finite element simulation of buckling of extended beam-to-girder shear tab connections under gravity induced shear force, SSRC Annual Stability Conference, Orlando, FL., 2016.
- [26] ASTM A6 /A6M, General requirements for rolled structural steel bars, plates, shapes, and sheet piling, ASTM International, 2004.
- [27] CSA-G40.20-13/G40.21-13, General requirements for rolled or welded structural quality steel/ structural quality steel, Canadian Standards Association, Toronto, ON., 2013.
- [28] CISC, Handbook of steel construction, Canadian Institute of Steel Construction, Markham, ON., 2016.
- [29] A. Elkady, D.G. Lignos, Analytical investigation of the cyclic behavior and plastic hinge formation in deep wide-flange steel beam-columns, Bull. Earthq. Eng., 13(4) (2015) 1097-1118.

- [30] J.J. Wallaert, J.W. Fisher, Shear strength of high-strength bolts, Lehigh University, Bethlehem, PA, 1964.
- [31] J. Wallaert, J. Fisher, Shear strength of high-strength bolts, J. Struct. Div. ASCE, 91(3) (1965) 99-126.

# Link between Chapter 4 and Chapter 5

In Chapter 4 are proposed the design recommendations for the single-sided configuration of the full-depth stiffened extended beam-to-girder shear tab connection. However, the girder web flexibility caused a different load transfer mechanism for the single- and double-sided configurations. Furthermore, Chapters 3 and 4 were based on the connection behaviour under gravity induced shear force, while large axial force may develop in the double-sided configurations. To address this shortcoming, the author tested two full-scale double-sided specimens of the full-depth stiffened extended beam-to-girder shear tabs under coupled axial and shear forces. Chapter 5 contains a detail description of these laboratory tests as well as the results of complementary FE simulations.

# 5 Chapter 5: Full-scale Testing of Stiffened Extended Shear Tab Connections under Combined Axial and Shear Forces

Engineering Structures (2018), Under Review (Submission No.: ENGSTRUCT\_2018\_528)

Mohammad Motallebi<sup>1</sup>, Dimitrios G. Lignos<sup>2</sup>, Colin A. Rogers<sup>3</sup>

Colin A. Rogers, Associate Professor, Department of Civil Engineering and Applied Mechanics, McGill University, Montreal, QC. Email: colin.rogers@mcgill.ca

817 Sherbrooke Street West Montreal QC, Canada, H3A 0C3 Tel. 514 398-6449

Fax. 514 398-7361

<sup>&</sup>lt;sup>1</sup> Graduate Research Assistant, Department of Civil Engineering and Applied Mechanics, McGill University, Montreal, QC. Email: mohammad.motallebinasrabadi@mail.mcgill.ca

<sup>&</sup>lt;sup>2</sup> Dimitrios G. Lignos, Associate Professor, School of Architecture, Civil and Environmental Engineering, Swiss Federal Institute of Technology, Lausanne (EPFL), Lausanne, Switzerland, Email: dimitrios.lignos@epfl.ch

<sup>&</sup>lt;sup>3</sup> Corresponding author

# **Abstract**

Owing to the lack of a comprehensive published procedure for the design of stiffened extended shear tabs, practicing engineers usually follow design guides for unstiffened shear tabs. The results of recent laboratory experiments and numerical analyses have demonstrated that improvements to this design approach are warranted. Furthermore, design methods for this connection type under loading scenarios including combined axial and shear forces are not well established. To address these shortcomings, full-scale laboratory tests were carried out on the double-sided configuration of stiffened extended beam-to-girder shear tabs with full depth shear plates. These experiments were complemented by a thoroughly validated finite element (FE) study. Based on the results of these experiments and FE simulations, the connection failure modes were characterized and the axial force along with the other main parameters that affect the connection behaviour were further examined. The current design practice for the double-sided configuration of the full-depth extended beam-to-girder shear tab was also evaluated.

**Keywords**: extended shear tab, double-sided configuration, gross section yielding, plate out-ofplane deformation, net section fracture

## 5.1 Introduction

Shear connections transfer the end reactions of simply supported beams to supporting columns or girders without transmitting more than 20% of the nominal plastic moment resistance of the supported beam [1]. These connections must have sufficient ductility to sustain the rotational demands at the ends of the supported beams. A simple shear connection may be subjected to axial force demands due to wind and/or earthquake while it is resisting gravity-induced shear force; hence, design for combined axial and shear force demands would be necessary. Furthermore, extreme loading scenarios, such as the removal of a column, lead to the development of significant axial tension in these connections. Despite this need, there is little guidance in the literature for the design of shear connections under combined axial and shear forces [4, 14, 15]. Past editions of the American Institute of Steel Construction (AISC) Steel Construction Manual [28] addressed only gravity induced shear demand in the design of shear connections. The design of these connections under combined axial and shear forces was mainly left to the judgment of the engineer. The AISC Steel Construction Manual [28] did, however, introduce ductility checks for the designed connection under combined loading. The most recent edition of the AISC Steel Construction Manual (15<sup>th</sup> edition) [4] contains a requirement for the engineer to consider the interaction limit states due to the orthogonal loading in the connection in addition to the individual shear and axial limit states. Further, the AISC Steel Construction Manual [4] refers to its companion document, the AISC Design Examples [15], for design examples of simple shear connections under combined axial and shear forces. The procedure found in the AISC Design Examples [15] is similar to that described in the Steel Connection Handbook [14]; however, reference is not provided to laboratory tests or finite element (FE) simulations in support of this design procedure.

A shear tab is a common type of simple shear connection used in steel construction (Fig. 5-1). The  $15^{th}$  edition of the AISC Steel Construction Manual [4] classifies this connection into conventional and extended types based on the distance between the support face and the vertical bolt line closest to the support; this is noted as the a distance in Fig. 5-1. If this distance is larger than 89 mm (3.5 in.), the connection is classified as an extended shear tab.

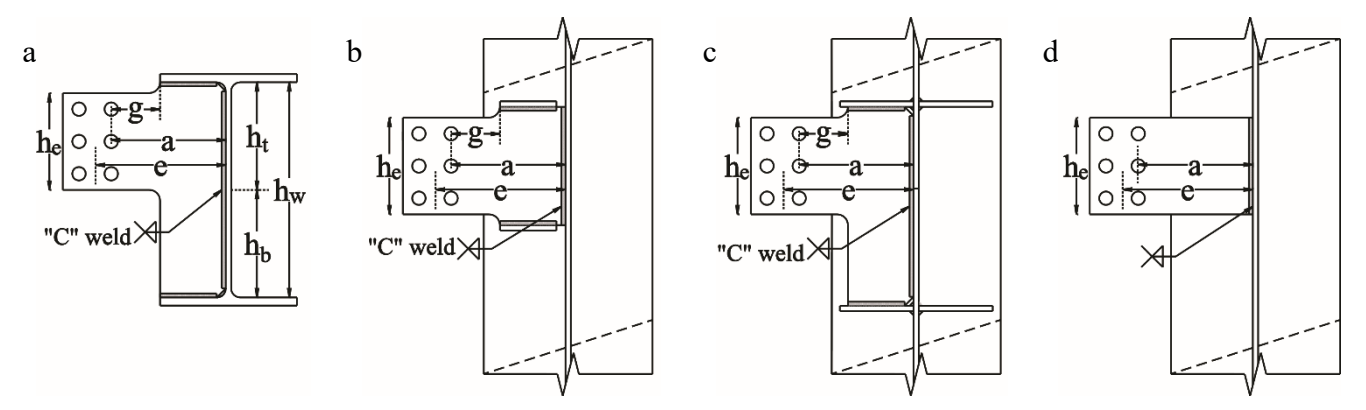


Fig. 5-1.Single-sided extended shear tab configurations: (a) stiffened beam-to-girder with full-depth shear plate (h<sub>w</sub> definition based on CSA-S16 [2]), (b) stiffened beam-to-column, (c) stiffened beam-to-column with continuity plates, (d) unstiffened beam-to-column

Extended shear tab connections are considered as a practical and economical solution to join a simply supported beam to a column or girder web. The long plate moves the bolts clear of the support; as such, access is provided to install the bolts, and also, there is no need for coping of the beam's flange(s). The extended shear tab is a common connection configuration. A full-depth stiffener detail can also be implemented in such a connection when so desired; designated as a "stiffened" configuration. The shear plate is shop-welded to the girder web and both flanges (Fig. 5-1a). In the case of a beam-to-column web connection (Figs. 5-1b and 5-1c), a similar detail can be achieved if the shear plate is welded to the column web and to two stabilizer plates, which in turn are welded to the column flanges. Although the stiffened extended shear tab connection has been used in steel construction in the USA and Canada, only a few recommendations [17, 18, 24, 25, 41] have been published for its design due to its rarity. The current AISC design approach for

extended shear tab connections [4] was developed for unstiffened connections (Fig. 5-1d). In this configuration, only the vertical edge of the plate is welded to the support; its horizontal edges are laterally unrestrained. Prior studies demonstrated that plate buckling is often the governing failure mode for stiffened full-depth configurations of either beam-to-girder [17, 24, 25, 41] or beam-to-column shear tab connections [18]. The focus of these research programs was limited to the single-sided configuration of stiffened extended shear tabs under gravity induced shear force.

Regarding the behaviour of stiffened extended shear tab connections under combined axial and shear forces, Thomas et al. [20, 21] focused on the single-sided configuration, similar to that shown in Fig. 5-1b. This configuration would need to be modified if continuity plates were incorporated into a fully restrained beam-to-column connection (Fig. 5-1c). In this case, the horizontal stiffeners (continuity plates) are placed along the beam flanges connected to the column's strong axis, which is usually much deeper than the simply supported beam connected to the column's weak axis. The top surface of the beams are typically specified to be at the same height, which would require the shear tab to be placed closer to the upper horizontal stiffener as shown in Fig. 5-1c. Thomas et al. [20, 21] determined the shear plate's out-of-plane deformation to be the critical failure mode of their ten tests, while acknowledging that the plate completely yielded prior to failure of the connection. In these tests, the specimens were subjected to a limited axial force range due to the relatively low stiffness of the column's weak-axis. Nevertheless stiffened extended shear tabs may experience large axial forces in real word applications; e.g. the double-sided configuration, which provides a load path to transfer axial force. Even the singlesided stiffened extended beam-to-girder shear tab may experience a large axial force, with lateral forces transferring to the supported concrete slab (diaphragm). Furthermore, the single-sided shear tab may resist large axial force due to wind load on the cladding of a building. Hence, the behaviour of stiffened extended shear tab connections should be evaluated under a wider range of axial force to provide information for engineers, who may be presented with the challenge of designing such a connection under combined axial and shear forces.

This paper presents the results of a coordinated experimental-numerical study aiming to deepen our understanding of the behaviour of the stiffened extended beam-to-girder shear tab under combined axial and shear forces. The full-scale connection tests allowed for an improved comprehension of the inelastic behaviour of the stiffened extended shear tab, and were used to validate the complementary finite element (FE) models. Based on the experimental and numerical results, probable failure modes and their influential parameters were determined. The current design practice was evaluated to improve this design approach for double-sided stiffened extended beam-to-girder shear tab connections with full depth shear plates.

# 5.2 Full-scale laboratory testing

Two full-scale connection specimens representing the current design practice in the USA and Canada were tested in the Jamieson Structures Laboratory at McGill University to examine the behaviour of stiffened extended shear tabs under combined axial and shear forces. These experiments were part of an extensive laboratory testing program [32, 42-46] aiming toward improving the current design and detailing provisions for shear tab connections. The test specimens were chosen to represent the double-sided configuration of a beam-to-girder extended shear tab connection with full-depth shear plates. The rationale behind choosing the double-sided configuration was its ability to provide a load path for pass-through forces, allowing the connection to experience a wide range of axial and shear forces. Therefore, a shear-axial force interaction curve could be developed in consideration of a shear tab's failure modes.

## **5.2.1** Description of test specimens

The specimens varied with respect to the number of rows of bolts lines and the dimensions of the shear plate, including its depth, length, and thickness (Fig. 5-2). The specimen ID, e.g. BG3-2-13-F-200C, identifies the following: BG stands for beam-to-girder configuration, 3 represents the number of rows of bolts, 2 shows the number of vertical bolt lines, 13 demonstrates the thickness of shear plate (mm), F indicates that a full-depth shear plate was used, and 200C represents the magnitude (200 kN) and direction (Compression) of the applied axial force.

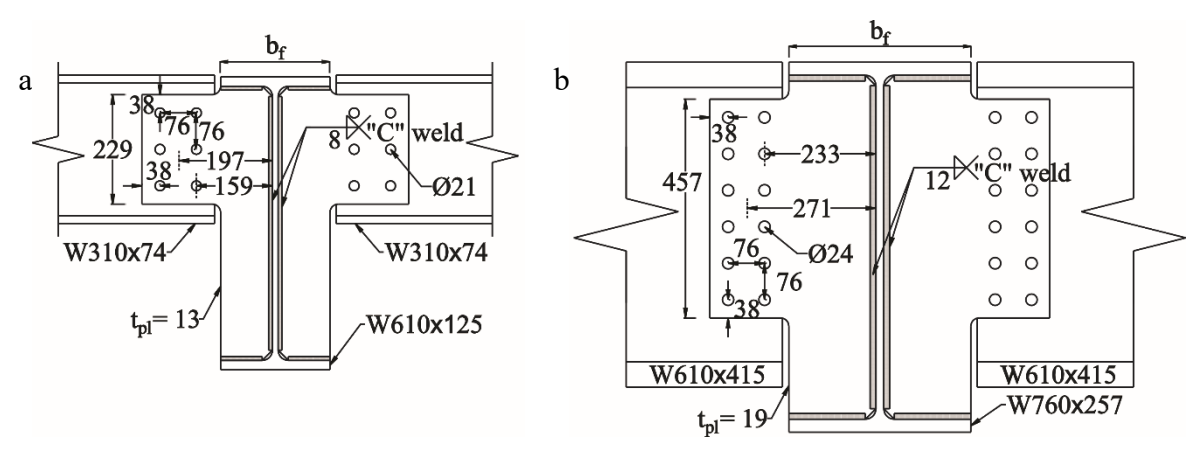


Fig. 5-2. Double-sided configuration of test specimens: (a) BG3-2-13-F-200C, (b) BG6-2-19-F-500C

In both specimens, the slenderness ratio ( $b_f/2t_{pl}$ ) of the shear plate satisfied the CSA-S16 compactness requirement [2] for plate girder stiffeners ( $200/\sqrt{F_y}=10.7$ ). However, this is not a requirement for the existing AISC design method [4] because local buckling is not a concern for an unstiffened extended shear tab. Prior studies [24, 25, 41] demonstrated the influence of the shear plate compactness on the ductile response of single-sided shear tab connections.

Considering the symmetry of a double-sided shear tab along the girder axis, the laboratory specimens consisted of only half of the girder and the shear tab connection on that side (Fig. 5-3). Prior research indicated that the behaviour of single- and double-sided shear tabs is different due to the distortion of the girder web [41]. To simulate one side of the girder two steel plates were

joined to the column flange using a complete joint penetration (CJP) weld. The plate dimensions were chosen to be representative of the half width of the girder flange. The shear plate was connected to the girder flanges, as well as to the column flange, through a fillet weld, which was detailed based on the requirements of the AISC Manual [4] for the weld of the extended shear tab. The in-plane displacement of the column was restricted using two back-braces, which were attached to the strong-floor of the laboratory as described in Section 5.2.2. These braces, in addition to the strong-axis stiffness of the column, provided a rigid support to the connection being tested and prevented all possible failure modes of the simulated girder.

Furthermore, the bottom flange of both test beams was coped to increase the beam-plate gap, and consequently delay beam binding, i.e. contact between the beam's bottom flange and the edge of the shear tab. Preliminary FE analyses suggested that these short copes would not affect the connection's global response, although the out-of-plane deformation of the beam and plate might increase slightly.

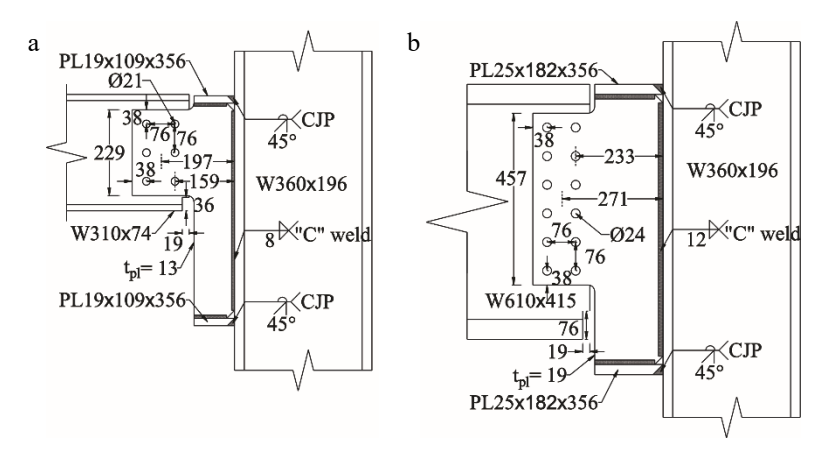


Fig. 5-3. Details of test specimens: (a) BG3-2-13-F-200C, (b) BG6-2-19-F-500C

The beams and girders were fabricated from ASTM A992 Grade 50 ( $F_y$  = 345 MPa) steel [47], while the shear plates were made of ASTM A572 Grade 50 ( $F_y$  = 345 MPa) steel [48]. To attach the shear tab to the fabricated supporting girder, an E71T electrode ( $X_u$  = 490 MPa) [49] was used

in a flux-cored arc welding process with additional shielding gas (CO<sub>2</sub>) to provide a fillet weld on both sides of the plate. Each beam was snug-tightened to the shear tab using ASTM F3125 Grade A490 bolts [34] in standard size holes, 2mm (1/16") larger in diameter than the bolts. Figure 5-4 shows these two specimens prior to testing.

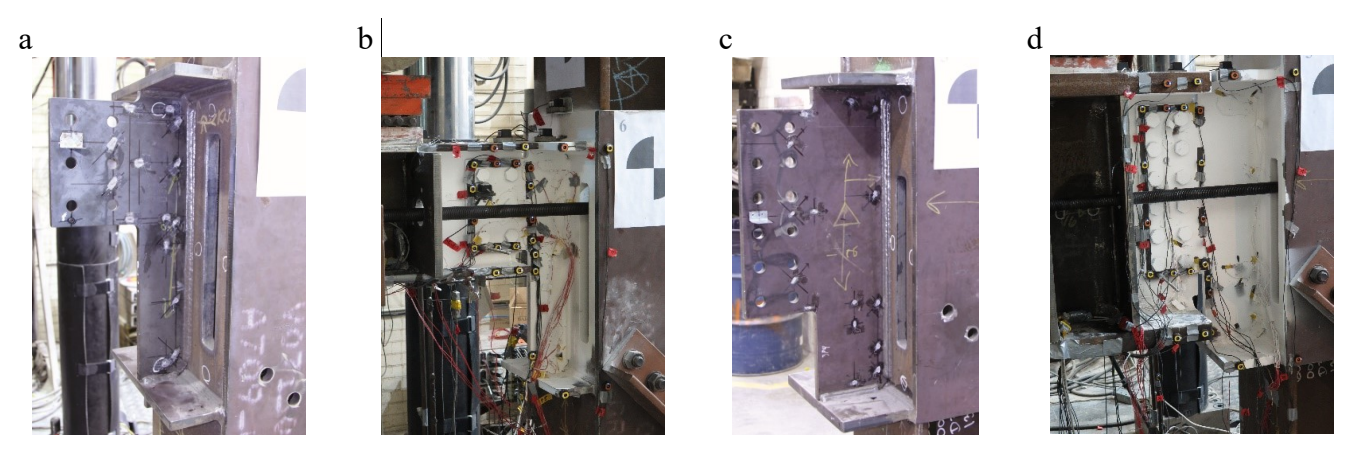


Fig. 5-4. Specimens: (a & b) BG3-2-13-F-200C, (c&d) BG6-2-19-F-500C

Table 5-1 shows the nominal and expected strength of the connection components, along with their measured material properties obtained by ancillary tests in the form of steel and all-weld tensile coupon tests. The test coupons of the shear plates and beams (including web and flanges) were extracted from the same batch of full-scale test components. For each beam, four coupons were cut from the flanges, while three were cut from the web. Six coupons were taken from each plate thickness, three along and three perpendicular to the grain direction.

Table 5-1. Material properties of connection components

Connection components		Nominal		Probable 1		Measured	
		F <sub>y</sub>	$F_{u}$	$F_{y}$	$F_{u}$	$F_{y}$	$F_{\rm u}$
		(MPa)	(MPa)	(MPa)	(MPa)	(MPa)	(MPa)
W310×74	Flange	345	448	379	493	374	490
$(W12\times50)$	Web	345	448	379	493	379	495
W610×415	Flange	345	448	379	493	372	513
$(W24 \times 279)$	Web	345	448	379	493	377	507
13mm (1/2") plates		345	448	379	538	432	508
19mm (3/4") plates		345	448	379	538	377	527
E71T electrode		400	490			548	620
A490 bolts		896	1034				

 $<sup>^{1}\</sup> R_{y}F_{y}\ and\ R_{T}F_{u}; for\ steel\ plates\ 1.1\ F_{y}\ and\ 1.2\ F_{u}\ while\ 1.1\ F_{y}\ and\ 1.1\ F_{u}\ for\ hot-rolled\ structural\ shapes\ [50]$ 

All steel coupons were tested based on ASTM A370 [51], except that the two all-weld coupons were tested based on AWS A5.20 [52]. All-weld coupons were extracted from a groove welded assembly of two plates, fabricated from the same electrodes used for the shear tab specimens [52, 53]. As neither bolt fracture, nor bolt deformation was observed in these tests, bolt shear tests were not conducted.

The connection specimens were designed based on the current AISC procedure [4] for unstiffened extended shear tabs. To calculate the capacity of the bolt group, the geometric eccentricity (e), i.e. the distance between the support face and the centre of the bolt group, was chosen as the bolt group eccentricity. As such, the bolt group was designed for the beam end shear reaction (V) and its eccentric bending moment (V × e). The effect of the axial force (P) was accounted by controlling the bolt group capacity for the resultant of the axial and shear forces (  $R=\sqrt{V^2+P^2}$  ) and the eccentric bending moment (V × e). The weld line was designed to concentrically resist the beam end reaction (R). To ensure sufficient ductility of the shear tab connection, the weld throat and the plate thickness were detailed such that yielding can develop over the full height of the shear plate's extended portion ( $h_e$  in Fig. 5-1) in advance of bolt shear fracture and weld tearing. The flexural buckling strength of the shear plate was calculated using both the current [4] and previous [28] versions of the AISC design method.

To address the higher probability of occurrence of shear plate instability, because of its large eccentricity, the latest AISC design method [4] can be used to estimate the shear tab's buckling strength based on the rectangular plate buckling model [1, 31]. Earlier editions [28] used models representative of the flexural buckling of a doubly coped beam [9, 27, 29]. To calculate the buckling strength, the distance between the girder web and the interior bolt line (a distance) was conservatively chosen to be the unbraced length of the shear plate. Both methods predicted that

buckling would not prevent the shear plate from reaching its fully plastic flexural capacity  $(M_p=F_yZ_p)$ . Regarding the shear tab design, the AISC Steel Construction Manual [4] considers the interaction of the shear and bending moment using an elliptical interaction equation (Eq. (5-1)). AISC Design Examples (Example IIA-19B) [15] and the Steel Connection Handbook (Section 2.5.3) [14] use Eq. (5-2) to calculate yielding strength of the plate due to the interaction of the bending moment, shear, and axial force. This equation was based on Eq. (5-1) and the design requirement of Section H1.1 of the AISC 360 Specification [1] for doubly symmetric members subjected to flexure and axial force.

$$\left(\frac{M}{M_{P}}\right)^{2} + \left(\frac{V}{V_{P}}\right)^{2} \le 1 \tag{5-1}$$

$$\left(\frac{P}{2P_{P}} + \frac{M}{M_{P}}\right)^{2} + \left(\frac{V}{V_{P}}\right)^{2} \le 1 \qquad \frac{P}{P_{P}} < 0.2$$

$$\left(\frac{P}{P_{P}} + \frac{8}{9} \frac{M}{M_{P}}\right)^{2} + \left(\frac{V}{V_{P}}\right)^{2} \le 1 \qquad 0.2 \ge \frac{P}{P_{P}}$$
(5-2)

Table 5-2 contains a summary of the calculated connection strengths corresponding to the probable failure modes. In addition to the design strength, the expected capacity of the connection was calculated based on the probable material properties of the steel plate (Table 5-1), whereas the nominal properties of the bolt and the welding electrode were implemented. Furthermore, the resistance factors ( $\phi$  factors) were excluded from the calculation of the connections' expected strengths. Referring to Table 5-2, bolt shear fracture was predicted to be the connections' governing failure mode in the calculation of the design and expected strengths. Although this prediction was in contrast with the findings from prior research [17, 18, 20, 21, 24, 25, 41], it should be noted that an aim of the AISC design method is to provide a reasonably conservative estimate of the connection's capacity, without requiring an overly complex design procedure. To

this end, the AISC calculated bolt group capacity is based on the geometric eccentricity (e), as depicted in Fig. 5-1.

In addition to the nominal and expected material properties, the measured properties of the beam, girder, plate, and weld (Table 5-1) were used to conduct these AISC-based calculations, whereas the nominal properties of the bolts were relied on in this process.

Table 5-2. AISC predicted strength of shear tab test specimens

	BG3-2-13-F-200C		BG6-2-19-F-500C			
Failure mode	Design strength (kN)	Expected strength <sup>1</sup> (kN)	Expected strength <sup>2</sup> (kN)	Design strength (kN)	Expected strength <sup>1</sup> (kN)	Expected strength <sup>3</sup> (kN)
Flexural-shear-axial yielding	254	329	365	991	1180	1171
Shear yielding of shear plate	616	678	761	1835	2018	1976
Bolt bearing	250	367	367	1137	1820	1725
Flexural buckling of shear plate	333	407	456	1351	1651	1616
Shear rupture at net section of shear plate	430	688	648	1207	1931	1824
Bolt shear	221	327	327	746	1105	1105
Weld tearing	1512	2016	2544	2657	3543	4505

<sup>&</sup>lt;sup>1</sup>Expected strength based on probable material properties i.e. $R_yF_y$  (1.1  $F_y$ ) and  $R_TF_u$  (1.2  $F_u$ ) for steel plates [50]

### 5.2.2 Test setup

The test setup (Fig. 5-5a) consisted of a 12 MN and a 445 kN hydraulic actuator, a lateral bracing system for the steel beam, supporting elements for the connection, and an axial load application system. The 12 MN actuator was located near the shear tab connection; it developed the main shear force in the connection. The 445 kN actuator, placed near the far end of the beam, facilitated the vertical displacement control of the beam tip, as well as the connection rotation. The lateral bracing system was installed to restrict the lateral displacement of the beam, without affecting its vertical displacement. The overall setup has been successfully used in prior research [24, 25, 32, 33, 42-46, 54].

 $<sup>^{2}</sup>$  Expected strength based on measured material properties i.e F<sub>v</sub>=432MPa and F<sub>v</sub>=508MPa for 13mm plate

<sup>&</sup>lt;sup>3</sup> Expected strength based on measured material properties i.e F<sub>v</sub>=377MPa and F<sub>v</sub>=527MPa for 19mm plate

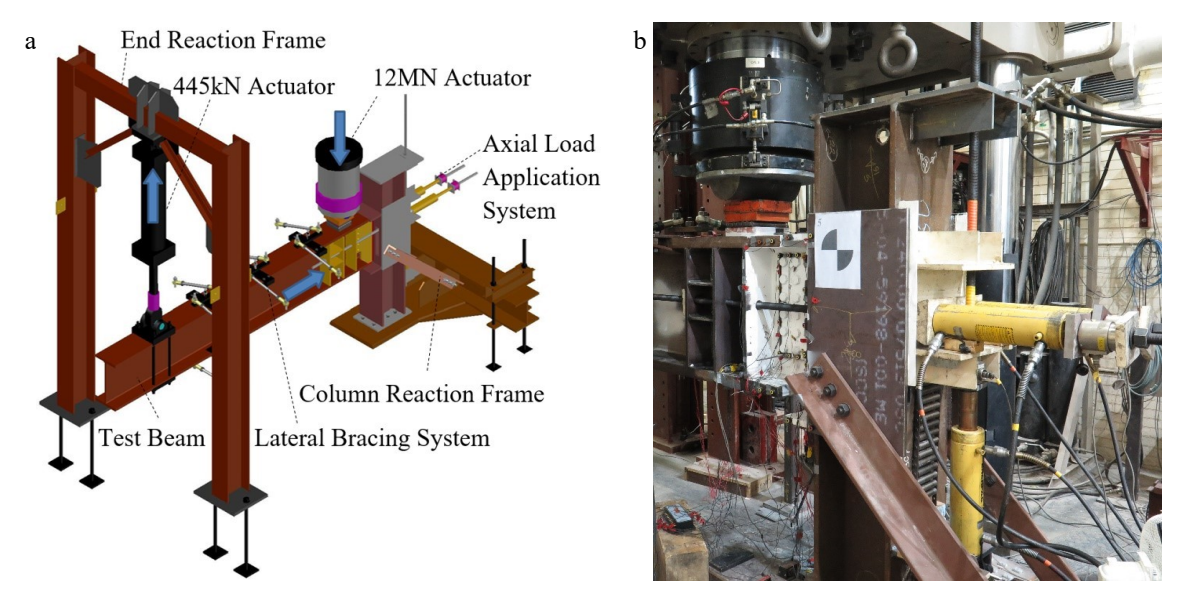


Fig. 5-5. Laboratory tests: (a) test setup, (b) axial load application system

The axial load application system (Fig. 5-5b) was used to maintain a constant axial force on the connection, while following the beam end rotation to maintain a force normal to the beam's cross-section. Slots on the column flanges allowed two threaded 31.8 mm (1 1/4") steel rods to pass through and transfer the axial load to a heavily reinforced region of the beam. Further, these rods passed through the moving plate and half cylinder, which allowed for control of the rods' rotation and vertical displacement, respectively. The axial force was generated by two horizontal Enerpac RRH-3010 hydraulic jacks, while the vertical displacement of the moving plate was controlled by a vertical 31.8 mm (1 1/4") steel rods pass through another similar Enerpac cylinder.

#### 5.2.3 Instrumentation

The implemented test setup was similar to that used in prior research [44], other than the beam lateral bracing system. The new bracing system provided enough free space to implement an optical Coordinate-Measuring Machine (CMM) for 3D measurement of the connection deformation at discrete points (Fig. 5-6a). Linear Variable Differential Transformers (LVDTs) were installed to measure the out-of-plane deformations as a backup of the optical CMM system

(Fig. 5-6b). Inclinometers measured the in-plane rotation of the beam, top girder flange, shear plate, and column. The out-of-plane rotations of the shear plate and beam were also measured. String potentiometers were used to measure the vertical deformation of the beam and shear plate, as well as the horizontal displacement of the column capping plate. To observe the yielding pattern of the connection, it was whitewashed and strain gauges were installed on the shear plate, beam web and flanges adjacent to the connection (Fig. 5-6c). Load cells were used to monitor the applied vertical and horizontal forces. Vishay Model 5100B scanners and the Vishay System 5000 StrainSmart software were used to record the measured data.

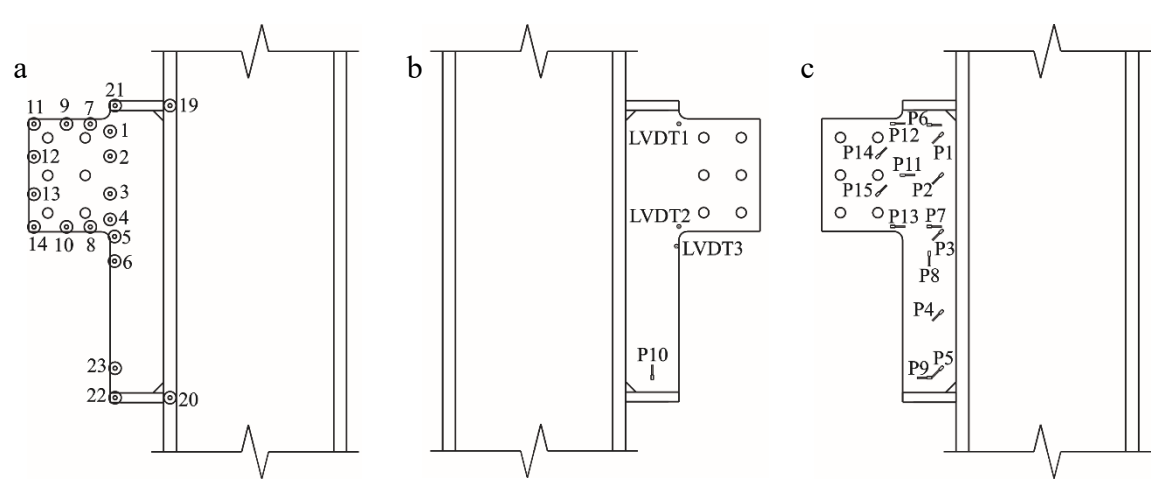


Fig. 5-6. Instrumentation of Specimen BG3-2-13-F-200C: (a) targets of optical CMM system, (b) LVDTs, (c) strain gauges

# 5.2.4 Loading protocol

The loading protocol was chosen to simulate the end demands of a simply supported beam when subjected to coupled axial and shear force demands. As such, each test specimen was first subjected to its service level of shear load, followed by the application of the axial force. From this point in the loading protocol, the axial force was kept constant, under load control, while the shear demand (deformation/rotation control) was increased until failure of the connection. Because previous research [44] suggested that prior to reaching the service shear load on the connection,

only local yielding of the shear tab is typically observed, the axial force was applied in advance of yielding onset based on real time monitoring of strain gauge data. For both specimens, axial force was applied at a connection rotation of approximately 0.0085 rad.

To replicate the rotational demand at the end of a simply supported beam under gravity induced shear force, 0.02 rad relative rotation between the beam and column was set as a target. This target rotation was achieved at the connection's probable shear resistance, which was calculated based on the expected material properties in lieu of measured ones, as coupons tests were conducted after the full-scale tests. The probable resistance was calculated according to the AISC design method with the resistance factors equal to one. This was deemed a rational approach based on prior research [33, 54]. To follow the loading protocol, the ratio between the displacement rates of the actuators was adjusted constantly up to the target rotation / load point; after reaching this level, the ratio between displacement rates of the actuators was held constant.

### 5.2.5 Experimental results

Figure 5-7 shows the response of both specimens versus the connection rotation, relative rotation between the beam and girder (i.e. the girder top flange). The measured connection shear force was normalized by the shear force corresponding to the plastic shear resistance of the plate's gross section (h<sub>e</sub> in Fig. 5-1), which is equal to 761 kN and 1976 kN for Specimens BG3-2-13-F and BG6-2-19-F, respectively.

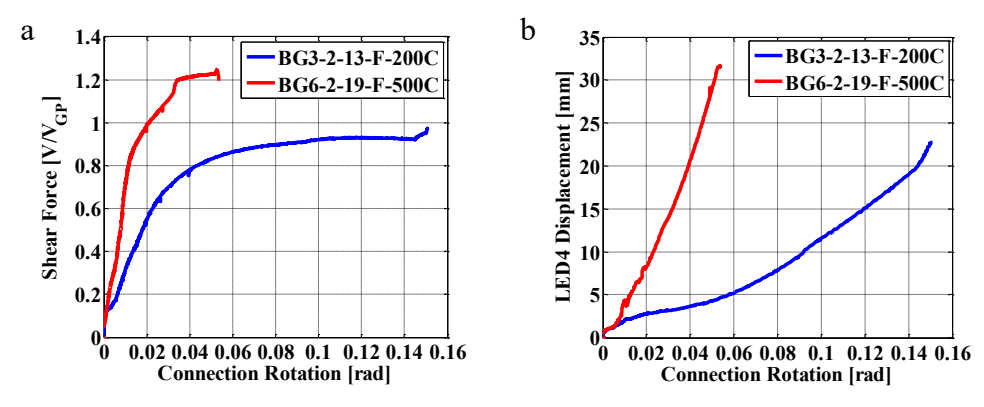


Fig. 5-7. Measured response vs. connection rotation: (a) connection shear force, (b) shear plate out-of-plane deformation

Referring to Fig. 5-8a, the axial load was applied to Specimen BG3-2-13-F-200C prior to yielding of the shear tab. Afterward, the extended portion of the shear plate started to yield along its bottom edge (Strain gauge 13 in Fig. 5-6c) where the compression stress was developed due to the combination of eccentric shear force and the axial compression. Then, plate yielding was observed along the interior bolt line (Strain gauges 14 and 15 in Fig. 5-6c). The top edge of the shear plate yielded after the bottom because the compression force counterbalanced a portion of the developed flexural tensile stress due to the eccentric shear. The connection stiffness reduced at 0.026 rad due to yielding of the extended portion of the shear plate.

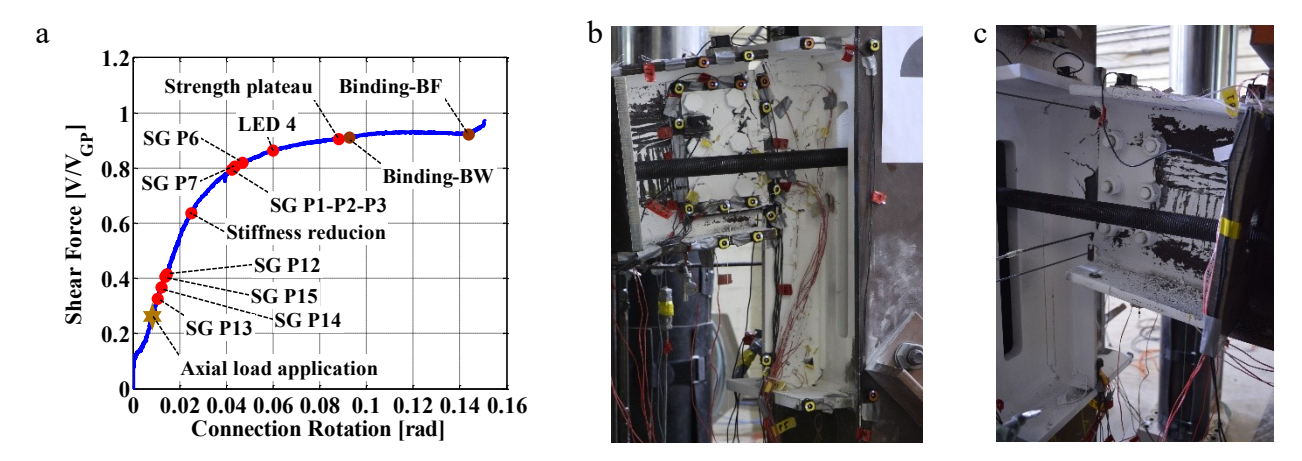


Fig. 5-8. Specimen BG3-2-13-F-200C: (a) damage propagation (SG: Strain Gauge experienced strain larger than yield strain), (b) deformed shape at strength plataeu (West view), (b) deformed shape at strength plataeu (East view)

The connection shear force still increased and yielding propagated toward the girder web at the upper portion of the stiffener. Strain gauges P6 and P7 indicated that there was flexural yielding due to the eccentric shear force. The stiffener strain gauges, installed adjacent to the girder web, demonstrated the non-uniform distribution of the shear force along the stiffener. Strain gauges P1, P2 and P3 reported yielding stress, while the recorded shear strain of strain gauges P4 and P5 was negligible. The connection stiffness decreased again when the slope of the curve representing the out-of-plane deformation of the plate bottom edge (LED4, Fig. 5-6a) largely increased. The connection shear force still increased, while the out-of-plane deformation of the plate increased. Following a shear strength plateau (Figs. 5-8b and 5-8c), binding between the shear plate and the bottom edge of the beam web slightly increased the shear resistance of Specimen BG3-2-13-F-200C. The test was terminated when the beam's bottom flange started to bind on the shear plate (Fig. 5-9a). The out-of-plane deformation of the shear plate was obvious at the end of the test (Figs. 5-9b to 5-9d). The two tested specimens responded similarly to the combined axial and shear forces other than the extent of the strength plateau, which was limited by binding at the bottom flange / stiffener interface in Specimen BG6-2-19-F-500C.



Fig. 5-9. Specimen BG3-2-13-F-200: (a) binding between beam and shear plate, (b-d) deformed shape at end of test

Through post-test examination, bolt bearing damage was evident along the interior vertical bolt line of both shear plates. Referring to Fig. 5-10, the bearing deformation was larger at the

upper portion of the plate where the tensile and shear stress developed simultaneously due to the applied bending moment and shear force, respectively.

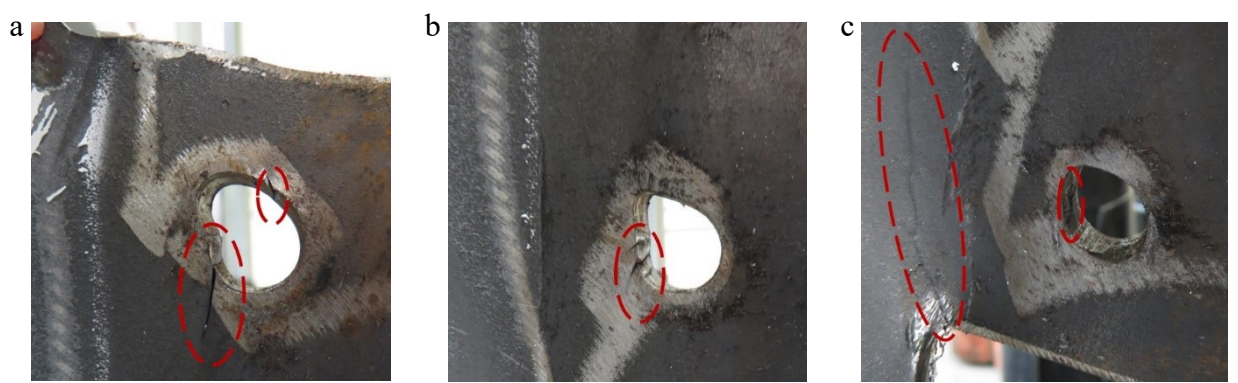


Fig. 5-10. Bearing deformation and fracture along the interior bolt line of specimen BG3-2-13-F-200C at: (a) top bolt hole, (b) middle bolt hole, (c) bottom bolt hole

In comparison to Specimen BG6-2-19-F-500C (Fig. 5-11), small fractures and more extensive bearing deformation were observed along the interior bolt holes in Specimen BG3-2-13-F-200C (Fig. 5-10). After unloading the specimens, a diagonal crack was observed at the bottom re-entrant corner of the shear plate (Figs. 5-10c and 5-11c). It is believed that this occurred due to the out-of-plane deformation of the shear plate and binding between the beam web and the shear plate.

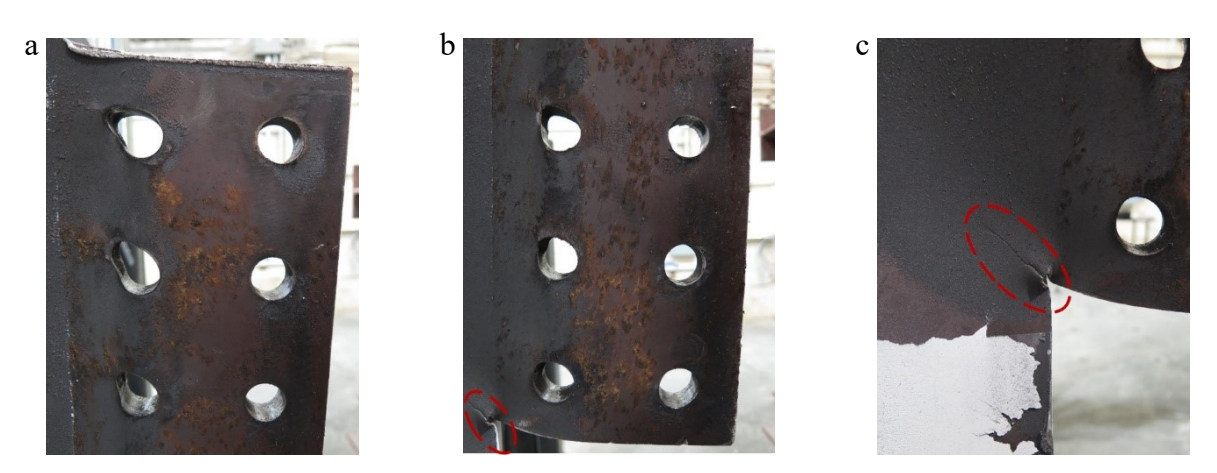


Fig. 5-11. Specimen BG6-2-19-F-500C: (a) bolt bearing at plate top half, (b) bolt bearing at plate bottom half, (c) diagonal crack at bottom re-entrant corner

A comparison was carried out of the predictions obtained using the current AISC design procedure for extended shear tab connections with the laboratory observations, even though this

Table 5-2, the current design method suggests that bolt shear fracture should be the governing failure mode. However, bolt fracture was not observed during the shear tab tests. Furthermore, no evidence of bolt deformation leading to fracture was observed through post-test examination. The connection stiffness started to decrease at a shear force which was much larger than the expected resistance corresponding to the flexural and shear yielding of the shear plate. These discrepancies can be explained by the fact that the current design method, which was developed for unstiffened extended shear tabs, relies on the geometric eccentricity (the *e* distance in Fig. 5-1) as the bolt group eccentricity. The complementary FE simulations (Section 5.3.2) showed that the bolt group eccentricity was shorter than the *e* distance because the inflection point formed far from the column face and the b, beyond the bolt group centre.

Although the use of the stabilizer plates significantly increased the connection capacity, the out-of-plane deformation of the shear plate started to increase rapidly when yielding propagated into the stiffened portion of the plate. This deformation would likely have been more severe if the shear plate had not satisfied the CSA-S16 compactness requirements [2] for the plate girder stiffeners. At this point in loading, a reduction of the connection stiffness was also observed. Of note, the out-of-plane deformation was the result of the combined compression and flexural moment of the shear tab, as demonstrated in subsequent FE analyses (Section 5.3).

In addition to the plate yielding, the bolt bearing contributed to the connections' ductility. Although the bearing deformation was quite large along the interior vertical bolt line of the shear plate, the connection resistance was not governed by the bearing resistance based on observations. The connection shear force became larger than the predicted strength corresponding to the net section fracture, while minor tearing around the bolt holes was observed only in Specimen BG3-

2-13-F-200C. This could be attributed to the compressive force influence and the inherent conservatism of the design equation for net section fracture. Furthermore, it was not possible to determine the connections' ultimate failure mode because binding between the beam web and shear plate changed the load transfer mechanism at the end of the test. Through subsequent finite element simulations that excluded the beam binding it was possible to extend the experimental load deformation curve and identify a conceivable ultimate failure mode (Section 5.3).

## 5.3 Complementary finite element simulations

Complementary finite element (FE) simulations were conducted to further understand the load transfer mechanism in stiffened extended shear tab connections subjected to coupled gravity and axial loads. Several parameters were studied that were not evaluated through the laboratory experiments, including the direction of the axial force. Furthermore, FE simulation was used to extrapolate from the experimental results and estimate the ultimate strength of the tested connections, which could not be observed in the experiments due to the beam binding. The FE models were developed in the commercial software ABAQUS-6.11-3 [23]. The features of the FE models were chosen to be representative of those seen in the laboratory experiments; including geometry, imperfections, boundary conditions, material properties, element size and element type, contacts and interactions, and the imposed loading protocol [41]. Because the initial position of each bolt in its hole could not be controlled in the laboratory tests, the bolts were placed at the centre of the bolt hole in the FE model, resulting in a 1 mm (1/32 in.) gap around the entire perimeter.

The employed material properties were defined based on true stress-strain curves of the various components shown in Fig. 5-12. Other than the bolt's characteristic response, the implemented stress-strain curves were obtained from the testing of tensile coupons. The bolts'

material properties were defined based on typical stress-strain curves reported in Kulak et al. [55], which were scaled to meet the minimum specified values for ASTM F3125 Grade A490 bolts [34]. Of note, the constitutive material models of all components were defined up to the ultimate strain.

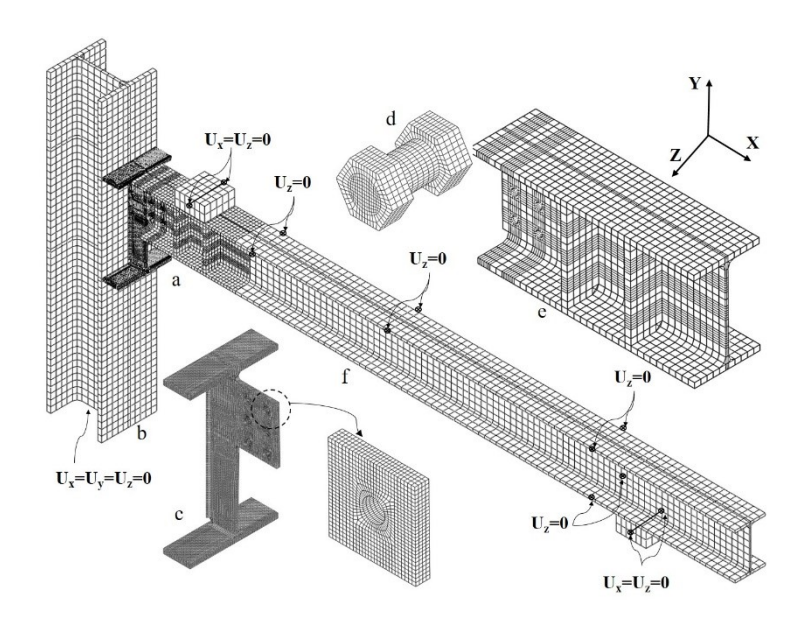


Fig. 5-12. Finite element model specifics: (a) overall model, (b) column mesh (typical element size of 40 mm), (c) shear plate mesh (typical element size of 3 mm), (d) bolt mesh (typical element size of 1.5 mm), (e) mesh of the beam in the vicinity of connection (typical element size of 20 mm), (f) beam mesh (typical element size of 40 mm)

First-order fully-integrated 3D solid elements (C3D8) were utilized to mesh the components. Based on a mesh refinement analysis, the element size (Fig. 5-12) was determined. The loading protocol was simulated by applying the displacements of the two actuators, recorded during the tests, to the centerline of the load cubes, while the horizontal  $(U_x)$  and out-of-plane  $(U_z)$  deformations of the load cubes' centerline were prevented. The lateral displacement of the beam flanges at the locations of the lateral braces was restricted. The column's supporting system was replaced by a fixed boundary condition at the column base to increase the computational efficiency of the FE model. The axial load application system was simulated by applying uniform compression  $(P_x)$  to the beam's stiffener while it was counterbalanced by applying opposite force to the column. Frictionless interaction was defined for surface-to-surface contact pairs between the

load cubes and the beam flanges. For all other components in contact, surface-to-surface contact pairs with a friction coefficient of 0.3 [1] were used to allow transmission of tangential force. The hard contact formulation, with the capability of separation after closure, was implemented to define the normal behaviour of all contact pairs. Both normal and frictional constraints were enforced using the stiffness method (penalty method). Instead of an infinite stiffness in the sticking phase of the contact, the penalty method assumed a finite stiffness to decrease computational cost and convergence issues. In other words, small slip (elastic slip) can occur between two surfaces even though they are in the sticking frictional state. The Abaqus default value for allowable elastic slip is 0.005 of the characteristic contact surface length, which is calculated in each increment. A value for the coefficient of friction (0.30) was chosen based on the AISC 360-16 specification. Furthermore, local instabilities of the shear tab connection were triggered by the introduction of local imperfections into the shear plate. These local imperfections, an estimate based on the connection bifurcation buckling, were proportioned to the limits of manufacturing tolerances for the web and flange of W-sections [5, 56, 57]. This approach has been successfully implemented in prior FE studies concerned with member and local instabilities [58]. Additional details of the FE model simulations can be found in [41].

#### 5.3.1 Model validation

To evaluate the accuracy of the numerical analyses, the predictions obtained from the FE model were compared with the experimental measurements, as shown in Fig. 5-13. The developed connection shear force and the out-of-plane deformation of the shear plate were chosen as the FE model verification criteria.

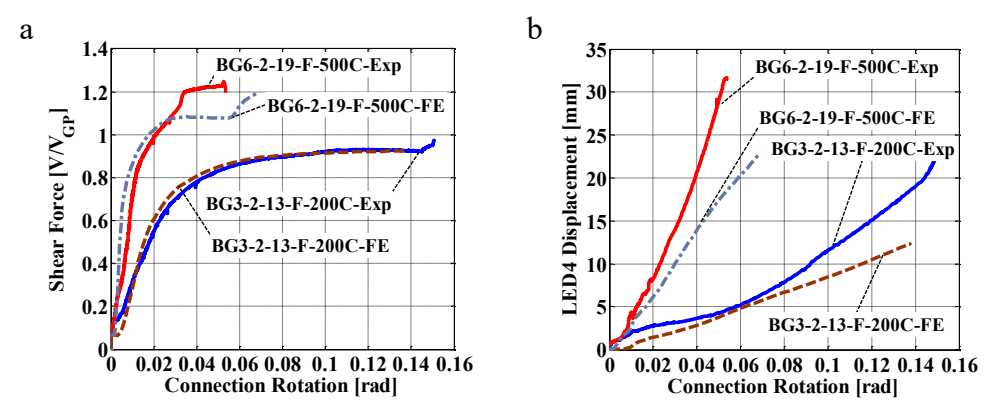


Fig. 5-13. FE model verification: (a) shear force, (b) shear plate out-of-plane deformation

Referring to Fig. 5-13, the FE model predicted reasonably well the connection response up to the point where the beam's web started bearing on the stiffened portion of the shear plate due to the out-of-plane deformations. The side binding between the beam web and the stiffened portion of the shear plate (Fig. 5-9a) occurred prior to beam flange binding. This side binding significantly increased the connection shear force in Specimen BG6-2-16-F-500C, while there were minor effects on Specimen BG3-2-13-F-200C (Fig. 5-13a). This discrepancy was due to the uncertainties related to the contact between the beam web's bottom edge and the shear plate. In addition to the fabrication tolerance and installation of the respective test specimens, these uncertainties arise because of the imperfections introduced into the FE model. The applied imperfections were an estimate based on the connection bifurcation buckling and allowable manufacturing tolerance of W sections. Of note, structural engineers typically neglect the over-strength in a connection due to beam binding because it is neither desirable nor dependable.

As a snug-tightened connection, the initial response of a shear tab connection depended greatly on the contact between shanks of the bolts and the bolt holes. As mentioned before, each bolt was placed conservatively at the centre of its bolt hole in the FE model; the initial contact conditions of the bolts in the laboratory test specimens may been different from those assumed for the FE

model. Due to this discrepancy, the predictions of the connection shear force obtained from the FE model deviated from the test measurements in the initial increments of the applied loading.

#### 5.3.2 Simulation results

Figures 5-14 and 5-15 show the normalized predictions of the FE models. Referring to Figs. 5-14a and 5-15a, the shear force along the outer end of the shear plate's re-entrant corners was normalized based on the plastic shear resistance of the gross section ( $V_{GP} = 0.6F_yA_g$ ), while the plate's plastic shear resistance of the net section ( $V_{NP} = 0.6F_yA_{net}$ ) was implemented to normalize the shear force along the bolt line (Figs. 5-14b and 5-15b). The plastic bending moment resistance of the gross section ( $M_{GP} = F_yZ_g$ ) was used to normalize the bending moment at the plate's gross section, as shown in Figs. 5-14c and 5-15c. The bending moment along the plate's interior bolt line (Figs. 5-14d and 5-15d) was normalized based on the flexural capacity of the plate's net section ( $M_{NP} = F_yZ_{net}$ ). The plastic section modulus was defined for an odd number of bolt rows as  $Z_{net} = 1/4t_{pl}(s-d_h)(n^2s+d_h)$ , while  $Z_{net} = 1/4t_{pl}(s-d_h)(n^2s)$  was used for an even number bolt rows [59]. In these equations, n=number of rows of bolts, s=bolt spacing,  $d_h=$ diameter of bolt hole,  $d_p=$ plate thickness, and  $d_p=$ plate depth. The aforementioned plastic capacities of the shear plate, shown in Table 5-3, were calculated based on its measured dimensions and yield stress.

Table 5-3. Calculated plastic capacities of shear tab test specimens

Specimens	BG3-2-13-F	BG6-2-19-F	
$P_{GP} (F_y A_g = F_y d_{pl} t_{pl})$	1268 kN	3294 kN	
$P_{NP} (F_y A_{net} = F_y (d_{pl} - nd_h) t_{pl})$	950 kN	2331 kN	
$V_{GP} (0.6F_y A_g = 0.6F_y d_{pl} t_{pl})$	761 kN	1976 kN	
$V_{NP} (0.6F_y A_{net} = 0.6F_y (d_{pl} - nd_h)t_{pl}$	) 570 kN	1398 kN	
$M_{GP} (F_y Z_g = F_y t_{pl} d_{pl}^2 / 4)$	72.5 kN.m	376.5 kN.m	
$M_{NP} (F_y Z_{net})$	54.0 kN.m	256.8 kN.m	

Regarding Specimen BG3-2-13-F-200C, a comparison between the normalized shear flow and the connection rotation (Figs. 5-14a and 5-14b) demonstrates that only a fraction of the connection shear force was transferred through the net section along the centerline of the bolt holes, i.e. the critical section with the smallest cross-sectional area along the plate. Referring to Fig. 5-14a, Specimen BG3-2-13-F-200C experienced a connection shear force equal to 614 kN (V/V<sub>GP</sub> =0.81) at 0.04 rad rotation, while the net section was subjected to only 463 kN shear force ( $V_n/V_{NP}$  =0.81 in Fig. 5-14b). Figures 5-15a and 5-15b show a similar trend for Specimen BG6-2-19-F-500C. This observation, which coincided with prior research studies [22], was due to the bearing mechanism between the bolt shanks and the bolt holes, which is further elaborated in Section 4.2. A larger bending moment developed at the gross section (Figs. 5-14c and 5-15c) in comparison to the net section (Figs. 5-14d and 5-15d) because the inflection point (Figs. 5-14e and 5-15e) formed far from the column face, away from the centroid of the bolt group.

To evaluate the influence of the axial load on the observed connection behaviour and failure modes, additional FE analyses were carried out for each specimen. Only gravity-induced shear force was applied to the connection in the first FE analysis (models BG3-2-13-F and BG6-2-16-F), while the connection was subjected to combined tensile and shear forces in the second. These FE models were subjected to the same loading protocols imposed in the experimental program; to maintain simplicity, the magnitude of the tensile force in the analysis was set equal to the magnitude of the compression force used during testing (BG3-2-13-F-200T and BG6-2-16-F-500T).

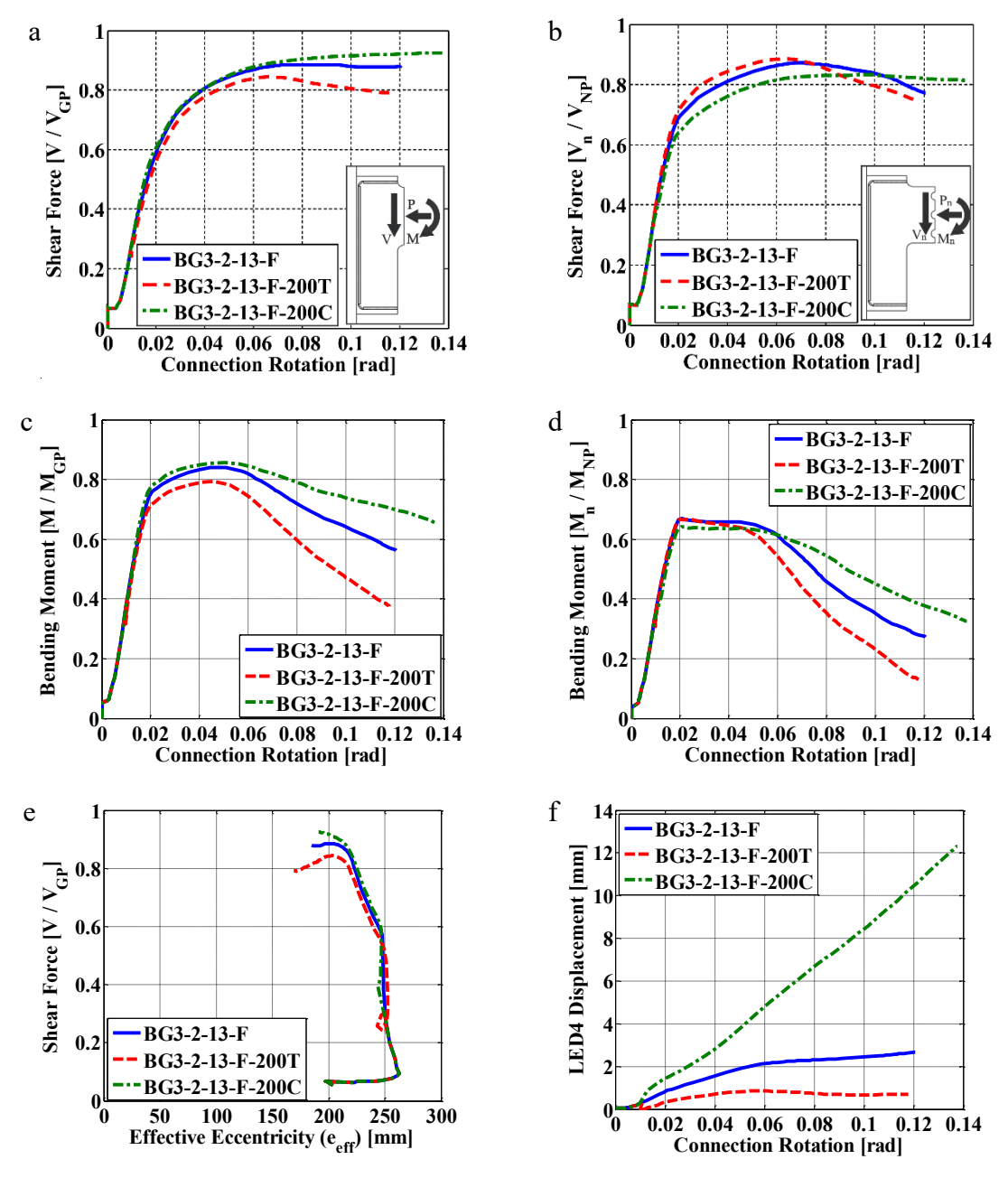


Fig. 5-14. Simulated response of Specimen BG3-2-13-F: (a) connection shear force, (b) net section shear force, (c) gross section bending moment, (d) net section bending moment, (e) effective eccentricity, (f) plate out-of-plane deformation

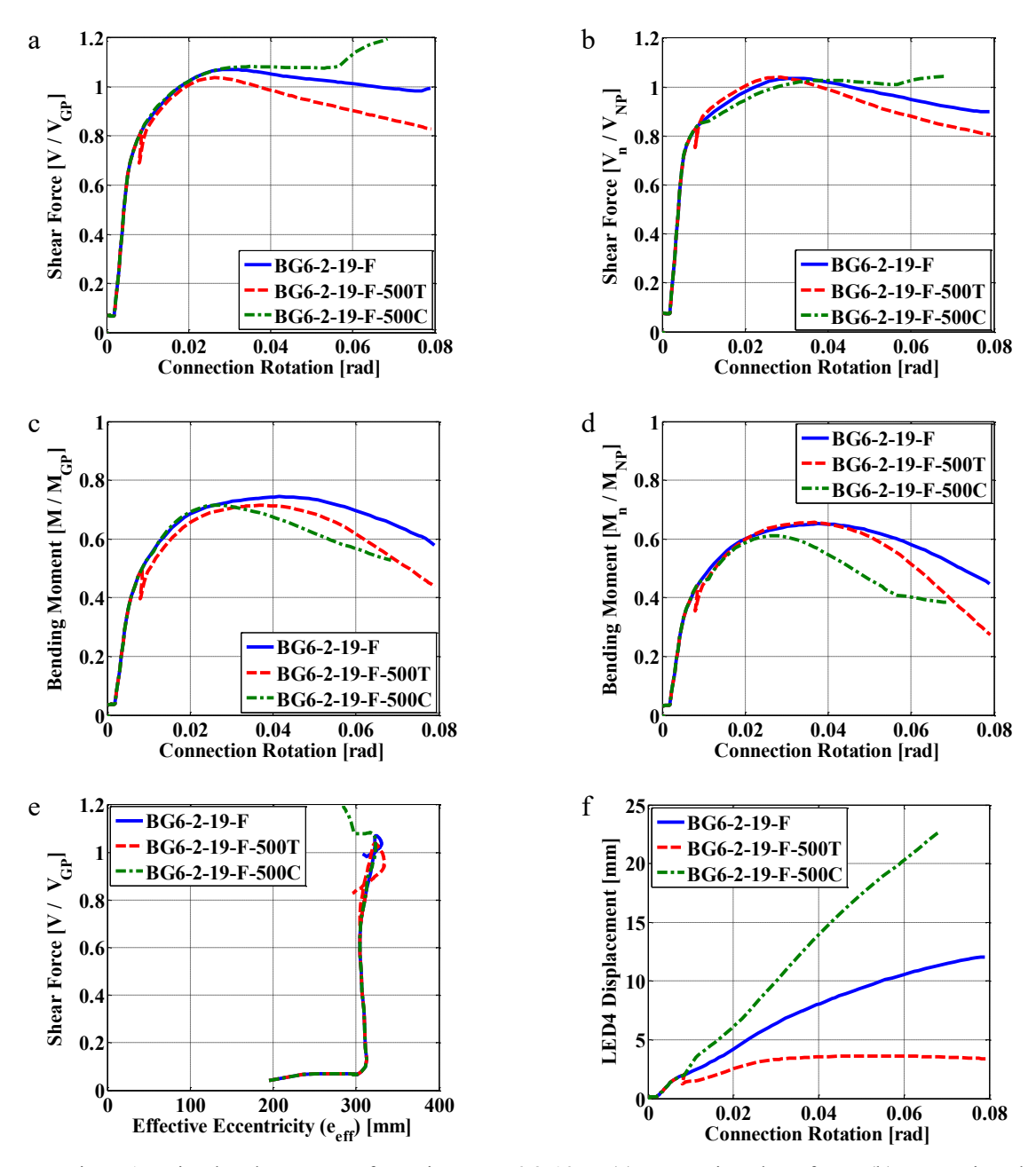


Fig. 5-15. Simulated response of Specimen BG6-2-19-F: (a) connection shear force, (b) net section shear force, (c)gross section bending moment, (d) net section bending moment, (e) effective eccentricity, (f) plate out-of-plane deformation

In all FE models, gross and net section yielding of the shear plate were observed and the net section fracture along the plate interior bolt line was determined as the connection's ultimate failure mode. Of note, the capability of this simulation procedure to capture the net section fracture was verified. The FE models, developed based on this simulation procedure, replicated accurately

the ultimate strength of unstiffened extended shear tabs, which ultimately failed due to net section fracture. The details and verification of this simulation procedure can be found in [60]. Referring to Figs. 5-14 and 5-15, the axial force affected the connection's response slightly because the level of the applied axial load was small ( $P/P_{GY}=0.16$  and 0.15 for Specimens BG3-2-13-F and BG6-2-19-F, respectively).

#### 5.4 Discussion

### 5.4.1 Shear plate yielding

Referring to Fig. 5-16, Neal's interaction equation [40] was used to account for the interaction of axial, shear, and flexural loads at the plate gross and net sections. It was observed that the results of Neal's [40] and the AISC interaction equations [4] (Eqs. (5-3) and (5-4), respectively) were almost equal in the range of this study. Of note, Astaneh [61] proposed Eq. (5-4) as a simplified version of Neal's interaction equation, which later was incorporated into the AISC Steel Construction Manual [4] for the rectangular connecting element under in-plane loading. Equations (5-3) and (5-4) were more accurate as compared to Eq. (5-2), although this equation resulted in conservative predictions for the connection resistance corresponding to the yielding of the gross section.

$$\left(\frac{M}{M_P}\right) + \left(\frac{P}{P_P}\right)^2 + \left(\frac{(V/V_P)^4}{1 - (P/P_P)^2}\right) \le 1$$
(5-3)

$$\left(\frac{M}{M_{P}}\right) + \left(\frac{P}{P_{P}}\right)^{2} + \left(\frac{V}{V_{P}}\right)^{4} \le 1$$
 (5-4)

The behaviour of the FE model of connections BG3-2-13-F-200C and BG6-2-19-F-500C was similar to the test specimens. Yielding began from the re-entrant corners of the shear plate, then propagated toward the interior bolt line. The FE models showed that the connection stiffness

slightly decreased when a large portion of the shear plate along the interior bolt line yielded. The full depth of the shear plate along the net section yielded after yielding of the gross section of connection BG3-2-13-F-200C, while they occurred at the same time for connection BG6-2-19-F-500C. Following the yielding of the shear plate, its out-of-plane deformation increased. Furthermore, the FE models demonstrated that the net section fracture would determine the connection's ultimate strength in the absence of beam binding. To further illustrate this point, the maximum equivalent plastic strain (PEEQ) developed at the bottom re-entrant corner and at the bolt holes of the plate's upper portion is shown in Fig. 5-17.

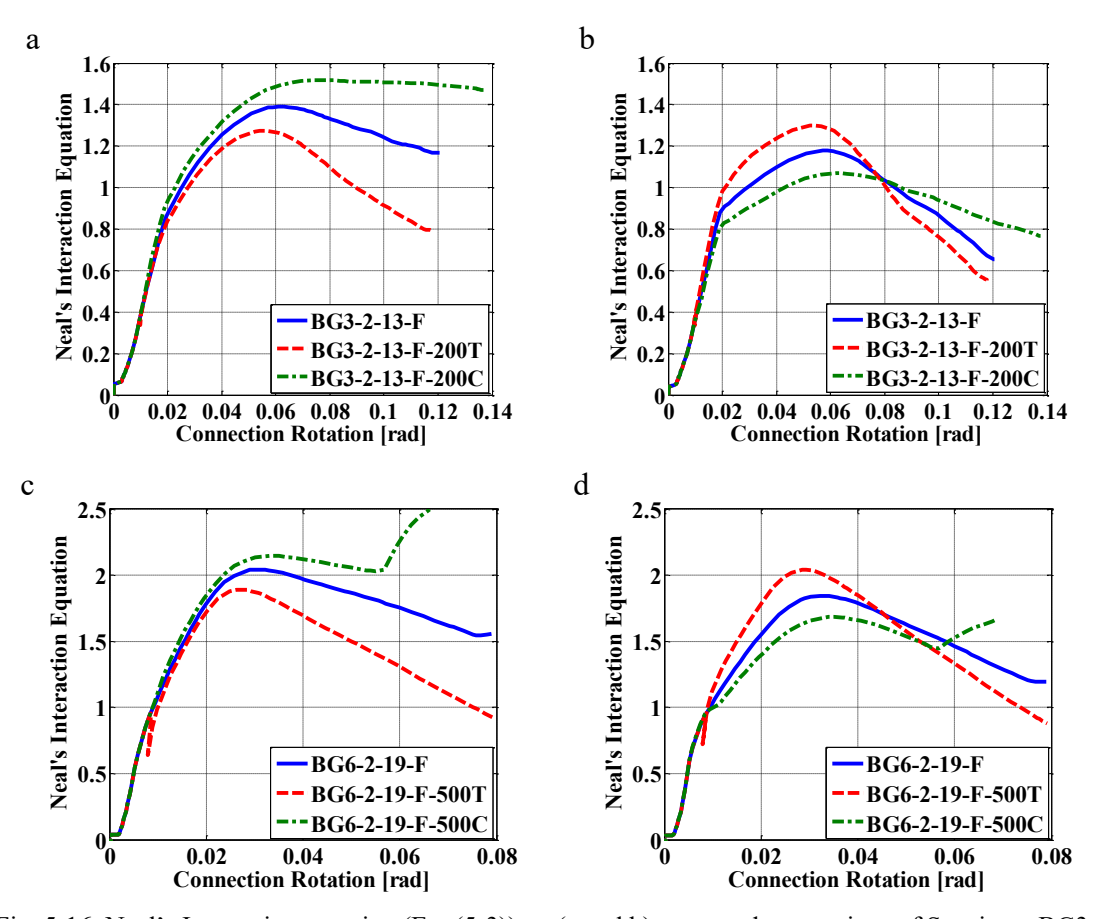


Fig. 5-16. Neal's Interaction equation (Eq. (5-3)) at: (a and b) gross and net sections of Specimen BG3-2-13-F, respectively, (c and d) gross and net sections of Specimen BG6-2-19-F, respectively

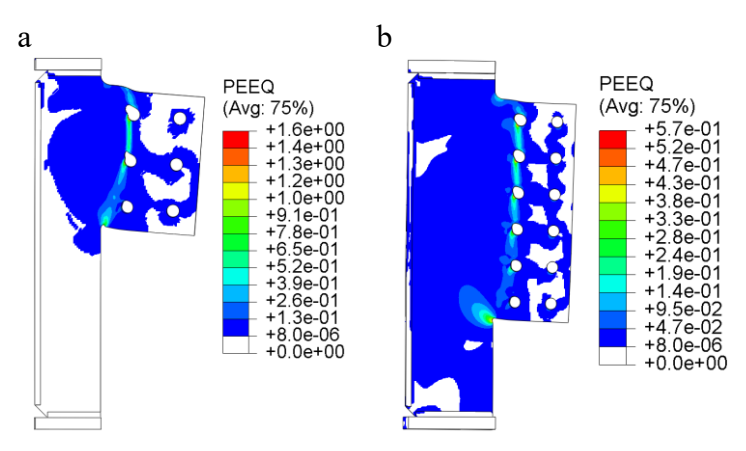


Fig. 5-17. Shear plate equivalent plastic strain (PEEQ) corresponding to the net section fracture at: (a) BG3-2-1-13-F-200C, (b) BG6-2-1-9-F-500C

### 5.4.2 Shear plate internal forces along the interior bolt line

Referring to Table 5-3, the plate's plastic shear resistance at the net section ( $V_{NP}$ ) is a fraction ( $A_{net}/A_g$ ) of its plastic shear resistance at the gross section ( $V_{GP}$ ). However, Figs. 5-14 and 5-15 show that the  $V/V_{GP}$  ratio was larger than  $V_n/V_{NP}$ . This observation demonstrates that the net section, the section along the bolt line centerline, was subjected to only a portion of the connection shear force. Furthermore, applying the axial force changed the shear demand at the net section (Figs. 5-14b & 5-15b). To clarify this fact, the net section's shear and axial forces ( $V_n$  and  $P_n$  in Fig 5-14b, respectively) were compared with corresponding values from the gross section of the plate (Fig. 5-18). Referring to Figs. 5-18a and 5-18b, the tensile force increased the ratio between the shear force at the net and gross sections, while the compression force decreased it. Referring to Figs. 5-18c and 5-18d, the axial force along the net section was compared with the applied axial force ( $P_a$ ), 200 kN and 500 kN for connections BG3-2-13-F and BG6-2-19-F, respectively. In comparison to the tensile force, the net section was subjected to a smaller portion of the applied axial force in the presence of the compression force. Furthermore, Figs. 5-18c and 5-18d show that the tensile force was developed along the net section even under gravity-induced shear force.

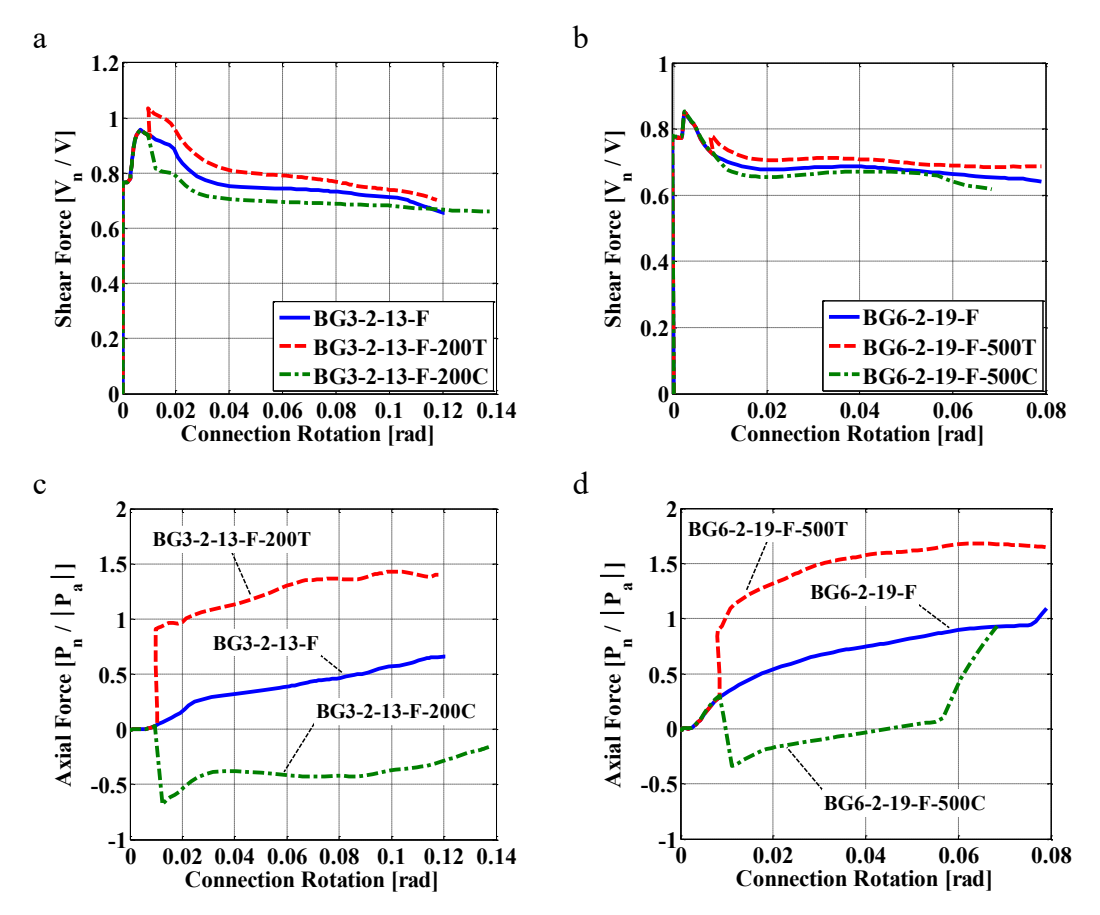


Fig. 5-18. FE model predictions for: (a) shear force of BG3-2-13-F models, (b) shear force of BG6-2-19-F models, (c) Axial force of BG3-2-13-F models,(d) Axial force of BG6-2-19-F models (|Pa| is the magnitude of the applied axial force, 200 kN and 500 kN for connections BG3-2-13-F and BG6-2-19-F, respectively; Pn and Vn stand for the axial and shear demands along the plate net section, respectively)

The bearing mechanism between the bolt shanks and the bolt holes was further studied to explain the reasons for the aforementioned observations. Figure 5-19a shows the bolt group, which was subjected to the eccentric shear force. In addition to the vertical shear force, a horizontal force was developed in the top and bottom bolts due to the eccentric shear force and its consequent bending moment. Referring to Fig 5-19b, the horizontal force moved the top bolt away from the centerline of the bolt hole, while the bottom bolt moved closer to the support.

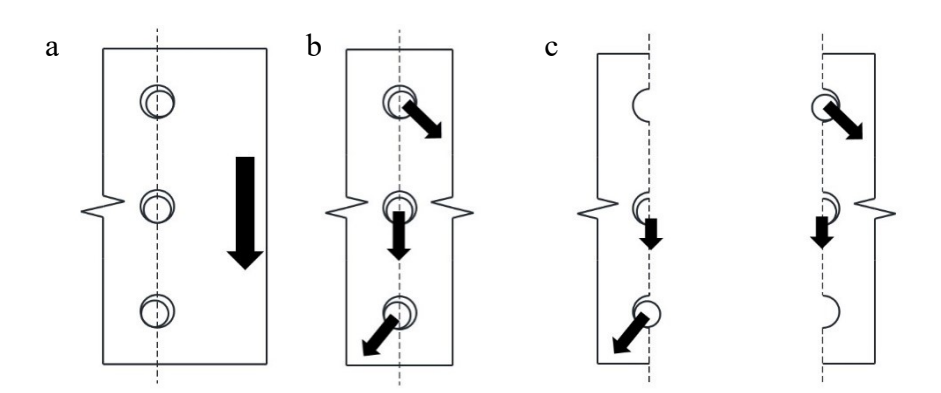


Fig. 5-19. Bolt group under an eccentric shear force, (a) applied shear force, (b) resultant force at each bolt due to the applied eccentric shear force, (c) the distribution of the resultant force along the bolt line centerline

The middle bolt (Fig. 5-20a) transferred a shear force to the plate while it was placed along the centerline of the bolt hole. Therefore, half of the bolts' shear force was transferred through the net section. In the presence of the tensile force (the top bolt), the net section was subjected to a larger portion of the shear and axial forces as the bolt moved away from the support and crossed the bolt line centerline (Fig. 5-20b). Therefore, the horizontal force of the top bolt subjected the net section to the tensile force (Fig. 5-19c). That was the reason behind development of an extra tension in Figs. 5-18c and 5-18d. In contrast, an applied axial compression force pushed the bottom bolt toward the support (Fig. 5-20c) and the net section resisted a smaller component of the shear and axial force. This observation is used in Section 6.3.9 to provide detailed design recommendation for shear plate yielding and rupture along the interior bolt line.

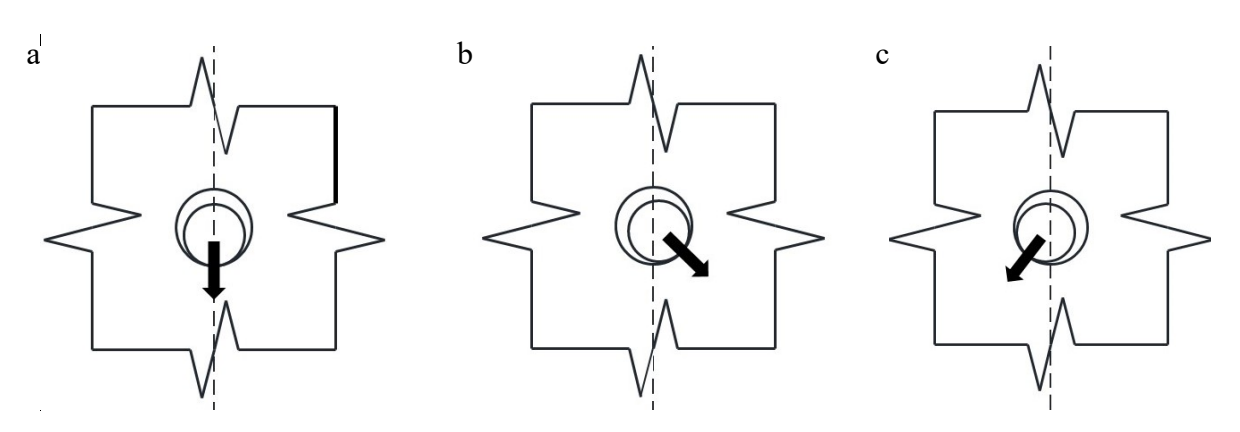


Fig. 5-20. Bolt under: (a) shear force, (b) shear and tension, (c) shear and compression

#### 5.4.3 Effect of axial force

Referring to Figs. 5-14a and 5-15a, the axial tensile force decreased the ultimate shear resistance of the connection, while the axial compression force increased it. This occurred because the tensile force increased the force demands on the interior bolt line of the shear plate, while the compression force decreased those demands (Figs. 5-14b and 5-15b). Then, the tensile force hastened the onset of the connection's ultimate failure mode, i.e. net section fracture of the shear plate, while the axial compression force delayed the onset of this failure mode. The same observations held true for the connection resistance corresponding to the net section yielding. Referring to Table 5-4, the tension force caused the net section yielding to precede the gross section yielding. However, the difference between the yielding strength of the net and gross sections was small; hence, the connection could still resist much larger shear after the gross section yielding. In addition to the axial force, the ratio between the gross and net section areas affected the yielding sequence of the gross and net sections. In model BG3-2-13-F, the net section yielded shortly after the gross section, while they occurred at the same time in the BG6-2-19-F model. The aforementioned ratio, A<sub>net</sub>/A<sub>g</sub>, was equal to 0.73 and 0.69 for Specimens BG3-2-13-F and BG6-2-19-F, respectively.

Table 5-4. FE model predictions for connection resistance

		BG3-2-13-F	1		BG6-2-19-F	1
Axial Load	200C	0	200T	500C	0	500T
Failure mode	Measured strength (kN)	Measured strength (kN)	Measured strength (kN)	Measured strength (kN)	Measured strength (kN)	Measured strength (kN)
Gross section yielding	507	518	517	1674	1676	1631
Net section yielding	631	545	450	1767	1676	1544
Out-of-plane deformation	662			1995	2021	
Net section fracture	688	666	634	2120	2103	2046

Referring to Figs 5-14f and 5-15f, the axial compression force increased the plate's out-ofplane deformation, while the tension force decreased it. This observation suggested that the compression could trigger the shear plate buckling and change the connection's ultimate failure mode, especially in the case of a slender shear plate or larger compressive force.

### 5.4.4 Evaluation of the current design procedure

Various failure modes were observed in the studied connection configurations, both tested and numerical, including the gross and net section yielding of the shear plate, the shear plate out-ofplane deformation, and the net section fracture. Of note, the shear plate yielded at its gross and net sections because of the interaction of moment, shear and axial force. Referring to Table 5-5, to evaluate the accuracy of the current AISC design method [2], the results obtained from it were compared with those determined from the laboratory measurements and the FE model. The accuracy of the design method improved if the geometric eccentricity was replaced with the measured eccentricity corresponding to the gross section yielding of the shear plate. Furthermore, the current design method correctly predicted the governing failure mode when the measured eccentricity was implemented. Of note, the AISC design method [2] allows one to design the bolt group based on an alternative eccentricity, obtained from a rational procedure. In this case, the supporting member should be designed for the effect of shear force at the same alternative eccentricity. Referring to Table 5-5, Eq. (5-2) resulted in a conservative estimate of the momentshear-axial force yielding of the shear plate gross section. The accuracy of this prediction could be increased if Eqs. (5-3) and (5-4) were implemented in lieu of Eq. (5-2). Based on Eqs. (5-3) and (5-4), the shear plate gross section of connections BG3-2-13-F-200C and BG6-2-19-F-500C yielded at a connection shear force equal to 496 kN and 1642 kN, respectively. Furthermore, the current design procedure might significantly overestimate the buckling strength of connection

BG6-2-19-F-500C, because it neglects the detrimental effects of the axial and shear forces on the plate's flexural capacity. To address this issue, Dowswell & Whyte [28] used Eq. (5-3) to determine the available flexural buckling strength in the presence of the shear and axial forces. If this advice was taken for the test specimens, the buckling strength of the extended portion of the shear plate would be equal to the applied force corresponding to the gross section yielding of the shear plate. Notably, the 15<sup>th</sup> edition of the AISC Steel Construction Manual [2] introduced the simplified form of Neal's interaction equation (Eq. (5-4)) to consider the interaction of in-plane loads for a rectangular connecting plate. To calculate the weld group capacity under an eccentric shear force, the Instantaneous Centre of Rotation (ICR) method was implemented for the C-Shape weld group, while only the vertical weld lines were considered in the calculation of the weld group capacity under a concentric shear force.

Table 5-5. Connection resistance to different failure modes

	BC	3-2-13-F-20	00C	В	G6-2-19-F-5	Measured strength (kN)  1674  1976 3  1995 <sup>5</sup> 2120		
Failure mode	Expected strength <sup>1</sup> (kN)	Expected strength <sup>2</sup> (kN)	Measured strength (kN)	Expected strength <sup>1</sup> (kN)	Expected strength <sup>2</sup> (kN)	strength		
Plate moment-shear-axial force yielding	365	$452^{3}$	507	1171	1621 <sup>3</sup>	1674		
Plate Shear yielding	761	761		1976	1976	1976		
Bolt bearing	367	965	3	1725	4204	3		
Plate flexural buckling	456	$625^{4}$	$662^{5}$	1616	$2885^{4}$	$1995^{5}$		
Shear rupture at net section of shear plate	648	648	687	1824	1824	2120		
Bolt shear	327	858	>687	1105	2743	>2120		
Weld tearing	2544	$2334^{6}$		4505	$4777^{6}$			

<sup>&</sup>lt;sup>1</sup>Expected strength based on geometric eccentricity (e)

Among the observed failure modes, the gross section yielding of the shear plate occurred earlier under a smaller shear force. Furthermore, other failure modes occurred when the connection

<sup>&</sup>lt;sup>2</sup>Expected strength based on measured eccentricity

<sup>&</sup>lt;sup>3</sup>Although large bearing deformation was observed, bearing failure did not occur

<sup>&</sup>lt;sup>4</sup>Flexural buckling strength of the extended portion of the shear plate

<sup>&</sup>lt;sup>5</sup> Shear resistance corresponding to the shear plate out-of-plane deformation

<sup>&</sup>lt;sup>6</sup>Strength of C-shape weld group

underwent large deformation and rotation, which negatively affected the supported beam's serviceability. Therefore, the moment-shear-axial force yielding of the shear plate's gross section should be considered as a conservative estimate of the connection's capacity. In the presence of the axial tensile force, yielding of the net section preceded yielding of the gross section (i.e. BG3-2-13-F-200T and BG6-2-19-F-500T). However, the yield strength of the gross section was still a conservative estimate of the connection's capacity because the difference between the yield strength of the gross and net sections was small and the connection was able to resist a much larger shear force.

#### 5.5 Conclusions

Two full-scale specimens were tested to deepen our understanding of the behaviour of the double-sided configuration of the full-depth extended beam-to-girder shear tab under coupled gravity and axial force demands. The test specimens were constructed of different features, including shear plate dimensions, bolt size, bolt group configuration, geometric eccentricity, beam and girder sizes. Furthermore, finite element models, which were validated up to web and flange binding, were adopted to investigate the dependency of the connection's behaviour on critical parameters including the axial force direction and the force distribution along the plate net section. The main findings of the paper are summarized as follows:

- The double-sided configuration of the full-depth extended beam-to-girder shear tab yielded through its net section along the bolt line, the closest to the girder. Furthermore, the gross section yielding of the shear plate occurred along the outer end of its re-entrant corners.
- The net section fracture was determined as the ultimate failure mode of the studied connections.
- The net section along the centerline of the plate's interior bolt line was subjected to a portion of the connection axial and shear forces. This amount depended on the number of vertical bolt lines, bolt hole

diameter, the distance between bolt holes, the axial load direction and magnitude, and the initial position of the bolt in its hole.

- The compressive axial load increased the out-of-plane deformation of the shear plate, which could result into plate buckling in the case of the slender shear plate or a larger compression force. The axial compression force decreased the shear force demand on the net section.
- The tensile axial force accelerated the plate yielding and fracture along the interior bolt line by
  increasing the force demands on the shear plate's net section. Furthermore, the tensile force decreased
  the shear plate's out-of-plane deformation and delayed the plate buckling.
- The gross section yielding strength of the shear plate could be considered as a conservative estimate of
  the connection capacity as the connection resisted much larger shear force following the gross section
  yielding of the shear plate. Further analyses are needed to validate this finding in the presence of a large
  tensile force.
- The current design method significantly underestimated the connection shear capacity due to the
  assumption that the inflection point formed at the girder web's face. In contrast, the inflection point
  formed far away from the girder web, beyond the bolt group centroid.

To extend this research to the point where recommendations for design can be made a numerical parametric study is needed to validate the observations described herein for a greater range of stiffened extended shear tab connections. This work is ongoing.

# 5.6 Acknowledgments

The authors would like to thank the ADF Group Inc. and DPHV Structural Consultants for their generous technical and financial support, as well as the Natural Sciences and Engineering Research Council of Canada. The finite element computations were conducted on the McGill University supercomputer Guillimin, which is managed by Calcul Québec and Compute Canada. The

supercomputer operation is funded by the Canada Foundation for Innovation (CFI), NanoQuébec, RMGA and the Fonds de recherche du Québec - Nature et technologies (FRQ-NT).

#### 5.7 References

- [1] AISC 360-16, Specification for structural steel buildings, American Institute of steel Construction, Chicago, IL, 2016.
- [2] Steel construction manual, 15<sup>th</sup> edition, American Institute of steel Construction, Chicago, IL, 2017.
- [3] Design examples companion to the aisc steel construction manual, version 15.0, American Institute of steel Construction, Chicago, IL, 2017.
- [4] A.R. Tamboli, Handbook of structural steel connection design and details, Third edition, McGraw-Hill, New York, NY., 2016.
- [5] Steel construction manual, 14<sup>th</sup> edition, American Institute of steel Construction, Chicago, IL, 2011.
- [6] CSA-S16-14, Design of steel structures, Canadian Standards Association, Mississauga, ON., 2014.
- [7] D.R. Sherman, A. Ghorbanpoor, Design of extended shear tabs, University of Wisconsin-Milwaukee, Milwaukee, WI, 2002.
- [8] J. Hertz, Testing of extended shear tab connections subjected to shear, Master's Thesis, McGill University, Montreal, QC, 2014.
- [9] N. Goldstein Apt, Testing of extended shear tab and coped beam-to-girder connections subject to shear loading, Master's Thesis, McGill University, Montreal, QC, 2015.

- [10] M. Motallebi, D.G. Lignos, C.A. Rogers, Behavior of stiffened extended shear tab connections under gravity induced shear force., J. Constr. Steel Res., 148 (2018) 336-350.
- [11] W. Goodrich, Behavior of extended shear tabs in stiffened beam-to-column web connections, Master's Thesis, Vanderbilt University, Nashville, TN, 2005.
- [12] K. Thomas, Design and behaviour of extended shear tabs under combined loads, Master's Thesis, University of Alberta, Edmonton, AB, 2014.
- [13] K. Thomas, R.G. Driver, S.A. Oosterhof, L. Callele, Full-scale tests of stabilized and unstabilized extended single-plate connections, Structures, 10 (2017) 49-58.
- [14] M. Marosi, M. D'Aronco, R. Tremblay, C.A. Rogers, Multi-row bolted beam to column shear tab connections, 6th European Conference on Steel and Composite Structures, Budapest, Hungary, 2011.
- [15] M. Marosi, Behaviour of single and double row bolted shear tab connections and weld retrofits, Master's Thesis, McGill University, Montreal, QC, 2011.
- [16] M. D'Aronco, Behaviour of double and triple vertical rows of bolts shear tab connections and weld retrofits, Master's Thesis, École Polytechnique de Montréal, Montreal, QC, 2013.
- [17] A. Mirzaei, Steel shear tab connections subjected to combined shear and axial forces, PhD Thesis, McGill University, Montreal, QC, 2014.
- [18] J. Hertz, D.G. Lignos, C.A. Rogers, Full scale testing of extended beam-to-column and beam to-girder shear tab connections subjected to shear, 8th International Conference on Behavior of Steel Structures in Seismic Areas, Shanghai, China, 2015.

- [19] C.A. Rogers, M. Marosi, J. Hertz, D.G. Lignos, R. Tremblay, M. D'Aronco, Performance of weld-retrofit beam-to-column shear tab connections, 8th Int. Workshop on Connections in Steel Structures, Boston, MA., 2016.
- [20] ASTM A992 / A992M-11(2015), Standard specification for structural steel shapes, ASTM International, West Conshohocken, PA, 2015.
- [21] ASTM A572 / A572M-15, Standard specification for high-strength low-alloy columbium-vanadium structural steel, ASTM International, West Conshohocken, PA, 2015.
- [22] AWS D1.1/D1.1M:2015, Structural welding code-steel, American Welding Society, Miami, FL., 2015.
- [23] ASTM F3125 / F3125M-15a, Standard specification for high strength structural bolts, steel and alloy steel, heat treated, 120 ksi (830 mpa) and 150 ksi (1040 mpa) minimum tensile strength, inch and metric dimensions, ASTM International, West Conshohocken, PA, 2015.
- [24] AISC 341-16, Seismic provisions for structural steel buildings, American Institute of steel Construction, Chicago, IL, 2016.
- [25] ASTM A370-17, Standard test methods and definitions for mechanical testing of steel products, ASTM International, West Conshohocken, PA, 2017.
- [26] AWS A5.20/A5.20M:2005 (R2015), Carbon steel electrodes for flux cored arc welding, American Welding Society, Miami, FL., 2015.
- [27] A.M. Kanvinde, I.R. Gomez, M. Roberts, B.V. Fell, G.Y. Grondin, Strength and ductility of fillet welds with transverse root notch, J. Constr. Steel Res., 65 (2009) 11.
- [28] B. Dowswell, R. Whyte, Local stability of double-coped beams, Eng. J. AISC, 51(1) (2014) 43-52.

- [29] J.-J. Cheng, J. Yura, C. Johnson, Design and behavior of coped beams, University of Texas at Austin, Austin, TX, 1984.
- [30] L.S. Muir, C.M. Hewitt, Design of unstiffened extended single-plate shear connections, Eng. J. AISC, 46(2) (2009) 67-80.
- [31] L. Muir, W. Thornton, A direct method for obtaining the plate buckling coefficient for double-coped beams, Eng. J. AISC, 41 (2004) 133-134.
- [32] A. Astaneh, Demand and supply of ductility in steel shear connections, J. Constr. Steel Res., 14(1) (1989) 1-19.
- [33] A. Astaneh, K.M. McMullin, S.M. Call, Behavior and design of steel single plate shear connections, J. Struct. Eng. ASCE, 119(8) (1993) 2421-2440.
- [34] ABAQUS 6.11-3, [Computer software], Dassault Systemes Simulia Corp., Providence, RI.
- [35] G.L. Kulak, J.W. Fisher, J.H. Struik, Guide to design criteria for bolted and riveted joints, AISC, Chicago, IL, 2001.
- [36] ASTM A6 /A6M, General requirements for rolled structural steel bars, plates, shapes, and sheet piling, ASTM International, 2004.
- [37] CSA-G40.20-13/G40.21-13, General requirements for rolled or welded structural quality steel/ structural quality steel, Canadian Standards Association, Toronto, ON., 2013.
- [38] CISC, Handbook of steel construction, Canadian Institute of Steel Construction, Markham, ON., 2016.
- [39] A. Elkady, D.G. Lignos, Analytical investigation of the cyclic behavior and plastic hinge formation in deep wide-flange steel beam-columns, Bull. Earthq. Eng., 13(4) (2015) 1097-1118.

- [40] B.A. Mohr, T.M. Murray, Bending strength of steel bracket and splice plates, Eng. J. AISC, 45(2) (2008) 97-106.
- [41] P. Salem, Unified design criteria for steel cantilever plate connection elements, PhD Thesis, University of Alberta, Edmonton, AB, 2016.
- [42] M. Motallebi, Behavior of extended shear tab connections under combined axial and shear forces, PhD Thesis, McGill University, Montreal, QC, 2018.
- [43] B.G. Neal, The effect of shear and normal forces on the fully plastic moment of a beam of rectangular cross section, Journal of Applied Mechanics, 28(2) (1961) 269-274.
- [44] A. Astaneh, Seismic behavior and design of gusset plates, Steel Tips, Structural Steel Education Council, Moraga, CA., 1998.

# Link between Chapter 5 and Chapter 6

The findings of the laboratory tests and complementary FE simulations, presented in Chapter 5, should be evaluated through a wider range of connection configurations and applied axial force. To do this, a parametric FE simulation was conducted on the double-sided configuration of the full-depth stiffened extended beam-to-girder shear tabs. Chapter 6 includes the results of this parametric study, while modifications to the current AISC design method for extended shear tabs are introduced to improve its accuracy with respect to stiffened extended shear tab connections.

# 6 Chapter 6: Parametric Study of Stiffened Extended Shear Tab Connections under Combined Axial and Shear Forces

Mohammad Motallebi<sup>1</sup>, Dimitrios G. Lignos<sup>2</sup>, Colin A. Rogers<sup>3</sup>

<sup>&</sup>lt;sup>1</sup> Graduate Research Assistant, Department of Civil Engineering and Applied Mechanics, McGill University, Montreal, QC. Email: mohammad.motallebinasrabadi@mail.mcgill.ca

<sup>&</sup>lt;sup>2</sup> Dimitrios G. Lignos, Associate Professor, School of Architecture, Civil and Environmental Engineering, Swiss Federal Institute of Technology, Lausanne (EPFL), Lausanne, Switzerland, Email: dimitrios.lignos@epfl.ch

<sup>&</sup>lt;sup>3</sup> Corresponding author
Colin A. Rogers, Associate Professor, Department of Civil Engineering and Applied Mechanics, McGill University,
Montreal, QC. Email: colin.rogers@mcgill.ca
817 Sherbrooke Street West
Montreal QC, Canada, H3A 0C3
Tel. 514 398-6449
Fax. 514 398-7361

**Abstract** 

This paper presents the findings from a parametric finite element (FE) study on the double-

sided configuration of full-depth stiffened extended shear tab connections. In addition to gravity

induced shear force, the connection behaviour was studied under loading scenarios including

combined axial and shear forces. The parametric FE simulation demonstrated that the connection

behaviour depended on the plate thickness, the number of horizontal and vertical bolt lines, the

girder depth, the bolt group offset from the girder, the direction and the magnitude of the axial

force. The current design practice was evaluated and a set of recommendations is proposed for the

improved design of the double-sided configuration of the full-depth extended beam-to-girder shear

tab connection.

**Keywords**: extended shear tab, double-sided configuration, gross section yielding, plate buckling,

net section fracture

167

## 6.1 Introduction

The current AISC design procedure [4] for shear tab connections considers only gravity induced shear force. Despite traditional perspectives on shear tab connections as being part of the gravity load carrying system, their ability to resist simultaneous shear and axial demands may affect a building's response to wind and earthquake. Furthermore, the presence of an axial force may be detrimental to the shear tab's rotational capacity and its influential contribution to sustain the integrity of the gravity frame in the case of extreme loading scenarios such as column loss. As a result, there is a need for a comprehensive design procedure of extended shear tab connections under combined axial and shear forces. Although the AISC design method [4] does not address the shear tab connection under combined axial and shear force, the AISC Design Examples [15] and the Steel Connection Handbook [14] introduced a few minor adjustments to the AISC design method to use it for design extended shear tabs under combined axial and shear forces. These adjustments need to be validated through either laboratory tests or finite element simulations. This situation is further warranted in the case of stiffened extended shear tabs with full depth shear plates (Figs. 6-1a and 6-1b), where the current design procedure fails to predict accurately the connection behaviour even under gravity induced shear force [21, 24, 25]. Although the current AISC design approach was originally developed for unstiffened extended shear tabs (Fig. 6-1c), structural engineers often rely on it for stiffened shear tabs due to the lack of an alternative published design method for this type of connection.

In comparison to conventional shear tab connections, extended shear tabs have large a distance, i.e. larger than 89 mm (3.5 in.), the distance between the support face and the vertical bolt line, closest to the support. This large distance facilitates the joining of a simply supported beam to the supporting column or girder web without coping of the beam flanges. In the full-depth

stiffened extended shear tab, the shear plate is shop-welded to the girder web and both flanges (column web and two stabilizer plates in case of a beam-to-column web connection).

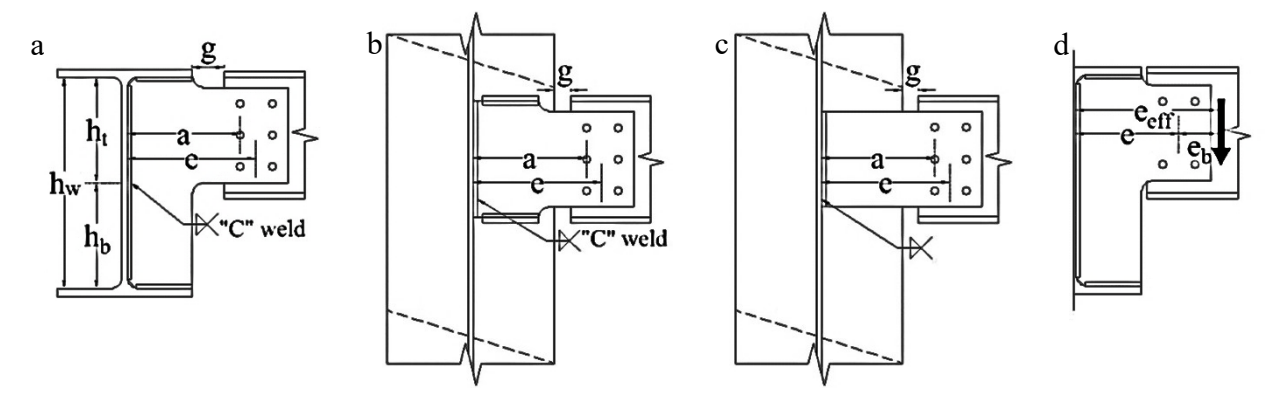


Fig. 6-1. Configuration of single-sided extended shear tab connections: (a) stiffened beam-to-girder with full-depth shear plate, (b) stiffened beam-to-column, (c) unstiffened beam-to-column, (d) definition of e, e<sub>eff</sub>, and e<sub>b</sub>

A few experimental and numerical studies were carried out to examine the behaviour of full-depth stiffened extended shear tabs. Under gravity induced shear force, the plate buckling was determined as the governing failure mode for single-sided stiffened extended shear tabs with full depth shear plates [17, 18, 21, 25, 41, 45, 62]. To improve the current design provisions for full-depth stiffened extended shear tabs, Fortney and Thornton [36] recommended to consider the inflection point at the toe of a stabilizer plate and design the extended portion of the shear tab based on a shorter eccentricity. This recommendation was based on the assumption that the stiffened portion of the shear plate transfer a pure shear force, while the total bending moment was transferred to the supporting member through the stiffeners. Neither published laboratory tests nor finite element analyses were provided to fully explain this recommendation.

Regarding the behaviour of stiffened extended shear tab under combined axial and shear forces, Thomas et al. [21] determined the shear plate's out-of-plane deformation as the critical failure mode of all ten tests. The shear plate yielded throughout prior to failure of the connection. However, the range of the applied axial force was limited because the single-sided shear tab

experiences small axial force in real world applications due to low weak-axis stiffness of the supporting girder.

In comparison to the single-sided shear tab, the double-sided configuration may be subjected to much higher axial force because this pass-through force is transferred from one beam to the next through the girder. The full-scale tests under combined compression and shear forces, conducted by the authors [63], showed a variety of failure modes. Yielding was observed along the plate's interior bolt line, as well as in the gross section along the outer edge of the re-entrant corners. Following yielding of the plate, its out-of-plane deformation largely increased, although the width-to-thickness ratio of the tested shear tabs ( $b_f/2t_f$ ) satisfied the CSA-S16 [2] compactness criterion for plate girder stiffeners ( $200/\sqrt{F_y}$ ). In addition to the large bearing deformation, small fractures propagated from the bolt holes of the shear plate's interior bolt line.

These shear tab experiments built a foundation for complementary numerical simulations, using finite element (FE) software, which were used in validation of the models [9]. The FE simulations demonstrated that net shear fracture was the test connections' ultimate failure mode. Furthermore, the connection behaviour's dependency on the axial force was evaluated by removing axial force as well as applying tension in lieu of compression. Although the connection tolerated much larger shear force following the plate gross section yielding, the authors conservatively considered the yield strength of the plate gross section as the connection design capacity because the rotation and deformation, required for developing larger shear force, would be detrimental to the supported beam serviceability.

To propose design recommendations for stiffened extended shear tab connections, the aforementioned observations [63] had to be evaluated over a variety of configurations under a wider range of axial force magnitudes. To this end, a parametric finite element study was

conducted. Presented herein are the results of this parametric study aiming to evaluate the crucial parameters that formed the connection behaviour, including; the plate length and thickness, the number of horizontal and vertical bolt lines, the girder depth, the bolt group offset from the girder, the direction and the magnitude of the axial force. Based on these observations, several recommendations were proposed for the design of stiffened extended beam-to-girder shear tab connections with full depth shear plates subjected to combined shear and axial forces.

#### **6.2** Finite element simulations

Parametric finite element (FE) simulations were conducted to expand upon the findings from the laboratory tests conducted by the authors [63]. The FE models were developed in the commercial software ABAQUS-6.11-3 [23]. As the laboratory tests, the FE models and their validation procedure were already described in detail in a previous publication [63]; only the highlights are contained herein. Figure 6-2 presents the predictions of the FE model along with the experiment measurements for Specimen BG3-2-13-F-200C. Of note, the specimen ID represented its features including the beam-to-girder configuration (BG), the number of horizontal bolt lines (1), the number of vertical bolt lines (2), the shear plate thickness (13 mm), and its full-depth detailing (F). Referring to Fig. 6-2a, the FE model predicted accurately the connection response under coupled compression and shear demands. Furthermore, the FE model was capable of capturing the plate yielding and damage propagation. The plate yielding started from the outer end of the shear plate's re-entrant corners. Then yielding propagated along the plate's interior bolt line as well as the stiffened portion of the shear plate, which was confined between the girder web and flanges. In addition to the failure modes, the FE model's deformed shape (Fig. 6-2) was a close mimic of the test observed deformation (Fig. 6-2c).

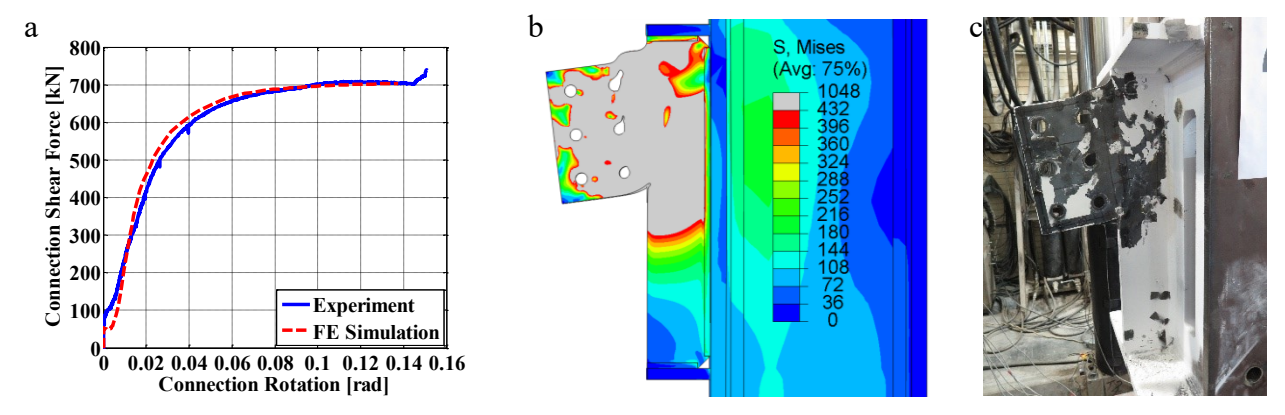


Fig. 6-2. Specimen BG3-2-13-F-200: (a) FE model verification, (b) deformed shaped at end of analysis, (c) deformed shape at end of test

#### 6.1.1 Numerical parametric study

The laboratory tests and complementary FE simulations [63] demonstrated the connections' critical failure modes and damage propagation due to material nonlinearity and/or geometric instabilities. A closer look was taken into these observations through the numerical parametric analyses, which allowed the systematic evaluation of each failure mode and its influential parameters. The matrix of the FE simulations included 23 different configurations, each represented by two model classes. The first class (noted as PL models) was employed to determine the connection capacity, as well as the interactions between different failure modes, under gravity induced shear force. In these models, all connection components could exhibit inelastic behaviour except for the beams. As the connection behaviour was the main interest of these analyses, elastic material properties were assigned to beams. Among these configurations, four representative configurations were chosen to further investigate the effect of axial force on the connection's capacity and governing failure modes. In addition to gravity induced shear force, these four connections were subjected simultaneously to an axial force, which ranged between the connection's axial tensile and compressive capacities. The second class (noted as E-Bo models) was employed to determine the shear capacity of the bolt group. In these models, only the bolts

could experience yielding, while the other components in the model remained elastic. Furthermore, the concentric shear capacity of the bolt group was determined when only an axial force was applied to the connection. Referring to Table 6-1, the 23 configurations were divided into four groups in order to facilitate the interpretation of the FE simulations.

Table 6-1. Connection configurations for parametric FE study

	ID.		Gi	rder		Bolt		Centroid of Bolt		Shear Plate				
	ID.	Beam Section	Section	h <sub>w</sub> (mm)	b <sub>f</sub> (mm)	$\begin{array}{c ccccccccccccccccccccccccccccccccccc$	t <sub>pl</sub> (mm)	$\frac{h_t}{h_w}$	$\frac{b_{\rm f}}{2t_{\rm pl}}$					
	BG3-2-10-F	W310×74	W610×125	573	229	2	3	203	229	10	0.43	11.4		
up 1	BG3-2-13-F °	W310×74	W610×125	573	229	2	3	203	229	13	0.43	8.8		
Group 1	BG6-2-16-F	W610×140	W30×173	719	381	2	6	279	457	16	0.34	12.0		
J	BG6-2-19-F °	W610×140	W30×173	719	381	2	6	279	457	19	0.34	10.0		
	BG2-1-10-F	W250×49	W610×125	573	229	1	2	165	152	10	0.30	11.4		
	BG3-1-10-F	W310×74	W610×125	573	229	1	3	165	229	10	0.43	11.4		
	BG4-1-10-F	W410×74	W610×125	573	229	1	4	165	305	10	0.56	11.4		
2	BG5-1-10-F	W460×82	W610×125	573	229	1	5	165	381	10	0.70	11.4		
Group 2	BG6-1-10-F	W530×82	W610×125	573	229	1	6	165	457	10	0.83	11.4		
Ţ	BG2-2-10-F	W250×49	W610×125	573	229	2	2	203	152	10	0.30	11.4		
	BG4-2-10-F	W410×74	W610×125	573	229	2	4	203	305	10	0.56	11.4		
	BG5-2-10-F	W460×82	W610×125	573	229	2	5	203	381	10	0.70	11.4		
	BG6-2-10-F	W530×82	W610×125	573	229	2	6	203	457	10	0.83	11.4		
	BG3-2-10-F-GD0.93	W310×74	W610×125bd	264	229	2	3	203	229	10	0.93	11.4		
	BG3-2-10-F-GD0.80	W310×74	$W610{\times}125b^{d}$	308	229	2	3	203	229	10	0.80	11.4		
$\omega$	BG3-2-10-F-GD0.60	W310×74	$W610{\times}125b^{d}$	410	229	2	3	203	229	10	0.60	11.4		
Group 3	BG3-2-10-F-GD0.30	W310×74	$W610{\times}125b^{d}$	821	229	2	3	203	229	10	0.30	11.4		
Ţ	BG3-2-10-F-GD0.27	W310×74	$W610{\times}125b^{d}$	900	229	2	3	203	229	10	0.27	11.4		
	BG3-2-10-F-GD0.24	W310×74	$W610{\times}125b^{\rm d}$	1027	229	2	3	203	229	10	0.24	11.4		
	BG3-2-10-F-GD0.20	W310×74	W610×125b	1232	229	2	3	203	229	10	0.20	11.4		
4	BG3-2-10-F-G25	W310×74	W610×125	573	229	2	3	216	229	10	0.43	11.4		
Group 4	BG3-2-10-F-G38	W310×74	W610×125	573	229	2	3	229	229	10	0.43	11.4		
Ţ	BG3-2-10-F-G50	W310×74	W610×125	573	229	2	3	241	229	10	0.43	11.4		

<sup>&</sup>lt;sup>a</sup> Distance between centroid of bolt group and the centre of girder web

<sup>&</sup>lt;sup>b</sup> Depth of the extended portion of the shear plate

<sup>&</sup>lt;sup>c</sup> Tested specimen

<sup>&</sup>lt;sup>d</sup> The girder section is created based on W610×125. Although girder web is different, width and thickness of the girder flange is same as W610×125 section ( $b_f$ =229mm,  $t_f$ =19.6mm).

The purpose of the first group, which included four configurations, was to study the effect of the shear tab slenderness on the connection behaviour. In addition to the two tested configurations, i.e. BG3-2-13-F and BG6-2-19-F, this group contained two additional configurations, i.e. BG3-2-10-F and BG6-2-16-F, detailed as per the test specimens except for a change in the thickness of the shear plate. The thinner shear plates did not satisfy the CSA-S16 [2] compactness requirements for plate girder stiffeners.

The second group contained configurations with different numbers of vertical and horizontal bolt lines, while all other aspects were identical to specimen BG3-2-10-F. The main goal of this group was to determine the effect of the number of bolt lines on the connection's eccentricity and shear capacity.

The third group included connections with different girder web depth and thickness, while other features including the  $h_w/t_w$  ratio were set to be the same as those of specimen BG3-2-10-F. This group was formed to investigate the dependency of the shear plate's instabilities on the ratio between the height of the top part of the stiffener and the height of the girder web ( $h_t/h_w$ ), as shown in Fig. 6-1a. This ratio represented the relative distance between the bottom edge of the extended portion of the shear plate and the bottom flange of the girder. The shallowest member corresponded to the depth of the shear plate (having two vertical lines of three bolts, 229 mm (9 in.)), while the deepest member is 203 mm (8 in.) deeper than the deepest available AISC section (W1100×499). Of note, the girder of the second group connections did not represent the available AISC sections. They were identical to W610×125 section other then the height and thickness of the web, changed to study the effect of the  $h_v/h_w$  ratio on the connection behaviour. The thickness of the girder web was kept constant to keep their  $h_w/t_w$  ratio equal to W610×125.

The purpose of the fourth group was to determine the impact of the gap distance (g distance as shown in Fig.6-1) on the shear plate instability, assuming that a large gap might cause buckling to occur prior to yielding of the extended portion of the shear plate. The gap distance ranged between 13 mm (Specimen BG3-2-10-F) and 50 mm, i.e. the worst-case scenario when a large gap was required due to fireproofing between the beam and girder. Other than the *a* distance and the shear plate length, all other aspects were identical to Specimen BG3-2-10-F. The third and fourth group were denoted by adding suffixes "-GD(h<sub>t</sub>/h<sub>w</sub> ratio)" and "-G(Gap distance)" to the regular alphanumerical label of the specimens.

It should be noted that snug tight 19 mm (3/4 in.) bolts were used in all configurations other than BG6-2-16-F and BG6-2-19-F, where snug tight 22 mm (7/8 in.) bolts were implemented. For the 20 configurations with a 10 mm thick shear plate, ASTM F3125 Grade A325 bolts [34] were used, while the beam was attached to the shear tab using ASTM F3125 Grade A490 bolts [34] in the remaining three configurations. The girders and beams were made of ASTM A992 Grade 50 steel [47], while the shear plates were fabricated from ASTM A572 Grade 50 steel [48]. Referring to Table 6-2, the probable material properties were assigned to the shear plate and girder, while nominal material properties were used for the bolt and weld. To decrease computational costs, symmetric boundary conditions were implemented along the girder axis in lieu of the supporting column.

Table 6-2. Material properties of connection components

	Non	ninal	Expe	ected
Connection components	$F_{y}$	$F_{u}$	$F_{y}$	$F_{u}$
	(MPa)	(MPa)	(MPa)	(MPa)
ASTM A992 Grade 50 steel	345	448	379	493
(Hot-rolled structural shapes)	343	440	319	493
ASTM A572 Grade 50 steel	345	448	379	538
(Plate)	343	440	319	336
E71T electrode	400	490		
A325 bolts	634	827		
A490 bolts	896	1034		

<sup>&</sup>lt;sup>1</sup> Based on probable material properties i.e. R<sub>v</sub>F<sub>v</sub> (1.1 F<sub>v</sub>) and R<sub>T</sub>F<sub>u</sub> (1.1 F<sub>u</sub>) for hot-rolled structural shapes [50]

<sup>&</sup>lt;sup>2</sup> Based on probable material properties i.e.  $R_yF_y$  (1.1  $F_y$ ) and  $R_TF_u$  (1.2  $F_u$ ) for steel plates [50]

#### 6.1.2 Simulation results

The finite element method was adopted to further our understanding on how double-sided stiffened extended shear tabs behave under combined axial and shear forces. Furthermore, the free body cut option of the Abaqus software was implemented to determine the force demands on the gross and net sections of the shear plate. Figure 6-3 shows the normalized predictions of the FE models for configurations BG3-2-10-F and BG3-2-13-F.

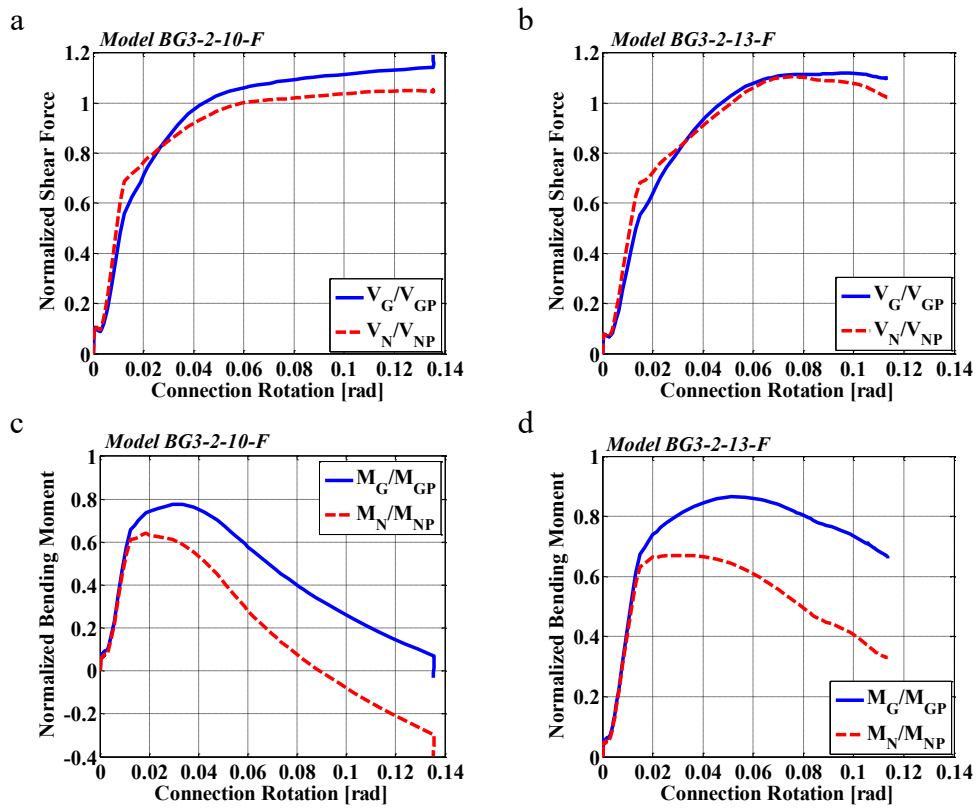


Fig. 6-3. FE model predictions for: shear force of configurations (a) BG3-2-10-F and (b) BG3-2-13-F, bending moment of configurations (c) BG3-2-10-F and (d) BG3-2-13-F

The shear force and bending moment along the outer end of the shear plate's re-entrant corners were normalized based on the plastic shear ( $V_{GP}=0.6F_yA_g$ ) and plastic flexural ( $M_{GP}=F_yZ_g$ ) capacities of the plate's gross section, respectively. Furthermore, the plastic shear ( $V_{NP}=0.6F_yA_{net}$ ) and plastic flexural capacities ( $M_{NP}=F_yZ_{net}$ ) of the plate's net section were implemented to

normalize the shear force and bending moment along the bolt line, respectively. For an odd number of horizontal bolt lines  $Z_{net} = 1/4t_{pl}(s-d_h)(n^2s+d_h)$  while  $Z_{net} = 1/4t_{pl}(s-d_h)(n^2s)$  for an even number of horizontal bolt lines [59]. In these equations, n=number of horizontal bolt lines, s=bolt spacing, d<sub>h</sub>=diameter of bolt hole, t<sub>pl</sub>=plate thickness, and d<sub>pl</sub>=plate depth. Referring to Table 6-3, the connection plastic capacities were calculated based on the plate's probable yield strength.

Table 6-3. Predicted plastic capacities of shear tab connection specimens

Spacimana	$P_{GP}$	P <sub>NP</sub>	P <sub>cr</sub>	$V_{GP}$	$V_{NP}$	$M_{GP}$	$M_{NP}$
Specimens	(kN)	(kN)	(kN)	(kN)	(kN)	(kN.m)	(kN.m)
BG2-(1, 2)-10-F <sup>1</sup>	555	404	499	333	243	21.1	15.4
BG3-(1, 2)-10-F <sup>1</sup>	832	607	748	499	364	47.5	35.7
BG4-(1, 2)-10-F <sup>1</sup>	1109	809	998	666	485	84.5	61.6
BG5-(1, 2) -10-F <sup>1</sup>	1387	1011	1248	832	607	132.1	98.1
BG6-(1, 2)-10-F <sup>1</sup>	1664	1213	1497	998	728	190.2	139.7
BG3-2-13-F <sup>1</sup>	1102	804	1061	661	482	63.0	47.3
BG6-2-16-F <sup>1</sup>	2794	1921	2556	1676	1153	319.4	219.6
BG6-2-19-F <sup>1</sup>	3353	2305	3170	2012	1383	383.3	263.5
BG3-2-10-F-G25 <sup>1</sup>	832	607	735	499	364	47.5	35.7
BG3-2-10-F-G38 <sup>1</sup>	832	607	721	499	364	47.5	35.7
BG3-2-10-F-G50 <sup>1</sup>	832	607	707	499	364	47.5	35.7

<sup>&</sup>lt;sup>1</sup> Based on probable material properties, i.e. R<sub>v</sub>F<sub>v</sub> (1.1 F<sub>v</sub>) and R<sub>T</sub>F<sub>u</sub> (1.2 F<sub>u</sub>) for steel plates [50]

Referring to Figs. 6-3a and 6-3b, both models reached their strength plateau. At this point, the shear force of model BG3-2-13-F started to decrease, while model BG3-2-10-F was able to maintain its shear resistance. This observation was due to their different ultimate failure modes: shear plate buckling and net section fracture for models BG3-2-10-F and BG3-2-13-F, respectively. Referring to Fig. 6-4a, the plastic strain concentrated at both re-entrant corners of model BG3-2-10-F, while the plastic strain concentration was observed along the top half of the plate interior bolt line in model BG3-2-13-F. Due to buckling of the stiffened portion of the shear plate, which was confined between the girder web and flanges, the connection stiffness decreased significantly; the inflection point then moved rapidly toward the girder and the negative bending moment mobilized along the interior bolt line. Referring to Figs. 6-3c and 6-3d, a larger bending moment was developed at the gross section of the shear plate. It was due to the fact that the inflection point formed away from the girder web, beyond the centre of the bolt group.

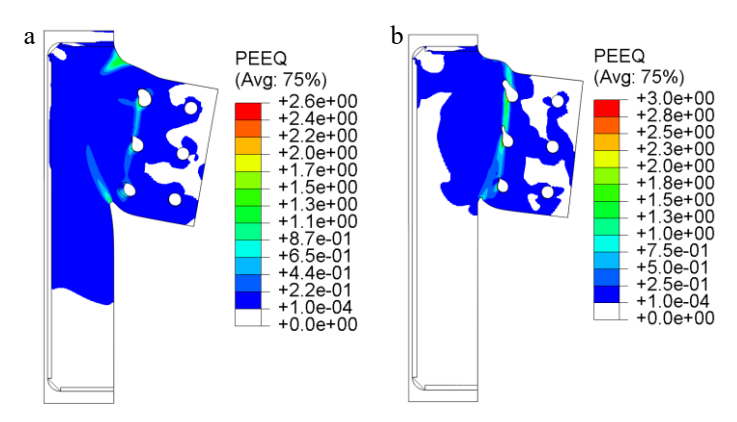


Fig. 6-4. Deformed shape of shear tab at end of analysis for models: (a) BG3-2-10-F, (b) BG3-2-13-F

Table 6-4 presents a quantitative summary of the FE models' responses under gravity induced shear force.

Table 6-4. Connection response under gravity induced shear force

	Table 6-4. Connection response under gravity induced shear force												
	ID.		section		ection		f-plane	Buc	kling		ection	Bolt	shear
		yie	lding	yiel	ding	defori	nation	Bue	5		ture	Bon	511041
		V	$e_{\rm eff}$	V	$e_{\rm eff}$	V	$e_{\rm eff}$	V	$e_{\rm eff}$	V	$e_{\rm eff}$	V	$e_{\rm eff}$
		(kN)	(mm)	(kN)	(mm)	(kN)	(mm)	(kN)	(mm)	(kN)	(mm)	(kN)	(mm)
	BG3-2-10-F	358	233	372	231	478	211	530	188			$570^{\rm a}$	141
Group	BG3-2-13-F	464	239	464	239					727	208		
iro	BG6-2-16-F	1401	337	1348	338	1718	338	1756	332				
	BG6-2-19-F	1686	341	1555	343					2160	344		
	BG2-1-10-F	281	174			331	173	360	170			312	171
	BG3-1-10-F	426	186			521	184	529	182			455	183
	BG4-1-10-F	566	207			697	203	752	197			602	196
Group 2	BG5-1-10-F	696	229			887	219	923	211			719	215
onl	BG6-1-10-F	836	254			1003	245	1062	230			828	236
Ġ	BG2-2-10-F	225	211	311	190	336	184	356	171			351ª	160
	BG4-2-10-F	504	253	489	253	657	227	706	208			$770^{\rm a}$	138
	BG5-2-10-F	629	280	606	280	733	267	846	230			943ª	139
	BG6-2-10-F	745	319	694	316	805	311	901	268			1097ª	142
	BG3-2-10-F-GD0.93	361	234	375	231					560	204	565ª	190
	BG3-2-10-F-GD0.80	354	236	383	229	512	209	561	193			583ª	151
53	BG3-2-10-F-GD0.60	352	235	395	226	504	208	542	191			573ª	142
Group 3	BG3-2-10-F-GD0.30	360	232	403	223	486	205	526	189			573ª	140
Ğ	BG3-2-10-F-GD0.27	361	232	404	222	486	205	521	192			574ª	140
	BG3-2-10-F-GD0.24	356	233	408	222	469	207	518	184			567ª	139
	BG3-2-10-F-GD0.20	362	232	426	218	487	205	523	193			577ª	140
4	BG3-2-10-F-G25	341	243	390	230	425	220	461	208			538a	140
Group 4	BG3-2-10-F-G38	328	252	385	227	385	227	423	207			508a	140
Ď	BG3-2-10-F-G50	317	260	383	219	351	241	383	219			484ª	140

<sup>&</sup>lt;sup>a</sup> Bolt axial deformation increased due to shear plate buckling.

Various failure modes were observed in these specimens, including; gross and net section yielding of the shear plate, shear plate buckling, net section fracture, and bolt shear fracture. A comparison between Tables 6-3 and 6-4 demonstrates that the shear plate yielded at its gross and net sections because of the interaction of moment, shear and axial force. Among the observed failure modes, yielding of the plate's gross and net sections occurred earlier under a smaller shear force. Furthermore, other failure modes occurred when the connection underwent large deformation and rotation, which could negatively affect the supported beam's serviceability. Therefore, the moment-shear-axial force yielding of the shear plate was considered a conservative estimate of the connection's shear capacity.

Of note, the reported resistance for the gross and net section yielding of the shear plate corresponded to the shear force caused yielding through the full depth of the shear plate. The comparison of the plate's plastic capacities (Table 6-3) with the observed connection resistance corresponding to yield of the plate demonstrated that yielding occurred due to the interaction of axial, shear, and flexural loads.

The predictions from the FE model were compared with available bolt shear experiments [64, 65] to validate the numerical model's capability to capture the bolt shear strength. Although the FE model accurately simulated the bolt's strength plateau (continuous increase of the bolt deformation while the bolt force remained constant) in the shear test, it was not possible to capture the bolt's post ultimate (softening) response. This may result in concern regarding the capability of the FE model to capture the shear capacity of the bolt group under an eccentric shear force, in which the bolts would experience shear fracture progressively. To address this issue, the force-deformation response of each individual bolt was monitored during the analysis; the minimum level of the connection shear force corresponding to the time when the first bolt reached its strength

plateau was considered as the shear capacity of the bolt group. Referring to Table 6-4, the bolt shear fracture was observed as the ultimate failure mode only in connections with a single vertical bolt line. In connections with a 10mm shear plate and two vertical bolt lines, bolt fracture was observed as the secondary mode, following shear plate buckling and consequent bolt elongation. Although connections with a single vertical bolt line did not satisfy the maximum thickness requirement of the AISC design procedure [4], the bolt shear fracture occurred after full yielding of the gross section of the shear plate.

Since yielding of the shear plate precluded the bolt shear fracture in most configurations, the *E-Bo* FE models were utilized to determine the connection shear strength corresponding to the bolt shear fracture. The results of the *E-Bo* FE models are summarized in Table 6-5.

Among the 23 configurations, four members of Group 1 were chosen to study the impact of the axial load on the stiffened extended shear tab behaviour because they failed due to various damage states. Further, these configurations varied in the number of bolt rows, plate slenderness, the bolt size and bolt grades, and the offset of the bolt group from the girder web. First, their behaviour under pure tension and compression was determined. Their behaviour was then studied under a wide range of coupled axial and shear forces. Table 6-6 summarizes the response of the connections under axial forces. Both tension and compression resulted in gross section yielding of the shear plate, while net section yielding occurred only under tension.

Table 6-5.bolt shear strength based on FE-E-Bo models

			FE n	nodels	Currer	nt Design M	ethod	New R	Recommend	lations
	ID.	Inflection point a (mm)	e <sub>b</sub> b (mm)	V <sub>FE</sub> c (kN)	e <sub>b</sub> b (mm)	V <sub>A</sub> d (kN)	$\frac{V_{\text{FE}}}{V_{\text{A}}}$	e <sub>b</sub> <sup>b</sup> (mm)	V <sub>A</sub> d (kN)	$\frac{V_{\text{FE}}}{V_{\text{A}}}$
	BG3-2-10-F	237	34	798	197	270	2.96	35	732	1.09
Group 1	BG3-2-13-F	245	42	918	197	337	2.72	35	915	1.00
iroı	BG6-2-16-F	338	59	2856	271	1169	2.44	61	2623	1.09
_	BG6-2-19-F	337	58	2878	271	1169	2.46	61	2623	1.10
	BG2-1-10-F	173	8	315	159	68	4.63	10	274	1.15
	BG3-1-10-F	186	21	452	159	138	3.28	20	408	1.11
	BG4-1-10-F	191	26	666	159	246	2.42	34	532	1.12
7	BG5-1-10-F	205	40	813	159	370	1.94	50	648	1.11
Group 2	BG6-1-10-F	223	58	940	159	508	1.61	70	752	1.09
Ġ	BG2-2-10-F	210	7	650	197	146	3.94	17	519	1.11
	BG4-2-10-F	234	28	1306	197	445	2.25	58	934	1.07
	BG5-2-10-F	247	44	1594	197	647	1.81	86	1092	1.07
	BG6-2-10-F	268	64	1831	197	885	1.49	119	1220	1.08
	BG3-2-10-F-GD0.93	221	18	998	197	270	2.97	35	732	1.09
	BG3-2-10-F-GD0.80	221	18	993	197	270	3.03	35	732	1.12
$\tilde{\omega}$	BG3-2-10-F-GD0.60	221	18	995	197	270	3.02	35	732	1.11
Group 3	BG3-2-10-F-GD0.30	221	18	995	197	270	2.97	35	732	1.10
J	BG3-2-10-F-GD0.27	221	18	991	197	270	2.93	35	732	1.08
	BG3-2-10-F-GD0.24	221	18	993	197	270	3.09	35	732	1.14
	BG3-2-10-F-GD0.20	221	18	992	197	270	2.91	35	732	1.07
4	BG3-2-10-F-G25	233	17	996	210	255	3.22	30	752	1.09
Group 4	BG3-2-10-F-G38	244	16	997	223	242	3.40	27	766	1.07
Ţ	BG3-2-10-F-G50	256	15	1004	235	231	3.74	24	780	1.11
					Minimum	1.50			1.00	
				Mean	2.84			1.09		
						Maximum	4.63			1.15
					Standard	d deviation	0.74			0.03
						COV	0.26			0.03

<sup>&</sup>lt;sup>a</sup> The distance between the inflection point and the weld line.

To study the shear tab's behaviour under combined axial and shear forces, these four configurations were subjected to a wide range of axial force while resisting their service shear

<sup>&</sup>lt;sup>b</sup> The distance between the inflection point and the centre of the bolt group.

<sup>&</sup>lt;sup>c</sup> The estimated shear capacity of the bolt group based on FE simulations.

<sup>&</sup>lt;sup>d</sup> The estimated shear capacity of the bolt group based on design recommendations.

force. The axial force varied between the connection tensile and compressive capacities, which was obtained from the FE model. The axial load was kept constant while the displacement based shear loading was continued until failure of the connection. In the calculation of the service shear force, the dead and live loads of an archetype office building [66] were considered. Further analyses were conducted to determine the dependency of the connection's behaviour on the magnitude of the service shear force. These analyses revealed that the magnitude of the service shear force does not affect the connection's ultimate response, unless the shear plate has already yielded under the service shear force.

Table 6-6. FE models predictions for connection axial capacities

Twenty of the meaning productions for commentation and an adjustment												
ID.	Gro Sect yield	ion	Net se Yield			f-plane nation	Bucl	kling	Net se		Bolt s	hear
	F <sub>FE</sub> (kN)	$\frac{F_{\text{FE}}}{F_{\text{GP}}}$	F (kN)	$\frac{F_{\text{fe}}}{F_{\text{NP}}}$	F (kN)	$\frac{F_{\text{FE}}}{P_{\text{cr}}}$	F (kN)	$\frac{F_{\text{FE}}}{P_{\text{cr}}}$	F (kN)	$\frac{F_{_{FE}}}{F_{_{NU}}}$	F (kN)	$\frac{F_{\text{FE}}}{F_{\text{BSH}}}$
BG3-2-10-F-PC <sup>a</sup>	834	1.00			734	0.98	836	1.12				
BG3-2-13-F-PCa	1102	1.00			987	0.93	1205	1.14			1192 <sup>b</sup>	1.08
BG6-2-16-F-PC <sup>a</sup>	2564°	0.92			2059	0.81	2564	1.00			$2489^{b}$	0.83
BG6-2-19-F-PCa	3141°	0.91			2505	0.79	3141	0.99			$3094^{b}$	1.03
BG3-2-10-F-PT <sup>d</sup>	825	0.99	671	1.11					926	1.09	926	1.05
BG3-2-13-F-PT <sup>d</sup>	1118	1.01	831	1.04					1239	1.04	1162	1.05
BG6-2-16-F-PT <sup>d</sup>	2781	1.00	2055	1.07					3073	1.12	3062	1.02
BG6-2-19-F-PT <sup>d</sup>	3359	1.00	2457	1.07					3698	1.11	3112	1.04

<sup>&</sup>lt;sup>a</sup> PC: Pure compression

Referring to Table 6-7, all FE models experienced yielding of the gross section of the shear plate, except for model BG6-2-16-F-2000C, which buckled prior to yielding due to the presence of a large compressive force, i.e. 0.78 P<sub>GP</sub>. As the axial force increased, the shear force corresponding to yielding of the gross section decreased.

<sup>&</sup>lt;sup>b</sup> secondary failure mode

<sup>&</sup>lt;sup>c</sup> Gross section yielding was not observed due to buckling

<sup>&</sup>lt;sup>d</sup> PT: Pure tension

Table 6-7. FE models predictions for connection capacities under combined axial and shear forces

		section		ns for con	Out-of					ection		1
ID.	yiel	ding	yiel	ding	deform	nation	Buck	ding	frac	ture	Bolt	shear
	V	$e_{ m eff}$	V	$e_{ m eff}$	V	e <sub>eff</sub>	V	$e_{ m eff}$	V	$e_{ m eff}$	V	e <sub>eff</sub>
	(kN)	(mm)	(kN)	(mm)	(kN)	(mm)	(kN)	(mm)	(kN)	(mm)	(kN)	(mm)
BG3-2-10-F-700C	182	199			182	199	198	179				
BG3-2-10-F-600C	245	204			201	231	245	204				
BG3-2-10-F-400C	291	241	362	177	322	230	358	200			297ª	85
BG3-2-10-F-200C	332	240	440	207	408	220	458	191			$477^{a}$	126
BG3-2-10-F	358	233	372	231	478	211	530	188			570a	141
BG3-2-10-F-200T	344	231	285	239					525	196		
BG3-2-10-F-400T	308	226	225 b	244					455	201		
BG3-2-10-F-600T	233	211	195 b	214					366	195		
BG3-2-10-F-800T	78	188	43 <sup>b</sup>	205					209	190		
BG3-2-13-F-1000C	226 b	219			282	215	367	191			339	166
BG3-2-13-F-800C	300	244	520	194	350	237	520	191			481ª	162
BG3-2-13-F-600C	339	250	632	195	598	208	632	195			622a	169
BG3-2-13-F-400C	396	243	610	220	665	211	724	195			721ª	175
BG3-2-13-F-200C	443	244	545	230	647	219			758	199	768ª	188
BG3-2-13-F	464	239	464	239					727	208		
BG3-2-13-F-200T	454	235	394	243					696	207		
BG3-2-13-F-400T	422	235	319	247					649	204		
BG3-2-13-F-600T	380	228	298 b	237					578	202		
BG3-2-13-F-800T	311	214	268 b	216					494	194		
BG3-2-13-F-1000T	209	191	209 b	191					367	187		
BG6-2-16-F-2000C	1084 <sup>d</sup>	247			886 °	311	1084	247			887 a	149
BG6-2-16-F-1500C	1151	333	1395	284	1151	333	1376	292			1314 a	169
BG6-2-16-F-1000C	1294	339	1540	320	1466	328	1676	275				
BG6-2-16-F-500C	1367	338	1451	335	1569	337	1748	310				
BG6-2-16-F-250C	1359	339	1409	338	1629	340	1763	321				
BG6-2-16-F	1401	337	1348	338	1718	338	1756	332				
BG6-2-16-F-250T	1386	334	1268	336	1603	340			1737	337		
BG6-2-16-F-500T	1359	333	1156	336					1689	339		
BG6-2-16-F-1000T	1277	335	885	345					1560	336		
BG6-2-16-F-1500T	1102	331	800 b	343					1391	325		
BG6-2-16-F-2000T	971	315	715 b	325					1164	309		
BG6-2-16-F-2500T	588	287	564 b	288					908	283		
BG6-2-19-F-2500C	1125	296			929°	308	1250	270			1194	233
BG6-2-19-F-2000C	1267	332	1728	278	1134°	337	1752	266			1722	230
BG6-2-19-F-1500C	1457	340	1964	300	1824	321	2078	262			2057a	235
BG6-2-19-F-1000C	1547	342	1851	339	1877	338	2218	292				
BG6-2-19-F-500C	1647	342	1702	341	1997	344			2221	324		
BG6-2-19-F-250C	1639	342	1639	342	2040	345			2194	337		
BG6-2-19-F	1686	341	1555	343	2066	346			2160	344		
BG6-2-19-F-250T	1670	339	1452	342	2048	346			2111	346		
BG6-2-19-F-500T	1648	336	1430	339					2059	344		
BG6-2-19-F-1000T	1574	336	1144	344					1942	339		
BG6-2-19-F-1500T	1461	332	992 <sup>b</sup>	348					1792	330		
BG6-2-19-F-2000T	1283	323	933 <sup>b</sup>	338					1650	316		
BG6-2-19-F-2500T	1137	301	896 <sup>b</sup>	307					1439	296	1392	296
BG6-2-19-F-3000T	788	274	644 b	273					1189	279	788	274
a Rolt avial defor									1107	-17	, 50	

<sup>&</sup>lt;sup>a</sup> Bolt axial deformation increased due to shear plate buckling
<sup>b</sup> minimum shear force after applying axial force, the section yielded during applying axial force.

<sup>&</sup>lt;sup>c</sup> Out-of-plane deformation occurred in advance of the gross section yielding <sup>d</sup> It buckled in advance of the shear plate yielding.

## 6.3 Discussion

## 6.3.1 Shear plate yielding under gravity induced shear force

Referring to Table 6-4, yielding of the gross and sections of the shear plate was observed in all configurations of Group 1. The small differences between the yield strength of the gross and net sections of these configurations demonstrated that these two failure modes occurred almost at the same time, although the net section properties, i.e.  $A_{net}$  and  $Z_{net}$  were much smaller than those of the gross section. This was due to the different loading rates at the gross and net sections. In comparison to the net section, the gross section was subjected to a larger bending moment, because the aforementioned cross section was farther from the inflection point. Furthermore, the gross section was subjected to a larger shear force as compared to the net section along the centerline of the bolt holes. Regarding Group 1, the gross section yielded shortly prior to the net section in specimens with 19 mm (3/4") bolts, while yielding of the net section occurred earlier than that of the gross section in specimens with 22 mm (7/8") bolts. This observation can be attributed to the ratios between the net and gross sections, which were smaller in shear plates with larger bolt holes, i.e.  $A_{net}/A_g$ =0.73 and 0.69 for the specimens with 19 mm and 22 mm bolts when the bolt holes distance was 76 mm.

Referring to Table 6-4, yielding of the gross section of the shear plate occurred in all FE models, whereas yielding of the net section did not. The net section yielding was not observed in Group 2 configurations with a single vertical line of bolts because less than 60% of the connection's shear force was transferred through the net section along the centerline of the bolt holes, the section with the smallest cross-sectional area along the plate. For other members of Group 2, configurations with two vertical bolt lines, yielding of the net section occurred shortly after the gross section yielding. The results obtained from the FE models with varied horizontal

and vertical bolt lines (Group 2) demonstrated that the inflection point forms farther from the girder web as the number of horizontal bolt lines increases. Furthermore, adding a vertical bolt line moved the inflection point away from the girder.

A comparison between the response of Group 3 configurations and BG3-2-10-F configuration of the first group demonstrated that the configurations with varied stiffener depth showed similar response under gravity induced shear force. The shear plate yielded at its gross and net sections.

Regarding the members of fourth group (configurations with a beam-girder gap larger than 13 mm), the shear plate resistance associated with gross section yielding decreased as the gap distance and consequently the eccentricity increased. In comparison with the BG3-2-10-F configuration, the greater unbraced length led to a larger out-of-plane deformation and a faster reduction of the eccentricity following yielding of the gross section. Therefore, the net section yield strength of the Group 4 configurations was larger than the corresponding resistance of BG3-2-10-10.

A global survey of the results of the FE models demonstrated that the conclusion of the previous study [63] was valid; i.e. yielding of the gross section of the shear plate could be considered conservatively as the connection design strength. As mentioned in Section 6.2.2, the development of a higher shear force required a larger connection rotation and deformation, which probably overshadowed the supported beam serviceability. Furthermore, a comparison between the predictions of the FE model for the shear plate's gross section yielding and the plate's shear yield capacity (V<sub>GP</sub> Table 6-3) demonstrated the need for consideration of the axial-shear-moment interaction.

To take into account the effect of the axial and shear forces on the plastic bending capacity of the structural members with a rectangular section, Neal proposed a plastic interaction equation (Eq. (6-1)) [40]. Previous research [22, 63] showed its accuracy in detecting plate yielding under

combined loads. Astaneh proposed Eq. (6-2) as a simplified version of Neal's interaction equation [61]. This simplified equation was later introduced in the AISC Steel Construction Manual [4] to consider the interaction of axial, shear, and flexural demands. In the absence of axial load, these two equations resulted in equal values. Of note, the AISC used an elliptical interaction equation (Eq. (6-3)) to consider the interaction of the shear and bending moment in shear tabs [4].

$$\left(\frac{M}{M_{P}}\right) + \left(\frac{P}{P_{P}}\right)^{2} + \left(\frac{(V/V_{P})^{4}}{1 - (P/P_{P})^{2}}\right) \le 1$$
(6-1)

$$(\frac{M}{M_P}) + (\frac{P}{P_P})^2 + (\frac{V}{V_P})^4 \le 1$$
 (6-2)

$$\left(\frac{M}{M_{P}}\right)^{2} + \left(\frac{V}{V_{P}}\right)^{2} \le 1 \tag{6-3}$$

The main prerequisite for the accurate prediction of the connection strength was the precise estimation of the location of the inflection point. To estimate the distance between the centre of the bolt group and the inflection point, an empirical equation was proposed. Equation (6-4) can be relied on to predict the bolt group eccentricity corresponding to the gross section yielding of the shear plate as a function of the parameter  $t_{pl}d_{pl}^3/a^4$ . This parameter was found to be the statistically significant variable at the 95% level based on the standard t- and F-test. The coefficient of determination is  $R^2$ =0.924 and  $0.05 \le t_{pl}d_{pl}^3/a^4 \le 1.22$  is the applicability range.

$$e_b(mm) = 95.30 \left(\frac{t_{pl}d_{pl}^3}{a^4}\right)^{0.66}$$
 (6-4)

in which,  $e_b$  is the bolt group eccentricity, the distance between the inflection point and the centre of the bolt group,  $t_{pl}$  is the shear plate thickness,  $d_{pl}$  is depth of the extended portion of the shear plate, a is the distance between the girder web centre and the interior bolt line.

Table 6-8 presents estimates of the bolt group eccentricity using Eq. (6-4) in comparison with the predictions from the FE models. The bolt group eccentricity increased as the shear plate stiffness increased due to either a decrease of the *a* distance or an increase of the shear plate depth and/or thickness. Eqs. (6-2) and (6-3) were used to estimate the shear strength corresponding to yielding of the gross section of the shear plate. Both interaction equations provided reasonably conservative predictions for the yield strength, while elliptical interaction equation, Eq. (6-3), was easier to be implemented.

Table 6-8. Gross section yielding strength

-	ID.	Gaomat	ric param	atars		FE mode	1 <sub>c</sub>			recomm		n	
	ID.	Geomei	nc param	CICIS		TE mode	15	Eccen	tricity	Eq. (6	5-2)	Eq. (	6-3)
		a (mm)	$\begin{array}{c} e_g \\ (mm) \end{array}$	$\frac{t_{pl}d_{pl}^3}{a^4}$	e <sub>b</sub> (mm)	$\begin{array}{c} e_{\rm eff} \\ (mm) \end{array}$	V <sub>FE</sub> (kN)	e <sub>b</sub> (mm)	e <sub>eff</sub> (mm)	V <sub>A</sub> (kN)	$\frac{V_{\text{FE}}}{V_{\text{A}}}$	V <sub>A</sub> (kN)	$\frac{V_{\text{FE}}}{V_{\text{A}}}$
1	BG3-2-10-F	165	203	0.152	30	233	358	28	231	350	1.02	339	1.06
Group 1	BG3-2-13-F	165	203	0.205	36	239	464	33	236	452	1.03	435	1.07
Gro	BG6-2-16-F	241	279	0.450	58	337	1401	56	335	1363	1.03	1379	1.02
	BG6-2-19-F	241	279	0.541	62	341	1686	64	343	1614	1.04	1625	1.04
	BG2-1-10-F	165	165	0.045	9	174	281	12	177	262	1.07	262	1.07
	BG3-1-10-F	165	165	0.152	21	186	426	28	193	407	1.05	412	1.03
	BG4-1-10-F	165	165	0.361	42	207	566	49	214	544	1.04	551	1.03
Group 2	BG5-1-10-F	165	165	0.705	64	229	696	76	241	672	1.04	677	1.03
rou	BG6-1-10-F	165	165	1.219	89	254	836	109	274	790	1.06	792	1.06
Ö	BG2-2-10-F	165	203	0.045	8	211	225	12	215	205	1.10	195	1.15
	BG4-2-10-F	165	203	0.361	50	253	504	49	252	487	1.04	476	1.06
	BG5-2-10-F	165	203	0.705	77	280	629	76	279	615	1.02	603	1.04
	BG6-2-10-F	165	203	1.219	116	319	745	109	312	733	1.02	718	1.04
	BG3-2-10-F-GD0.93	165	203	0.152	31	234	361	28	231	350	1.03	339	1.07
	BG3-2-10-F-GD0.80	165	203	0.152	33	236	354	28	231	350	1.01	339	1.05
р3	BG3-2-10-F-GD0.60	165	203	0.152	32	235	352	28	231	350	1.01	339	1.04
Group 3	BG3-2-10-F-GD0.30	165	203	0.152	29	232	360	28	231	350	1.03	339	1.06
Ö	BG3-2-10-F-GD0.27	165	203	0.152	29	232	361	28	231	350	1.03	339	1.07
	BG3-2-10-F-GD0.24	165	203	0.152	30	233	356	28	231	350	1.02	339	1.05
	BG3-2-10-F-GD0.20	165	203	0.152	29	232	362	28	231	350	1.03	339	1.07
4 c	BG3-2-10-F-G25	178	216	0.113	27	243	341	23	239	338	1.01	325	1.05
Group 4	BG3-2-10-F-G38	191	229	0.085	23	252	328	19	248	325	1.01	310	1.06
9	BG3-2-10-F-G50	203	241	0.067	19	260	317	16	257	312	1.02	296	1.07
									Minimum		1.01		1.02
		Mean				Mean	1.03		1.05				
		Maximum Standard deviation				1.10		1.15					
							S	standard d	eviation	0.02		0.03	
									COV	0.02		0.03	

## 6.3.2 Shear plate buckling under gravity induced shear force

Referring to Table 6-4, the specimens with compact shear plates, i.e. BG3-2-13-F and BG6-2-19-F, reached their ultimate strength due to the net section fracture, while slender shear tabs (i.e. BG3-2-10-F and BG6-2-16-F) experienced large out-of-plane deformation and buckling which defined their capping strength. Figure 6-5 presents a comparison of the response of Configuration BG3-2-10-F with that of configuration BG3-2-13-F. Referring to Fig. 6-5a both configurations reached their capping strength, while only the configuration with the slender shear plate (BG3-2-10-F) experienced a large out-of-plane deformation along its bottom edge (LED4), which was subjected to compressive stress due to an eccentric shear force. Of note, the shear plate's out-of-plane deformation, both slender and compact plates (Fig. 6-5b), started to increase after yielding of the full depth of the shear plate along the gross section. However, only in the configuration with the slender shear plate (BG3-2-10-F), did the connection stiffness decrease while the slope of the curve representing the plate's out-of-plane deformation versus the connection rotation increased significantly.

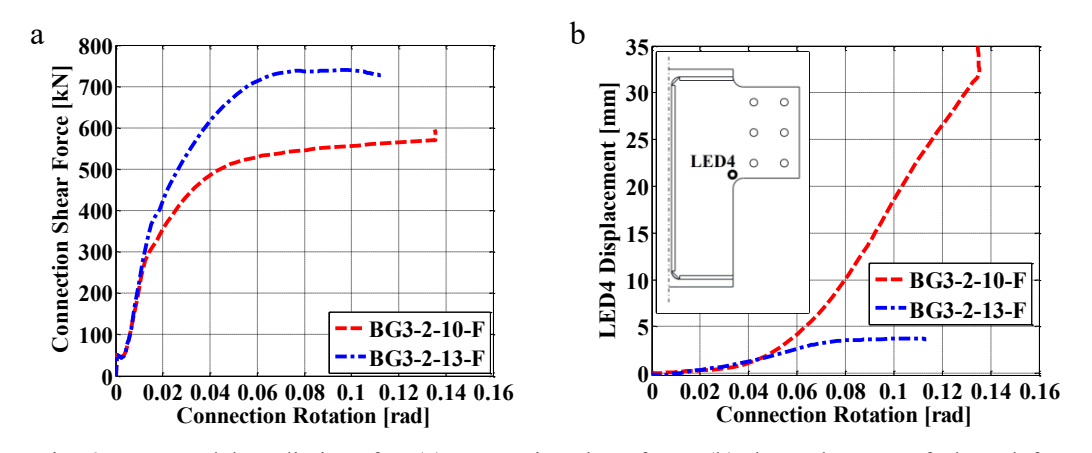


Fig. 6-5. FE model predictions for: (a) connection shear force, (b) shear plate out-of-plane deformation

For the configurations with a single vertical bolt line, bolt shear fracture was observed in the model after gross section yielding of the shear plate. In these models, bolt shear precluded the

shear plate from experiencing its ultimate strength. To deepen our understanding about the shear plate's ultimate failure mode, these models were rerun with elastic material properties assigned to the bolts. The ultimate strength of these models was controlled by shear plate buckling. In comparison to the shear tab with a single vertical bolt line, the buckling strength of the corresponding configuration with two vertical bolt lines was lower due to its larger effective eccentricity, the distance between the inflection point and the centre of the girder web.

Shear plate buckling was observed as the ultimate failure mode in all members of Group 3 other than BG3-2-10-F-GD0.93, which failed due to net section fracture. In this model, the bottom girder flange, placed at the shear plate's lower re-entrant corner, introduced extra restraint against the out-of-plane deformation of the shear plate, which prevented buckling. Results from Group 4 demonstrated that an increase in eccentricity reduced the plate yielding and buckling resistances. In configurations with a larger gap between the beam and girder, the bolt group was placed farther from the girder; that is, the connection eccentricity and the unbraced length were increased.

# 6.3.3 Shear capacity of bolt group

For the configurations with a single vertical bolt line, bolt shear fracture was observed as the ultimate failure mode. The bolt fracture was observed after gross section yielding of the shear plate, even though these connections did not satisfy the requirement of the AISC design method for the maximum plate thickness. Bolt shear fracture was observed as the secondary failure mode in configurations with two vertical bolt lines and two vertical bolt line, in which axial elongation of the interior bottom bolt occurred due to the shear plate buckling and large out-of-plane deformation.

Referring to Table 6-5, results of the *E-Bo* models demonstrated that the bolt group eccentricity corresponding to the bolt shear fracture was much smaller than the geometric eccentricity, *e* distance (as shown in Fig. 6-1d). The current AISC design procedure [4] uses this distance to calculate the capacity of the bolt group because of the assumption that the inflection point is formed at the support face, i.e. the web of the girder. Therefore, the observed bolt group capacity in the FE model was much larger (at least 1.50) than the current design method predictions. A comparison between *E-Bo* and *PL* models of configurations with a single vertical bolt line (Tables 6-4 and 6-5, respectively) demonstrated the slight influence of the shear plate yielding on the strength and effective eccentricity corresponding to the bolt shear fracture. The *PL* models of connection with a single vertical bolt line experience slightly larger bolt shear strength due to the stress redistribution following the yield of the shear plate.

To estimate the distance between the inflection point and the centre of the bolt group, Eq. (6-5) was proposed based on regression analysis. This equation predicted the bolt group eccentricity with a  $R^2$ =0.976 and a range of applicability of  $0.92 \le d_{pl} / a \le 2.77$  and c=1 & 2.

$$e_b(mm) = 11.23 c^{0.78} \left(\frac{d_{pl}}{a}\right)^{1.79}$$
 (6-5)

in which  $e_b$  is the distance between inflection point and the centre of bolt group as shown in Fig. 6-1d, c is the number of vertical bolt lines,  $d_{pl}$  is the depth of the extended portion of the shear plate, and a is the distance between the interior bolt line and the girder web.

The predicted eccentricity of the bolt group was used with the Instantaneous Centre of Rotation (ICR) method to determine the connection shear resistance corresponding to the bolt shear fracture. As shown in Table 6-5, the proposed eccentricity resulted in a reasonably conservative prediction of the bolt shear strength, compared to the current design recommendations. The predictions based

on this recommendation were conservative for FE-PL models with a single vertical line of bolts in which bolt shear fracture occurred after yielding of the shear plate.

#### 6.3.4 Shear plate resistance under tension

Referring to Table 6-6, the shear plate yielding began at the internal vertical bolt line of the shear plate. Then yielding propagated to the shear plate's gross section. In other words, net section yielding occurred prior to gross section yielding under pure tensile force applied to the beam. The bolt shear fracture was the ultimate failure mode of these models, except for BG3-2-10-F-PT in which the net section rupture and bolt shear fracture occurred simultaneously. To determine the net section fracture resistance of these configuration, the FE model was again run, where only elastic material properties were assigned to the bolts. Based on the current AISC design procedure [1], the fracture strength  $F_{UN} = F_u A_{net}$ , in which  $A_{net}$  and  $F_u$  are the plate net area and ultimate stress, respectively. The AISC predictions were reasonably conservative as compared to the predictions obtained from the FE models. Referring to Table 6-6, the reported bolt group resistance under tensile force represented the bolt group shear resistance under concentric shear force. These values were obtained from the E-Bo FE model under tensile force. The predictions obtained from the FE model for bolt shear fracture showed the reasonable conservativism of the current AISC equation for the bolt's nominal shear strength ( $F_{nv} = 0.625 F_u$ ), although the 0.90 length reduction factor was not considered.

# 6.3.5 Shear plate resistance under compression

The net section yielding did not occur in the shear plate under pure compression. For two configurations with a large *a* distance, i.e. BG6-2-16-F and BG6-2-19-F, plate buckling precluded the gross section yielding. In configurations BG3-2-10-F and BG3-2-13-F, shear plate yielding

occurred prior to buckling. The shear plate's buckling strength (P<sub>cr</sub>) was calculated based on the procedure proposed by Tamboli [14] for unstiffened extended shear tabs under pure compression. In this method, 0.65a was considered as the effective length of the shear plate. This method's predictions were reasonably accurate, although the ratio between the FE results and the analytical prediction for buckling strength decreased as the a distance increased. In comparison to the P<sub>cr</sub> values, the shear plate's out-of-plane deformation started to increase rapidly at a compressive force lower than the buckling strength. The bolt shear fracture was a secondary failure mode under compression. Following shear plate buckling, the large out-of-plane deformation of the shear plate resulted in the axial elongation of the bolts; as such, a smaller compressive force in the beam resulted in bolt shear fracture as compared to the tensile force in the beam required to fracture the bolts in shear.

#### 6.3.6 Effects of ht/hw ratio

Referring to Table 6-4, the results of the Group 3 members demonstrated the effect of the h<sub>t</sub>/h<sub>w</sub> ratio. This ratio involved the relative distance between the girder bottom flange and the lower edge of the extended portion of the shear plate. As this distance decreased, the girder flange provided a stiffer lateral bracing along the bottom re-entrant corner of the shear plate, where maximum compressive stress developed due to the bending moment. Shear plate buckling did not occur in configuration BG3-2-10-F-GD0.93, where the bottom flange was placed at the shear plate's lower re-entrant corner. As a general trend, the connection resistances corresponding to the plate out-of-plane deformation and buckling slightly decreased as the h<sub>t</sub>/h<sub>w</sub> ratio increased. However, the gross section yielding was greatly independent of the h<sub>t</sub>/h<sub>w</sub> ratio, as shown in Table 6-4.

# 6.3.7 Effect of the gap between beam and girder

Referring to Table 6-4, the connection resistance associated with gross section yielding decreased as the connection eccentricity increased due to the larger gap between the beam and girder. The larger gap amplified the plate's out-of-plane deformation by increasing the plate's unbraced length. The larger unbraced length also resulted in a reduction of the buckling strength. Due to the larger out-of-plane deformation of the shear plate, the connection eccentricity decreased rapidly after gross section yielding, which resulted in a lower flexural demand on the interior bolt line of the shear plate. A larger shear force was needed to develop the net section yielding.

#### 6.3.8 Effect of axial force

Referring to Table 6-7, axial force (either compression or tension) decreased the shear resistance corresponding to the gross section yielding due to the interaction of moment, shear, and axial force as shown in Eqs. (6-1) and (6-2). Regarding net section yielding, the axial compression force increased the shear resistance by reducing the shear demand on the net section, along the centerline of the bolt hole. In contrast, the applied axial tension force increased the shear demand on the net section, which resulted in the reduction of the shear resistance corresponding to net section yielding. In this case, net section yielding preceded gross section yielding.

The compressive force increased the out-of-plane deformation of the shear plate, which buckled under a smaller shear force as compared with its base model under gravity induced shear force alone. In several cases, buckling was followed by bolt shear fracture due to bolt elongation, i.e. the bolts experienced a combination of axial tension and shear. The shear fracture of these bolts was considered as the secondary failure mode. Contrary to the compression-loading scenario, the

axial tensile force placed on the beam reduced the out-of-plane deformation of the shear plate resulting in a larger buckling-related shear strength.

Net section fracture was the connections' ultimate failure mode under combined shear and tensile forces. Referring to Fig. 6-6a, the model that demonstrated net section fracture under coupled shear and tension force demands shows a markedly different strain distribution compared with that which failed due to buckling under combined compression and shear forces (Fig. 6-6b).

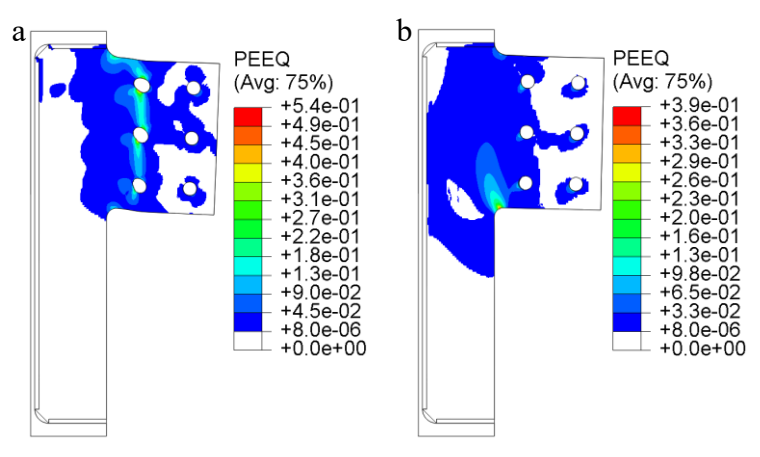


Fig. 6-6. Plastic strain propagation corresponding to capping strength at: (a) model BG3-2-10-F-400T (400kN tensile force), (b) model BG3-2-10-F-400C (400kN compression force)

Referring to Table 6-7, bolt shear fracture was observed as the ultimate failure mode only in five connections; this occurred after the full yielding of the shear plate.

Referring to Table 6-9, applying a small axial tensile force to the beam moves the inflection point toward the girder web. A further increase of the tensile force resulted in a larger reduction in the eccentricity. In contrast, a small axial compression force in the beam increased the effective eccentricity slightly, up to maximum of 7% for Specimen BG3-2-13-F-600C. However, further increasing the compressive force resulted in a decrease of the eccentricity. This observation can be attributed to the axial compressive force in the beam, which decreases the shear demand along the net section and delays yielding of the shear plate along the net section. This results in the delay

of the reduction in the stiffness and eccentricity of the connection. On the other hand, a further increase of the compressive force in the beam increased the out-of-plane deformation of the shear plate, which resulted in a rapid decrease of the connection stiffness and consequently the connection eccentricity. Referring to Table 6-9, the connection strength associated with yielding due to the moment-shear-axial force interaction was calculated based on three different interaction equations including; Eqs. (6-1), (6-2), (6-6), and (6-7). Equation (6-6) was identical to Eq. (6-2) other than the compressive capacity where P<sub>cr</sub> (shear plate buckling capacity, defined previously in Section 6.3.5) was used in lieu of P<sub>GY</sub>. Further, Eq. (6-7) was used to take into account the interaction of bending, shear and axial moment. This equation was introduced by the AISC Design Examples (Example IIA-19B) [15] and Steel Connection Handbook (Section 2.5.3) [14] based on Eq. (6-3) and design requirement of Section H1.1 of the AISC 360 Specification [1] for doubly symmetric members subjected to flexure and axial force.

$$\left(\frac{M}{M_{P}}\right) + \left(\frac{P}{P_{cr}}\right)^{2} + \left(\frac{V}{V_{P}}\right)^{4} \le 1$$
 (6-6)

$$\left(\frac{P}{2P_{u}} + \frac{M}{M_{u}}\right)^{2} + \left(\frac{V}{V_{u}}\right)^{2} \le 1 \qquad \frac{P}{P_{u}} < 0.2$$

$$\left(\frac{P}{P_{u}} + \frac{8}{9} \frac{M}{M_{u}}\right)^{2} + \left(\frac{V}{V_{u}}\right)^{2} \le 1 \qquad 0.2 \ge \frac{P}{P_{u}}$$

$$(6-7)$$

Both Eqs. (6-1) and (6-2) provided a reasonably accurate prediction of the yield strength. As the axial force increased, these predictions became less accurate. For most levels of axial force, the Eq. (6-2) predictions were almost equal to those of Eq. (6-1). These predictions deviated from each other under large axial forces when both equations significantly underestimated the shear yield strength. Therefore, Eq. (6-2) could be used in lieu of Eq. (6-1). Based on the comparison between predictions of Eqs. (6-2) and (6-6), the accuracy of Eq. (6-6) gained little benefit from the

implementation of  $P_{cr}$  instead of  $P_{GP}$  in the case of combined compressive and shear force. It was observed that Eq. (6-2) underestimated the shear yield strength by 16% and 20% under compressive and tensile forces equal to  $0.75P_{cr}$  and  $0.72P_{GY}$ , respectively. Equation (6-7) predicted conservatively the yield strength of all connection while its underestimation was more significant as compared to Eq. (6-1) and Eq. (6-2).

However, the shear strength corresponding to the gross section yielding was smaller than the connections' ultimate capacity. As the rotation and vertical displacement of the shear plate during the gross section yielding was still close to that of the net section yielding, the shear force corresponding to gross section yielding was considered as the connections' design strength.

Table 6-9. Connection capacities under combined axial and shear forces

			1 4016 0-3	New Recommendation										
ID.	]	FE Mode	1	F	ccentricit	h.	Fa	(6-1)	Eq. (		Eq. (	(6-6)	Eq. (	(6-7)
				L			Eq.	Ì	Eq. (		Eq. (	ì	Eq. (	<del>`                                    </del>
	$e_b^{\;FE}$	$e_{ m eff}^{ m FE}$	$V^{FE}$	e <sub>b</sub> A	$e_{\rm eff}{}^{A}$	$e_{\rm eff}^{\rm FE}$	$V_{A}$	$V_{\scriptscriptstyle  ext{FE}}$	$V_{A}$	$\overline{\mathrm{V}_{\scriptscriptstyle\mathrm{FE}}}$	$V_{A}$	$V_{\scriptscriptstyle  ext{FE}}$	$V_{A}$	$V_{\scriptscriptstyle  ext{FE}}$
	(mm)	(mm)	(kN)	(mm)	(mm)	$e_{\rm eff}^{\rm A}$	(kN)	$\overline{V_A}$	(kN)	$\overline{V_A}$	(kN)	$V_{A}$	(kN)	$\overline{V_{A}}$
BG3-2-10-F-700C	-4	199	182	28	231	0.86	128	1.42	132	1.37	57	3.18	76	2.39
BG3-2-10-F-600C	-4 1	204	245	28	231	0.88	128	1.42	208	1.18	160	1.53	127	1.92
BG3-2-10-F-000C BG3-2-10-F-400C	38	204	243 291	28 28	231	1.05	288	1.24	208 297	0.98	282	1.03	218	1.92
BG3-2-10-F-200C	38 37	241	332	28	231	1.03	335	0.99	338	0.98	335	0.99	218	1.13
BG3-2-10-F-200C	30	233	352 358	28	231	1.04	350	1.02	350 350	1.02	350	1.02	339	1.13
BG3-2-10-F BG3-2-10-F-200T	28	233	338 344	28 28	231		335	1.02	338	1.02	338		339 294	1.06
BG3-2-10-F-2001 BG3-2-10-F-400T	28	231	308	28 28	231	1.00 0.98	288	1.03	338 297	1.02	338 297	1.02 1.04	218	1.17
BG3-2-10-F-600T	8	211	233	28 28	231	0.98	200 198	1.07	208	1.12	208	1.12	127	1.42
BG3-2-10-F-800T	-15	188	233 78	28	231	0.92	35	2.25	35	2.24	35	2.24	20	3.99
BG3-2-13-F-1000C	16	219	226 b	33	236	0.82	100	2.25	102	2.24	64	3.50	58	3.99
BG3-2-13-F-1000C BG3-2-13-F-800C	41	219	300	33	236	1.03	249	1.21	260	1.16	239	1.25	38 159	3.92 1.89
BG3-2-13-F-600C	47	250	339	33	236	1.05	345	0.98	357	0.95	348	0.97	249	1.36
BG3-2-13-F-400C	40	243	339 396	33	236	1.00	407	0.98	413	0.95	410	0.97	328	1.21
BG3-2-13-F-200C	40	243 244	443	33	236	1.03	407 441	1.01	443	1.00	442	1.00	328 405	1.21
BG3-2-13-F	36	239	443 464	33	236	1.03	452	1.01	443	1.03	452	1.00	435	1.09
BG3-2-13-F-200T	32	235	454	33	236	0.99	432 441	1.03	432	1.03	443	1.03	405	1.12
BG3-2-13-F-400T	32	235	422	33	236	0.99	441	1.03	443	1.03	443	1.03	328	1.12
BG3-2-13-F-600T	25	233	380	33	236	0.99	345	1.04	357	1.02	357	1.02	249	1.53
BG3-2-13-F-800T	11	214	311	33	236	0.90	249	1.10	260	1.20	260	1.20	159	1.95
BG3-2-13-F-1000T	-12	191	209	33	236	0.91	100	2.08	102	2.05	102	2.05	58	3.62
BG6-2-16-F-2000C	-32	247	1084	56	335	0.74	851	1.27	940	1.15	808	1.34	596	1.82
BG6-2-16-F-1500C	-32 54	333	1151	56	335	0.74	1097	1.05	1162	0.99	1114	1.03	868	1.33
BG6-2-16-F-1000C	60	339	1294	56	335	1.01	1250	1.03	1282	1.01	1265	1.03	1091	1.33
BG6-2-16-F-500C	59	338	1367	56	335	1.01	1335	1.03	1343	1.01	1340	1.02	1304	1.19
BG6-2-16-F-250C	60	339	1357	56	335	1.01	1356	1.02	1343	1.02	1340	1.02	1342	1.03
BG6-2-16-F	58	339 337	1401	56	335 335	1.01	1363	1.00	1363	1.00	1363	1.00	1342	1.01
BG6-2-16-F-250T	55	334	1386	56	335	1.01	1356	1.03	1358	1.03	1358	1.03	1342	1.02
BG6-2-16-F-500T	53 54	333	1359	56	335	0.99	1335	1.02	1343	1.02	1343	1.02	1342	1.03
BG6-2-16-F-1000T	56	335 335	1339	56	335 335	1.00	1250	1.02	1343	1.01	1282	1.01	1091	1.04
BG6-2-16-F-1500T	52	333	1102	56	335 335	0.99	1097	1.02	1162	0.95	1162	0.95	868	1.17
BG6-2-16-F-2000T	36	315	971	56	335	0.99	851	1.14	940	1.03	940	1.03	596	1.63
BG6-2-16-F-2500T	8	287	588	56	335	0.94	430	1.14	940 468	1.03	468	1.03	255	2.31
DG0-2-10-F-23001	0	201	200	50	333	0.00	430	1.37	400	1.20	400	1.20	233	2.31

Table 6.9 (Continued). Connection capacities under combined axial and shear forces

ID.		FE Mode			omicero				ecomme					
	e <sub>b</sub> FE (mm)	e <sub>eff</sub> <sup>FE</sup> (mm)	V <sup>FE</sup> (kN)	e <sub>b</sub> <sup>A</sup> (mm)	e <sub>eff</sub> A (mm)	$\frac{e_{eff}^{FE}}{e_{eff}^{A}}$	V <sub>A</sub> (kN)	$\frac{V_{FE}}{V_{A}}$	V <sub>A</sub> (kN)	$\frac{V_{\text{FE}}}{V_{\text{A}}}$	V <sub>A</sub> (kN)	$\frac{V_{FE}}{V_{A}}$	V <sub>A</sub> (kN)	$\frac{V_{\text{FE}}}{V_{\text{A}}}$
BG6-2-19-F-2500C	17	296	1125	64	343	0.86	935	1.20	1033	1.09	921	1.22	632	1.78
BG6-2-19-F-2000C	53	332	1267	64	343	0.97	1212	1.05	1298	0.98	1250	1.01	914	1.39
BG6-2-19-F-1500C	61	340	1457	64	343	0.99	1399	1.04	1454	1.00	1432	1.02	1154	1.26
BG6-2-19-F-1000C	63	342	1547	64	343	1.00	1522	1.02	1547	1.00	1539	1.01	1360	1.14
BG6-2-19-F-500C	63	342	1647	64	343	1.00	1592	1.03	1598	1.03	1596	1.03	1551	1.06
BG6-2-19-F-250C	63	342	1639	64	343	1.00	1609	1.02	1610	1.02	1610	1.02	1589	1.03
BG6-2-19-F	62	341	1686	64	343	1.00	1614	1.04	1614	1.04	1614	1.04	1625	1.04
BG6-2-19-F-250T	60	339	1670	64	343	0.99	1609	1.04	1610	1.04	1610	1.04	1589	1.05
BG6-2-19-F-500T	57	336	1648	64	343	0.98	1592	1.04	1598	1.03	1598	1.03	1551	1.06
BG6-2-19-F-1000T	57	336	1574	64	343	0.98	1522	1.03	1547	1.02	1547	1.02	1360	1.16
BG6-2-19-F-1500T	53	332	1461	64	343	0.97	1399	1.04	1454	1.00	1454	1.00	1154	1.27
BG6-2-19-F-2000T	44	323	1283	64	343	0.94	1212	1.06	1298	0.99	1298	0.99	914	1.40
BG6-2-19-F-2500T	22	301	1137	64	343	0.88	935	1.22	1033	1.10	1033	1.10	632	1.80
BG6-2-19-F-3000T	-5	274	788	64	343	0.80	498	1.58	536	1.47	536	1.47	293	2.69
				M	inimum	0.74		0.97		0.95		0.95		1.01
					Mean	0.96		1.16		1.13		1.22		1.55
				Ma	aximum	1.06		2.25		2.24		3.50		3.99
			St	andard d	eviation	0.07		0.30		0.29		0.52		0.72
					COV	0.08		0.26		0.26		0.43		0.47

<sup>&</sup>lt;sup>a</sup> Bolt axial deformation increased due to shear plate buckling
<sup>b</sup> Minimum shear force after applying axial force, the section yielded during applying axial force.
<sup>c</sup> Out-of-plane deformation occurred in advance of the gross section yielding

#### 6.3.9 Shear plate internal forces along the bolt line

The net section along the centerline of the interior bolt line was subjected to a portion of a connection's shear and axial forces, referring to Fig. 6-7. Figures 6-7a and 6-7b show that more than 95% of the tensile force was transferred through the interior bolt line, while less than 60% of the compressive force was carried by the net section along the centerline of the bolt holes. Referring to Fig. 6-7c, in the case of gravity induced shear force, the ratio between the shear force at the net and gross sections,  $\eta$  factor, decreased to 0.78 after an initial peak. Applying an axial force affected this ratio significantly. The tensile force increased the  $\eta$  factor, while the compression force decreased it. Referring to Fig. 6-7d, the same trend was observed for the  $\eta'$  ratio, the ratio of axial force at the net section and the magnitude of the applied axial force. In the presence of a tensile axial force, the  $\eta'$  ratio became larger than 1 because the existing bending due to the eccentric shear load developed tension at the plate's net section. The  $\eta'$  ratio reduced to less than 0.6 at 0.02 rad connection rotation in the presence of axial compression. The existing bending due to the eccentric shear load started to decrease this ratio. Previous research [63] showed that the axial force moved the bolt shank in the bolt hole and consequently changed the  $\eta$  and  $\eta'$  ratios.

In order to develop an analytical equation to predict the  $\eta$  and  $\eta'$  ratios, it was assumed that a bolt group with  $n_v$  vertical bolt lines (Fig. 6-8a) was subjected to a concentric shear force with the bolts placed along the centerline of bolt holes. The plate's interior bolt line was subjected to half of the shear load from the interior bolts in addition to shear loads from the other  $n_v$ -1 bolt lines. By assuming a uniform force distribution between the bolts, Eq. (6-8) estimated a portion of the connection shear force transferring through the plate interior bolt line.

$$\eta = \frac{n_{v} - 1}{n_{v}} + \frac{1}{2n_{v}} = 1 - \frac{1}{2n_{v}} \tag{6-8}$$

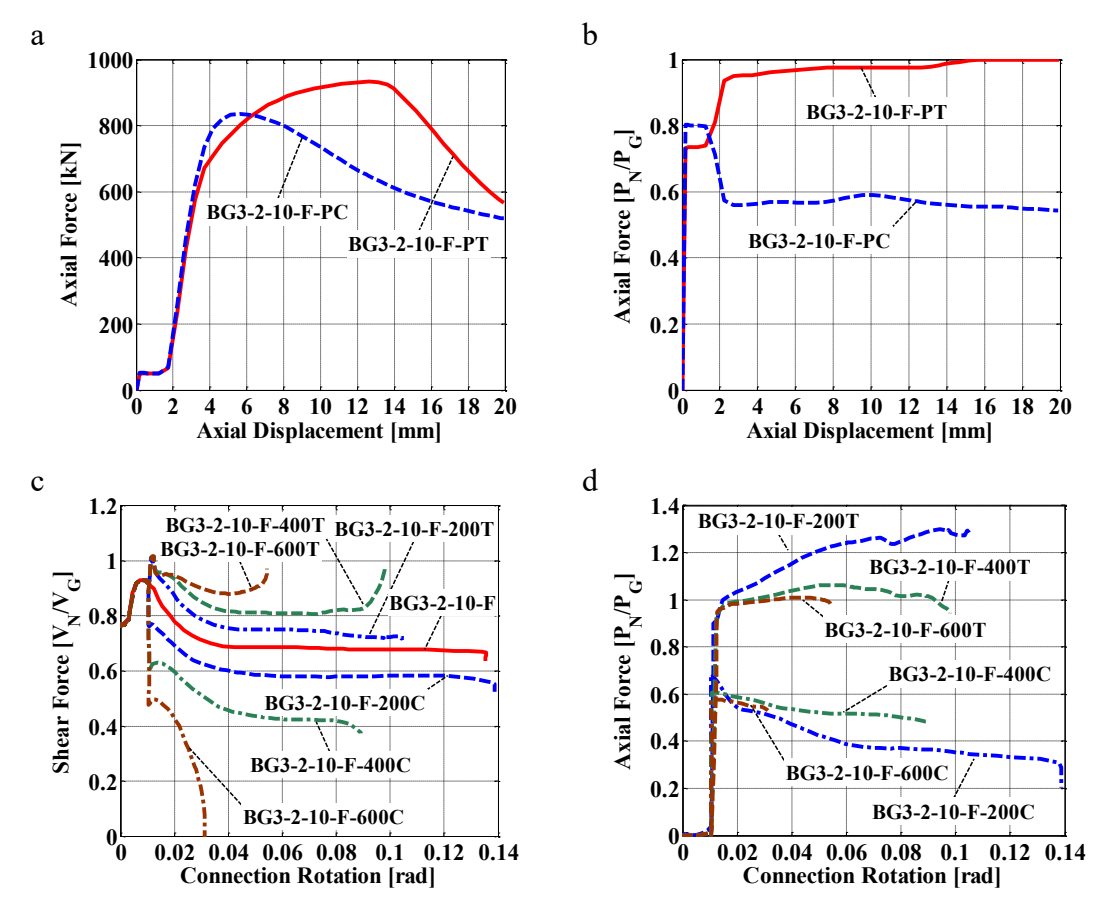


Fig. 6-7 P<sub>n</sub>/P<sub>a</sub> under combined axial and shear forces

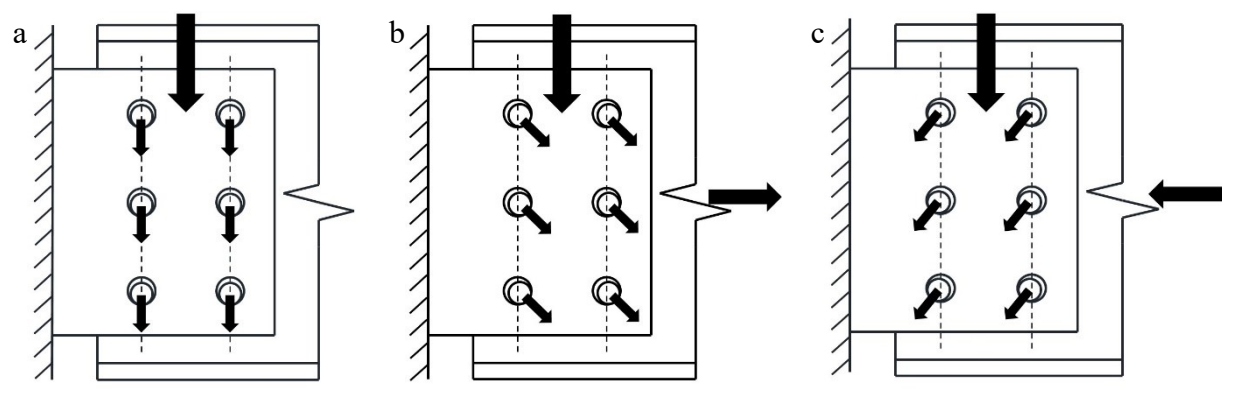


Fig. 6-8. Interior vertical bolt line under: (a) concentric shear force, (b) tension and concentric shear, (c) compression and concentric shear

Referring to Fig. 6-8b, the bolts moved away from the support and crossed the bolt-line centerline if they were subjected to enough tensile force from the beam in addition to the shear force. In this case, the total shear force of the interior bolts was transferred through the net section.

The ratio between the transferred shear force and connection shear force could be calculated using Eq. (6-9).

$$\eta = \frac{(n_v - 1)}{n_v} + \frac{1}{n_v} = 1 \tag{6-9}$$

In contrast, if the bolt group was subjected to enough compression force from the beam in addition to the shear load (Fig. 6-8c), the bolts moved toward the supports and the net section transferred the shear force from the other n<sub>v</sub>-1 bolt lines (Eq. (6-10)). However, this equation might be unconservative, if the magnitude of compression was not sufficient to move the bolts towards the support. In this case, Eq. (6-11), the average of Eqs. (6-8) and (6-10), was a more rational option.

$$\eta = \frac{n_{v} - 1}{n_{v}} = 1 - \frac{1}{n_{v}} \tag{6-10}$$

$$\eta = \frac{1}{2} \left[ \left( 1 - \frac{1}{2n_v} \right) + \left( 1 - \frac{1}{n_v} \right) \right] = 1 - \frac{3}{4n_v}$$
 (6-11)

Equations (6-8) to (6-11) could be used to determine the  $\eta'$  ratio, the ratio between axial force at the gross and net sections, as well. Of note, these equations were obtained based on the assumption that the bolt group was subjected to the eccentric axial and shear forces. Referring to Figs. 6-7c and 6-7d, these estimations slightly deviated from those observed in the FE models due to the existing bending moment. Referring to 6c, Eq. (6-8) predicted the  $\eta$  ratio (0.75) reasonably well in the case of gravity induced shear force (0.78 at 0.02 rad connection rotation in model BG3-2-10-F). In the case of combined tension and shear forces, Eq. (6-9) gave conservative estimations. Fig. 6-7c shows that Eq. (6-11) conservatively predicted the  $\eta$  value in FE models under combined shear and compression other than BG3-2-10-F-200C in which the observed  $\eta$  value (0.69 at 0.02 rad connection rotation) was slightly larger than Eq. (6-11) prediction, 0.625. Referring to Fig. 6-7d, Eq. (6-11) conservatively predicted the  $\eta'$  value for the FE models under combined compressive and

shear forces. Referring to Fig. 6-7d, the  $\eta'$  value became larger than unity in the FE models under combined shear and tension. This extra tensile force arose from bending moment due to the existing eccentricity of the shear force. However, this extra tension could be taken into account implicitly in the interaction equations (Eqs. (6-1) and (6-2)) by assuming bending moment along the net section equal to the product of the connection shear force and the distance between the inflection point and the interior bolt line. Referring to Table 6-10, Eq. (6-8) predictions resulted in a conservative estimation of the net section yielding strength of models under gravity induced shear force.

Table 6-10. Net section yielding strength of connection under gravity shear

			, .		raing sire	8				ommend	ation		
	ID.		netric neters	I	FE model	S	Eq.	(6-4)	Eq. (6-8)	Eq. (	6-2)	Eq. (	6-3)
		a (mm)	e <sub>g</sub> (mm)	e <sub>b</sub> (mm)	e <sub>eff</sub> - a (mm)	V <sub>FE</sub> (kN)	e <sub>b</sub> (mm)	e <sub>eff</sub> - a (mm)	η	V <sub>A</sub> (kN)	$\frac{V_{\text{FE}}}{V_{\text{A}}}$	V <sub>A</sub> (kN)	$\frac{V_{\text{FE}}}{V_{\text{A}}}$
	BG3-2-10-F	165	203	28	66	372	28	66	0.75	366	1.02	362	1.03
Group 1	BG3-2-13-F	165	203	36	74	464	33	71	0.75	472	0.98	461	1.01
iro	BG6-2-16-F	241	279	59	97	1348	56	94	0.75	1265	1.07	1283	1.05
	BG6-2-19-F	241	279	64	102	1555	64	102	0.75	1488	1.05	1503	1.03
	BG2-1-10-F	165	165				12	12	0.50	438		453	
	BG3-1-10-F	165	165				28	28	0.50	799		803	
	BG4-1-10-F	165	165				49	49	0.50	767		770	
Group 2	BG5-1-10-F	165	165				76	76	0.50	900		886	
no.	BG6-1-10-F	165	165				109	109	0.50	998		964	
5	BG2-2-10-F	165	203	-13	25	311	12	50	0.75	230	1.35	222	1.40
	BG4-2-10-F	165	203	50	88	489	49	87	0.75	485	1.01	478	1.02
	BG5-2-10-F	165	203	77	115	606	76	114	0.75	600	1.01	590	1.03
	BG6-2-10-F	165	203	113	151	694	109	147	0.75	697	1.00	680	1.02
	BG3-2-10-F-GD0.93	165	203	28	66	375	28	66	0.75	366	1.02	362	1.03
	BG3-2-10-F-GD0.80	165	203	26	64	383	28	66	0.75	366	1.05	362	1.06
Group 3	BG3-2-10-F-GD0.60	165	203	23	61	395	28	66	0.75	366	1.08	362	1.09
noı	BG3-2-10-F-GD0.30	165	203	20	58	403	28	66	0.75	366	1.10	362	1.11
G	BG3-2-10-F-GD0.27	165	203	19	57	404	28	66	0.75	366	1.10	362	1.11
	BG3-2-10-F-GD0.24	165	203	19	57	408	28	66	0.75	366	1.11	362	1.13
	BG3-2-10-F-GD0.20	165	203	15	53	426	28	66	0.75	366	1.16	362	1.18
Group 4	BG3-2-10-F-G25	178	216	14	52	390	23	74	0.75	351	1.11	343	1.14
ron	BG3-2-10-F-G38	191	229	-2	36	385	19	83	0.75	334	1.15	323	1.19
<u> </u>	BG3-2-10-F-G50	203	241	-22	16	383	16	92	0.75	317	1.21	303	1.26
									M	inimum	0.98		1.01
										Mean	1.09		1.10
										iximum	1.35		1.40
								St	andard de		0.09		0.10
										COV	0.08		0.09

Referring to Table 6-10, Eq. (6-4) provided a reasonable estimate of the location of the inflection point corresponding to the net section yielding in all models. Regarding the FE models under combined axial and shear forces, Fig. 6-9 shows the results of interaction equation along the interior bolt line. Referring to Fig. 6-9, Eq. (6-2) predictions was much close to Eq. (6-1) estimates until net section yielding. Since after, their results became larger than unity and the difference between their predictions started to increase.

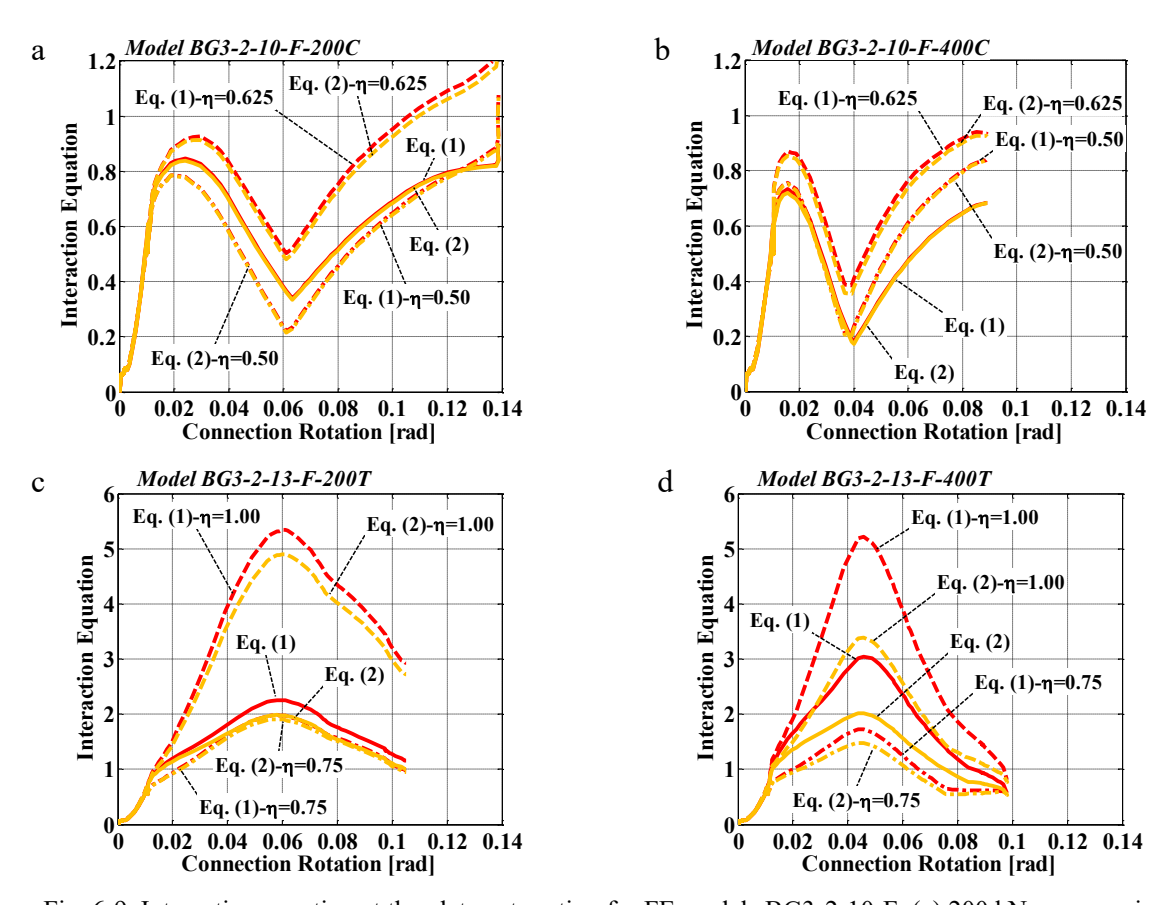


Fig. 6-9. Interaction equation at the plate net section for FE models BG3-2-10-F: (a) 200 kN compression, (b) 400 kN compression, (c) 200kN tension, (d) 400 kN tension

Referring to Fig. 6-9b, the results of both Eqs. (6-10) and (6-11), i.e.  $\eta = \eta' = 0.625$  and  $\eta = \eta' = 0.50$ , respectively, caused an overestimation of the interaction effects for model BG3-2-10-400C, in which the connection was subjected to a larger axial compression as compared to model BG3-2-10-F-200C. A general survey over the results of the FE models under combined shear and

compression demonstrated that Eq. (6-11) predictions ended in a conservative estimate of the net section interaction yielding unless the compressive force was smaller than 0.10  $P_{GY}$ . In this case, Eq. (6-8) would result in a conservative prediction for the interaction effect. Figures. 6-9c and 6-9d demonstrates that estimates of Eq. (6-9) ( $\eta = \eta' = 1.00$ ) occasioned a conservative estimation of the interaction yielding in connection under coupled tension and shear demands. These aforementioned trends were also observed in other configurations under combined axial and shear forces. Table 6-11 present estimates of Eqs. (6-1) and (6-2) for the connection shear force corresponding to the yielding of the net section.

Table 6-11. Net section yielding strength of the connections under combined axial and shear force

Table	6-11. Ne	t section	yielding s	strength of	the conn		inder con ew Recor			ear force	
ID.	]	FE Mode	1	Eqs. (6-8 9), and (6		Eq.	(6-4)	Eq.	(6-1)	Eq.	(6-2)
	e <sub>b</sub> (mm)	e <sub>eff</sub> - a (mm)	V <sup>FE</sup> (kN)	η	$\frac{P}{P_{NP}}$	e <sub>b</sub> (mm)	e <sub>eff</sub> - a (mm)	V <sub>A</sub> (kN)	$\frac{\mathrm{V_{FE}}}{\mathrm{V_{A}}}$	V <sub>A</sub> (kN)	$\frac{\mathrm{V_{FE}}}{\mathrm{V_{A}}}$
BG3-2-10-F-700C				0.625	0.72	28	66	232		244	
BG3-2-10-F-600C				0.625	0.62	28	66	284		297	
BG3-2-10-F-400C	-26	12	362	0.625	0.41	28	66	358	1.01	366	0.99
BG3-2-10-F-200C	4	42	440	0.625	0.21	28	66	396	1.11	398	1.10
BG3-2-10-F	28	66	372	0.75	0.00	28	66	366	1.02	366	1.02
BG3-2-10-F-200T	36	74	285	1.00	0.33	28	66	277	1.29	283	1.26
BG3-2-10-F-400T	41	79	225 b	1.00	0.66	28	66	206	1.09	226	1.00
BG3-2-10-F-600T	11	49	195 <sup>b</sup>	1.00	0.99	28	66	11	18.15°	11	18.12 <sup>c</sup>
BG3-2-10-F-800T	2	40	43 b	1.00	1.32	28	66				
BG3-2-13-F-1000C				0.625	0.78	33	71	244		253	
BG3-2-13-F-800C	-13	26	520	0.625	0.62	33	71	359	1.45	373	1.39
BG3-2-13-F-600C	-8	30	632	0.625	0.47	33	71	434	1.46	445	1.42
BG3-2-13-F-400C	17	55	610	0.625	0.31	33	71	486	1.26	492	1.24
BG3-2-13-F-200C	27	65	545	0.625	0.16	33	71	514	1.06	516	1.06
BG3-2-13-F	36	74	464	0.75	0.00	33	71	472	0.98	472	0.98
BG3-2-13-F-200T	40	78	394	1.00	0.25	33	71	372	1.06	377	1.05
BG3-2-13-F-400T	44	82	319	1.00	0.50	33	71	322	0.99	338	0.94
BG3-2-13-F-600T	34	72	298 b	1.00	0.75	33	71	222	1.34	246	1.21
BG3-2-13-F-800T	13	51	$268^{\mathrm{b}}$	1.00	1.00	33	71				
BG3-2-13-F-1000T	-12	26	209 b	1.00	1.24	33	71				
BG6-2-16-F-2000C				0.625	0.65	56	94	1000		1077	
BG6-2-16-F-1500C	5	43	1395	0.625	0.49	56	94	1209	1.15	1263	1.10
BG6-2-16-F-1000C	41	79	1540	0.625	0.33	56	94	1344	1.15	1370	1.12
BG6-2-16-F-500C	56	94	1451	0.625	0.16	56	94	1424	1.02	1431	1.01
BG6-2-16-F-250C	59	97	1409	$0.75^{d}$	0.10	56	94	1256	1.12	1258	1.12
BG6-2-16-F	59	97	1348	0.75	0.00	56	94	1265	1.07	1265	1.07
BG6-2-16-F-250T	57	95	1268	1.00	0.13	56	94	992	1.28	996	1.27
BG6-2-16-F-500T	57	95	1156	1.00	0.26	56	94	962	1.20	976	1.18
BG6-2-16-F-1000T	66	104	885	1.00	0.52	56	94	833	1.06	887	1.00
BG6-2-16-F-1500T	64	102	$800^{\mathrm{b}}$	1.00	0.78	56	94	567	1.41	662	1.21
BG6-2-16-F-2000T	46	84	715 b	1.00	1.04	56	94				
BG6-2-16-F-2500T	9	47	564 b	1.00	1.30	56	94				
BG6-2-19-F-2500C				0.625	0.68	64	102	1098		1180	
BG6-2-19-F-2000C	-1	37	1728	0.625	0.54	64	102	1340	1.29	1407	1.23
BG6-2-19-F-1500C	21	59	1964	0.625	0.41	64	102	1498	1.31	1541	1.27
BG6-2-19-F-1000C	60	98	1851	0.625	0.27	64	102	1611	1.15	1632	1.13
BG6-2-19-F-500C	62	100	1702	0.625	0.14	64	102	1673	1.02	1678	1.01
BG6-2-19-F-250C	63	101	1639	$0.75^{d}$	0.08	64	102	1475	1.11	1478	1.11
BG6-2-19-F	64	102	1555	0.75	0.00	64	102	1488	1.05	1488	1.05
BG6-2-19-F-250T	63	101	1452	1.00	0.11	64	102	1178	1.23	1181	1.23
BG6-2-19-F-500T	60	98	1430	1.00	0.22	64	102	1152	1.24	1164	1.23
BG6-2-19-F-1000T	65	103	1144	1.00	0.43	64	102	1051	1.09	1094	1.05
BG6-2-19-F-1500T	69	107	992 <sup>b</sup>	1.00	0.65	64	102	851	1.17	940	1.06
BG6-2-19-F-2000T	59	97	933 <sup>b</sup>	1.00	0.87	64	102	477	1.95	559	1.67
BG6-2-19-F-2500T	28	66	896 <sup>b</sup>	1.00	1.08	64	102				
BG6-2-19-F-3000T	-6	32	644 <sup>b</sup>	1.00	1.30	64	102				
DG0-2-17-1-30001	-0	34	077	1.00	1.50	U <del>1</del>	102				

Table 6.11 (Continued). Net section yielding strength of the connections under combined axial and shear force

			Eqs. (6- 9), and (		Eq.	(6-4)	Eq. (6-1)		Eq.	(6-2)
e <sub>b</sub> (mm)	e <sub>eff</sub> - a (mm)	V <sup>FE</sup> (kN)	η	$\frac{P}{P_{NP}}$	e <sub>b</sub> (mm)	e <sub>eff</sub> - a (mm)	V <sub>A</sub> (kN)	$\frac{V_{FE}}{V_A}$	V <sub>A</sub> (kN)	$\frac{\mathrm{V}_{\mathrm{FE}}}{\mathrm{V}_{\mathrm{A}}}$
						Mi	inimum	0.97		0.94
							Mean	1.18		1.14
						Ma	iximum	1.95		1.67
					St	andard de	eviation	0.20		0.16
							COV	0.17		0.14

<sup>&</sup>lt;sup>a</sup> Based on Eq. (6-8) for connection under gravity induced shear force, Eq. (6-9) for models under combined tension and shear, and Eq. (6-11) for models under combined compression and shear

#### **6.3.10** The net section fracture

Referring to Table 6-6, the current AISC design method [1] conservatively predicted the tensile strength corresponding to the net section fracture. This observation can be explained by the average ultimate stress at the net section being higher than the test coupons' ultimate stress; the holes in the shear tab prevent development of free lateral contraction at the net section [55]. For the case when the net section was subjected to a concentric shear force, the AISC design procedure [1] estimated  $V_{UN} = 0.6F_uA_{net}$  as the shear fracture strength, while it assumed that the net section resisted the total connection shear force. Of note, the AISC design method for extended shear tabs ignored the shear-moment interaction along the net section and separately checked the net section fracture under shear and bending loads. For the cases where the net section was subjected to combined shear and tension forces, the AISC method contains no interaction equation. Based on Eqs. (6-1) and (6-2), Eqs. (6-12) and (6-13) were proposed, respectively, in order to consider the interaction of the axial force, shear, and moment at the net section of the shear plate. Furthermore, an elliptical interaction equation between the shear and axial forces (Eq. (6-14)) was used to calculate the net section fracture strength, referring to Table 6-12.

<sup>&</sup>lt;sup>b</sup> Minimum shear force after applying axial force, the section yielded during applying axial force

<sup>&</sup>lt;sup>c</sup> This value was not included in statistic analysis

<sup>&</sup>lt;sup>d</sup> Based on Eq. (6-8) because  $P/P_{GP} \le 0.10$ 

$$\left(\frac{M}{M_{NU}}\right) + \left(\frac{P}{P_{NU}}\right)^2 + \left(\frac{(V/V_{NU})^4}{1 - (P/P_{NU})^2}\right) \le 1 \tag{6-12}$$

$$\left(\frac{M}{M_{NU}}\right) + \left(\frac{P}{P_{NU}}\right)^2 + \left(\frac{V}{V_{NU}}\right)^4 \le 1$$
 (6-13)

$$\left(\frac{P}{P_{NU}}\right)^2 + \left(\frac{V}{V_{NU}}\right)^2 \le 1 \tag{6-14}$$

Table 6-12. Shear strength corresponding to net section fracture

				icai stici	igtii corre	New R	ecomme					
ID.		FE Mode	I	E	ccentricit	ty	Eq. (6		Eq. (	6-13)	Eq. (	6-14)
-	e <sub>b</sub> FE	e <sub>eff</sub> FE	VFE	Δ	Δ	e <sub>eff</sub> eff	37	$V_{FE}$		$V_{\text{FE}}$	17	$V_{FE}$
			•	e <sub>b</sub> A	e <sub>eff</sub> A	eff A	$V_A$		$V_A$		$V_A$	FE -
	(mm)	(mm)	(kN)	(mm)	(mm)	$e_{\text{eff}}^{A}$	(kN)	$V_{_{A}}$	(kN)	$V_{_{A}}$	(kN)	$\overline{V_{A}}$
BG3-2-10-F-200T	-7	196	525	28	231	0.85	404	1.30	409	1.28	497	1.06
BG3-2-10-F-400T	-2	201	455	28	231	0.87	358	1.27	374	1.22	451	1.01
BG3-2-10-F-600T	-8	195	366	28	231	0.85	270	1.35	299	1.23	365	1.00
BG3-2-10-F-800T	-13	190	209	28	231	0.82	84	2.50	88	2.38	174	1.20
BG3-2-13-F-200C	-4	199	758	33	236	0.84	532	1.42	536	1.42	665	1.14
BG3-2-13-F	5	208	727	33	236	0.88	544	1.34	544	1.34	676	1.08
BG3-2-13-F-200T	4	207	696	33	236	0.88	532	1.31	536	1.30	665	1.05
BG3-2-13-F-400T	1	204	649	33	236	0.86	500	1.30	512	1.27	633	1.02
BG3-2-13-F-600T	-1	202	578	33	236	0.85	439	1.32	464	1.25	573	1.01
BG3-2-13-F-800T	9	194	494	33	236	0.82	341	1.45	375	1.32	476	1.04
BG3-2-13-F-1000T	-16	187	367	33	236	0.79	174	2.11	188	1.95	308	1.19
BG6-2-16-F-250T	58	337	1737	56	335	1.01	1399	1.24	1401	1.24	1610	1.08
BG6-2-16-F-500T	60	339	1689	56	335	1.01	1376	1.23	1387	1.22	1588	1.06
BG6-2-16-F-1000T	57	336	1560	56	335	1.00	1290	1.21	1330	1.17	1502	1.04
BG6-2-16-F-1500T	46	325	1391	56	335	0.97	1126	1.24	1213	1.15	1340	1.04
BG6-2-16-F-2000T	30	309	1164	56	335	0.92	871	1.34	1001	1.16	1088	1.07
BG6-2-16-F-2500T	4	283	908	56	335	0.84	374	2.43	427	2.13	594	1.53
BG6-2-19-F-500C	45	324	2221	64	343	0.95	1642	1.35	1649	1.35	1918	1.16
BG6-2-19-F-250C	58	337	2194	64	343	0.98	1657	1.32	1660	1.32	1934	1.13
BG6-2-19-F	65	344	2160	64	343	1.00	1664	1.30	1664	1.30	1940	1.11
BG6-2-19-F-250T	67	346	2111	64	343	1.01	1657	1.27	1660	1.27	1934	1.09
BG6-2-19-F-500T	65	344	2059	64	343	1.00	1642	1.25	1649	1.25	1918	1.07
BG6-2-19-F-1000T	60	339	1942	64	343	0.99	1567	1.24	1600	1.21	1844	1.05
BG6-2-19-F-1500T	51	330	1792	64	343	0.96	1444	1.24	1514	1.18	1723	1.04
BG6-2-19-F-2000T	37	316	1650	64	343	0.92	1242	1.33	1359	1.21	1522	1.08
BG6-2-19-F-2500T	17	296	1439	64	343	0.86	954	1.51	1100	1.31	1238	1.16
BG6-2-19-F-3000T	0	279	1189	64	343	0.81	427	2.79	476	2.50	713	1.67
						M	inimum	1.21		1.15		1.00
							Mean	1.48		1.40		1.12
							aximum	2.79		2.50		1.67
					Sta	andard d		0.42		0.36		0.15
							COV	0.28		0.26		0.13

Referring to Table 6-12, all equations conservatively predicted the fracture shear strength.

Among these equations, Eq. (6-14) presented the most accurate results. This observation could be

attributed to movement of the inflection point toward the girder web after gross section yielding. As such, the eccentricity corresponding to the net section fracture was smaller than the implemented eccentricity corresponding to the gross section yielding, calculated based on Eq. (6-4).

#### **6.3.11** Design procedure

To evaluate the accuracy of the current design method for extended shear tabs, the ultimate shear capacity of the connections under gravity induced shear force was compared with the predicted strength (Table 6-13). In addition to the AISC design recommendation, the connection capacity was estimated based on Fortney's and Thornton's recommendation to consider the inflection point at the toe of the horizontal stiffeners (tip of the girder flange). Furthermore, the connection capacity was calculated based on the connection eccentricity ( $e_{eff} = e_b + e_g$ ). The effective eccentricity was estimated in accordance with the prediction of Eq. (6-4) for the bolt group eccentricity (e<sub>b</sub>) and the connection's geometric eccentricity (e<sub>g</sub>). Referring to Table 6-13, the AISC design method is the most conservative. Implementation of Fortney's and Thornton's recommendation for the location of the inflection point significantly increased the accuracy of the predictions for the ultimate shear capacity of the connection. However, this recommendation resulted in overestimation of the connection resistance corresponding to the yielding of the gross section of the plate. The large rotation and deformation following the yielding of the shear plate may be detrimental to the serviceability of the supported beam. In comparison to the AISC and Fortney's and Thornton's recommendations for the design of extended shear tabs, implementation of the effective eccentricity, calculated based on Eq. (6-4), resulted in the most accurate predictions. Further, this method gave reasonable predictions for the connection shear force corresponding to the yield of the gross section of the shear plate.

Referring to Table 6-14, the accuracy of the aforementioned design recommendations was evaluated in the presence of the axial force, Of note, the interaction of the bending moment, shear and axial was taken into account by Eq. (6-2) for the yield of the gross section of the shear plate. Referring to Section 3.10, only the interaction of the axial and shear force was considered to calculate the rupture strength of the plate's net section. The bolt group capacity was calculated for the resultant force of the axial and shear in accordance to the ICR method. The comparison between observed ultimate strength and predicted strength demonstrated that the AISC design recommendation was still most conservative method. Although Fortney's and Thornton's recommendations resulted in the most accurate prediction (the mean value of for the observed-to-predicted strength ratio), this method overestimated the connection capacity of a few connections in the presence of medium to large axial compression. Referring to Table 6-14, the calculation based on the effective eccentricity (Eq. 6-4) still resulted in a reasonably conservative estimate of the connection shear capacity in the presence of combined axial and shear force.

Referring to Tables 6-4 and 6-7, the connection's inflection point moved toward the girder web following yielding of the shear plate. Referring to Tables 6-13 and 6-14, the infection point passed through the interior bolt line and moved closer to the girder web following the shear plate buckling. This behaviour may overshadow the reliability of the calculated bolt shear capacity based on the Eq. (6-5) in connections with too slender shear plate or a very large gap between the beam and girder. In this case, the Fortney's and Thornton's recommendation for the location of the inflection point, being the toe of the stiffener, may result in more conservative predictions for the bolt shear strength. However, it should be noted that the bolt group capacity of all studied configurations was predicted conservatively even when the estimate of Eq. (6-4) was used as the bolt group

eccentricity. This equation resulted in higher shear capacity as compared to those calculated based on Eq. (6-5).

Table 6-13. Ultimate capacity of the connections under gravity shear force

			nulations		арасну	AISC reco			Fortney and recomm	d Thorn		New re	comme	ndation		
	Model	Ultimate failure mode	V <sub>FE</sub> (kN)	e <sub>eff</sub> (mm)	$\frac{e_{\text{eff}}}{a}$	$\frac{\mathrm{e_{eff}}}{\mathrm{e_{g}}}$	Governing failure mode	V <sub>A</sub> (kN)	$\frac{V_{_{FE}}}{V_{_{A}}}$	Governing failure mode	V <sub>A</sub> (kN)	$\frac{V_{\text{FE}}}{V_{\text{A}}}$	Governing failure mode	V <sub>A</sub> (kN)	$\frac{V_{_{FE}}}{V_{_{A}}}$	$\frac{e_{\rm eff}^{\rm FE}}{e_{\rm eff}^{\rm A}}$
	BG3-2-10-F	PB	530	188	1.14	0.93	GSP	249	2.13	GSP	441	1.20	GSP	339	1.57	1.23
Group 1	BG3-2-13-F	NSR	727	208	1.26	1.02	BSF	325	2.24	GSP	584	1.24	GSP	435	1.67	1.14
iro	BG6-2-16-F	PB	1756	332	1.38	1.19	GSP	1040	1.69	NSR	1617	1.09	GSP	1379	1.27	1.01
	BG6-2-19-F	NSR	2160	344	1.43	1.23	BSF	1133	1.91	NSR	1940	1.11	GSP	1625	1.33	1.00
	BG2-1-10-F	BSF	312	171	1.04	1.04	BSF	65	4.80	BSF	174	1.80	GSP	262	1.19	1.04
	BG3-1-10-F	BSF	455	183	1.11	1.11	BSF	132	3.45	BSF	328	1.39	BSF	394	1.16	1.05
	BG4-1-10-F	BSF	602	196	1.19	1.19	BSF	238	2.53	BSF	489	1.23	BSF	494	1.22	1.09
Group 2	BG5-1-10-F	BSF	719	215	1.30	1.30	BSF	358	2.01	BSF	647	1.11	BSF	573	1.25	1.12
lno.	BG6-1-10-F	BSF	828	236	1.43	1.43	BSF	494	1.68	BSF	802	1.03	BSF	637	1.30	1.16
5	BG2-2-10-F	BSF	356	171	1.04	0.84	GSP	119	2.98	GSP	260	1.37	GSP	195	1.83	1.26
	BG4-2-10-F	PB	706	208	1.26	1.02	GSP	406	1.74	GSP	619	1.14	GSP	476	1.48	1.21
	BG5-2-10-F	PB	879	205	1.24	1.01	GSP	577	1.52	GSP	793	1.11	GSP	603	1.46	1.36
	BG6-2-10-F	PB	1010	198	1.20	0.98	GSP	755	1.34	GSP	965	1.05	GSP	718	1.41	1.57
	BG3-2-10-F-GD0.93	NSF	560	204	1.24	1.00	GSP	249	2.25	GSP	441	1.27	GSP	339	1.65	1.13
	BG3-2-10-F-GD0.80	PB	561	193	1.17	0.95	GSP	249	2.25	GSP	441	1.27	GSP	339	1.66	1.19
Group 3	BG3-2-10-F-GD0.60	PB	542	191	1.16	0.94	GSP	249	2.17	GSP	441	1.23	GSP	339	1.60	1.21
lno.	BG3-2-10-F-GD0.30	PB	526	189	1.14	0.93	GSP	249	2.11	GSP	441	1.19	GSP	339	1.55	1.22
5	BG3-2-10-F-GD0.27	PB	521	192	1.16	0.94	GSP	249	2.09	GSP	441	1.18	GSP	339	1.54	1.20
	BG3-2-10-F-GD0.24	PB	518	184	1.11	0.91	GSP	249	2.08	GSP	441	1.18	GSP	339	1.53	1.25
	BG3-2-10-F-GD0.20	PB	523	193	1.17	0.95	GSP	249	2.10	GSP	441	1.19	GSP	339	1.54	1.19
4	BG3-2-10-F-G25	PB	492	187	1.05	0.87	GSP	235	2.09	GSP	415	1.19	GSP	325	1.52	1.27
Group 4	BG3-2-10-F-G38	PB	462	179	0.94	0.78	GSP	223	2.07	GSP	389	1.19	GSP	310	1.49	1.39
5	BG3-2-10-F-G50	PB	431	182	0.90	0.75	GSP	212	2.03	GSP	365	1.18	GSP	296	1.46	1.41
			M	inimum	0.90	0.75			1.34			1.03			1.16	1.00
				Mean	1.18	1.01			2.23			1.21			1.46	1.20
			Ma	aximum	1.43	1.43			4.80			1.80			1.83	1.57
		Sta	andard d	eviation	0.13	0.16			0.70			0.15			0.17	0.13
	_			COV	0.11	0.16			0.31			0.12			0.12	0.11

Table 6-14. Ultimate capacity of the connections under combined axial and shear forces

			nulations		<u></u>	AISC reco			Fortney an recomn	d Thorn	ton's		ecomme	ndation	
Model	Ultimate failure mode	V <sub>FE</sub> (kN)	e <sub>eff</sub> (mm)	$\frac{e_{\text{eff}}}{a}$	$\frac{\mathrm{e_{eff}}}{\mathrm{e_{g}}}$	Governing failure mode	V <sub>A</sub> (kN)	$\frac{V_{FE}}{V_A}$	Governing failure mode	V <sub>A</sub> (kN)	$\frac{V_{FE}}{V_A}$	Governing failure mode	V <sub>A</sub> (kN)	$\frac{V_{FE}}{V_A}$	$\frac{e_{\rm eff}^{\rm FE}}{e_{\rm eff}^{\rm A}}$
BG3-2-10-F-700C	PB	198	179	1.08	0.88	GSP	84	2.36	GSP	231	0.86	GSP	132	1.50	0.75
BG3-2-10-F-600C	PB	245	204	1.24	1.00	GSP	137	1.79	GSP	310	0.79	GSP	208	1.18	0.86
BG3-2-10-F-400C	PB	358	200	1.21	0.98	BSF	208	1.72	GSP	386	0.93	GSP	297	1.21	0.84
BG3-2-10-F-200C	PB	458	191	1.16	0.94	BSF	250	1.84	GSP	419	1.09	GSP	338	1.36	0.80
BG3-2-10-F	PB	530	188	1.14	0.93	BSF	262	2.02	GSP	429	1.24	GSP	350	1.52	0.79
BG3-2-10-F-200T	NSR	525	196	1.19	0.96	BSF	250	2.10	GSP	419	1.25	GSP	338	1.55	0.82
BG3-2-10-F-400T	NSR	455	201	1.22	0.99	BSF	208	2.19	GSP	386	1.18	GSP	297	1.53	0.84
BG3-2-10-F-600T	NSR	366	195	1.18	0.96	GSP	137	2.68	GSP	310	1.18	GSP	208	1.76	0.82
BG3-2-10-F-800T	NSR	209	190	1.15	0.94	GSP	22	9.62	GSP	71	2.96	GSP	35	6.01	0.80
BG3-2-13-F-1000C	PB	367	191	1.16	0.94	BSF	67	5.49	GSP	208	1.76	GSP	102	3.61	0.79
BG3-2-13-F-800C	PB	520	191	1.16	0.94	BSF	171	3.05	GSP	408	1.27	GSP	260	2.00	0.79
BG3-2-13-F-600C	PB	632	195	1.18	0.96	BSF	241	2.63	GSP	493	1.28	GSP	357	1.77	0.81
BG3-2-13-F-400C	PB	724	195	1.18	0.96	BSF	290	2.49	GSP	538	1.35	GSP	413	1.75	0.81
BG3-2-13-F-200C	NSR	758	199	1.21	0.98	BSF	320	2.37	GSP	561	1.35	GSP	443	1.71	0.82
BG3-2-13-F	NSR	727	208	1.26	1.02	BSF	328	2.22	GSP	568	1.28	GSP	452	1.61	0.86
BG3-2-13-F-200T	NSR	696	207	1.25	1.02	BSF	320	2.18	GSP	561	1.24	GSP	443	1.57	0.86
BG3-2-13-F-400T	NSR	649	204	1.24	1.02	BSF	290	2.24	GSP	538	1.21	GSP	413	1.57	0.85
BG3-2-13-F-600T	NSR	578	202	1.22	0.99	BSF	241	2.40	GSP	493	1.17	GSP	357	1.62	0.84
BG3-2-13-F-800T	NSR	494	194	1.18	0.95	BSF	171	2.90	GSP	408	1.21	GSP	260	1.90	0.80
BG3-2-13-F-1000T	NSR	367	187	1.13	0.92	GSP	67	5.45	GSP	208	1.76	GSP	102	3.61	0.77
BG6-2-16-F-2000C	PB	1084	247	1.02	0.92	BSF	600	1.81	GSP	1233	0.88	GSP	940	1.15	0.77
BG6-2-16-F-1500C	PB	1376	292	1.02	1.05	BSF	817	1.68	GSP	1402	0.98	GSP	1162	1.13	0.62
BG6-2-16-F-1000C	PB	1676	275	1.14	0.99	BSF	971	1.73	GSP	1496	1.12	GSP	1282	1.31	0.58
BG6-2-16-F-500C	PB	1748	310	1.28	1.11	GSP	1066	1.64	GSP	1546	1.13	GSP	1343	1.30	0.66
BG6-2-16-F-250C	PB	1763	321	1.33	1.15	GSP	1083	1.63	GSP	1557	1.13	GSP	1358	1.30	0.68
BG6-2-16-F	PB	1756	332	1.38	1.19	GSP	1089	1.61	GSP	1561	1.12	GSP	1363	1.29	0.70
BG6-2-16-F-250T	NSR	1737	337	1.40	1.21	GSP	1083	1.60	GSP	1557	1.12	GSP	1358	1.28	0.71
BG6-2-16-F-500T	NSR	1689	339	1.40	1.22	GSP	1066	1.58	GSP	1546	1.09	GSP	1343	1.26	0.72
BG6-2-16-F-1000T	NSR	1560	336	1.39	1.20	BSF	971	1.61	GSP	1496	1.04	GSP	1282	1.22	0.71
BG6-2-16-F-1500T	NSR	1391	325	1.35	1.16	BSF	817	1.70	GSP	1340	1.04	GSP	1162	1.20	0.69
BG6-2-16-F-2000T	NSR	1164	309	1.28	1.11	BSF	600	1.94	GSP	1088	1.07	GSP	940	1.24	0.65
BG6-2-16-F-2500T	NSR	908	283	1.17	1.01	GSP	263	3.45	GSP	594	1.53	GSP	468	1.94	0.60

Table6.14 (Continued). Ultimate capacity of the connections under combined axial and shear forces

	FE Simulations Ultimate					AISC reco	mmend	ation	Fortney and recomm			New recommendation			
Model	Ultimate failure mode	V <sub>FE</sub> (kN)	e <sub>eff</sub> (mm)	$\frac{e_{\text{eff}}}{a}$	$\frac{e_{\rm eff}}{e_{\rm g}}$	Governing failure mode	V <sub>A</sub> (kN)	$\frac{V_{_{FE}}}{V_{_{A}}}$	Governing failure mode	V <sub>A</sub> (kN)	$\frac{V_{_{FE}}}{V_{_{A}}}$	Governing failure mode	V <sub>A</sub> (kN)	$\frac{V_{\text{FE}}}{V_{\text{A}}}$	$\frac{e_{eff}^{FE}}{e_{eff}^{A}}$
BG6-2-19-F-2500C	BSF	1194	233	0.97	0.84	BSF	554	2.15	BSF	1333	0.90	BSF	1014	1.18	0.49
BG6-2-19-F-2000C	BSF	1722	230	0.95	0.82	BSF	756	2.28	GSP	1629	1.06	GSP	1298	1.33	0.48
BG6-2-19-F-1500C	PB	2078	262	1.09	0.94	BSF	901	2.31	GSP	1748	1.19	GSP	1454	1.43	0.55
BG6-2-19-F-1000C	PB	2218	292	1.21	1.05	BSF	1013	2.19	GSP	1821	1.22	GSP	1547	1.43	0.61
BG6-2-19-F-500C	NSR	2221	324	1.34	1.16	BSF	1087	2.04	GSP	1861	1.19	GSP	1598	1.39	0.68
BG6-2-19-F-250C	NSR	2194	337	1.40	1.21	BSF	1115	1.97	GSP	1871	1.17	GSP	1610	1.36	0.71
BG6-2-19-F	NSR	2160	344	1.43	1.23	BSF	1133	1.91	GSP	1874	1.15	GSP	1614	1.34	0.72
BG6-2-19-F-250T	NSR	2111	346	1.43	1.24	BSF	1115	1.89	GSP	1871	1.13	GSP	1610	1.31	0.73
BG6-2-19-F-500T	NSR	2059	344	1.43	1.23	BSF	1087	1.89	GSP	1861	1.11	GSP	1598	1.29	0.72
BG6-2-19-F-1000T	NSR	1942	339	1.40	1.22	BSF	1013	1.92	GSP	1821	1.07	GSP	1547	1.25	0.71
BG6-2-19-F-1500T	NSR	1792	330	1.37	1.18	BSF	901	1.99	GSP	1723	1.04	GSP	1454	1.23	0.69
BG6-2-19-F-2000T	NSR	1650	316	1.31	1.13	BSF	756	2.18	GSP	1522	1.08	GSP	1298	1.27	0.66
BG6-2-19-F-2500T	BSF	1392	296	1.23	1.06	BSF	554	2.51	BSF	1198	1.16	BSF	1014	1.37	0.62
BG6-2-19-F-3000T	BSF	788	274	1.14	0.98	BSF	266	2.97	BSF	645	1.22	BSF	490	1.61	0.58
		M	inimum	0.95	0.82			1.58			0.89			1.15	0.48
			Mean	1.23	1.04			2.43			1.26			1.53	0.72
		Ma	aximum	1.43	1.24			5.49			3.12			3.61	0.86
	Sta	andard d	eviation	0.12	0.12			0.81			0.35			0.50	0.10
			COV	0.10	0.12			0.33			0.28			0.33	0.14

# 6.4 Conclusions

This paper presents the findings of a finite element study on the double-sided configuration of full-depth stiffened extended shear tab connections. The finite element models were validated with prior full-scale experiments of such connections conducted by the authors. First, the connection behaviour under gravity induced shear force was examined for a wide range of configurations. Then the connection axial capacity was determined. The effect of the axial force on the connection response was further evaluated under coupled axial and shear. The applied axial demand ranged between a connection's tensile and compressive capacities. The main findings are summarized as follows:

- The current AISC design method for extended shear tabs resulted in over conservative predictions for the capacity of the connection. This was likely due to this method having been developed for unstiffened shear tabs; i.e. it neglects the presence of the stabilizer plates (girder flanges)
- Implementation of Fortney's and Thornton's recommendation for the location of the inflection point, i.e. the toe of the stiffener (the tip of the girder flange), resulted in more accurate predictions for the ultimate capacity of the connection.
- Regarding the double-sided configuration of full-depth extended beam-to-girder shear tabs, the
  connection shear strength corresponding to the plate's gross section yielding was a
  conservative estimate of the connection's shear capacity, even in the presence of a large tensile
  axial force where the net section yielding preceded the gross section yielding.
- To determine the shear force corresponding to the plate's gross section yielding, the interaction of moment, shear, and axial load should be taken into account using Eqs. (6-1) and (6-2). In the absence of the axial load, Eq. (6-3) can be used instead of the aforementioned equations.

Furthermore, Eq. (6-4) can be used to estimate the location of the inflection point when the gross section yields.

- Implementation of the effective eccentricity (e<sub>eff</sub> = e<sub>b</sub>+ e<sub>g</sub> in which e<sub>b</sub> was calculated based on Eq. (6-4)) resulted in the most accurate predictions for the ultimate capacity of the connections under gravity shear demand.
- Under gravity induced shear force, the shear plate's out-of-plane deformation started to increase after yielding of the full depth of the shear plate along the gross section. Plate buckling was the ultimate failure mode of the slender shear tab connection in which the plate did not satisfy the CSA-S16 requirements for bearing stiffeners ( $200/\sqrt{F_y}$ ). For the connections with a compact shear tab, net section fracture was determined as the ultimate failure mode.
- To calculate the shear capacity of the bolt group, the ICR method was implemented along with the bolt group eccentricity, obtained from Eq. (6-5). If the shear plate satisfied the requirement of the AISC design procedure for the maximum plate thickness, the bolt group eccentricity could be considered conservatively as the distance between the bolt group centre and the toe of the stiffener. In this case, calculation based on Eq. (6-4) also resulted in a conservative estimate for the bolt group capacity. An increase of the gap distance between the beam and girder flanges resulted in an increase of the connection's eccentricity, as well as the shear plate's unbraced length. Therefore, the connection strength corresponding to the gross section yielding and shear plate buckling decreased. The plate buckled after the gross section had first yielded.
- The connections under pure tension failed due to net section fracture. The AISC design equation for net section fracture,  $F_{UN} = F_u A_{net}$ , predicted reasonably well the fracture tensile force. In the scenario of pure compression loading, plate buckling was the ultimate failure

- mode. Considering the shear plate as a column with an effective length of 0.65*a* resulted in a reasonably accurate prediction of the buckling resistance.
- An increase of the axial force, either in tension or compression, decreased the connection's shear strength corresponding to the gross section yielding. The use of Eqs. (6-1) and (6-2) provided a conservative estimate of the connection's capacity, although the presence of a compressive or tensile force decreased the shear force corresponding to plate buckling and net section yielding, respectively.
- A tensile axial force triggers net section fracture by increasing the force demands on the shear plate's net section along the centerline of bolt holes. Furthermore, an axial tensile force decreases the shear plate's out-of-plane deformation and delays plate buckling.
- It was observed that the calculation in accordance with Fortney's and Thornton's recommendation resulted in an overestimation of the ultimate resistance of the connection if it is subjected to a large axial compression. In this case, the calculation should be conducted based on the AISC's recommendation for connection eccentricity or Eq. (6-4).
- To determine the net section yielding along the plate's interior bolt line, Eqs. (6-1) and (6-2) were used. In this case, the product of the connection's shear force and the distance between the inflection point and the interior bolt line provided a reasonable estimate of the bending moment along the net section. Equation (6-4) could be used to determine the location of the inflection point. In the case of a gravity induced shear load, Eq. (6-8) resulted in a reasonable estimate of the axial and shear force along the net section. Under combined shear and tension, Eq. (6-9) conservatively considered the total connection shear and axial forces as the internal forces along the interior bolt line. Equation (6-11) gave reasonably accurate estimates for the net section shear and axial forces in the case of coupled shear and compression.

• The plate's fracture strength along its interior bolt line was estimated conservatively through Eqs. (6-13) and (6-14). The former considers the interaction of moment, shear and axial force while the shear-axial force interaction is accounted in the latter.

# 6.5 Acknowledgments

The authors would like to thank the ADF Group Inc. and DPHV Structural Consultants for their generous technical and financial support, as well as the Natural Sciences and Engineering Research Council of Canada. The finite element computations were conducted on the McGill University supercomputer Guillimin, which is managed by Calcul Québec and Compute Canada. The supercomputer operation is funded by the Canada Foundation for Innovation (CFI), NanoQuébec, RMGA and the Fonds de recherche du Québec - Nature et technologies (FRQ-NT).

### 6.6 References

- [1] Steel construction manual, 15<sup>th</sup> edition, American Institute of steel Construction, Chicago, IL, 2017.
- [2] Design examples companion to the aisc steel construction manual, version 15.0, American Institute of steel Construction, Chicago, IL, 2017.
- [3] A.R. Tamboli, Handbook of structural steel connection design and details, Third edition, McGraw-Hill, New York, NY., 2016.
- [4] J. Hertz, Testing of extended shear tab connections subjected to shear, Master's Thesis, McGill University, Montreal, QC, 2014.
- [5] N. Goldstein Apt, Testing of extended shear tab and coped beam-to-girder connections subject to shear loading, Master's Thesis, McGill University, Montreal, QC, 2015.

- [6] K. Thomas, R.G. Driver, S.A. Oosterhof, L. Callele, Full-scale tests of stabilized and unstabilized extended single-plate connections, Structures, 10 (2017) 49-58.
- [7] D.R. Sherman, A. Ghorbanpoor, Design of extended shear tabs, University of Wisconsin-Milwaukee, Milwaukee, WI, 2002.
- [8] J. Hertz, D.G. Lignos, C.A. Rogers, Full scale testing of extended beam-to-column and beam to-girder shear tab connections subjected to shear, 8th International Conference on Behavior of Steel Structures in Seismic Areas, Shanghai, China, 2015.
- [9] M. Motallebi, D.G. Lignos, C.A. Rogers, Behavior of stiffened extended shear tab connections under gravity induced shear force., J. Constr. Steel Res., Under Review (2018).
- [10] M. Motallebi, D.G. Lignos, C.A. Rogers, Stability of stiffened extended shear tab connections under gravity induced shear force, J. Constr. Steel Res., Under Review (2018).
- [11] W. Goodrich, Behavior of extended shear tabs in stiffened beam-to-column web connections, Master's Thesis, Vanderbilt University, Nashville, TN, 2005.
- [12] P.J. Fortney, W.A. Thornton, Analysis and design of stabilizer plates in single-plate shear connections, Eng. J. AISC, 53(1) (2016) 1-28.
- [13] M. Motallebi, D.G. Lignos, C.A. Rogers, Full-scale testing of stiffened extended shear tab connections under combined axial and shear forces, Eng. Struct., Under Review (2018).
- [14] CSA-S16-14, Design of steel structures, Canadian Standards Association, Mississauga, ON., 2014.
- [15] ABAQUS 6.11-3, [Computer software], Dassault Systemes Simulia Corp., Providence, RI.

- [16] ASTM F3125 / F3125M-15a, Standard specification for high strength structural bolts, steel and alloy steel, heat treated, 120 ksi (830 mpa) and 150 ksi (1040 mpa) minimum tensile strength, inch and metric dimensions, ASTM International, West Conshohocken, PA, 2015.
- [17] ASTM A992 / A992M-11(2015), Standard specification for structural steel shapes, ASTM International, West Conshohocken, PA, 2015.
- [18] ASTM A572 / A572M-15, Standard specification for high-strength low-alloy columbium-vanadium structural steel, ASTM International, West Conshohocken, PA, 2015.
- [19] AISC 341-16, Seismic provisions for structural steel buildings, American Institute of steel Construction, Chicago, IL, 2016.
- [20] B.A. Mohr, T.M. Murray, Bending strength of steel bracket and splice plates, Eng. J. AISC, 45(2) (2008) 97-106.
- [21] J. Wallaert, J. Fisher, Shear strength of high-strength bolts, J. Struct. Div. ASCE, 91(3) (1965) 99-126.
- [22] J.J. Wallaert, J.W. Fisher, Shear strength of high-strength bolts, Lehigh University, Bethlehem, PA, 1964.
- [23] NIST GCR 10-917-8, Evaluation of the fema p695 methodology for quantification of building seismic performance factors, NEHRP consultants Joint Venture, Redwood City, CA., 2010.
- [24] B.G. Neal, The effect of shear and normal forces on the fully plastic moment of a beam of rectangular cross section, Journal of Applied Mechanics, 28(2) (1961) 269-274.
- [25] P. Salem, Unified design criteria for steel cantilever plate connection elements, PhD Thesis, University of Alberta, Edmonton, AB, 2016.

- [26] A. Astaneh, Seismic behavior and design of gusset plates, Steel Tips, Structural Steel Education Council, Moraga, CA., 1998.
- [27] AISC 360-16, Specification for structural steel buildings, American Institute of steel Construction, Chicago, IL, 2016.
- [28] G.L. Kulak, J.W. Fisher, J.H. Struik, Guide to design criteria for bolted and riveted joints, AISC, Chicago, IL, 2001.

# Link between Chapter 6 and Chapter 7

The unstiffened extended shear tab connection is more common than the unstiffened configuration in steel construction practice. Chapters 3-6 focused on the stiffened extended shear tabs, whereas the results of four full-scale tests of the unstiffened extended beam-to-column shear tabs are presented in Chapter 7. These connections were subjected to gravity shear demand as well as to coupled axial force and gravity shear. In addition to the experimental results, a detailed description of the parametric FE study on the unstiffened extended shear tabs is provided in Chapter 7. During these numerical simulations, the dependence of the connection's behaviour on the geometric parameters of the shear plate was determined. Further, the impact of the axial force's direction and magnitude on the connection response was evaluated. Finally, modifications to the current AISC design method to take into account the presence of the axial force in the design procedure are proposed in Chapter 7.

# 7 Chapter 7: Unstiffened Extended Shear Tabs under Combined Axial and Shear Forces

Mohammad Motallebi<sup>1</sup>, Dimitrios G. Lignos<sup>2</sup>, Colin A. Rogers<sup>3</sup>

<sup>&</sup>lt;sup>1</sup> Graduate Research Assistant, Department of Civil Engineering and Applied Mechanics, McGill University, Montreal, QC. Email: mohammad.motallebinasrabadi@mail.mcgill.ca

<sup>&</sup>lt;sup>2</sup> Dimitrios G. Lignos, Associate Professor, School of Architecture, Civil and Environmental Engineering, Swiss Federal Institute of Technology, Lausanne (EPFL), Lausanne, Switzerland, Email: dimitrios.lignos@epfl.ch

<sup>&</sup>lt;sup>3</sup> Corresponding author Colin A. Rogers, Associate Professor, Department of Civil Engineering and Applied Mechanics, McGill University, Montreal, QC. Email: colin.rogers@mcgill.ca 817 Sherbrooke Street West Montreal QC, Canada, H3A 0C3 Tel. 514 398-6449 Fax. 514 398-7361

# **Abstract**

This paper presents the findings from an experimental-numerical study on unstiffened extended shear tab connections. Full-scale laboratory tests were carried out to study their behaviour under gravity induced shear force, as well as under coupled shear and axial demands. The results of these tests were then implemented to validate the finite element models and to conduct a parametric study on unstiffened extended shear tabs under gravity induced shear force. The parametric study demonstrated the validity of the current AISC design method for extended shear tabs, as well as the dependency of the connection's response to loading on different parameters, such as; the number of the vertical bolt lines and bolt rows, the depth and thickness of the plate, and the bolt group offset from the column face. Refinements were proposed to increase the accuracy of the current design method. Furthermore, the connection behaviour was evaluated under combined axial and shear demand, with axial force levels ranging between the connection's axial tension and compression capacities. Based on the FE simulations, a refined AISC method for the design of extended shear tab connections under combined axial and shear forces.

**Keywords**: unstiffened extended shear tab, weld tearing, net section fracture, plate buckling, effective eccentricity

# 7.1 Introduction

Unstiffened extended shear tab connections are widely used in beam-to-column connections due to their ease of fabrication and erection. The shear plate is welded to either the flange or the web of a supporting column (Figs. 7-1a and 7-1b, respectively). Furthermore, unstiffened extended shear tabs can be used to connect the beam web to the web of a supporting girder (Fig. 7-1c). Among these configurations, the beam-to-column flange configuration provides a rigid support for the shear tab, while the web of the supporting column or girder provide a flexible support for single-sided shear tabs where the beam is placed only on one side of the supporting element. The double-sided configuration, in which the web of either the girder or the column supports a beam on each side (Figs. 7-1d and 7-1e), provides a rigid support for shear tab connections. The back stiffeners (Fig. 7-1f) also provide a rigid support for shear tab connections.

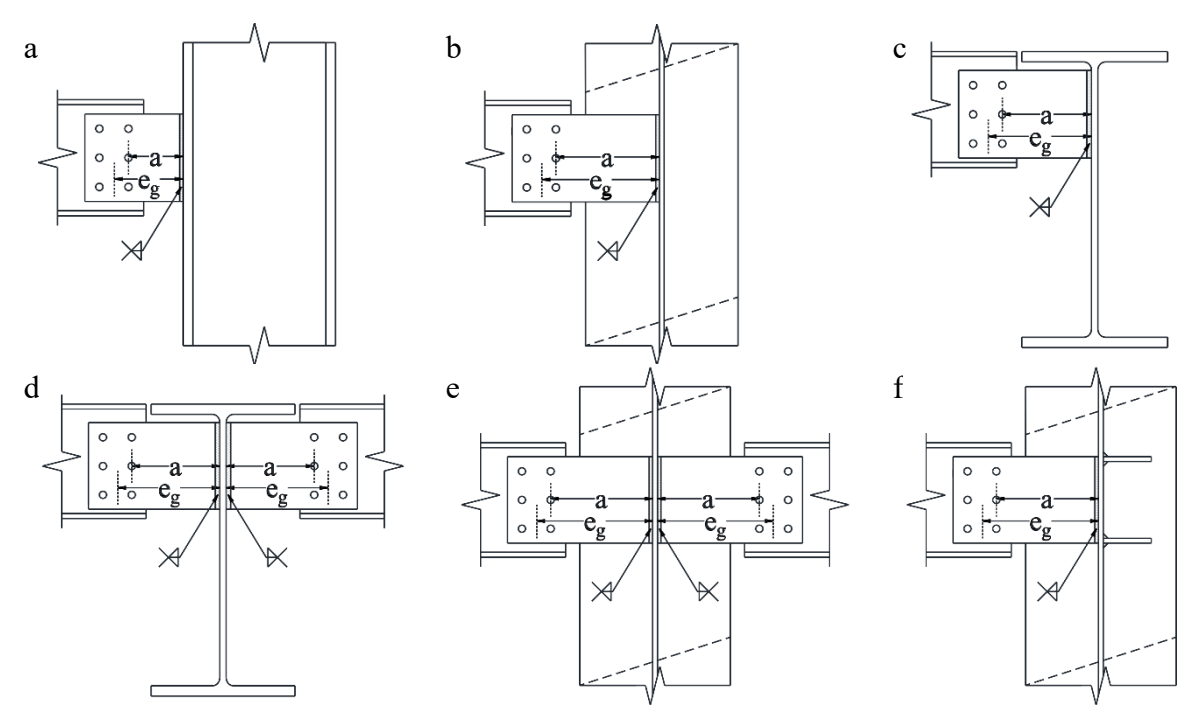


Fig. 7-1. Different configurations for unstiffened extended shear tabs: (a) beam-to-column flange (single-sided), (b) beam-to-column web (single-sided), (c) beam to girder web (single-sided), (d) beam-to-column web (double-sided), (e) beam-to-girder web (double-sided), (f) beam-to-column web with back stiffeners

The AISC Steel Construction Manual [4] implemented a lower bound theorem to provide a safe, simple, and easy to use design method for extended shear tab connections [9]. Of note, this method should be used for all connections with multiple vertical bolt lines even when the distance between the support and the interior bolt line, the a distance, is shorter than the AISC limit [4] (89) mm, 3.5 in.) for conventional shear tabs. In this method, using the geometric eccentricity (e<sub>g</sub>) (Fig. 7-1) the bolt group is designed to resist the shear force. The interaction of the shear force and the bending moment is considered in design as a function of the yield of the gross section of the shear plate. Given that the required ductility of a shear tab is provided through yielding of the shear plate, the brittle failure modes of the connection, i.e. weld tearing and bolt fracture, should have a higher factored resistance than that associated with the full yielding of the shear plate. To this end, the thickness of the shear plate is limited to an upper bound  $(t_{max})$ , while a minimum weld size (5/8t<sub>p</sub>≤a<sub>w</sub>) is required. The AISC design method [4] does not address the shear tab connection under combined axial and shear forces, e.g. when the building is subjected to lateral loads such as wind and earthquake in addition to the gravity induced shear force. However, the Steel Connection Handbook [14] and AISC Design Examples [15] make a few minor adjustments to the AISC design method in order to implement it for design of extended shear tabs under combined axial and shear forces. In this adjusted method, the capacity of bolt group and weld lines is controlled for the resultant force of axial and shear demands. The interaction of axial and shear forces is taken into account for control of the block shear rupture. The main adjustment is introduction of an equation to consider the axial-shear-bending interaction to control the gross section yield and the net section rupture of the shear plate. Neither published laboratory tests nor finite element analyses have been provided to validate these adjustments.

Despite a long history of use, limited research has been conducted on extended shear tabs. Based on experimental research of beam-to-column shear tabs, Moore and Owens [16] demonstrated that extended shear tabs with flexible supports fail along the bolt line, while weld tearing is the governing failure mode of extended shear tabs with rigid supports. Furthermore, they concluded that the large rotation and vertical deformation of extended shear tabs, especially in the case of a beam-to-column web configuration, could be detrimental to the serviceability of the supported beam. Sherman and Ghorbanpoor [17] found the yielding of the supporting column web as the failure mode of the unstiffened extended shear tabs, which were connected to supporting members having a high web slenderness. Furthermore, large torsion of the shear tab plate was observed in unstiffened extended connections for which the beam was not laterally supported near the connection.

Metzger [19] tested beam-to-column flange shear tabs to evaluate the AISC design method [8] for shear tabs, which had been revised in 2005. Weld tearing was observed as the ultimate failure mode for two short shear tabs (a = 51 mm (2 in.)) with two vertical bolt lines; their weld size ( $a_w=1/2t_p$ ) was smaller than the limit proposed by the AISC ( $5/8t_p \le a_w$ ). Beam lateral buckling precluded the shear tab from reaching its ultimate capacity in the other two extended shear tabs, which satisfied the minimum weld size requirement.

Marosi et al. [42, 43] observed net section shear fracture as the governing failure mode of shear tab connections with either a single or two vertical bolt lines, for which the *a* distance was relatively short (less than 64mm, 2.5 in). Of note, weld tearing was observed in most of these tests, but it was a ductile failure mode and the connection could reach higher shear force following the onset of the weld tearing. Hertz et al. [24, 45] observed weld tearing in extended beam-to-column flange shear tabs connected with two vertical bolt lines even though they met the AISC minimum

weld size requirement  $(5/8t_p \le a_w)$  [28]. Weld tearing was determined to be the ultimate failure mode for three tested shallow shear tabs (having three bolt rows), whereas net section fracture was observed as the ultimate failure mode of a tested deep shear tab with six bolt rows. In advance of weld tearing, yielding of the plate occurred in these tests due to the interaction of shear and bending moment. Furthermore, out-of-plane deformation of the shear tab plate was observed in all cases.

Only few research programs addressed the behaviour of extended shear tabs under combined shear and a relatively small axial force. Mirzaei et al. [44, 67] conducted an experimental-numerical study on beam-to-column flange shear tabs with two vertical bolt lines and a short *a* distance. Following the yield of the shear plate due to the interaction of shear and bending, weld tearing initiated in these specimens. The presence of the axial compression stabilized the weld tearing propagation and the connections failed due to net section fracture. For the connections under combined axial tension and shear forces, the presence of an axial tensile force applied higher demand on the tensile portion of the weld line; as such, weld tearing was observed as the ultimate failure mode. The tensile force resulted in a decrease of the connection shear capacity, in contrast with a slight increase in connection shear capacity when subjected to a small axial compression force.

Thomas et al. [20, 21] conducted a series of full-scale tests to study the behaviour of extended shear tabs under combined axial and shear forces. All the unstiffened extended shear tabs had a large a distance (233 mm, 9 3/16 in.) as they connected the web of the supported beams to the web of the supporting columns. Relatively small axial force was applied to these connections; it varied between zero and 0.30  $P_{GP}$  ( $P_{GP} = F_y A_g$ ). Following the yield of the shear plate (along the interior bolt line in most cases), the shear plate failed due to either bolt shear fracture or weld tearing. Of note, weld tearing was observed in all specimens although they satisfied the minimum weld size

requirement of the AISC Manual [28]. Further, the web of the supporting column yielded in most specimens due to its low out-of-plane bending capacity.

Salem [22] observed bolt shear fracture after the yielding and severe out-of-plane deformation of the shear plate in extended beam-to-column flange shear tabs. In these long shear tabs (a=233 mm (9 3/16 in.) or 195 mm (7 2/3 in.)), small weld tearing was observed although their weld size was (a<sub>w</sub>=4/5t<sub>p</sub>) much larger than the minimum AISC requirement (5/8t<sub>p</sub> <a<sub>w</sub>). In addition to the extended beam-to-column flange shear tabs, Salem tested several beam-to-column web shear tabs, in which the web of the column was stiffened by using horizontal stabilizer plates in the backside of the column (Fig. 7-1f). The majority of connections failed due to weld tearing, although the weld size was almost equal to the minimum AISC requirement. Of note, Salem laboratory testing program [22] was limited to the extended shear tabs with three bolt rows while the applied axial force varied between zero and 0.22P<sub>GP</sub>.

In summary, there exists limited research involving the behaviour of extended shear tab connections under combined axial and shear force. The past studies mainly focused on long shear tabs under relatively small axial force. To address this shortcoming, a series of full-scale laboratory tests were conducted on medium-length extended shear tab connections subjected to combined axial and shear force at McGill University. These connections were further investigated for a wider range of configurations and loads by making use of finite element models validated to testing. The numerical models included 32 extended shear tab configurations that considered variations in the the number of bolt rows and the vertical bolt lines, the *a* distance, and the thickness of the shear plate. Furthermore, four connection configurations were chosen to be studied under a wide range of axial and shear forces. This paper presents the results of this experimental-numerical study.

Based on these results, several recommendations are presented for the design of unstiffened extended shear tabs under combined axial and shear forces.

## 7.2 Full-scale laboratory testing

To study the behaviour of medium-length extended shear tabs, four full-scale connection specimens were tested in the Jamison Structures Laboratory at McGill University. The specimens were representative of two different configurations of unstiffened extended beam-to-column shear tabs in which the shear plate is welded to the flange of the supporting column. Two identical specimens were fabricated for each configuration. The behaviour of the connection was determined under gravity induced shear force during the first test. In the second test, a compressive axial force was applied to the connection in addition to the gravity demand. A comparison of the results of these two tests allowed for an improved understanding of the impact of axial force on the behaviour of each shear tab connection configuration.

## 7.2.1 Description of test specimens

The specimens varied with respect to the bolt size and the number of bolt rows, while they all had two vertical bolt lines and a medium-length *a* distance ((114 mm) 4.5 in.) and reflect the current practice in steel construction in the USA and Canada. To label each specimen an alphanumerical ID was used, e.g. BC3-2-10-200C, in which BC indicates the beam-to-column configuration, 3 is the number of bolt rows, 2 represents the number of the vertical bolt lines, 10 stands for the thickness of the plate (10 mm), 200C indicates the magnitude (200 kN) and direction of the applied axial force (Compression).

The connections were designed for gravity induced shear force based on the AISC design method for extended shear tabs. Although the weld size was detailed to be slightly larger than the minimum AISC weld size requirement, pretest measurements demonstrated that the weld size was much larger than the minimum size (6 mm) for shallow shear tabs, i.e. BC3-2-10 and BC3-2-10-200C (11 mm and 11.6 mm, respectively). Other than the weld size, all other measurements remained within the limits for fabrication tolerance of the connection. Figure 7-2 shows the asbuilt dimensions of the four specimens.

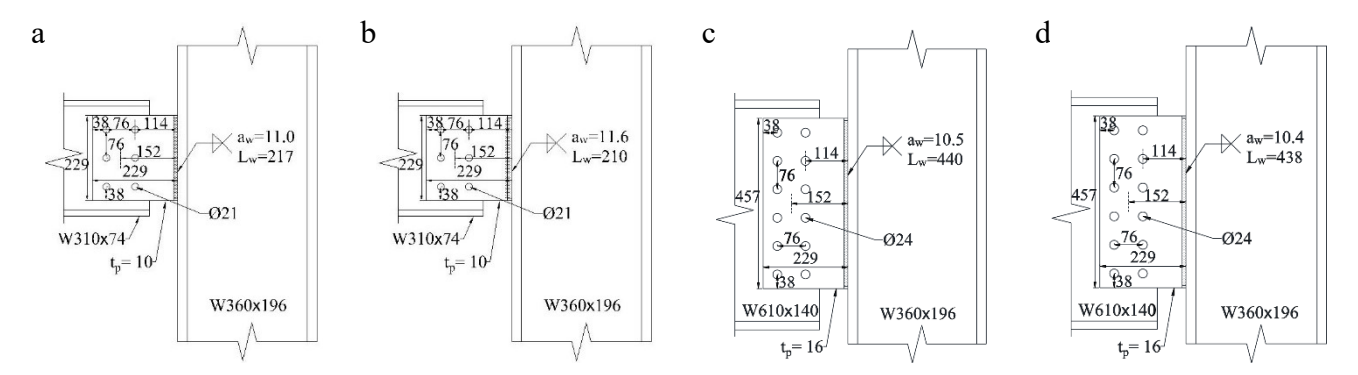


Fig. 7-2. As built dimensions of the specimens: (a) BC3-2-10, (b) BC3-2-10-200C, (c) BC6-2-16, (d) BC6-2-16-500C (All dimensions in mm)

The shear plate was fabricated from ASTM A572 Grade 50 ( $F_y$  = 345 MPa) steel [48], while the beams and girders were made of ASTM A992 Grade 50 ( $F_y$  = 345 MPa) steel [47]. Each beam was snug-tightened to the shear tab using ASTM F3125 Grade A490 bolts [34] in standard size holes, 2mm (1/16") larger in diameter than the bolts. To attach the shear tab to the fabricated supporting girder, an E71T electrode ( $X_u$  = 490 MPa) [52] was used in a flux-cored arc welding process with additional shielding gas (CO<sub>2</sub>) to provide a fillet weld on both sides of the plate. Figure 7-3 shows these specimens prior to testing.

To determine the constitutive material model for each component of the connection, steel and all-weld tensile coupons were tested following ASTM A370 [51] and AWS A5.20 [52], respectively. The steel coupons were taken from the same parent plates and beams, as used for the connections. For each thickness of plate, two sets of three tensile coupons were fabricated: one set along and one set perpendicular to the plate's grain direction. The reported value for the yield and

tensile strength of the beam's web was the average of three coupons, cut from the beam web. For the beam's flanges, the reported values were derived from two sets of two coupons: one set from top flange and the other set from the bottom flange. For the welding electrode, two all-weld coupon were extracted from a groove weld assembly of two plates, fabricated from the same electrode used for the shear tab specimen [52]. Table 7-1 lists the measured yield and tensile stress of each component, in addition to the nominal and probable values.

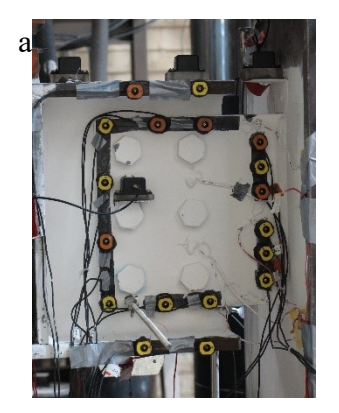








Fig. 7-3. Specimens: (a) BC3-2-10, (b) BC3-2-10-200C, (c) BC6-2-16, (d) BC6-2-16-500C

Table 7-1. Material properties of connection components

		1				1	
		Non	ninal	Prob	able <sup>1</sup>	Meas	sured
Connection co	mponents	F <sub>y</sub>	Fu	Fy	Fu	$F_{y}$	Fu
		(MPa)	(MPa)	(MPa)	(MPa)	(MPa)	(MPa)
W310×74	Flange	345	448	379	493	374	490
$(W12\times50)$	Web	345	448	379	493	379	495
W610×140	Flange	345	448	379	493	420	534
$(W24\times94)$	Web	345	448	379	493	444	544
10mm (3/8"	) plates	345	448	379	538	449	522
16mm (5/8"	) plates	345	448	379	538	371	518
E71T elec	trode	400	490			548	620
A490 b	olts	896	1034				

 $<sup>^{1}</sup>$  R<sub>y</sub>F<sub>y</sub> and R<sub>T</sub>F<sub>u</sub>; for steel plates 1.1 F<sub>y</sub> and 1.2 F<sub>u</sub>, whereas 1.1 F<sub>y</sub> and 1.1 F<sub>u</sub> for W-shapes [50]

All specimens satisfied the requirements of the AISC design method [4] for extended shear tabs. Of note, the impact of the axial force was not considered in design and detailing of the specimens. In accordance with the AISC design method, the connection capacity was calculated for the different probable failure modes (Table 7-2). In addition to the nominal and probable

properties, the connection capacity was calculated based on the measured material properties of the connection components including the shear plate, beam and weld. In all cases, the shear capacity of the bolt group was calculated based on the nominal properties of A490 bolts.

Table 7-2. AISC predicted shear strength of shear tab test specimens

•		BC3-2-10		•	BC6-2-16	
	Design	Expected	Expected	Design	Expected	Expected
Failure mode	strength	strength1	strength <sup>2</sup>	strength	strength1	strength <sup>3</sup>
	(kN)	(kN)	(kN)	(kN)	(kN)	(kN)
Flexural and shear yielding of shear plate	277	325	385	1238	1404	1371
Shear yielding of shear plate	461	507	601	1488	1637	1599
Bolt bearing	305	463	463	1200	1760	1934
Buckling of shear plate	346	423	501	2232	2728	2665
Rupture at net section of shear plate	325	521	505	990	1538	1525
Bolt shear	280	414	414	1213	1797	1797
Weld tearing	744	992	1256	1444	1924	2436

<sup>&</sup>lt;sup>1</sup>Expected strength based on probable material properties i.e.R<sub>y</sub>F<sub>y</sub> (1.1 F<sub>y</sub>) and R<sub>T</sub>F<sub>u</sub> (1.2 F<sub>u</sub>) for steel plates [50]

The reported values for the buckling capacity of the shear plate were calculated in accordance with the current and the previous versions of the AISC design method [4, 28]. Both methods showed that the shear plate could reach its plastic bending resistance and resulted in the shear force corresponding to the plastic bending moment capacity of the shear plate (Fy Zg/a). In these calculations, the distance between the column face and the interior bolt line, the a distance, was considered as the unbraced length of the shear tab. Regarding the weld capacity, the reported values were the concentric shear capacity of the weld line, calculated in accordance with the AISC design method. Referring to Table 7-2, flexural and shear yielding of the shear plate resulted in the lowest shear resistance for the specimens; 385kN and 1371 kN were chosen as the expected shear capacity of the two connections, respectively. In calculating these values, measured material of all component, other than bolts, were used while the unity safety factor was assumed. For bolts, minimum specified strength was implemented.

 $<sup>^2</sup>$ Expected strength based on measured material properties i.e  $F_y$ =449MPa and  $F_y$ =522MPa for 10mm plate

<sup>&</sup>lt;sup>3</sup>Expected strength based on measured material properties i.e F<sub>y</sub>=371MPa and F<sub>y</sub>=518MPa for 16mm plate

### 7.2.2 Test Setup

A beam-to-column setup was used for the testing of the shear tab connections (Fig. 7-4). Similar to prior research on these connections [6, 24, 42-45, 67], two actuators were incorporated in the test setup to apply coupled shear and rotation to the extended shear tabs. The connection shear force was developed mainly by the actuator near the connection (12MN actuator), while the connection rotation was controlled mainly by the actuator at the far end of the beam (445 kN actuator). The top flange of the test beam was laterally supported along its entire length, while the bottom flange was restrained from out-of-plane deformation near the tip actuator. Two Enerpac RRH-3010 hydraulic jacks were installed in line with the beam on the back side of the column (Fig. 7-4b) to apply the axial force on the connection. The position of these jacks was adjusted during the test to follow the beam end rotation, while maintaining a constant axial force on the connection. To control the vertical displacement of the moving parts of the axial load application system one Enerpac RRH-3010 hydraulic jack was placed vertically in the setup (Fig. 7.4b).

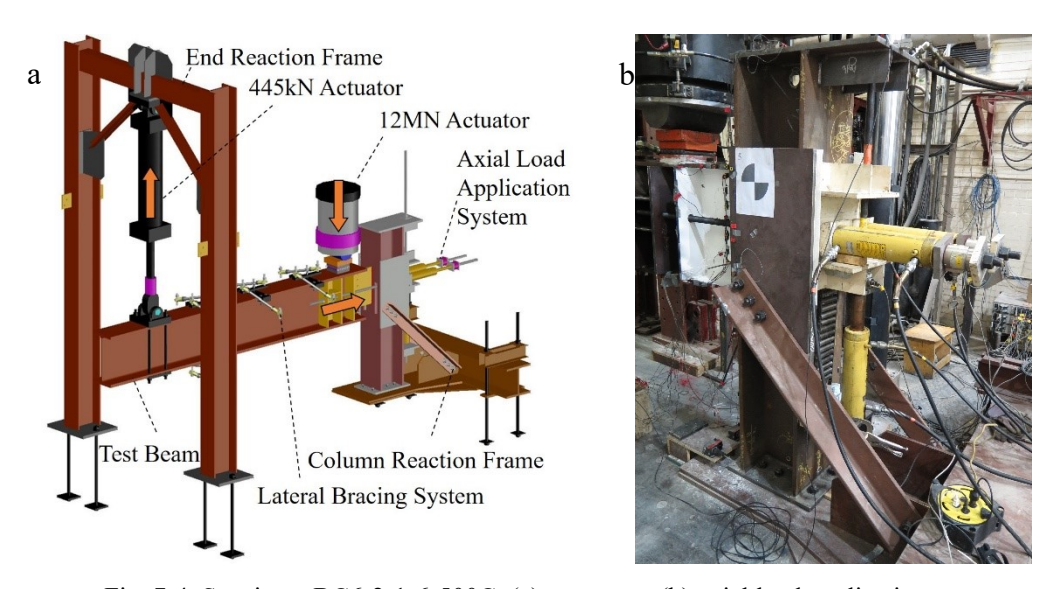


Fig. 7-4. Specimen BC6-2-1-6-500C: (a) test setup, (b) axial load application system

## 7.2.3 Loading Protocol

The connection was subjected to a coupled shear and rotation, representing the end demands of a uniformly loaded simply supported beam. It was assumed that the connection would reach its probable resistance at 0.02 rad relative rotation between the beam and the column. Of note, prior research [6, 33] demonstrated 0.02 rad as a reasonable value for the target rotation. As the tensile coupons could not be tested in advance of the full-scale tests, the probable material properties were used to calculate the expected strength of the connections (Table 7-2) in accordance with the AISC Construction Manual [4]. In these calculations, the resistance factors were considered equal to one. To apply this loading protocol, the ratio between the displacement rates of the actuators was adjusted up to the target rotation/load point; this ratio was kept constant once the target load was achieved. To replicate a real world situation in which the shear tab will likely carry the service level gravity forces prior to the application of a lateral force (axial force in beam), the test connection was subjected to an axial force only after the applied shear force reached a specific level, representative of its service level gravity in a real world situation. The axial force was then kept constant, while the shear demand was further increased up to the failure of the connection. During the tests, the axial force was applied to the specimens as soon as the onset of the plate yielding based on real time monitoring of the strain gauge data. This method was consistent with the loading approach used in previous research [44]; the shear tab experienced only minor local yielding under the service level of the gravity induced shear force.

#### 7.2.4 Instrumentation

To record the connection shear and axial forces, load cells were installed on all actuators and hydraulic jacks. The in-plane rotation of the column, as well as the in-plane and out-of-plane rotations of the beam and shear plate were measured using inclinometers. To detect the connection

yield pattern, strain gauges were installed on the shear plate (Fig. 7-5a), as well as the web and flanges of the test beam near the connection. Further, the specimens were whitewashed, which allowed for visual observation of damage. Referring to Fig. 7-5b, the connection deformation was measured in the 3D space using an optical Coordinate-Measuring Machine (CMM). As a backup measurement, Linear Variable Differential Transformers (LVDTs) recorded the out-of-plane deformations of the shear plate (Fig. 7-5c). In addition to the horizontal deformation of the column capping plate, the vertical deformation of the beam and shear plate were measured using string potentiometers. All the measured data was recorded using Vishay Model 5100B scanners and the Vishay System 5000 StrainSmart software.

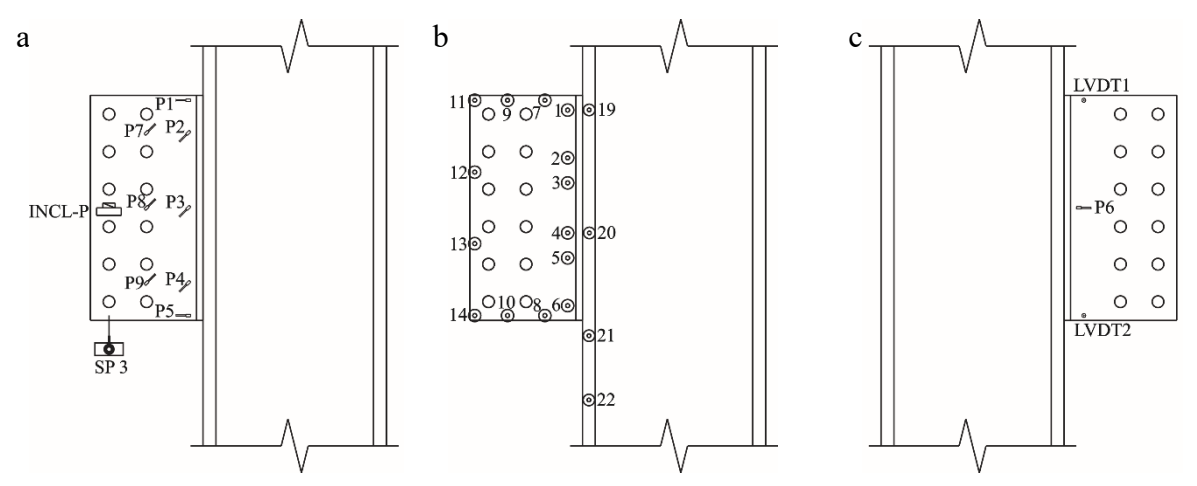


Fig. 7-5. Instrumentation of Specimen BC6-2-16-500C: (a) strain gauges, (b) targets of optical CMM system, (c) LVDTs

### 7.2.5 Experimental Results

Various damage states were observed including; shear plate yielding, out-of-plane deformation of the shear plate, plate buckling, weld tearing, and net section rupture. Bolt shear fracture was not observed. Of note, the reported value for yielding of the gross and net sections corresponds to the connection shear force at the time when yield strain was reported by all strain gauges installed on the gross and nest sections of the plate, respectively. The out-of-plane and

buckling damage states were determined based on the out-of-plane deformation of the plate as well as the stiffness of the shear-rotation curve of the connection. In addition to the visual inspection during the tests, curves representing the shear force versus the connection rotation the plate deformation (both vertical and horizontal) were implemented to determine weld tearing damage state. The damage state of the net section rupture was determined based on post-test inspection as well as the curve representing the shear force-vertical deformation of the connection. It should be noted that some of these damage states occurred simultaneously while other damage states were in progression.

Figure 7-6 presents the measured shear force of the connection versus the connection rotation, and the relative rotation between the beam and column. In connections under gravity shear demand, the installed strain gauges (SG) demonstrated that the shear plate yielded at its gross and net sections (GSP and NSP, respectively). The gross section yielded prior to the net section in Specimen BG3-2-10, while yielding of the net section occurred first in specimen BG6-2-16. This observation can be attributed to the fact that ratios between the net and gross sections were smaller in shear plates with larger bolt holes, i.e.  $A_{net}/A_g=0.73$  and 0.69 for the specimens with 19 mm and 22 mm bolts when the bolt holes distance was 76 mm. Further, the net section yielded due to the interaction of shear and bending while different flexural stiffness of these connection developed varied bending moment at these critical sections. Following the shear plate yielding, the weld line started to tear from its top edge (WTO), subjected to tensile stress due to the eccentric shear force. Although the connection stiffness significantly decreased due to weld tearing, the specimen could reach a higher level of the shear force following the onset of the weld tearing while the weld tearing was propagating slowly. Weld tearing decreased the depth of the shear plate effectively contributed in resisting the applied demands and consequently the out-of-plane deformation of the bottom edge of the shear plate started to increase rapidly (OPD). The Specimen BC3-2-10 reached its strength plateau (SP) when the weld tearing started to propagate rapidly (WTP). The rapid propagation of the weld tearing resulted in another significant decrease of the connection stiffness in Specimens BC6-2-16. Post-test examinations demonstrated that this specimen failed due to net section rupture (NSR) along the interior bolt line of the shear plate. The strength plateau occurred due to combination of the rapid propagation of the weld tearing and the excessive deformation of the shear plate along the interior bolt line.

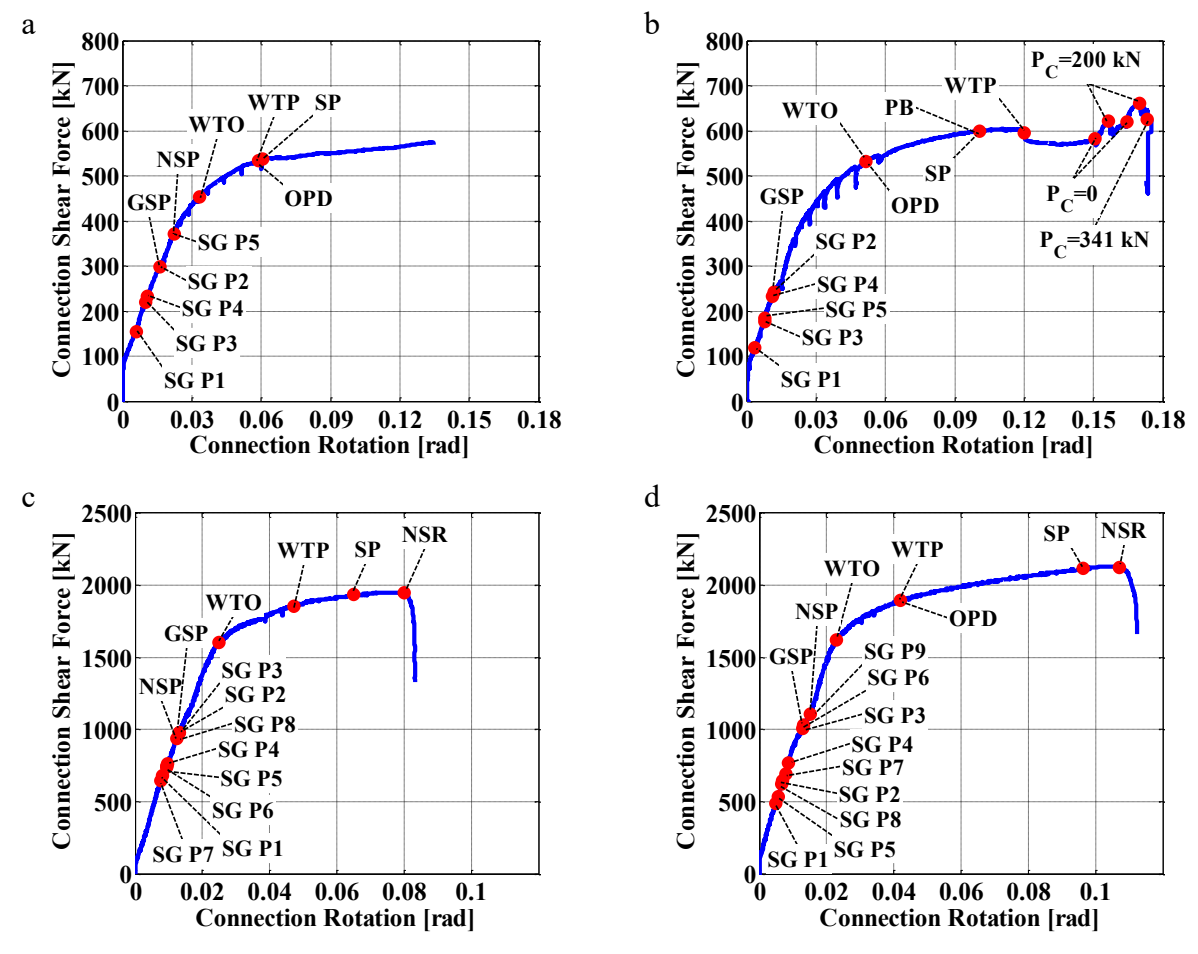


Fig. 7-6. Damage propagation of Specimen: (a) BC3-2-10, (b) BC3-2-10-200C, (c) BC6-2-16, (d) BC6-2-16-500C (GSP: plastic gross section, NSP: plastic net section, WTO: onset of weld tearing, WTP: propagation of weld tearing, OPD: Out-of-plane deformation, SP: strength plateau, NSR: net section rupture, SG: strain gauge reported yielding strain)

In the presence of an axial compression, the Specimen BC3-2-10-200C experienced a strength plateau due to plate buckling (PB) when the beam started to get close to the column rapidly and the out-of-plane deformation of the shear plate increased quickly. In this specimen, the rapid propagation of the weld tearing, which occurred after the strength plateau, resulted in small drop of the connection shear force. Following this drop, the specimens started to regain the shear force due to stress redistribution. Removing the axial force (P<sub>c</sub>=0) resulted in rapid increase of the shear force. The connection shear force of Specimen BC3-2-10-200C dropped when the axial compression increased to 341kN. In the presence of the axial compression, Specimen BC6-2-16-500C failed due to the net section fracture at larger shear force as compared to Specimen BC6-2-16.

As shown in Fig. 7-7, applying axial compression resulted in larger out-of-plane deformation of the shear plate (Figs. 7-7a and 7-7b versus Figs. 7-7d and 7-7e), while slightly decrease the tensile demand on top edge of the weld line. Regarding Specimens BC6-2-1-6 and BC6-2-16-500C, applying axial compression decreased the weld tearing length, while the out-of-plane deformation of the shear plate increased (Fig. 7-8), a similar observation to the two BC3 specimens. Furthermore, the axial compression decreased the rupture length along the interior bolt line. The photographs in Figs. 7-9 and 7-10 illustrate that the axial compression force prevented the fracture from propagating into the bottom portion of the plate in Specimen BC6-2-1-6-500C. Of note, the rupture did not propagate through the top bolt holes of the interior bolt line of either Specimen BC6-2-16 or BC6-2-16-500C. The weld tearing relieved the stress demands on this upper portion of the shear plate, and hence fracture between the bolt holes did not develop.



Fig. 7-7. Deformed shape of Specimens: (a-c) BC3-2-10, (d-f) BC3-2-10-200C



Fig. 7-8. Deformed shape of Specimens: (a-c) BC6-2-16, (d-f) BC6-2-16-500C

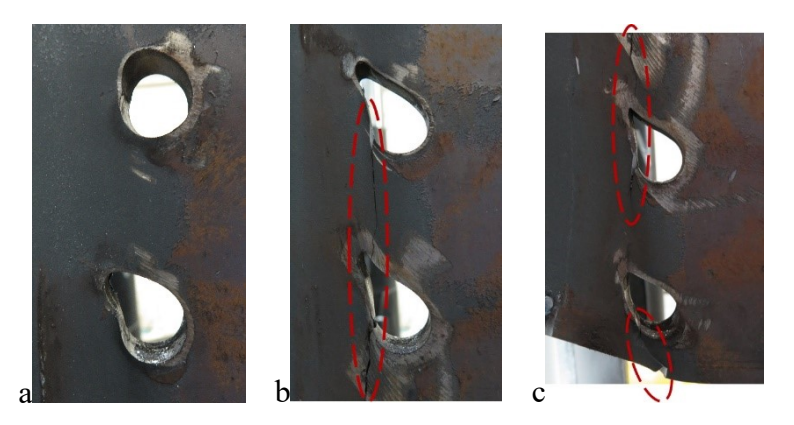


Fig. 7-9. The interior vertical bolt line of Specimen BC6-2-16 at: (a) bearing at top bolt holes, (b) net section rupture at middle bolt holes, (c) net section rupture at bottom bolt holes

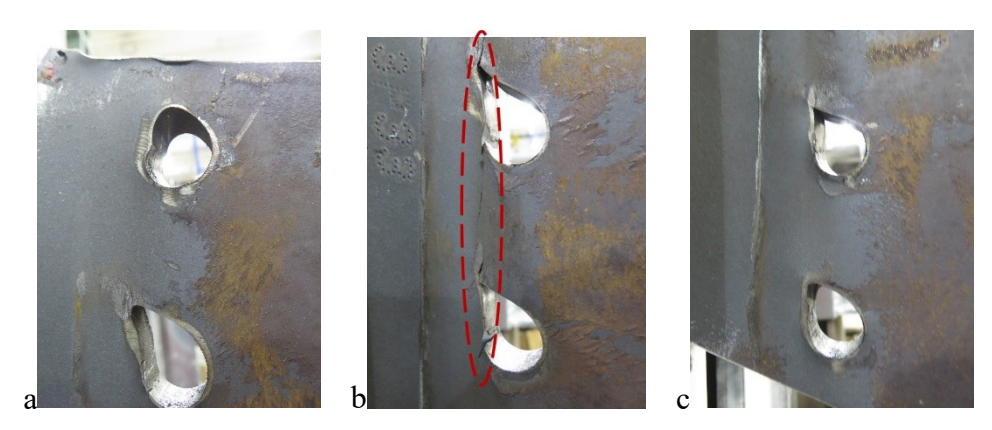


Fig. 7-10. The interior vertical bolt line of Specimen BC6-2-16-500C at: (a) bearing at top bolt holes, (b) net section rupture at middle bolt holes, (c) bearing at bottom bolt holes

The shear resistance corresponding to each damage state is summarized in Table 7-3. The effective eccentricity of the connection, that is, the distance between the inflection point and the weld line, was calculated based on the developed bending moment at the face of the column and the connection shear force ( $e_{eff}$ =M/V). The bending moment at the face of the column was calculated based on the actuators' recorded forces and their distance to the column face (M= $F_{main} \times L_{main}$  -  $F_{tip} \times L_{tip}$ ).

Table 7-3 Specimen measured response

ID.	Gross	section	Net s	ection	Weld	tearing	Duo	lelina	Weld	tearing	Net so	ection
	yie	lding	yiel	ding	(On	iset)	***		(Propa	gation)	rup	ture
	V	$e_{ m eff}$	V	$e_{ m eff}$	V	$e_{ m eff}$	V	$e_{ m eff}$	V	$e_{ m eff}$	V	$e_{ m eff}$
	(kN)	(mm)	(kN)	(mm)	(kN)	(mm)	(kN)	(mm)	(kN)	(mm)	(kN)	(mm)
BC3-2-10	299	197	371	167	454	145			533	135		
BC3-2-10-200C	231	227	<sup>a</sup>		531	128	599	125	596	120		
BC6-2-16	980	239	935	243	1560	149			1853	98	1940	83
BC6-2-16-500C	1006	257	1108	242	1621	160			1898	128	2130	107

a yield along the net section could not be determined due to malfunction of strain gauge P6

A comparison of the expected and measured resistances (Table 7-2 and 7-3, respectively) demonstrated that the current design method overestimated the shear resistance corresponding to yielding of the plate gross section. This was because the connection eccentricity was larger than the *a* distance used in the calculations. However, the connection shear force reached the expected flexural-shear yielding resistance at a connection rotation lower than 0.02 rad, (Fig. 7-6). Although Specimens BC3-2-10 and BC3-2-10-200C could attain a shear force larger than the expected buckling resistance, significant out-of-plane deformation was observed in these specimens. The design assumptions resulted in a conservative estimate of the net section rupture in all specimens. Regarding the bolt shear fracture, the design method lead to a conservative prediction because the bolt group eccentricity (e<sub>b</sub>: the distance between the inflection point and the bolt group centre) was smaller than the geometric eccentricity (e<sub>g</sub>: the distance between weld line and the bolt group centre).

Referring to Table 7-3, weld tearing was observed even in Specimen BC3-2-10-200C in which the weld line with a large weld size ( $a_w$ =1.20  $t_p$ ) was subjected to transverse compression force in addition to the eccentric shear force. Weld tearing was the ultimate failure mode only in Specimen BC3-2-10, where a larger than designed weld ( $a_w$ =1.14  $t_p$ ) was used to connect the shear plate to the column flange. Weld tearing did show a ductile behaviour, and the force applied to the connection continued to increase after the onset of the tearing. Yielding in the gross section of the

shear plate, occurred in advance of the onset of the weld tearing, which allowed for a stress redistribution in the connection and the movement of the inflection point toward the weld line. Furthermore, weld tearing decreased the rotational stiffness of the plate and shifted the inflection point to be located closer to the weld line. Therefore, the capacity of the weld line increased because a lower bending moment was imposed to the weld line. This mechanism demonstrated that the extended shear tab behaved in a ductile manner because of shear plate yielding prior to weld tearing. The design procedure found in the AISC Construction Manual [4] proposes a minimum weld size requirement to assure the aforementioned failure mode hierarchy. This requirement was developed based on the nominal yield and tensile stress of ASTM A572 Grade 50 steel and an E70 electrode, respectively [9]. In the case where the yield stress of the shear plate is higher than the nominal value, as found for the specimens included in the research described herein, the minimum weld size may not be sufficient to guarantee the ductile response of the shear tab. This observation was consistent with the conclusion of the previous research [20, 24]. Therefore, it seems sensible to determine the minimum fillet weld size based on the expected yield stress  $(R_yF_y, [50])$  and nominal tensile strength of the steel and weld, respectively. In this case, the minimum weld size would increase to 11/16 t<sub>p</sub> for A572 steel and an E70 electrode. Of note, this new recommendation resulted in 7 mm weld size for Specimen BC3-2-10, which was still smaller than their oversized weld lines.

The observed resistance corresponding to the weld tearing was much lower than the concentric shear capacity of the weld line as shown in Table 7-4. This was due to the existing eccentricity between the weld line and the inflection point. As a conservative assumption, the weld capacity was calculated for an eccentric shear force, placed at the centre of the bolt group [9]. Referring to Table 7-4, the eccentric capacity of the weld line was calculated based on the current AISC [4]

and CISC [5] design methods for the weld group under combined shear and bending. The AISC design method was originally developed for in-plane bending based on the Instantaneous Centre of Rotation (ICR) method, whereas the CISC method was based on the model proposed by Kwan and Grondin [68] for a weld line subjected to out-of-plane bending. In these calculation the measured size and length of the weld line was used, in addition to the measured weld tensile strength, reported in Table 7-1. Furthermore, the resistance factor  $(\phi_w)$  was assumed equal to unity in all calculations. The measured resistance corresponding to the propagation of the weld tearing was considered conservatively as the weld group capacity. All calculations were conducted based on the geometric eccentricity (e<sub>g</sub>=152mm) in the absence of an axial force. The AISC method overestimated the weld capacity of Specimen BC3-2-10, where the weld line was subjected to a large eccentricity in comparison to its depth (e<sub>g</sub>/l<sub>w</sub>=0.70). In this case, the Kwan and Grondin method conservatively predicted the weld group capacity. This method overestimated the weld group capacity when the eccentricity-length ratio was small. (e<sub>g</sub>/l<sub>w</sub>=0.35). The third method, in which the CISC method was used with  $0.6F_{EEX}$  in lieu of  $0.67X_u$  as the shear strength of the fillet weld, resulted in a conservative estimate for all configurations. Of note, the tensile strength of the welding electrode was shown by  $F_{EXX}$  and  $X_u$  in AISC and CISC handbooks, respectively [4, 5].

Table 7-4. Weld line resistance under an eccentric shear force

-									
		Concent	ric capacity			Eccentric	capacity	7	
	Experiment	A	ISC <sup>a</sup>	AIS	SC <sup>b</sup>	CIS	SC °	CIS	SC <sup>d</sup>
		$F_v=0$ .	$.60~\mathrm{F_{EEX}}$	$F_v=0.6$	$50 \; \mathrm{F_{EEX}}$	$F_v=0$ .	67 X <sub>u</sub>	$F_v=0.6$	$50 F_{\rm EEX}$
Specimens	V <sub>WTP</sub> (kN)	V <sub>A</sub> (kN)	$\frac{V_{\text{WTP}}}{V}$						
-	(KIV)	(KIV)	$V_{A}$	(KIN)	$V_{A}$	(KIV)	$V_A$	(KIV)	V A
BC3-2-10	533	1256	0.42	585	0.91	466	1.14	450	1.18
BC3-2-10-200C	596	1275	0.47	578	1.03	440	1.35	428	1.39
BC6-2-16	1853	2436	0.76	1870	0.99	1949	0.95	1779	1.04
BC6-2-16-500C	1898	2396	0.79	1834	1.03	1915	0.99	1749	1.09

<sup>&</sup>lt;sup>a</sup> concentric shear capacity of the weld line [4]

<sup>&</sup>lt;sup>b</sup> Eccentric shear capacity of the weld line based on ICR method [4]

<sup>&</sup>lt;sup>c</sup> shear capacity of the weld line under shear force and out-of-plane bending moment [5, 68]

d shear capacity of the weld line under shear force and out-of-plane bending moment [68]

To evaluate the validity of the AISC design method [4], the predicted and ultimate resistance of the specimens were compared. As mentioned in Section 7.2.1, the AISC design method predicts the combined flexural and shear yield of the shear plate as the governing failure mode. Referring to Table 7-5, all specimens exceeded by 38% to 56% the predicted strength according to the AISC design method. These large measured-to-predicted ratios can be attributed to the AISC design method, which was developed based on the lower bound theorem as a conservative, straight forward, and simple to use procedure [9]. Of note, applying a relatively small axial compression ( $\approx 0.2 F_y A_g$ ) increased the ultimate resistance of the connection. The axial compression delayed both weld tearing and net section rupture, the ultimate failure mode of the connection under gravity induced shear force.

Table 7-5 Observed and predicted failure modes and corresponding resistances

1 4	ole / 5 Observed and predict	oa rarrare	modes and corresponding resist	ances	
	Experiment		AISC Design Me	thod	
Specimens	Ultimate failure mode	V <sub>u</sub> (kN)	Governing failure mode	V <sub>A</sub> (kN)	$\frac{V_u}{V_A}$
BC3-2-10	Weld tearing-propagation	533	Flexural and shear yielding	385	1.38
BC3-2-10-200C	Plate Buckling	599	Flexural and shear yielding	385	1.56
BC6-2-16	Net section rupture	1940	Flexural and shear yielding	1371	1.41
BC6-2-16-500C	Net section rupture	2130	Flexural and shear yielding	1371	1.55

### 7.3 Finite element simulation

Finite element (FE) simulation was adopted to expand our understanding of the behaviour of the unstiffened extended shear tab under combined axial and shear force. The FE models of the tested specimens, developed in the commercial program ABAQUS-6.11-3 [23], were compared with the laboratory results to validate the simulations. The dependence of a connection's behaviour on different parameters was then studied through FE simulations. In particular, the parameters that were investigated were as follows: the number of the vertical bolt lines and bolt rows, the plate's depth and thickness, the offset of the bolt group from the column face, the bolt grade, and the magnitude and direction of the axial load.

### 7.3.1 Description of FE models

The features of the FE model were chosen to be representative of the laboratory tests, including; the geometry, boundary conditions, material properties, element size and type, contacts and interactions, and the loading protocol. To decrease the computational cost of the FE model (Fig. 7-11), the column's supporting system was replaced by a fixed boundary condition at the column base. Further, the out-of-plane deformation of the beam flanges was restricted at the location of the lateral brace. The displacement of the two actuators, recorded during each test, was applied to the centerline of the load cubes to replicate the experimental loading protocol. Of note, the horizontal and out-of-plane deformations (U<sub>x</sub> and U<sub>z</sub>, respectively) of the load cube centerline were restrained.

The surface-to-surface contact pairs were defined to allow force transmission between all components in contact. Both normal and tangential behaviours of the contact pair were enforced using the penalty method. The normal behaviour of the contact pair, capable of separation after closure, was defined using a hard contact formulation. The tangential behaviour of the contact pairs between the load cubes and the flanges of the beam was defined by a frictionless interaction. For all other contact pairs, a friction coefficient of 0.3 was used to define the tangential behaviour.

The FE models were meshed using first-order fully-integrated 3D solid elements, and a mesh sensitivity analysis was conducted to determine the element size. The material properties were defined up to the ultimate strain based on the true stress-strain curves of connection components. Other than the bolts' material properties, these stress-strain curves were obtained from tensile coupon tests. The material properties of the bolts were defined based on typical stress-strain curves reported in Kulak et al. [55], which were scaled to meet the minimum specified values for ASTM F3125 Grades A325 and A490 bolts [34].

As the exact location of the bolt shanks in the bolt holes was not determined prior to each laboratory test, due to the complexity of such measurements, the bolts were consistently placed at the bolt hole centre in the FE model. This resulted in an initial 0.8 mm (1/32 in.) gap around the entire perimeter of the bolt shank, which matches the fabrication tolerance of a standard 21 mm (13/16 in.) hole. In this case, a small amount of bolt pretension, i.e. 50 MPa based on prior related studies [36], was applied to prevent rigid body motion of the beam.

Regarding the validity and convergence issues of the current damage simulation models in capturing the weld tearing propagation, the focus of the FE model simulations was narrowed to the behaviour of the plate and bolts. Although the weld geometry was included in the FE models due to their action as a lateral brace of the plate at the face of the column, only elastic material properties were assigned to the weld material.

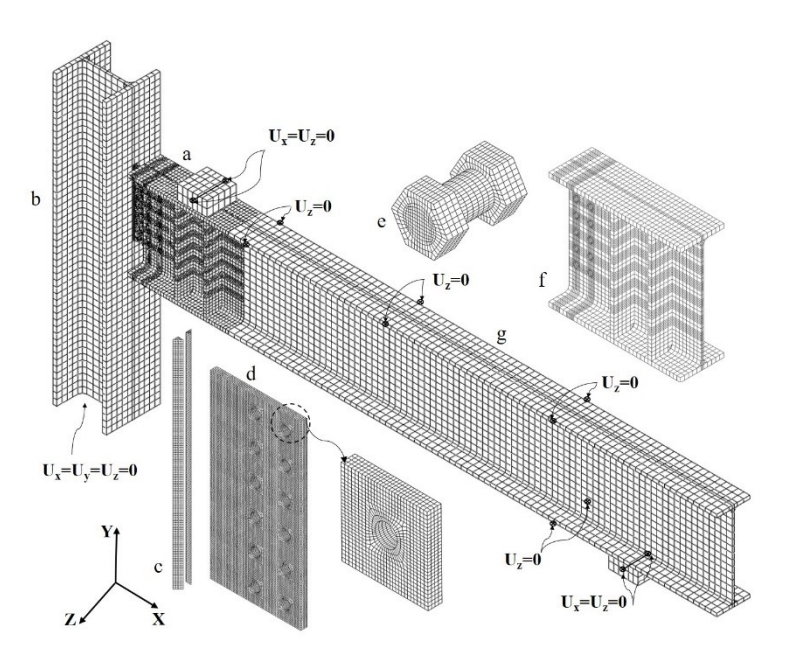


Fig. 7-11. Details of FE model: (a) overall model, (b) column mesh (typical element size of 40 mm), (c) Weld line mesh shear (typical element size of 3 mm), (d) plate mesh (typical element size of 3 mm), (e) bolt mesh (typical element size of 1.5 mm), (f) mesh of the beam in the vicinity of connection (typical element size of 20 mm), (g) beam mesh (typical element size of 40 mm)

#### 7.3.2 Model Validation

Referring to Fig. 7-12, the response of the FE models deviated from the test measurements in the initial increments of loading. This discrepancy was due to the bolt bearing conditions in the FE models, which were different from those in the laboratory tests. The initial response of the shear tab, as a snug-tightened connection, relied on the contact between the bolt shank and bolt hole. Nonetheless, placing the bolts in the centre of bolt hole for the FE model was selected as a conservative approach, necessary because the exact location of the bolt in the bolt hole was not available.

Referring to Figs. 7-12a and 7-12b, the FE model of Specimen BC3-2-10 reasonably captured the strength plateau and the vertical deformation of the shear plate along its exterior vertical bolt line, although the weld damage was not included in the model. The FE model showed large plastic strain and deformation at the gross section of the shear plate near the weld line (Fig. 7-13a), which resembled the base metal failure in the welded connection. For Specimen BC3-2-10-200C in which buckling was determined as the ultimate failure mode, the FE model predicted reasonably well the connection shear force and rotation as well as the out-of-plane deformation of the shear plate, as shown in Figs. 7-12c and 7-12d. Although the FE model could not capture the small drop of the shear force, which occurred due to rapid propagation of the weld tearing, it was able to detect the connection resistance corresponding to the plate buckling. Figure 7-13 presents the deformed shape of the FE model of Specimen BC3-2-10-200C.

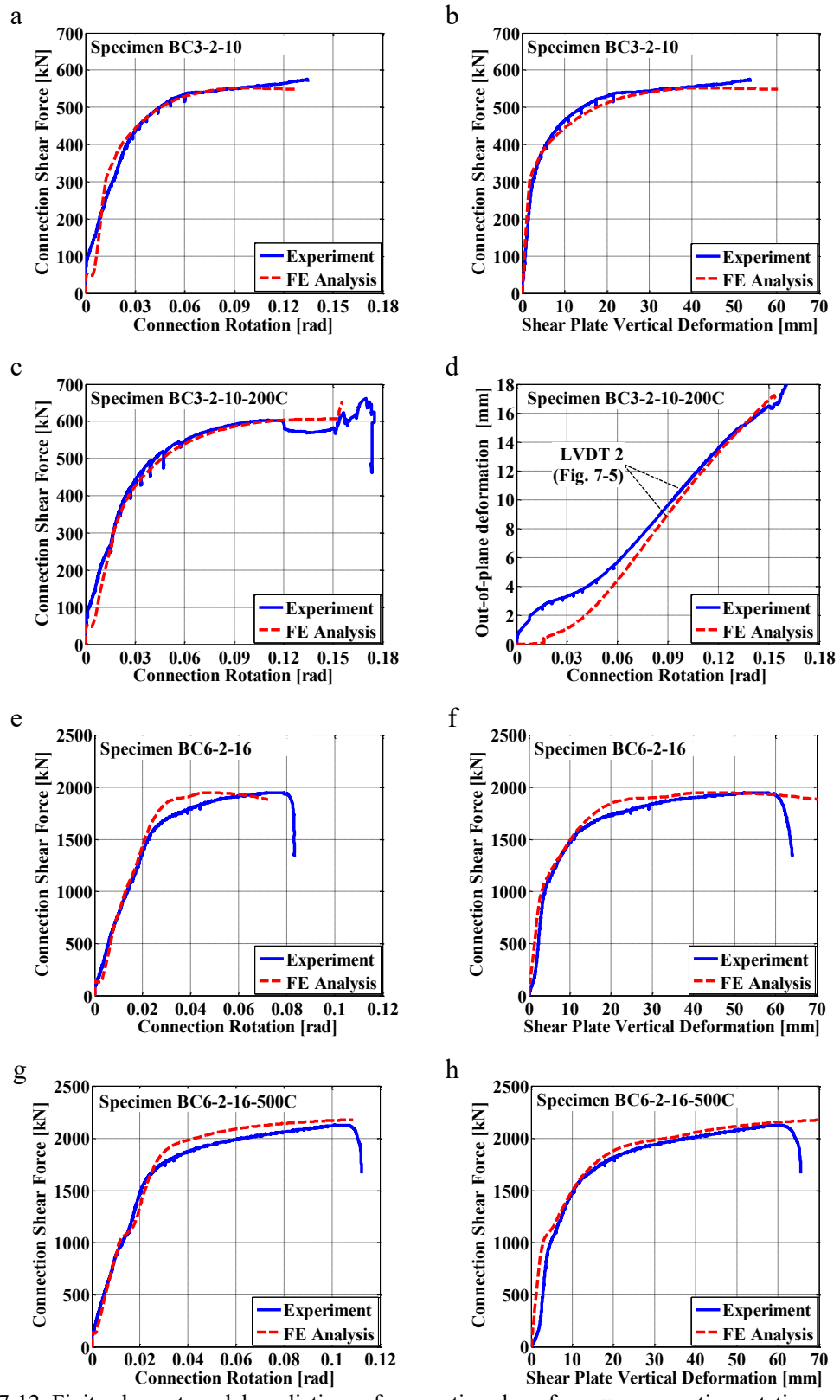


Fig. 7-12. Finite element model predictions of connection shear force vs. connection rotation and shear plate vertical deformation

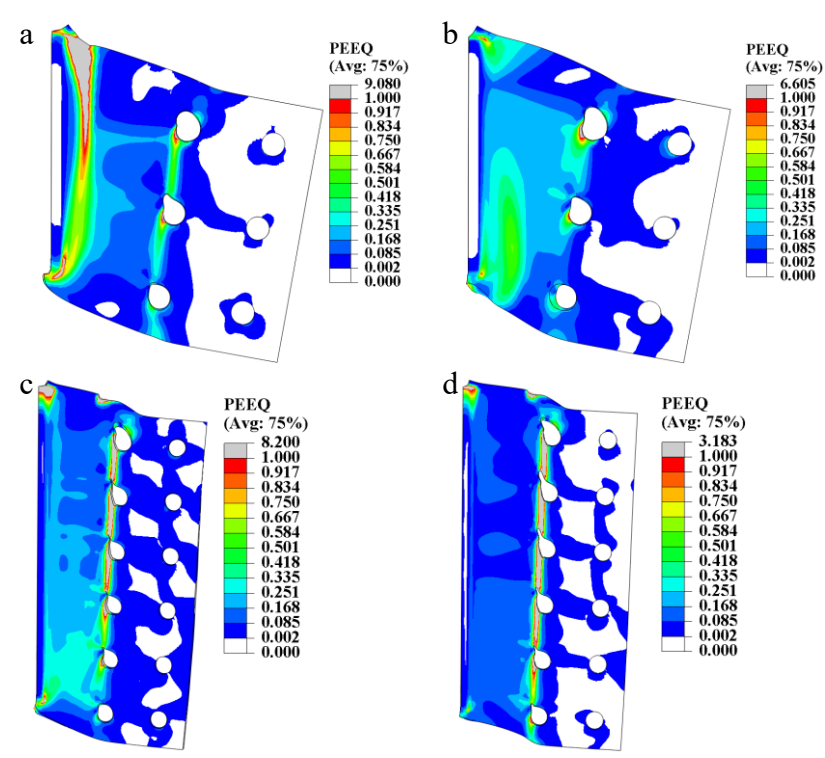


Fig. 7-13. Deformed shape of FE model: (a) BC3-2-10, (b) BC3-2-10-200C, (c) BC6-2-16, (d) BC6-2-16-500C

Referring to Figs. 7-12e and 7-12g, the predicted behaviour slightly deviated from the measured response when the stiffness of Specimens BC6-2-16 and BC6-2-1-6-500C decreased due to the onset of the weld tearing. However, the FE models accurately predicted the connection shear resistance corresponding to the net section rupture. As a conclusion, although the FE models could not capture the softening response of the specimens, they accurately predicted the connection resistance corresponding to the weld tearing, buckling and net section rupture as a strength plateau.

## 7.3.3 FE Parametric study

To determine the influential parameters of the unstiffened extended shear tab, a parametric FE study was carried out. Referring to Table 7-6, the FE simulation matrix consisted of 32 configurations varied in the number of bolt rows and vertical bolt lines, the offset of the bolt group from the column face, the plate thickness, the bolt grade and bolt size. To facilitate the

interpretation of the FE simulations, the configurations were classified into six main groups; the number of the bolt rows as well as the bolt size were kept constant in each group.

Table 7-6. Unstiffened shear tab connection configurations for parametric FE study

		1 abic	/ <b>-6.</b> Unstiffe	siled silea		ear Plate	Jonnigura	110118 101	paramen	•	
	ID.	Bolt	Vertical	$d_{pl}$	t <sub>pl</sub>	a	eg	$a_{\mathrm{w}}$	d <sub>b</sub>	Beam	Column
		rows	bolt lines	(mm)	(mm)	(mm)	(mm)	(mm)	(mm)	Section	Section
	BC2-1-10		1	152	10	114	114	6			
1	BC2-2-10		2	152	10	114	152	6		W250×49	W360×196
Group 1	BC2-2-10-a1	2	2	152	10	152	191	6	19	(W10×33)	
Gr	BC2-2-10-a2		2	152	10	203	241	6		( W10×33)	(W14×132)
	BC2-2-10-a3		2	152	10	254	292	6			
	BC3-1-10		1	229	10	114	114	6			
7	BC3-2-10		2	229	10	114	152	6			
dn	BC3-2-13	3	2	229	13	114	152	8	19	W310×74	W360×196
Group 2	BC3-2-10-a1	3	2	229	10	152	191	6	19	$(W12\times50)$	(W14×132)
$\circ$	BC3-2-10-a2		2	229	10	203	241	6			
	BC3-2-10-a3		2	229	10	254	292	6			
	BC4-1-10		1	305	10	114	114	6			
Group 3	BC4-2-10		2	305	10	114	152	6		W410×74	W360×196
no.	BC4-2-10-a1	4	2	305	10	152	191	6	19	$(W16\times50)$	(W14×132)
Ğ	BC4-2-10-a2		2	305	10	203	241	6		(W10^30)	( W14^132)
	BC4-2-10-a3		2	305	10	254	292	6			
	BC5-1-10		1	381	10	114	114	6			
Group 4	BC5-2-10		2	381	10	114	152	6		W460×82	W360×196
lno	BC5-2-10-a1	5	2	381	10	152	191	6	19	(W18×55)	(W14×132)
Ğ	BC5-2-10-a2		2	381	10	203	241	6		(W16^33)	( W14^132)
	BC5-2-10-a3		2	381	10	254	292	6			
	BC6-1-10		1	457	10	114	114	6			
p 5	BC6-2-10		2	457	10	114	152	6		W530×82	W360×196
Group 5	BC6-2-10-a1	6	2	457	10	152	191	6	19	$(W21\times55)$	(W14×132)
Ğ	BC6-2-10-a2		2	457	10	203	241	6		(W21^33)	( W14^132)
	BC6-2-10-a3		2	457	10	254	292	6			
	BC6-1-16		1	457	16	114	114	10			
9	BC6-2-16		2	457	16	114	152	10			
Group 6	BC6-2-13	6	2	457	13	114	152	8	22	W610×140	W360×196
iro	BC6-2-16-a1	U	2	457	16	152	191	10	<i>LL</i>	(W24×94)	(W14×132)
$\circ$	BC6-2-16-a2		2	457	16	203	241	10			
	BC6-2-16-a3		2	457	16	254	292	10			

In the first five groups 19 mm (3/4 in.) bolts were used to connect the plate to the beam while

22 mm (7/8 in.) bolts were implemented in the sixth group. The reference configuration of each group had two vertical bolt lines and an *a* distance of 114 mm (4.5mm). In addition to the reference configuration, each group included a configuration with a single vertical bolt line and the *a* distance equal to that of the reference model. A comparison between these two configurations allowed one to determine the effect of adding a vertical bolt line on the behaviour of extended shear tabs. At

least three configurations with two vertical bolt lines were added to these two configuration to shape a group. These three configurations were identical to the reference configuration, other than the a distance, which was increased to determine the impact of a larger eccentricity on the connection response. These configurations were labeled by adding the suffix "a1, a2, and a3 to the ID of the reference configuration. In these configurations, a1 stands for a=152 mm (6 in.), while the a2 and a3 stand for a=203 mm (8 in.) and a=254 mm (10 in.), respectively. To study the effect of the plate thickness on the behaviour of an extended shear tab connection, a configuration with different plate thickness was added to the second and sixth groups.

The material properties of the shear plates were defined based on the probable yield and tensile strength ( $R_yF_y$  and  $R_TF_u$ ), whereas the nominal material properties were assigned to the bolts. As the main interest of this research was the connection behaviour, only elastic material properties were assigned to the beam, column and weld lines. To determine the effect of the bolt grade on the behaviour of shear tab, each FE model was run two times: one time with Grade A325 and a second time with Grade A490 ASTM F3125 bolts [34].

To investigate the behaviour of the shear tabs under combined axial and shear forces, four representative configurations were chosen among these 32 configurations. These four configurations, i.e. BC3-2-10, BC3-2-10-a2, BC6-2-16, BC6-2-16-a2, were subjected to a wide range of the axial force while they were resisting their service level of the gravity demand, representative calculated based on the dead and live load of an archetype office building [66]. Among chosen configurations, two medium-length shear tabs (BC3-2-10 and BC6-2-1-6) were representative of the extended beam-to-column flange connections while the long configurations (BC3-2-10-a2 and BC6-2-10-a2) were representative of double-sided configuration when the beam was framed into the column web.

#### 7.3.4 Simulation Results

Table 7-7 presents the response of the FE models under gravity induced shear force. Various damage states were observed, including; shear plate yielding, the plate buckling, the rupture at the plate's gross section, and the net section rupture. Of note, the damage state of plate yielding was determine through monitoring the equivalent plastic strain (PEEQ). The plate buckling was determined through inspection of the out-of-plane deformation of the plate and the stiffness of the shear-rotation curve of the connection. The net section rupture was determined by survey of the plastic strain and vertical deformation of the plate along the interior bolt line. The plastic strain at the critical gross section was implemented along the vertical and horizontal deformation of the plate to determine the gross section rupture damage state.

First, the critical gross section of the plate, i.e. the section at the face of the weld line, fully yielded. Although the yield of the critical gross section slightly decreased the connection stiffness, it could still resist a higher shear force as the yielding propagated toward the bolt line. When a significant length of the shear plate had yielded, the out-of-plane deformation of the plate started to increase rapidly, however, the connection shear force still increased. The section of the plate along the interior bolt line (the critical net section) completely yielded only after the full yield of the critical gross section had occurred, although the yield of the net section began prior to that of the gross section in some configurations. This observation was due to the fact that the yield occurred due to the interaction of the shear and bending while a larger bending moment was applied to the gross section in comparison to the critical net section. The inflection point of the connection moved toward the column face while the rotational stiffness of the connection decreased due to the yield and out-of-plane deformation of the shear plate. This allowed the connection to resist higher shear force under a smaller bending moment. Following a large rotation

and deformation, the connection reached its ultimate strength. In several shallow shear tabs, e.g. connection BC2-2-10, the connection reached its strength plateau due to the rupture of the plate's critical gross section. Although the onset of plate rupture, i.e. development of large plastic strain and deformation at top edge of the critical gross section, was observed in almost all configurations, only in a few configurations did the rupture propagate significantly and the connection reached its strength plateau due to the plate rupture.

Table 7-7. Connection response under gravity induced shear force based on FE analyses

			section	Net so	ection	Out-of	-plane		kling	Net s		Gross	section	Bolt fi	racture	Bolt fi	
		V	ding -	yiele V	_	deforr V		V		rup V	1	rup V		(A3	r ′	(A4	
	Models	(kN)	e <sub>eff</sub> (mm)	(kN)	e <sub>eff</sub> (mm)	v (kN)	e <sub>eff</sub> (mm)	(kN)	e <sub>eff</sub> (mm)	(kN)	e <sub>eff</sub> (mm)	(kN)	e <sub>eff</sub> (mm)	(kN)	e <sub>eff</sub> (mm)	(kN)	e <sub>eff</sub> (mm)
	BC2-1-10	175	117	319	96	301	101				/	317	97	296	105	324 <sup>a</sup>	91
_	BC2-1-10 BC2-2-10	173	183	326	90	255	1113					347	83	323	93		
ф	BC2-2-10 BC2-2-10-a1		213	290	107	250	113					300	99	285	108		
Group 1		101	247	234				240	124								
9	BC2-2-10-a2	90			134	199	163	240	124					232	125		
	BC2-2-10-a3	77	287	195	163	166	196	191	171					190a	143	 5.619	
	BC3-1-10	325	128	536	112	477	116					544	111	481	118	561ª	96
2	BC3-2-10	232	204	515	118	472	127					567	104	582ª	91		
dno	BC3-2-13	299	202	666	121		1.40		100			760	89	737 <sup>a</sup>	110	775ª	96
Group 2	BC3-2-10-a1	210	231	491	124	420	148	517	109					517 <sup>a</sup>	98		
	BC3-2-10-a2	180	269	432	115	341	185	437	107					419a	117		
	BC3-2-10-a3	156	308	349	128	292	219	348	137					341ª	132	7.10	107
~	BC4-1-10	460	143	663	132	663	132			706	110			616	132	742	127
Group 3	BC4-2-10	362	224	667	146	667	146	726	1.02	786	119			7200			
rou	BC4-2-10-a1	333	251	647	151	567	172	736	103					730 <sup>a</sup>	87		
G	BC4-2-10-a2	302	287	601	125	474	209	601	125					602ª	102		
	BC4-2-10-a3	253	326	493	144	396	252	493	144								1.10
	BC5-1-10	618	154	907	142	812	147							753	144	907	142
Group 4	BC5-2-10	506	238	737	180	814	172			960	147						
ron	BC5-2-10-a1	461	279	812	172	649	208	942	106					936ª	77	915ª	51
9	BC5-2-10-a2	425	311	760	143	547	256	786	122					780ª	86		
	BC5-2-10-a3	382	346	645	147	497	291	645	147								
	BC6-1-10	748	178	1082	164	973	172							873	167	1043	167
p 5	BC6-2-10	643	264	868	200	929	212			1115	186						
Group :	BC6-2-10-a1	564	313	882	217	776	239	1134	109					1138ª	74	1160a	47
Ğ	BC6-2-10-a2	547	340	836	198	692	276	950	124					905ª	70		
	BC6-2-10-a3	517	372	793	139	601	329	793	139					729 <sup>a</sup>	95		
	BC6-1-16	1300	157	1521	134									1225	150	1573	130
9	BC6-2-16	1143	219	1602	151					1956	127						
dn	BC6-2-13	911	228	1361	146					1580	126						
Group 6	BC6-2-16-a1	1066	255	1768	155					1935	142						
Û	BC6-2-16-a2	997	290	1733	176					1908	165						
	BC6-2-16-a3	923	320	1504	212					1831	185						

<sup>&</sup>lt;sup>a</sup> Secondary failure mode

Note: --- means the damage state was not occured

Plate rupture was also observed along the interior bolt line in a few configuration, e.g. connection BC4-2-10 in which large deformation was observed along the interior bolt line while the connection reached its strength plateau. Most of the long shear tabs, such as connection BC3-2-10-a3, experienced their strength plateau following large out-of-plane deformation of the shear plate. The plate buckling was considered as the ultimate failure mode of these connections.

In a few configurations, such as connection BC5-2-10-a2, the bolt shear fracture was considered as the secondary failure mode. In these configuration, the inflection point moved quickly toward the column face once the connection had reached its strength plateau and the connection stiffness diminished due to the before mentioned ultimate failure modes; i.e. the gross section rupture, the net section rupture, and the plate buckling. As the inflection moved toward the column face, the eccentricity of the shear force for the bolt group increased and the bolt group then was subjected to a shear force with a large eccentricity and bolt shear fracture occurred following the ultimate failure mode. Furthermore, the bolts experienced a large axial elongation following the plate buckling. The bolt shear fracture was considered as the ultimate failure mode in few configurations when the bolt group reached its capacity following plate yielding. Of note, the FE model prediction was compared with the available bolt shear experiments [64, 65] to evaluate the capability of the FE model to accurately capture the bolt shear strength. The FE model's prediction for a bolt's post ultimate response was not in agreement with the measured response; however, the FE model was able to replicate the strength plateau corresponding to bolt shear. As such, the FE model would overestimate the shear capacity of the bolt group under an eccentric shear force, in which the bolt fracture occurred progressively. To cope with this shortcoming, the forcedeformation response of each individual bolt was recorded during the analysis, and the shear capacity of the bolt group was considered as the connection shear force corresponding to the time when the first bolt reached its strength plateau.

In addition to the analyses of the shear tab connections under gravity induced shear force, four configurations were subjected to a coupled axial and shear force. The applied axial force ranged between the connection's axial compressive and tensile capacities, shown in Table 7-8.

Table 7-8. FE models predictions for connection axial capacities

ID.	Gro Sect yield	ion	Net se Yield			f-plane nation	Buck	kling	Net se		Bolt s	hear
	F <sub>FE</sub> (kN)	$\frac{F_{\text{FE}}}{F}$	F (kN)	$\frac{F_{\text{FE}}}{F}$	F (kN)	$\frac{F_{\text{FE}}}{D}$	F (kN)	$\frac{F_{\text{FE}}}{D}$	F (kN)	$\frac{F_{\text{FE}}}{F}$	F (kN)	$\frac{F_{\text{FE}}}{F}$
	(KIN)	$F_{GP}$	(KIN)	$F_{NP}$	(KIV)	$\mathbf{P}_{\mathrm{cr}}$	(KIN)	$\mathbf{P}_{\mathrm{cr}}$	(KIV)	$F_{NU}$	(KIN)	$F_{BSH}$
BC3-2-10-PC <sup>a</sup>	822	0.98			804	1.02	822	1.04				
BC3-2-10-a2-PC <sup>a</sup>	$507^{b}$	0.61			689	0.98	749	1.07				
BC6-2-16-PC a	2653	0.97			2040	0.75	3205	1.20			3047	1.01
BC6-2-16-a2-PC <sup>a</sup>					1995	0.78	2289	0.90			1965°	0.65
BC3-2-10-PT d	845	1.01	662	1.09					914	1.06		
BC3-2-10-a2-PT <sup>d</sup>	842	1.01	624	1.02					926	1.07		
BC6-2-16-PT <sup>d</sup>	2747	1.01	2072	1.10					2958	1.11	3046	1.01
BC6-2-16-a2-PTd	2745	1.01	2051	1.09					2976	1.12	2980	0.99

<sup>&</sup>lt;sup>a</sup> PC: Pure compression

As mentioned in Section 7.3.1, four configurations were subjected to combined axial and shear forces. Referring to Table 7-9, applying the axial tensile force decreased the out-of-plane deformation of the shear plate while the demand on the net section of the plate as well as the weld line increased. The presence of the axial compression decreased the connection resistance corresponding to the out-of-plane deformation and buckling of the shear plate. Following buckling of the plate, bolt fracture was observed as the secondary mode in several connections.

<sup>&</sup>lt;sup>b</sup> Gross section yielding observed after the plate buckling due to large out-of-plane deformation

<sup>&</sup>lt;sup>c</sup> Secondary failure mode

d PT: Pure tension

Table 7-9. Connection response under gravity induced shear force based on FE analysis

	Axial		section ding	Net s	ection ding	Out-o	f-plane nation	Buc	kling	Net s	ection ture	Gross	section ture		racture 190)
	Force (kN)	V (kN)	e <sub>eff</sub> (mm)	V (kN)	e <sub>eff</sub> (mm)	V (kN)	e <sub>eff</sub> (mm)	V (kN)	e <sub>eff</sub> (mm)	V (kN)	e <sub>eff</sub> (mm)	V (kN)	e <sub>eff</sub> (mm)	V (kN)	e <sub>eff</sub> (mm)
	700C	113ª	167			146	159	242	99						
	600C	147ª	186			234	148	333	100						
0	400C	183	204	456	63	380	134	471	99					453 <sup>b</sup>	61
BC3-2-10	200C	215	206	524	114	437	133	553	103				104		
3-	0 200T	232	204	515	118	472	127					567	104		
B(	200T 400T	224 194	202 191	434 222	125 183							533 499	103 94		
	600T	150a	160	150a	160					421	93	499	9 <del>4</del> 		
	800T	73 <sup>a</sup>	104	73 <sup>a</sup>	104					261	107				
	600C	94ª	220			94	220	95	204						
	500C	128ª	254			135	249	141	242						
$\mathcal{C}_{\mathbf{J}}$	400C	142	263	190	90	168	250	198	168						
BC3-2-10-a2	200C	174	268	333	94	252	218	333	94						
2-1	0	180	269	432	115	341	185	437	107						
5-	200T	174	263	428	147	374	167					446	134		
B	400T	149	250	289	176							402	136		
	600T	135	241	135	241							346	131		
	800T	44	142	44 <sup>a</sup>	142					231	145				
	2750C	495ª	167			668	158	749	141					780 <sup>b</sup>	120
	2500C	579ª	183			876	163	1104	119					1117 <sup>b</sup>	105
	2000C	700 <sup>a</sup>	216	1653	109	1051	185	1653	109					1679 <sup>b</sup>	97
	1500C	868	234	1943	117	1121	202	2007	112	2110				2019 <sup>b</sup>	110
9	1000C	1025	232	1994	124	1201	202			2110	117				
BC6-2-16	500C	1107	222	1847	136					2059	122				
-5	250C	1133	222 219	1762 1602	142 151					2011 1956	124 127				
BC	0 250T	1143 1124	219	1406	170					1930	127				
	500T	1167	207	1094	220					1823	132				
	1000T	1063	218	797	239					1670	135				
	1500T	865	227	732ª	236					1479	138				
	2000T	692	209	643 <sup>a</sup>	210					1252	139				
	2500T	552a	171	552a	171					946	140				
	2750T	422ª	146	422ª	146					735	135				
	2000C	489°	187			489	187	515	173						
	1500C	684°	230			618	251	718	208						
	1000C	782	266			782	266	1072	152						
	500C	846	293	1633	161	1073	251	1745	145					1707	153
-a2	250C	934	293	1685	178	1248	230	1965	163					1981 <sup>b</sup>	163
BC6-2-16-a2	0	939	293	1789	172	1543	191			1946	165				
-2-	250T	997	290	1733	176					1908	165				
92j	500T	948	291	1666	180					1863	166				
В	1000T	912	291	1558	185					1821	167				
	1500T	856 752	293	856	293					1672	170				
	2000T	753 500	281	676	284					1482	174				
	2500T	590	261	590ª	261					1243	180				
	2750T	414 <sup>a</sup>	220 shear force	414 <sup>a</sup>	220	· 1.C		· · · · · · · · · · · · · · · · · · ·	1 1 1 .	917	190				

<sup>&</sup>lt;sup>a</sup> minimum shear force after applying axial force, the section yielded during applying axial force. <sup>b</sup> Secondary failure mode

<sup>&</sup>lt;sup>c</sup> It buckled in advance of the shear plate yielding.

<sup>---</sup> means that the damage state was not occurred.

# 7.4 Discussion

# 7.4.1 Ultimate resistance under gravity induced shear force

Tables 7-10 and 7-11 present the ultimate resistance of each connection configuration when Grade A325 and A490 ASTM F3125 bolts were implemented, respectively.

Table 7-10. Ultimate strength of the connection with A325 bolts under gravity shear demand

14616 / 1	o. Ommate	FE simu		<u> </u>		1020 001	Current d	•	
	Ultimate						Governing		
Model	failure	$V_{FE}$	$\theta_{\rm c}$	$e_{\mathrm{eff}}$	$e_{eff}$	$\frac{\mathbf{e}_{b}}{}$	failure	V <sub>A</sub>	$\frac{V_{FE}}{}$
	mode	(kN)	(rad)	(mm)	$\mathbf{e}_{\mathrm{g}}$	$\mathbf{e}_{\mathrm{g}}$	mode	(kN)	$V_A$
BC2-1-10	BSF	296	0.065	105	0.92	-0.08	BSF	92	3.21
BC2-2-10	BSF	323	0.093	93	0.61	-0.39	GSP	163	1.98
BC2-2-10-a1	BSF	285	0.095	108	0.57	-0.43	GSP	129	2.21
BC2-2-10-a2	BSF	232	0.092	125	0.52	-0.48	GSP	100	2.33
BC2-2-10-a3	PB	191	0.060	171	0.58	-0.42	GSP	81	2.35
BC3-1-10	BSF	481	0.050	118	1.04	0.04	BSF	188	2.56
BC3-2-10	GSR	567	0.087	104	0.68	-0.32	GSP	322	1.76
BC3-2-13	GSR	760	0.110	89	0.58	-0.42	BSF	332	2.29
BC3-2-10-a1	PB	517	0.085	109	0.57	-0.43	GSP	267	1.94
BC3-2-10-a2	PB	437	0.086	107	0.44	-0.56	GSP	213	2.05
BC3-2-10-a3	PB	348	0.063	137	0.47	-0.53	GSP	176	1.97
BC4-1-10	BSF	616	0.036	132	1.16	0.16	BSF	322	1.91
BC4-2-10	NSR	786	0.088	119	0.78	-0.22	GSP	499	1.58
BC4-2-10-a1	PB	736	0.088	103	0.54	-0.46	GSP	430	1.71
BC4-2-10-a2	PB	601	0.063	125	0.52	-0.48	GSP	355	1.69
BC4-2-10-a3	PB	493	0.051	144	0.49	-0.51	GSP	299	1.65
BC5-1-10	BSF	753	0.032	144	1.26	0.26	BSF	469	1.61
BC5-2-10	NSR	960	0.069	147	0.97	-0.03	GSP	681	1.41
BC5-2-10-a1	PB	942	0.087	106	0.56	-0.44	GSP	605	1.56
BC5-2-10-a2	PB	786	0.063	122	0.51	-0.49	GSP	516	1.52
BC5-2-10-a3	PB	645	0.048	147	0.50	-0.50	GSP	444	1.45
BC6-1-10	BSF	873	0.029	167	1.46	0.46	BSF	623	1.40
BC6-2-10	NSR	1115	0.059	186	1.22	0.22	GSP	865	1.29
BC6-2-10-a1	PB	1134	0.086	109	0.57	-0.43	GSP	788	1.44
BC6-2-10-a2	PB	950	0.063	124	0.51	-0.49	GSP	690	1.38
BC6-2-10-a3	PB	793	0.051	139	0.47	-0.53	GSP	605	1.31
BC6-1-16	BSF	1225	0.019	150	1.32	0.32	BSF	847	1.45
BC6-2-16	NSR	1956	0.028	127	0.83	-0.17	GSP	1407	1.39
BC6-2-13	NSR	1580	0.027	126	0.83	-0.17	GSP	1135	1.39
BC6-2-16-a1	NSR	1935	0.029	142	0.75	-0.25	BSF	1235	1.57
BC6-2-16-a2	NSR	1908	0.031	165	0.69	-0.31	BSF	1027	1.86
BC6-2-16-a3	NSR	1831	0.030	185	0.63	-0.37	BSF	876	2.09
			M	inimum	0.44	-0.56			1.29
				Mean	0.74	-0.26			1.79
			Ma	aximum	1.46	0.46			3.21
		Sta	andard de	eviation	0.28	0.28			0.43
				COV	0.38				0.24

The following ultimate failure modes were observed from the FE models; bolt shear fracture (BSF), gross section rupture (GSR), net section rupture (NSR), and plate buckling (PB).

Table 7-11. Ultimate strength of the connection with A490 bolts under gravity shear demand

Table /-1				onnection	i With A	1490 001	Cumant d	•	
		FE simu	nanon				Current d	esign me	
Model	Ultimate failure	$V_{\text{FE}}$	$\theta_{\mathrm{c}}$	$e_{\rm eff}$	$e_{eff}$	$e_b$	Governing failure	$V_{A}$	$\overline{V_{\scriptscriptstyle FE}}$
Model	mode	(kN)	(rad)	(mm)	$\mathbf{e}_{\mathrm{g}}$	$\mathbf{e}_{\mathrm{g}}$	mode	(kN)	$\overline{\mathrm{V}_{_{\mathrm{A}}}}$
BC2-1-10	GSR	317	0.079	97	0.85	-0.15	BSF	115	2.75
BC2-1-10 BC2-2-10	GSR	347	0.079	83	0.83	-0.13 -0.46	GSP	163	2.73
BC2-2-10 BC2-2-10-a1	GSR	300		83 99	0.54	-0.48	GSP	103	
			0.108				GSP		2.33
BC2-2-10-a2	PB	240	0.089	124	0.51	-0.49		100	2.40
BC2-2-10-a3	PB	191	0.060	171	0.58	-0.42	GSP	81	2.35
BC3-1-10	GSR	544	0.072	111	0.97	-0.03	BSF	235	2.32
BC3-2-10	GSR	567	0.087	104	0.68	-0.32	GSP	322	1.76
BC3-2-13	GSR	760	0.110	89	0.58	-0.42	BSF	414	1.83
BC3-2-10-a1	PB	517	0.085	109	0.57	-0.43	GSP	267	1.94
BC3-2-10-a2	PB	437	0.086	107	0.44	-0.56	GSP	213	2.05
BC3-2-10-a3	PB	348	0.063	137	0.47	-0.53	GSP	176	1.97
BC4-1-10	BSF	742	0.063	127	1.11	0.11	BSF	403	1.84
BC4-2-10	NSR	786	0.088	119	0.78	-0.22	GSP	499	1.58
BC4-2-10-a1	PB	736	0.088	103	0.54	-0.46	GSP	430	1.71
BC4-2-10-a2	PB	601	0.063	125	0.52	-0.48	GSP	355	1.69
BC4-2-10-a3	PB	493	0.051	144	0.49	-0.51	GSP	299	1.65
BC5-1-10	BSF	907	0.051	142	1.25	0.25	BSF	586	1.55
BC5-2-10	NSR	960	0.069	147	0.97	-0.03	GSP	681	1.41
BC5-2-10-a1	PB	942	0.087	106	0.56	-0.44	GSP	605	1.56
BC5-2-10-a2	PB	786	0.063	122	0.51	-0.49	GSP	516	1.52
BC5-2-10-a3	PB	645	0.048	147	0.50	-0.50	GSP	444	1.45
BC6-1-10	BSF	1043	0.043	167	1.47	0.47	BSF	778	1.34
BC6-2-10	NSR	1115	0.059	186	1.22	0.22	GSP	865	1.29
BC6-2-10-a1	PB	1134	0.086	109	0.57	-0.43	GSP	788	1.44
BC6-2-10-a2	PB	950	0.063	124	0.51	-0.49	GSP	690	1.38
BC6-2-10-a3	PB	793	0.051	139	0.47	-0.53	GSP	605	1.31
BC6-1-16	BSF	1573	0.024	130	1.14	0.14	BSF	1059	1.49
BC6-2-16	NSR	1956	0.028	127	0.83	-0.17	GSP	1407	1.39
BC6-2-13	NSR	1580	0.027	126	0.83	-0.17	GSP	1135	1.39
BC6-2-16-a1	NSR	1935	0.029	142	0.75	-0.25	GSP	1281	1.51
BC6-2-16-a2	NSR	1908	0.031	165	0.69	-0.31	GSP	1122	1.70
BC6-2-16-a3	NSR	1831	0.030	185	0.63	-0.37	GSP	983	1.86
			M	inimum	0.44	-0.56		·	1.29
				Mean	0.72	-0.28			1.75
			Ma	aximum	1.47	0.47			2.75
		Sta	andard de	eviation	0.27	0.27			0.37
				COV	0.38				0.21

Although, the current AISC design method predicted either the flexural-shear yield of the shear plate (GSP) or the bolt shear fracture (BSF) as the governing failure mode of the connection, the design method conservatively predicted the connection's ultimate resistance. The observed-to-

predicted strength ratio ranged between 1.29 and 3.21 for the connections with A325 bolts, while this ratio remained in the range of 1.29 to 2.75 for configurations with A490 bolts. These large ratios occurred because a lower bound theorem had been implemented to develop the AISC design method as a conservative, straight forward and simple to use design procedure [9].

### 7.4.2 Shear capacity of the bolt group

Referring to Table 7-10, all six configurations with a single vertical bolt line failed due to bolt shear fracture when ASTM Grade A325 bolts were implemented. The bolt shear occurred after full yielding of the shear plate, although these configurations did not satisfy the ductility requirement of the AISC Steel Construction Manual for the maximum plate thickness. Furthermore, bolt shear fracture was observed as the ultimate failure mode of configurations with two bolt rows, other than BC2-2-10-a3 which failed due to plate buckling.

Referring to Table 7-11, only four configurations failed due to bolt shear fracture when the higher bolt grade (ASTM Grade A490) was implemented. These four configurations all had a single vertical bolt line. The observed bolt group eccentricity in the configurations, that failed due to the bolt shear fracture, ranged between -0.48e<sub>g</sub> and 0.46e<sub>g</sub>. Of note, the negative bolt group eccentricity means the connection inflection point was formed between the bolt group centre and the face of the column, whereas the inflection point formed beyond the bolt group centre in the case of the positive bolt group eccentricity. This observation suggests that Salem's recommendation [22] for the bolt group eccentricity, i.e. 0.5e<sub>g</sub>, would result in reasonably conservative predictions. Furthermore, the bolt group eccentricity remained in the range of -0.56e<sub>g</sub> and 0.47e<sub>g</sub> if all configurations were considered.

The comparison between Tables 7-10 and 7-11 demonstrated that the connections with A490 bolts experienced slightly longer bolt group eccentricity in comparison to the connections with

A325 bolts. This observation can be attributed to the fact that the bolt yielding in the connections with A325 fasteners kept the inflection point closer to the bolt group centre by preventing the yielding from propagating over a larger portion of the shear plate.

### 7.4.3 Yielding of the shear plate under shear force

Yielding of the gross and net sections of the shear plate was observed in all configurations. Yielding started at the top and bottom edges of the shear plate adjacent to the weld line. The yielding then propagated along the depth and length of the shear plate. In addition to the plate's gross section, the net section of the shear plate started to yield along the interior bolt line. In all cases, the gross section of the shear plate completely yielded in advance of the full yield of the net section because the yield occurred due to the interaction of the shear and bending while a larger bending moment was applied to the gross section in comparison to the critical net section. Referring to Table 7-12, the connection resistance corresponding to the gross section of the shear plate was compared with the predictions for flexural-shear yield of the shear plate. In these calculations, the bending demand was calculated based on the AISC assumption for the arm of the shear force, the a distance. The connection resistance corresponding to the flexural-shear yield of the gross section was calculated using two interaction equations: the elliptical interaction equation (Eq. (7-1)) and the Neal's interaction [40] equation for rectangular sections (Eq. (7-2)). Equation (7-1) is used in the current AISC design method to consider the interaction of bending and shear force in extended shear tabs. Further, Eq. (7-3), proposed by Astaneh [61] as the simplified version of Neal's equation, was implemented by the AISC steel manual [4] to account the bending-shearaxial force interaction for the connecting elements. In the absence of an axial force, both Eqs. (7-2) and (7-3) are identical.

$$\left(\frac{M}{M_P}\right)^2 + \left(\frac{V}{V_P}\right)^2 \le 1$$
 (7-1)

$$\left(\frac{M}{M_P}\right) + \left(\frac{P}{P_P}\right)^2 + \left(\frac{(V/V_P)^4}{1 - (P/P_P)^2}\right) \le 1$$
 (7-2)

$$\left(\frac{M}{M_P}\right) + \left(\frac{P}{P_P}\right)^2 + \left(\frac{V}{V_P}\right)^4 \le 1$$
 (7-3)

Table 7-12. Yielding of the plate's critical gross section

		F	E models		craing c		$(7-1)^a$	Eq. (		Eq. (	7-1) <sup>b</sup>	Eq. (	7-3) <sup>b</sup>
_	$V_{ ext{FE}}$	$e_{ m eff}$	$\theta_{\rm c}$		e <sub>eff</sub>	V <sub>A</sub>	$V_{\text{FE}}$	$V_{A}$	$ m V_{FE}$	V <sub>A</sub>	$V_{\text{FE}}$	$V_{A}$	$V_{\text{FE}}$
	(kN)	(mm)	(rad)	$\frac{e_{\text{eff}}}{a}$	e <sub>g</sub>	(kN)	$\frac{V_{FE}}{V_{A}}$	(kN)	$\frac{V_{FE}}{V_{A}}$	(kN)	$\frac{V_{FE}}{V_A}$	(kN)	$\frac{V_{\text{FE}}}{V_{\text{A}}}$
BC2-1-10	175	117	0.017	1.03	1.03	163	1.08	173	1.01	163	1.08	173	1.01
BC2-2-10	120	183	0.017	1.60	1.20	163	0.74	173	0.69	129	0.93	136	0.88
BC2-2-10-a1	101	213	0.014	1.40	1.12	129	0.78	136	0.74	106	0.95	110	0.92
BC2-2-10-a2	90	247	0.014	1.22	1.03	100	0.90	103	0.87	85	1.06	88	1.03
BC2-2-10-a3	77	287	0.013	1.13	0.98	81	0.95	83	0.93	71	1.09	72	1.06
BC3-1-10	325	128	0.017	1.12	1.12	322	1.01	336	0.97	322	1.01	336	0.97
BC3-2-10	232	204	0.015	1.79	1.34	322	0.72	336	0.69	267	0.87	283	0.82
BC3-2-13	299	202	0.017	1.77	1.33	423	0.71	441	0.68	350	0.85	371	0.81
BC3-2-10-a1	210	231	0.013	1.52	1.22	267	0.79	283	0.74	225	0.93	239	0.88
BC3-2-10-a2	180	269	0.011	1.32	1.11	213	0.84	226	0.80	185	0.98	194	0.93
BC3-2-10-a3	156	308	0.010	1.21	1.05	176	0.89	185	0.84	156	1.00	162	0.96
BC4-1-10	460	143	0.016	1.26	1.26	499	0.92	505	0.91	499	0.92	505	0.91
BC4-2-10	362	224	0.016	1.97	1.48	499	0.73	505	0.72	430	0.84	448	0.81
BC4-2-10-a1	333	251	0.014	1.65	1.32	430	0.78	448	0.74	372	0.89	394	0.84
BC4-2-10-a2	302	287	0.012	1.41	1.19	355	0.85	377	0.80	312	0.97	332	0.91
BC4-2-10-a3	253	326	0.010	1.28	1.12	299	0.84	318	0.80	267	0.95	282	0.90
BC5-1-10	618	154	0.017	1.35	1.35	681	0.91	675	0.91	681	0.91	675	0.91
BC5-2-10	506	238	0.017	2.08	1.56	681	0.74	675	0.75	605	0.84	617	0.82
BC5-2-10-a1	461	279	0.015	1.84	1.47	605	0.76	617	0.75	537	0.86	560	0.82
BC5-2-10-a2	425	311	0.013	1.53	1.29	516	0.82	541	0.79	461	0.92	488	0.87
BC5-2-10-a3	382	346	0.011	1.36	1.18	444	0.86	471	0.81	400	0.96	425	0.90
BC6-1-10	748	178	0.017	1.56	1.56	866	0.86	847	0.88	866	0.86	847	0.88
BC6-2-10	643	264	0.017	2.32	1.74	866	0.74	847	0.76	789	0.82	790	0.81
BC6-2-10-a1	564	313	0.014	2.06	1.65	789	0.72	790	0.71	714	0.79	732	0.77
BC6-2-10-a2	547	340	0.013	1.67	1.41	690	0.79	712	0.77	625	0.87	655	0.83
BC6-2-10-a3	517	372	0.012	1.46	1.27	605	0.85	637	0.81	551	0.94	584	0.89
BC6-1-16	1300	157	0.019	1.37	1.37	1407	0.92	1377	0.94	1407	0.92	1377	0.94
BC6-2-16	1143	219	0.015	1.92	1.44	1407	0.81	1377	0.83	1282	0.89	1283	0.89
BC6-2-13	911	228	0.014	2.00	1.50	1136	0.80	1112	0.82	1035	0.88	1036	0.88
BC6-2-16-a1	1066	255	0.013	1.68	1.34	1282	0.83	1283	0.83	1161	0.92	1189	0.90
BC6-2-16-a2	997	290	0.012	1.43	1.20	1122	0.89	1157	0.86	1017	0.98	1065	0.94
BC6-2-16-a3	923	320	0.010	1.26	1.09	984	0.94	1035	0.89	896	1.03	949	0.97
		M	inimum	1.03	0.98		0.71		0.68		0.79		0.77
			Mean	1.55	1.29		0.84		0.81		0.93		0.90
			aximum	2.32	1.74		1.07		1.01		1.09		1.06
	Sta	andard d		0.32	0.19		0.09		0.08		0.07		0.07
a C 1 1 1:			COV	0.21	0.15		0.11		0.10		0.08		0.08

 $<sup>^</sup>a$  Calculations were conducted based on M=V×a  $^b$  Calculations were conducted based on M=V×e  $_g$ 

Referring to Table 7-12, Eq. (7-1) resulted in lower estimations as compared with Eq. (7-3). However, both equations overestimated the connection shear force corresponding to yielding of the plate's gross section because the connection eccentricity was larger than the a distance. The results listed in Table 7-10 demonstrated that the addition of bolt rows and vertical bolt lines significantly increased a connection's effective eccentricity. Furthermore, the observed connection effective eccentricity became closer to the a distance in configurations with longer a distance; however, the change of the plate thickness was not overly influential on the connection eccentricity. Further, the yielding of the gross section of the shear plate allowed for the plate's stress redistribution, which resulted in the connection reaching a much larger shear force in comparison to that associated with the plate's yield resistance. As shown in Section 7.4.1, the plate's flexural-shear yield resistance, calculated based on the a distance, was overly conservative to be used for the connection's ultimate resistance. However, the large rotation and deformation, required to develop the ultimate resistance, could be detrimental to the serviceability of the supported beam. In this case, the author suggests that the required service level of the shear force shall be compared with the connection resistance corresponding to the gross section yielding. Referring to Table 7-10, the lower mean value and the standard deviation indicate that the geometric eccentricity (eg) is a more realistic estimate for the connection effective eccentricity ( $e_{\text{eff}}$ ). The calculation based on the  $e_g$  distance resulted in a more accurate prediction for the gross section yielding of the shear plate, although the mean value of the observed-to-predicted strength was still lower than unity.

Referring to Table 7-13, use of the plastic shear strength of the net section ( $V_{NP}$ =0.60 $F_yA_{net}$ ) overestimated the connection resistance corresponding to the yield of the plate's critical net section

in configurations with a relatively long a distance, i.e. a=254 mm. This was due to the shear-bending interaction.

Table 7-13 Yielding of the plate's critical net section

	I	FE model	ls		ear ngth	Eq. (	7-1) a	Eq. (	7-3) a	Eq. (	7-1) <sup>b</sup>	Eq. (	7-3) <sup>b</sup>
	$ m V_{FE}$	$e_{ m eff}$	e	V <sub>NP</sub>	$V_{\text{FE}}$	V <sub>A</sub>	$V_{\text{FE}}$	$V_{A}$	$V_{\text{FE}}$	V <sub>A</sub>	$V_{\text{FE}}$	V <sub>A</sub>	$\frac{V_{FE}}{V_{FE}}$
	(kN)	(mm)	$\frac{e_{\text{eff}}}{a}$	(kN)	$\frac{V_{\text{FE}}}{V_{\text{NP}}}$	(kN)	$\frac{V_{\text{FE}}}{V_{\text{A}}}$	(kN)	$\frac{V_{\text{FE}}}{V_{\text{A}}}$	(kN)	$\frac{V_{\text{FE}}}{V_{\text{A}}}$	(kN)	$\frac{V_{\text{FE}}}{V_{\text{A}}}$
BC2-1-10	319	96	0.84	244	1.31	119	2.67	127	2.51	159	2.00	169	1.89
BC2-2-10	326	92	0.81	244	1.33	119	2.73	127	2.57	159	2.05	169	1.93
BC2-2-10-a1	290	107	0.71	244	1.19	95	3.07	100	2.91	126	2.30	133	2.18
BC2-2-10-a2	234	134	0.66	244	0.96	73	3.19	76	3.07	98	2.39	101	2.31
BC2-2-10-a3	195	163	0.64	244	0.80	60	3.27	61	3.19	79	2.46	82	2.39
BC3-1-10	536	112	0.98	367	1.46	240	2.24	249	2.15	320	1.68	332	1.61
BC3-2-10	515	118	1.04	367	1.40	240	2.15	249	2.07	320	1.61	332	1.55
BC3-2-13	666	121	1.06	481	1.38	315	2.12	327	2.04	419	1.59	436	1.53
BC3-2-10-a1	491	124	0.82	367	1.34	199	2.46	211	2.32	266	1.85	282	1.74
BC3-2-10-a2	432	115	0.57	367	1.18	160	2.70	170	2.55	213	2.02	226	1.91
BC3-2-10-a3	349	128	0.50	367	0.95	133	2.63	139	2.51	177	1.97	186	1.88
BC4-1-10	663	132	1.16	489	1.36	364	1.82	369	1.80	486	1.36	492	1.35
BC4-2-10	667	146	1.28	489	1.36	364	1.83	369	1.81	486	1.37	492	1.36
BC4-2-10-a1	647	151	0.99	489	1.32	314	2.06	327	1.98	419	1.54	437	1.48
BC4-2-10-a2	601	125	0.61	489	1.23	260	2.31	276	2.18	347	1.73	368	1.63
BC4-2-10-a3	493	144	0.57	489	1.01	219	2.25	233	2.12	292	1.69	310	1.59
BC5-1-10	907	142	1.24	611	1.48	499	1.82	494	1.84	665	1.36	659	1.38
BC5-2-10	737	180	1.58	611	1.21	499	1.48	494	1.49	665	1.11	659	1.12
BC5-2-10-a1	812	172	1.13	611	1.33	444	1.83	453	1.79	592	1.37	603	1.35
BC5-2-10-a2	760	143	0.70	611	1.24	380	2.00	398	1.91	506	1.50	530	1.43
BC5-2-10-a3	645	147	0.58	611	1.06	327	1.97	347	1.86	436	1.48	463	1.39
BC6-1-10	1082	164	1.44	735	1.47	631	1.71	617	1.75	841	1.29	823	1.31
BC6-2-10	868	200	1.75	735	1.18	631	1.38	617	1.41	841	1.03	823	1.05
BC6-2-10-a1	882	217	1.43	735	1.20	575	1.53	576	1.53	766	1.15	767	1.15
BC6-2-10-a2	836	198	0.98	735	1.14	503	1.66	519	1.61	671	1.25	692	1.21
BC6-2-10-a3	793	139	0.55	735	1.08	441	1.80	464	1.71	588	1.35	619	1.28
BC6-1-16	1521	134	1.17	1127	1.35	967	1.57	947	1.61	1290	1.18	1262	1.21
BC6-2-16	1602	151	1.33	1127	1.42	967	1.66	947	1.69	1290	1.24	1262	1.27
BC6-2-13	1361	146	1.28	910	1.50	781	1.74	764	1.78	1041	1.31	1019	1.34
BC6-2-16-a1	1768	155	1.02	1127	1.57	881	2.01	882	2.00	1175	1.50	1176	1.50
BC6-2-16-a2	1733	176	0.87	1127	1.54	771	2.25	795	2.18	1029	1.68	1061	1.63
BC6-2-16-a3	1504	212	0.83	1127	1.33	676	2.22	711	2.11	902	1.67	949	1.59
	M	inimum	0.50		0.80		1.38		1.41		1.11		1.05
		Mean	0.97		1.27		2.13		2.06		1.60		1.55
	Ma	aximum	1.75		1.57		3.27		3.19		2.46		2.39
Sta	ndard d	eviation	0.32		0.18		0.49		0.44		0.37		0.33
		COV	0.33		0.14		0.23		0.21		0.23		0.21

<sup>&</sup>lt;sup>a</sup> Calculations were conducted based on V<sub>N</sub>=V<sub>G</sub>

To consider the interaction of the shear and bending moment, Eqs (7-1) and (7-3) were employed, while the a distance was considered as the eccentricity of the shear force. These

 $<sup>^{</sup>b}$  Calculations were conducted based on  $V_{N}\!\!=\!\!0.75V_{G}$ 

equations largely underestimated the connection shear force because it was assumed that the critical net section was subjected to the total shear force of the connection. Referring to Section 6.3.10, this assumption was overly conservative for the shear plate under gravity induced shear force where the critical net section was subjected to a fraction of the connection shear force ( $\approx$  0.75). Therefore, the connection shear force corresponding to yielding of the plate's net section was recalculated using Eqs. (7-1) and (7-3) and  $V_N$ =0.75V. Although these estimates were more accurate than predictions of other methods, they were still conservative; the mean observed-to-predicted strength ratio was 2.46 and 2.39 for Eqs. (7-1) and (7-3), respectively..

## 7.4.4 Shear plate buckling

Referring to Table 7-11, plate buckling was identified as the ultimate failure mode of 14 configurations, in which the shear plate was larger than the reference configuration with a = 114mm (4.5 in.). The plate's buckling strength was calculated based on the AISC requirements for the buckling strength of double-coped beams [4]. In these calculations, the a distance was considered as the unbraced length of the shear plate. The AISC method predicted that the flexural buckling would not occur in any configuration; instead, the flexural capacity of the shear plate was governed by the plastic flexural strength ( $M_p = F_y Z_g$ ). Table 7-14 presents the predictions using the AISC method for the buckling strength of the shear plate. Although this method did not consider the interaction of flexural and shear force, it conservatively predicted the buckling strength of the shear plate in all configurations, other than BC6-2-16-a1. This observation was attributed to the fact that the distance between the inflection point and the column face was much shorter than the a distance when buckling occurred. In configuration BC6-2-16-a1, the shear plate was deep but the eccentricity was short, hence, the interaction of the flexural-shear was more influential in comparison to the other configurations. If the shear-bending interaction had been considered in the

calculation of the buckling strength, while the a distance was assumed to be the shear force eccentricity, the shear resistance corresponding to the full yield of the plate gross section (V<sub>GSP</sub>) the buckling strength of the shear plate. Referring to Table 7-14, the flexural-shear yield resistance provided an overly conservative estimate (the mean observed-to-predicted strength ratio of 1.74) for the buckling strength of the shear plate. This could be attributed to the fact that the out-of-plane deformation of the shear plate started to increase following the yielding of the shear plate, while the connection's rotational stiffness started to decrease. Therefore, the inflection point moved toward the column face as yielding propagated along the plate length and the plate was subjected to a lower bending moment. To predict the buckling strength more accurately, Eqs. (7-1) and (7-3) were implemented to calculate the interaction of the shear and bending moment. In these calculations,  $0.5e_g$  was used as the eccentricity of the shear force. These assumptions resulted in a reasonably conservative estimate of the buckling strength of the shear plate.

Table 7-14 Plate buckling strength

	FE simulation					cural ngth	Flexura yie	ld <sup>a</sup>	Eq. (	7-1) <sup>b</sup>	Eq. (7-3) <sup>b</sup>	
	V <sub>FE</sub> (kN)	$\begin{array}{c} e_{\rm eff} \\ (mm) \end{array}$	$\frac{e_{\rm eff}}{a}$	$\frac{\mathrm{e_{eff}}}{\mathrm{e_{g}}}$	V <sub>cr</sub> (kN)	$\frac{V_{\text{FE}}}{V_{\text{cr}}}$	V <sub>GSP</sub> (kN)	$\frac{V_{_{FE}}}{V_{_{GSP}}}$	V <sub>cr</sub> (kN)	$\frac{V_{_{FE}}}{V_{_{cr}}}$	V <sub>cr</sub> (kN)	$\frac{V_{_{FE}}}{V_{_{cr}}}$
BC2-2-10-a2	240	124	0.61	0.51	105	2.29	100	2.40	156	1.54	165	1.45
BC2-2-10-a3	191	171	0.67	0.58	84	2.28	81	2.35	133	1.43	141	1.36
BC3-2-10-a1	517	109	0.72	0.57	315	1.64	267	1.94	356	1.45	364	1.42
BC3-2-10-a2	437	107	0.53	0.44	235	1.86	213	2.05	311	1.40	326	1.34
BC3-2-10-a3	348	137	0.54	0.47	188	1.85	176	1.97	274	1.27	291	1.20
BC4-2-10-a1	736	103	0.67	0.54	559	1.32	430	1.71	537	1.37	534	1.38
BC4-2-10-a2	601	125	0.61	0.52	419	1.44	355	1.69	486	1.24	496	1.21
BC4-2-10-a3	493	144	0.57	0.49	335	1.47	299	1.65	440	1.12	457	1.08
BC5-2-10-a1	942	106	0.70	0.56	874	1.08	605	1.56	719	1.31	704	1.34
BC5-2-10-a2	786	122	0.60	0.51	654	1.20	516	1.52	668	1.18	666	1.18
BC5-2-10-a3	645	147	0.58	0.50	523	1.23	444	1.45	617	1.05	627	1.03
BC6-2-10-a1	1134	109	0.72	0.57	1264	0.90	788	1.44	903	1.26	876	1.30
BC6-2-10-a2	950	124	0.61	0.51	946	1.00	690	1.38	853	1.11	838	1.13
BC6-2-10-a3	793	139	0.55	0.47	756	1.05	605	1.31	801	0.99	799	0.99
	M	inimum	0.53	0.44		0.90		1.31		0.99		0.99
		Mean	0.62	0.52		1.47		1.74		1.27		1.24
	Ma	aximum	0.72	0.58		2.29		2.40		1.54		1.45
Sta	Standard deviation		0.06	0.04		0.47		0.34		0.16		0.14
	COV			0.08		0.32		0.20		0.13		0.11

<sup>&</sup>lt;sup>a</sup> Calculations were conducted based on M=V×a

<sup>&</sup>lt;sup>b</sup> Calculations were conducted based on M=V×e<sub>g</sub>

## 7.4.5 Gross section rupture

Referring to Table 7-11, only six configurations failed due to the rupture of the critical gross section, that is, the section in the vicinity of the weld line (Fig. 7-13a). As mentioned in Section 7.3.4, this failure mode corresponded to the base metal failure in the welded connection. To control the base metal failure mode of the fillet joint under a concentric shear force, the AISC 360 Specification [1] controls the transmitted force with the shear rupture resistance of the connecting element (V<sub>Gu</sub>=0.60F<sub>u</sub> A<sub>g</sub>). Referring to Table 7-15, the V<sub>GU</sub> value of the shear plate overestimated the connection resistance corresponding to the plate's gross section rupture. This observation was due to the fact that the critical gross section of the extended shear tab is subjected to shear and bending simultaneously. To consider the interaction of these demands, Eqs. (7-4) to (7-6) were proposed based on Eqs. (7-1) to (7-3), respectively. In the new equations, the plate's plastic resistances were replaced by rupture resistances. Table 7-15 presents the predicted shear resistance corresponding to the base metal failure in accordance with Eqs. (7-4) and (7-6). To calculate the bending demand, the a distance was implemented as the eccentricity of the shear force. Both equations predicted conservatively the plate's rupture strength. The observed-to-predicted ratio ranged between 1.19 and 1.64 for Eq. (7-4), while this ratio fluctuated between 1.14 and 1.56 for Eq. (7-6).

$$\left(\frac{M}{M_{v}}\right)^{2} + \left(\frac{V}{V_{v}}\right)^{2} \le 1 \tag{7-4}$$

$$\left(\frac{M}{M_{u}}\right) + \left(\frac{P}{P_{u}}\right)^{2} + \left(\frac{(V/V_{u})^{4}}{1 - (P/P_{u})^{2}}\right) \le 1$$
(7-5)

$$\left(\frac{M}{M_u}\right) + \left(\frac{P}{P_u}\right)^2 + \left(\frac{V}{V_u}\right)^4 \le 1$$
 (7-6)

Table 7-15. Connection resistance corresponding to gross section rupture

					Shear	rupture	Eq. (	(7-4)	Eq. (	(7-6)
	V <sub>FE</sub> (kN)	$\begin{array}{c} e_{\rm eff} \\ (mm) \end{array}$	$\frac{e_{\rm eff}}{a}$	$\frac{e_{\text{eff}}}{e_{\text{g}}}$	V <sub>GU</sub> (kN)	$\frac{V_{_{FE}}}{V_{_{GU}}}$	V <sub>A</sub> (kN)	$\frac{V_{\text{FE}}}{V_{\text{A}}}$	V <sub>A</sub> (kN)	$\frac{V_{_{FE}}}{V_{_{A}}}$
BC2-1-10	317	97	0.85	0.85	475	0.67	231	1.37	245	1.29
BC2-2-10	347	83	0.72	0.54	475	0.73	231	1.50	245	1.41
BC2-2-10-a1	300	99	0.65	0.52	475	0.63	183	1.64	193	1.56
BC3-1-10	544	111	0.97	0.97	712	0.76	456	1.19	476	1.14
BC3-2-10	567	104	0.91	0.68	712	0.80	456	1.24	476	1.19
BC3-2-13	760	89	0.78	0.58	935	0.81	598	1.27	624	1.22
	M	inimum	0.65	0.52		0.63		1.19		1.14
		Mean	0.81	0.69		0.73		1.37		1.30
	Ma	aximum	0.97	0.97		0.81		1.64		1.56
Sta	andard d	eviation	0.11	0.17		0.07		0.16		0.14
		COV	0.14	0.25		0.10		0.12		0.11

<sup>&</sup>lt;sup>a</sup> Calculations were conducted based on M=V×a

## 7.4.6 Net section rupture

Referring to Table 7-11, eight configurations failed due to the net section rupture under gravity induced shear force. In these configurations, the strength plateau was observed in the curves corresponding to force-rotation and force-vertical deformation while large plastic strain developed along the interior bolt line (Fig. 7-13c). The observed shear resistance of these configurations was compared with the shear rupture strength of the plate's net section ( $V_{Nu}$ =0.60F<sub>u</sub>A<sub>net</sub>). Although the interaction of the shear and bending moment was not considered in these calculations, the shear rupture strength was a reasonably conservative estimate of the connection's shear resistance corresponding to the net section rupture (Table 7-16). This observation was due to the fact that the critical net section, along the centerline of the bolt hole, was subjected to a fraction of the connection shear force, while this calculation was based on the conservative assumption that the total value of shear force is transferred through this critical section. In contrast, the flexural rupture strength of the net section ( $V=M_{Nu}/a=F_u$   $Z_{net}/a$ ), gave an unsafe prediction for the connection shear force corresponding to the net section rupture. For the purpose of the comparison, the shear rupture resistance was calculated using Eqs. (7-4) and (7-6) as well. In these calculations, a-0.50e<sub>g</sub> was

assumed as the arm of the shear force to calculate the corresponding bending demand along the interior bolt line. Referring to Table 7-16, these equations predicted lower shear resistance corresponding to the net section rupture as compared to the plate's shear rupture strength  $V_{\rm Nu}$ .

Table 7-16. Connection resistance corresponding to net section rupture

					Shear	rupture	Flexural rupture a		Eq. (7-4) <sup>b</sup>		Eq. (	7-6) <sup>b</sup>
	V <sub>FE</sub> (kN)	e <sub>eff</sub> (mm)	$\frac{e_{eff}-a}{a}$	$\frac{e_{eff} - a}{e}$	V <sub>A</sub> (kN)	$\frac{\mathrm{V_{FE}}}{\mathrm{V_{A}}}$	V <sub>A</sub> (kN)	$\frac{V_{FE}}{V_A}$	V <sub>A</sub> (kN)	$\frac{V_{_{FE}}}{V_{_{A}}}$	V <sub>A</sub> (kN)	$\frac{V_{FE}}{V_A}$
DC4 2 10	` ′		a 0.04	e <sub>g</sub>			. ,		, ,		` '	
BC4-2-10	786	119	0.04	0.03	692	1.14	774	1.02	663	1.19	639	1.23
BC5-2-10	960	147	0.29	0.22	865	1.11	1222	0.79	842	1.14	812	1.18
BC6-2-10	1115	186	0.63	0.47	1041	1.07	1741	0.64	1021	1.09	988	1.13
BC6-2-16	1956	127	0.11	0.08	1596	1.23	2668	0.73	1565	1.25	1514	1.29
BC6-2-13	1580	126	0.11	0.08	1288	1.23	2153	0.73	1263	1.25	1222	1.29
BC6-2-16-a1	1935	142	-0.07	-0.05	1596	1.21	2001	0.97	1529	1.27	1472	1.31
BC6-2-16-a2	1908	165	-0.19	-0.16	1596	1.20	1498	1.27	1465	1.30	1414	1.35
BC6-2-16-a3	1831	185	-0.27	-0.23	1596	1.15	1197	1.53	1388	1.32	1355	1.35
	M	inimum	-0.27	-0.23		1.07		0.64		1.09		1.13
		Mean	0.08	0.06		1.17		0.96		1.23		1.27
	Ma	aximum	0.63	0.47		1.23		1.53		1.32		1.35
Sta	andard d	eviation	0.26	0.21		0.05		0.29		0.07		0.08
		COV				0.04		0.30		0.06		0.06

<sup>&</sup>lt;sup>a</sup> Calculations were conducted based on M=V×a

#### 7.4.7 Connection resistance under axial force

Referring to Table 7-8, the connections under axial compression failed due to the plate buckling, whereas net section rupture was their ultimate failure mode under axial tension. In the FE models subjected to axial tension, the plate first yielded along the interior bolt line. Then the gross section of the shear plate yielded, and finally the connection failed due to net section rupture. The AISC design method ( $T_{UN} = F_u A_{net}$ ) was found to provide a reasonable estimate of the connection's ultimate resistance. This was due to the fact that the average ultimate stress at the net section being higher than the ultimate stress as obtained from coupon tests, because the holes prevent the development of free lateral contraction at the net section [55].

<sup>&</sup>lt;sup>a</sup> Calculations were conducted based on M=V×(a-0.5e<sub>g</sub>)

In the connections under axial compression, the out-of-plane deformation of the shear tab started to increase rapidly prior to plate buckling. For the medium-length shear tabs, i.e. BC3-2-10-PC and BC6-2-16-PC, the plate's gross section yielded no later than the shear plate buckling. Contrary to the medium-length shear tabs, long shear tabs could not reach the level of the axial force corresponding to the yielding of the plate gross section. The gross section of the connection BC3-2-10-a2 yielded long after the plate buckling due to the extensive large out-of-plane deformation. For the specimen BC6-2-16-a2, the shear plate yielded partially due to the out-ofplane deformation. The employed procedure, proposed in Steel Connection Handbook (Section 2.5.3) [14] and AISC Design Examples (Example IIA-19B) [15], conservatively predicted the buckling resistance of all connections other than BC6-2-16-a2. In this configuration, the lateral brace of the top flange of the supported beam did not provided enough lateral support for this long and deep shear tab. In other words, the effective length of this shear tab was longer than the 0.65a. If a 1.2a distance was implemented as the effective length of the connection BC6-2-16-a2, the predicted buckling strength would decrease to 1545 kN and the observed-to-predicted ratio (V<sub>FE</sub>/V<sub>cr</sub>) increase to 1.48. The large out-of-plane deformation of the connection BC6-2-16-a2-PC caused the axial elongation of the bolts. Therefore, the bolt failure in this configuration was considered as the secondary failure mode, while the bolt group reached its shear capacity in the connection BC6-2-16-PC.

#### 7.4.8 Effect of axial force

Referring to Table 7-9, the impact of the axial force on the connection behaviour depends greatly on the magnitude and direction of the axial force, as well as the ultimate failure mode of the connection under gravity induced shear force. The presence and increase of axial compression decreased the connection's ultimate resistance in configurations such as BC3-2-10-a2, which

failed due to the plate buckling even under gravity induced shear force. Nevertheless, the ultimate shear resistance of connections BC6-2-16 and BC6-2-16-a2 increased as the applied axial compression was amplified up to  $0.37P_{GP}$  and  $0.18P_{GP}$ , respectively, in which,  $P_{GP}=F_yA_g$ . This observation was due to the thick shear plate failing by net section rupture under gravity induced shear force. The axial compression increased the shear rupture resistance of the plate and consequently the connection's ultimate resistance. An axial compression force, larger than the above mentioned limits  $(0.37P_{GP})$  and  $0.18P_{GP}$  for connections BC6-2-16 and BC6-2-16-a2, respectively), caused a decline of the connection's ultimate shear resistance due to plate buckling.

The applied axial tension decreased the ultimate resistance of all connections, other than the BC3-2-10-a2 model. The connection's capacity slightly increased because a small tensile force  $(0.24P_{GP})$  prevented the plate buckling, which was the ultimate failure mode of the BC3-2-10-a2 configuration under gravity induced shear forces. The connection capacity decreased when the BC3-2-10-a2 connection was subjected to a tensile force larger than  $0.24\ P_{GP}$ . In the presence of a tensile force, connections BC3-2-10 and BC3-2-10-a2 failed mostly due to the gross section rupture of the plate, while all BC6-2-16 and BC6-2-1-6a2 configurations failed due to the net section rupture. This occurred because the response of the BC3-2-10 and BC3-2-10-a2 configurations under gravity induced shear force was governed primarily by the bending moment  $(e_g/d_p=0.67$  and 1.06, respectively), while the behaviour of configurations BC6-2-16 and BC6-2-16-a2  $(e_g/d_p=0.33)$  and 0.53, respectively) depends greatly on the interaction of the shear and bending moment. The bolt fracture was observed as the ultimate failure mode only for connection BC6-2-16-1000C. In some connections, subjected to combined shear and compression, the bolt fracture following the plate buckling as the secondary failure mode.

To estimate the ultimate resistance of the extended shear tabs under combined axial and shear forces, the AISC design method for extended shear tabs was adjusted. Equation (7-3) was employed in lieu of Eq. (7-1) to predict the yielding strength of the critical gross section under the interaction of the bending, shear, and axial force. The plate rupture was controlled at the critical gross and net sections by Eq. (7-6). In these calculations, the bending demand was estimated based on the *a* distance eccentricity of the shear force. The shear resistance corresponding to the interaction yielding of the critical gross section had the minimum value for all cases. This shear force was employed along with the applied axial force to calculate the magnitude and angle of the resultant force.

Based on the angle of the resultant force, the bolt group capacity was determined in accordance with the Instantaneous Centre of Rotation (ICR) method. In most cases, the bolt group could resist the resultant force; the interaction yield of the critical gross section was determined as the governing failure mode. In a few cases, where the bolt group capacity was lower than the resultant force, the bolt group capacity was reported as the connection resistance. Referring to Table 7-17, the adjusted version of the AISC design method could not be used for three connections in which the applied axial force was larger than P<sub>GP</sub>. Among remaining connections that their capacity was calculated based on the adjusted AISC method, the adjusted method conservatively predicted the ultimate shear resistance of all except four models. In these four models, printed in bold in Table 7-17, the connections BC3-2-10-a2 and BC6-2-16-a2 buckled soon after applying a large axial force, close to their axial buckling resistance. Referring to Table 7-8, these two configuration buckled prior to yielding of the plate under axial compression force. The observed-to-predicted strength varied between 0.84 and 3.48 with the mean of 1.68 and 0.50 as the coefficient of variation.

Table 7-17. Ultimate capacity of shear tabs under combined axial and shear force

Table	e 7-17. U				bs under	combir	ned axial	l and shear for			
	FE simulation Current design methoda  P Ultimate T Governing T V										
	$\underline{P_{FE}}$	Ultimate	$ m V_{FE}$	$\theta_{\mathrm{c}}$	Α	$e_{\rm eff}$	e.	Governing	$V_{A}$	$\overline{\mathrm{V}_{\scriptscriptstyle\mathrm{FE}}}$	
Model	$\overline{P_{GP}}$	failure	(kN)	(rad)	e <sub>eff</sub> (mm)		$\frac{e_b}{e_b}$	failure	(kN)		
	1 GP	mode	(KIN)	(lau)	(111111)	$\mathbf{e}_{\mathrm{g}}$	$\mathbf{e}_{\mathrm{g}}$	mode	(KIV)	$V_{A}$	
BC3-2-10-700C	0.83	PB	242	0.023	99	0.65	-0.35	GSP	129	1.88	
BC3-2-10-600C	0.72	PB	333	0.032	100	0.66	-0.34	GSP	193	1.72	
BC3-2-10-400C	0.48	PB	471	0.057	99	0.65	-0.35	GSP	282	1.67	
BC3-2-10-200C	0.24	PB	553	0.082	103	0.68	-0.32	GSP	323	1.71	
BC3-2-10	0.00	GSR	567	0.087	104	0.68	-0.32	GSP	336	1.69	
BC3-2-10-200T	0.24	GSR	533	0.070	103	0.68	-0.32	GSP	323	1.65	
BC3-2-10-400T	0.48	GSR	499	0.068	94	0.62	-0.38	GSP	282	1.77	
BC3-2-10-600T	0.72	NSR	421	0.058	93	0.61	-0.39	GSP	193	2.18	
BC3-2-10-800T	0.95	NSR	261	0.034	107	0.70	-0.30	GSP	41	$6.38^{b}$	
BC3-2-10-a2-600C	0.72	PB	95	0.006	204	0.85	-0.15	GSP	113	0.84	
BC3-2-10-a2-500C	0.60	PB	141	0.008	242	1.00	0.00	GSP	149	0.95	
BC3-2-10-a2-400C	0.48	PB	198	0.019	168	0.70	-0.30	GSP	178	1.11	
BC3-2-10-a2-200C	0.24	PB	333	0.058	94	0.39	-0.61	GSP	214	1.55	
BC3-2-10-a2	0.00	PB	437	0.086	107	0.44	-0.56	GSP	226	1.93	
BC3-2-10-a2-200T	0.24	GSR	446	0.078	134	0.55	-0.45	GSP	214	2.08	
BC3-2-10-a2-400T	0.48	GSR	402	0.061	136	0.56	-0.44	GSP	178	2.26	
BC3-2-10-a2-600T	0.72	GSR	346	0.054	131	0.54	-0.46	GSP	113	3.07	
BC3-2-10-a2-800T	0.95	NSR	231	0.037	145	0.60	-0.40	GSP	23	$10.05^{b}$	
BC6-2-16-2750C	1.01	PB	749	0.012	141	0.93	-0.07	GSP			
BC6-2-16-2500C	0.91	PB	1104	0.015	119	0.79	-0.21	GSP	455	2.43	
BC6-2-16-2000C	0.73	PB	1653	0.022	109	0.72	-0.28	BSF	955	1.73	
BC6-2-16-1500C	0.55	PB	2007	0.029	112	0.73	-0.27	GSP	1179	1.70	
BC6-2-16-1000C	0.37	NSR	2110	0.032	117	0.77	-0.23	GSP	1296	1.63	
BC6-2-16-500C	0.18	NSR	2059	0.031	122	0.80	-0.20	GSP	1359	1.52	
BC6-2-16-250C	0.09	NSR	2011	0.030	124	0.82	-0.18	GSP	1373	1.47	
BC6-2-16	0.00	NSR	1956	0.028	127	0.83	-0.17	GSP	1377	1.42	
BC6-2-16-250T	0.09	NSR	1912	0.029	128	0.84	-0.16	GSP	1373	1.39	
BC6-2-16-500T	0.18	NSR	1823	0.027	132	0.87	-0.13	GSP	1359	1.34	
BC6-2-16-1000T	0.37	NSR	1670	0.026	135	0.89	-0.11	GSP	1296	1.29	
BC6-2-16-1500T	0.55	NSR	1479	0.025	138	0.91	-0.09	GSP	1179	1.25	
BC6-2-16-2000T	0.73	NSR	1252	0.024	139	0.91	-0.09	BSF	936	1.34	
BC6-2-16-2500T	0.91	NSR	946	0.023	140	0.92	-0.08	GSP	455	2.08	
BC6-2-16-2750T	1.01	NSR	735	0.022	135	0.89	-0.11	GSP			
BC6-2-16-a2-2000C	0.73	PB	515	0.006	173	0.72	-0.28	BSF	582	0.88	
BC6-2-16-a2-1750C	0.64	PB	718	0.009	208	0.86	-0.14	BSF	727	0.99	
BC6-2-16-a2-1500C	0.55	PB	1072	0.016	152	0.63	-0.37	BSF	881	1.22	
BC6-2-16-a2-1000C	0.37	BSF	1731	0.031	127	0.53	-0.47	GSP	1059	1.63	
BC6-2-16-a2-500C	0.18	NSR	1965	0.033	163	0.67	-0.33	GSP	1135	1.73	
BC6-2-16-a2-250C	0.09	NSR	1946	0.033	165	0.68	-0.32	GSP	1152	1.69	
BC6-2-16-a2	0.00	NSR	1908	0.031	165	0.69	-0.31	GSP	1157	1.65	
BC6-2-16-a2-250T	0.09	NSR	1863	0.030	166	0.69	-0.31	GSP	1152	1.62	
BC6-2-16-a2-500T	0.18	NSR	1821	0.030	167	0.69	-0.31	GSP	1135	1.60	
BC6-2-16-a2-1000T	0.37	NSR	1672	0.028	170	0.71	-0.29	GSP	1059	1.58	
BC6-2-16-a2-1500T	0.55	NSR	1482	0.027	174	0.72	-0.28	BSF	881	1.68	
BC6-2-16-a2-2000T	0.73	NSR	1243	0.025	180	0.75	-0.25	BSF	582	2.14	
BC6-2-16-a2-2500T	0.91	NSR	917	0.023	190	0.79	-0.21	GSP	263	3.48	
BC6-2-16-a2-2750T	1.01	NSR	726	0.022	193	0.80	-0.20	GSP			

Tr 11 7 17 /	(C) (1)	T T1/'	• ,	C 1	, 1 1	1	1 . 1	1 1 C
Lable /-1 / (	( onfinited)	Ulfimate car	าลดาโพด	t shear	tabs under	combined	I	nd shear force
14010 / 1 / (	Commuca	. Citimate eap	Jucity 0.	Bilear	tuos anaci	comonica	i uzriai a	iid biicai ioicc

			FE s							
Model	$\frac{P_{\text{FE}}}{P_{\text{GP}}}$	Ultimate failure mode	V <sub>FE</sub> (kN)	$\theta_c$ (rad)	e <sub>eff</sub> (mm)	$\frac{\mathrm{e_{eff}}}{\mathrm{e_{g}}}$	$\frac{\mathrm{e_{b}}}{\mathrm{e_{g}}}$	Governing failure mode	V <sub>A</sub> (kN)	$\frac{V_{_{FE}}}{V_{_{A}}}$
			Mi	-0.61			0.84			
					Mean	0.73	-0.27			1.68
				Ma	ximum	1.00	0.00			3.48
		Standard deviation 0.1								0.50
								0.30		

<sup>&</sup>lt;sup>a</sup> Calculations were conducted based on M=V×a

The response of the connection, failed due to the plate buckling, was reviewed in Table 7-18. As mentioned in Section 7.4.4, the interaction of the internal forces should be considered in the calculation of the connection buckling strength. For connections under gravity induced shear force, 0.5eg, as a conservative estimate of the eccentricity, was used to calculate the connection bending demand in the case of plate buckling.

Table 7-18 buckling strength under combined axial and shear forces

					Eq.	(7-2) <sup>a</sup>	Eq. (	7-3) <sup>a</sup>	Eq. (	7-7) <sup>a</sup>	Eq. (	7-8) <sup>a</sup>
Models	$V_{\text{FE}}$	$e_{\rm eff}$	$e_{\rm eff}$	$\underline{e_{eff}}$	$V_{cr}$	$V_{\scriptscriptstyle  m FE}$	$ m V_{GSP}$	$V_{\text{FE}}$	$V_{cr}$	$\overline{V_{_{ m FE}}}$	$V_{cr}$	$V_{\scriptscriptstyle  m FE}$
Wiodels	(kN)	(mm)	a	$\mathbf{e}_{\mathrm{g}}$	(kN)	$V_{cr}$	(kN)	${ m V}_{ m GSP}$	(kN)	$V_{cr}$	(kN)	$V_{cr}$
BC3-2-10-700C	242	99	0.86	0.65	125	1.93	129	1.88	75	3.23	92	2.63
BC3-2-10-600C	333	100	0.88	0.66	186	1.79	193	1.72	119	2.80	173	1.92
BC3-2-10-400C	471	99	0.87	0.65	274	1.71	282	1.67	205	2.30	275	1.71
BC3-2-10-200C	553	103	0.90	0.68	321	1.72	323	1.71	279	1.98	322	1.72
BC3-2-10-a2-600C	95	204	1.00	0.85	112	0.85	113	0.84	71	1.33	63	1.51
BC3-2-10-a2-500C	141	242	1.19	1.00	148	0.95	149	0.95	101	1.40	115	1.23
BC3-2-10-a2-400C	198	168	0.83	0.70	177	1.12	178	1.11	129	1.53	156	1.26
BC3-2-10-a2-200C	333	94	0.46	0.39	214	1.56	214	1.55	183	1.82	209	1.59
BC3-2-10-a2	437	107	0.53	0.44	226	1.93	226	1.93	213	2.05	226	1.93
BC6-2-16-2750C	749	141	1.24	0.93								
BC6-2-16-2500C	1104	119	1.05	0.79	409	2.70	455	2.43	243	4.54	339	3.25
BC6-2-16-2000C	1653	109	0.96	0.72	852	1.94	959	1.72	610	2.71	927	1.78
BC6-2-16-1500C	2007	112	0.98	0.73	1104	1.82	1179	1.70	891	2.25	1169	1.72
BC6-2-16-a2-2000C	515	173	0.85	0.72	638	0.81	671	0.77	409	1.26	572	0.90
BC6-2-16-a2-1750C	718	208	1.02	0.86	777	0.92	814	0.88	530	1.35	749	0.96
BC6-2-16-a2-1500C	1072	152	0.75	0.63	885	1.21	920	1.16	641	1.67	879	1.22
	M	inimum	0.46	0.39		0.81		0.77		1.26		0.90
		Mean	0.90	0.71		1.53		1.47		2.15		1.69
	Ma	aximum	1.24	1.00		2.70		2.43		4.54		3.25
St	andard d	eviation	0.20	0.15		0.52		0.47		0.86		0.59
		COV	0.22	0.21		0.34		0.32		0.40		0.35

<sup>&</sup>lt;sup>a</sup> Calculations were conducted based on M=V×a

<sup>&</sup>lt;sup>b</sup> This value was not included in statistic analysis

Referring to Table 7-18, the application of a large axial force prevented the inflection point from moving toward the column face. Therefore, the 0.5e<sub>g</sub> would not be a safe estimate of the connection eccentricity corresponding to the plate buckling under combined shear and compression. For this loading scenario, the *a* distance was employed as the connection eccentricity. In addition to Eqs. (7-2) and (7-3), shear-bending- axial force interaction was taken into account using Eqs. (7-7) and (7-8). Equations (7-2) and (7-3) overstimated the buckling strength of the four configuration in which the applied axial force was close to their buckling strength, much lower than the plastic axial capacity of the plate.

Steel Connection Handbook (Section 2.5.3) [14] and AISC Design Examples (Example IIA-19B) [15] used Eq. (7-7) to control the interaction of the internal forces of the shear tab. This equation was based on Eq. (7-1) and design requirement of Section H1.1 of the AISC 360 Specification [1] for doubly symmetric members subjected to flexure and axial force. Unlike Eqs. (7-2) and (7-3), this equation could be used to predict the buckling strength of all connections safely, but it was overly conservative. This observation was consistent with the conclusion of the previous research by Thomas [20]; this equation was overly conservative for extended shear tab connections. Equation (7-8) was identical to Eq. (7-3), except that the connection's plastic axial capacity was replaced by the predicted buckling strength. This equation could not safely predict the buckling strength of two connections (BC6-2-16-2000C and BC6-2-16-1500C). The implemented method overestimated the buckling axial strength of this configuration, referring to Table 7-8. This equation predicted the buckling resistance of BC3-2-10-a2-600C and BC3-2-10a2-500C because their axial buckling strength was estimated conservatively. Referring to Table 7-18, Eq. (7-3) was determined as the appropriate equation to consider the interaction of bending, shear, and axial force in the presence of a small to medium axial force. Under a large axial force,

(0.8P<sub>cr</sub>≤P), a more conservative equation such as Eq. (7-8) should be implemented to take into account the interaction of the internal forces.

$$\left(\frac{P}{2P_{P}} + \frac{M}{M_{P}}\right)^{2} + \left(\frac{V}{V_{P}}\right)^{2} \le 1 \qquad \frac{P}{P_{P}} < 0.2$$

$$\left(\frac{P}{P_{P}} + \frac{8}{9} \frac{M}{M_{P}}\right)^{2} + \left(\frac{V}{V_{P}}\right)^{2} \le 1 \qquad 0.2 \ge \frac{P}{P_{P}}$$
(7-7)

$$(\frac{M}{M_P}) + (\frac{P}{P_{cr}})^2 + (\frac{V}{V_P})^4 \le 1$$
 (7-8)

The rupture of the critical gross section occurred with six of the modelled connections. Referring to Table 7-19, the *a* distance is a conservative estimate of the shear force eccentricity to calculate the bending demand at the critical gross section.

Table 7-19 Rupture strength of the critical gross section under combined axial and shear demands

					Eq. (	7-5) <sup>a</sup>	Eq. (	7-6) <sup>a</sup>	Eq. (	7-9) <sup>a</sup>	Eq. (′	7-10) <sup>a</sup>
	$V_{FE}$	$e_{\rm eff}$	$\underline{e_{\text{eff}}}$	$\underline{e_{\text{eff}}}$	$V_A$	$\underline{V_{\text{FE}}}$	$V_A$	$\underline{V_{\text{FE}}}$	$V_A$	$\underline{V_{\text{FE}}}$	$V_A$	$\underline{V_{\scriptscriptstyle FE}}$
	(kN)	(mm)	a	$e_g$	(kN)	$V_{_{ m A}}$	(kN)	$V_{_{ m A}}$	(kN)	$V_{_{ m A}}$	(kN)	$V_{_{ m A}}$
BC3-2-10	567	104	0.91	0.68	476	1.19	476	1.19	456	1.24	712	0.80
BC3-2-10-200T	533	103	0.90	0.68	465	1.15	467	1.14	426	1.25	702	0.76
BC3-2-10-400T	499	94	0.82	0.62	434	1.15	440	1.13	354	1.41	670	0.74
BC3-2-10-a2-200T	446	134	0.66	0.55	312	1.43	312	1.43	279	1.60	702	0.64
BC3-2-10-a2-400T	402	136	0.67	0.56	286	1.40	287	1.40	229	1.75	670	0.60
BC3-2-10-a2-600T	346	131	0.65	0.54	242	1.43	244	1.42	174	1.99	615	0.56
	M	inimum	0.65	0.54		1.15		1.13		1.24		0.56
		Mean	0.77	0.61		1.29		1.29		1.54		0.68
	M	aximum	0.91	0.68		1.43		1.43		1.99		0.80
Sta	andard d	eviation	0.11	0.06		0.13		0.13		0.27		0.09
		COV	0.14	0.10		0.10		0.10		0.18		0.13

<sup>&</sup>lt;sup>a</sup> Calculations were conducted based on M=V×a

In addition to Eqs. (7-5) and (7-6), the connection resistance corresponding to the gross section rupture was calculated using Eqs. (7-9) and (7-10). Equation (7-9) was derived based on Eq. (7-8) to consider the impact of the bending-shear-axial force interaction on the rupture strength of the plate while Eq. (7-10) took into account only the interaction of the axial and shear forces. Equation (7-9) resulted in the most conservative estimate of the rupture strength, while Eq. (7-10)

overestimated the strength. Although both Eqs. (7-5) and (7-6) predicted the rupture strength most accurately, Eq. (7-6) was determined as the most appropriate equation due to its simplicity.

$$\left(\frac{P}{2P_{u}} + \frac{M}{M_{u}}\right)^{2} + \left(\frac{V}{V_{u}}\right)^{2} \le 1 \qquad \frac{P}{P_{u}} < 0.2$$

$$\left(\frac{P}{P_{u}} + \frac{8}{9} \frac{M}{M_{u}}\right)^{2} + \left(\frac{V}{V_{u}}\right)^{2} \le 1 \qquad 0.2 \ge \frac{P}{P_{u}}$$
(7-9)

$$(\frac{P}{P_u})^2 + (\frac{V}{V_u})^2 \le 1 \tag{7-10}$$

Referring to Table 7-20, The rupture strength of the critical net section was determined by the above mentioned four equations; Eqs. (7-5), (7-6), (7-9), and (7-10). Like the case of shear tabs under gravity induced shear force, *a*-0.5e<sub>g</sub> was considered as the eccentricity of the shear force for the critical net section. Referring to Table 7-20, it was a conservative assumption. Contrary to the gross section rupture, Eq. (7-10) resulted in the most accurate estimate of the plate rupture strength, although it considered only the axial-shear interaction. Among three equations that considered the interaction of bending-shear-axial force, Eq. (7-6) was the most accurate one.

Table 7-20. Rupture strength of the critical net section under combined axial and shear forces

	Table 7-20. Rupture s					(7-5) <sup>a</sup>	Eq. (		Eq. (		Eq. (7	7-10)a
	$V_{FE}$	$e_{ m eff}$	e <sub>eff</sub> -a	e <sub>eff</sub> -a	$V_{A}$	$V_{\text{FE}}$	$V_{A}$	$V_{\text{FE}}$	$V_{A}$	$V_{\scriptscriptstyle  m FE}$	$V_{A}$	$V_{\text{FE}}$
	(kN)	(mm)	a	$\overline{\mathbf{e}_{\mathrm{g}}}$	(kN)	$\overline{\mathrm{V}_{_{\mathrm{A}}}}$	(kN)	$\overline{\mathrm{V}_{_{\mathrm{A}}}}$	(kN)	$\overline{\mathrm{V}_{\mathrm{A}}}$	(kN)	$\overline{V_{_{ m A}}}$
BC3-2-10-600T	421	93	0.81	0.61	320	1.32	365	1.15	259	1.63	374	1.13
BC3-2-10-800T	261	107	0.94	0.70	142	1.84	176	1.48	90	2.90	197	1.32
BC3-2-10-a2-800T	231	145	0.72	0.60	86	2.69	88	2.61	49	4.72	197	1.17
BC6-2-16-1000C	2110	117	1.02	0.77	1399	1.51	1450	1.45	1360	1.55	1479	1.43
BC6-2-16-500C	2059	122	1.07	0.80	1488	1.38	1501	1.37	1532	1.34	1568	1.31
BC6-2-16-250C	2011	124	1.09	0.82	1509	1.33	1512	1.33	1551	1.30	1589	1.27
BC6-2-16	1956	127	1.11	0.83	1516	1.29	1516	1.29	1567	1.25	1596	1.23
BC6-2-16-250T	1912	128	1.12	0.84	1509	1.27	1512	1.26	1551	1.23	1589	1.20
BC6-2-16-500T	1823	132	1.16	0.87	1488	1.23	1501	1.21	1532	1.19	1568	1.16
BC6-2-16-1000T	1670	135	1.18	0.89	1399	1.19	1450	1.15	1360	1.23	1479	1.13
BC6-2-16-1500T	1479	138	1.21	0.91	1238	1.19	1353	1.09	1156	1.28	1318	1.12
BC6-2-16-2000T	1252	139	1.22	0.91	971	1.29	1173	1.07	854	1.47	1052	1.19
BC6-2-16-2500T	946	140	1.22	0.92	462	2.05	681	1.39	341	2.78	545	1.74
BC6-2-16-2750T	735	135	1.19	0.89								
BC6-2-16-a2-500C	1965	163	0.80	0.67	1390	1.41	1401	1.40	1411	1.39	1568	1.25
BC6-2-16-a2-250C	1946	165	0.81	0.68	1411	1.38	1414	1.38	1442	1.35	1589	1.22
BC6-2-16-a2	1908	165	0.81	0.69	1419	1.35	1419	1.35	1470	1.30	1596	1.20
BC6-2-16-a2-250T	1863	166	0.82	0.69	1411	1.32	1414	1.32	1442	1.29	1589	1.17
BC6-2-16-a2-500T	1821	167	0.82	0.69	1390	1.31	1401	1.30	1411	1.29	1568	1.16
BC6-2-16-a2-1000T	1672	170	0.84	0.71	1301	1.29	1344	1.24	1201	1.39	1479	1.13
BC6-2-16-a2-1500T	1482	174	0.86	0.72	1139	1.30	1232	1.20	972	1.52	1318	1.12
BC6-2-16-a2-2000T	1243	180	0.89	0.75	871	1.43	1017	1.22	666	1.87	1052	1.18
BC6-2-16-a2-2500T	917	190	0.93	0.79	358	2.56	421	2.18	216	4.25	545	1.68
BC6-2-16-a2-2750T	726	193	0.95	0.80								
	M	inimum	-0.28	-0.24		1.19		1.07		1.19		1.12
		Mean	-0.02	-0.02		1.50		1.38		1.80		1.25
	Ma	iximum	0.22	0.17		2.69		2.61		4.72		1.74
Sta	ndard de	eviation	0.16	0.13		0.41		0.34		0.96		0.16
		COV				0.26		0.25		0.53		0.13

<sup>&</sup>lt;sup>a</sup> Calculations were conducted based on M=V×(a-0.5e<sub>g</sub>)

## 7.5 Conclusions

This paper presents the results of corroborating experimental and numerical study on the behaviour of extended beam-to-column shear tab connections. The intent was to determine the dependency of the connection behaviour on various parameters such as the number of vertical bolt lines and bolt rows, the grade of bolts, the distance between the weld and bolt lines, the weld size, and the applied axial force. First, two configurations were chosen for laboratory testing. In addition to the number of bolt rows, the chosen configurations varied in the depth and thickness of the shear plate. Two identical specimens of each configuration were tested under different loading protocols;

gravity induced shear force and the coupled gravity and axial demands. The Impact of the axial force was determined based on the comparison between the results of two tests of each configuration, while the comparison between responses of different configurations shed light on the influence of different parameters on the connection behaviour. These tests also founded a baseline for validation of the FE simulations, conducted to expand upon the findings from the laboratory tests. These validated finite element models were then implemented to conduct a parameter study on the behaviour of the extended shear tabs under gravity induced shear force. Further, a parametric study were carried out to determine the impact of the magnitude and direction of the axial force on the behaviour of the extended shear tabs. The main findings are summarized as follows:

- Shear plate yielding provides the required ductility of a shear tab connection through stress redistribution within the shear plate. To postpone the weld tearing until after full yielding of the shear plate, the minimum weld size should be chosen based on the probable yield stress (R<sub>y</sub>F<sub>y</sub>) in lieu of the nominal yield stress (F<sub>y</sub>). In comparison with the current recommendation of the AISC Steel Construction Manual for the minimum weld size (a<sub>w</sub>=5/8t<sub>p</sub>) based on the nominal yield stress of the shear plate, the implementation of the new recommendation resulted in a slightly larger weld size 11/16t<sub>p</sub>.
- Although the current AISC design method is deemed to provide a safe estimate of the connection resistance under gravity induced shear force, the predicted failure modes deviated from the observed ultimate failure modes.
- A shorter distance (0.5e<sub>g</sub>) should be used to determine the bolt group capacity in accordance with the Instantaneous Centre of Rotation (ICR) method. This eccentricity may be used if the connection's shear plate satisfies the maximum thickness requirement of the AISC manual.

- The rupture strength of the critical gross section of the shear plate should be determined using Eq. (7-4) to take into account shear-bending interaction, calculated based on the *a* distance eccentricity of the shear force.
- To predict the bending demand on the critical net section at the time corresponding to its rupture, a-0.5eg was a conservative estimate of the eccentricity of the shear force. However, there was no need to consider the interaction of the bending and shear force to calculate the connection resistance corresponding to the net section rupture. It was observed that the shear rupture strength (0.6Fu Anet) was a conservative estimate for the net section rupture resistance of the connection under gravity induced shear force.
- In the case of the connections under gravity induced shear force, shear-bending interaction (Eq. (7-1)) should be considered to determine the connection resistance corresponding to plate buckling. The 0.5e<sub>g</sub> seems to be a conservative estimate of the connection eccentricity corresponding to plate buckling under gravity induced shear force.
- In the case of extended shear tabs under combined axial and shear forces, the current AISC design method shall be adjusted to consider the impact of the axial force. Most accurate equation was determined to consider the shear-bending-axial force interaction and estimate the connection resistance corresponding to the yield of the gross section. Furthermore, the bolt group capacity should be determined for the resultant force of the shear and axial force in accordance with the ICR method. In most cases, the revised method could predict conservatively the connection resistance.
- Regarding the buckling capacity of the shear tabs under combined axial and shear force, the shear-bending-axial force interaction should be taken into account the a distance was considered as the connection eccentricity. In the case of the large axial compression (0.8P<sub>cr</sub> ≤

- P), the shear-bending-axial force interaction should be calculated based on the predicted buckling strength of the connection in lieu of connection's plastic axial capacity.
- The equation was proposed to take into account the shear-bending-axial force interaction and
  calculate connection resistance corresponding to the rupture of the critical gross section in the
  case of the connections under combined axial and shear forces.
- If the connection is subjected to coupled axial tension and shear forces, the interaction of the tension and shear forces should be considered to determine the connection resistance corresponding to the rupture of the critical net section. The *a*-0.5e<sub>g</sub> distance was still a conservative estimate of the eccentricity of the shear force.

## 7.6 Acknowledgments

The authors would like to thank the ADF Group Inc. and DPHV Structural Consultants for their generous technical and financial support, as well as the Natural Sciences and Engineering Research Council of Canada. The finite element computations were conducted at the McGill University's supercomputer Guillimin, which is managed by Calcul Québec and Compute Canada. The supercomputer operation is funded by the Canada Foundation for Innovation (CFI), NanoQuébec, RMGA and the Fonds de recherche du Québec - Nature et technologies (FRQ-NT).

#### 7.7 References

- [1] AISC 360-16, Specification for structural steel buildings, American Institute of steel Construction, Chicago, IL, 2016.
- [2] CSA-S16-14, Design of steel structures, Canadian Standards Association, Mississauga, ON., 2014.

- [3] R. Bjorhovde, A. Colson, J. Brozzetti, Classification system for beam-to-column connections,J. Struct. Eng. ASCE, 116(11) (1990) 3059-3076.
- [4] Steel construction manual, 15<sup>th</sup> edition, American Institute of steel Construction, Chicago, IL, 2017.
- [5] CISC, Handbook of steel construction, Canadian Institute of Steel Construction, Markham, ON., 2016.
- [6] A. Astaneh, S.M. Call, K.M. McMullin, Design of single plate shear connections, Eng. J. AISC, 26(1) (1989) 21-32.
- [7] Manual of steel construction, volume ii connection, 9th asd edition/1st lrfd edition, American Institute of steel Construction, Chicago, IL, 1992.
- [8] Steel construction manual, 13<sup>th</sup> edition, American Institute of steel Construction, Chicago, IL, 2005.
- [9] L.S. Muir, C.M. Hewitt, Design of unstiffened extended single-plate shear connections, Eng. J. AISC, 46(2) (2009) 67-80.
- [10] UFC 4-023-03, Unified facilities criteria, design of buildings to resist progressive collapse,U.S. Department of Defence, Washington, DC., 2013.
- [11] IBC-2015, International building code,, International Code Council, Falls Church, VA., 2015.
- [12] BS EN 1991-1-7: 2006, Eurocode 1: Actions on structures, part7: General actions-accidental actions, British Standards Institution, London, England, 2010.
- [13] ASCE 7-16, Minimum design loads for buildings and other structures, American Society of Civil Engineers, Reston, VA, 2016.

- [14] A.R. Tamboli, Handbook of structural steel connection design and details, Third edition, McGraw-Hill, New York, NY., 2016.
- [15] Design examples companion to the aisc steel construction manual, version 15.0, American Institute of steel Construction, Chicago, IL, 2017.
- [16] D.B. Moore, G.W. Owens, Verification of design methods for finplate connections, The Struct. Eng., 70(3) (1992).
- [17] D.R. Sherman, A. Ghorbanpoor, Design of extended shear tabs, University of Wisconsin-Milwaukee, Milwaukee, WI, 2002.
- [18] W. Goodrich, Behavior of extended shear tabs in stiffened beam-to-column web connections, Master's Thesis, Vanderbilt University, Nashville, TN, 2005.
- [19] K.A. Baldwin Metzger, Experimental verification of a new single plate shear connection design model, Master's Thesis, Virginia Polytechnic Institute and State University, Blacksburg, VA, 2006.
- [20] K. Thomas, Design and behaviour of extended shear tabs under combined loads, Master's Thesis, University of Alberta, Edmonton, AB, 2014.
- [21] K. Thomas, R.G. Driver, S.A. Oosterhof, L. Callele, Full-scale tests of stabilized and unstabilized extended single-plate connections, Structures, 10 (2017) 49-58.
- [22] P. Salem, Unified design criteria for steel cantilever plate connection elements, PhD Thesis, University of Alberta, Edmonton, AB, 2016.
- [23] ABAQUS 6.11-3, [Computer software], Dassault Systemes Simulia Corp., Providence, RI.

- [24] J. Hertz, Testing of extended shear tab connections subjected to shear, Master's Thesis, McGill University, Montreal, QC, 2014.
- [25] N. Goldstein Apt, Testing of extended shear tab and coped beam-to-girder connections subject to shear loading, Master's Thesis, McGill University, Montreal, QC, 2015.
- [26] W.A. Thornton, P.J. Fortney, On the need for stiffeners for and the effect of lap eccentricity on extended single-plate connections, Eng. J. AISC, 48(2) (2011) 117-125.
- [27] J.-J. Cheng, J. Yura, C. Johnson, Design and behavior of coped beams, University of Texas at Austin, Austin, TX, 1984.
- [28] Steel construction manual, 14<sup>th</sup> edition, American Institute of steel Construction, Chicago, IL, 2011.
- [29] L. Muir, W. Thornton, A direct method for obtaining the plate buckling coefficient for double-coped beams, Eng. J. AISC, 41 (2004) 133-134.
- [30] AISC 360-10, Specification for structural steel buildings, American Institute of steel Construction, Chicago, IL, 2010.
- [31] B. Dowswell, R. Whyte, Local stability of double-coped beams, Eng. J. AISC, 51(1) (2014) 43-52.
- [32] M. D'Aronco, Behaviour of double and triple vertical rows of bolts shear tab connections and weld retrofits, Master's Thesis, École Polytechnique de Montréal, Montreal, QC, 2013.
- [33] A. Astaneh, Demand and supply of ductility in steel shear connections, J. Constr. Steel Res., 14(1) (1989) 1-19.

- [34] ASTM F3125 / F3125M-15a, Standard specification for high strength structural bolts, steel and alloy steel, heat treated, 120 ksi (830 mpa) and 150 ksi (1040 mpa) minimum tensile strength, inch and metric dimensions, ASTM International, West Conshohocken, PA, 2015.
- [35] A. Abou-zidan, Y. Liu, Numerical study of unstiffened extended shear tab connections, J. Constr. Steel Res., 107 (2015) 70-80.
- [36] P.J. Fortney, W.A. Thornton, Analysis and design of stabilizer plates in single-plate shear connections, Eng. J. AISC, 53(1) (2016) 1-28.
- [37] M.F. Suleiman, B.M. Shahrooz, H.L. Bill, P.J. Fortney, W.A. Thornton, 3-d finite element modeling of extended single plate shear connections: Predicting the mode of failure, International Journal of Steel Structures, 17(2) (2017) 525-534.
- [38] S.J. Guravich, J.L. Dawe, Simple beam connections in combined shear and tension, Can. J. Civil Eng., 33(4) (2006) 357-372.
- [39] G. Johnston, Strength and behaviour of double-coped steel beams under combined loads, Master's Thesis, University of Alberta, Edmonton, AB, 2015.
- [40] B.G. Neal, The effect of shear and normal forces on the fully plastic moment of a beam of rectangular cross section, Journal of Applied Mechanics, 28(2) (1961) 269-274.
- [41] M. Motallebi, D.G. Lignos, C.A. Rogers, Behavior of stiffened extended shear tab connections under gravity induced shear force., J. Constr. Steel Res., 148 (2018) 336-350.
- [42] M. Marosi, M. D'Aronco, R. Tremblay, C.A. Rogers, Multi-row bolted beam to column shear tab connections, 6th European Conference on Steel and Composite Structures, Budapest, Hungary, 2011.

- [43] M. Marosi, Behaviour of single and double row bolted shear tab connections and weld retrofits, Master's Thesis, McGill University, Montreal, QC, 2011.
- [44] A. Mirzaei, Steel shear tab connections subjected to combined shear and axial forces, PhD Thesis, McGill University, Montreal, QC, 2014.
- [45] J. Hertz, D.G. Lignos, C.A. Rogers, Full scale testing of extended beam-to-column and beam to-girder shear tab connections subjected to shear, 8th International Conference on Behavior of Steel Structures in Seismic Areas, Shanghai, China, 2015.
- [46] C.A. Rogers, M. Marosi, J. Hertz, D.G. Lignos, R. Tremblay, M. D'Aronco, Performance of weld-retrofit beam-to-column shear tab connections, 8th Int. Workshop on Connections in Steel Structures, Boston, MA., 2016.
- [47] ASTM A992 / A992M-11(2015), Standard specification for structural steel shapes, ASTM International, West Conshohocken, PA, 2015.
- [48] ASTM A572 / A572M-15, Standard specification for high-strength low-alloy columbium-vanadium structural steel, ASTM International, West Conshohocken, PA, 2015.
- [49] AWS D1.1/D1.1M:2015, Structural welding code-steel, American Welding Society, Miami, FL., 2015.
- [50] AISC 341-16, Seismic provisions for structural steel buildings, American Institute of steel Construction, Chicago, IL, 2016.
- [51] ASTM A370-17, Standard test methods and definitions for mechanical testing of steel products, ASTM International, West Conshohocken, PA, 2017.
- [52] AWS A5.20/A5.20M:2005 (R2015), Carbon steel electrodes for flux cored arc welding, American Welding Society, Miami, FL., 2015.

- [53] A.M. Kanvinde, I.R. Gomez, M. Roberts, B.V. Fell, G.Y. Grondin, Strength and ductility of fillet welds with transverse root notch, J. Constr. Steel Res., 65 (2009) 11.
- [54] A. Astaneh, K.M. McMullin, S.M. Call, Behavior and design of steel single plate shear connections, J. Struct. Eng. ASCE, 119(8) (1993) 2421-2440.
- [55] G.L. Kulak, J.W. Fisher, J.H. Struik, Guide to design criteria for bolted and riveted joints, AISC, Chicago, IL, 2001.
- [56] ASTM A6 /A6M, General requirements for rolled structural steel bars, plates, shapes, and sheet piling, ASTM International, 2004.
- [57] CSA-G40.20-13/G40.21-13, General requirements for rolled or welded structural quality steel/ structural quality steel, Canadian Standards Association, Toronto, ON., 2013.
- [58] A. Elkady, D.G. Lignos, Analytical investigation of the cyclic behavior and plastic hinge formation in deep wide-flange steel beam-columns, Bull. Earthq. Eng., 13(4) (2015) 1097-1118.
- [59] B.A. Mohr, T.M. Murray, Bending strength of steel bracket and splice plates, Eng. J. AISC, 45(2) (2008) 97-106.
- [60] M. Motallebi, Behavior of extended shear tab connections under combined axial and shear forces, PhD Thesis, McGill University, Montreal, QC, 2018.
- [61] A. Astaneh, Seismic behavior and design of gusset plates, Steel Tips, Structural Steel Education Council, Moraga, CA., 1998.
- [62] M. Motallebi, D.G. Lignos, C.A. Rogers, Stability of stiffened extended shear tab connections under gravity induced shear force, J. Constr. Steel Res., 148 (2018) 336-350.

- [63] M. Motallebi, D.G. Lignos, C.A. Rogers, Full-scale testing of stiffened extended shear tab connections under combined axial and shear forces, Eng. Struct., Under Review (2018).
- [64] J. Wallaert, J. Fisher, Shear strength of high-strength bolts, J. Struct. Div. ASCE, 91(3) (1965) 99-126.
- [65] J.J. Wallaert, J.W. Fisher, Shear strength of high-strength bolts, Lehigh University, Bethlehem, PA, 1964.
- [66] NIST GCR 10-917-8, Evaluation of the fema p695 methodology for quantification of building seismic performance factors, NEHRP consultants Joint Venture, Redwood City, CA., 2010.
- [67] A. Mirzaei, C.A. Rogers, R. Tremblay, Full-scale testing of shear tab connections subjected to combined axial and shear forcess, 3rd specility conference om material engineering & applied Mechanics, Canadian Society for civil engineering, Montreal, 2013.
- [68] Y.K. Kwan, G.Y. Grondin, Strength of welded joints under combined shear and out-of-plane bending, Structural Engineering Report No. 280, University of Alberta, Edmonton, AL, 2008.

## 8 Chapter 8: Summary and conclusions

## 8.1 Summary

Among the various possible configurations for shear connections, the shear tab has gained popularity due to its simplicity in terms of fabrication and erection. This connection is classified into two main categories: conventional and extended configurations. In the conventional shear tab, the a distance, the distance between the weld line and the single vertical bolt line, is not larger than 89mm (3.5in.), whereas for the extended configuration there is no limit for the a distance. Further, the extended configuration may have multiple vertical bolt lines. Even though the extended shear tab is widely used in Canada, the CISC Handbook of Steel Construction remains silent as to its design. For this reason, Canadian engineers usually implement the procedure found in the AISC Steel Construction Manual for the design of extended shear tab connections. Although the AISC method was developed for design of unstiffened extended shear tabs under gravity induced shear force, practicing structural engineers use this method for design of stiffened extended shear tabs owing to the lack of a validated comprehensive design procedure. Because this design procedure is applicable only to the connection under gravity induced shear force, the AISC Design Examples and Steel Connection Handbook introduce a few minor adjustments to this method in order to cover the loading scenario including axial tension or compression in addition to the gravity shear.

To address these shortcomings, an experimental-numerical study was conducted. First, the validity of the current design practice of the extended shear tab was evaluated in the case of the single-sided configuration of the full-depth stiffened extended beam-to-girder shear tab under gravity shear demand. This task was achieved through a parametric FE study, the numerical model for which was calibrated using the results of laboratory tests that had previously been conducted at McGill University.

In the second phase of the study, six full-scale tests were conducted on extended shear tab connections under combined axial and shear forces. These tests consisted of four beam-to-column flange connections, as well as two full-depth stiffened beam-to-girder configurations. The tested connections varied in the number of vertical bolt lines and bolt rows, the thickness and depth of the shear plate, the bolt size, the offset of the bolt group from the support face, and the magnitude of the applied axial compression. These tests shed light on the inelastic response of the extended shear tab connections, and shaped a baseline for validation of the FE models.

In the third phase of the study, the findings of the laboratory test program were validated for a wider range of applied axial force and connection configurations. To this end, the validated FE models were implemented in a parametric study for both stiffened and unstiffened configurations of the extended shear tab connections. The influence of a number of parameters on the connection behaviour was evaluated; among them, the number of vertical bolt lines and bolt rows, the thickness of the shear plate, the offset of the bolt group from the girder face, the depth of shear plate and the direction and magnitude of the applied axial force. Based on the experimental-numerical results, modifications to the current AISC procedure for the design of the extended shear tabs are introduced, and applied in the case of coupled axial and shear demands.

#### 8.2 Conclusions

The main findings of this research can be concluded as follows:

#### Full-depth stiffened extended beam-to-girder shear tab connections:

• The inflection point of the connection formed away from the girder centreline (i.e. beyond the centre of the bolt group) in both the single- and double-sided configurations. Hence, the current practice for design of these connections may not always be conservative as it underestimates

the force demands on the stiffened portion of the shear tab as well as the bending demands on the supporting element.

- The stiffened portion of a shear tab (including single-sided and double-sided configurations) was subjected to vertical axial and horizontal shear forces simultaneously. The force demands developed at the shear plate's critical section (section along the bottom edge of the extended part of the shear plate) were strongly influenced by the girder web flexibility and the relative distance between the girder bottom flange and the bottom edge of the extended part of the shear plate.
- The stiffness of the single-sided configuration reduced following the yielding of the critical section of the shear plate. The use of shear plates that satisfied the CSA S16 compactness ratio for stiffeners  $(200/\sqrt{F_y})$  resulted in a more stable behaviour following the local yielding of the shear plate.
- In the case of the double-sided configuration under gravity induced shear force, yielding was
  observed at the plate's gross and net sections along the outer end of the re-entrant corners and
  the interior bolt line, respectively.
- For the double-sided configuration, the shear plate's out-of-plane deformation started to increase after yielding of the full depth of the shear plate along the gross section. Plate buckling was the ultimate failure mode of the slender shear tab connection in which the plate did not satisfy the CSA-S16 requirements for bearing stiffeners ( $200/\sqrt{F_y}$ ). For the connections with a compact shear tab, net section fracture was determined as the ultimate failure mode.
- An increase of the gap distance between the beam and girder flanges resulted in an increase of
  the connection's eccentricity, as well as the shear plate's unbraced length. Therefore, the

connection strength corresponding to the gross section yielding and shear plate buckling decreased.

- The current design method significantly underestimated the ultimate shear capacity (plateau of shear force) of the double-sided stiffened extended shear tabs under gravity induced shear force. This was due to the assumption that the inflection point forms at the face of the girder web. If the extended portion of the shear plate was design based on Thornton's and Fortney's recommendation, i.e. the inflection point is formed at the toe of the stiffener (the tip of the girder flange), the design procedure predicted more accurately the ultimate strength of the connection.
- Although Thornton's and Fortney's suggestion for the location of the inflection point results in more accurate predictions for the ultimate strength of the connection, it creates an overestimation of the connection resistance corresponding to the yielding of the gross section of the shear plate. The observed large rotation and deformation, following the shear plate yield, may be detrimental to the serviceability of the supported beam.
- In order to determine the shear force corresponding to the plate's gross section yielding in the double-sided configuration, a regression equation (Eq. (6-4)) used to estimate the location of the inflection point was introduced. It was observed that the calculation based on this eccentricity would result in a conservative prediction for the connection resistance corresponding to the gross section yield and consequently the connection ultimate resistance.
- To calculate the shear capacity of the bolt group, the ICR method was implemented along with the bolt group eccentricity, obtained from Eq. (6-5). If the shear plate satisfied the requirement of the AISC design procedure for the maximum plate thickness, the bolt group eccentricity could be considered conservatively as the distance between the bolt group centre and the toe

- of the stiffener. In this case, calculation based on Eq. (6-4) also resulted in a conservative estimate for the bolt group capacity.
- In the presence of axial force, the interaction of moment, shear, and axial load should be taken into account in the estimation of the connection resistance corresponding to the yielding of plate's gross section. It was observed that the calculation in accordance with Thornton's and Fortney's recommendation resulted in an overestimation of the ultimate resistance of the connection if it is subjected to a large axial compression. In this case, the calculation should be conducted based on the AISC's recommendation for connection eccentricity or Eq. (6-4).
- The shear rupture strength of the plate (0.6F<sub>u</sub> A<sub>net</sub>) was observed as a conservative estimate for the net section rupture resistance of the connection under gravity induced shear force. In the case of combined tension and shear force, the interaction of the shear and tensile forces should be taken into account.

#### Unstiffened extended beam-to-column shear tab connections

- The current AISC design method predicted conservatively the ultimate capacity of the unstiffened extended shear tab connections under gravity shear demand.
- It is suggested to determine the minimum fillet weld size based on the probable yield stress of the plate (R<sub>y</sub>F<sub>y</sub>) in lieu of the nominal yield stress (F<sub>y</sub>). In comparison to the current recommendation of the AISC Steel Construction Manual for the minimum weld size (a<sub>w</sub>=5/8t<sub>p</sub>), the implementation of the new recommendation results in a slightly larger weld size 11/16t<sub>p</sub>.
- If the connection satisfies the requirement of the AISC Steel Construction Manual for the maximum thickness of the shear plate, a shorter bolt group eccentricity (e.g. 0.50eg) would result in a more accurate prediction for the bolt group capacity.

- In the case of extended shear tabs under combined axial and shear forces, the current AISC design method should be adjusted to take into account the interaction of the bending moment, shear and axial force. The studied method conservatively predicted the connection ultimate resistance, except for the case when a large axial compression (0.8P<sub>cr</sub> ≤ P) was applied to the connection.
- For a connection under combined axial and shear forces, the bolt group capacity should be determined for the resultant force of the shear and axial force in accordance with the ICR method.
- The rupture strength of the critical gross section of the shear plate should be determined by considering the interaction of the shear force and bending moment, calculated based on the *a* distance eccentricity of the shear force. In the presence of the axial force, the interaction of bending, shear and axial demand should be taken into account.
- The shear rupture strength of the plate (0.6F<sub>u</sub> A<sub>net</sub>) was observed as a conservative estimate for
  the net section rupture resistance of the connection under gravity induced shear force. In the
  case of combined tension and shear force, the interaction of the shear and tensile forces should
  be taken into account.

## 8.3 Original contribution

The current AISC method for the design of extended shear tabs was evaluated comprehensively
and modifications were introduced to make its predictions more accurate in the case of the
unstiffened and full-depth stiffened configurations of extended shear tabs under gravity shear
demand.

- The behaviour of Full-depth and unstiffened shear tab was studied under a wide range of combined axial and shear forces. The axial force ranged from tensile to compressive capacities of the connection.
- Required modifications to the current AISC design method were introduced in order to implement this method for design of the unstiffened and full-depth stiffened extended shear tabs under combined axial and shear forces.

#### 8.4 Recommendations for future research

The author's recommendation for future research can be classified as follows:

- In the case of beam-to-girder shear tabs, the effect of the girder length on the connection response requires further research. It is recommended for future research to compare the efficiency of the full-depth stiffened configuration with that of the unstiffened and partial-depth stiffened configurations.
- Although the contribution of the concrete slab is conservatively ignored in the design of steel
  connections, it can significantly affect the connection's response to load. Future research is
  needed to quantify the impact of the concrete slab, as well as the reliability of the slab's
  contribution in a connection.
- The column stiffness may affect the behaviour of the stiffened beam-to-column extended shear tab connection. It is recommended to study the behaviour of stiffened extended beam-to-column shear tabs under gravity shear, as well as coupled axial and shear demands. Furthermore, it is recommended to study the impact of the column axial force on the stiffness of the beam-to-column shear tab connections.

- In this study, the fabrication tolerance was implemented as the amplitude of the initial imperfection. Although this method is safe, it may exaggerated the effect of the out-of-plane plane deformation. Parametric study should be carried out to determine the influence of the initial imperfection (shape and amplitude) on the connection capacity.
  - To determine the location of the inflection point, structural mechanics can be used in lieu of the regression analysis. This method will results in more robust estimates.
  - An analytical approach should be developed to determine the buckling capacity of too slender shear plates.

# **Appendix A: Design Calculations**

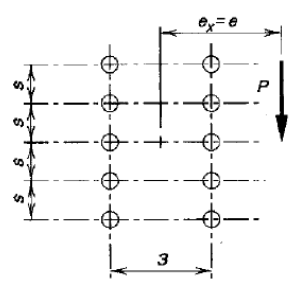
## Specimen BC3-2-10

## **Configuration parameter**

Supporting Ccolumn			W360×	196	
Supported beam			W310	×76	
Offset of bol group, a	=	4 1/2	in.	114.3	mm
Bolt diameter, d <sub>b</sub>	=	3/4	in.	19.1	mm
Bolt diameter, d <sub>h</sub>	=	13/16	in.	21.1	mm
Number of bolt lines, m	=	2		2	
Number of bolts rows, n	=	3		3	
Plate Depth, d	=	9.0	in.	228.6	mm

# **Bolt Shear & Bolt Bearing**

Compute ICR coefficient (C)			Table '	7-8	
		A	AISC Har	ldbook	
			(15th Ver	rsion)	
Number of bolt lines, m	=	2		2	
Moment arm, e	=	6.0	in.	152.4	mm
gage, s	=	3.0	in.	76.2	mm
Pitch, p	=	3.0	in.	76.2	mm
Vertical edge distances	=	1 1/2	in.	38.1	mm
Horizontal edge distances	=	1 1/2	in.	38.1	mm
Number of bolt rows, n	=	3		3	
L1	=	6.0	in.	152.4	mm
C1	=	2.25		2.25	
L2	=	7.0	in.	177.8	mm
C2	=	1.99		1.99	
ICR coefficient (C)	=	2.25		2.25	



## **Bolt Shear**

$V_r\!\!=\!\!\phi_V\phi_b\phi_tA_b(0.625F_u)C$		Eq. (J3-1), AISC 360-15				
Reduction factor for shear	=	0.75		0.75		
rupture, φ <sub>v</sub> Reduction factor for uneven	=	0.9		0.9		
force distribution, φ <sub>d</sub> Reduction factor for shear plan  are not excluded from the	=	1.0		1.0		
threaded part, $\phi_t$ Number of shear planes, m	=	1.0		1.0		
Bolt area, A <sub>b</sub>	=	0.442	in. <sup>2</sup>	285	$\mathrm{mm}^2$	
Nominal ultimate strength of bolts, F <sub>U</sub>	=	150	ksi	1034.2	MPa	
Factored bolt group capacity, V <sub>r</sub>	=	62.9	kips	280	kN	
Expected bolt group capacity, $V_e(\phi_v=\phi_d=1.0)$	=	93.1	kips	414	kN	

## **Bolt Bearing**

$B_r=3\phi_{br}d_bmin[(tF_u)_{plate},(tF_u)_{web}]$	Eq. (J3-10), AISC 360-15					
Modification factor, φ <sub>br</sub>	=	0.75		0.75		
Plate thickness, t <sub>p</sub>	=	3/8	in.	9.76	mm	

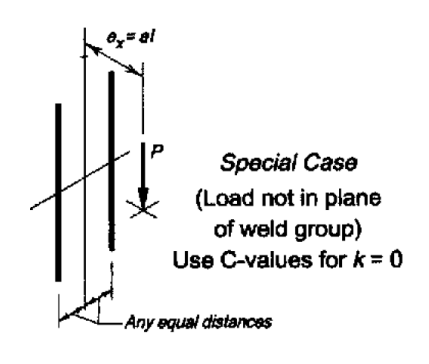
Beam web thickness, t <sub>w</sub>	=	0.395	in.	10.04	mm
Bolt Diameter, d <sub>b</sub>	=	3/4	in.	19.05	mm
Clear edge distance	=	1.09	in.	27.58	mm
Nominal tensile strength of plate, $F_{u,plate}$	=	65.0	ksi	448.2	MPa
Nominal tensile strength of beam $F_{u,beam}$	=	65.0	ksi	448.2	MPa
Expected plate strength,	=	78.0	ksi	537.8	MPa
$R_y F_{u,plate}$ Expected beam strength, $R_y F_{u,beam}$	=	72.0	ksi	495.0	MPa
Tensile strength of plate, $F_{u,plate}$	=	75.7	ksi	522.0	MPa
Tensile strength of beam F <sub>u,beam</sub>	=	71.8	ksi	495.0	MPa
Factored bearing resistance, B <sub>r</sub>	=	69.1	kips	305	kN
<u> </u>			•		
Expected bearing strength, $B_r$ $(\phi=1.0,R_yF_u)$	=	104.8	kips	463	kN
Measured bearing resistance, B <sub>r</sub>	=	104.8	kips	463	kN
Plat	te Dı	ıctility			
$t_{pmax}=6M_{max}/F_yd_{pl}^2$				10-5)	
M F / (A CD)		AISC S	Steel Man	ual (15 <sup>th</sup> E	dition)
$M_{\text{max}} = F_{\text{nv}} / \varphi_{\text{d}}(A_{\text{b}}C')$	_	011	ksi	5017	MDa
Bolt Shear Strength, F <sub>nV</sub>	=	84.4 0.442	in. <sup>2</sup>	581.7 285	MPa mm <sup>2</sup>
Bolt Area, A <sub>b</sub> Compute ICR coefficient for	_	0.442	Tabl		111111
moment only case (C')		AISC S		e 7-8 ual (15 <sup>th</sup> E	dition)
	=		steer iviair	uai (13 E	aition)
Number of bolt lines, m	=	2	:		****
Column spacing		3	in.	76	mm
Row spacing, s	=	3	in.	76	mm
Number of bolts rows, n	=	3		3	
		150			
ICR coefficient, C'	=	15.8	1.1.1.	15.8	1.3.1
$ m M_{max}$	=	654.1	kip.in	73.9	kN.m
$\begin{array}{c} M_{max} \\ Nominal \ yield \ stress, \ F_y \end{array}$	=	654.1 50.0	kips	73.9 344.7	MPa
$M_{max}$ Nominal yield stress, $F_y$ Expected yield stress, $R_y$ $F_y$	= = =	654.1 50.0 55.0	kips kips	73.9 344.7 379.2	MPa MPa
$M_{max}$ Nominal yield stress, $F_y$ Expected yield stress, $R_y F_y$ Measured yield stress, $F_{ym}$	= = =	654.1 50.0 55.0 65.1	kips kips kips	73.9 344.7 379.2 449.0	MPa
$M_{max}$ Nominal yield stress, $F_y$ Expected yield stress, $R_y F_y$ Measured yield stress, $F_{ym}$ Plate depth, d	= = =	654.1 50.0 55.0 65.1 9.0	kips kips kips in.	73.9 344.7 379.2 449.0 228.6	MPa MPa
$M_{max}$ Nominal yield stress, $F_y$ Expected yield stress, $R_y F_y$ Measured yield stress, $F_{ym}$ Plate depth, d Plate thickness, $t_{pl}$	= = =	654.1 50.0 55.0 65.1 9.0 0.384	kips kips kips in. in.	73.9 344.7 379.2 449.0 228.6 9.76	MPa MPa MPa
$M_{max}$ Nominal yield stress, $F_y$ Expected yield stress, $R_y$ $F_y$ Measured yield stress, $F_{ym}$ Plate depth, d Plate thickness, $t_{pl}$ Maximum plate thickness, $t_{max}$ $(F_y)$	= = =	654.1 50.0 55.0 65.1 9.0	kips kips kips in.	73.9 344.7 379.2 449.0 228.6	MPa MPa MPa mm
$M_{max}$ Nominal yield stress, $F_y$ Expected yield stress, $R_y$ $F_y$ Measured yield stress, $F_{ym}$ Plate depth, d Plate thickness, $t_{pl}$ Maximum plate thickness, $t_{max}$ $(F_y)$ Is this requirement satisfied? $(t_p)$	= = = =	654.1 50.0 55.0 65.1 9.0 0.384	kips kips kips in. in.	73.9 344.7 379.2 449.0 228.6 9.76	MPa MPa MPa mm mm
$M_{max}$ Nominal yield stress, $F_y$ Expected yield stress, $R_y$ $F_y$ Measured yield stress, $F_{ym}$ Plate depth, d Plate thickness, $t_{pl}$ Maximum plate thickness, $t_{max}$ $(F_y)$ Is this requirement satisfied? $(t_p$ $< t_{max})$ Maximum plate thickness, $t_{max}$	= = = =	654.1 50.0 55.0 65.1 9.0 0.384 0.969	kips kips kips in. in.	73.9 344.7 379.2 449.0 228.6 9.76	MPa MPa MPa mm mm
$M_{max}$ Nominal yield stress, $F_y$ Expected yield stress, $R_y$ $F_y$ Measured yield stress, $F_{ym}$ Plate depth, $d$ Plate thickness, $t_{pl}$ Maximum plate thickness, $t_{max}$ $(F_y)$ Is this requirement satisfied? $(t_p$ $< t_{max})$ Maximum plate thickness, $t_{max}$ $(R_y F_y)$ Is this requirement satisfied? $(t_p$	= = = =	654.1 50.0 55.0 65.1 9.0 0.384 0.969	kips kips kips in. in. in.	73.9 344.7 379.2 449.0 228.6 9.76 24.61	MPa MPa MPa mm mm
$M_{max}$ Nominal yield stress, $F_y$ Expected yield stress, $R_y$ $F_y$ Measured yield stress, $F_{ym}$ Plate depth, $d$ Plate thickness, $t_{pl}$ Maximum plate thickness, $t_{max}$ $(F_y)$ Is this requirement satisfied? $(t_p < t_{max})$ Maximum plate thickness, $t_{max}$ $(R_y F_y)$ Is this requirement satisfied? $(t_p < t_{max})$ Maximum plate thickness, $t_{max}$	= = = =	654.1 50.0 55.0 65.1 9.0 0.384 0.969 Yes	kips kips kips in. in. in.	73.9 344.7 379.2 449.0 228.6 9.76 24.61	MPa MPa MPa mm mm
$M_{max} \\ Nominal yield stress, F_y \\ Expected yield stress, R_y F_y \\ Measured yield stress, F_{ym} \\ Plate depth, d \\ Plate thickness, t_{pl} \\ Maximum plate thickness, t_{max} \\ (F_y) \\ Is this requirement satisfied? (t_p < t_{max}) \\ Maximum plate thickness, t_{max} \\ (R_y F_y) \\ Is this requirement satisfied? (t_p < t_{max}) \\ Maximum plate thickness, t_{max} \\ (F_{ym}) \\ Is this requirement satisfied? (t_p < t_{max}) \\ Maximum plate thickness, t_{max} \\ (F_{ym}) \\ Is this requirement satisfied? (t_p < t_{max}) \\ Naximum plate thickness, t_{max} \\ (F_{ym}) \\ Is this requirement satisfied? (t_p < t_{max}) \\ Naximum plate thickness, t_{max} \\ (F_{ym}) \\ Is this requirement satisfied? (t_p < t_{max}) \\ Naximum plate thickness, t_{max} \\ (F_{ym}) \\ Is this requirement satisfied? (t_p < t_{max}) \\ Naximum plate thickness, t_{max} \\ (F_{ym}) \\ Is this requirement satisfied? (t_p < t_{max}) \\ Naximum plate thickness, t_{max} \\ (F_{ym}) \\ Is this requirement satisfied? (t_p < t_{max}) \\ Naximum plate thickness, t_{max} \\ (F_{ym}) \\ Is this requirement satisfied? (t_p < t_{max}) \\ Naximum plate thickness, t_{max} \\ (F_{ym}) \\ Is this requirement satisfied? (t_p < t_{max}) \\ Naximum plate thickness, t_{max} \\ (F_{ym}) \\ Naximum plate thickness \\ Naximum plate \\ Nax$	= = = =	654.1 50.0 55.0 65.1 9.0 0.384 0.969 Yes 0.881	kips kips kips in. in. in.	73.9 344.7 379.2 449.0 228.6 9.76 24.61	MPa MPa MPa mm mm mm
$\begin{array}{c} M_{max} \\ \text{Nominal yield stress, } F_y \\ \text{Expected yield stress, } R_y  F_y \\ \text{Measured yield stress, } F_{ym} \\ \text{Plate depth, d} \\ \text{Plate thickness, } t_{pl} \\ \text{Maximum plate thickness, } t_{max} \\ (F_y) \\ \text{Is this requirement satisfied? } (t_p \\ < t_{max}) \\ \text{Maximum plate thickness, } t_{max} \\ (R_y  F_y) \\ \text{Is this requirement satisfied? } (t_p \\ < t_{max}) \\ \text{Maximum plate thickness, } t_{max} \\ (F_{ym}) \\ \text{Is this requirement satisfied? } (t_p \\ < t_{max}) \\ \end{array}$	= = = =	654.1 50.0 55.0 65.1 9.0 0.384 0.969 Yes 0.881 Yes	kips kips kips in. in. in.	73.9 344.7 379.2 449.0 228.6 9.76 24.61	MPa MPa MPa mm mm mm
$\begin{array}{c} M_{max} \\ \text{Nominal yield stress, } F_y \\ \text{Expected yield stress, } R_y  F_y \\ \text{Measured yield stress, } F_{ym} \\ \text{Plate depth, d} \\ \text{Plate thickness, } t_{pl} \\ \text{Maximum plate thickness, } t_{max} \\ (F_y) \\ \text{Is this requirement satisfied? } (t_p \\ < t_{max}) \\ \text{Maximum plate thickness, } t_{max} \\ (R_y  F_y) \\ \text{Is this requirement satisfied? } (t_p \\ < t_{max}) \\ \text{Maximum plate thickness, } t_{max} \\ (F_{ym}) \\ \text{Is this requirement satisfied? } (t_p \\ < t_{max}) \\ \\ \text{She} \\ \end{array}$	= = = =	654.1 50.0 55.0 65.1 9.0 0.384 0.969 Yes 0.881 Yes 0.744 Yes	kips kips kips in. in. in.	73.9 344.7 379.2 449.0 228.6 9.76 24.61	MPa MPa MPa mm mm mm
$M_{max} \\ Nominal yield stress, F_y \\ Expected yield stress, R_y F_y \\ Measured yield stress, F_{ym} \\ Plate depth, d \\ Plate thickness, t_{pl} \\ Maximum plate thickness, t_{max} \\ (F_y) \\ Is this requirement satisfied? (t_p < t_{max}) \\ Maximum plate thickness, t_{max} \\ (R_y F_y) \\ Is this requirement satisfied? (t_p < t_{max}) \\ Maximum plate thickness, t_{max} \\ (F_{ym}) \\ Is this requirement satisfied? (t_p < t_{max}) \\ Maximum plate thickness, t_{max} \\ (F_{ym}) \\ Is this requirement satisfied? (t_p < t_{max}) \\ She \\ V_{GP} = 0.60 \phi F_y A_g$	= = = =	654.1 50.0 55.0 65.1 9.0 0.384 0.969 Yes 0.881 Yes 0.744 Yes	kips kips kips in. in. in.	73.9 344.7 379.2 449.0 228.6 9.76 24.61	MPa MPa MPa mm mm mm
$\begin{array}{c} M_{max} \\ \text{Nominal yield stress, } F_y \\ \text{Expected yield stress, } R_y  F_y \\ \text{Measured yield stress, } F_{ym} \\ \text{Plate depth, d} \\ \text{Plate thickness, } t_{pl} \\ \text{Maximum plate thickness, } t_{max} \\ (F_y) \\ \text{Is this requirement satisfied? } (t_p \\ < t_{max}) \\ \text{Maximum plate thickness, } t_{max} \\ (R_y  F_y) \\ \text{Is this requirement satisfied? } (t_p \\ < t_{max}) \\ \text{Maximum plate thickness, } t_{max} \\ (F_{ym}) \\ \text{Is this requirement satisfied? } (t_p \\ < t_{max}) \\ \\ \text{She} \\ \end{array}$	= = = =	654.1 50.0 55.0 65.1 9.0 0.384 0.969 Yes 0.881 Yes 0.744 Yes	kips kips kips in. in. in.	73.9 344.7 379.2 449.0 228.6 9.76 24.61	MPa MPa MPa mm mm mm

Expected yield stress, R <sub>y</sub> F <sub>y</sub>	=	55.0	ksi	379.2	MPa
Measured yield stress, F <sub>ym</sub>	=	65.1	ksi	449.0	MPa
Plate thickness, t <sub>pl</sub>	=	3/8	in.	9.76	mm
Plate depth, d <sub>pl</sub>	=	9.0	in.	228.6	mm
Gross plate area, Ag	=	3.456	in. <sup>2</sup>	2230	$\text{mm}^2$
Factored shear yielding resistance, V <sub>GP</sub>	=	103.7	kips	461	kN
Expected yielding strength, $V_{GP}$ ( $\phi$ =1.0, $R_yF_y$ )	=	114.1	kips	507	kN
Shear yielding resistance, V <sub>GP</sub>	=	135.1	kips	601	kN
She	ar R	upture			
$V_{N}\!\!=\!\!0.60\phi F_{u}A_{net}$			Eq. (J4	-4), AISC	360-15
Resistance Factor, φ	=	0.75		0.75	
Nominal tensile strength, F <sub>u</sub>	=	65.0	ksi	448.2	MPa
Expected tensile strength, R <sub>y</sub> F <sub>u</sub>	=	78.0	ksi	537.8	MPa
Measured tensile strength, F <sub>um</sub>	=	75.7	ksi	522.0	MPa
Plate thickness, t <sub>pl</sub>	=	3/8	in.	9.76	mm
Net depth, d <sub>net</sub>	=	6.6	in.	165.5	mm
Net area, A <sub>net</sub>	=	2.520	in. <sup>2</sup>	1614	$\mathrm{mm}^2$
Factored rupture strength, V <sub>N</sub>	=	73.7	kips	325	kN
Expected rupture strength, $V_N$ ( $\phi$ =1.0, $R_YFu$ )	=	118.0	kips	521	kN
Measured rupture strength, V <sub>N</sub>	=	114.5	kips	505	kN
ricasarea raptare strength, v		11	F		
	Shear	r Ruptur	•		
		r Ruptur	·e	1-5) AISC	360-15
Block S		r Ruptur	·e		360-15
$\label{eq:block} \begin{array}{c} \textbf{Block S} \\ V_{BS} \!\!=\!\! \phi_u \! [U_{bs} A_{nt} F_u \!\!+\!\! min(0.6 A_{gv} F_y \!\!-\!\! min(0.6 A_{gv} $	,0.6A	r Ruptur AnvFu)]	·e	1-5) AISC	360-15
$\begin{aligned} & \textbf{Block S} \\ V_{BS} = & \phi_u [U_{bs} A_{nt} F_u + min(0.6 A_{gv} F_y \\ & \text{Resistance Factor, } \phi_U \end{aligned}$	,0.6A =	r Ruptur AnvF <sub>U</sub> )] 0.75	·e	1-5) AISC 0.75	360-15 MPa
$\begin{aligned} & \textbf{Block S} \\ & V_{BS} \!\!=\!\! \phi_u \! [U_{bs} A_{nt} F_u \!\!+\!\! \min(0.6 A_{gv} F_y \!\!, \\ & \text{Resistance Factor, } \phi_U \\ & \text{Efficiency Factor, } U_{bs} \end{aligned}$	,0.6A = =	r Ruptur AnvF <sub>U</sub> )] 0.75 0.5	e Eq. (J <sup>2</sup>	0.75 0.5	
$\begin{aligned} & \textbf{Block S} \\ & V_{BS} = & \phi_u [U_{bs} A_{nt} F_u + min(0.6 A_{gv} F_y \\ & \text{Resistance Factor, } \phi_U \\ & \text{Efficiency Factor, } U_{bs} \\ & \text{Nominal yield stress, } F_y \end{aligned}$	,0.6A = = =	r Ruptur AnvF <sub>U</sub> )] 0.75 0.5 50.0	Eq. (J <sup>2</sup>	0.75 0.5 344.7	MPa
Block S $V_{BS} = \phi_u [U_{bs} A_{nt} F_u + min(0.6 A_{gv} F_y)]$ Resistance Factor, $\phi_U$ Efficiency Factor, $U_{bs}$ Nominal yield stress, $F_y$ Nominal tensile strength, $F_u$	,0.6A = = = =	n Ruptur AnvF <sub>U</sub> )] 0.75 0.5 50.0 65.0	Eq. (J4 ksi ksi	4-5) AISC 0.75 0.5 344.7 448.2	MPa MPa
$\begin{aligned} \textbf{Block S} \\ V_{BS} = & \phi_u [U_{bs} A_{nt} F_u + min(0.6 A_{gv} F_y \\ & \text{Resistance Factor, } \phi_U \\ & \text{Efficiency Factor, } U_{bs} \\ & \text{Nominal yield stress, } F_y \\ & \text{Nominal tensile strength, } F_u \\ & \text{Expected yield stress, } R_y F_y \end{aligned}$	,0.6A = = = = =	n Ruptur AnvF <sub>U</sub> )] 0.75 0.5 50.0 65.0 55.0	Eq. (J4  ksi ksi ksi	0.75 0.5 344.7 448.2 379.0	MPa MPa MPa
$\begin{aligned} & \textbf{Block S} \\ & V_{BS} \!\! = \!\! \phi_u [U_{bs} A_{nt} F_u \!\! + \!\! \min(0.6 A_{gv} F_y \!\! \\ & \text{Resistance Factor, } \phi_U \\ & \text{Efficiency Factor, } U_{bs} \\ & \text{Nominal yield stress, } F_y \\ & \text{Nominal tensile strength, } F_u \\ & \text{Expected yield stress, } R_y F_y \\ & \text{Expected tensile strength, } R_u F_u \end{aligned}$	,0.6A = = = = = =	n Ruptur 0.75 0.5 50.0 65.0 55.0 78.0	Eq. (J4 ksi ksi ksi ksi	4-5) AISC 0.75 0.5 344.7 448.2 379.0 537.8	MPa MPa MPa MPa
$\begin{aligned} & \textbf{Block S} \\ & V_{BS} \!\! = \!\! \phi_u [U_{bs} A_{nt} F_u \!\! + \!\! \min(0.6 A_{gv} F_y \\ & \text{Resistance Factor, } \phi_U \\ & \text{Efficiency Factor, } U_{bs} \\ & \text{Nominal yield stress, } F_y \\ & \text{Nominal tensile strength, } F_u \\ & \text{Expected yield stress, } R_y F_y \\ & \text{Expected tensile strength, } R_u F_u \\ & \text{Measured yield stress, } F_{ym} \\ & \text{Measured tensile strength, } F_{um} \end{aligned}$	,0.6A = = = = = = =	n Ruptur (20,000 AnvFu)] 0.75 0.5 50.0 65.0 78.0 65.1	ksi ksi ksi ksi ksi ksi	1-5) AISC 0.75 0.5 344.7 448.2 379.0 537.8 449.0	MPa MPa MPa MPa MPa
$\begin{aligned} & \textbf{Block S} \\ & V_{BS} = & \phi_u [U_{bs} A_{nt} F_u + \min(0.6 A_{gv} F_y \\ & \text{Resistance Factor, } \phi_U \\ & \text{Efficiency Factor, } U_{bs} \\ & \text{Nominal yield stress, } F_y \\ & \text{Nominal tensile strength, } F_u \\ & \text{Expected yield stress, } R_y F_y \\ & \text{Expected tensile strength, } R_u F_u \\ & \text{Measured yield stress, } F_{ym} \\ & \text{Measured tensile strength, } F_{um} \\ & \text{Net area in tension, } A_{nt} \end{aligned}$	,0.6A = = = = = = =	r Ruptur 0.75 0.5 50.0 65.0 55.0 78.0 65.1 75.7	ksi ksi ksi ksi ksi	1-5) AISC 0.75 0.5 344.7 448.2 379.0 537.8 449.0 522.0	MPa MPa MPa MPa MPa MPa
$\begin{aligned} & \textbf{Block S} \\ & V_{BS} \!\! = \!\! \phi_u [U_{bs} A_{nt} F_u \!\! + \!\! \min(0.6 A_{gv} F_y \\ & \text{Resistance Factor, } \phi_U \\ & \text{Efficiency Factor, } U_{bs} \\ & \text{Nominal yield stress, } F_y \\ & \text{Nominal tensile strength, } F_u \\ & \text{Expected yield stress, } R_y F_y \\ & \text{Expected tensile strength, } R_u F_u \\ & \text{Measured yield stress, } F_{ym} \\ & \text{Measured tensile strength, } F_{um} \end{aligned}$	,0.6A = = = = = = = = =	r Ruptur 0.75 0.5 50.0 65.0 55.0 78.0 65.1 75.7 0.840 5.761	ksi ksi ksi ksi ksi ksi in.2	1-5) AISC 0.75 0.5 344.7 448.2 379.0 537.8 449.0 522.0 538 3717	MPa MPa MPa MPa MPa MPa mm²
$V_{BS} = \phi_u [U_{bs} A_{nt} F_u + min(0.6 A_{gv} F_y \\ Resistance \ Factor, \ \phi_U \\ Efficiency \ Factor, \ U_{bs} \\ Nominal \ yield \ stress, \ F_y \\ Nominal \ tensile \ strength, \ F_u \\ Expected \ yield \ stress, \ R_y F_y \\ Expected \ tensile \ strength, \ R_u F_u \\ Measured \ yield \ stress, \ F_{ym} \\ Measured \ tensile \ strength, \ F_{um} \\ Net \ area \ in \ tension, \ A_{nt} \\ Gross \ area \ in \ shear, \ A_{gv} \\ Net \ area \ in \ shear, \ A_{nv} \\ Factored \ block \ shear \ rupture,$	0.64	(anyFu)] 0.75 0.5 50.0 65.0 55.0 78.0 65.1 75.7 0.840	ksi ksi ksi ksi ksi ksi in. <sup>2</sup> in. <sup>2</sup>	4-5) AISC 0.75 0.5 344.7 448.2 379.0 537.8 449.0 522.0 538	MPa MPa MPa MPa MPa MPa mm² mm²
$\begin{aligned} & \textbf{Block S} \\ & V_{BS} = & \phi_u [U_{bs} A_{nt} F_u + \min(0.6 A_{gv} F_y \\ & \text{Resistance Factor, } \phi_U \\ & \text{Efficiency Factor, } U_{bs} \\ & \text{Nominal yield stress, } F_y \\ & \text{Nominal tensile strength, } F_u \\ & \text{Expected yield stress, } R_y F_y \\ & \text{Expected tensile strength, } R_u F_u \\ & \text{Measured yield stress, } F_{ym} \\ & \text{Measured tensile strength, } F_{um} \\ & \text{Net area in tension, } A_{nt} \\ & \text{Gross area in shear, } A_{gv} \\ & \text{Net area in shear, } A_{nv} \\ & \text{Factored block shear rupture, } \\ & V_{BS} \\ & \text{Expected block shear rupture, } \end{aligned}$	0.6A = = = = = = = = = = = = =	(a) Ruptur (a) AnvFu)] (a) 75 (a) 5 (b) 65.0 (c) 65.0 (c) 78.0 (c) 65.1 (c) 75.7 (c) 840 (c) 761 (d) 4.201	ksi ksi ksi ksi ksi in. <sup>2</sup> in. <sup>2</sup>	4-5) AISC 0.75 0.5 344.7 448.2 379.0 537.8 449.0 522.0 538 3717 2690	MPa MPa MPa MPa MPa MPa mm² mm²
$\begin{aligned} & \textbf{Block S} \\ & V_{BS} = & \phi_u [U_{bs} A_{nt} F_u + \min(0.6 A_{gv} F_y \\ & \text{Resistance Factor, } \phi_U \\ & \text{Efficiency Factor, } U_{bs} \\ & \text{Nominal yield stress, } F_y \\ & \text{Nominal tensile strength, } F_u \\ & \text{Expected yield stress, } R_y F_y \\ & \text{Expected tensile strength, } R_u F_u \\ & \text{Measured yield stress, } F_{ym} \\ & \text{Measured tensile strength, } F_{um} \\ & \text{Measured tensile strength, } F_{um} \\ & \text{Net area in tension, } A_{nt} \\ & \text{Gross area in shear, } A_{gv} \\ & \text{Net area in shear, } A_{nv} \\ & \text{Factored block shear rupture, } \\ & V_{BS} \end{aligned}$	0.6A = = = = = = = = = = = = = = = = = = =	(AnvFu)] 0.75 0.5 50.0 65.0 55.0 78.0 65.1 75.7 0.840 5.761 4.201 143	ksi ksi ksi ksi ksi in. <sup>2</sup> in. <sup>2</sup> kips	1-5) AISC 0.75 0.5 344.7 448.2 379.0 537.8 449.0 522.0 538 3717 2690 633	MPa MPa MPa MPa MPa MPa mm² mm² kN
$\begin{aligned} & \textbf{Block S} \\ & V_{BS} \!\!=\!\! \phi_u [U_{bs} A_{nt} F_u \!\!+\!\! \min(0.6 A_{gv} F_y \\ & \text{Resistance Factor, } \phi_U \\ & \text{Efficiency Factor, } U_{bs} \\ & \text{Nominal yield stress, } F_y \\ & \text{Nominal tensile strength, } F_u \\ & \text{Expected yield stress, } R_y F_y \\ & \text{Expected tensile strength, } R_u F_u \\ & \text{Measured yield stress, } F_{ym} \\ & \text{Measured tensile strength, } F_{um} \\ & \text{Measured tensile strength, } F_{um} \\ & \text{Net area in tension, } A_{nt} \\ & \text{Gross area in shear, } A_{gv} \\ & \text{Net area in shear, } A_{nv} \\ & \text{Factored block shear rupture, } \\ & V_{BS} \\ & \text{Expected block shear rupture, } \\ & V_{BS} (\phi \!=\! 1.0, R_y F_y \& R_y F_u) \\ & \text{Measured block shear rupture, } V_{BS} \end{aligned}$	0.6A = = = = = = = = = = = = = = = = = = =	r Ruptur 0.75 0.5 50.0 65.0 55.0 78.0 65.1 75.7 0.840 5.761 4.201 143	ksi ksi ksi ksi ksi in.² in.² kips	1-5) AISC 0.75 0.5 344.7 448.2 379.0 537.8 449.0 522.0 538 3717 2690 633	MPa MPa MPa MPa MPa MPa mm² mm² kN
Block Struck $V_{BS} = \phi_u [U_{bs} A_{nt} F_u + \min(0.6 A_{gv} F_y Resistance Factor, \phi_U Efficiency Factor, U_{bs} Nominal yield stress, F_y Nominal tensile strength, F_u Expected yield stress, R_yF_y Expected tensile strength, R_uF_u Measured yield stress, F_ym Measured tensile strength, F_um Net area in tension, A_{nt} Gross area in shear, A_{gv} Net area in shear, A_{nv} Factored block shear rupture, V_{BS} Expected block shear rupture, V_{BS} (\phi=1.0, R_yF_y &R_yF_u) Measured block shear rupture, V_BS Flexural (V_r/V_c)^2 + (V_re/M_c)^2 = 1$	0.6A = = = = = = = = = = = = = = = = = = =	r Ruptur 0.75 0.5 50.0 65.0 55.0 78.0 65.1 75.7 0.840 5.761 4.201 143 223 223 ar yieldi	ksi ksi ksi ksi ksi in.² in.² kips kips	1-5) AISC 0.75 0.5 344.7 448.2 379.0 537.8 449.0 522.0 538 3717 2690 633	MPa MPa MPa MPa MPa MPa mm² mm² kN kN
$\label{eq:block-state} \textbf{Block S} \\ V_{BS} = \varphi_u[U_{bs}A_{nt}F_u + \min(0.6A_{gv}F_y \\ \text{Resistance Factor, } \varphi_U \\ \text{Efficiency Factor, } U_{bs} \\ \text{Nominal yield stress, } F_y \\ \text{Nominal tensile strength, } F_u \\ \text{Expected yield stress, } R_yF_y \\ \text{Expected tensile strength, } R_uF_u \\ \text{Measured yield stress, } F_{ym} \\ \text{Measured tensile strength, } F_{um} \\ \text{Net area in tension, } A_{nt} \\ \text{Gross area in shear, } A_{gv} \\ \text{Net area in shear, } A_{nv} \\ \text{Factored block shear rupture, } V_{BS} \\ \text{Expected block shear rupture, } V_{BS} \\ \text{Measured block shear rupture, } V_{BS} \\ \text{Flexura} \\ Flexu$	0.6A = = = = = = = = = = = = = = = = = = =	r Ruptur 0.75 0.5 50.0 65.0 55.0 78.0 65.1 75.7 0.840 5.761 4.201 143 223 223 ar yieldi	ksi ksi ksi ksi ksi in.² in.² kips kips	1-5) AISC 0.75 0.5 344.7 448.2 379.0 537.8 449.0 522.0 538 3717 2690 633 990 983	MPa MPa MPa MPa MPa MPa mm² mm² kN kN

$V_n = 0.6 F_y A_g$					
Nominal yield stress, F <sub>y</sub>	=	50.0	ksi	344.7	MPa
Expected yield stress, R <sub>y</sub> F <sub>y</sub>	=	55.0	ksi	379.0	MPa
Measured yield stress, F <sub>ym</sub>	=	65.1	ksi	449.0	MPa
Gross area of plate, Ag	=	3.456	in. <sup>2</sup>	2230	$\mathrm{mm}^2$
Factored shear Capacity, Vc	=	104	kips	461	kN
Expected shear Capacity, Ve	=	114	kips	507	kN
Measured shear capacity, V <sub>m</sub>	=	135	kips	601	kN
a distance	=	4.5	in.	114	mm
$M_c = \phi_b M_n$					
Resistance factor, φ <sub>b</sub>	=	0.90		0.90	
$M_n = F_y Z_{pl}$					
Plastic section modulus, $Z_{pl}$	=	7.777	in. <sup>3</sup>	127.44	$10^3 \text{ mm}^3$
Factored moment capacity, Mc	=	350.0	kip.in	39.5	kN.m
Expected moment capacity, Me	=	427.7	kip.in	48.3	kN.m
Measured moment capacity, M <sub>m</sub>	=	506.5	kip.in	57.2	kN.m
Factored shear-flexural yielding	=	62.2	kips	277	kN
resistance, V <sub>r</sub>					
Expected shear-flexural yielding resistance, $V_e$ ( $\phi$ =1.0, $R_yF_y$ )	=	73.0	kips	325	kN
Measured shear-flexural	=	86.5	kips	385	kN
yielding resistance, V <sub>m</sub>			1		
Plat	e Bı	ıckling			
$V_r = \phi_b F_{cr} S_{net} / e$	Ec	q. (9-6), A			
Resistance Factor, φ <sub>b</sub>	=	0.90	h Edition	0.90	
$S_{net} = 1/6 t_p h_o^2$	=	5.18	in. <sup>3</sup>	85	$10^{3}$ m
					$m^3$
$Z_{\text{net}} = 1/4 t_{\text{p}} h^2_{\text{o}}$	=	7.78	in. <sup>3</sup>	127.44	$10^3$ m m <sup>3</sup>
depth of top cope, dc	=	1.6	in.	40.0	mm
Beam Depth, d	=	12.2	in.	309.0	mm
Eccentricity, e	=	4 1/2	in.	114.3	mm
Unsupported Length of Plate, c	=	4 1/2	in.	114.3	mm
$d_c < 0.2d \& c < 2d$ ?		YES, fd	equation	valid	
f <sub>d</sub> equation (Cheng et al. 1984)			1		
. , ,			Eq. (	(9-12)	
$F_{cr} = 0.62\pi E f_d \frac{t_w^2}{ch_0} \le F_y$		AISC S	teel Man	ual (14th E	dition)
Modulus of Elasticity, E	=	29000	ksi	200000	MPa
Thickness of Plate, tp	=	3/8	in.	9.76	mm
Plate Depth, h <sub>o</sub>	=	9	in.	228.6	mm
$c = 2.5 \cdot 7.5 (d_{ct})$				(9-13)	
$f_d = 3.5 - 7.5(\frac{d_{ct}}{d_b})$			teel Man	ual (14th E	dition)
Adjustment Factor, f <sub>d</sub>	=	2.52		2.52	
Critical Stress, F <sub>cr</sub>	=	519.0	ksi	3579	MPa

Nominal yield stress, F <sub>y</sub>	=	50.0	ksi	344.7	MPa
Expected yield stress, R <sub>y</sub> F <sub>y</sub>	=	55.0	ksi	379.2	MPa
Measured yield stress, F <sub>ym</sub>	=	65.1	ksi	449.0	MPa
Factored buckling resistance	=	77.8	kips	346	kN
Ğ			•		
Expected buckling resistance $(R_yF_y, \varphi=1.0)$	=	95.1	kips	423	kN
Measured buckling resistance	=	112.5	kips	501	kN
Q equation (classical plate b	uckli	ing)			
$F_{cr} = F_{y}Q$			Eq. (	9-14)	
		AISC S		ual (14th E	Edition)
$\lambda = h_0$ $F_y$		A ICC C		9-18)	2.122
$\lambda = \frac{h_0}{10t_w} \sqrt{\frac{F_y}{475 + 280(\frac{h_0}{c})^2}}$		AISC S	teel Man	ual (14th E	dition)
Nominal Yield Stress of Plate, F <sub>Y</sub>	=	50	ksi	345	MPa
Expected Yield Stress, RyFy	=	55	ksi	379	MPa
Yield Stress of Plate, F <sub>Y</sub>	=	65	ksi	449	MPa
Nominal slenderness of coped section, λ	=	0.41			
Expected slenderness of coped section, $\lambda_e$	=	0.44			
Measured slenderness of coped section, $\lambda_m$	=	0.47			
Nominal strength reduction factor, Q	=	1.00			
Expected strength reduction factor, Q <sub>e</sub>	=	1.00			
Measured strength reduction factor, Q <sub>m</sub>	=	1.00			
Nominal critical stress, F <sub>cr</sub>	=	50.0	ksi	344.7	MPa
Expected critical stress, F <sub>cr,e</sub>	=	55.0	ksi	379.2	MPa
Measured critical stress, F <sub>cr,m</sub>	=	65.1	ksi	449.0	MPa
Factored buckling resistance, V <sub>r</sub>	=	77.8	kips	346	kN
Expected buckling resistance, $V_{r,e}$ ( $\phi$ =1.0, $R_yF_y$ )	=	95.1	kips	423	kN
Measured buckling resistance, $V_{r,m}(\varphi=1.0,F_{ym})$	=	112.5	kips	501	kN
Rectangular Bar Buckling		Sectio	n F11, A	ISC 360-1	5
$M_n(cd/t^2)$					
Nominal yield stress, F <sub>y</sub>	=	50.0	ksi	344.7	MPa
Expected yield stress, R <sub>y</sub> F <sub>y</sub>	=	55.0	ksi	379.2	MPa
Measured yield stress, Fym	=	65.1	ksi	449.0	MPa
c	=	4 1/2	in.	114	mm
d	=	9.0	in.	229	mm
t	=	3/8	in.	9.76	mm
$\lambda = cd/t^2$	=	275		275	
Nominal 0.08 E/F <sub>y</sub>	=	46		46	
Expected 0.08 E/F <sub>y</sub>	=	42		42	

Measured 0.08 E/F <sub>y</sub>	=	36		36	
Nominal 1.9 E/F <sub>y</sub>	=	1102		1102	
Expected 1.9 E/F <sub>y</sub>	=	1002		1002	
Measured 1.9 E/F <sub>y</sub>	=	846		846	
$C_b = \left[ 3 + \ln(\frac{a}{d_b}) \right] (1 - \frac{d_{ct}}{d_b}) \ge 1.84$		AISC Ste	Eq. (9- el Manu	-15) al (15 <sup>th</sup> Edi	tion)
$C_{b}$	=	1.84		1.84	
Factored buckling resistance, $V_r$	=	77.8	kips	346	kN
Expected buckling resistance, $V_{re} (\phi=1.0, R_yF_y)$	=	95.1	kips	423	kN
Measured buckling resistance,	=	112.5	kips	501	kN
V <sub>rm</sub> Weld to Su	ıppo	rting Eler	nent		
$D_{\min} = 5/8 t_{pl}$	••	8	Section	n 10	
				al (15 <sup>th</sup> Edi	tion)
Thickness of Plate, t <sub>p</sub>	=	3/8	in.	9.76	mm
Minimum Weld Thickness, D <sub>min</sub>	=	0.240	in.	6.10	mm
Take Weld Thickness, D <sub>w</sub>	=	13/30	in.	11.00	mm
Longitdunal Length of Weld, L	=	8.54	in.	217.00	mm
$V_w = 2 \phi_w 0.6 F_{EXX} 0.707 D_w (1)$	Eq. (J2-5) AISC 360-15				
$X_c$		0.00	in.	0.0	mm
$Y_c$		4.3	in.	108.5	mm
aL		6.0	in.	152.4	mm
K		0		0	
a		0.70		0.70	
Factored Weld Resistance, V <sub>w</sub>					
$Vw=2*CC_1DL(\phi_w=0.75)$		AICC Ctoo	Table	-	tion)
D=Dw/(1/16)		6.93	ei iviaiiua	ıl (15th Edi 6.93	uon)
$\mathbf{C}_1$		1.00		1.00	
C <sub>1</sub> (Measured)		1.26		1.26	
al		0.7			
<i>a2</i>		0.8			
C1-1		1.76			
C1-2		1.56			
C		1.76			
Resistance Factor, φ <sub>w</sub>	=	0.75		0.75	
Nominal ultimate strength, F <sub>EXX</sub>	=	71.1	ksi	490.0	Mpa
Measured ultimate strength,	=	89.9	ksi	620.0	Mpa
$F_{EXX} \\ Factored Weld Resistance, V_w$	=	78.2	kips	348	kN
Expected Weld Strength, $V_w$ $(\phi=1.0)$	=	104.2	kips	464	kN
Expected Weld Strength, V <sub>w</sub> (measured properties)	=	131.5	kips	585	kN



Failure Modes	Factored		Expe	ected	Meas	ured
	kips	kN	kips	kN	kips	kN
Shear -flexural yielding resistance, Vr	62.2	277	73.0	325	86.5	385
Shear yielding resistance, VG	103.7	461	114.1	507	135.1	601
Block shear rupture resistance, vbs	143.3	633	222.9	990	222.6	983
Shear rupture strength over net area, vn	73.7	325	118.0	521	114.5	505
Plate buckling(f <sub>d</sub> equation)	77.8	346	95.1	423	112.5	501
Plate buckling(Q equation)	77.8	346	95.1	423	112.5	501
Rectangular bar buckling	77.8	346	95.1	423	112.5	501
Bearing resistance, b <sub>r</sub>	69.1	305	104.8	463	104.8	463
Shear resistance of bolts, vr	62.9	280	93.1	414		
Weld resistance, vw	78.2	348	104.2	464	131.5	585

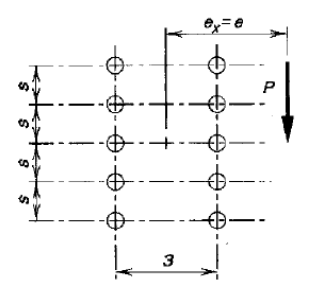
#### Specimen BC3-2-10-200C

#### **Configuration parameter**

Supporting column	W360×196					
Supported beam	W310×76					
Offset of bolt group, a	=	4 1/2	in.	114.3	mm	
Bolt diameter, d <sub>b</sub>	=	3/4	in.	19.1	mm	
Bolt diameter, d <sub>h</sub>	=	13/16	in.	21.1	mm	
Number of bolt lines, m	=	2		2		
Number of bolts rows, n	=	3		3		
Plate Depth, d	=	9.0	in.	228.6	mm	

#### **Bolt Shear & Bolt Bearing**

	8						
Compute ICR coefficient (C)	Table 7-8						
-	AISC Handbook						
	(15 <sup>th</sup> Version)						
Number of bolt lines, m	=	2	•	2			
Moment arm, e	=	6.0	in.	152.4	mm		
gage, s	=	3.0	in.	76.2	mm		
Pitch, p	=	3.0	in.	76.2	mm		
Vertical edge distances	=	1 1/2	in.	38.1	mm		
Horizontal edge distances	=	1 1/2	in.	38.1	mm		
Number of bolt rows, n	=	3		3			
L1	=	6.0	in.	152.4	mm		
C1	=	2.25		2.25			
L2	=	7.0	in.	177.8	mm		
C2	=	1.99		1.99			
ICR coefficient (C)	=	2.25		2.25			



#### **Bolt Shear**

$V_r\!\!=\!\!\phi_V\phi_b\phi_tA_b(0.625F_u)C$		Eq. (J3-1), AISC 360-15						
Reduction factor for shear rupture,	=	0.75		0.75				
$\phi_{ m v}$								
Reduction factor for uneven force	=	0.9		0.9				
distribution, φ <sub>d</sub>								
Reduction factor for shear plan are	=	1.0		1.0				
not excluded from the threaded								
part, $\phi_t$								
Number of shear planes, m	=	1.0		1.0				
Bolt area, Ab	=	0.442	in. <sup>2</sup>	285	$\mathrm{mm}^2$			
Nominal ultimate strength of bolts,	=	150	ksi	1034.2	MPa			
$\mathrm{F}_{\mathrm{U}}$								
Factored bolt group capacity, V <sub>r</sub>	=	62.9	kips	280	kN			
Expected bolt group capacity, V <sub>e</sub>	=	93.1	kips	414	kN			
$(\phi_{\rm v} = \phi_{\rm d} = 1.0)$			•					
Bolt Bearing								

$B_r=3\phi_{br}d_bmin[(tF_u)_{plate},(tF_u)_{web}] C$	Eq. (J3-10), AISC 360-15				
Modification factor, φ <sub>br</sub>	= 0.75 0.75				
Plate thickness, t <sub>p</sub>	=	3/8	in.	9.76	mm

Beam web thickness, tw	=	0.395	in.	10.04	mm
Bolt Diameter, d <sub>b</sub>	=	3/4	in.	19.05	mm
Clear edge distance	=	1.09	in.	27.58	mm
Nominal tensile strength of plate,	=	65.0	ksi	448.2	MPa
F <sub>u,plate</sub> Nominal tensile strength of beam	=	65.0	ksi	448.2	MPa
F <sub>u,beam</sub> Expected plate strength, R <sub>y</sub> F <sub>u,plate</sub>	=	78.0	ksi	537.8	MPa
Expected beam strength, RyFu,beam	=	72.0	ksi	495.0	MPa
Tensile strength of plate, F <sub>u,plate</sub>	=	75.7	ksi	522.0	MPa
Tensile strength of beam F <sub>u,beam</sub>	=	71.8	ksi	495.0	MPa
Factored bearing resistance, B <sub>r</sub>	=	69.1	kips	305	kN
	=	104.8	_		kN
Expected bearing strength, B <sub>r</sub> (φ=1.0,R <sub>y</sub> F <sub>u</sub> )	_	104.8	kips	463	KIN
Measured bearing resistance, B <sub>r</sub>	=	104.8	kips	463	kN
Plat	te Du	ıctility			
$t_{\text{pmax}} = 6M_{\text{max}}/F_{\text{y}}d_{\text{pl}}^{2}$			Eq. (	10-5)	
		AISC	Steel Man	ual (15 <sup>th</sup> Eo	dition)
$M_{\text{max}} = F_{\text{nv}}/\phi_{\text{d}}(A_{\text{b}}C')$				-01-	
Bolt Shear Strength, F <sub>nV</sub>	=	84.4	ksi	581.7	MPa
Bolt Area, A <sub>b</sub>	=	0.442	in. <sup>2</sup>	285	mm <sup>2</sup>
Compute ICR coefficient for		AICC	Table Steel Man		dition)
moment only case (C') Number of bolt lines, m	=	2	Steel Mail	uai (13 E)	1111011)
Column spacing	=	3	in.	76	mm
Row spacing, s	=	3	in.	76	mm
Number of bolts rows, n	=	3		3	
ICR coefficient, C'	=	15.8		15.8	
$ m M_{max}$	=	654.1	kip.in	73.9	kN.m
Nominal yield stress, F <sub>y</sub>	=	50.0	kips	344.7	MPa
Expected yield stress, R <sub>y</sub> F <sub>y</sub>	=	55.0	kips	379.2	MPa
Measured yield stress, F <sub>ym</sub>	=	65.1	kips	449.0	MPa
Plate depth, d	=	9.0	in.	228.6	mm
Plate thickness, t <sub>pl</sub>	=	0.384	ın.	9.76	mm
Maximum plate thickness, $t_{max}(F_y)$	=	0.969	ın.	24.61	mm
Is this requirement satisfied? (t <sub>p</sub> <		Yes		Yes	
$t_{max}$ ) Maximum plate thickness, $t_{max}$ ( $R_y$ $F_y$ )	=	0.881	in.	22.37	mm
Is this requirement satisfied? ( $t_p$ <		Yes		Yes	
$t_{ m max})$ Maximum plate thickness, $t_{ m max}$ $(F_{ m ym})$	=	0.744	in.	17.90	mm
Is this requirement satisfied? (t <sub>p</sub> <		Yes		Yes	
$t_{max}$ )					
She	ar Y	ielding			
$V_{GP}\!=0.60\phi F_y A_g$		E	q. (J4-3), A	AISC 360-1	5
Resistance factor, φ	=	1.00		1.00	
Nominal yield stress, F <sub>y</sub>	=	50.0	ksi	344.7	MPa
Expected yield stress, R <sub>y</sub> F <sub>y</sub>	=	55.0	ksi	379.2	MPa
Measured yield stress, Fym	=	65.1	ksi	449.0	MPa

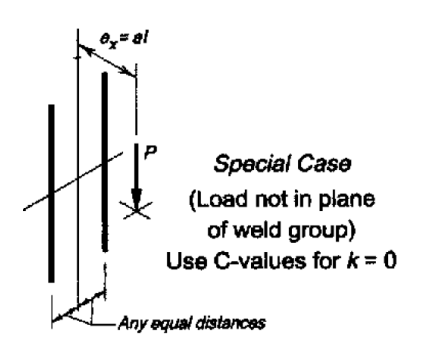
Plate thickness, t <sub>pl</sub>	=	3/8	in.	9.76	mm
Plate depth, d <sub>pl</sub>	=	9.0	in.	228.6	mm
Gross plate area, Ag	=	3.456	in. <sup>2</sup>	2230	$mm^2$
Factored shear yielding resistance, $V_{GP}$	=	103.7	kips	461	kN
Expected yielding strength, $V_{GP}$ $(\phi=1.0,R_vF_v)$	=	114.1	kips	507	kN
Shear yielding resistance, V <sub>GP</sub>	=	135.1	kips	601	kN
She	ar R	upture			
$V_N\!\!=\!\!0.60\phi F_u A_{net}$			Eq. (J	4-4), AISC	360-15
Resistance Factor, φ	=	0.75		0.75	
Nominal tensile strength, Fu	=	65.0	ksi	448.2	MPa
Expected tensile strength, R <sub>y</sub> F <sub>u</sub>	=	78.0	ksi	537.8	MPa
Measured tensile strength, F <sub>um</sub>	=	75.7	ksi	522.0	MPa
Plate thickness, t <sub>pl</sub>	=	3/8	in.	9.76	mm
Net depth, d <sub>net</sub>	=	6.6	in.	165.5	mm
Net area, A <sub>net</sub>	=	2.520	in. <sup>2</sup>	1614	$\text{mm}^2$
Factored rupture strength, V <sub>N</sub>	=	73.7	kips	325	kN
Expected rupture strength, $V_N$ ( $\phi$ =1.0, $R_YFu$ )	=	118.0	kips	521	kN
Measured rupture strength, V <sub>N</sub>	=	114.5	kips	505	kN
Block	Shear	r Ruptui	-		
$V_{BS} = \varphi_u[U_{bs}A_{nt}F_u + min(0.6A_{gv}F_y)]$	0.6A <sub>r</sub>	$_{\mathrm{nv}}\mathrm{F}_{\mathrm{U}})]$	Eq. (J	4-5) AISC	360-15
Resistance Factor, $\phi_{\mathrm{U}}$	=	0.75		0.75	
Efficiency Factor, Ubs	=	0.5		0.5	
Nominal yield stress, F <sub>y</sub>	=	50.0	ksi	344.7	MPa
Nominal tensile strength, Fu	=	65.0	ksi	448.2	MPa
Expected yield stress, R <sub>y</sub> F <sub>y</sub>	=	55.0	ksi	379.0	MPa
Expected tensile strength, R <sub>u</sub> F <sub>u</sub>	=	78.0	ksi	537.8	MPa
Measured yield stress, Fym	=	65.1	ksi	449.0	MPa
Measured tensile strength, F <sub>um</sub>	=	75.7	ksi	522.0	MPa
Net area in tension, Ant	=	0.840	in. <sup>2</sup>	538	$mm^2$
Gross area in shear, $A_{\rm gv}$	=	5.761	in. <sup>2</sup>	3717	$mm^2$
Net area in shear, A <sub>nv</sub>	=	4.201	in. <sup>2</sup>	2690	$mm^2$
Factored block shear rupture, $V_{\rm BS}$	=	143	kips	633	kN
Expected block shear rupture, $V_{\text{BS}}$	=	223	kips	990	kN
$(\phi = 1.0,R_yF_y\&R_yF_u)$ Measured block shear rupture, $V_{BS}$	=	223	kips	983	kN
Flexura	l-she	ar yieldi	ng		
$(V_r/V_c)^2 + (V_r e/M_c)^2 = 1$		AISC	Equati Steel Man	on 10-5 ual (15 <sup>th</sup> E	dition),
$V_c = \phi_v V_n$					
Resistance Factor, φ <sub>v</sub>	=	1.00		1.00	
$V_n = 0.6F_y A_g$		<b>7</b> 0.0	1 .	244=	1.00
Nominal yield stress, F <sub>y</sub>	=	50.0	ksi	344.7	MPa

Expected yield stress, R <sub>y</sub> F <sub>y</sub>	=	55.0	ksi	379.0	MPa
Measured yield stress, Fym	=	65.1	ksi	449.0	MPa
Gross area of plate, Ag	=	3.456	in. <sup>2</sup>	2230	$mm^2$
Factored shear Capacity, Vc	=	104	kips	461	kN
Expected shear Capacity, Ve	=	114	kips	507	kN
Measured shear capacity, V <sub>m</sub>	=	135	kips	601	kN
a distance	=	4.5	in.	114	mm
$\mathbf{M}_{\mathrm{c}} = \mathbf{\phi}_{\mathrm{b}}  \mathbf{M}_{\mathrm{n}}$					
Resistance factor, φ <sub>b</sub>	=	0.90		0.90	
$M_n = F_y Z_{pl}$					
Plastic section modulus, $Z_{pl}$	=	7.777	in. <sup>3</sup>	127.44	$\begin{array}{c} 10^3 \\ mm^3 \end{array}$
Factored moment capacity, Mc	=	350.0	kip.in	39.5	kN.m
Expected moment capacity, Me	=	427.7	kip.in	48.3	kN.m
Measured moment capacity, $M_{\text{m}}$	=	506.5	kip.in	57.2	kN.m
Factored shear-flexural yielding resistance, V <sub>r</sub>	=	62.2	kips	277	kN
Expected shear-flexural yielding	=	73.0	kips	325	kN
resistance, V <sub>e</sub> (φ=1.0, R <sub>y</sub> F <sub>y</sub> ) Measured shear-flexural yielding	=	86.5	kips	385	kN
resistance, V <sub>m</sub>	te Bu	ickling			
$V_{r} = \phi_{b} F_{cr} S_{net} / e$		_	AISC Steel	Manual	
·		(14	th Edition	)	
Resistance Factor, φ <sub>b</sub>	=	0.90	2	0.90	2
$S_{net} = 1/6 t_p h_o^2$	=	5.18	in. <sup>3</sup>	85	$10^{3}$ mm
$Z_{\text{net}} = 1/4 t_{\text{p}} h^2_{\text{o}}$	=	7.78	in. <sup>3</sup>	127.44	$10^3$ mm
depth of top cope, d <sub>c</sub>	=	1.6	in.	40.0	mm
Beam Depth, d	=	12.2	in.	309.0	mm
Eccentricity, e	=	4 1/2	in.	114.3	mm
Unsupported Length of Plate, c	=	4 1/2	in.	114.3	mm
$d_c \le 0.2d \& c \le 2d$ ?		YES, f <sub>d</sub>	equation	valid	
$f_d$ equation (Cheng et al. 1984)					
$F_{cr} = 0.62\pi E f_d  \frac{t_w^2}{ch_0} \le F_y$		AISC		(9-12) ual (14th Eo	dition)
Modulus of Elasticity, E	=	29000	ksi	200000	MPa
Thickness of Plate, t <sub>p</sub>	=	3/8	in.	9.76	mm
Plate Depth, h <sub>o</sub>	=	9	in.	228.6	mm
$f_d = 3.5 - 7.5(\frac{d_{ct}}{d_h})$		AISC		(9-13) ual (14th Eo	dition)
Adjustment Factor, f <sub>d</sub>	=	2.52		2.52	
Critical Stress, F <sub>cr</sub>	=	519.0	ksi	3579	MPa
Nominal yield stress, F <sub>y</sub>	=	50.0	ksi	344.7	MPa
1 tollillar flora birobb, 1 y		20.0	1101	5 1 1.7	1,11 0

Expected yield stress, R <sub>y</sub> F <sub>y</sub>	=	55.0	ksi	379.2	MPa
Measured yield stress, F <sub>ym</sub>	=	65.1	ksi	449.0	MPa
Factored buckling resistance	=	77.8	kips	346	kN
Expected buckling resistance	=	95.1	kips	423	kN
$(R_yF_y, \varphi=1.0)$		75.1	тро	123	III (
Measured buckling resistance	=	112.5	kips	501	kN
Q equation (classical plate bi	ucklin	ıg)			
$F_{cr} = F_y Q$				9-14)	
		AISC S		ual (14th E	dition)
$\lambda = \frac{h_0}{1 - \frac{1}{2} \frac{h_0}{h_0}}$		AISC S		(9-18) ual (14th Eo	dition)
$\lambda = \frac{h_0}{10t_w} \sqrt{\frac{F_y}{475 + 280(\frac{h_0}{c})^2}}$		Alse	occi wian	uai (14tii E	uition)
Nominal Yield Stress of Plate, F <sub>Y</sub>	=	50	ksi	345	MPa
Expected Yield Stress, R <sub>Y</sub> F <sub>Y</sub>	=	55	ksi	379	MPa
Yield Stress of Plate, F <sub>Y</sub>	=	65	ksi	449	MPa
Nominal slenderness of coped section, $\lambda$	=	0.41			
Expected slenderness of coped section, $\lambda_e$	=	0.44			
Measured slenderness of coped section, $\lambda_m$	=	0.47			
Nominal strength reduction factor,	=	1.00			
Expected strength reduction factor, $Q_e$	=	1.00			
Measured strength reduction factor, Q <sub>m</sub>	=	1.00			
Nominal critical stress, F <sub>cr</sub>	=	50.0	ksi	344.7	MPa
Expected critical stress, F <sub>cr,e</sub>	=	55.0	ksi	379.2	MPa
Measured critical stress, F <sub>cr,m</sub>	=	65.1	ksi	449.0	MPa
Factored buckling resistance, V <sub>r</sub>	=	77.8	kips	346	kN
Expected buckling resistance, $V_{r,e}$ ( $\phi$ =1.0, $R_yF_y$ )	=	95.1	kips	423	kN
Measured buckling resistance, $V_{r,m}(\phi=1.0,F_{ym})$	=	112.5	kips	501	kN
Rectangular Bar Buckling		Section	on F11, A	ISC 360-15	;
$M_n(cd/t^2)$					
Nominal yield stress, F <sub>y</sub>	=	50.0	ksi	344.7	MPa
Expected yield stress, R <sub>y</sub> F <sub>y</sub>	=	55.0	ksi	379.2	MPa
Measured yield stress, Fym	=	65.1	ksi	449.0	MPa
c	=	4 1/2	in.	114	mm
d	=	9.0	in.	229	mm
t	=	3/8	in.	9.76	mm
$\lambda = cd/t^2$	=	275		275	
Nominal 0.08 E/F <sub>y</sub>	=	46		46	
Expected 0.08 E/F <sub>y</sub>	=	42		42	
Measured 0.08 E/F <sub>y</sub>	=	36		36	

Expected Weld Strength, Vw

(measured properties)



kips

576

kN

129.5

=

Failure Modes	Factored		Expected		Meas	ured
	kips	kN	kips	kN	kips	kN
Shear -flexural yielding resistance, Vr	62.2	277	73.0	325	86.5	385
Shear yielding resistance, VG	103.7	461	114.1	507	135.1	601
Block shear rupture resistance, vbs	143.3	633	222.9	990	222.6	983
Shear rupture strength over net area, vn	73.7	325	118.0	521	114.5	505
Plate buckling(fd equation)	77.8	346	95.1	423	112.5	501
Plate buckling(Q equation)	77.8	346	95.1	423	112.5	501
Rectangular bar buckling	77.8	346	95.1	423	112.5	501
Bearing resistance, b <sub>r</sub>	69.1	305	104.8	463	104.8	463
Shear resistance of bolts, vr	62.9	280	93.1	414		
Weld resistance, vw	77.0	342	102.6	457	129.5	576

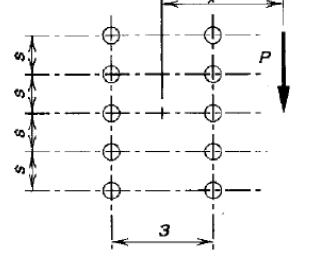
#### Specimen BC6-2-16

#### **Configuration parameter**

Supporting column		W360×196						
Supported beam		W610×140						
Offset of bolt group, a	=	4 1/2	in.	114.3	mm			
Bolt diameter, d <sub>b</sub>	=	7/8	in.	22.2	mm			
Bolt diameter, d <sub>h</sub>	=	15/16	in.	24.2	mm			
Number of bolt lines, m	=	2		2				
Number of bolts rows, n	=	6		6				
Plate Depth, d	=	18.0	in.	457.2	mm			

## Bolt Shear & Bolt Bearing

Compute ICD as afficient (C)			Table	7 0		
Compute ICR coefficient (C)	Table 7-8					
		AISC Handbook				
			$(15^{th} Ve$	rsion)		
Number of bolt lines, m	=	2		2		
Moment arm, e	=	6.0	in.	152.4	mm	
gage, s	=	3.0	in.	76.2	mm	
Pitch, p	=	3.0	in.	76.2	mm	
Vertical edge distances	=	1 1/2	in.	38.1	mm	
Horizontal edge distances	=	1 1/2	in.	38.1	mm	
Number of bolt rows, n	=	6		6		
L1	=	6.0	in.	152.4	mm	
C1	=	7.17		7.17		
L2	=	7.0	in.	177.8	mm	
C2	=	6.46		6.46		
ICR coefficient (C)	=	7.17		7.17		



#### **Bolt Shear**

$V_r\!\!=\!\!\phi_V\phi_b\phi_tA_b(0.625F_u)C$	Eq. (J3-1), AISC 360-15					
Reduction factor for shear	=	0.75		0.75		
rupture, $\phi_v$ Reduction factor for uneven force distribution, $\phi_d$	=	0.9		0.9		
Reduction factor for shear plan are not excluded from the threaded part, $\phi_t$	=	1.0		1.0		
Number of shear planes, m	=	1.0		1.0		
Bolt area, Ab	=	0.601	in. <sup>2</sup>	388	$\mathrm{mm}^2$	
Nominal ultimate strength of bolts, F <sub>U</sub>	=	150	ksi	1034.2	MPa	
Factored bolt group capacity, V <sub>r</sub>	=	272.7	kips	1213	kN	
Expected bolt group capacity, $V_e(\phi_v=\phi_d=1.0)$	=	404.0	kips	1797	kN	

$B_r=3\phi_{br}d_bmin[(tF_u)_{plate},(tF_u)_{web}]$		5			
Modification factor, φ <sub>br</sub>	=	0.75		0.75	
Plate thickness, t <sub>p</sub>	=	5/8	in.	15.74	mm

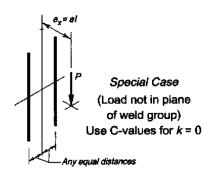
Beam web thickness, tw	=	0.515	in.	12.72	mm
Bolt Diameter, d <sub>b</sub>	=	7/8	in.	22.2	mm
Clear edge distance	=	1.03	in.	25.99	mm
Nominal tensile strength of	=	65.0	ksi	448.2	MPa
plate, F <sub>u,plate</sub>					
Nominal tensile strength of beam F <sub>u,beam</sub>	=	65.0	ksi	448.2	MPa
Expected plate strength, $R_yF_{u,plate}$	=	78.0	ksi	537.8	MPa
Expected beam strength,	=	72.0	ksi	495.0	MPa
$R_y F_{u,beam}$ Tensile strength of plate, $F_{u,plate}$	=	75.1	ksi	518.0	MPa
Tensile strength of beam F <sub>u,beam</sub>	=	78.9	ksi	544.0	MPa
Factored bearing resistance, B <sub>r</sub>	=	279.6	kips	1200	kN
•			•		
Expected bearing strength, B <sub>r</sub> (φ=1.0,R <sub>y</sub> F <sub>u</sub> )	=	410.1	kips	1760	kN
Measured bearing resistance, B <sub>r</sub>	=	450.7	kips	1934	kN
Pla	te D	uctility			
$t_{\rm pmax}=6M_{\rm max}/F_{\rm y}d_{\rm pl}^{2}$				(10-5)	
M E / (A CI)		AISC	Steel Mar	nual (15 <sup>th</sup> I	Edition)
$M_{max}=F_{nv}/\varphi_d(A_bC')$ Bolt Shear Strength, $F_{nV}$	=	84.4	ksi	581.7	MPa
Bolt Area, Ab	_	0.601	in. <sup>2</sup>	388	mm <sup>2</sup>
Compute ICR coefficient for		0.001		le 7-8	111111
moment only case (C')		AISC		nual (15 <sup>th</sup> I	Edition)
Number of bolt lines, m	=	2	Steel Mai	2	zamon)
Column spacing	=	3	in.	76	mm
Row spacing, s	=	3	in.	76	mm
Number of bolts rows, n	=	6	111.	6	111111
ICR coefficient, C'	=	54.2		54.2	
M <sub>max</sub>	=	3053.9	kip.in	345.0	kN.m
Nominal yield stress, F <sub>y</sub>	=	50.0	kips	344.7	MPa
Expected yield stress, R <sub>y</sub> F <sub>y</sub>	=	55.0	kips	379.2	MPa
Measured yield stress, F <sub>ym</sub>	=	53.7	kips	370.5	MPa
Plate depth, d	=	18.0	in.	457.2	mm
Plate thickness, t <sub>pl</sub>		0.619	in.	15.74	mm
Maximum plate thickness, t <sub>max</sub>	=	1.13	in.	28.73	
$(F_y)$		1.13	111.	20.73	mm
Is this requirement satisfied? ( $t_p$ $< t_{max}$ )		Yes		Yes	
Maximum plate thickness, $t_{max}$	=	1.03	in.	26.12	mm
$(R_y F_y)$ Is this requirement satisfied? $(t_p$		Yes		Yes	
< t <sub>max</sub> )  Maximum plate thickness, t <sub>max</sub>	=	1.05	in.	26.73	mm
(F <sub>ym</sub> ) Is this requirement satisfied? (t <sub>p</sub>		Yes		Yes	
< t <sub>max</sub> )	ear V	ielding			
$V_{GP} = 0.60 \phi F_y A_g$		_	n (I4-3)	AISC 360-	-15
	_		4. (* T-2 <i>)</i> ,		15
Resistance factor, φ	=	1.00		1.00	
Nominal yield stress, F <sub>y</sub>	=	50.0	ksi	344.7	MPa

Expected yield stress, R <sub>y</sub> F <sub>y</sub>	=	55.0	ksi	379.2	MPa					
Measured yield stress, F <sub>ym</sub>	=	53.7	ksi	370.5	MPa					
Plate thickness, t <sub>pl</sub>	=	5/8	in.	15.74	mm					
Plate depth, d <sub>pl</sub>	=	18.0	in.	457.2	mm					
Gross plate area, Ag	=	11.151	in. <sup>2</sup>	7194	$\text{mm}^2$					
Factored shear yielding resistance, V <sub>GP</sub>	=	334.5	kips	1488	kN					
Expected yielding strength, $V_{GP}$ ( $\phi$ =1.0, $R_yF_y$ )	=	368.0	kips	1637	kN					
Shear yielding resistance, V <sub>GP</sub>	=	359.5	kips	1599	kN					
Shear Rupture										
$V_N = 0.60 \phi F_u A_{net}$			Eq. (J	4-4), AISC	2 360-15					
Resistance Factor, φ	=	0.75		0.75						
Nominal tensile strength, F <sub>u</sub>	=	65.0	ksi	448.2	MPa					
Expected tensile strength, R <sub>y</sub> F <sub>u</sub>	=	78.0	ksi	537.8	MPa					
Measured tensile strength, F <sub>um</sub>	=	75.1	ksi	518.0	MPa					
Plate thickness, t <sub>pl</sub>	=	3/8	in.	9.76	mm					
Net depth, d <sub>net</sub>	=	12.4	in.	311.9	mm					
Net area, A <sub>net</sub>	=	7.666	in. <sup>2</sup>	4907	$\text{mm}^2$					
Factored rupture strength, $V_{\mathrm{N}}$	=	224.2	kips	990	kN					
Expected rupture strength, $V_N$ ( $\phi$ =1.0, $R_YFu$ )	=	358.8	kips	1583	kN					
Measured rupture strength, V <sub>N</sub>	=	345.6	kips	1525	kN					
Block Shear Rupture										
Block	Shea	ır Ruptu	re							
$\begin{aligned} & \textbf{Block} \\ & V_{BS} \!\!=\!\! \phi_u \! [U_{bs} A_{nt} F_u \!\!+\!\! min(0.6 A_{gv} F_y \end{aligned}$		-		4-5) AISC	360-15					
		-		4-5) AISC 0.75	360-15					
$V_{BS}\!\!=\!\!\phi_u[U_{bs}A_{nt}F_u\!\!+\!\!min(0.6A_{gv}F_y$	,0.6	$\Lambda_{\rm nv}F_{\rm U})]$			360-15					
$\begin{split} V_{BS} \!\! = \!\! \phi_u \! [U_{bs} A_{nt} F_u \!\! + \!\! min(0.6 A_{gv} F_y \\ Resistance \ Factor, \ \! \phi_U \end{split}$	,0.6 <i>A</i> =	$\Lambda_{\rm nv}F_{\rm U})]$ 0.75		0.75	2360-15 MPa					
$V_{BS} = \phi_u [U_{bs} A_{nt} F_u + min(0.6 A_{gv} F_y$ Resistance Factor, $\phi_U$ Efficiency Factor, $U_{bs}$	,0.6 <i>A</i> = =	0.75 0.5	Eq. (J	0.75 0.5						
$V_{BS} = \phi_u [U_{bs} A_{nt} F_u + min(0.6 A_{gv} F_y \ Resistance\ Factor,\ \phi_U \ Efficiency\ Factor,\ U_{bs} \ Nominal\ yield\ stress,\ F_y$	,0.6A = = =	0.75 0.5 50.0	Eq. (J	0.75 0.5 344.7	MPa					
$\begin{split} V_{BS} = & \phi_u [U_{bs} A_{nt} F_u + min(0.6 A_{gv} F_y \\ & Resistance\ Factor,\ \phi_U \\ & Efficiency\ Factor,\ U_{bs} \\ & Nominal\ yield\ stress,\ F_y \\ & Nominal\ tensile\ strength,\ F_u \end{split}$	,0.6A = = = = =	0.75 0.5 50.0 65.0	Eq. (J ksi ksi	0.75 0.5 344.7 448.2	MPa MPa					
$V_{BS}$ = $\phi_u[U_{bs}A_{nt}F_u+min(0.6A_{gv}F_y)]$ Resistance Factor, $\phi_U$ Efficiency Factor, $U_{bs}$ Nominal yield stress, $F_y$ Nominal tensile strength, $F_u$ Expected yield stress, $R_yF_y$	,0.6A = = = = = =	A <sub>nv</sub> F <sub>U</sub> )] 0.75 0.5 50.0 65.0 55.0	Eq. (J ksi ksi ksi	0.75 0.5 344.7 448.2 379.0	MPa MPa MPa					
$\begin{split} V_{BS} = & \phi_u [U_{bs} A_{nt} F_u + min(0.6 A_{gv} F_y \\ & Resistance\ Factor,\ \phi_U \\ & Efficiency\ Factor,\ U_{bs} \\ & Nominal\ yield\ stress,\ F_y \\ & Nominal\ tensile\ strength,\ F_u \\ & Expected\ yield\ stress,\ R_y F_y \\ & Expected\ tensile\ strength,\ R_u F_u \end{split}$	,0.6A = = = = = = =	AnvF <sub>U</sub> )] 0.75 0.5 50.0 65.0 55.0 78.0	Eq. (J ksi ksi ksi ksi	0.75 0.5 344.7 448.2 379.0 537.8	MPa MPa MPa MPa					
$\begin{split} V_{BS} = & \phi_u [U_{bs} A_{nt} F_u + min(0.6 A_{gv} F_y \\ & \text{Resistance Factor, } \phi_U \\ & \text{Efficiency Factor, } U_{bs} \\ & \text{Nominal yield stress, } F_y \\ & \text{Nominal tensile strength, } F_u \\ & \text{Expected yield stress, } R_y F_y \\ & \text{Expected tensile strength, } R_u F_u \\ & \text{Measured yield stress, } F_{ym} \end{split}$	,0.6A = = = = = = = =	AnvF <sub>U</sub> )] 0.75 0.5 50.0 65.0 55.0 78.0 53.7	Eq. (J ksi ksi ksi ksi	0.75 0.5 344.7 448.2 379.0 537.8 370.5 518.0	MPa MPa MPa MPa MPa					
$\begin{split} V_{BS} = & \phi_u [U_{bs} A_{nt} F_u + min(0.6 A_{gv} F_y \\ & \text{Resistance Factor, } \phi_U \\ & \text{Efficiency Factor, } U_{bs} \\ & \text{Nominal yield stress, } F_y \\ & \text{Nominal tensile strength, } F_u \\ & \text{Expected yield stress, } R_y F_y \\ & \text{Expected tensile strength, } R_u F_u \\ & \text{Measured yield stress, } F_{ym} \\ & \text{Measured tensile strength, } F_{um} \end{split}$	,0.6A = = = = = = = = =	AnvF <sub>U</sub> )] 0.75 0.5 50.0 65.0 55.0 78.0 53.7 75.1	ksi ksi ksi ksi ksi ksi	0.75 0.5 344.7 448.2 379.0 537.8 370.5 518.0 818	MPa MPa MPa MPa MPa					
$V_{BS} = \phi_u [U_{bs} A_{nt} F_u + min(0.6 A_{gv} F_y \\ Resistance Factor, \phi_U \\ Efficiency Factor, U_{bs} \\ Nominal yield stress, F_y \\ Nominal tensile strength, F_u \\ Expected yield stress, R_y F_y \\ Expected tensile strength, R_u F_u \\ Measured yield stress, F_{ym} \\ Measured tensile strength, F_{um} \\ Net area in tension, A_{nt} \\$	,0.6A = = = = = = = = = =	AnvF <sub>U</sub> )] 0.75 0.5 50.0 65.0 55.0 78.0 53.7 75.1 1.278	ksi ksi ksi ksi ksi ksi in.2	0.75 0.5 344.7 448.2 379.0 537.8 370.5 518.0 818 13189	MPa MPa MPa MPa MPa MPa mm²					
V <sub>BS</sub> =φ <sub>u</sub> [U <sub>bs</sub> A <sub>nt</sub> F <sub>u</sub> +min(0.6A <sub>gv</sub> F <sub>y</sub> Resistance Factor, φ <sub>U</sub> Efficiency Factor, U <sub>bs</sub> Nominal yield stress, F <sub>y</sub> Nominal tensile strength, F <sub>u</sub> Expected yield stress, R <sub>y</sub> F <sub>y</sub> Expected tensile strength, R <sub>u</sub> F <sub>u</sub> Measured yield stress, F <sub>ym</sub> Measured tensile strength, F <sub>um</sub> Net area in tension, A <sub>nt</sub> Gross area in shear, A <sub>gv</sub> Net area in shear, A <sub>nv</sub> Factored block shear rupture,	(0.6A) = = = = = = = = = = = = = = = = = = =	AnvFu)] 0.75 0.5 50.0 65.0 55.0 78.0 53.7 75.1 1.278 20.443	ksi ksi ksi ksi ksi in. <sup>2</sup> in. <sup>2</sup>	0.75 0.5 344.7 448.2 379.0 537.8 370.5 518.0 818	MPa MPa MPa MPa MPa MPa mm² mm²					
$V_{BS} = \varphi_u [U_{bs} A_{nt} F_u + min(0.6 A_{gv} F_y \\ Resistance Factor, \ \varphi_U \\ Efficiency Factor, \ U_{bs} \\ Nominal yield stress, \ F_y \\ Nominal tensile strength, \ F_u \\ Expected yield stress, \ R_y F_y \\ Expected tensile strength, \ R_u F_u \\ Measured yield stress, \ F_{ym} \\ Measured tensile strength, \ F_{um} \\ Net area in tension, \ A_{nt} \\ Gross area in shear, \ A_{gv} \\ Net area in shear, \ A_{nv} \\ Factored block shear rupture, \\ V_{BS} \\ Expected block shear rupture, \\$	,0.6A = = = = = = = = = = = = = = = = = = =	AnvFu)] 0.75 0.5 50.0 65.0 55.0 78.0 53.7 75.1 1.278 20.443 14.055	ksi ksi ksi ksi ksi in. <sup>2</sup> in. <sup>2</sup>	0.75 0.5 344.7 448.2 379.0 537.8 370.5 518.0 818 13189 8996	MPa MPa MPa MPa MPa MPa mm² mm²					
$V_{BS} \!\!=\!\! \phi_u [U_{bs} A_{nt} F_u \!\!+\!\! min(0.6 A_{gv} F_y \\ Resistance Factor, \phi_U \\ Efficiency Factor, U_{bs} \\ Nominal yield stress, F_y \\ Nominal tensile strength, F_u \\ Expected yield stress, R_y F_y \\ Expected tensile strength, R_u F_u \\ Measured yield stress, F_{ym} \\ Measured tensile strength, F_{um} \\ Net area in tension, A_{nt} \\ Gross area in shear, A_{gv} \\ Net area in shear, A_{nv} \\ Factored block shear rupture, \\ V_{BS} \\ \label{eq:VBS}$	,0.6A = = = = = = = = = = = = = = = = = = =	AnvFu)] 0.75 0.5 50.0 65.0 55.0 78.0 53.7 75.1 1.278 20.443 14.055 442.2	ksi ksi ksi ksi ksi in. <sup>2</sup> in. <sup>2</sup> kips	0.75 0.5 344.7 448.2 379.0 537.8 370.5 518.0 818 13189 8996 1952	MPa MPa MPa MPa MPa MPa mm² mm² kN					
$V_{BS} = \varphi_u[U_{bs}A_{nt}F_u + min(0.6A_{gv}F_y \\ Resistance\ Factor,\ \varphi_U \\ Efficiency\ Factor,\ U_{bs} \\ Nominal\ yield\ stress,\ F_y \\ Nominal\ tensile\ strength,\ F_u \\ Expected\ yield\ stress,\ R_yF_y \\ Expected\ tensile\ strength,\ R_uF_u \\ Measured\ yield\ stress,\ F_{ym} \\ Measured\ tensile\ strength,\ F_{um} \\ Net\ area\ in\ tension,\ A_{nt} \\ Gross\ area\ in\ shear,\ A_{gv} \\ Net\ area\ in\ shear,\ A_{nv} \\ Factored\ block\ shear\ rupture,\ V_{BS} \\ Expected\ block\ shear\ rupture,\ V_{BS}(\phi=1.0,\ R_yF_y\&R_y\ F_u) \\ Measured\ block\ shear\ rupture,\ V_{BS}$	,0.6A = = = = = = = = = = = = = = = = = = =	AnvFu)] 0.75 0.5 50.0 65.0 78.0 53.7 75.1 1.278 20.443 14.055 442.2 707.6	ksi ksi ksi ksi ksi in.² in.² kips	0.75 0.5 344.7 448.2 379.0 537.8 370.5 518.0 818 13189 8996 1952 3123	MPa MPa MPa MPa MPa MPa mm² mm² kN					
$V_{BS} = \varphi_u[U_{bs}A_{nt}F_u + min(0.6A_{gv}F_y \\ Resistance\ Factor,\ \varphi_U \\ Efficiency\ Factor,\ U_{bs} \\ Nominal\ yield\ stress,\ F_y \\ Nominal\ tensile\ strength,\ F_u \\ Expected\ yield\ stress,\ R_yF_y \\ Expected\ tensile\ strength,\ R_uF_u \\ Measured\ yield\ stress,\ F_{ym} \\ Measured\ tensile\ strength,\ F_{um} \\ Net\ area\ in\ tension,\ A_{nt} \\ Gross\ area\ in\ shear,\ A_{gv} \\ Net\ area\ in\ shear,\ A_{nv} \\ Factored\ block\ shear\ rupture,\ V_{BS} \\ Expected\ block\ shear\ rupture,\ V_{BS}(\phi=1.0,\ R_yF_y\&R_y\ F_u) \\ Measured\ block\ shear\ rupture,\ V_{BS}$	,0.6A = = = = = = = = = = = = = = = = = = =	AnvFu)] 0.75 0.5 50.0 65.0 78.0 53.7 75.1 1.278 20.443 14.055 442.2 707.6 681.5 ear yieldi	Eq. (J ksi ksi ksi ksi in. <sup>2</sup> in. <sup>2</sup> kips kips kips	0.75 0.5 344.7 448.2 379.0 537.8 370.5 518.0 818 13189 8996 1952 3123	MPa MPa MPa MPa MPa MPa mm² mm² kN kN					
$V_{BS} = \varphi_u[U_{bs}A_{nt}F_u + min(0.6A_{gv}F_y) \\ Resistance Factor, \ \varphi_U \\ Efficiency Factor, \ U_{bs} \\ Nominal yield stress, \ F_y \\ Nominal tensile strength, \ F_u \\ Expected yield stress, \ R_yF_y \\ Expected tensile strength, \ R_uF_u \\ Measured yield stress, \ F_{ym} \\ Measured tensile strength, \ F_{um} \\ Net area in tension, \ A_{nt} \\ Gross area in shear, \ A_{gv} \\ Net area in shear, \ A_{nv} \\ Factored block shear rupture, \ V_{BS} \\ Expected block shear rupture, \ V_{BS} (\phi=1.0, R_yF_y\&R_yF_u) \\ Measured block shear rupture, \ V_{BS} \\ Flexure$	,0.6A = = = = = = = = = = = = = = = = = = =	AnvFu)] 0.75 0.5 50.0 65.0 78.0 53.7 75.1 1.278 20.443 14.055 442.2 707.6 681.5 ear yieldi	Eq. (J ksi ksi ksi ksi in. <sup>2</sup> in. <sup>2</sup> kips kips kips	0.75 0.5 344.7 448.2 379.0 537.8 370.5 518.0 818 13189 8996 1952 3123 3008	MPa MPa MPa MPa MPa MPa mm² mm² kN kN					

$V_n = 0.6F_v A_g$									
Nominal yield stress, F <sub>v</sub>	=	50.0	ksi	344.7	MPa				
Expected yield stress, R <sub>y</sub> F <sub>y</sub>	=	55.0	ksi	379.0	MPa				
Measured yield stress, F <sub>vm</sub>	=	53.7	ksi	370.5	MPa				
Gross area of plate, A <sub>g</sub>	=	11.151	in. <sup>2</sup>	7194	mm <sup>2</sup>				
Factored shear Capacity, V <sub>c</sub>	=	334.5	kips	1488	kN				
Expected shear Capacity, V <sub>e</sub>	=	368.0	kips	1637	kN				
Measured shear capacity, V <sub>m</sub>	=	359.5	kips	1599	kN				
a distance	=	4.5	in.	114	mm				
$M_c = \varphi_b M_n$		1.5	111.	111	111111				
Resistance factor, φ <sub>b</sub>	=	0.90		0.90					
$M_n = F_v Z_{pl}$		0.70		0.70					
Plastic section modulus, Z <sub>pl</sub>	=	50.179	in. <sup>3</sup>	822.28	$10^{3}$				
rastic section modulus, 2pi		30.177	111.	022.20	$mm^3$				
Factored moment capacity, Mc	=	2258.0	kip.in	255.1	kN.m				
Expected moment capacity, Me	=	2759.8	kip.in	311.8	kN.m				
Measured moment capacity, $\ensuremath{M_{m}}$	=	2696.4	kip.in	304.7	kN.m				
Factored shear-flexural yielding resistance, V <sub>r</sub>	=	278.3	kips	1238	kN				
Expected shear-flexural yielding	=	315.5	kips	1404	kN				
resistance, V <sub>e</sub> (φ=1.0, R <sub>y</sub> F <sub>y</sub> ) Measured shear-flexural	=	308.3	kips	1371	kN				
yielding resistance, V <sub>m</sub>	4. D								
Plate Buckling $V_r = \phi_b F_{cr} S_{net} / e$ Eq. (9-6), AISC Steel Manual									
		_	ISC Steel	l Manual					
$V_r = \phi_b \; F_{cr}  S_{net} / \; e$		ı. (9-6), A	ISC Steel						
		ı. (9-6), A							
$V_r = \phi_b \; F_{cr}  S_{net} \! / \; e$	Eq	i. (9-6), A (14t		)	$10^3$ mm <sup>3</sup>				
$V_r = \phi_b \; F_{cr}  S_{net} \! / \; e \label{eq:Vr}$ Resistance Factor, $\phi_b$	Eq	(14t) 0.90	h Edition	0.90	$10^3 \text{mm}^3$ $10^3 \text{mm}^3$				
$V_r = \phi_b \; F_{cr}  S_{net} / \; e$ $Resistance \; Factor, \; \phi_b$ $S_{net} = 1/6 \; t_p  h^2_{\; o}$	Eq = =	(14t) 0.90 33.45	h Edition	0.90 548.19					
$V_r = \phi_b \; F_{cr}  S_{net} / \; e$ Resistance Factor, $\phi_b$ $S_{net} = 1/6 \; t_p  h^2_o$ $Z_{net} = 1/4 \; t_p  h^2_o$	Eq = = = =	0.90 33.45 50.18	in. <sup>3</sup> in. <sup>3</sup>	0.90 548.19 822.28	$10^3$ mm <sup>3</sup>				
$V_r = \phi_b \; F_{cr}  S_{net} / \; e$ $Resistance \; Factor, \; \phi_b$ $S_{net} = 1/6 \; t_p  h^2_o$ $Z_{net} = 1/4 \; t_p  h^2_o$ $depth \; of \; top \; cope, \; d_c$	Eq	0.90 33.45 50.18 3.2	in. <sup>3</sup> in. in.	0.90 548.19 822.28 80.4	10 <sup>3</sup> mm <sup>3</sup> mm				
$V_r = \phi_b \; F_{cr}  S_{net} / \; e$ Resistance Factor, $\phi_b$ $S_{net} = 1/6 \; t_p  h^2_o$ $Z_{net} = 1/4 \; t_p  h^2_o$ depth of top cope, $d_c$ Beam Depth, $d$	Eq	0.90 33.45 50.18 3.2 24.3	in. <sup>3</sup> in. <sup>3</sup> in. in.	0.90 548.19 822.28 80.4 618.0	10 <sup>3</sup> mm <sup>3</sup> mm mm				
$V_r = \phi_b \; F_{cr}  S_{net} / \; e$ $Resistance \; Factor, \; \phi_b$ $S_{net} = 1/6 \; t_p \; h^2_o$ $Z_{net} = 1/4 \; t_p \; h^2_o$ $depth \; of \; top \; cope, \; d_c$ $Beam \; Depth, \; d$ $Eccentricity, \; e$	Eq	0.90 33.45 50.18 3.2 24.3 4.5	in.3 in.3 in. in. in. in. in. in.	0.90 548.19 822.28 80.4 618.0 114.3 114.3	10 <sup>3</sup> mm <sup>3</sup> mm mm mm				
$\begin{split} V_r &= \phi_b \; F_{cr}  S_{net} / \; e \\ \\ Resistance \; Factor, \; \phi_b \\ S_{net} &= 1/6 \; t_p  h^2_{\; o} \\ Z_{net} &= 1/4 \; t_p  h^2_{\; o} \\ \\ depth \; of \; top \; cope, \; d_c \\ \\ Beam \; Depth, \; d \\ \\ Eccentricity, \; e \\ \\ Unsupported \; Length \; of \; Plate, \; c \end{split}$	Eq	0.90 33.45 50.18 3.2 24.3 4.5	in.3 in.3 in. in. in. in. in. in.	0.90 548.19 822.28 80.4 618.0 114.3 114.3	10 <sup>3</sup> mm <sup>3</sup> mm mm mm				
$V_r = \phi_b \; F_{cr}  S_{net} / \; e$ $Resistance \; Factor, \; \phi_b$ $S_{net} = 1/6 \; t_p \; h^2_o$ $Z_{net} = 1/4 \; t_p \; h^2_o$ $depth \; of \; top \; cope, \; d_c$ $Beam \; Depth, \; d$ $Eccentricity, \; e$ $Unsupported \; Length \; of \; Plate, \; c$ $d_c < 0.2d \; \& \; c < 2d?$	Eq	1. (9-6), A (14t) 0.90 33.45 50.18 3.2 24.3 4.5 4.5 YES, fd o	in.3 in.3 in. in. in. in. equation	0.90 548.19 822.28 80.4 618.0 114.3 114.3	10 <sup>3</sup> mm <sup>3</sup> mm mm mm				
$V_r = \phi_b \; F_{cr}  S_{net} / \; e$ $Resistance \; Factor, \; \phi_b$ $S_{net} = 1/6 \; t_p \; h^2_o$ $Z_{net} = 1/4 \; t_p \; h^2_o$ $depth \; of \; top \; cope, \; d_c$ $Beam \; Depth, \; d$ $Eccentricity, \; e$ $Unsupported \; Length \; of \; Plate, \; c$ $d_c < 0.2d \; \& \; c < 2d?$ $f_d \; equation \; (Cheng \; et \; al. \; 1984)$	Eq	1. (9-6), A (14t) 0.90 33.45 50.18 3.2 24.3 4.5 4.5 YES, fd o	in.3 in.3 in. in. in. in. equation	0.90 548.19 822.28 80.4 618.0 114.3 114.3 valid	10 <sup>3</sup> mm <sup>3</sup> mm mm mm				
$V_r = \phi_b \; F_{cr}  S_{net} / \; e$ $Resistance \; Factor, \; \phi_b$ $S_{net} = 1/6 \; t_p  h^2_o$ $Z_{net} = 1/4 \; t_p  h^2_o$ $depth \; of \; top \; cope, \; d_c$ $Beam \; Depth, \; d$ $Eccentricity, \; e$ $Unsupported \; Length \; of \; Plate, \; c$ $d_c < 0.2d \; \& \; c < 2d?$ $\textit{f_d} \; equation \; (Cheng \; et \; al. \; 1984)$ $F_{cr} = 0.62\pi E f_d \; \frac{t_w^2}{ch_0} \leq F_y$	Eq	1. (9-6), A (14t 0.90 33.45 50.18 3.2 24.3 4.5 4.5 YES, f <sub>d</sub> o	in.3 in.3 in. in. in. in. equation  Eq. Steel Mar	0.90 548.19 822.28 80.4 618.0 114.3 114.3 valid (9-12) nual (14th 1	10 <sup>3</sup> mm <sup>3</sup> mm mm mm mm				
$V_r = \phi_b \; F_{cr}  S_{net} / \; e$ $Resistance \; Factor, \; \phi_b$ $S_{net} = 1/6 \; t_p  h^2_o$ $Z_{net} = 1/4 \; t_p  h^2_o$ $depth \; of \; top \; cope, \; d_c$ $Beam \; Depth, \; d$ $Eccentricity, \; e$ $Unsupported \; Length \; of \; Plate, \; c$ $d_c < 0.2d \; \& \; c < 2d?$ $f_d \; equation \; (Cheng \; et \; al. \; 1984)$ $F_{cr} = 0.62\pi E f_d \; \frac{t_w^2}{ch_0} \leq F_y$ $Modulus \; of \; Elasticity, \; E$	Eq	1. (9-6), A (14t) 0.90 33.45 50.18 3.2 24.3 4.5 4.5 YES, f <sub>d</sub> o	in.3 in.3 in. in. in. in. equation  Eq. Steel Marksi	0.90 548.19 822.28 80.4 618.0 114.3 114.3 valid (9-12) nual (14th)	10 <sup>3</sup> mm <sup>3</sup> mm mm mm mm MPa				
$V_r = \phi_b \; F_{cr}  S_{net} / \; e$ $Resistance \; Factor, \; \phi_b$ $S_{net} = 1/6 \; t_p \; h^2_o$ $Z_{net} = 1/4 \; t_p \; h^2_o$ $depth \; of \; top \; cope, \; d_c$ $Beam \; Depth, \; d$ $Eccentricity, \; e$ $Unsupported \; Length \; of \; Plate, \; c$ $d_c < 0.2d \; \& \; c < 2d?$ $f_d \; equation \; (Cheng \; et \; al. \; 1984)$ $F_{cr} = 0.62\pi E f_d \; \frac{t_w^2}{ch_0} \leq F_y$ $Modulus \; of \; Elasticity, \; E$ $Thickness \; of \; Plate, \; t_p$ $Plate \; Depth, \; h_o$	Eq	1. (9-6), A (14t) 0.90 33.45 50.18 3.2 24.3 4.5 4.5 YES, fd 6	in.3 in.3 in. in. in. in. equation  Eq. Steel Marksi in. in. in.	0.90 548.19 822.28 80.4 618.0 114.3 114.3 valid (9-12) rual (14th)	10 <sup>3</sup> mm <sup>3</sup> mm mm mm mm MPa mm				
$V_{\rm r} = \varphi_{\rm b} \; F_{\rm cr}  S_{\rm net} / \; e$ $Resistance \; Factor, \; \varphi_{\rm b}$ $S_{\rm net} = 1/6 \; t_{\rm p}  h^2_{\rm o}$ $Z_{\rm net} = 1/4 \; t_{\rm p}  h^2_{\rm o}$ $depth \; of \; top \; cope, \; d_{\rm c}$ $Beam \; Depth, \; d$ $Eccentricity, \; e$ $Unsupported \; Length \; of \; Plate, \; c$ $d_{\rm c} < 0.2d \; \& \; c < 2d?$ $\textit{f_d} \; equation \; (Cheng \; et \; al. \; 1984)$ $F_{cr} = 0.62\pi E f_d \; \frac{t_w^2}{c h_0} \leq F_y$ $Modulus \; of \; Elasticity, \; E$ $Thickness \; of \; Plate, \; t_p$	Eq	1. (9-6), A (14t) 0.90 33.45 50.18 3.2 24.3 4.5 4.5 YES, f <sub>d</sub> 6 29000 5/8 18	in.3 in.3 in. in. in. in. equation  Eq. Steel Marksi in. in. Eq.	0.90 548.19 822.28 80.4 618.0 114.3 114.3 valid (9-12) nual (14th) 200000 15.74 457.2	10 <sup>3</sup> mm <sup>3</sup> mm mm mm mm MPa mm mm				
$V_r = \phi_b \; F_{cr}  S_{net} / \; e$ $Resistance \; Factor, \; \phi_b$ $S_{net} = 1/6 \; t_p \; h^2_o$ $Z_{net} = 1/4 \; t_p \; h^2_o$ $depth \; of \; top \; cope, \; d_c$ $Beam \; Depth, \; d$ $Eccentricity, \; e$ $Unsupported \; Length \; of \; Plate, \; c$ $d_c < 0.2d \; \& \; c < 2d?$ $f_d \; equation \; (Cheng \; et \; al. \; 1984)$ $F_{cr} = 0.62\pi E f_d \; \frac{t_w^2}{ch_0} \leq F_y$ $Modulus \; of \; Elasticity, \; E$ $Thickness \; of \; Plate, \; t_p$ $Plate \; Depth, \; h_o$	Eq	1. (9-6), A (14t) 0.90 33.45 50.18 3.2 24.3 4.5 4.5 YES, f <sub>d</sub> 6 29000 5/8 18	in.3 in.3 in. in. in. in. equation  Eq. Steel Marksi in. in. Eq.	0.90 548.19 822.28 80.4 618.0 114.3 114.3 valid (9-12) nual (14th) 200000 15.74 457.2 (9-13)	10 <sup>3</sup> mm <sup>3</sup> mm mm mm mm MPa mm mm				

Nominal yield stress, F <sub>y</sub>	=	50.0	ksi	344.7	MPa
Expected yield stress, R <sub>y</sub> F <sub>y</sub>	=	55.0	ksi	379.2	MPa
Measured yield stress, F <sub>ym</sub>	=	53.7	ksi	370.5	MPa
Factored buckling resistance	=	501.8	kips	2232	kN
Expected buckling resistance $(R_yF_y, \varphi=1.0)$	=	613.3	kips	2728	kN
Measured buckling resistance	=	599.2	kips	2665	kN
Q equation (classical plate b	uckli	ing)			
$F_{cr} = F_{v}Q$			Ea	(9-14)	
- u - y Q		AISC S	-	iual (14th 1	Edition)
$h_{\circ}$ $F_{\circ}$			Eq.	(9-18)	
$\lambda = \frac{h_0}{10t_w} \sqrt{\frac{F_y}{475 + 280(\frac{h_0}{c})^2}}$		AISC S	Steel Mar	nual (14th 1	Edition)
Nominal Yield Stress of Plate,	=	50	ksi	345	MPa
F <sub>Y</sub> Expected Yield Stress, R <sub>Y</sub> F <sub>Y</sub>	=	55	ksi	379	MPa
Yield Stress of Plate, F <sub>Y</sub>	=	53.7	ksi	370.5	MPa
Nominal slenderness of coped	=	0.29	noi	370.5	wii a
section, $\lambda$		0.29			
Expected slenderness of coped section, $\lambda_e$	=	0.31			
Measured slenderness of coped section, $\lambda_m$	=	0.30			
Nominal strength reduction factor, Q	=	1.00			
Expected strength reduction factor, Q <sub>e</sub>	=	1.00			
Measured strength reduction factor, Q <sub>m</sub>	=	1.00			
Nominal critical stress, F <sub>cr</sub>	=	50.0	ksi	344.7	MPa
Expected critical stress, F <sub>cr,e</sub>	=	55.0	ksi	379.2	MPa
Measured critical stress, F <sub>cr,m</sub>	=	53.7	ksi	370.5	MPa
Factored buckling resistance, V <sub>r</sub>	=	501.8	kips	2232	kN
Expected buckling resistance,	=	613.3	kips	2728	kN
$V_{r,e} (\phi=1.0, R_y F_y)$ Measured buckling resistance,	=	599.2	kips	2665	kN
$V_{r,m}(\phi=1.0,F_{ym})$		a	F11	100000	
Rectangular Bar Buckling		Secti	on FII, A	AISC 360-1	15
$M_n(cd/t^2)$					
Nominal yield stress, F <sub>y</sub>	=	50.0	ksi	344.7	MPa
Expected yield stress, R <sub>y</sub> F <sub>y</sub>	=	55.0	ksi	379.2	MPa
Measured yield stress, F <sub>ym</sub>	=	53.7	ksi	370.5	MPa
С	=	4 1/2	in.	114	mm
d	=	18.0	in.	457.2	mm
t	=	5/8	in.	15.74	mm
$\lambda = cd/t^2$	=	211		211	
Nominal 0.08 E/F <sub>y</sub>	=	46		46	
Expected 0.08 E/F <sub>y</sub>	=	42		42	

Measured 0.08 E/F <sub>y</sub>	=	43		43	
Nominal 1.9 E/F <sub>y</sub>	=	1102		1102	
Expected 1.9 E/F <sub>y</sub>	=	1002		1002	
Measured 1.9 E/F <sub>y</sub>	=	1025		1025	
$C_b = \left[ 3 + \ln(\frac{a}{d_b}) \right] (1 - \frac{d_{ct}}{d_b}) \ge 1.84$		AISC St	Eq. (9 seel Manu	1-15) ual (15 <sup>th</sup> Ed	ition)
$\mathrm{C}_{\mathrm{b}}$	=	1.84		1.84	
Factored buckling resistance, V <sub>r</sub>	=	501.8	kips	2232	kN
Expected buckling resistance, $V_{re}(\phi=1.0, R_yF_y)$ Measured buckling resistance,	=	613.3 599.2	kips kips	2728 2665	kN kN
$V_{\rm rm}$		377.2	трз	2002	1111
Weld to S	uppo	orting Ele	ement		
$D_{min} = 5/8 t_{pl}$			Sectio		
Thickness of Plate, tp	=	AISC St 5/8	eel Manu in.	al (15 <sup>th</sup> Edi 15.74	ition) mm
Minimum Weld Thickness, D <sub>min</sub>	=	0.387	in.	9.83	mm
Take Weld Thickness, D <sub>w</sub>	=	0.367	in.	10.50	mm
Longitudinal Length of Weld, L		17.36	in.	441.0	mm
$V_{\rm w} = 2  \phi_{\rm w}  0.6  F_{\rm EXX}  0.707  D_{\rm w}  (1)$				Eq. (J2-	
$\mathbf{v}_{\mathrm{W}} = 2 \; \mathbf{\psi}_{\mathrm{W}} \; 0.0 \; 1 \; \mathbf{E} \mathbf{\chi} \mathbf{\chi} \; 0.707 \; \mathbf{D}_{\mathrm{W}} (1)$	.0 1 0	.5 3111 0	,	AISC 360	
$X_{c}$		0.00	in.	0.0	mm
$Y_c$		8.68	in.	220.5	mm
aL		6.0	in.	152.4	mm
K		0		0	
a		0.35		0.35	
Factored Weld Resistance, $V_{\rm w}$					
$Vw=2*CC_1DL(\phi_w=0.75)$			Table	-	
D-D/(1/16)		AISC Sto	eel Manu	al (15th Ed	ition)
D=Dw/(1/16)				6.61 1.00	
$C_1$		1.00			
$C_1$ (Measured)  al		1.27 0.30		1.27	
		0.30			
a2 C1-1		3.09			
C1-2		2.66			
C1-2 C		2.89			
Resistance Factor, φ <sub>w</sub>	=			0.75	
		0.75	ksi	0.75	Mno
Nominal ultimate strength, F <sub>EXX</sub>	=	71.1		490.0	Mpa
Measured ultimate strength, $F_{EXX}$	=	89.9	ksi	620.0	Mpa
Factored Weld Resistance, V <sub>w</sub>	=	250.1	kips	1112	kN
Expected Weld Strength, $V_w$ ( $\phi$ =1.0)	=	333.4	kips	1483	kN
Expected Weld Strength, $V_{\rm w}$ (measured properties)	=	420.5	kips	1870	kN



	•						
Failure Modes	Factored		Expected		Meas	sured	
	kips	kN	kips	kN	kips	kN	
Shear -flexural yielding resistance, Vr	278.3	1238	315.5	1404	308.3	1371	
Shear yielding resistance, V <sub>G</sub>	334.5	1488	368.0	1637	359.5	1599	
Block shear rupture resistance, V <sub>bs</sub>	442.2	1952	707.6	3123	681.5	3008	
Shear rupture strength over net area, V <sub>n</sub>	224.2	990	358.8	1583	345.6	1525	
Plate buckling(f <sub>d</sub> equation)	501.8	2232	613.3	2728	599.2	2665	
Plate buckling(Q equation)	501.8	2232	613.3	2728	599.2	2665	
Rectangular bar buckling	501.8	2232	613.3	2728	599.2	2665	
Bearing resistance, B <sub>r</sub>	279.6	1200	410.1	1760	450.7	1934	
Shear resistance of bolts, V <sub>r</sub>	272.7	1213	404.0	1797			
Weld resistance, $V_{\rm w}$	250.1	1112	333.4	1483	420.5	1870	

#### Specimen BC6-2-16-500C

#### **Configuration parameter**

Supporting column	W360×196							
Supported beam	W610×140							
Offset of bolt group, a	=	4 1/2	in.	114.3	mm			
Bolt diameter, d <sub>b</sub>	=	7/8	in.	22.2	mm			
Bolt diameter, d <sub>h</sub>	=	15/16	in.	24.2	mm			
Number of bolt lines, m	=	2		2				
Number of bolts rows, n	=	6		6				
Plate Depth, d	=	18.0	in.	457.2	mm			

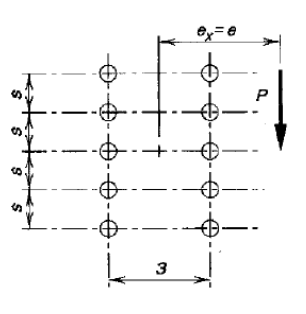
### **Bolt Shear & Bolt Bearing**

			0			
Compute ICR coefficient (C)	Table 7-8					
	AISC Handbook					
Number of bolt lines, m	=	2		2		
Moment arm, e	=	6.0	in.	152.4	mm	
gage, s	=	3.0	in.	76.2	mm	
Pitch, p	=	3.0	in.	76.2	mm	
Vertical edge distances	=	1 1/2	in.	38.1	mm	
Horizontal edge distances	=	1 1/2	in.	38.1	mm	
Number of bolt rows, n	=	6		6		
L1	=	6.0	in.	152.4	mm	
C1	=	7.17		7.17		
L2	=	7.0	in.	177.8	mm	
C2	=	6.46		6.46		
ICR coefficient (C)	=	7.17		7.17		



$V_{r}\!\!=\!\!\phi_{V}\phi_{b}\phi_{t}A_{b}(0.625F_{u})C$		Eq. (J3-1), AISC 360-15				
Reduction factor for shear rupture, φ <sub>v</sub>	=	0.75		0.75		
Reduction factor for uneven force distribution, φ <sub>d</sub>	=	0.9		0.9		
Reduction factor for shear plan are not excluded from the threaded part, φ <sub>t</sub>	=	1.0		1.0		
Number of shear planes, m	=	1.0		1.0		
Bolt area, Ab	=	0.601	in. <sup>2</sup>	388	$\mathrm{mm}^2$	
Nominal ultimate strength of bolts, F <sub>U</sub>	=	150	ksi	1034.2	MPa	
Factored bolt group capacity, V <sub>r</sub>	=	272.7	kips	1213	kN	
Expected bolt group capacity, $V_e(\phi_v=\phi_d=1.0)$	=	404.0	kips	1797	kN	

$B_r=3\phi_{br}d_bmin[(tF_u)_{plate},(tF_u)_{web}]$	Eq. (J3-10), AISC 360-15						
Modification factor, φ <sub>br</sub>	=	0.75					
Plate thickness, t <sub>p</sub>	=	5/8	in. 15.74				



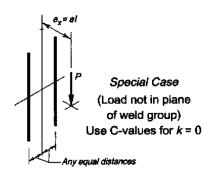
Beam web thickness, tw	=	0.515	in.	12.72	mm
Bolt Diameter, d <sub>b</sub>	=	7/8	in.	22.2	mm
Clear edge distance	=	1.03	in.	25.99	mm
Nominal tensile strength of	=	65.0	ksi	448.2	MPa
plate, F <sub>u,plate</sub>					
Nominal tensile strength of beam F <sub>u,beam</sub>	=	65.0	ksi	448.2	MPa
Expected plate strength, $R_yF_{u,plate}$	=	78.0	ksi	537.8	MPa
Expected beam strength,	=	72.0	ksi	495.0	MPa
$R_y F_{u,beam}$ Tensile strength of plate, $F_{u,plate}$	=	75.1	ksi	518.0	MPa
Tensile strength of beam F <sub>u,beam</sub>	=	78.9	ksi	544.0	MPa
Factored bearing resistance, B <sub>r</sub>	=	279.6	kips	1200	kN
•			•		
Expected bearing strength, B <sub>r</sub> (φ=1.0,R <sub>y</sub> F <sub>u</sub> )	=	410.1	kips	1760	kN
Measured bearing resistance, B <sub>r</sub>	=	450.7	kips	1934	kN
Pla	te D	uctility			
$t_{\rm pmax}=6M_{\rm max}/F_{\rm y}d_{\rm pl}^{2}$				(10-5)	
M E / (A CI)		AISC	Steel Mar	nual (15 <sup>th</sup> I	Edition)
$M_{max}=F_{nv}/\varphi_d(A_bC')$ Bolt Shear Strength, $F_{nV}$	=	84.4	ksi	581.7	MPa
Bolt Area, Ab	_	0.601	in. <sup>2</sup>	388	mm <sup>2</sup>
Compute ICR coefficient for		0.001		le 7-8	111111
moment only case (C')		AISC		nual (15 <sup>th</sup> I	Edition)
Number of bolt lines, m	=	2	Steel Mai	2	zamon)
Column spacing	=	3	in.	76	mm
Row spacing, s	=	3	in.	76	mm
Number of bolts rows, n	=	6	111.	6	111111
ICR coefficient, C'	=	54.2		54.2	
M <sub>max</sub>	=	3053.9	kip.in	345.0	kN.m
Nominal yield stress, F <sub>y</sub>	=	50.0	kips	344.7	MPa
Expected yield stress, R <sub>y</sub> F <sub>y</sub>	=	55.0	kips	379.2	MPa
Measured yield stress, F <sub>ym</sub>	=	53.7	kips	370.5	MPa
Plate depth, d	=	18.0	in.	457.2	mm
Plate thickness, t <sub>pl</sub>		0.619	in.	15.74	mm
Maximum plate thickness, t <sub>max</sub>	=	1.13	in.	28.73	
$(F_y)$		1.13	111.	20.73	mm
Is this requirement satisfied? (t <sub>p</sub> < t <sub>max</sub> )		Yes		Yes	
Maximum plate thickness, $t_{max}$	=	1.03	in.	26.12	mm
$(R_y F_y)$ Is this requirement satisfied? $(t_p$		Yes		Yes	
< t <sub>max</sub> )  Maximum plate thickness, t <sub>max</sub> (F. )	=	1.05	in.	26.73	mm
(F <sub>ym</sub> ) Is this requirement satisfied? (t <sub>p</sub>		Yes		Yes	
< t <sub>max</sub> )	ear V	ielding			
$V_{GP} = 0.60 \phi F_y A_g$		_	n (I4-3)	AISC 360-	-15
	_		4. (* T-2 <i>)</i> ,		15
Resistance factor, φ	=	1.00		1.00	
Nominal yield stress, F <sub>y</sub>	=	50.0	ksi	344.7	MPa

Expected yield stress, R <sub>y</sub> F <sub>y</sub>	=	55.0	ksi	379.2	MPa				
Measured yield stress, Fym	=	53.7	ksi	370.5	MPa				
Plate thickness, t <sub>pl</sub>	=	5/8	in.	15.74	mm				
Plate depth, d <sub>pl</sub>	=	18.0	in.	457.2	mm				
Gross plate area, Ag	=	11.151	in. <sup>2</sup>	7194	$\mathrm{mm}^2$				
Factored shear yielding resistance, V <sub>GP</sub>	=	334.5	kips	1488	kN				
Expected yielding strength, $V_{GP}$ $(\phi=1.0,R_yF_y)$	=	368.0	kips	1637	kN				
Shear yielding resistance, V <sub>GP</sub>	=	359.5	kips	1599	kN				
She	ear I	Rupture							
$V_N = 0.60 \phi F_u A_{net}$			Eq. (J	4-4), AISC	360-15				
Resistance Factor, φ	=	0.75		0.75					
Nominal tensile strength, F <sub>u</sub>	=	65.0	ksi	448.2	MPa				
Expected tensile strength, R <sub>y</sub> F <sub>u</sub>	=	78.0	ksi	537.8	MPa				
Measured tensile strength, F <sub>um</sub>	=	75.1	ksi	518.0	MPa				
Plate thickness, t <sub>pl</sub>	=	3/8	in.	9.76	mm				
Net depth, d <sub>net</sub>	=	12.4	in.	311.9	mm				
Net area, A <sub>net</sub>	=	7.666	in. <sup>2</sup>	4907	$mm^2$				
Factored rupture strength, $V_{\mathrm{N}}$	=	224.2	kips	990	kN				
Expected rupture strength, $V_N$ ( $\phi$ =1.0, $R_YFu$ )	=	358.8	kips	1583	kN				
Measured rupture strength, V <sub>N</sub>	=	345.6	kips	1525	kN				
Block Shear Rupture									
•	Shea		•						
•		ır Ruptu	re	(4-5) AISC	360-15				
Block		ır Ruptu	re	(4-5) AISC 0.75	360-15				
$\begin{aligned} & \textbf{Block} \\ & V_{BS} \!\!=\!\! \phi_u \! [U_{bs} A_{nt} F_u \!\!+\!\! min(0.6 A_{gv} F_y \!\!\! \\ \end{aligned} \label{eq:VBS}$	,0.6	r Ruptui A <sub>nv</sub> F <sub>U</sub> )]	re	ŕ	360-15				
$\begin{aligned} & \textbf{Block} \\ & V_{BS} \!\!=\!\! \phi_u \! [U_{bs} A_{nt} F_u \!\!+\!\! \min(0.6 A_{gv} F_y \\ & \text{Resistance Factor, } \phi_U \end{aligned}$	,0.6 <i>A</i> =	ar Ruptur A <sub>nv</sub> F <sub>U</sub> )] 0.75	re	0.75	2 360-15 MPa				
$\begin{aligned} & \textbf{Block} \\ & V_{BS} \!\!=\!\! \phi_u [U_{bs} A_{nt} F_u \!\!+\!\! \min(0.6 A_{gv} F_y \\ & \text{Resistance Factor, } \phi_U \\ & \text{Efficiency Factor, } U_{bs} \end{aligned}$	,0.6A = =	ar Ruptur $A_{nv}F_{U})] = 0.75 = 0.5$	re Eq. (J	0.75 0.5					
$\begin{aligned} \textbf{Block} \\ V_{BS} = & \phi_u [U_{bs} A_{nt} F_u + min(0.6 A_{gv} F_y \\ & \text{Resistance Factor, } \phi_U \\ & \text{Efficiency Factor, } U_{bs} \\ & \text{Nominal yield stress, } F_y \end{aligned}$	= = = =	AnvF <sub>U</sub> )] 0.75 0.5 50.0	Eq. (J	0.75 0.5 344.7	MPa				
$\begin{aligned} \textbf{Block} \\ V_{BS} = & \phi_u [U_{bs} A_{nt} F_u + min(0.6 A_{gv} F_y \\ & \text{Resistance Factor, } \phi_U \\ & \text{Efficiency Factor, } U_{bs} \\ & \text{Nominal yield stress, } F_y \\ & \text{Nominal tensile strength, } F_u \end{aligned}$	= = = = =	nr Ruptur 0.75 0.5 50.0 65.0	Eq. (J	0.75 0.5 344.7 448.2	MPa MPa				
$\begin{aligned} \textbf{Block} \\ V_{BS} = & \phi_u [U_{bs} A_{nt} F_u + \min(0.6 A_{gv} F_y \\ & \text{Resistance Factor, } \phi_U \\ & \text{Efficiency Factor, } U_{bs} \\ & \text{Nominal yield stress, } F_y \\ & \text{Nominal tensile strength, } F_u \\ & \text{Expected yield stress, } R_y F_y \end{aligned}$	= = = = = =	AnvFu)] 0.75 0.5 50.0 65.0 55.0	Eq. (J ksi ksi ksi	0.75 0.5 344.7 448.2 379.0	MPa MPa MPa				
$\label{eq:block} \begin{aligned} \textbf{Block} \\ V_{BS} = & \phi_u [U_{bs} A_{nt} F_u + \min(0.6 A_{gv} F_y \\ & \text{Resistance Factor, } \phi_U \\ & \text{Efficiency Factor, } U_{bs} \\ & \text{Nominal yield stress, } F_y \\ & \text{Nominal tensile strength, } F_u \\ & \text{Expected yield stress, } R_y F_y \\ & \text{Expected tensile strength, } R_u F_u \end{aligned}$	= = = = = = = = = = = = = = = = = = =	nr Ruptur 0.75 0.5 50.0 65.0 58.0 78.0	Eq. (J ksi ksi ksi ksi	0.75 0.5 344.7 448.2 379.0 537.8	MPa MPa MPa MPa				
$\label{eq:block} \begin{aligned} \textbf{Block} \\ V_{BS} = & \phi_u [U_{bs} A_{nt} F_u + \min(0.6 A_{gv} F_y \\ & \text{Resistance Factor, } \phi_U \\ & \text{Efficiency Factor, } U_{bs} \\ & \text{Nominal yield stress, } F_y \\ & \text{Nominal tensile strength, } F_u \\ & \text{Expected yield stress, } R_y F_y \\ & \text{Expected tensile strength, } R_u F_u \\ & \text{Measured yield stress, } F_{ym} \end{aligned}$	= = = = = = = = = = = = = = = = = = =	AnvFu)] 0.75 0.5 50.0 65.0 55.0 78.0 53.7	ksi ksi ksi ksi ksi	0.75 0.5 344.7 448.2 379.0 537.8 370.5 518.0	MPa MPa MPa MPa MPa				
$\label{eq:bounds} \textbf{Block} \\ V_{BS} \!\!=\!\! \phi_u [U_{bs} A_{nt} F_u \!\!+\!\! \min(0.6 A_{gv} F_y \\ \text{Resistance Factor, } \phi_U \\ \text{Efficiency Factor, } U_{bs} \\ \text{Nominal yield stress, } F_y \\ \text{Nominal tensile strength, } F_u \\ \text{Expected yield stress, } R_y F_y \\ \text{Expected tensile strength, } R_u F_u \\ \text{Measured yield stress, } F_{ym} \\ \text{Measured tensile strength, } F_{um} \\ \text{Net area in tension, } A_{nt} \\ \end{cases}$	= = = = = = = = = = = = = = = = = = =	AnvFu)] 0.75 0.5 50.0 65.0 55.0 78.0 53.7 75.1	ksi ksi ksi ksi ksi ksi	0.75 0.5 344.7 448.2 379.0 537.8 370.5 518.0 818	MPa MPa MPa MPa MPa				
$\begin{aligned} \textbf{Block} \\ V_{BS} = & \phi_u [U_{bs} A_{nt} F_u + \min(0.6 A_{gv} F_y \\ & \text{Resistance Factor, } \phi_U \\ & \text{Efficiency Factor, } U_{bs} \\ & \text{Nominal yield stress, } F_y \\ & \text{Nominal tensile strength, } F_u \\ & \text{Expected yield stress, } R_y F_y \\ & \text{Expected tensile strength, } R_u F_u \\ & \text{Measured yield stress, } F_{ym} \\ & \text{Measured tensile strength, } F_{um} \end{aligned}$	= = = = = = = = = = = = = = = = = = =	AnvFu)] 0.75 0.5 50.0 65.0 55.0 78.0 53.7 75.1 1.278	Eq. (J ksi ksi ksi ksi ksi ksi in. <sup>2</sup>	0.75 0.5 344.7 448.2 379.0 537.8 370.5 518.0 818 13189	MPa MPa MPa MPa MPa MPa mm²				
$\label{eq:bounds} \textbf{Block} \\ V_{BS} \!\!=\!\! \phi_u [U_{bs} A_{nt} F_u \!\!+\!\! \min(0.6 A_{gv} F_y \\ \text{Resistance Factor, } \phi_U \\ \text{Efficiency Factor, } U_{bs} \\ \text{Nominal yield stress, } F_y \\ \text{Nominal tensile strength, } F_u \\ \text{Expected yield stress, } R_y F_y \\ \text{Expected tensile strength, } R_u F_u \\ \text{Measured yield stress, } F_{ym} \\ \text{Measured tensile strength, } F_{um} \\ \text{Net area in tension, } A_{nt} \\ \text{Gross area in shear, } A_{gv} \\ \text{Net area in shear, } A_{nv} \\ \text{Factored block shear rupture,} \\ \end{aligned}$	,0.6A = = = = = = = = = = =	AnvFu)] 0.75 0.5 50.0 65.0 55.0 78.0 53.7 75.1 1.278 20.443	ksi ksi ksi ksi ksi in. <sup>2</sup> in. <sup>2</sup>	0.75 0.5 344.7 448.2 379.0 537.8 370.5 518.0 818	MPa MPa MPa MPa MPa MPa mm² mm²				
$\begin{aligned} & \textbf{Block} \\ & V_{BS} \!\!=\!\! \phi_u [U_{bs} A_{nt} F_u \!\!+\!\! \min(0.6 A_{gv} F_y \\ & \text{Resistance Factor, } \phi_U \\ & \text{Efficiency Factor, } U_{bs} \\ & \text{Nominal yield stress, } F_y \\ & \text{Nominal tensile strength, } F_u \\ & \text{Expected yield stress, } R_y F_y \\ & \text{Expected tensile strength, } R_u F_u \\ & \text{Measured yield stress, } F_{ym} \\ & \text{Measured tensile strength, } F_{um} \\ & \text{Measured tensile strength, } F_{um} \\ & \text{Net area in tension, } A_{nt} \\ & \text{Gross area in shear, } A_{gv} \\ & \text{Net area in shear, } A_{nv} \\ & \text{Factored block shear rupture,} \\ & V_{BS} \\ & \text{Expected block shear rupture,} \end{aligned}$	,0.6A = = = = = = = = = = = = = = = = = = =	AnvFu)] 0.75 0.5 50.0 65.0 55.0 78.0 53.7 75.1 1.278 20.443 14.055	ksi ksi ksi ksi ksi in. <sup>2</sup> in. <sup>2</sup>	0.75 0.5 344.7 448.2 379.0 537.8 370.5 518.0 818 13189 8996	MPa MPa MPa MPa MPa MPa mm² mm²				
$\label{eq:bounds} \textbf{Block} \\ V_{BS} \!\!=\!\! \phi_u [U_{bs} A_{nt} F_u \!\!+\!\! \min(0.6 A_{gv} F_y \\ \text{Resistance Factor, } \phi_U \\ \text{Efficiency Factor, } U_{bs} \\ \text{Nominal yield stress, } F_y \\ \text{Nominal tensile strength, } F_u \\ \text{Expected yield stress, } R_y F_y \\ \text{Expected tensile strength, } R_u F_u \\ \text{Measured yield stress, } F_{ym} \\ \text{Measured tensile strength, } F_{um} \\ \text{Net area in tension, } A_{nt} \\ \text{Gross area in shear, } A_{gv} \\ \text{Net area in shear, } A_{nv} \\ \text{Factored block shear rupture, } \\ V_{BS} \\ \end{aligned}$	,0.6A = = = = = = = = = = = = = = = = = = =	AnvFu)] 0.75 0.5 50.0 65.0 55.0 78.0 53.7 75.1 1.278 20.443 14.055 442.2	ksi ksi ksi ksi ksi in.² in.² kips	0.75 0.5 344.7 448.2 379.0 537.8 370.5 518.0 818 13189 8996 1952	MPa MPa MPa MPa MPa MPa mm² mm² kN				
$\begin{aligned} & \textbf{Block} \\ & V_{BS} \!\!=\!\! \phi_u [U_{bs} A_{nt} F_u \!\!+\!\! \min(0.6 A_{gv} F_y \\ & \text{Resistance Factor, } \phi_U \\ & \text{Efficiency Factor, } U_{bs} \\ & \text{Nominal yield stress, } F_y \\ & \text{Nominal tensile strength, } F_u \\ & \text{Expected yield stress, } R_y F_y \\ & \text{Expected tensile strength, } R_u F_u \\ & \text{Measured yield stress, } F_{ym} \\ & \text{Measured tensile strength, } F_{um} \\ & \text{Measured tensile strength, } F_{um} \\ & \text{Net area in tension, } A_{nt} \\ & \text{Gross area in shear, } A_{gv} \\ & \text{Net area in shear, } A_{nv} \\ & \text{Factored block shear rupture, } \\ & V_{BS} \\ & \text{Expected block shear rupture, } \\ & V_{BS} (\phi \!=\! 1.0, R_y F_y \& R_y F_u) \\ & \text{Measured block shear rupture, } V_{BS} \end{aligned}$	,0.6A = = = = = = = = = = = = = = = = = = =	AnvFu)] 0.75 0.5 50.0 65.0 78.0 53.7 75.1 1.278 20.443 14.055 442.2	ksi ksi ksi ksi ksi in.² in.² kips	0.75 0.5 344.7 448.2 379.0 537.8 370.5 518.0 818 13189 8996 1952 3123	MPa MPa MPa MPa MPa MPa mm² mm² kN				
$\begin{aligned} & \textbf{Block} \\ & V_{BS} \!\!=\!\! \phi_u [U_{bs} A_{nt} F_u \!\!+\!\! \min(0.6 A_{gv} F_y \\ & \text{Resistance Factor, } \phi_U \\ & \text{Efficiency Factor, } U_{bs} \\ & \text{Nominal yield stress, } F_y \\ & \text{Nominal tensile strength, } F_u \\ & \text{Expected yield stress, } R_y F_y \\ & \text{Expected tensile strength, } R_u F_u \\ & \text{Measured yield stress, } F_{ym} \\ & \text{Measured tensile strength, } F_{um} \\ & \text{Measured tensile strength, } F_{um} \\ & \text{Net area in tension, } A_{nt} \\ & \text{Gross area in shear, } A_{gv} \\ & \text{Net area in shear, } A_{nv} \\ & \text{Factored block shear rupture, } \\ & V_{BS} \\ & \text{Expected block shear rupture, } \\ & V_{BS} (\phi \!=\! 1.0, R_y F_y \& R_y F_u) \\ & \text{Measured block shear rupture, } V_{BS} \end{aligned}$	,0.6A = = = = = = = = = = = = = = = = = = =	AnvFu)] 0.75 0.5 50.0 65.0 78.0 53.7 75.1 1.278 20.443 14.055 442.2 707.6 681.5 ear yieldi	ksi ksi ksi ksi ksi in.² in.² kips kips	0.75 0.5 344.7 448.2 379.0 537.8 370.5 518.0 818 13189 8996 1952 3123	MPa MPa MPa MPa MPa MPa mm² mm² kN kN				
$\label{eq:bounds} \textbf{Block} \\ V_{BS} = \varphi_u [U_{bs} A_{nt} F_u + \min(0.6 A_{gv} F_y \\ \text{Resistance Factor, } \phi_U \\ \text{Efficiency Factor, } U_{bs} \\ \text{Nominal yield stress, } F_y \\ \text{Nominal tensile strength, } F_u \\ \text{Expected yield stress, } R_y F_y \\ \text{Expected tensile strength, } R_u F_u \\ \text{Measured yield stress, } F_{ym} \\ \text{Measured tensile strength, } F_{um} \\ \text{Net area in tension, } A_{nt} \\ \text{Gross area in shear, } A_{gv} \\ \text{Net area in shear, } A_{nv} \\ \text{Factored block shear rupture, } V_{BS} \\ \text{Expected block shear rupture, } V_{BS}(\phi=1.0, R_y F_y \& R_y F_u) \\ \text{Measured block shear rupture, } V_{BS}$	,0.6A = = = = = = = = = = = = = = = = = = =	AnvFu)] 0.75 0.5 50.0 65.0 78.0 53.7 75.1 1.278 20.443 14.055 442.2 707.6 681.5 ear yieldi	ksi ksi ksi ksi ksi in.² in.² kips kips	0.75 0.5 344.7 448.2 379.0 537.8 370.5 518.0 818 13189 8996 1952 3123 3008 ion 10-5	MPa MPa MPa MPa MPa MPa mm² mm² kN kN				

$V_n = 0.6F_y A_g$					
Nominal yield stress, F <sub>y</sub>	=	50.0	ksi	344.7	MPa
Expected yield stress, R <sub>y</sub> F <sub>y</sub>	=	55.0	ksi	379.0	MPa
Measured yield stress, F <sub>ym</sub>	=	53.7	ksi	370.5	MPa
Gross area of plate, A <sub>g</sub>	=	11.151	in. <sup>2</sup>	7194	mm <sup>2</sup>
Factored shear Capacity, V <sub>c</sub>	=	334.5	kips	1488	kN
Expected shear Capacity, V <sub>e</sub>	=	368.0	kips	1637	kN
Measured shear capacity, V <sub>m</sub>	=	359.5	kips	1599	kN
a distance	=	4.5	in.	114	mm
$M_c = \varphi_b M_n$		1.0	111.	111	11111
Resistance factor, $\varphi_b$	=	0.90		0.90	
$M_n = F_v Z_{pl}$		0.50		0.50	
Plastic section modulus, Z <sub>pl</sub>	=	50.179	in. <sup>3</sup>	822.28	$10^{3}$
rastic section modulus, 2pi		30.177	111.	022.20	$mm^3$
Factored moment capacity, Mc	=	2258.0	kip.in	255.1	kN.m
Expected moment capacity, Me	=	2759.8	kip.in	311.8	kN.m
Measured moment capacity, $\ensuremath{M_{m}}$	=	2696.4	kip.in	304.7	kN.m
Factored shear-flexural yielding	=	278.3	kips	1238	kN
resistance, V <sub>r</sub> Expected shear-flexural yielding	=	315.5	kips	1404	kN
resistance, $V_e$ ( $\phi$ =1.0, $R_yF_y$ )		313.3	Kips	1707	KIN
Measured shear-flexural	=	308.3	kips	1371	kN
yielding resistance, V <sub>m</sub>					
	40 D	aldina			
Pla		uckling	ISC Stack	l Manual	
		ı. (9-6), A			
Pla		ı. (9-6), A	ISC Stee h Edition		
$V_{r} = \phi_{b} \; F_{cr}  S_{net} \! / \; e \label{eq:Vr}$	Eq	i. (9-6), A (14t)		)	$10^3$ mm <sup>3</sup>
$V_r = \phi_b \; F_{cr}  S_{net} \! / \; e$ $Resistance \; Factor, \; \phi_b$	Eq	(9-6), A (14t) 0.90	h Edition	0.90	10 <sup>3</sup> mm <sup>3</sup>
$V_r = \phi_b \; F_{cr}  S_{net} / \; e$ $Resistance \; Factor, \; \phi_b$ $S_{net} = 1/6 \; t_p  h^2_{\; o}$	Eq = =	(9-6), A (14t) 0.90 33.45	h Edition	0.90 548.19	
$\begin{aligned} V_r &= \phi_b \ F_{cr}  S_{net} / \ e \\ \\ Resistance \ Factor, \ \phi_b \\ \\ S_{net} &= 1/6 \ t_p \ h^2_o \\ \\ Z_{net} &= 1/4 \ t_p \ h^2_o \end{aligned}$	Eq = = = =	(9-6), A (14t) 0.90 33.45 50.18	in. <sup>3</sup> in. <sup>3</sup>	0.90 548.19 822.28	$10^3$ mm <sup>3</sup>
$V_r = \phi_b \; F_{cr}  S_{net} / \; e$ $Resistance \; Factor, \; \phi_b$ $S_{net} = 1/6 \; t_p  h^2_o$ $Z_{net} = 1/4 \; t_p  h^2_o$ $depth \; of \; top \; cope, \; d_c$	Eq	0.90 33.45 50.18 3.2	in. <sup>3</sup> in. <sup>3</sup> in.	0.90 548.19 822.28 80.4	10 <sup>3</sup> mm <sup>3</sup> mm
$V_r = \phi_b \; F_{cr}  S_{net} / \; e$ $Resistance \; Factor, \; \phi_b$ $S_{net} = 1/6 \; t_p  h^2_{\; o}$ $Z_{net} = 1/4 \; t_p  h^2_{\; o}$ $depth \; of \; top \; cope, \; d_c$ $Beam \; Depth, \; d$	Eq	0.90 33.45 50.18 3.2 24.3	in. <sup>3</sup> in. in. in.	0.90 548.19 822.28 80.4 618.0	10 <sup>3</sup> mm <sup>3</sup> mm mm
$V_r = \phi_b \; F_{cr}  S_{net} / \; e$ $Resistance \; Factor, \; \phi_b$ $S_{net} = 1/6 \; t_p \; h^2_o$ $Z_{net} = 1/4 \; t_p \; h^2_o$ $depth \; of \; top \; cope, \; d_c$ $Beam \; Depth, \; d$ $Eccentricity, \; e$	Eq	0.90 33.45 50.18 3.2 24.3 4.5	in.3 in.3 in. in. in. in. in. in.	0.90 548.19 822.28 80.4 618.0 114.3 114.3	10 <sup>3</sup> mm <sup>3</sup> mm mm mm
$V_r = \phi_b \; F_{cr}  S_{net} / \; e$ $Resistance \; Factor, \; \phi_b$ $S_{net} = 1/6 \; t_p \; h^2_{\; o}$ $Z_{net} = 1/4 \; t_p \; h^2_{\; o}$ $depth \; of \; top \; cope, \; d_c$ $Beam \; Depth, \; d$ $Eccentricity, \; e$ $Unsupported \; Length \; of \; Plate, \; c$	Eq	0.90 33.45 50.18 3.2 24.3 4.5	in.3 in.3 in. in. in. in. in. in.	0.90 548.19 822.28 80.4 618.0 114.3 114.3	10 <sup>3</sup> mm <sup>3</sup> mm mm mm
$V_r = \phi_b \; F_{cr}  S_{net} / \; e$ $Resistance \; Factor, \; \phi_b$ $S_{net} = 1/6 \; t_p \; h^2_{\; o}$ $Z_{net} = 1/4 \; t_p \; h^2_{\; o}$ depth of top cope, $d_c$ $Beam \; Depth, \; d$ $Eccentricity, \; e$ $Unsupported \; Length \; of \; Plate, \; c$ $d_c < 0.2d \; \& \; c < 2d?$ $f_d \; equation \; (Cheng \; et \; al. \; 1984)$	Eq	1. (9-6), A (14t) 0.90 33.45 50.18 3.2 24.3 4.5 4.5 YES, fd 6	in.3 in.3 in. in. in. in. equation	0.90 548.19 822.28 80.4 618.0 114.3 114.3 valid	10 <sup>3</sup> mm <sup>3</sup> mm mm mm
$V_r = \phi_b \; F_{cr}  S_{net} / \; e$ $Resistance \; Factor, \; \phi_b$ $S_{net} = 1/6 \; t_p \; h^2_{\; o}$ $Z_{net} = 1/4 \; t_p \; h^2_{\; o}$ depth of top cope, $d_c$ $Beam \; Depth, \; d$ $Eccentricity, \; e$ $Unsupported \; Length \; of \; Plate, \; c$ $d_c < 0.2d \; \& \; c < 2d?$ $f_d \; equation \; (Cheng \; et \; al. \; 1984)$	Eq	1. (9-6), A (14t) 0.90 33.45 50.18 3.2 24.3 4.5 4.5 YES, fd 6	in.3 in.3 in. in. in. in. equation	0.90 548.19 822.28 80.4 618.0 114.3 114.3 valid	10 <sup>3</sup> mm <sup>3</sup> mm mm mm
$V_{r} = \phi_{b} \; F_{cr}  S_{net} / \; e$ $Resistance \; Factor, \; \phi_{b}$ $S_{net} = 1/6 \; t_{p} \; h^{2}_{o}$ $Z_{net} = 1/4 \; t_{p} \; h^{2}_{o}$ $depth \; of \; top \; cope, \; d_{c}$ $Beam \; Depth, \; d$ $Eccentricity, \; e$ $Unsupported \; Length \; of \; Plate, \; c$ $d_{c} < 0.2d \; \& \; c < 2d?$ $f_{d} \; equation \; (Cheng \; et \; al. \; 1984)$ $F_{cr} = 0.62\pi E f_{d} \; \frac{t_{w}^{2}}{ch_{0}} \leq F_{y}$	Eq	1. (9-6), A (14t) 0.90 33.45 50.18 3.2 24.3 4.5 4.5 YES, f <sub>d</sub> 6	in.3 in.3 in. in. in. in. equation  Eq. Steel Mar	0.90 548.19 822.28 80.4 618.0 114.3 114.3 valid (9-12) nual (14th 1	10 <sup>3</sup> mm <sup>3</sup> mm mm mm mm
$V_r = \phi_b \ F_{cr} \ S_{net} / \ e$ $Resistance \ Factor, \phi_b$ $S_{net} = 1/6 \ t_p \ h^2_o$ $Z_{net} = 1/4 \ t_p \ h^2_o$ $depth \ of \ top \ cope, \ d_c$ $Beam \ Depth, \ d$ $Eccentricity, \ e$ $Unsupported \ Length \ of \ Plate, \ c$ $d_c < 0.2d \ \& \ c < 2d?$ $f_d \ equation \ (Cheng \ et \ al. \ 1984)$ $F_{cr} = 0.62\pi E f_d \ \frac{t_w^2}{c h_0} \le F_y$ $Modulus \ of \ Elasticity, \ E$	Eq	1. (9-6), A (14t) 0.90 33.45 50.18 3.2 24.3 4.5 4.5 YES, f <sub>d</sub> 6	in.3 in.3 in. in. in. in. equation Eq. Steel Marksi	0.90 548.19 822.28 80.4 618.0 114.3 114.3 valid (9-12) nual (14th)	10 <sup>3</sup> mm <sup>3</sup> mm mm mm mm MMPa
Pla $V_r = \varphi_b \; F_{cr}  S_{net} / \; e$ Resistance Factor, $\varphi_b$ $S_{net} = 1/6 \; t_p  h^2_o$ $Z_{net} = 1/4 \; t_p  h^2_o$ depth of top cope, $d_c$ Beam Depth, $d$ Eccentricity, $e$ Unsupported Length of Plate, $c$ $d_c < 0.2d \; \& \; c < 2d?$ $f_d \; equation \; (Cheng \; et \; al. \; 1984)$ $F_{cr} = 0.62\pi E f_d \; \frac{t_w^2}{ch_0} \leq F_y$ Modulus of Elasticity, $E$ Thickness of Plate, $t_p$	Eq	1. (9-6), A (14t) 0.90 33.45 50.18 3.2 24.3 4.5 4.5 YES, f <sub>d</sub> 6	in.3 in.3 in. in. in. in. equation  Eq. Steel Marksi in	0.90 548.19 822.28 80.4 618.0 114.3 114.3 valid (9-12) nual (14th 1)	10 <sup>3</sup> mm <sup>3</sup> mm mm mm mm MM MPa mm
$V_r = \phi_b \; F_{cr}  S_{net} / \; e$ $Resistance \; Factor, \; \phi_b$ $S_{net} = 1/6 \; t_p \; h^2_o$ $Z_{net} = 1/4 \; t_p \; h^2_o$ $depth \; of \; top \; cope, \; d_c$ $Beam \; Depth, \; d$ $Eccentricity, \; e$ $Unsupported \; Length \; of \; Plate, \; c$ $d_c < 0.2d \; \& \; c < 2d?$ $f_d \; equation \; (Cheng \; et \; al. \; 1984)$ $F_{cr} = 0.62\pi E f_d \; \frac{t_w^2}{ch_0} \leq F_y$ $Modulus \; of \; Elasticity, \; E$ $Thickness \; of \; Plate, \; t_p$ $Plate \; Depth, \; h_o$	Eq	1. (9-6), A (14t) 0.90 33.45 50.18 3.2 24.3 4.5 4.5 YES, f <sub>d</sub> 6	in.3 in.3 in. in. in. in. equation  Eq. Steel Marksi in. in. in.	0.90 548.19 822.28 80.4 618.0 114.3 114.3 valid (9-12) nual (14th) 200000 15.74 457.2	10 <sup>3</sup> mm <sup>3</sup> mm mm mm mm MMPa
$V_r = \phi_b \; F_{cr}  S_{net} / \; e$ $Resistance \; Factor, \; \phi_b$ $S_{net} = 1/6 \; t_p \; h^2_o$ $Z_{net} = 1/4 \; t_p \; h^2_o$ $depth \; of \; top \; cope, \; d_c$ $Beam \; Depth, \; d$ $Eccentricity, \; e$ $Unsupported \; Length \; of \; Plate, \; c$ $d_c < 0.2d \; \& \; c < 2d?$ $f_d \; equation \; (Cheng \; et \; al. \; 1984)$ $F_{cr} = 0.62\pi E f_d \; \frac{t_w^2}{ch_0} \leq F_y$ $Modulus \; of \; Elasticity, \; E$ $Thickness \; of \; Plate, \; t_p$ $Plate \; Depth, \; h_o$	Eq	1. (9-6), A (14t) 0.90 33.45 50.18 3.2 24.3 4.5 4.5 YES, f <sub>d</sub> 6 29000 5/8 18	in.3 in.3 in. in. in. in. equation  Eq. Steel Marksi in. in. Eq.	0.90 548.19 822.28 80.4 618.0 114.3 114.3 valid (9-12) nual (14th 1)	10 <sup>3</sup> mm <sup>3</sup> mm mm mm mm MPa mm mm
Pla $V_r = \varphi_b \ F_{cr} \ S_{net} / \ e$ Resistance Factor, $\varphi_b$ $S_{net} = 1/6 \ t_p \ h^2_o$ $Z_{net} = 1/4 \ t_p \ h^2_o$ depth of top cope, $d_c$ Beam Depth, $d$ Eccentricity, $e$ Unsupported Length of Plate, $c$ $d_c < 0.2d \ \& \ c < 2d?$ $f_d \ equation \ (Cheng \ et \ al. \ 1984)$ $F_{cr} = 0.62\pi E f_d \ \frac{t_w^2}{ch_0} \le F_y$ Modulus of Elasticity, $E$ Thickness of Plate, $E$ Plate Depth, $E$ $f_d = 3.5 - 7.5(\frac{d_{ct}}{d_b})$	Eq	AISC S  AISC S  AISC S  AISC S  AISC S  AISC S	in.3 in.3 in. in. in. in. equation  Eq. Steel Marksi in. in. Eq.	0.90 548.19 822.28 80.4 618.0 114.3 114.3 valid (9-12) nual (14th) 200000 15.74 457.2 (9-13) nual (14th)	10 <sup>3</sup> mm <sup>3</sup> mm mm mm mm MPa mm mm
$V_r = \phi_b \; F_{cr}  S_{net} / \; e$ $Resistance \; Factor, \; \phi_b$ $S_{net} = 1/6 \; t_p \; h^2_o$ $Z_{net} = 1/4 \; t_p \; h^2_o$ $depth \; of \; top \; cope, \; d_c$ $Beam \; Depth, \; d$ $Eccentricity, \; e$ $Unsupported \; Length \; of \; Plate, \; c$ $d_c < 0.2d \; \& \; c < 2d?$ $f_d \; equation \; (Cheng \; et \; al. \; 1984)$ $F_{cr} = 0.62\pi E f_d \; \frac{t_w^2}{ch_0} \leq F_y$ $Modulus \; of \; Elasticity, \; E$ $Thickness \; of \; Plate, \; t_p$ $Plate \; Depth, \; h_o$	Eq	1. (9-6), A (14t) 0.90 33.45 50.18 3.2 24.3 4.5 4.5 YES, f <sub>d</sub> 6 29000 5/8 18	in.3 in.3 in. in. in. in. equation  Eq. Steel Marksi in. in. Eq.	0.90 548.19 822.28 80.4 618.0 114.3 114.3 valid (9-12) nual (14th) 200000 15.74 457.2 (9-13)	10 <sup>3</sup> mm <sup>3</sup> mm mm mm mm MPa mm mm

Nominal yield stress, F <sub>y</sub>	=	50.0	ksi	344.7	MPa
Expected yield stress, R <sub>y</sub> F <sub>y</sub>	=	55.0	ksi	379.2	MPa
Measured yield stress, F <sub>ym</sub>	=	53.7	ksi	370.5	MPa
Factored buckling resistance	=	501.8	kips	2232	kN
Expected buckling resistance $(R_yF_y, \varphi=1.0)$	=	613.3	kips	2728	kN
Measured buckling resistance	=	599.2	kips	2665	kN
Q equation (classical plate b	uckli	ing)			
$F_{cr} = F_{v}Q$			Ea	(9-14)	
- u - y Q		AISC S	-	iual (14th 1	Edition)
$h_{\circ}$ $F_{\circ}$			Eq.	(9-18)	
$\lambda = \frac{h_0}{10t_w} \sqrt{\frac{F_y}{475 + 280(\frac{h_0}{c})^2}}$		AISC S	Steel Mar	nual (14th 1	Edition)
Nominal Yield Stress of Plate,	=	50	ksi	345	MPa
F <sub>Y</sub> Expected Yield Stress, R <sub>Y</sub> F <sub>Y</sub>	=	55	ksi	379	MPa
Yield Stress of Plate, F <sub>Y</sub>	=	53.7	ksi	370.5	MPa
Nominal slenderness of coped	=	0.29	noi	370.5	wii a
section, $\lambda$		0.29			
Expected slenderness of coped section, $\lambda_e$	=	0.31			
Measured slenderness of coped section, $\lambda_m$	=	0.30			
Nominal strength reduction factor, Q	=	1.00			
Expected strength reduction factor, Q <sub>e</sub>	=	1.00			
Measured strength reduction factor, Q <sub>m</sub>	=	1.00			
Nominal critical stress, F <sub>cr</sub>	=	50.0	ksi	344.7	MPa
Expected critical stress, F <sub>cr,e</sub>	=	55.0	ksi	379.2	MPa
Measured critical stress, F <sub>cr,m</sub>	=	53.7	ksi	370.5	MPa
Factored buckling resistance, V <sub>r</sub>	=	501.8	kips	2232	kN
Expected buckling resistance,	=	613.3	kips	2728	kN
$V_{r,e} (\phi=1.0, R_y F_y)$ Measured buckling resistance,	=	599.2	kips	2665	kN
$V_{r,m}(\phi=1.0,F_{ym})$		a	F11	100000	
Rectangular Bar Buckling		Secti	on FII, A	AISC 360-1	15
$M_n(cd/t^2)$					
Nominal yield stress, F <sub>y</sub>	=	50.0	ksi	344.7	MPa
Expected yield stress, R <sub>y</sub> F <sub>y</sub>	=	55.0	ksi	379.2	MPa
Measured yield stress, F <sub>ym</sub>	=	53.7	ksi	370.5	MPa
С	=	4 1/2	in.	114	mm
d	=	18.0	in.	457.2	mm
t	=	5/8	in.	15.74	mm
$\lambda = cd/t^2$	=	211		211	
Nominal 0.08 E/F <sub>y</sub>	=	46		46	
Expected 0.08 E/F <sub>y</sub>	=	42		42	

Measured 0.08 E/F <sub>y</sub>	=	43		43	
Nominal 1.9 E/F <sub>y</sub>	=	1102		1102	
Expected 1.9 E/F <sub>y</sub>	=	1002		1002	
Measured 1.9 E/F <sub>y</sub>	=	1025		1025	
$C_b = \left[ 3 + \ln(\frac{a}{d_b}) \right] (1 - \frac{d_{ct}}{d_b}) \ge 1.84$		AISC St	Eq. (9 eel Manu	-15) ual (15 <sup>th</sup> Ed	ition)
$\mathrm{C}_{\mathrm{b}}$	=	1.84		1.84	
Factored buckling resistance, V <sub>r</sub>	=	501.8	kips	2232	kN
Expected buckling resistance, $V_{re}(\phi=1.0, R_yF_y)$ Measured buckling resistance,	=	613.3 599.2	kips kips	2728 2665	kN kN
$V_{\rm rm}$		377.2	трз	2002	1111
Weld to S	uppo	orting Ele	ement		
$D_{\min} = 5/8 t_{pl}$			Sectio		
Thickness of Plate, tp	=	AISC St 5/8	eel Manu in.	al (15 <sup>th</sup> Edi 15.74	ition) mm
Minimum Weld Thickness, D <sub>min</sub>	=	0.387	in.	9.83	mm
Take Weld Thickness, D <sub>w</sub>	=	0.367	in.	10.40	mm
Longitudinal Length of Weld, L		17.24	in.	438.0	mm
$V_{\rm w} = 2  \phi_{\rm w}  0.6  F_{\rm EXX}  0.707  D_{\rm w}  (1)$				Eq. (J2-	
$\mathbf{v}_{\mathrm{W}} = 2 \; \mathbf{\psi}_{\mathrm{W}} \; 0.0 \; 1 \; \mathbf{E} \mathbf{\chi} \mathbf{\chi} \; 0.707 \; \mathbf{D}_{\mathrm{W}} (1)$	.0 1 0	.5 3111 0	,	AISC 360	
$X_{c}$		0.00	in.	0.0	mm
$Y_c$		8.62	in.	219	mm
aL		6.0	in.	152.4	mm
K		0		0	
a		0.35		0.35	
Factored Weld Resistance, $V_{\rm w}$					
$Vw=2*CC_1DL(\phi_w=0.75)$			Table	-	
D-D/(1/16)			eel Manu	al (15th Ed	ition)
D=Dw/(1/16)		6.61		6.61	
$C_1$		1.00		1.00	
$C_1$ (Measured)		1.27		1.27	
al		0.30			
a2 C1-1		0.40			
		3.09			
C1-2 C		2.66			
		2.88		0.75	
Resistance Factor, φ <sub>w</sub>	=	0.75	1:	0.75	М
Nominal ultimate strength, F <sub>EXX</sub>	=	71.1	ksi	490.0	Mpa
Measured ultimate strength, $F_{EXX}$	=	89.9	ksi	620.0	Mpa
Factored Weld Resistance, V <sub>w</sub>	=	245.1	kips	1090	kN
Expected Weld Strength, $V_w$ ( $\phi$ =1.0)	=	326.8	kips	1454	kN
Expected Weld Strength, V <sub>w</sub> (measured properties)	=	412.2	kips	1834	kN



Failure Modes	Factored		Expected		Measure	
	kips	kN	kips	kN	kips	kN
Shear -flexural yielding resistance, Vr	278.3	1238	315.5	1404	308.3	1371
Shear yielding resistance, V <sub>G</sub>	334.5	1488	368.0	1637	359.5	1599
Block shear rupture resistance, V <sub>bs</sub>	442.2	1952	707.6	3123	681.5	3008
Shear rupture strength over net area, V <sub>n</sub>	224.2	990	358.8	1583	345.6	1525
Plate buckling(f <sub>d</sub> equation)	501.8	2232	613.3	2728	599.2	2665
Plate buckling(Q equation)	501.8	2232	613.3	2728	599.2	2665
Rectangular bar buckling	501.8	2232	613.3	2728	599.2	2665
Bearing resistance, B <sub>r</sub>	279.6	1200	410.1	1760	450.7	1934
Shear resistance of bolts, V <sub>r</sub>	272.7	1213	404.0	1797		
Weld resistance, V <sub>w</sub>	245.1	1090	326.8	1454	412.2	1834

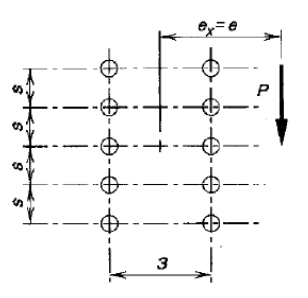
#### **Specimen BG3-2-13-200C**

#### **Configuration parameter**

Supporting girder	W610×125								
Supported beam		W310×76							
Offset of bolt group, a	=	4 1/2	in.	114.3	mm				
Bolt diameter, d <sub>b</sub>	=	3/4	in.	19.1	mm				
Bolt diameter, d <sub>h</sub>	=	13/16	in.	21.1	mm				
Number of bolt lines, m	=	2		2					
Number of bolts rows, n	=	3		3					
Plate Depth, d	=	9.0	in.	228.6	mm				
Plate Depth in Girder, dg	=	22.6	in	573	mm				

#### **Bolt Shear & Bolt Bearing**

Compute ICR coefficient (C)	Table 7-8				
. ,			AISC Ha	ndbook	
			$(15^{th} Ve$	rsion)	
Number of bolt lines, m	=	2		2	
Moment arm, e	=	7.75	in.	196.9	mm
gage, s	=	3.0	in.	76.2	mm
Pitch, p	=	3.0	in.	76.2	mm
Vertical edge distances	=	1 1/2	in.	38.1	mm
Horizontal edge distances	=	1 1/2	in.	38.1	mm
Number of bolt rows, n	=	3		3	
L1	=	7.0	in.	177.8	mm
C1	=	1.99		1.99	
L2	=	8.0	in.	203.2	mm
C2	=	1.78		1.78	
ICR coefficient (C)	=	1.83		1.83	



#### **Bolt Shear**

$V_r = \phi_V \phi_b \phi_t A_b (0.625 F_u) C$	Eq. (J3-1), AISC 360-15					
Reduction factor for shear	=	0.75		0.75		
rupture, $\phi_v$ Reduction factor for uneven force distribution, $\phi_d$	=	0.9		0.9		
Reduction factor for shear plan are not excluded from the threaded part, $\varphi_t$	=	1.0		1.0		
Number of shear planes, m	=	1.0		1.0		
Bolt area, A <sub>b</sub>	=	0.442	in. <sup>2</sup>	285	$\mathrm{mm}^2$	
Nominal ultimate strength of bolts, F <sub>U</sub>	=	150	ksi	1034.2	MPa	
Factored bolt group capacity, V <sub>r</sub>	=	51.2	kips	228	kN	
Expected bolt group capacity, $V_e(\phi_v=\phi_d=1.0)$	=	75.9	kips	337	kN	

$B_r=3\phi_{br}d_bmin[(tF_u)_{plate},(tF_u)_{web}]$		Eq. (J3	-10), AISC 360-15
C			
Modification factor, $\phi_{br}$	=	0.75	0.75

Plate thickness, t <sub>p</sub>	=	1/2	in.	12.84	mm
Beam web thickness, t <sub>w</sub>	=	0.395	in.	10.04	mm
Bolt Diameter, d <sub>b</sub>	=	3/4	in.	19.05	mm
Clear edge distance	=	1.09	in.	27.58	mm
<u> </u>	=	65.0	ksi	448.2	MPa
Nominal tensile strength of plate, $F_{u,plate}$	_	03.0	KSI	440.2	MPa
Nominal tensile strength of beam $F_{u,beam}$	=	65.0	ksi	448.2	MPa
Expected plate strength, $R_y F_{u,plate}$	=	78.0	ksi	537.8	MPa
Expected beam strength, $R_y F_{u,beam}$	=	72.0	ksi	495.0	MPa
Tensile strength of plate, F <sub>u,plate</sub>	=	73.7	ksi	508.0	MPa
Tensile strength of beam F <sub>u,beam</sub>	=	71.8	ksi	495.0	MPa
Factored bearing resistance, B <sub>r</sub>	=	58.2	kips	257	kN
			•		
Expected bearing strength, $B_r$ $(\phi=1.0,R_yF_u)$	=	85.3	kips	377	kN
Measured bearing resistance, B <sub>r</sub>	=_	85.3	kips	377	kN
_	te D	uctility			
$t_{pmax}=6M_{max}/F_yd_{pl}^2$		4100		(10-5)	3.10.0
$\mathbf{M} = \mathbf{F} / \alpha (\mathbf{A} C')$		AISC	Steel Mar	nual (15 <sup>th</sup> I	Edition)
$M_{max}=F_{nv}/\phi_d(A_bC')$ Bolt Shear Strength, $F_{nV}$	=	84.4	ksi	581.7	MPa
Bolt Area, A <sub>b</sub>	=	0.442	in. <sup>2</sup>	285	mm <sup>2</sup>
Compute ICR coefficient for		0.772		le 7-8	111111
moment only case (C')		AISC		nual (15 <sup>th</sup> I	Edition)
Number of bolt lines, m	=	2	Steel Mai	2	Januarij
Column spacing	=	3	in.	<del>-</del> 76	mm
Row spacing, s	=	3	in.	76	mm
Number of bolts rows, n	=	3		3	
ICR coefficient, C'	=	15.8		15.8	
$M_{ m max}$	=	654.1	kip.in	73.9	kN.m
Nominal yield stress, F <sub>y</sub>	=	50.0	kips	344.7	MPa
Expected yield stress, R <sub>y</sub> F <sub>y</sub>	=	55.0	kips	379.2	MPa
Measured yield stress, F <sub>ym</sub>	=	62.6	kips	432.0	MPa
Plate depth, d	=	9.0	in.	228.6	mm
Plate thickness, t <sub>pl</sub>		0.506	in.	12.84	mm
Maximum plate thickness, t <sub>max</sub>	=	0.969	in.	24.61	mm
$(F_y)$					
Is this requirement satisfied? $(t_p < t_{max})$		Yes			
Maximum plate thickness, $t_{max}$ $(R_y F_y)$	=	0.881	in.	22.37	mm
Is this requirement satisfied? (tp		Yes			
< t <sub>max</sub> )  Maximum plate thickness, t <sub>max</sub>	=	0.773	in.	19.64	mm
$(F_{ym})$ Is this requirement satisfied? $(t_p)$		Yes			
< t <sub>max</sub> )	oor L	ielding			
	cai I	_	a (IA 2)	A I C C 2 C O	1.5
$V_{GP} = 0.60 \phi F_y A_g$ Resistance factor, $\phi$	=	1.00	q. (J4-3), .	AISC 360- 1.00	·13
·					

Nominal yield stress, F <sub>y</sub>	=	50.0	ksi	344.7	MPa
Expected yield stress, R <sub>y</sub> F <sub>y</sub>	=	55.0	ksi	379.2	MPa
Measured yield stress, Fym	=	62.7	ksi	432.0	MPa
Plate thickness, t <sub>pl</sub>	=	1/2	in.	12.84	mm
Plate depth, d <sub>pl</sub>	=	9.0	in.	228.6	mm
Gross plate area, Ag	=	4.550	in. <sup>2</sup>	2935	$\mathrm{mm}^2$
Factored shear yielding	=	136.5	kips	607	kN
resistance, $V_{GP}$ Expected yielding strength, $V_{GP}$ $(\phi=1.0,R_{\nu}F_{\nu})$	=	150.1	kips	668	kN
Shear yielding resistance, $V_{GP}$	=	171.0	kips	761	kN
	ear F	Rupture	1		
$V_N=0.60 \phi F_u A_{net}$		<b>-</b>	Eg. (J	4-4), AISC	360-15
Resistance Factor, φ	=	0.75	1 (	0.75	
Nominal tensile strength, F <sub>u</sub>	=	65.0	ksi	448.2	MPa
Expected tensile strength, R <sub>y</sub> F <sub>u</sub>	=	78.0	ksi	537.8	MPa
Measured tensile strength, F <sub>um</sub>	=	73.7	ksi	508.0	MPa
Plate thickness, t <sub>pl</sub>	=	1/2	in.	12.84	mm
Net depth, d <sub>net</sub>	=	6.6	in.	165.5	mm
Net area, A <sub>net</sub>	=	3.317	in. <sup>2</sup>	2124	$mm^2$
Factored rupture strength, V <sub>N</sub>	=	97.0	kips	428	kN
Expected rupture strength, $V_N$	=	155.3	kips	685	kN
$(\varphi=1.0,R_YFu)$			-		
Measured rupture strength, V <sub>N</sub>	=	146.7	kips	648	kN
		r Ruptu			
$V_{BS} = \varphi_u[U_{bs}A_{nt}F_u + min(0.6A_{gv}F_y)]$	,0.6A	$I_{nv}F_{U})]$	Eq. (J	(4-5) AISC	360-15
Resistance Factor, φ <sub>U</sub>	=	0.75		0.75	
Efficiency Factor, U <sub>bs</sub>	=	0.5		0.5	
Nominal yield stress, F <sub>y</sub>	=	50.0	ksi	344.7	MPa
Nominal tensile strength, Fu	=	65.0	ksi	448.2	MPa
Expected yield stress, R <sub>y</sub> F <sub>y</sub>	=	55.0	ksi	379.0	MPa
Expected tensile strength, R <sub>u</sub> F <sub>u</sub>	=	78.0	ksi	537.8	MPa
Measured yield stress, Fym	=	62.7	ksi	432.0	MPa
Measured tensile strength, F <sub>um</sub>	=	73.7	ksi	508.0	MPa
Net area in tension, A <sub>nt</sub>	=	1.106	in. <sup>2</sup>	708.1	$mm^2$
Gross area in shear, Agv	=	7.583	in. <sup>2</sup>	4892.0	$mm^2$
Net area in shear, $A_{nv}$	=	5.529	in. <sup>2</sup>	3540.6	$mm^2$
Factored block shear rupture, $V_{\text{BS}}$	=	188.7	kips	833	kN
Expected block shear rupture, $V_{BS}(\phi=1.0, R_yF_y\&R_yF_u)$	=	293.4	kips 	1320	kN
Measured block shear rupture, V <sub>BS</sub>	=	285.2	kips •	1259	kN
	al-sh	ear yield	_	. 10.7	
$(V_r/V_c)^2 + (V_r e/M_c)^2 = 1$		AISC		ion 10-5 nual (15 <sup>th</sup> H	Edition)
$V_{c} \equiv \omega_{c} V_{c}$		1110C L	Jecoi iviai	(1.2 I	Zaiu011 <i>)</i> ,

 $V_c\!=\!\phi_v\,V_n$ 

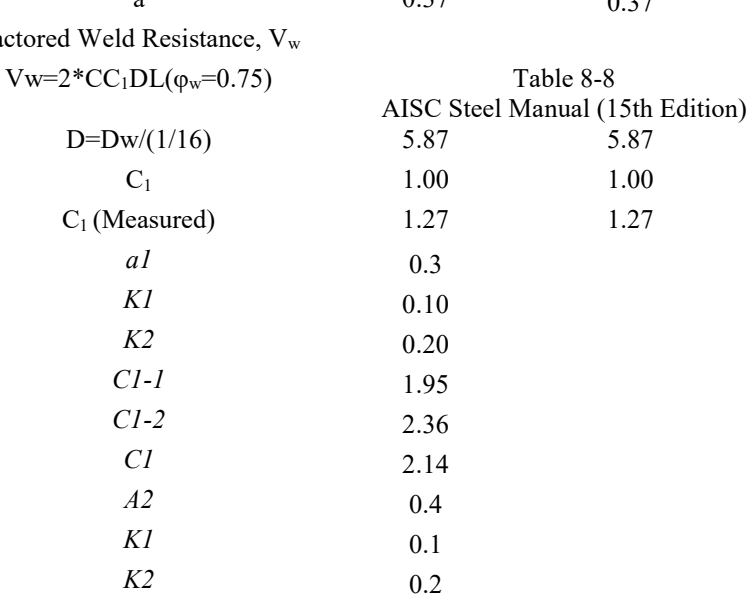
Resistance Factor, $\phi_v$	=	1.00		1.00	
$V_n = 0.6F_y A_g$					
Nominal yield stress, F <sub>y</sub>	=	50.0	ksi	344.7	MPa
Expected yield stress, R <sub>y</sub> F <sub>y</sub>	=	55.0	ksi	379.0	MPa
Measured yield stress, Fym	=	62.7	ksi	432.0	MPa
Gross area of plate, Ag	=	4.550	in. <sup>2</sup>	2935	$\text{mm}^2$
Factored shear Capacity, Vc	=	136	kips	607	kN
Expected shear Capacity, Ve	=	150	kips	668	kN
Measured shear capacity, V <sub>m</sub>	=	171	kips	761	kN
a distance	=	6.25	in.	158.8	mm
$M_c = \phi_b  M_n$					
Resistance factor, φ <sub>b</sub>	=	0.90		0.90	
$M_n = F_y Z_{pl}$					
Plastic section modulus, Z <sub>pl</sub>	=	10.237	in. <sup>3</sup>	167.75	$10^3 \\ mm^3$
Factored moment capacity, Mc	=	461	kip.in	52	kN.m
Expected moment capacity, Me	=	563	kip.in	64	kN.m
Measured moment capacity, $M_{\text{m}}$	=	641	kip.in	72	kN.m
Factored shear-flexural yielding resistance, V <sub>r</sub>	=	64.9	kips	288	kN
Expected shear-flexural yielding resistance, V <sub>e</sub> (φ=1.0, R <sub>y</sub> F <sub>y</sub> )	=	77.2	kips	344	kN
Measured shear-flexural yielding resistance, V <sub>m</sub>	=	88.0	kips	391	kN
	te B	uckling			
$V_r = \phi_b \; F_{cr} \; S_{net} \! / \; e$	Eq	ı. (9-6), A	ISC Steel h Edition		
Resistance Factor, φ <sub>b</sub>	=	0.90	ii Edition	0.90	
$S_{net} = 1/6 t_p h^2_o$	=	6.82	in. <sup>3</sup>	111.8	$10^3$ mm <sup>3</sup>
$Z_{\text{net}} = 1/4 t_{\text{p}} h^2_{\text{o}}$	=	10.24	in. <sup>3</sup>	167.7	$10^3$ mm <sup>3</sup>
depth of top cope, d <sub>c</sub>	=	1.6	in.	40	mm
Beam Depth, d	=	12.2	in.	309.0	mm
Eccentricity, e	=	6 1/4	in.	158.8	mm
Unsupported Length of Plate, c	=	6 1/4	in.	158.8	mm
$d_c < 0.2d \& c < 2d$ ?		YES, $f_d$			
f <sub>d</sub> equation (Cheng et al. 1984)		1 22, 1u		, 2227 22	
			Ea.	(9-12)	
$F_{cr} = 0.62\pi E f_d \frac{t_w^2}{ch_0} \le F_y$		AISC S	-	iual (14th 1	Edition)
Modulus of Elasticity, E	=	29000	ksi	200000	MPa
Thickness of Plate, tp	=	1/2	in.	12.84	mm
Plate Depth, ho	=	9	in.	228.6	mm
$f_d = 3.5 - 7.5(\frac{d_{ct}}{d_b})$		AISC S	-	(9-13) nual (14th 1	Edition)
Adjustment Factor, f <sub>d</sub>	=	2.52		2.52	

Critical Stress, F <sub>cr</sub>	=	647.4	ksi	4465	MPa
Nominal yield stress, F <sub>y</sub>	=	50.0	ksi	344.7	MPa
Expected yield stress, R <sub>y</sub> F <sub>y</sub>	=	55.0	ksi	379.2	MPa
Measured yield stress, F <sub>ym</sub>	=	62.7	ksi	432.0	MPa
Factored buckling resistance	=	73.7	kips	328	kN
Expected buckling resistance $(R_yF_y, \varphi=1.0)$	=	90.1	kips	401	kN
Measured buckling resistance	=	102.6	kips	456	kN
Q equation (classical plate b	uckli	ing)			
$F_{cr} = F_y Q$			-	(9-14)	
		AISC S		nual (14th I	Edition)
$\lambda = \frac{h_0}{10t_w} \sqrt{\frac{F_y}{475 + 280(\frac{h_0}{c})^2}}$		AISC S	-	(9-18) nual (14th I	Edition)
Nominal Yield Stress of Plate, Fy	=	50	ksi	345	MPa
Expected Yield Stress, R <sub>Y</sub> F <sub>Y</sub>	=	55	ksi	379	MPa
Yield Stress of Plate, F <sub>Y</sub>	=	62.7	ksi	432	MPa
Nominal slenderness of coped section, λ	=	0.39			
Expected slenderness of coped section, λ <sub>e</sub>	=	0.41			
Measured slenderness of coped section, $\lambda_m$	=	0.43			
Nominal strength reduction factor, Q	=	1.00			
Expected strength reduction factor, Q <sub>e</sub>	=	1.00			
Measured strength reduction factor, Q <sub>m</sub>	=	1.00			
Nominal critical stress, F <sub>cr</sub>	=	50	ksi	344.7	MPa
Expected critical stress, F <sub>cr,e</sub>	=	55	ksi	379.2	MPa
Measured critical stress, F <sub>cr,m</sub>	=	62.7	ksi	432.0	MPa
Factored buckling resistance, V <sub>r</sub>	=	73.7	kips	328	kN
Expected buckling resistance, $V_{r,e}$ ( $\phi$ =1.0, $R_vF_v$ )	=	90.1	kips	401	kN
Measured buckling resistance, $V_{r,m}(\varphi=1.0,F_{ym})$	=	102.6	kips	456	kN
Rectangular Bar Buckling		Secti	on F11, A	AISC 360-1	15
$M_n(cd/t^2)$					
Nominal yield stress, F <sub>v</sub>	=	50.0	ksi	344.7	MPa
Expected yield stress, R <sub>v</sub> F <sub>v</sub>	=	55.0	ksi	379.2	MPa
Measured yield stress, F <sub>ym</sub>	=	62.7	ksi	432.0	MPa
c	=	6 1/4	in.	158.8	mm
d	=	9.0	in.	229	mm
t	=	1/2	in.	12.84	mm
$\lambda = cd/t^2$	=	275		275	
Nominal 0.08 E/F <sub>y</sub>	=	46		46	

Factored Weld Resistance, Vw

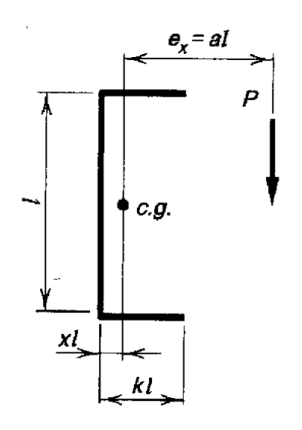
C2-1

C2-2



1.69

2.07



C2		1.86			
C		1.96			
Resistance Factor, $\phi_{\rm w}$	=	0.75		0.75	
Nominal ultimate strength, F <sub>EXX</sub>	=	71.1	ksi	490.0	Mpa
Measured ultimate strength, $F_{EXX}$	=	89.9	ksi	620.0	Mpa
Factored Weld Resistance, V <sub>w</sub>	=	350.5	kips	1559	kN
Expected Weld Strength, $V_w$ ( $\phi$ =1.0)	=	467.4	kips	2079	kN
Expected Weld Strength, V <sub>w</sub> (measured properties)	=	589.5	kips	2622	kN

Failure Modes	Factored		Expe	ected	Measured	
	kips	kN	kips	kN	kips	kN
Shear -flexural yielding resistance, Vr	64.9	288	77.2	344	88.0	391
Shear yielding resistance, VG	136.5	607	150.1	668	171.0	761
Block shear rupture resistance, vbs	188.7	833	293.4	1320	285.2	1259
Shear rupture strength over net area, vn	97.0	428	155.3	685	146.7	648
Plate buckling(f <sub>d</sub> equation)	73.7	328	90.1	401	102.6	456
Plate buckling(Q equation)	73.7	328	90.1	401	102.6	456
Rectangular bar buckling	73.7	328	90.1	401	102.6	456
Bearing resistance, b <sub>r</sub>	58.2	257	85.3	377	85.3	377
Shear resistance of bolts, vr	51.2	228	75.9	337		
Weld resistance, vw	350.5	1559	467.4	2079	589.5	2622

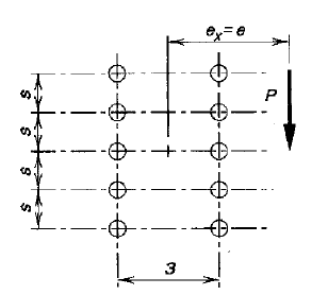
#### **Specimen BG6-2-19-500C**

#### **Configuration parameter**

Supporting girder		W760×257				
Supported beam		W610×415				
Offset of bolt group, a	=	9.2	in.	232.9	mm	
Bolt diameter, d <sub>b</sub>	=	7/8	in.	22.2	mm	
Bolt diameter, d <sub>h</sub>	=	15/16	in.	24.2	mm	
Number of bolt lines, m	=	2		2		
Number of bolts rows, n	=	6		6		
Plate Depth, d	=	18.0	in.	457.2	mm	
Plate Depth in Girder, $d_{\rm g}$	=	28.3	in	718.8	mm	

# Bolt Shear & Bolt Bearing Table 7-8

Compute ICR coefficient (C)			Tabl	e 7-8		
		AISC Handbook				
			$(15^{th} V$	ersion)		
Number of bolt lines, m	=	2	`	2		
Moment arm, e	=	10.67	in.	271.0	mm	
gage, s	=	3.0	in.	76.2	mm	
Pitch, p	=	3.0	in.	76.2	mm	
Vertical edge distances	=	1 1/2	in.	38.1	mm	
Horizontal edge distances	=	1 1/2	in.	38.1	mm	
Number of bolt rows, n	=	6		6		
L1	=	10.0	in.	254.0	mm	
C1	=	4.90		4.90		
L2	=	12.0	in.	304.8	mm	
C2	=	4.19		4.19		
ICR coefficient (C)	=	4.66		4.66		



#### **Bolt Shear**

$V_r = \phi_V \phi_b \phi_t A_b (0.625 F_u) C$	Eq. (J3-1), AISC 360-15				
Reduction factor for shear	=	0.75		0.75	
rupture, $\varphi_v$		0.0		0.0	
Reduction factor for uneven force distribution, φ <sub>d</sub>	=	0.9		0.9	
Reduction factor for shear plan are not excluded from the	=	1.0		1.0	
threaded part, $\phi_t$					
Number of shear planes, m	=	1.0		1.0	
Bolt area, A <sub>b</sub>	=	0.601	in. <sup>2</sup>	388	$\mathrm{mm}^2$
Nominal ultimate strength of bolts, F <sub>U</sub>	=	150	ksi	1034.2	MPa
Factored bolt group capacity, $V_{\rm r}$	=	177.3	kips	789	kN
Expected bolt group capacity, $V_e\left(\phi_v=\phi_d=1.0\right)$	=	262.7	kips	1169	kN

$B_r=3\phi_{br}d_bmin[(tF_u)_{plate},(tF_u)_{web}]$	Eq. (J3-10), AISC 360-15				
C					
Modification factor, $\phi_{br}$	=	0.75	0.75		

Plate thickness, t <sub>p</sub>	=	3/4	in.	19.11	mm		
Beam web thickness, t <sub>w</sub>	=	0.52	in.	29.22	mm		
Bolt Diameter, d <sub>b</sub>	=	7/8	in.	22.23	mm		
Clear edge distance	=	1.03	in.	25.99	mm		
Nominal tensile strength of	=	65.0	ksi	448.2			
plate, F <sub>u,plate</sub>	_	03.0	KSI	446.2	MPa		
Nominal tensile strength of	=	65.0	ksi	448.2	MPa		
beam $F_{u,beam}$ Expected plate strength,	=	78.0	ksi	537.8	MPa		
$R_y F_{u,plate}$ Expected beam strength,	=	72.0	ksi	495.0	MPa		
$R_y F_{u,beam}$							
Tensile strength of plate, F <sub>u,plate</sub>	=	74.0	ksi	510.0	MPa		
Tensile strength of beam $F_{u,beam}$	=	73.5	ksi	507.0	MPa		
Factored bearing resistance, B <sub>r</sub>	=	181.8	kips	1167	kN		
Expected bearing strength, B <sub>r</sub>	=	266.6	kips	1868	kN		
$(\phi=1.0,R_yF_u)$ Measured bearing resistance, $B_r$	=	273.1	kips	1771	kN		
Pl	ate l	Ductility					
$t_{pmax}=6M_{max}/F_yd_{pl}^2$			Eq.	(10-5)			
		AISC	Steel Ma	ınual (15 <sup>th</sup> 1	Edition)		
$M_{\text{max}} = F_{\text{nv}}/\phi_{\text{d}}(A_{\text{b}}C')$		0.4.4		501.5	1 (D		
Bolt Shear Strength, F <sub>nV</sub>	=	84.4	ksi in. <sup>2</sup>	581.7	MPa		
Bolt Area, A <sub>b</sub> Compute ICR coefficient for	=	0.601		388 ble 7-8	mm <sup>2</sup>		
moment only case (C')		Table 7-8 AISC Steel Manual (15 <sup>th</sup> Edition)					
Number of bolt lines, m	=	2	Steel Mid	2	Lamon		
Column spacing	=	3	in.	<del>-</del> 76	mm		
Row spacing, s	=	3	in.	76	mm		
Number of bolts rows, n	=	6		6			
ICR coefficient, C'	=	54.2		54.2			
$ m M_{max}$	=	3053.9	kip.in	345.0	kN.n		
Nominal yield stress, F <sub>y</sub>	=	50.0	kips	344.7	MPa		
Expected yield stress, R <sub>y</sub> F <sub>y</sub>	=	55.0	kips	379.2	MPa		
Measured yield stress, F <sub>ym</sub>	=	54.7	kips	377.0	MPa		
Plate depth, d	=	18	in.	457.2	mm		
Plate thickness, t <sub>pl</sub>		0.75	in.	19.11	mm		
Maximum plate thickness, $t_{max}$ ( $F_y$ )	=	1.13	in.	28.73	mm		
Is this requirement satisfied? ( $t_p$ < $t_{max}$ )		Yes		Yes			
Maximum plate thickness, t <sub>max</sub> (R <sub>y</sub> F <sub>y</sub> )	=	1.03	in.	26.12	mm		
Is this requirement satisfied? (tp		Yes		Yes			
< t <sub>max</sub> )  Maximum plate thickness, t <sub>max</sub>	=	1.03	in.	26.27	mm		
$(F_{ym})$ Is this requirement satisfied? $(t_p)$		Yes		Yes			
< t <sub>max</sub> )	100-	Viold:					
	iear	Yielding _					
$V_{GP} = 0.60 \varphi F_y A_g$		E	Eq. (J4-3),	, AISC 360	-15		

Resistance factor,  $\phi$ 

1.00

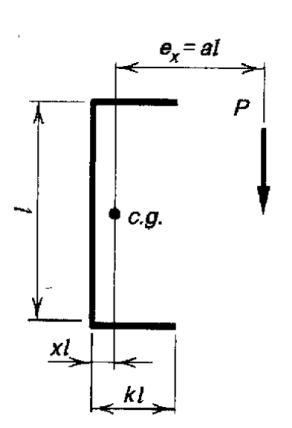
1.00

=	50.0	ksi	344.7	MPa
=	55.0	ksi	379.2	MPa
=	54.7	ksi	377.0	MPa
=	3/4	in.	19.11	mm
=	18.0	in.	457.2	mm
=	13.543	in. <sup>2</sup>	8737	$\mathrm{mm}^2$
=	406.3	kips	1807	kN
=	446.9	kips	1988	kN
=	444.3	kips	1976	kN
iear	Rupture			
		Eq. (	J4-4), AIS	C 360-15
=	0.75		0.75	
=	65.0	ksi	448.2	MPa
=	78.0	ksi	537.8	MPa
=	74.0	ksi	510.0	MPa
=	3/4	in.	19.11	mm
=	12.4	in.	311.9	mm
=	9.310	in. <sup>2</sup>	5959	$\mathrm{mm}^2$
=	272.3	kips	1202	kN
=	435.7	kips	1923	kN
=	413.2	kips	1824	kN
k She	ar Ruptu	ıre		
,0.6A	$\Lambda_{nv}F_{U})]$	Eq. (	J4-5) AIS	C 360-15
	0.75		0.75	
=	0.75		0.75	
=	0.75		0.75	
		ksi		MPa
=	0.5	ksi ksi	0.5	MPa MPa
=	0.5 50.0		0.5 344.7	
= = =	0.5 50.0 65.0	ksi	0.5 344.7 448.2	MPa
= = =	0.5 50.0 65.0 55.0	ksi ksi	0.5 344.7 448.2 379.0	MPa MPa
= = = =	0.5 50.0 65.0 55.0 78.0	ksi ksi ksi	0.5 344.7 448.2 379.0 537.8	MPa MPa MPa
= = = =	0.5 50.0 65.0 55.0 78.0 54.7	ksi ksi ksi ksi	0.5 344.7 448.2 379.0 537.8 377.0	MPa MPa MPa MPa
= = = = =	0.5 50.0 65.0 55.0 78.0 54.7 74.0	ksi ksi ksi ksi	0.5 344.7 448.2 379.0 537.8 377.0 510.0	MPa MPa MPa MPa MPa
= = = = = =	0.5 50.0 65.0 55.0 78.0 54.7 74.0 1.552	ksi ksi ksi ksi ksi in. <sup>2</sup>	0.5 344.7 448.2 379.0 537.8 377.0 510.0 993	MPa MPa MPa MPa MPa mm²
= = = = = =	0.5 50.0 65.0 55.0 78.0 54.7 74.0 1.552 24.828	ksi ksi ksi ksi in. <sup>2</sup> in. <sup>2</sup>	0.5 344.7 448.2 379.0 537.8 377.0 510.0 993 16018	MPa MPa MPa MPa MPa mm²
= = = = = = =	0.5 50.0 65.0 55.0 78.0 54.7 74.0 1.552 24.828 17.069	ksi ksi ksi ksi in. <sup>2</sup> in. <sup>2</sup>	0.5 344.7 448.2 379.0 537.8 377.0 510.0 993 16018 10926	MPa MPa MPa MPa MPa mm² mm²
= = = = = = = = = = = = = = = = = = = =	0.5 50.0 65.0 55.0 78.0 54.7 74.0 1.552 24.828 17.069 537.1	ksi ksi ksi ksi in. <sup>2</sup> in. <sup>2</sup> kips	0.5 344.7 448.2 379.0 537.8 377.0 510.0 993 16018 10926 2370	MPa MPa MPa MPa MPa mm² mm² kN
= = = = = = = = = = = = = = = = = = = =	0.5 50.0 65.0 55.0 78.0 54.7 74.0 1.552 24.828 17.069 537.1	ksi ksi ksi ksi in. <sup>2</sup> in. <sup>2</sup> kips	0.5 344.7 448.2 379.0 537.8 377.0 510.0 993 16018 10926 2370 3793	MPa MPa MPa MPa MPa mm² mm² kN
= = = = = = = = = = = = = = = = = = = =	0.5 50.0 65.0 55.0 78.0 54.7 74.0 1.552 24.828 17.069 537.1 859.4 814.9 hear yield	ksi ksi ksi ksi in.² in.² kips kips kips	0.5 344.7 448.2 379.0 537.8 377.0 510.0 993 16018 10926 2370 3793	MPa MPa MPa MPa MPa mm² mm² kN kN
	= = = = = = = = = = = = = = = = = = =	= 54.7 = 3/4 = 18.0 = 13.543 = 406.3 = 446.9 = 444.3 near Rupture = 0.75 = 65.0 = 78.0 = 74.0 = 3/4 = 12.4 = 9.310 = 272.3 = 435.7 = 413.2 x Shear Rupture, 0.6A <sub>nv</sub> F <sub>U</sub> )]	$= 54.7   ksi$ $= 3/4   in.$ $= 18.0   in.$ $= 13.543   in.^{2}$ $= 406.3   kips$ $= 446.9   kips$ $= 444.3   kips$ $= 444.3   kips$ $= 65.0   ksi$ $= 78.0   ksi$ $= 74.0   ksi$ $= 74.0   ksi$ $= 3/4   in.$ $= 12.4   in.$ $= 9.310   in.^{2}$ $= 272.3   kips$ $= 435.7   kips$ $= 413.2   kips$	= 54.7 ksi 377.0 = 3/4 in. 19.11 = 18.0 in. 457.2 = 13.543 in. <sup>2</sup> 8737 = 406.3 kips 1807 = 446.9 kips 1988 = 444.3 kips 1976 hear Rupture  Eq. (J4-4), AIS  = 0.75 0.75  = 65.0 ksi 448.2  = 78.0 ksi 537.8  = 74.0 ksi 510.0  = 3/4 in. 19.11  = 12.4 in. 311.9  = 9.310 in. <sup>2</sup> 5959  = 272.3 kips 1202  = 435.7 kips 1923  = 413.2 kips 1824  Shear Rupture

Resistance Factor, $\phi_{v}$	=	1.00		1.00	
$V_n = 0.6F_y A_g$					
Nominal yield stress, F <sub>y</sub>	=	50.0	ksi	344.7	MPa
Expected yield stress, R <sub>y</sub> F <sub>y</sub>	=	55.0	ksi	379.0	MPa
Measured yield stress, Fym	=	54.7	ksi	377	MPa
Gross area of plate, Ag	=	13.543	in. <sup>2</sup>	8737	$mm^2$
Factored shear Capacity, Vc	=	406.3	kips	1807	kN
Expected shear Capacity, Ve	=	446.9	kips	1988	kN
Measured shear capacity, V <sub>m</sub>	=	444.3	kips	1976	kN
a distance	=	9.2	in.	232.9	mm
$M_c\!=\phi_bM_n$					
Resistance factor, φ <sub>b</sub>	=	0.90		0.90	
$M_n = F_y Z_{pl}$					
Plastic section modulus, Z <sub>pl</sub>	=	60.941	in. <sup>3</sup>	998.65	$10^3\mathrm{mm}^3$
Factored moment capacity, Mc	=	2742.4	kip.in	309.8	kN.m
Expected moment capacity, Me	=	3351.8	kip.in	378.7	kN.m
Measured moment capacity, M <sub>m</sub>	=	3332.2	kip.in	376.5	kN.m
Factored shear-flexural yielding	=	240.8	kips	1071	kN
resistance, V <sub>r</sub>		202.0		1050	137
Expected shear-flexural yielding resistance, $V_e$ ( $\phi$ =1.0, $R_vF_v$ )	=	282.9	kips	1259	kN
Measured shear-flexural	=	281.3	kips	1251	kN
yielding resistance, V <sub>m</sub>	_		_		
		Buckling	Ta a a		
$V_r = \phi_b \; F_{cr}  S_{net} \! / \; e$	Ec	ı. (9-6), A (14t	ISC Stee h Edition		
Resistance Factor, φ <sub>b</sub>	=	0.90	n Lamon	0.90	
$S_{net} = 1/6 t_p h^2_o$	=	40.63	in. <sup>3</sup>	665.77	$10^3 \text{mm}^3$
$Z_{\rm net} = 1/4 t_{\rm p} h^2_{\rm o}$	=	60.94	in. <sup>3</sup>	998.65	$10^3 \text{mm}^3$
depth of top cope, d <sub>c</sub>	=	4.3	in.	110	mm
Beam Depth, d	=	26.7	in.	678.0	mm
Eccentricity, e	=	9.2	in.	232.9	mm
Unsupported Length of Plate, c	=	9.2	in.	232.9	mm
$d_c < 0.2d \& c < 2d$ ?		YES, f <sub>d</sub>	equation	valid	
f <sub>d</sub> equation (Cheng et al. 1984)		ŕ	•		
$t^2$			Eq.	(9-12)	
$F_{cr} = 0.62\pi E f_d \frac{t_w^2}{ch_0} \le F_y$		AISC	Steel Ma	nual (14th	Edition)
Modulus of Elasticity, E	=	29000	ksi	200000	MPa
Thickness of Plate, tp	=	3/4	in.	19.11	mm
Plate Depth, ho	=	18	in.	457.2	mm
$a = a = a = d_{at}$				(9-13)	
$f_d = 3.5 - 7.5(\frac{d_{ct}}{d_b})$		AISC	Steel Ma	nual (14th	Edition)
Adjustment Factor, $f_d$	=	2.28		2.28	
Critical Stress, F <sub>cr</sub>	=	441.2	ksi	3043	MPa
				- 0	

Naminal viold atwass E	=	50.0	ksi	344.7	MPa
Nominal yield stress, F <sub>y</sub>	=	55.0	ksi	379.2	MPa
Expected yield stress, R <sub>y</sub> F <sub>y</sub>	=	54.7	ksi	377.0	MPa
Measured yield stress, F <sub>ym</sub>	=				kN
Factored buckling resistance		299.1	kips	1330	
Expected buckling resistance $(R_yF_y, \varphi=1.0)$	=	365.5	kips	1626	kN
Measured buckling resistance	=	363.4	kips	1616	kN
Q equation (classical plate b	uckli	ing)			
$F_{cr} = F_y Q$			Eq.	(9-14)	
		AISC		nual (14th	Edition)
$\lambda = \frac{h_0}{1 - \frac{1}{2}} \left[ \frac{F_y}{1 - \frac{1}{2}} \right]$		AISC		(9-18) nual (14th	Edition)
$\lambda = \frac{h_0}{10t_w} \sqrt{\frac{F_y}{475 + 280(\frac{h_0}{c})^2}}$		AISC	Sicci Ma	nuar (1 <del>4</del> ur	Lattion)
Nominal Yield Stress of Plate, F <sub>Y</sub>	=	50	ksi	345	MPa
Expected Yield Stress, R <sub>Y</sub> F <sub>Y</sub>	=	55	ksi	379	MPa
Yield Stress of Plate, F <sub>Y</sub>	=	54.7	ksi	432	MPa
Nominal slenderness of coped	=	0.43			
section, λ Expected slenderness of coped	=	0.45			
section, λ <sub>e</sub> Measured slenderness of coped	=	0.45			
section, $\lambda_m$ Nominal strength reduction	=	1.00			
factor, Q Expected strength reduction	=	1.00			
factor, Q <sub>e</sub>		1.00			
Measured strength reduction factor, Q <sub>m</sub>	=	1.00			
Nominal critical stress, F <sub>cr</sub>	=	50.0	ksi	344.7	MPa
Expected critical stress, F <sub>cr,e</sub>	=	55.0	ksi	379.2	MPa
Measured critical stress, F <sub>cr,m</sub>	=	54.7	ksi	377.0	MPa
Factored buckling resistance, V <sub>r</sub>	=	299.1	kips	1330	kN
Expected buckling resistance, $V_{r,e} (\phi=1.0, R_y F_y)$	=	365.5	kips	1626	kN
Measured buckling resistance,	=	363.4	kips	1616	kN
V <sub>r,m</sub> (φ=1.0,F <sub>ym</sub> ) Rectangular Bar Buckling		Sect	tion F11,	AISC 360-	15
$M_n(cd/t^2)$					
Nominal yield stress, F <sub>y</sub>	=	50.0	ksi	344.7	MPa
Expected yield stress, R <sub>y</sub> F <sub>y</sub>	=	55.0	ksi	379.2	MPa
Measured yield stress, F <sub>ym</sub>	=	54.7	ksi	377.0	MPa
c	=	9.2	in.	233	mm
d	=	18.0	in.	457	mm
t	=	3/4	in.	19	mm
$\lambda = cd/t^2$	=	292		292	
Nominal 0.08 E/F <sub>y</sub>	=	46		46	
Expected 0.08 E/F <sub>y</sub>	=	42		42	

$$\begin{array}{rclrcl} \text{Measured } 0.08 \ E/F_y & = & 42 & 42 \\ \text{Nominal } 1.9 \ E/F_y & = & 1102 & 1102 \\ \text{Expected } 1.9 \ E/F_y & = & 1002 & 1002 \\ \text{Measured } 1.9 \ E/F_y & = & 1008 & 1008 \\ \hline \\ C_b = & \begin{bmatrix} 3 + \ln(\frac{a}{d_b}) \end{bmatrix} (1 - \frac{d_{cl}}{d_b}) \geq 1.84 & Eq. (9-15) \\ C_b & = & 1.84 & 1.84 \\ \hline \\ \text{Factored buckling resistance, } V_r & = & 299.1 & kips & 1330 & kN \\ \text{Expected buckling resistance, } V_r & = & 299.1 & kips & 1330 & kN \\ \text{Expected buckling resistance, } & & 365.5 & kips & 1626 & kN \\ \hline V_{re} (\phi=1.0, R_yF_y) & & & & 1616 & kN \\ \hline \\ Weld to Supporting Element & & & & \\ \hline D_{min} = 5/8 \ t_{pl} & & & & \\ \hline Weld to Supporting Element & & & \\ \hline D_{min} = 5/8 \ t_{pl} & & & & \\ \hline Weld to Supporting Element & & & \\ \hline D_{min} = 5/8 \ t_{pl} & & & \\ \hline Weld to Supporting Element & & \\ \hline D_{min} = 5/8 \ t_{pl} & & & \\ \hline Weld to Supporting Element & & \\ \hline D_{min} = 5/8 \ t_{pl} & & & \\ \hline Weld to Supporting Element & & \\ \hline D_{min} = 5/8 \ t_{pl} & & & \\ \hline Weld to Supporting Element & & \\ \hline D_{min} = 5/8 \ t_{pl} & & & \\ \hline Weld to Supporting Element & & \\ \hline D_{min} = 5/8 \ t_{pl} & & & \\ \hline Weld to Supporting Element & & \\ \hline D_{min} = 5/8 \ t_{pl} & & & \\ \hline Weld to Supporting Element & & \\ \hline D_{min} = 5/8 \ t_{pl} & & & \\ \hline Weld to Supporting Element & & \\ \hline D_{min} = 5/8 \ t_{pl} & & & \\ \hline Weld to Supporting Element & & \\ \hline D_{min} = 5/8 \ t_{pl} & & & \\ \hline Section 10 & & \\ \hline AISC Steel Manual (15th Edition) & & \\ \hline AISC Steel Manual (15th Edition) & & \\ \hline V_w = 2 \ \phi_w \ 0.6 \ F_{EXX} \ 0.707 \ D_w (1.0+0.5 \sin^{1.5}\theta) & & \\ \hline W_w = 2 \ \phi_w \ 0.6 \ F_{EXX} \ 0.707 \ D_w (1.0+0.5 \sin^{1.5}\theta) & & \\ \hline W_w = 2 \ \phi_w \ 0.6 \ F_{EXX} \ 0.707 \ D_w (1.0+0.5 \sin^{1.5}\theta) & & \\ \hline W_w = 2 \ \phi_w \ 0.6 \ F_{EXX} \ 0.707 \ D_w (1.0+0.5 \sin^{1.5}\theta) & & \\ \hline W_w = 2 \ \phi_w \ 0.6 \ F_{EXX} \ 0.707 \ D_w (1.0+0.5 \sin^{1.5}\theta) & & \\ \hline W_w = 2 \ \phi_w \ 0.6 \ F_{EXX} \ 0.707 \ D_w (1.0+0.5 \sin^{1.5}\theta) & & \\ \hline W_w = 2 \ \phi_w \ 0.6 \ F_{EXX} \ 0.707 \ D_w (1.0+0.5 \sin^{1.5}\theta) & & \\ \hline W_w = 2 \ \phi_w \ 0.6 \ F_{EXX} \ 0.707 \ D_w \ 0.707 \ D_w \ 0.707 \ D_w$$

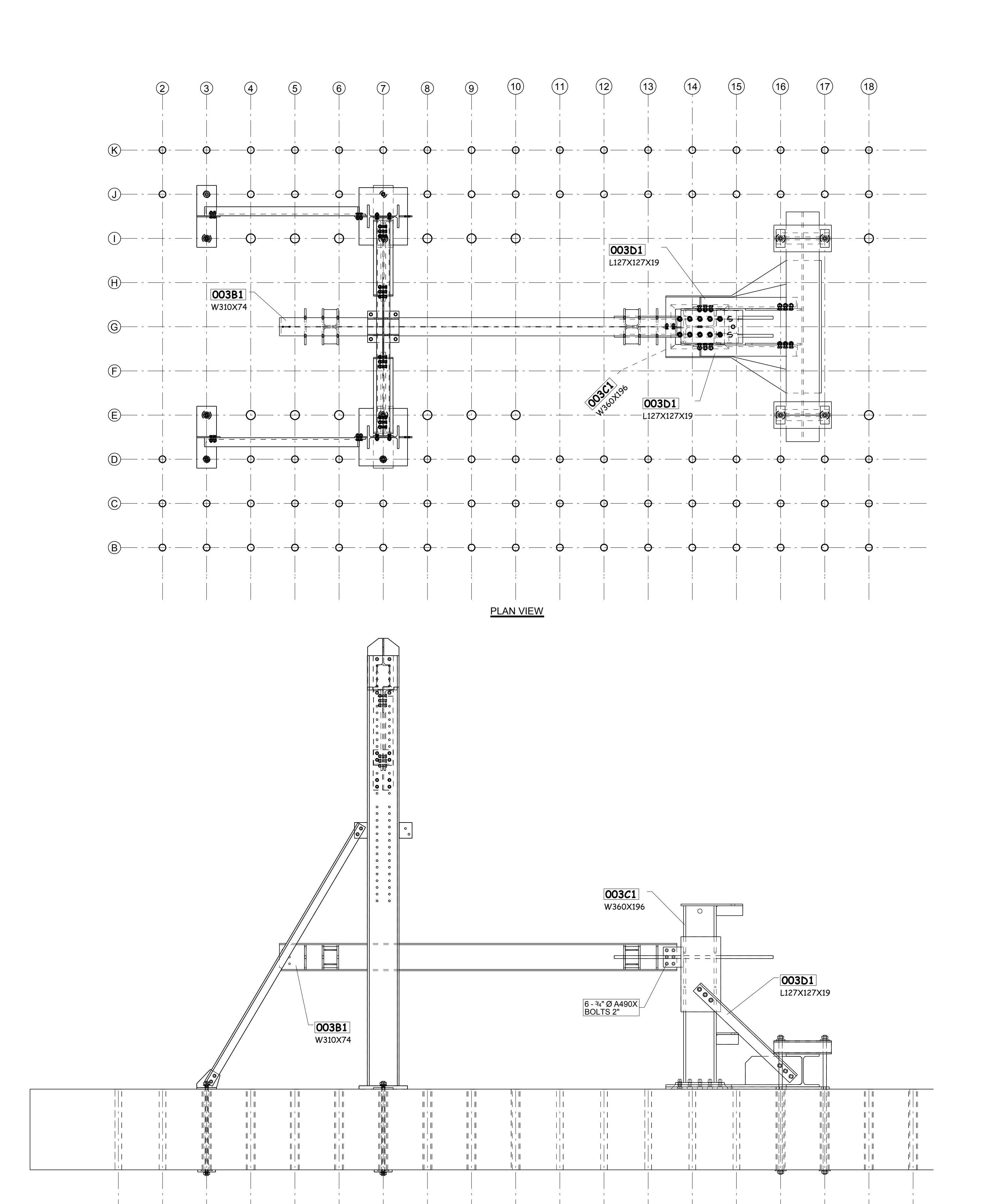


C		2.23			
Resistance Factor, $\phi_w$	=	0.75		0.75	
Nominal ultimate strength, $F_{EXX}$	=	71.1	ksi	490.0	MPa
Measured ultimate strength, $F_{EXX}$	=	89.9	ksi	620.0	MPa
Factored Weld Resistance, V <sub>w</sub>	=	698.1	kips	3105	kN
Expected Weld Strength, $V_w$ ( $\phi$ =1.0)	=	930.8	kips	4140	kN
Expected Weld Strength, V <sub>w</sub> (measured properties)	=	1174.0	kips	5222	kN

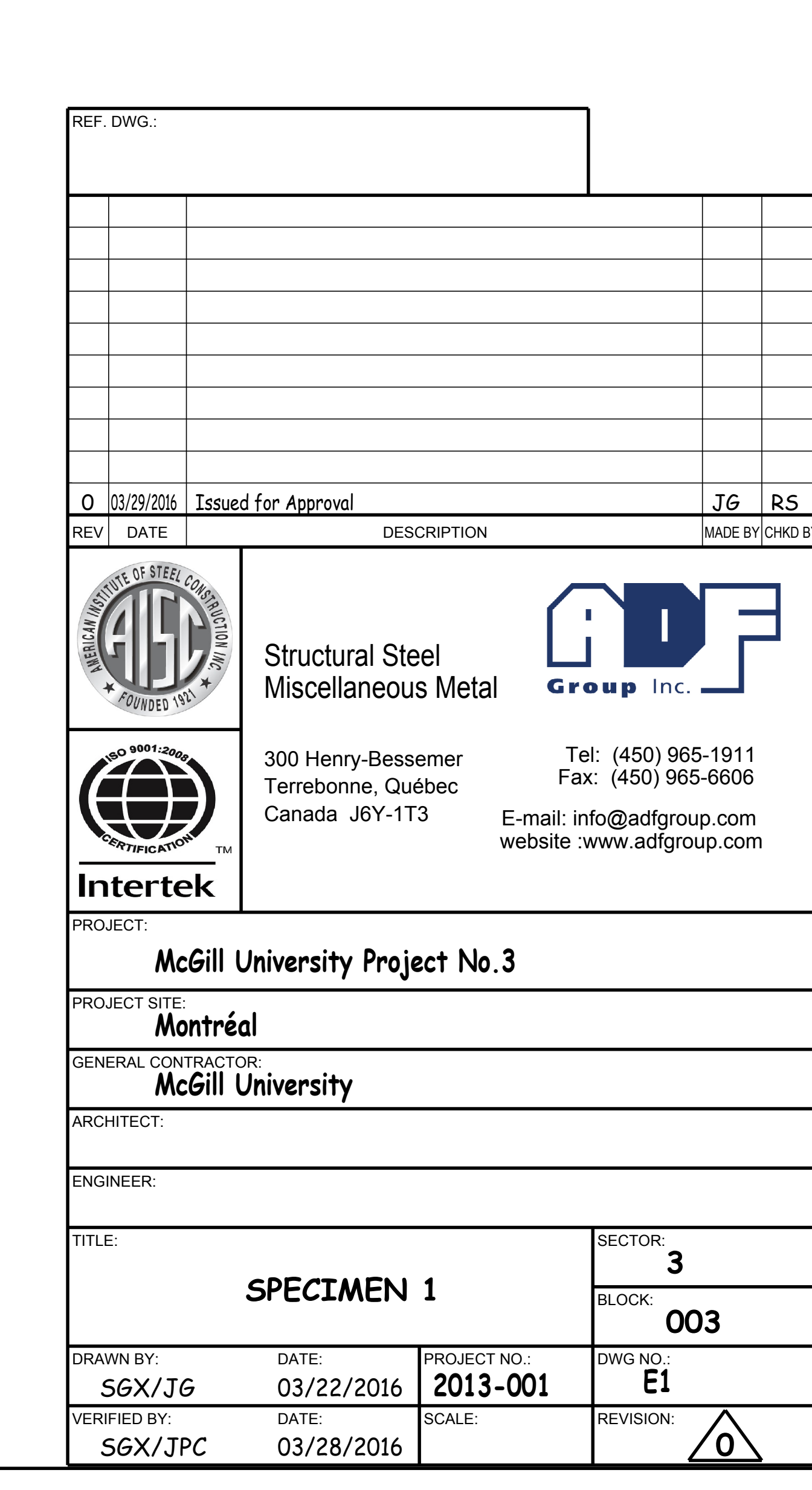
## **Summary**

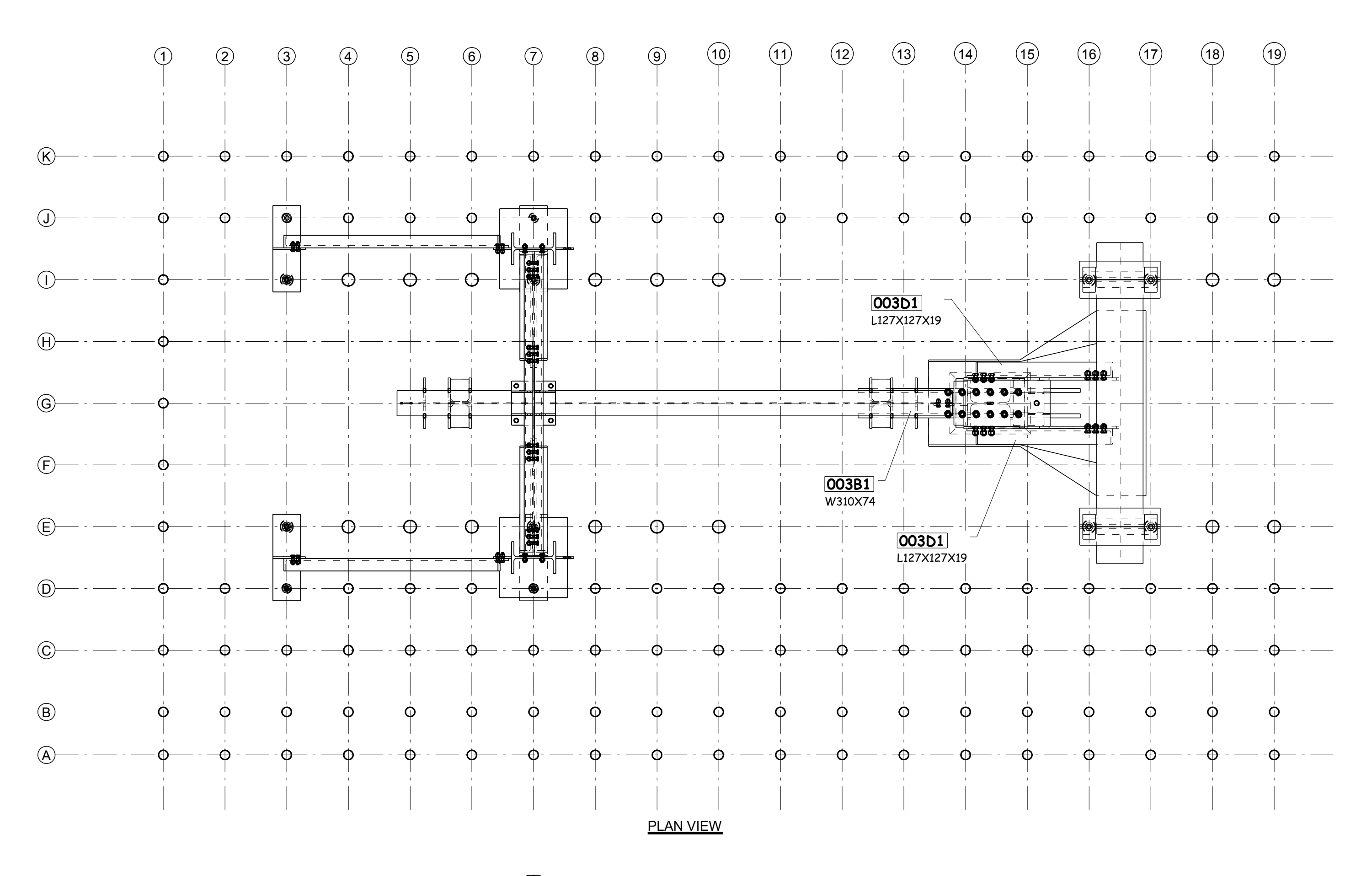
Failure Modes	Fact	ored	Expe	ected	Meas	ured
	kips	kN	kips	kN	kips	kN
Shear -flexural yielding resistance, Vr	240.8	1071	282.9	1259	281.3	1251
Shear yielding resistance, VG	406.3	1807	446.9	1988	444.3	1976
Block shear rupture resistance, vbs	537.1	2370	859.4	3793	814.9	3597
Shear rupture strength over net area, vn	272.3	1202	435.7	1923	413.2	1824
Plate buckling(f <sub>d</sub> equation)	299.1	1330	365.5	1626	363.4	1616
Plate buckling(Q equation)	299.1	1330	365.5	1626	363.4	1616
Rectangular bar buckling	299.1	1330	365.5	1626	363.4	1616
Bearing resistance, b <sub>r</sub>	181.8	1167	266.6	1868	273.1	1771
Shear resistance of bolts, vr	177.3	789	262.7	1169		
Weld resistance, vw	698.1	3105	930.8	4140	1174.0	5222

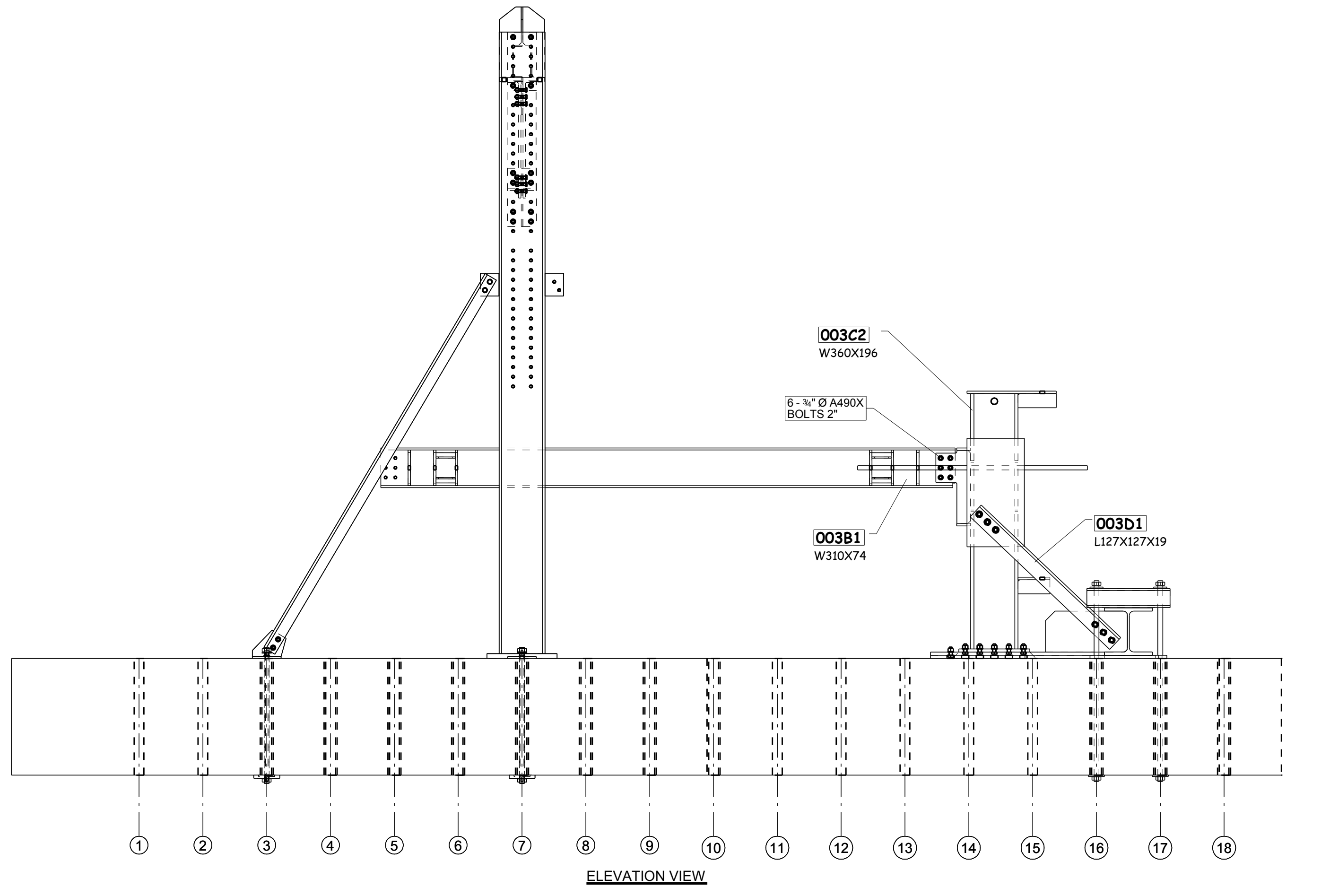
## **Appendix B: Fabrication Drawings**

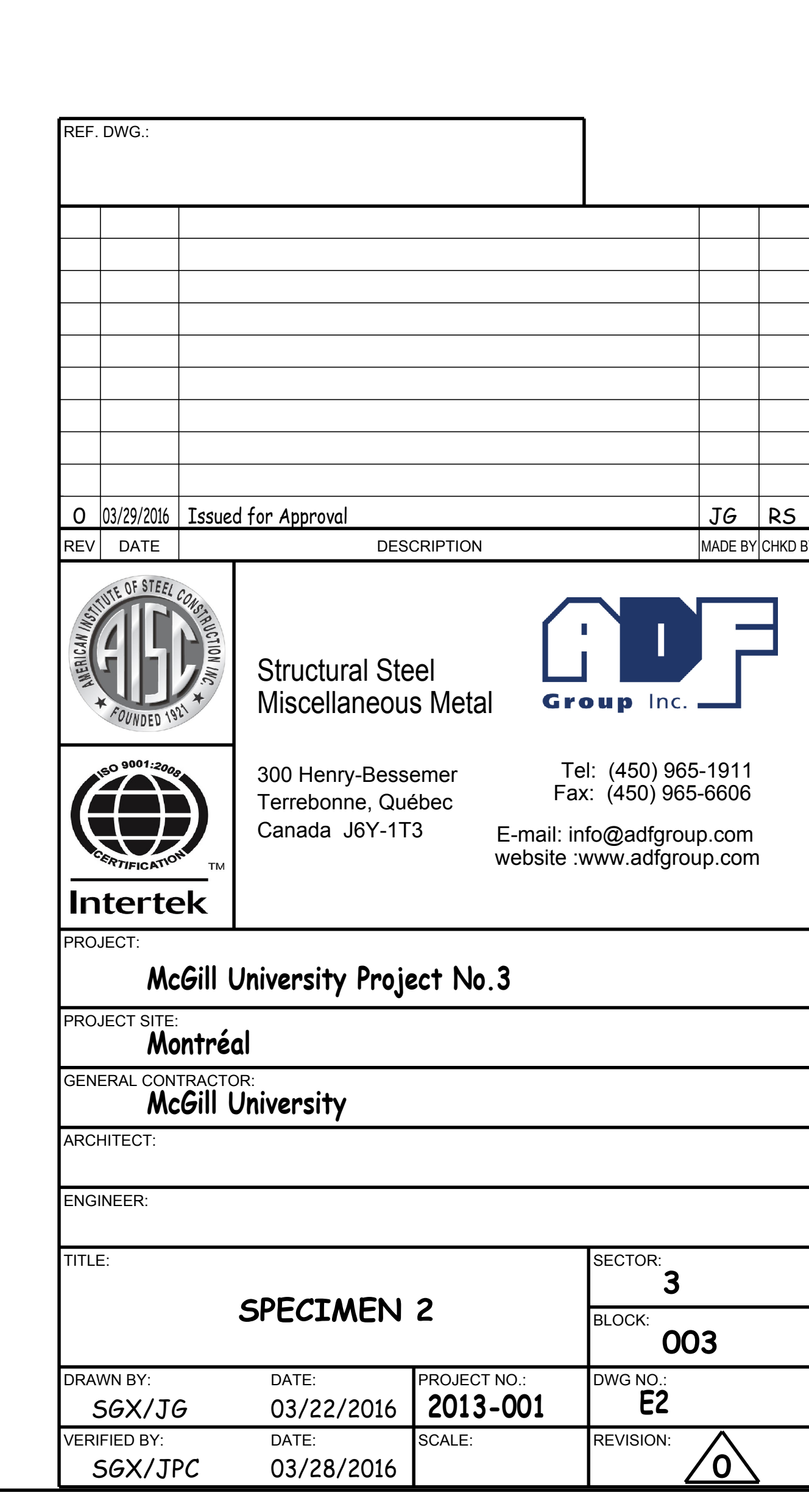


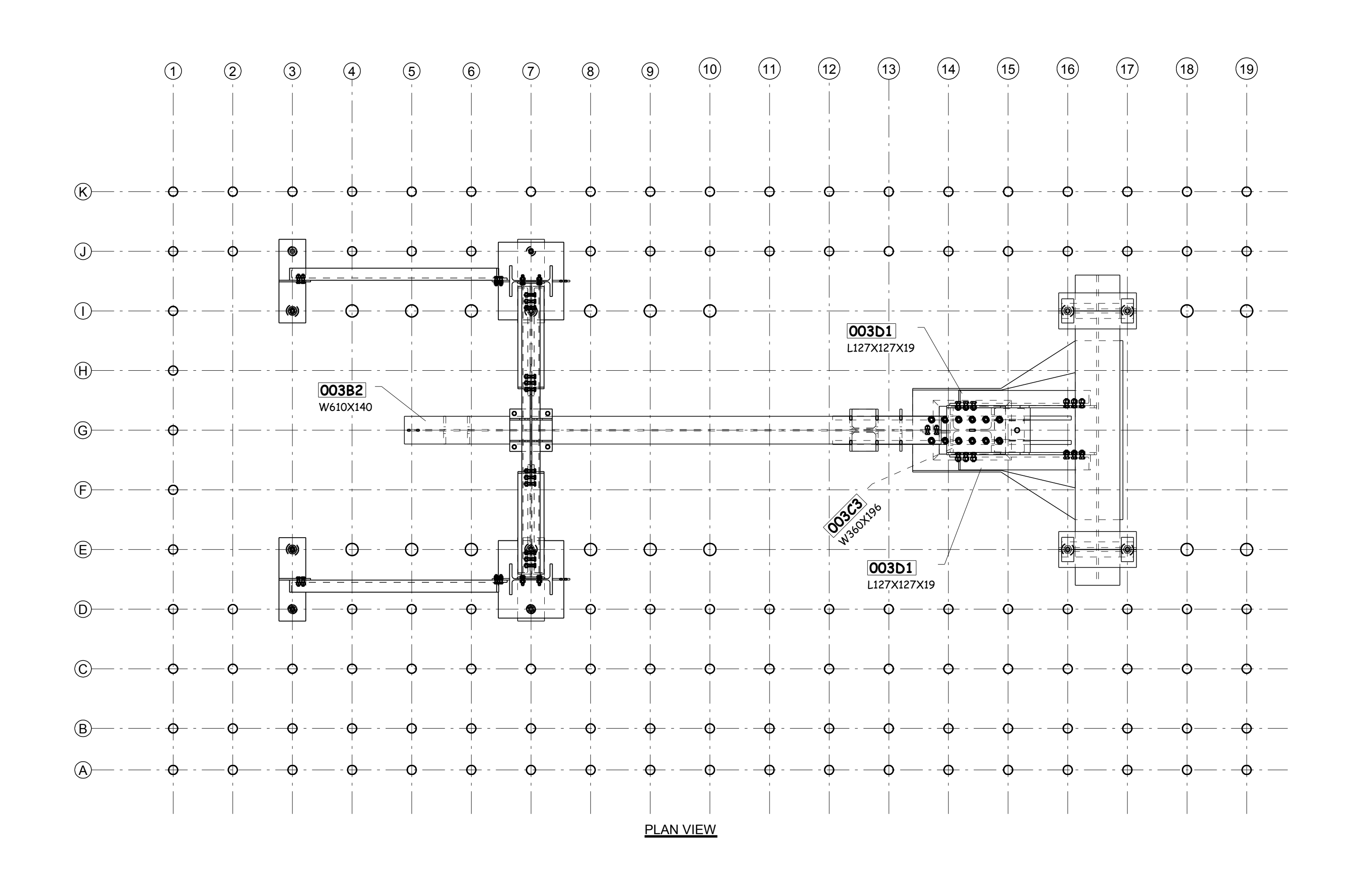
**ELEVATION VIEW** 

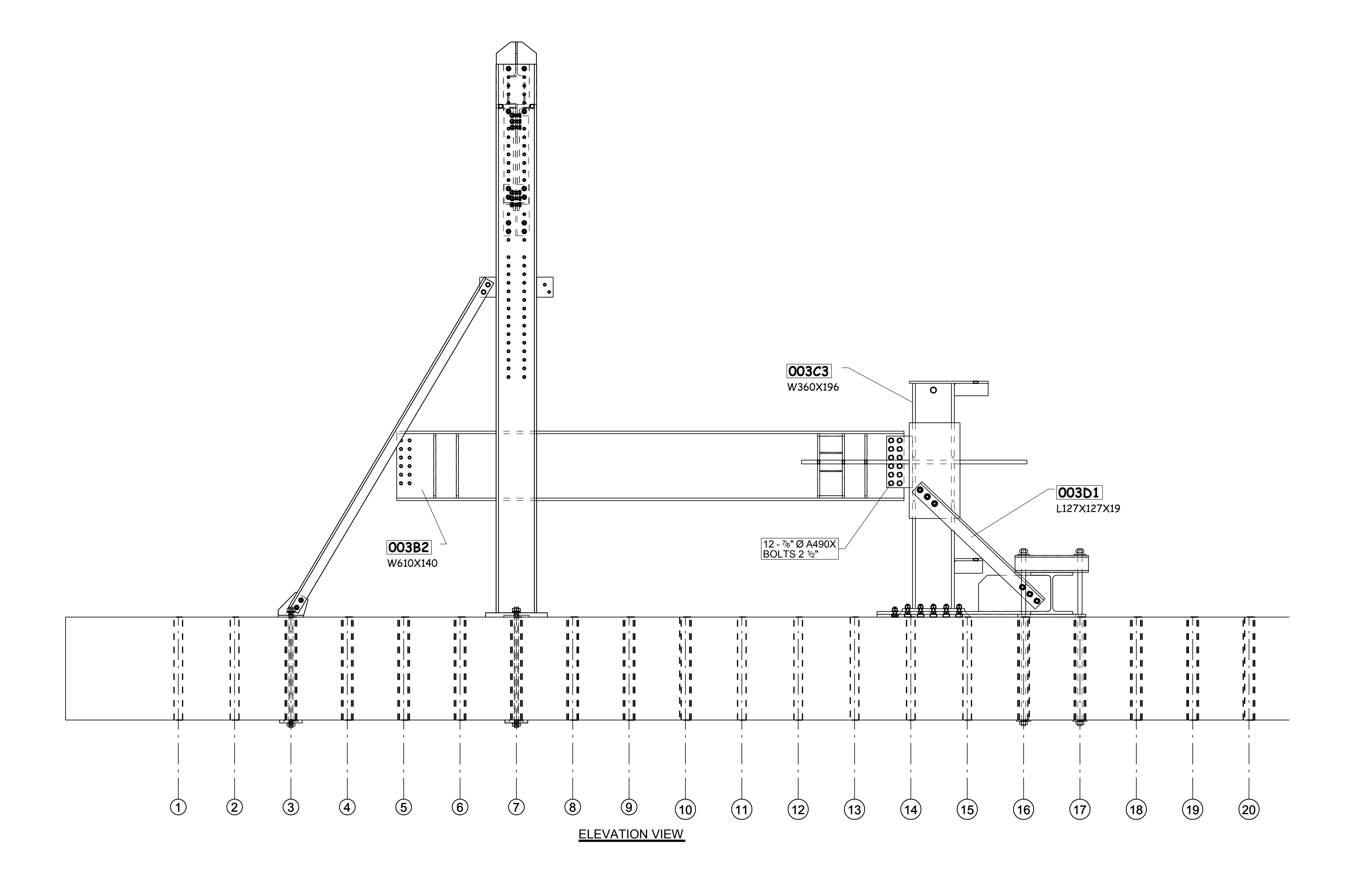


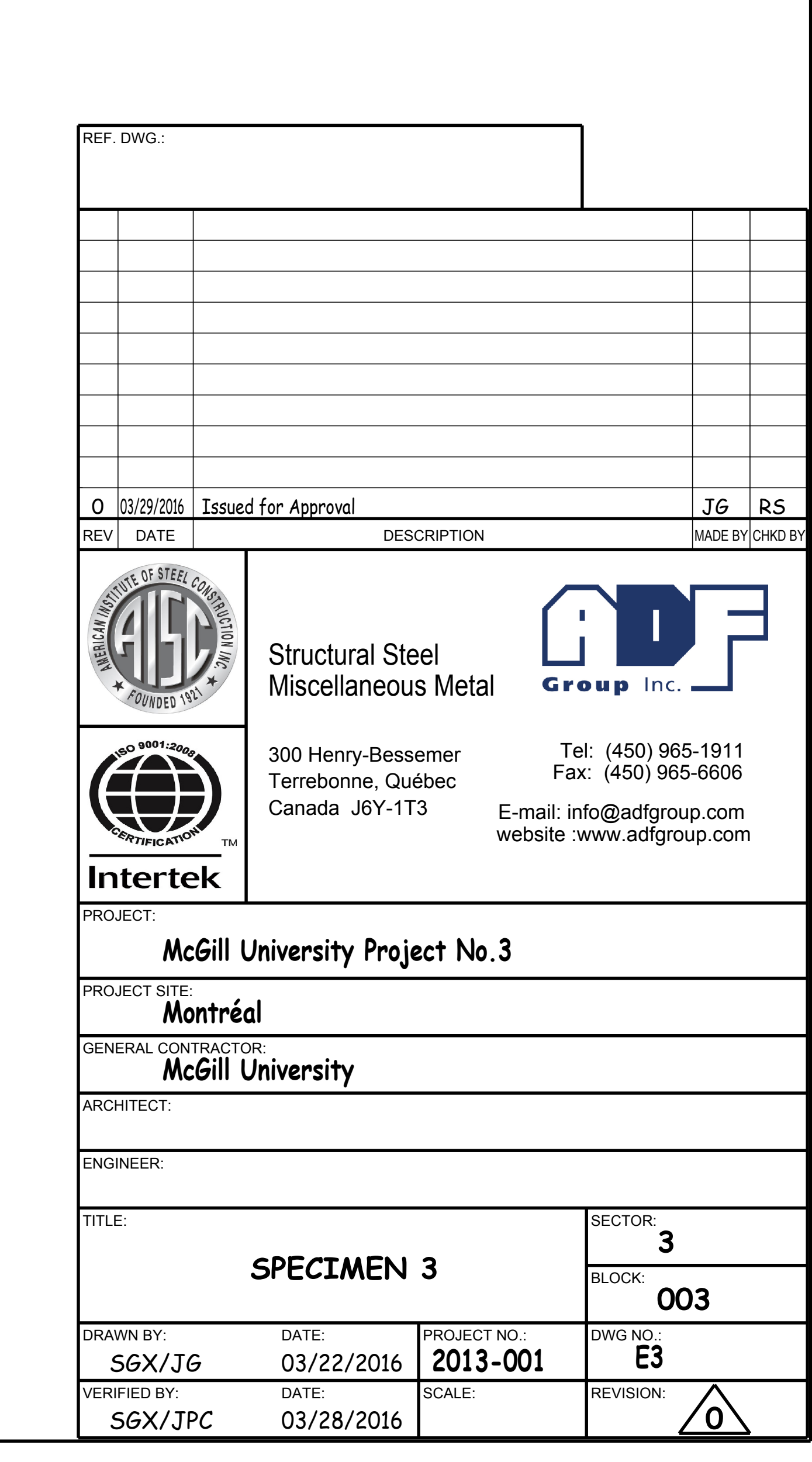


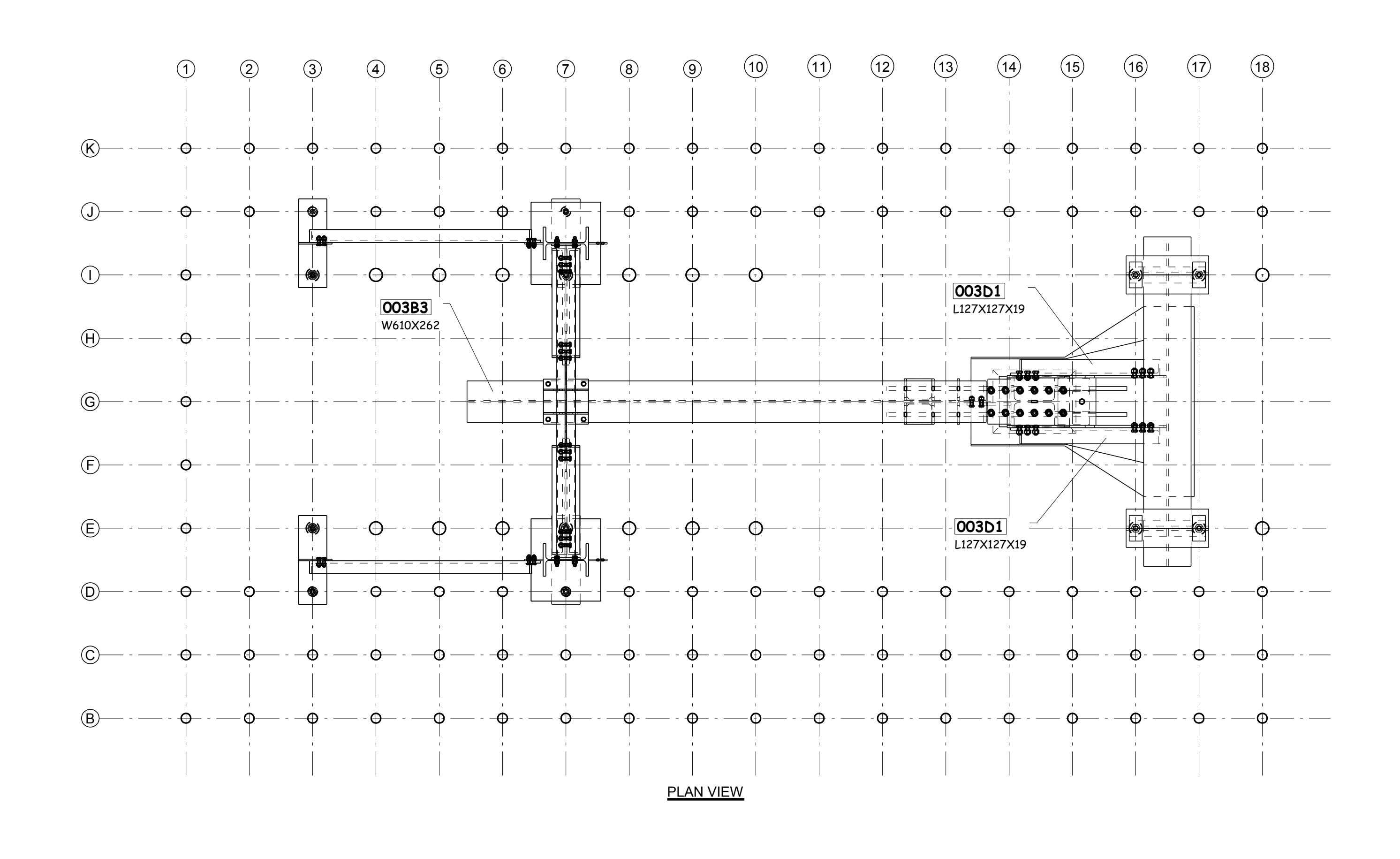


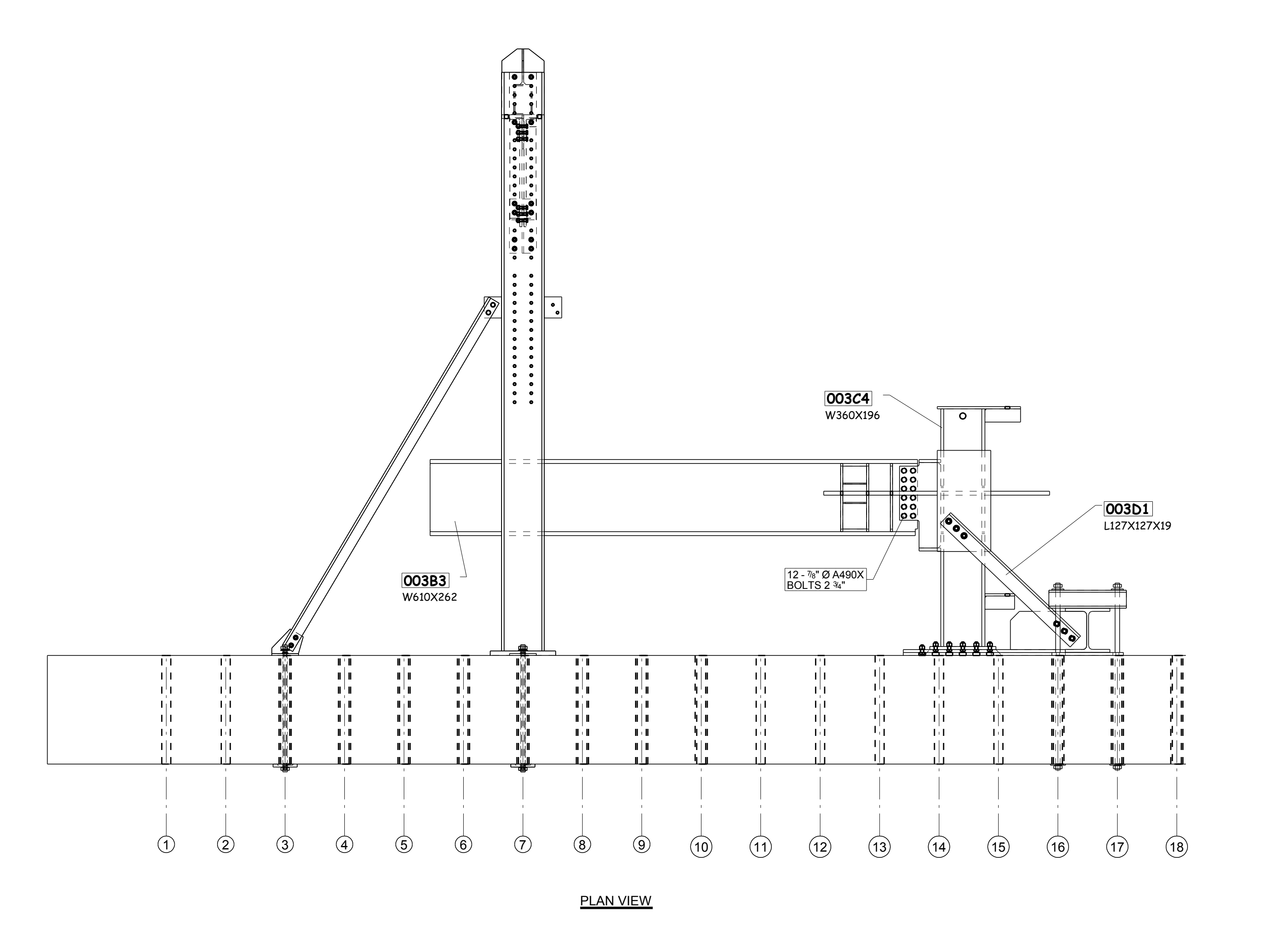


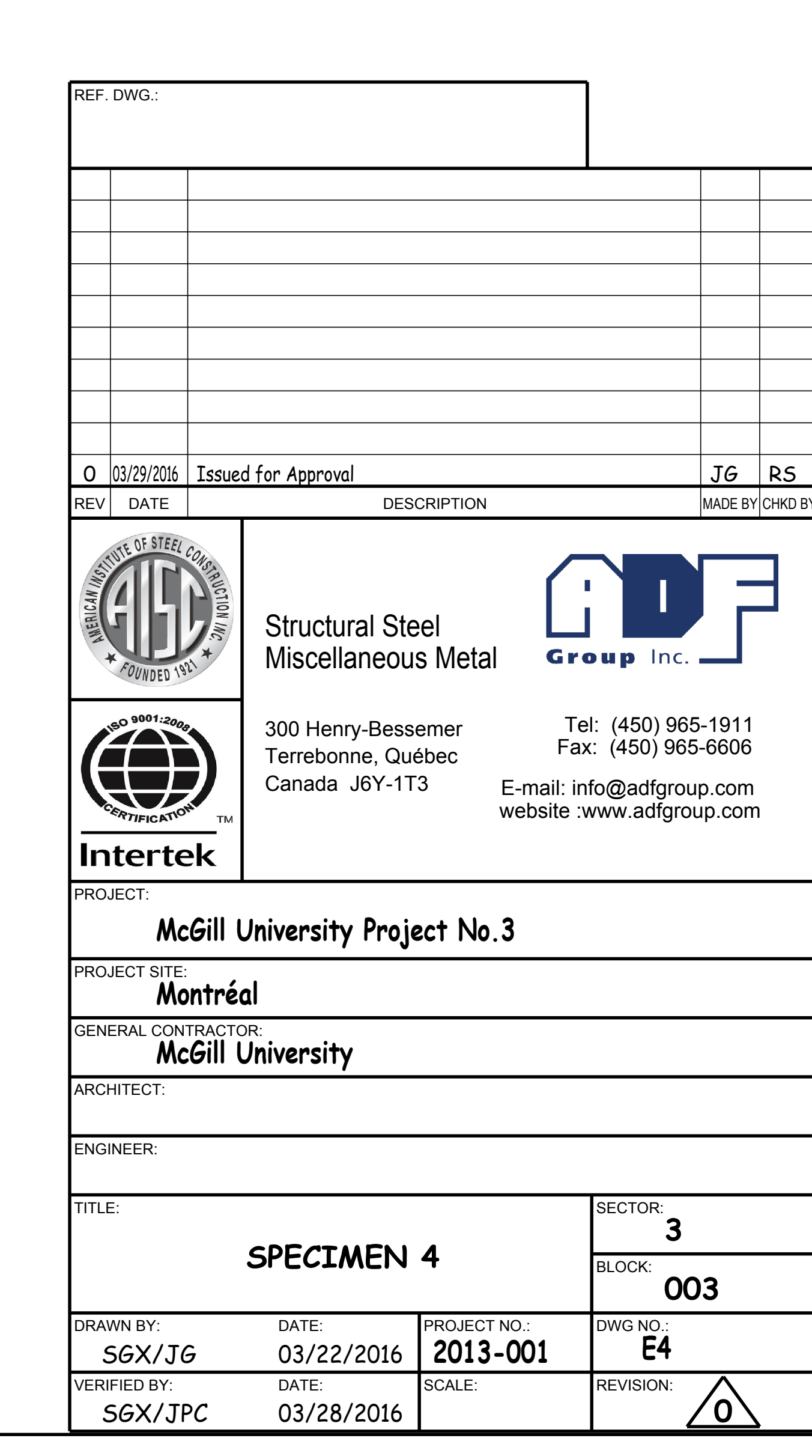


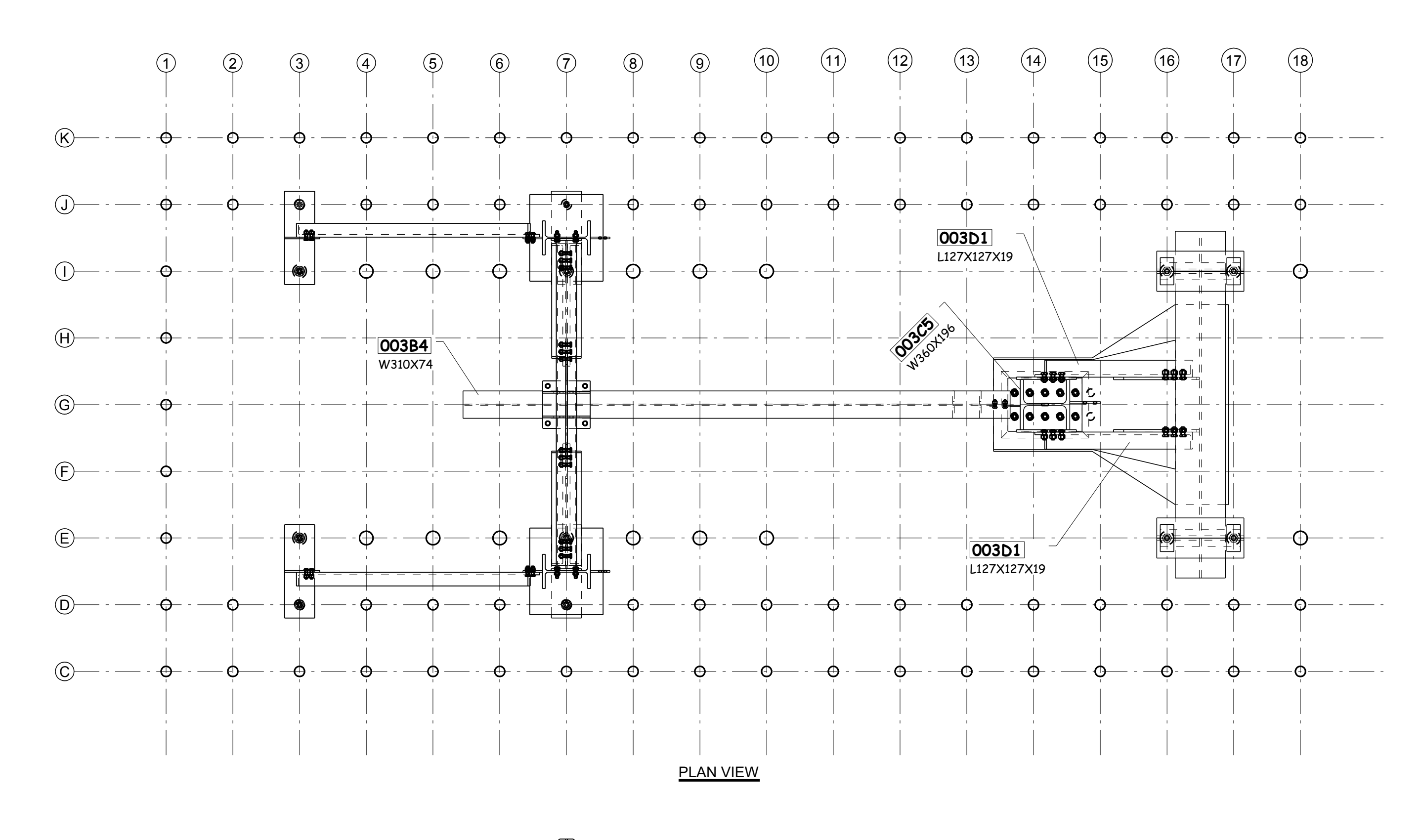


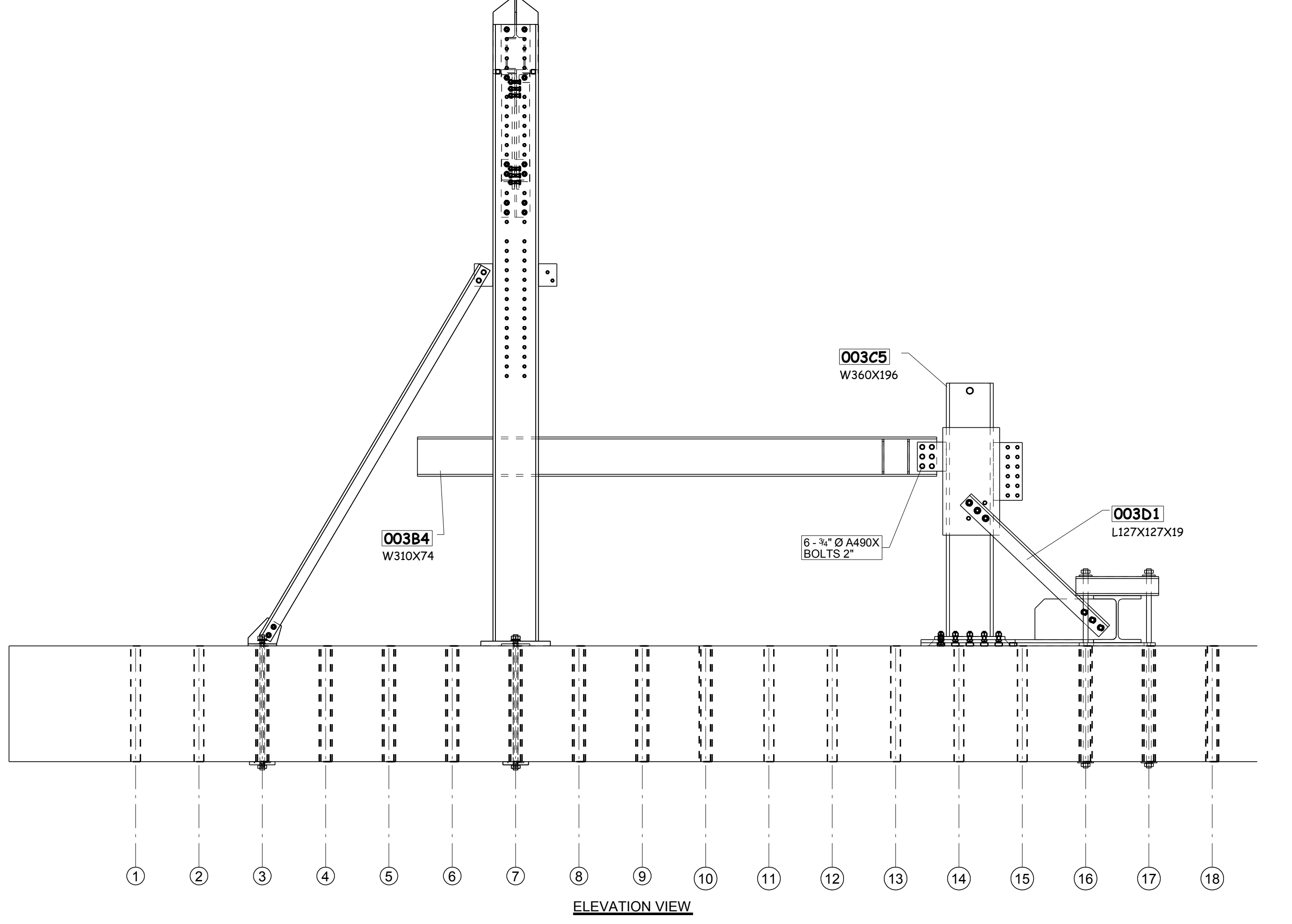


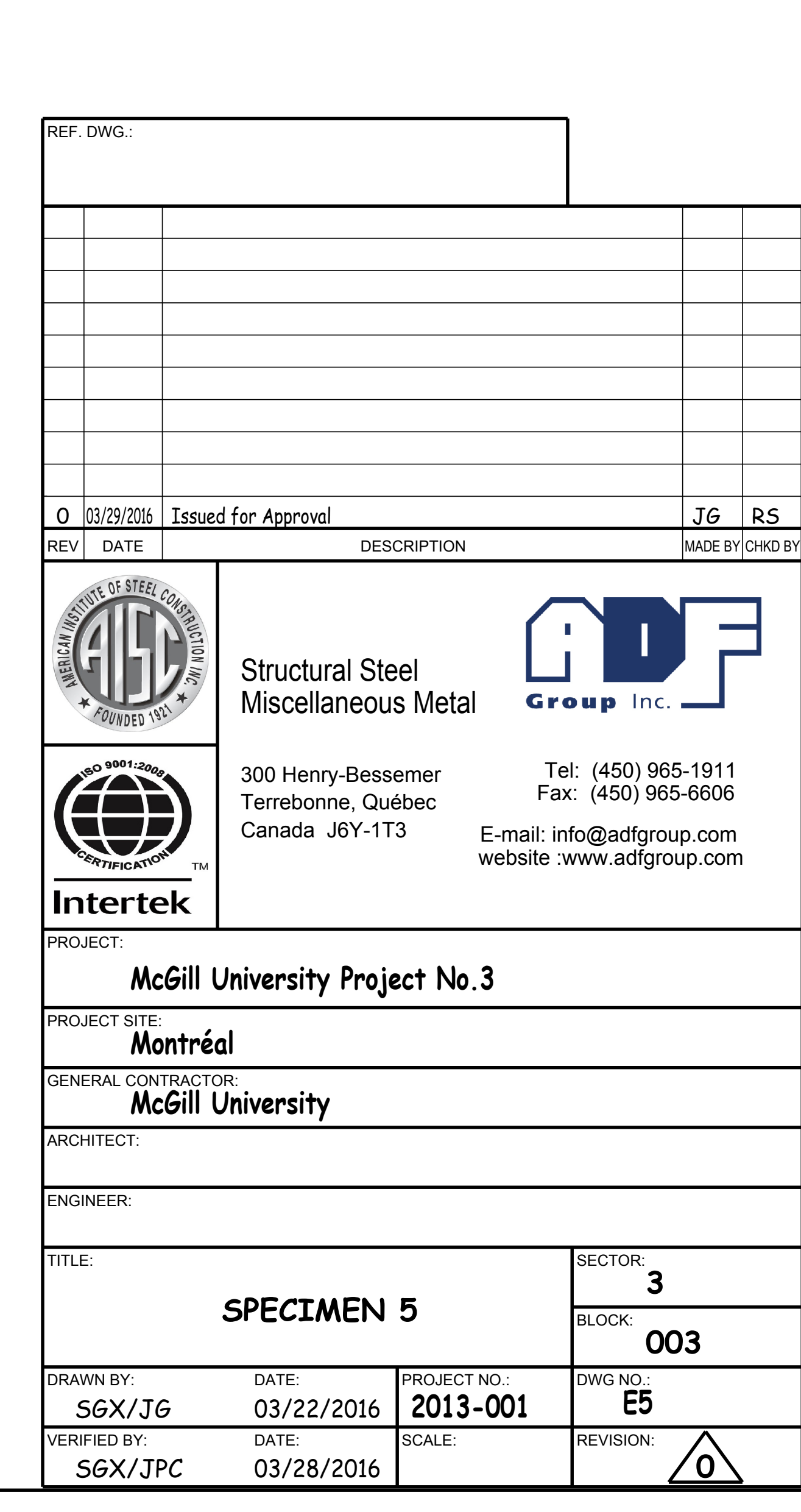


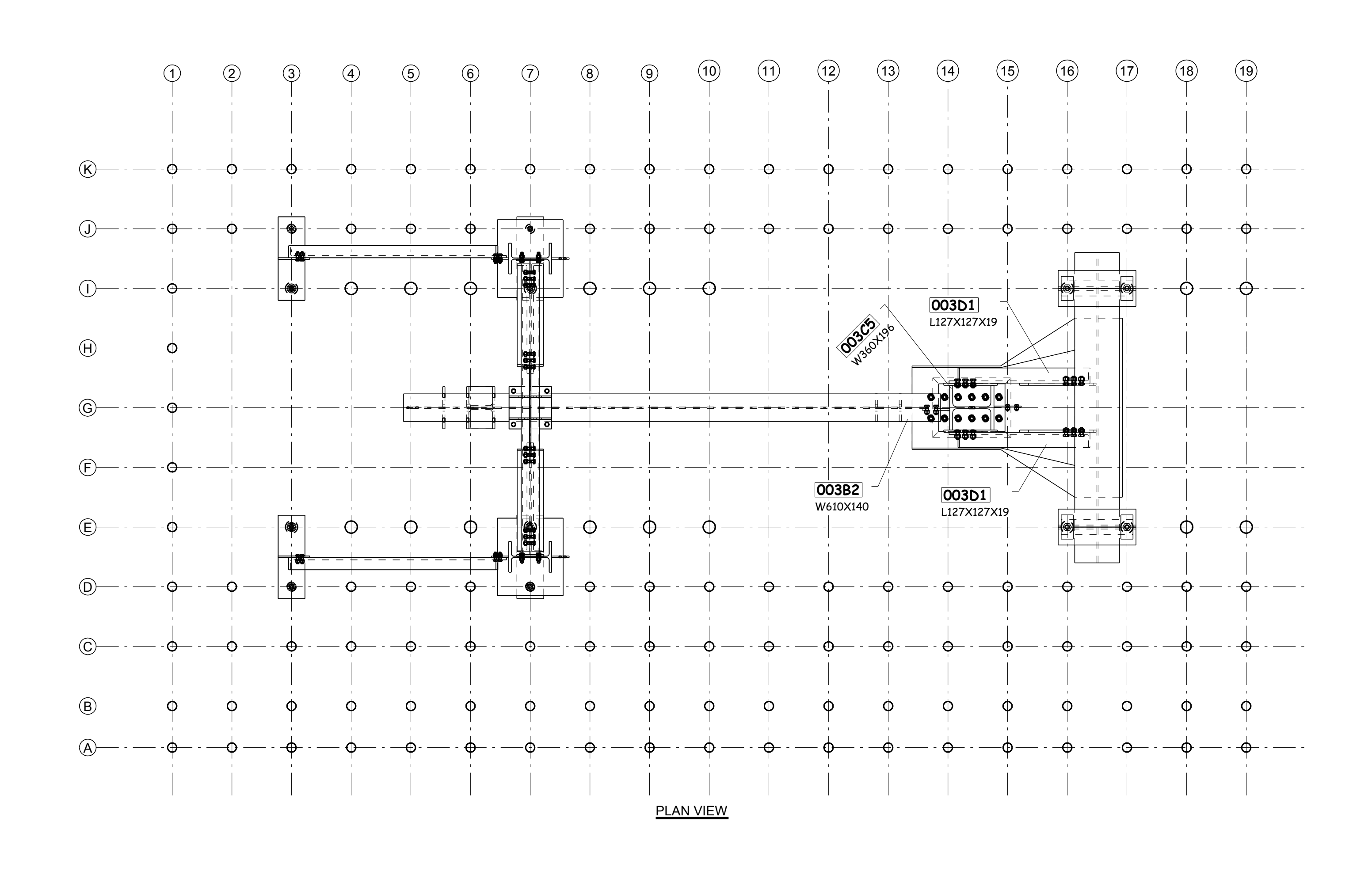


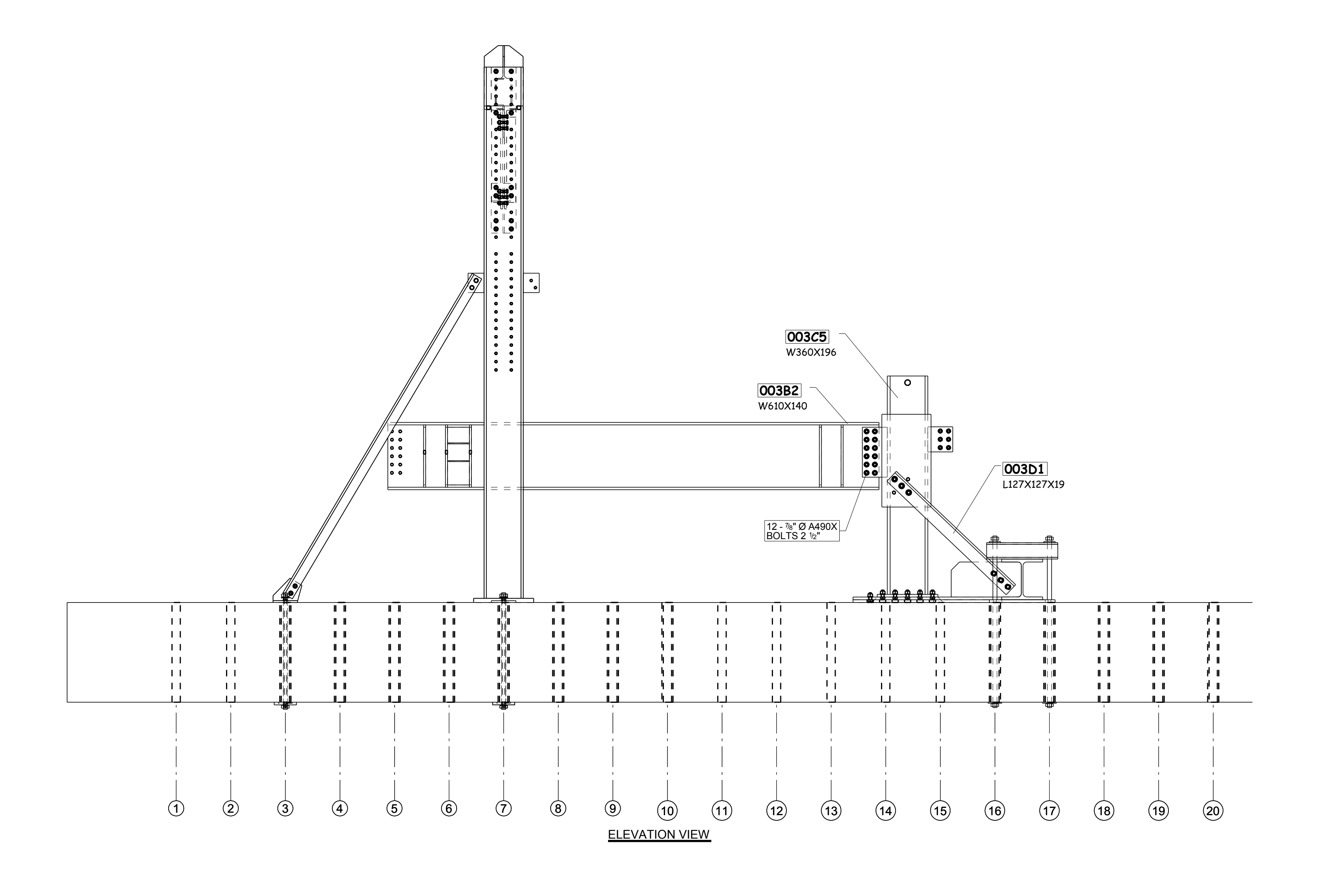


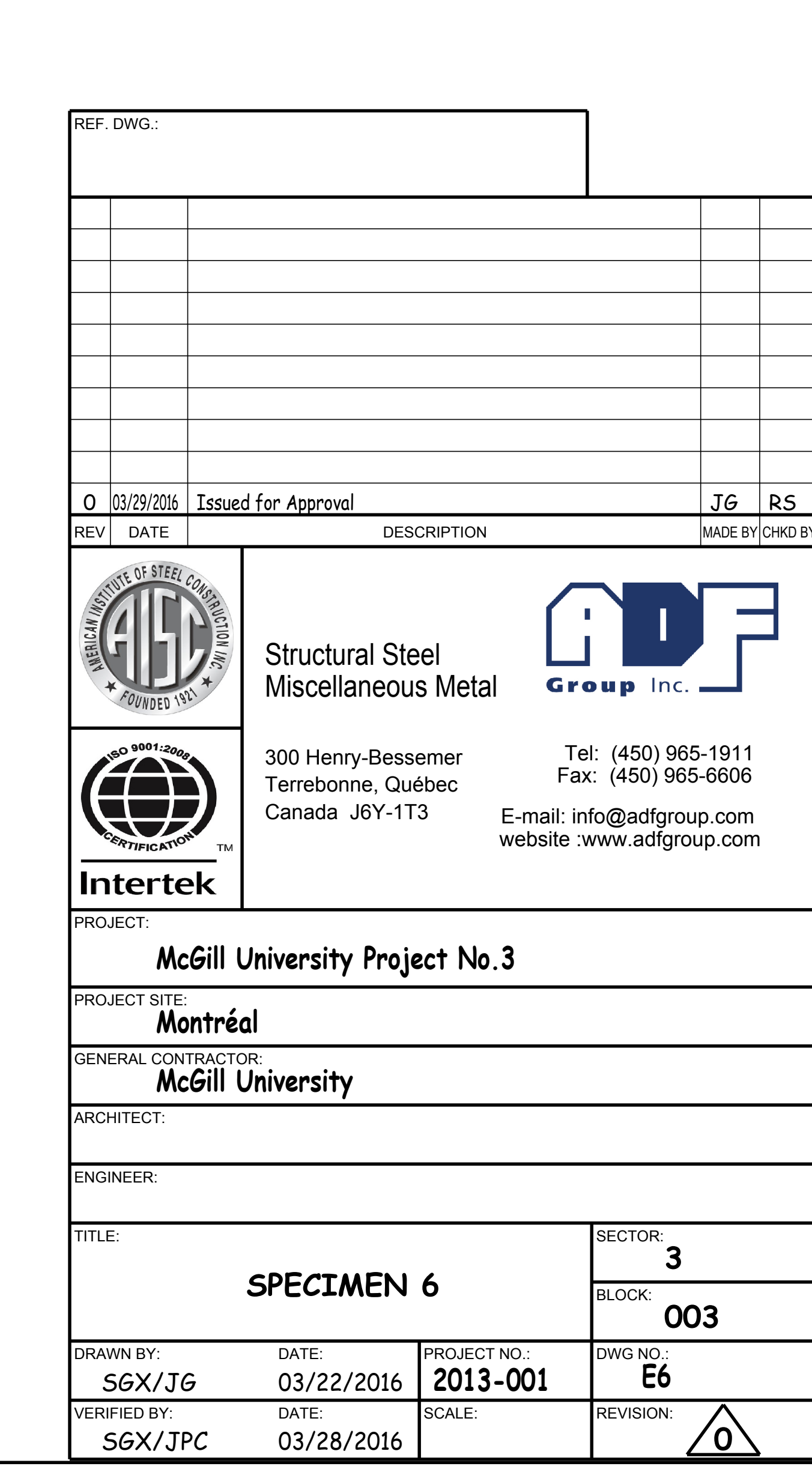


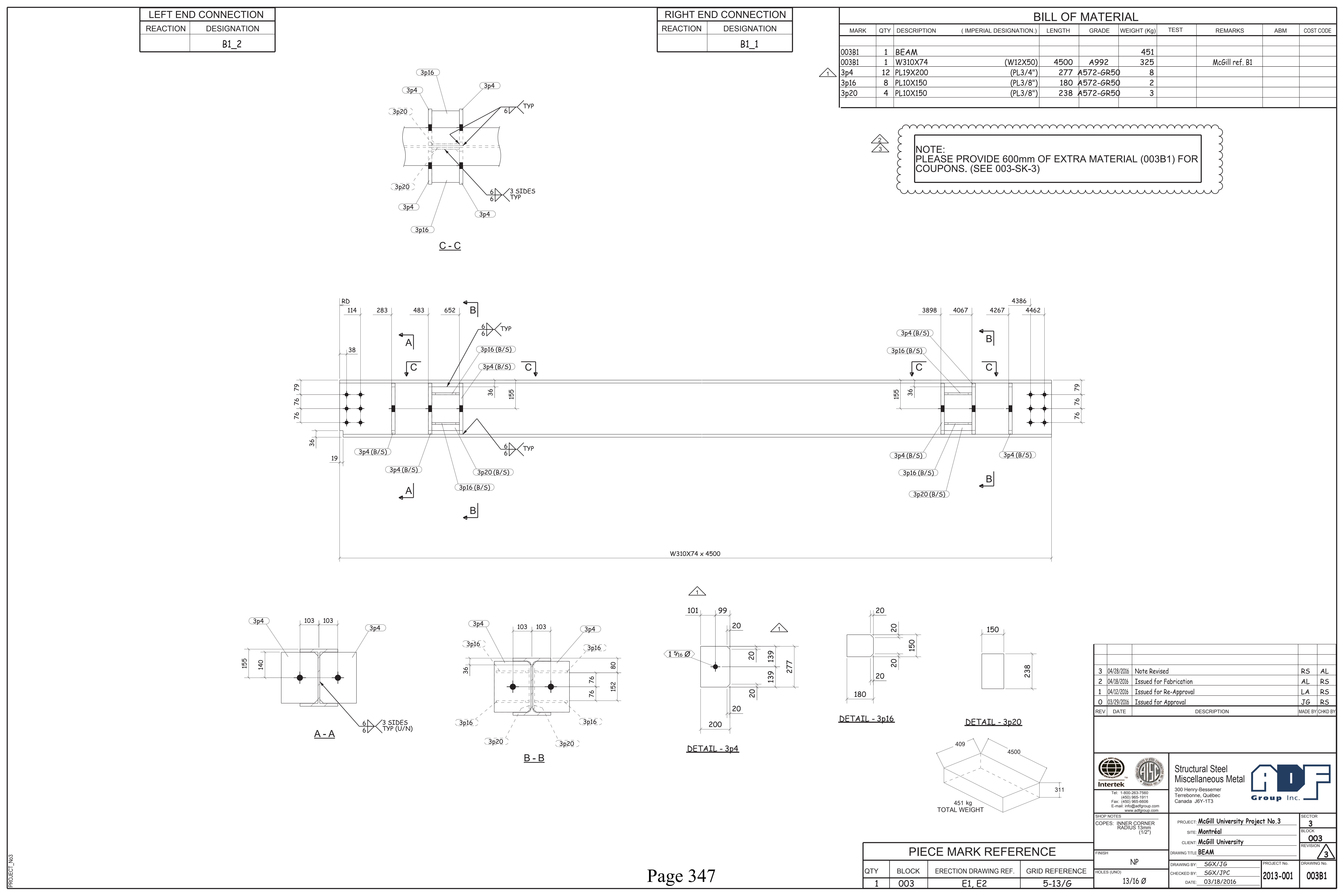


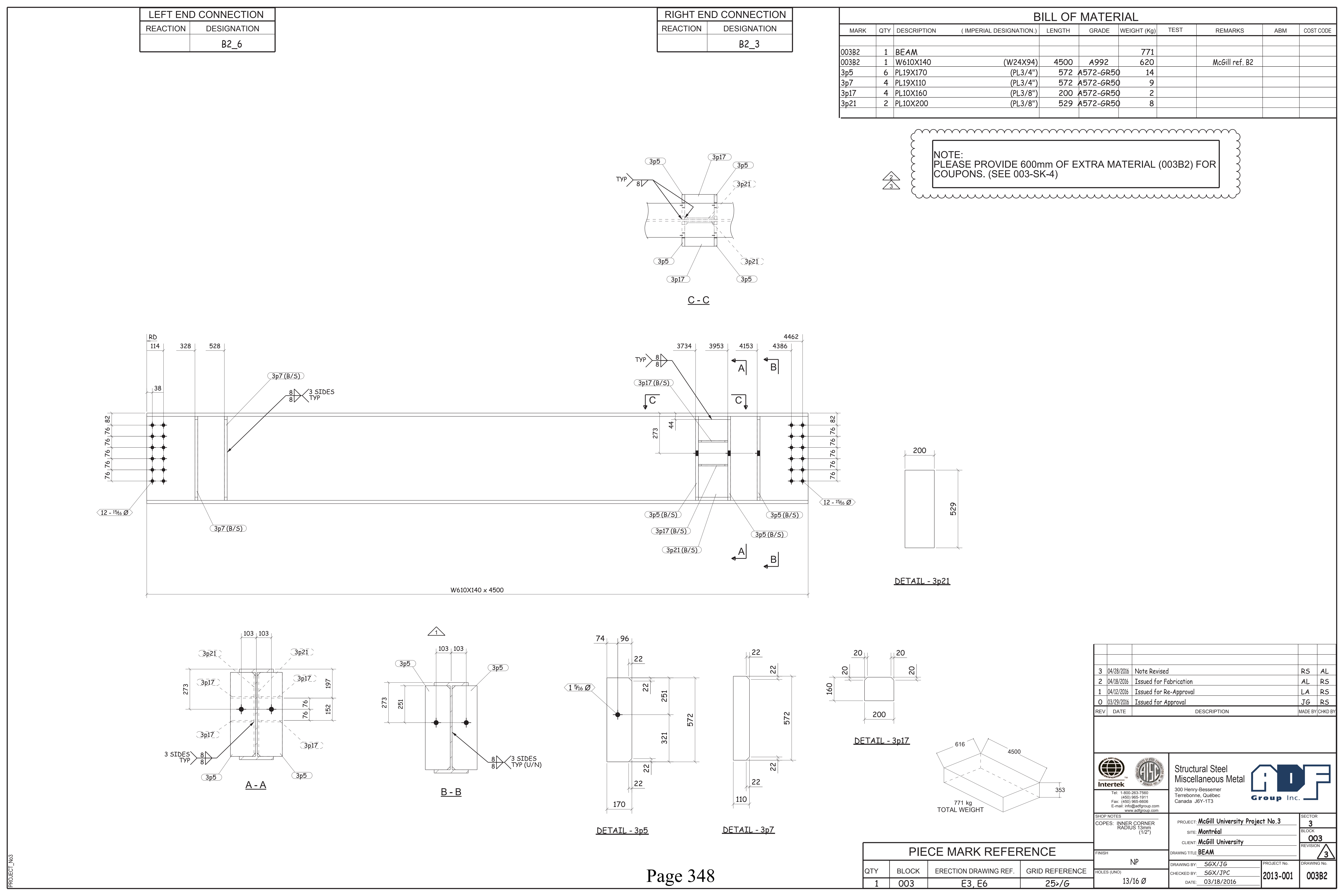


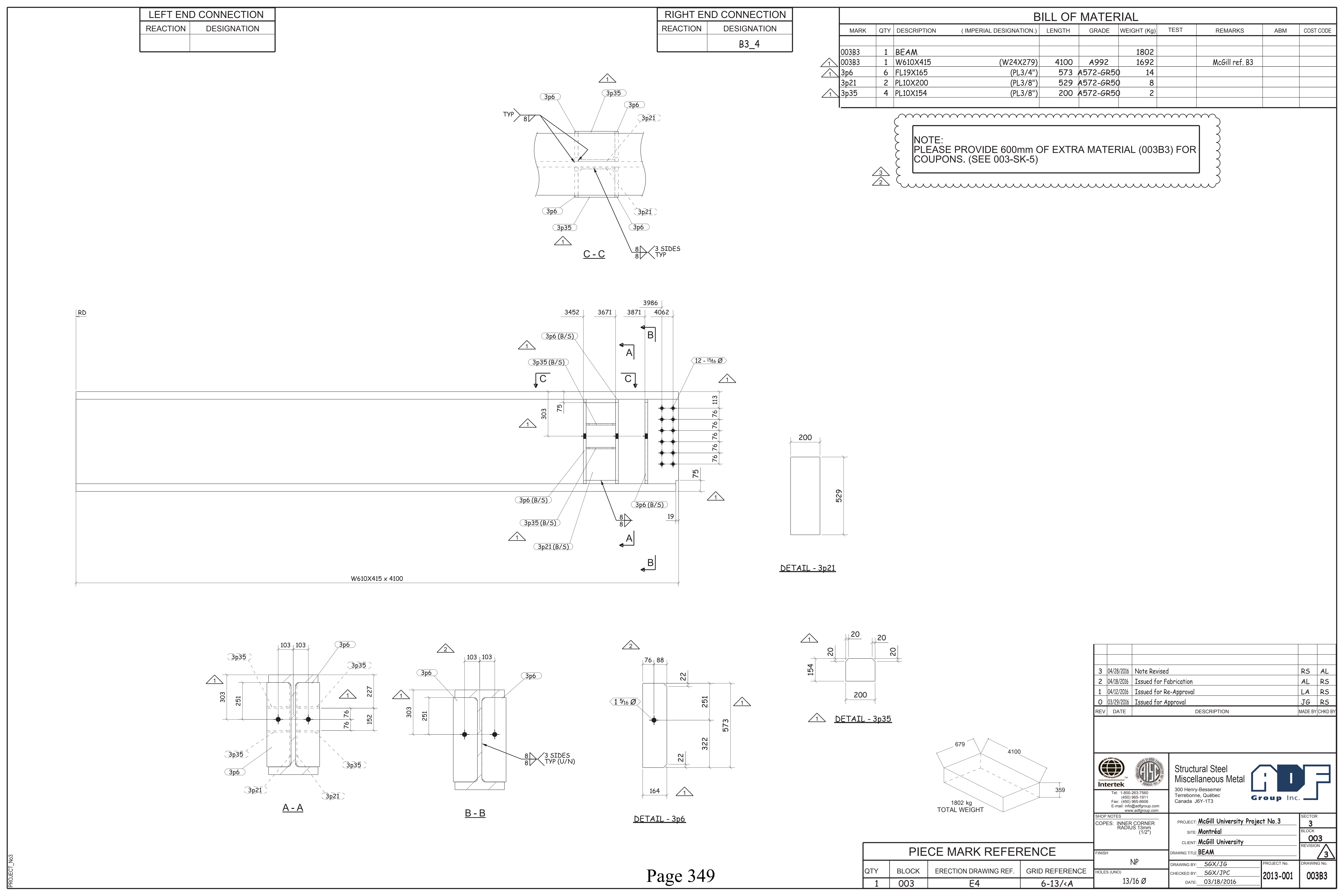


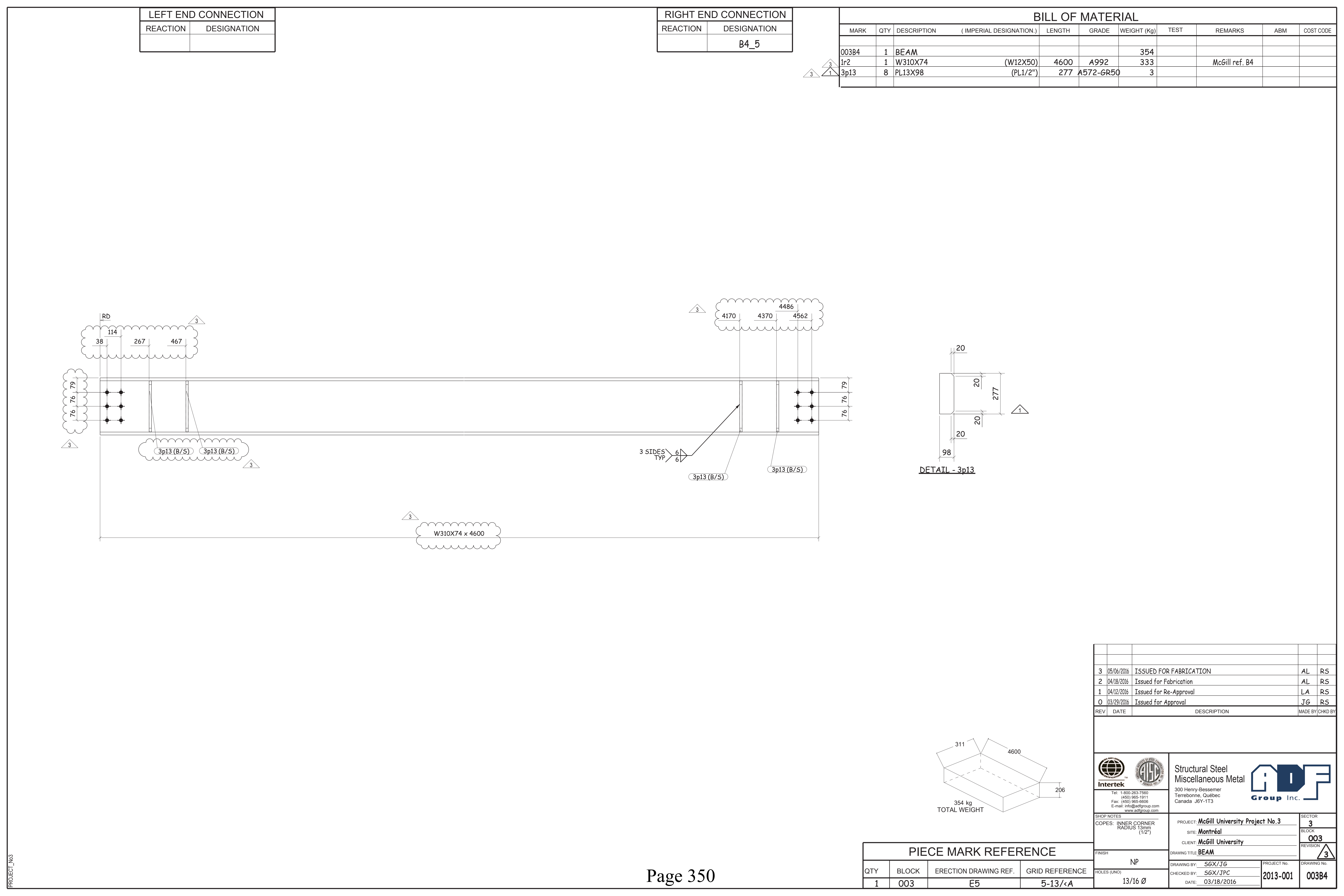


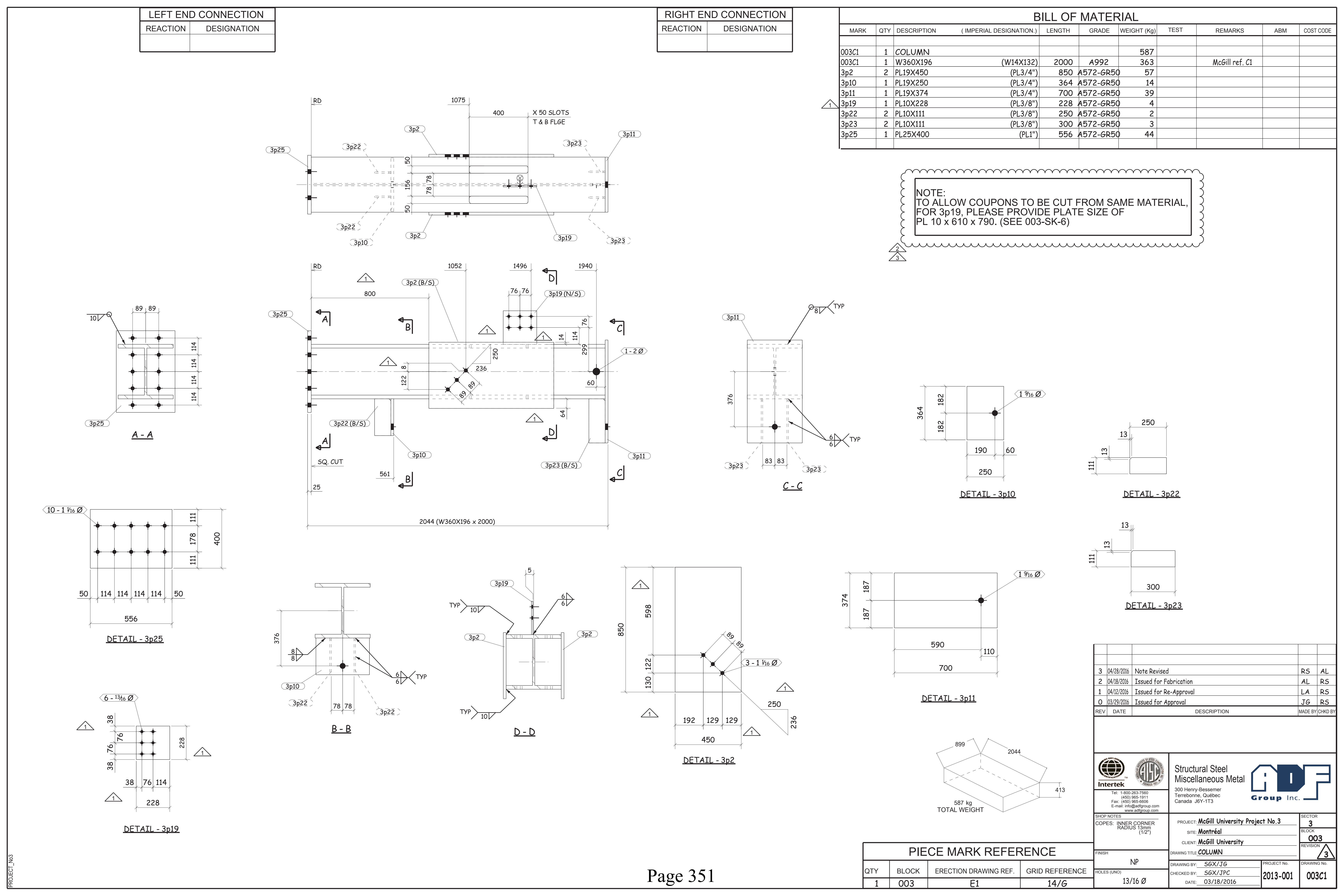


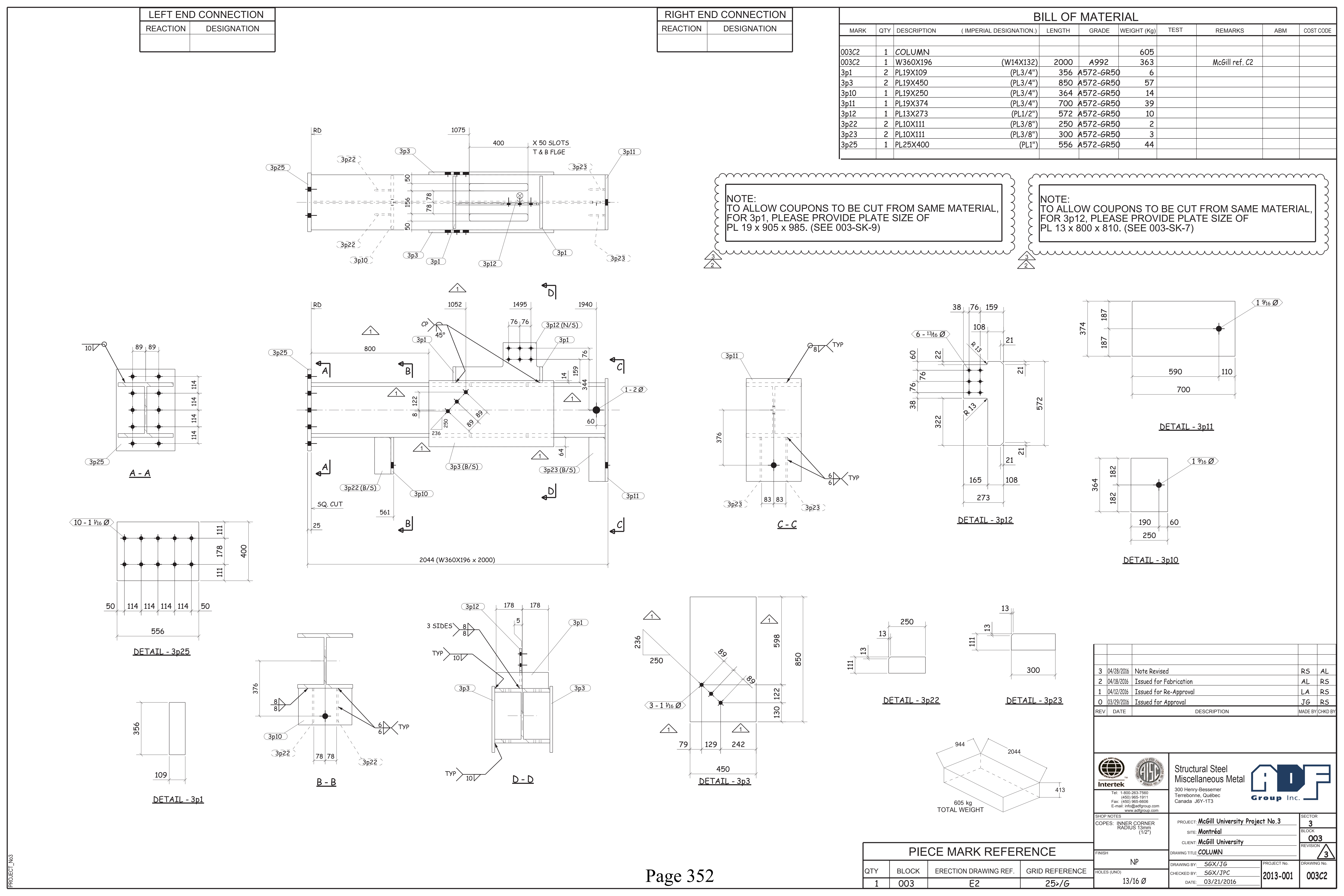


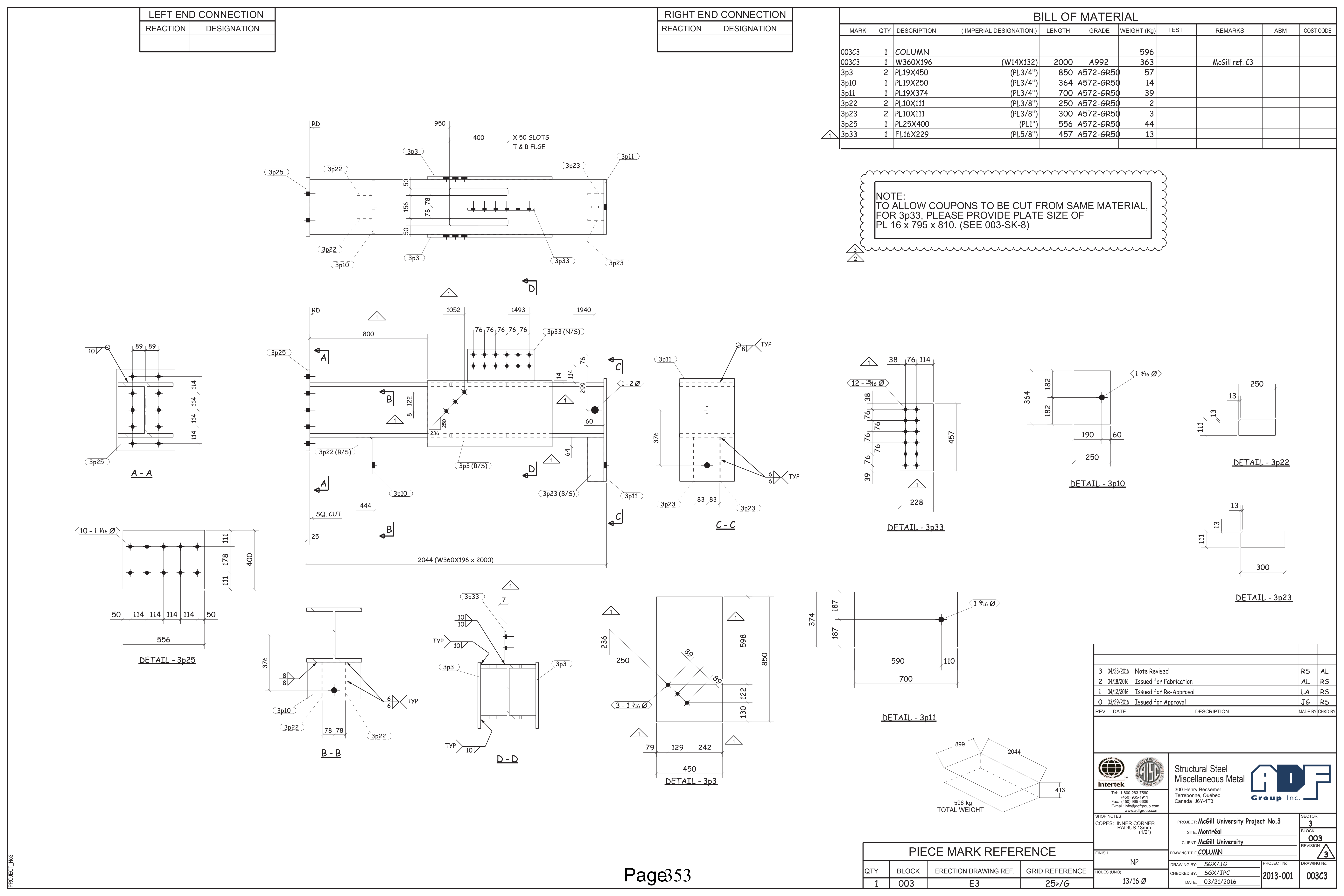


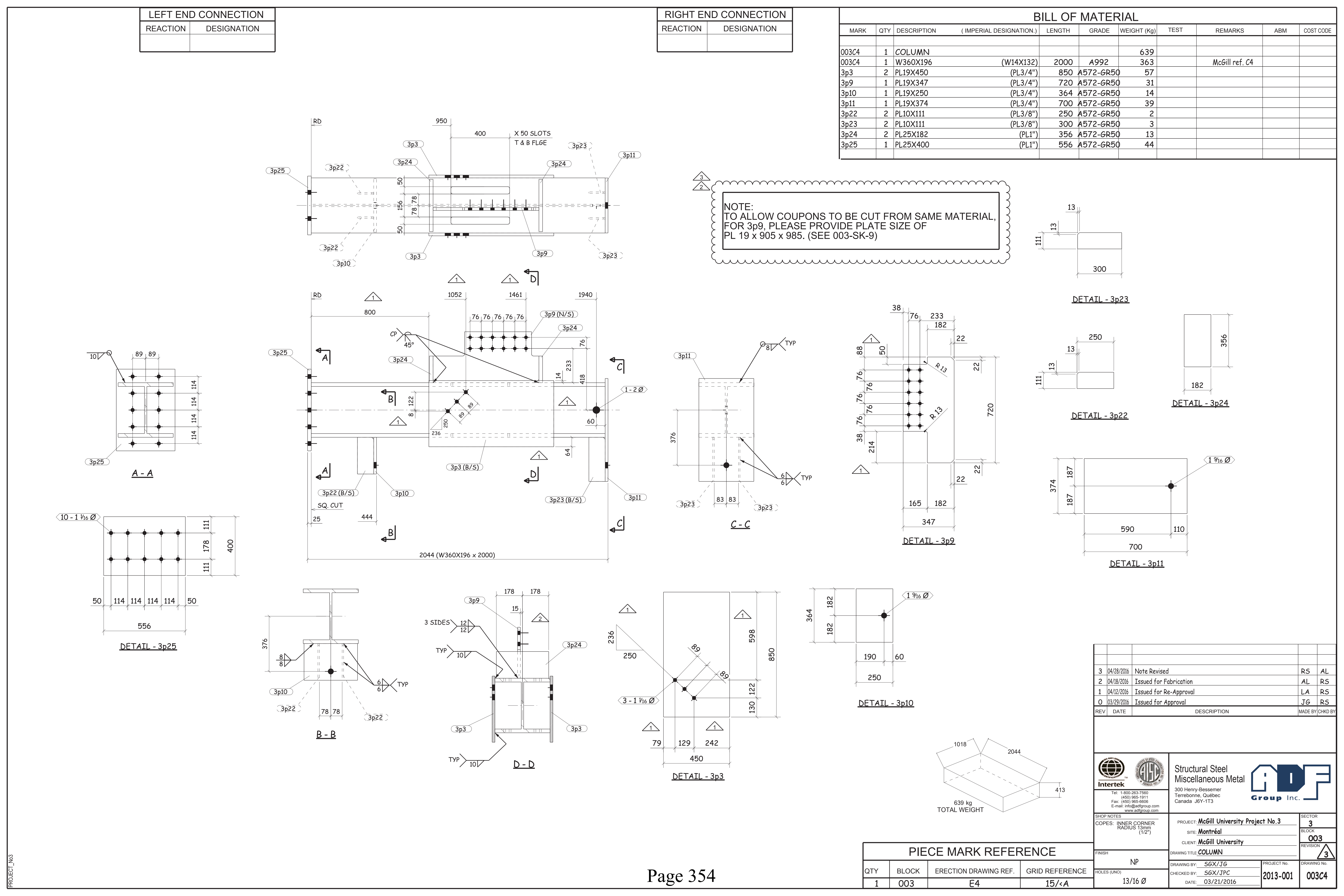










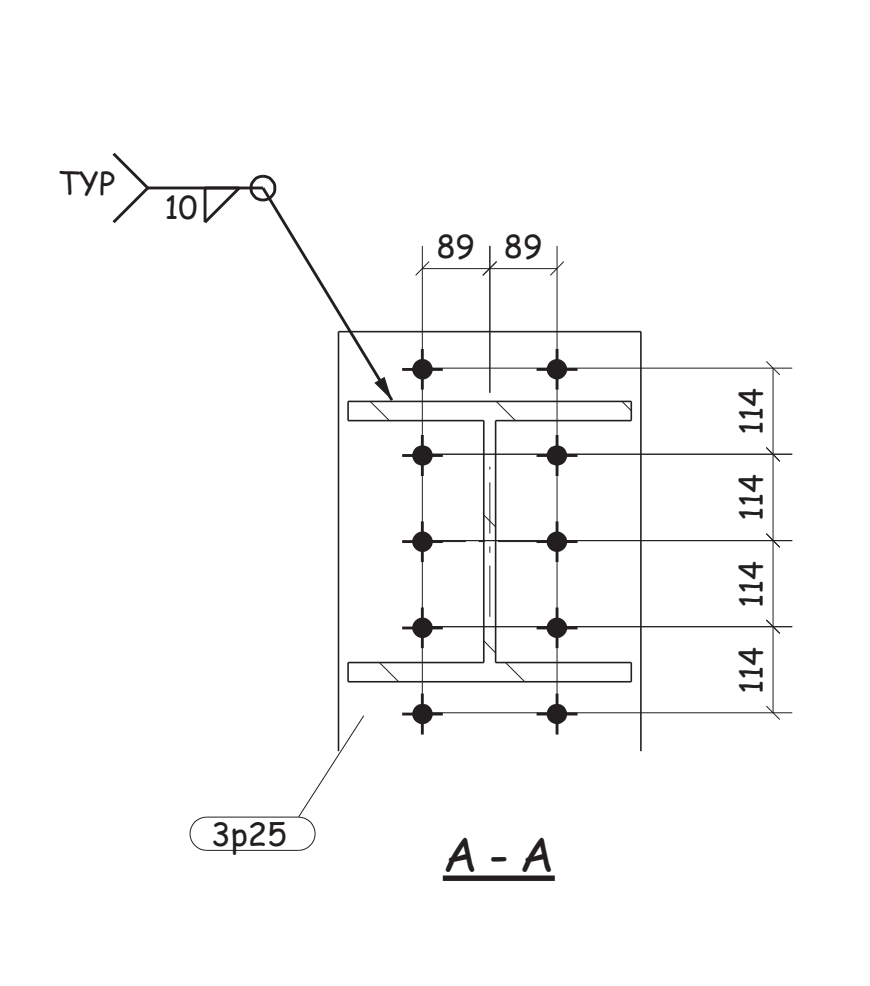


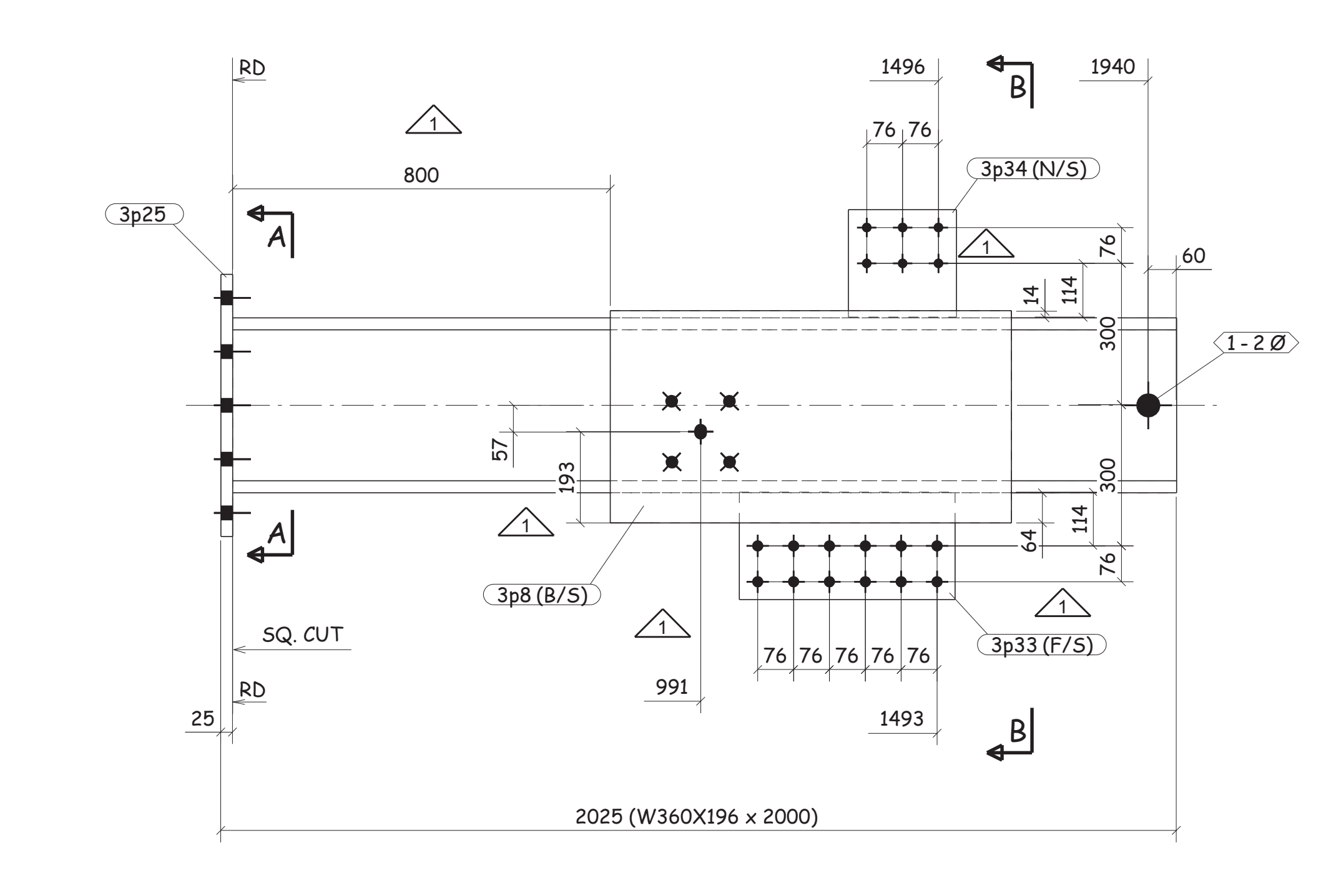
LEFT EN	D CONNECTION	
REACTION	DESIGNATION	

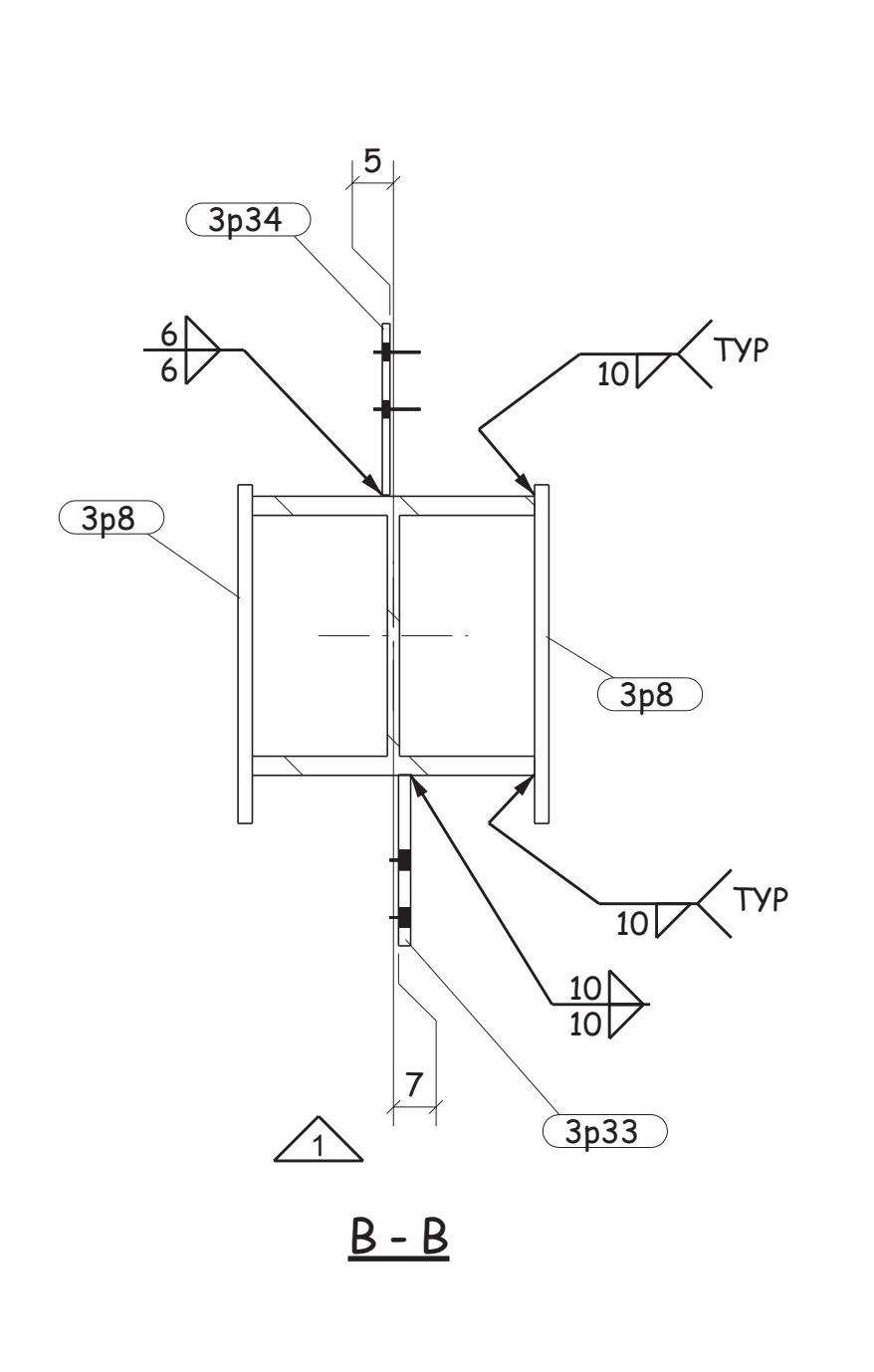
RIGHT EN	ND CONNECTION
REACTION	DESIGNATION

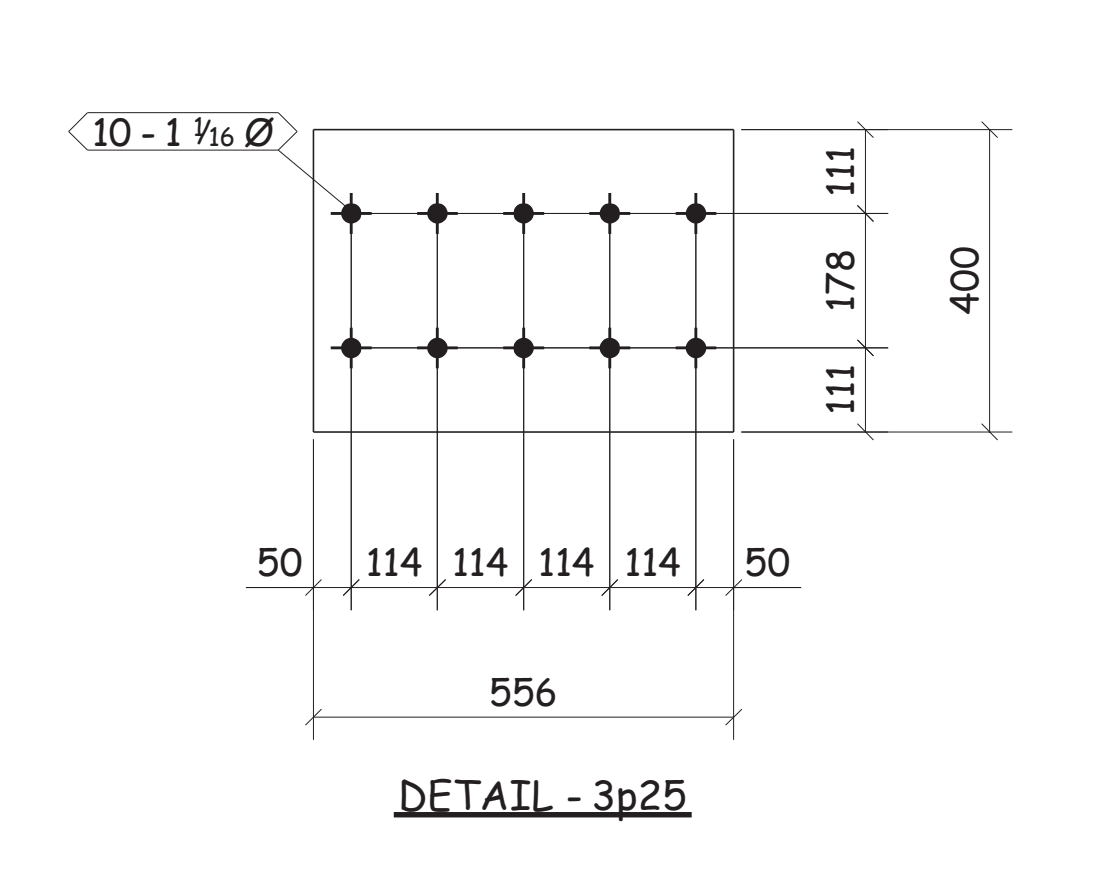
				В	ILL OF	MATER	RIAL				
	MARK	QTY	DESCRIPTION	( IMPERIAL DESIGNATION.)	LENGTH	GRADE	WEIGHT (Kg)	TEST	REMARKS	ABM	COST CODE
	003 <i>C</i> 5	1	COLUMN				554				
	003 <i>C</i> 5	1	W360X196	(W14X132)	2000	A992	379		McGill ref. C5		
	3p8	2	PL19X450	(PL3/4")	850	A572-GR50	57				
	3p25	1	PL25X400	(PL1")	556	A572-GR50	) 44				
$\sqrt{1}$	3p33	1	FL16X229	(PL5/8")	457	A572-GR50	13				
1	3p34	1	PL10X228	(PL3/8")	229	A572-GR50	) 4				

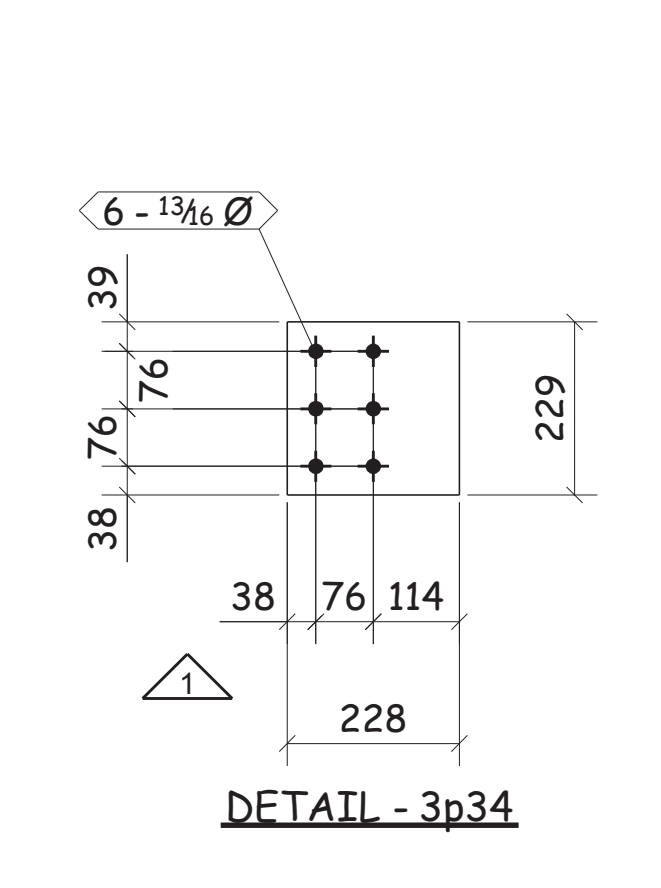
 $\mathcal{M}$ NOTE:
TO ALLOW COUPONS TO BE CUT FROM SAME MATERIAL,
FOR 3p33, PLEASE PROVIDE PLATE SIZE OF
PL 16 x 795 x 810. (SEE 003-SK-8)

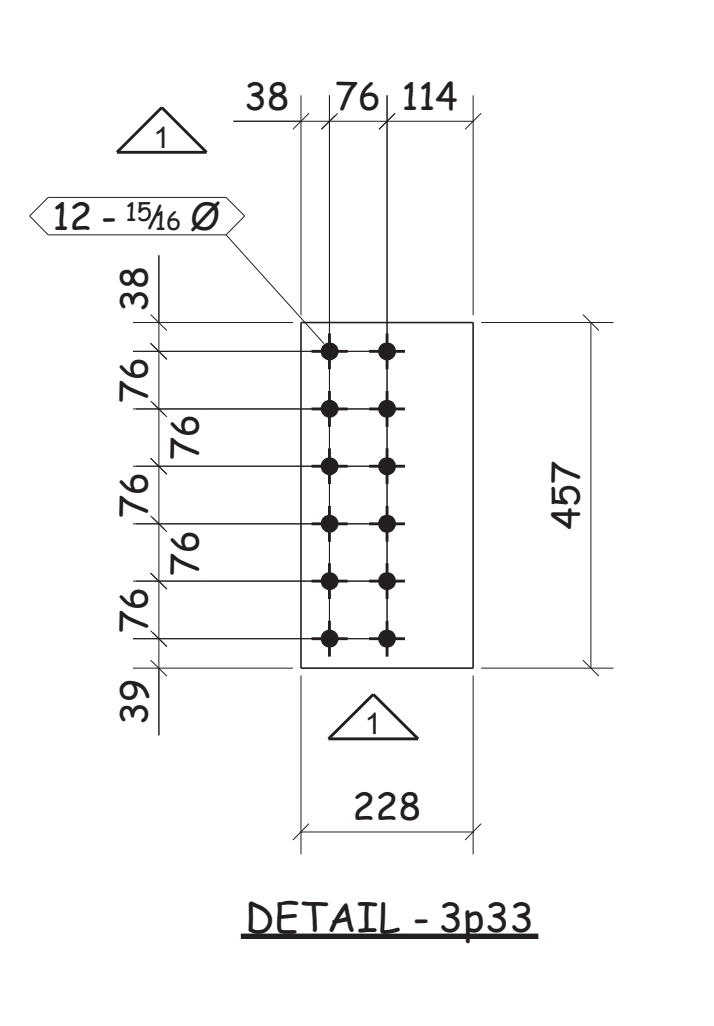


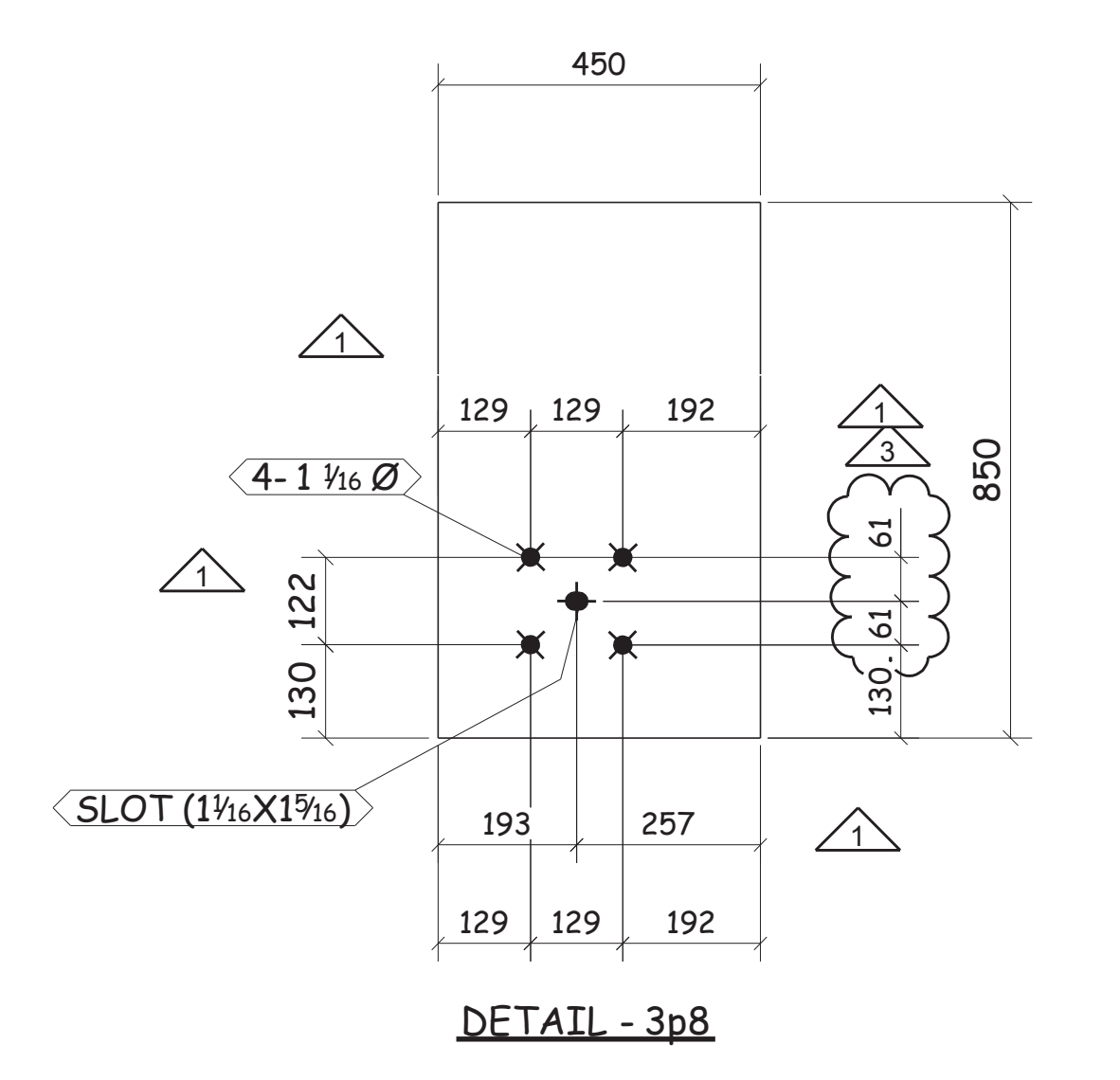






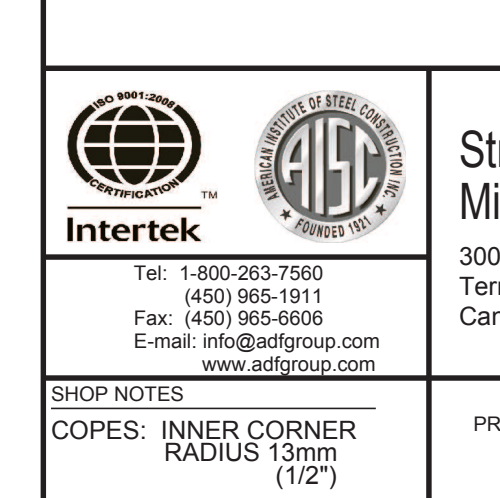






554 kg TOTAL WEIGHT

3	04/28/2016	Note Revised	RS	AL
2	04/18/2016	Issued for Fabrication	AL	RS
1	04/12/2016	Issued for Re-Approval	LA	RS
0	03/29/2016	Issued for Approval	JG	RS
REV	DATE	DESCRIPTION	MADE BY	CHKD



13/16 Ø

HOLES (UNO)

25>/<A

Structural Steel Miscellaneous Metal 300 Henry-Bessemer Terrebonne, Québec Canada J6Y-1T3

Group Inc.

PIECE MARK REFERENCE BLOCK ERECTION DRAWING REF. GRID REFERENCE

E5, E6

003

BLOCK
003
REVISION
RAWING No. PROJECT: McGill University Project No.3 site: Montréal CLIENT: McGill University WING TITLE: COLUMN NP AWING BY: SGX/JG HECKED BY: SGX/JPC
DATE: 03/21/2016 003*C*5 2013-001

## **Appendix C: Instrumentation**

